ISSN: 2249-6645

International Journal of Modern Engineering Research (IJMER)

Volume 4 Issue 11 November 2014

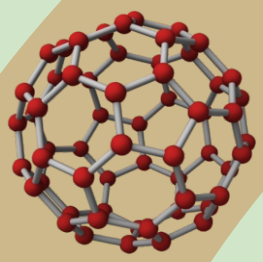

International Journal of Modern Engineering Research (IJMER)

Volume : 4 Issue : 11 (Version-1) ISSN : 2249-6645 November- 2014

Contents :

OPEN ACCESS

International
Journal
Of Modern Engineering Research (IJMER)

Development of a Smart Mechatronic Tracking System to Enhance Solar Cell Panels Performance

Osama A. Montasser
Mechanical Power Engineering Department, Faculty of Engineering, Ain Shams University, Egypt,
On leave to join the British University in Egypt, BUE,

Abstract: *Two degree of freedom Mechatronic solar tracking system was developed in the present study to improve the performance of photovoltaic cell panels. The present tracking control algorithm was applied on a small prototype, simulating a solar cells panel tracking system, designed and constructed in this work. The Mechatronic tracking hardware section consists mainly of a commercial arduino micro-controller with built in, two servo motor drivers, data input/output, and micro processor modules. Other components of the tracking hardware are, servo motors actuators and four LDR light intensity sensors. A feedback control soft ware program, designed and constructed in the present work, enables the solar tracker to automatically compensate for the sun location's change to enhance the PV cells efficiency. The LDR sensors are employed to continuously detect the sun rays intensity at four, light exposed isolated positions, representing up-right, up-left, down-right, and down-left sides of the solar panel. LDRs data is hence sent to the control software. The data is used to decide proper actuation actions and send them to the servomotors to redirect the PV cells panel perpendicular to incident sun rays. Sensors and actuation signals are exchanged via the in/out data module of the Arduino package. Results of the present experimental work show that using the present tracking system increases the PV cell out power by about 38% compared with that of a fixed collector.*

Keywords: *Dual axis tracking systems, micro controllers based Mechatronic systems, solar panel efficiency, solar trackers prototypes, solar tracking systems*

I. INTRODUCTION

Nowadays, clean renewable energy sources attract a great attention as an essential mean for solving the energy crisis around the globe. Solar energy is mostly available free of charge all over the world although it is not a continuous energy source. The increasing concern, in the world, about photovoltaic, PV, modules is mainly due to the fact that they convert solar energy directly into electrical energy without pollution, noise and other factors causing adverse changes in the environment. The cost of photovoltaic systems is systematically decreasing as well. They are extensively accepted as one of the renewable electricity resources. They are appropriate for most applications at moderate initial and low maintenance costs.

Applications of photovoltaic systems are classified as stand-alone, grid connected, and hybrid combinations in the form of a cells module or array. These systems are usually combined with batteries for energy storage. Solar tracking systems for maximizing the PV cells efficiency have a motivated great interest in many researches. Photovoltaic generators work most efficiently when the sun is directed perpendicular to their panel surfaces. Although, solar tracking systems significantly increase PV panel's initial and operational costs, the solar collecting system efficiency is reasonably increased in return.

Mechatronic tracking systems ensure the optimal positioning of the PV panels relative to the Sun's position. According to mobility degree classification, there are two basic types of tracking systems namely, mono axis and dual axis systems. The daily motion, tilting motion of the panel axis corresponding to the sun location's latitude angle, is achieved by the mono axis trackers [1, 2]. The dual axis trackers perform both daily and seasonal, tilting and elevation motions, and therefore, they precisely follow the Sun path all over the year. Dual axis tracking systems increase the PV cell efficiency up to 40–45% , than that of an equivalent fixed systems; compared to a lower increase with the mono axis systems of up to 30–35% [3, 4, 14].

Mono axis trackers have only one motion actuator and therefore they are simpler than dual axis trackers. They are of lower initial investment and their control algorithms for tracking the sun's trajectory are easier to be constructed. Although, the dual axis solar trackers can accurately follow the sun trajectory, any time all over the year and anywhere in the world they need two motion actuators and therefore they are complex to be controlled and more expensive [5, 6].

An ideal sun tracker correctly directs the photovoltaic panel to the sun by compensating for changes in the altitude and azimuth angles of the sun [7]. Sun trackers, in most applications, do not exactly follow trajectory motion of the sun. However, it was fortunately reported that sun's trajectory tracking deviation of 10% may cause an energy decrease of only 1.5% [13].

The orientation of the PV strings can be realized, in practice, in two ways, namely, the independent and the simultaneous orientations. In the independent orientation a separate motion actuator is used for each tracking axis. While, with simultaneous orientation the same motion actuator is used for both tracking axis. This is done by using motion transmitting mechanisms

Tracking control issues were approached in several research studies using different techniques, closed loop systems with photo sensors, open loop systems based on astronomical computerized systems, or hybrid combinations [8–11]. Different models, in the literature, for evaluating the sun radiation as an input data were used for designing tracking systems. The root mean square error was utilized as the main comparative analysis element, in constructing a model for estimating the monthly mean solar radiation [15]. Mathematical model for estimating the hourly and daily radiation incident on three-step tracking planes was developed by [12].

In the present work, a dual axis solar tracker was designed and implemented to maximize PV cells power generation from the incident sun energy. Mechatronic principles were used to construct the tracking control system. A commercial arduino UNO R3 micro controller with built in data input/output, servo motors driver, and micro processor modules was used to implement the tracking control software, designed and constructed in this study. Two degrees of freedom, small prototype was designed and constructed in the present work to simulate a PV cells panel tracking system. The prototype was used to check the success of the present tracking control software program. Servomotors actuators, driven by the drivers built in the arduino package and controlled by the present tracking software were used to move the prototype in horizontal and vertical directions. Four LDR light sensors were used to detect the intensity of the solar rays incident at the panel at its, up-right, up-left, down-right, and down-left positions. Experiments were carried out to check the effectiveness of the present solar tracking system. Present experimental results showed that using the present tracking system increases the PV cell out power by about 38% higher than that of a fixed collector.

The present paper is organized as follows. In the following section, section II, the design and construction of the present tracker model has been presented. The tracking control strategy and flow chart of the present study is over viewed in section III. The present experimental work and results are discussed in the section IV. Conclusions of the present study are summarized in the last section. Acknowledgement, references and list of abbreviations are presented at the end of this paper

II. CONSTRUCTION OF THE PRESENT SOLAR TRACKING MODEL

Implementation of a closed loop solar tracker model is presented in this section. The present Control strategy and software flow chart, used to control the present tracking model, are detailed in the next section. Same tracking control procedure can be applied on real much larger solar panels.

A model of a solar tracker was designed and constructed in this work to evaluate the solar tracking control software, developed in this work. It was used to study the effect of solar tracking on the efficiency of PV solar cells panels. The model composed mainly of the mechanical construction and the electronic hardware required for handling signals between the tracking system and the control software. The mechanical and electronic hard ware's components are described in what follows:

2.1 Model mechanical construction

The solar tracker model was designed to have 2 Degrees of freedom motion. This is achieved by utilizing the rotational motion of two groups of servo motors, one to rotate a vertical cylindrical rod, right and left, around *z* axis, azimuth axis, to follow the sun from east to west directions.

Two U shape brackets, one of them is fixed and the other is movable relative to the fixed one, are mounted by the cylindrical rod. The solar panel is attached to the rotating U bracket to be rotated over the hinges support between the 2 U brackets. The other servo motor, mounted on the fixed bracket, is used to rotate the movable bracket up and down around the x axis, altitude axis, to follow the tracking of the sun in north-south directions.

A conical base, carrying the rod and the brackets, is fixed on a flat plastic base board. The electronic circuits, used for signal handling is fixed on the base board.

Using the solid works 2012 soft ware commercial package, torque analysis was carried out for the rotation of the model around the *x* axis, with its holding brackets, solar panel and one motor attached, to determine the required size of the *x* axis rotation servo motor. Another analyses to decide the size of the *z* axis rotation motor, was performed for the rotation of the vertical rod, holding the whole tracker system, around the *z* axis. Torque around *x* axis was found to be equal to 0.34 N.m downward, thus two motors of 0.3 N.m torque

capacity, available in the market, both are total of 0.6 N.m, were chosen to do the job. It is therefore, a resultant torque for upward rotation of 0.26 N.m is available, which is enough to rotate the solar cells panel. But for downward rotations the resultant torque becomes 0.94 N.m downward, that is too much and therefore an opposing torque is needed to prevent the solar panel from falling. A suitable rubber seal was used to provide the required friction. Taking into consideration, the weight of the second motor, used, in the analyses didn't alter the calculated torque so much, since the motor is of a small weight, 44 g, relative to the total tracker weight of about 1200 g.

The torque required to overcome the friction forces, corresponding to the whole trucker weight, and to easily rotate the vertical cylindrical rod around *z* axis was found to equal to 2.0 N.m. A motor of a size 2.4 N.m, available in the market was selected to do the job. The final assembled solar tracking model is shown in Fig. 1 below.

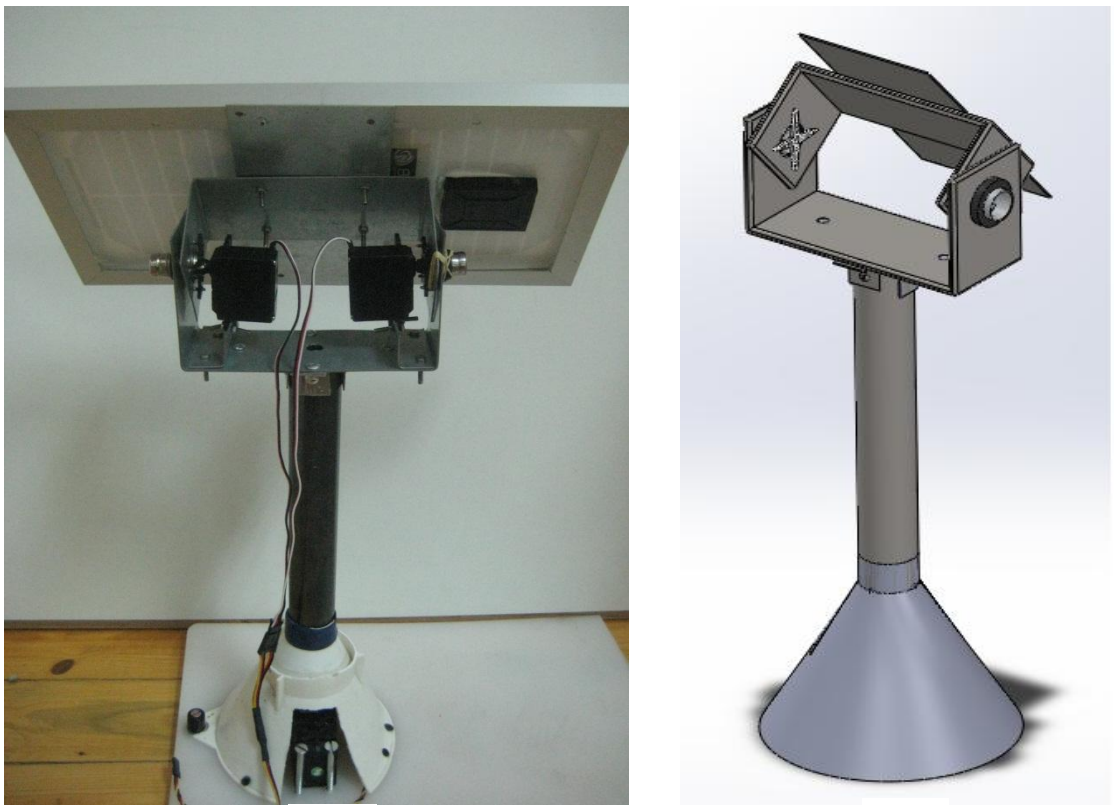

(a) **(b)**

Figure 1 (a) Photographic picture for the tracking model, (b) Final design using the solid works 2012

2.2 Electronic components and circuits

2.2.1. Light intensity detector, LDR

The LDR, light dependant resistance, was selected since it has no polarity, thus easy to interface with circuit, cheap, reliable, and is characterized by high spectral sensitivity, so that variation in light intensity is represented immediately by change in its resistance value. Four LDRs were used to detect light intensity, placed to represent the top-right, top-left, bottom-right and bottom-left directions of the solar panel as shown in Fig. 2 below. A light isolation barrier, 3 mm thick and black colored, shown in Fig. 2, was designed and constructed to prevent sunlight from hitting all the four sensors simultaneously so that the only case when the four sensors receive the same amount of sunlight is when the sun is perfectly normal on the surface of the panel.

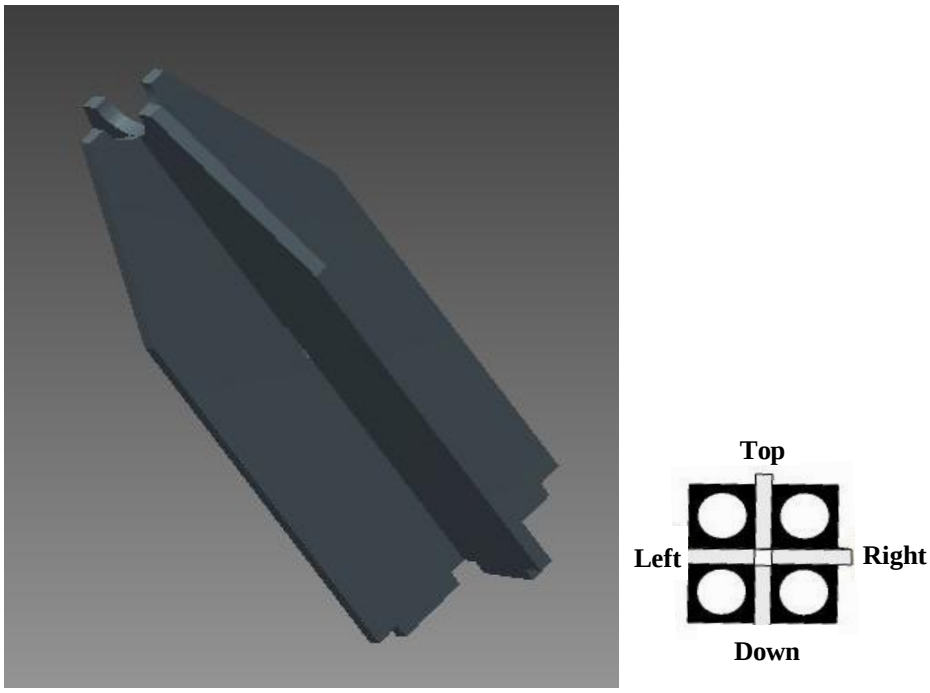

Figure 2 (a) The light isolation barrier, (b) RTDs are isolated by the barrier

2.2.2. Micro controller

Arduino UNO R3 microcontroller was selected in this work. It has two built in servo motor drivers, 8 digital Input/outputs, 6 analog inputs, flash memory of 32 KB and of low power consumption. These specifications are sufficient for the present required tracking task.

2.2.3. Servo motor actuators

As it is detailed above in the mechanical construction section, two motors of type Parallax 900.00005, 0.3 N.m torque and 44 g weight, were selected for the *x* axis rotational motion, and one motor of type Hitec 805BB+, 2.4 N.m torque is selected to rotate the present tracking system around *z* axis.

2.2.4. Solar Array

Mono-crystalline solar PV cells were chosen of model RYW-005-012. Although mono-crystalline cells are of less improved performance than the thin film cells, as interpreted from theoretical basis and literature review, they were selected due to their availability in the market. The PV cells were arranged in array assembly as a combination of series and parallel connections to give out put voltage of 5 V of maximum allowable current so that a load of 5 W can be applied. The dimensions of the assembled array are 330 long, 170 wide, and 17 mm thick of total mass with the carrying panel of 0.75 kg.

2.2.5. RTDs signal processing circuit

Voltage divider circuits, as shown in Fig. 3, are used to convert the change in the LDR resistance into analog voltage signal as a control usable signal. The resistance of LDR is theoretically equal to infinity and zero values in fully dark and fully bright conditions respectively. The variable resistance value was experimentally adjusted so that the circuit output voltage becomes near the zero value in the usual surrounding darkness time, 23 mV, and approaching the 5 V value as the light intensity approaches its usual maximum value at the noon time. Voltage divider circuit was repeated four times for the four LDRs used.

The RTDs output analog voltage signal is protected against loading effect, expected in case of utilizing voltage dividers, by using a buffer integrated circuit, IC. Voltage dividers signals are connected to the input of quad unity gain followers OP AMPs integrated circuit so that the OP AMPs output signals becomes loading error free. The RTDs circuit is shown in Fig. 3 below.

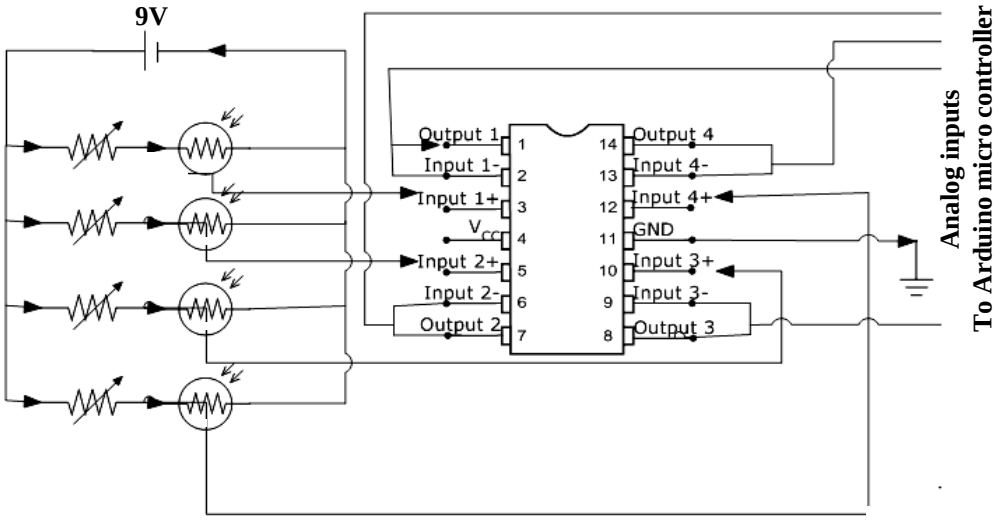

Figure 3 RTDs signal processing circuit

2.2.6. Arduino micro controller circuit

The buffered RTDs signals are connected to four analog inputs of the arduino micro controller package. One of the two servo motor driver, built in the arduino package, is used to drive the two motors of the tracker *x* axis rotation, as connecting in parallel. The tracker *z* axis rotation motor is driven by the other arduino driver. Fig. 4 below shows the arduino signals connection circuit.

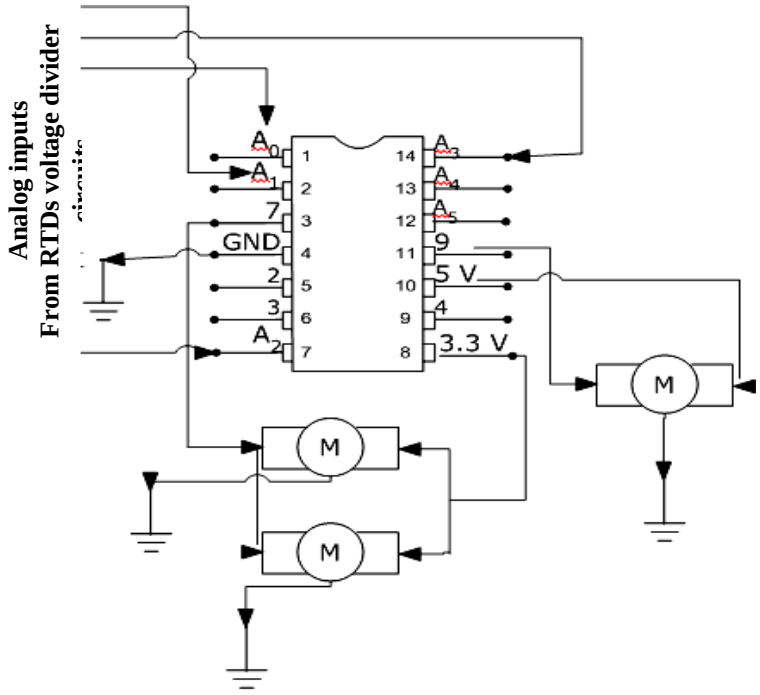

Figure 4 Arduino micro controller signal connections circuit

III. THE PRESENT CONTROL STRATEGY

Light intensity are detected at four panel positions, namely, the top-right, top-left, bottom-right and bottom-left positions. Four LDRs were used to do the job. A light isolation barrier is used to prevent sunlight from hitting all of the four sensors simultaneously so that the only case when the four sensors receive the same amount of sunlight is when the sun is perfectly perpendicular to the surface of the panel. The RTDs signals are sent to the tracking software to redirect the panel normal to the incident sun rays according to how the sun rays

hit the panel. Proper control actions are decided and sent to the servomotor drivers so that the change of the sun location is compensated for. The input/output data module of the arduino micro controller is used to exchange the control signals between the tracking control software and the tracking system. The tracking software is processed by the arduino micro processor and stored by its cash memory.

For example, if the top right and bottom right LDR's are receiving sunlight while the other two LDR's are in the shadow, then motor will move the panel to right until all the four sensors are receiving the same amount of the sunlight. Fig. 5 shows a schematic diagram for the tracking control soft ware.

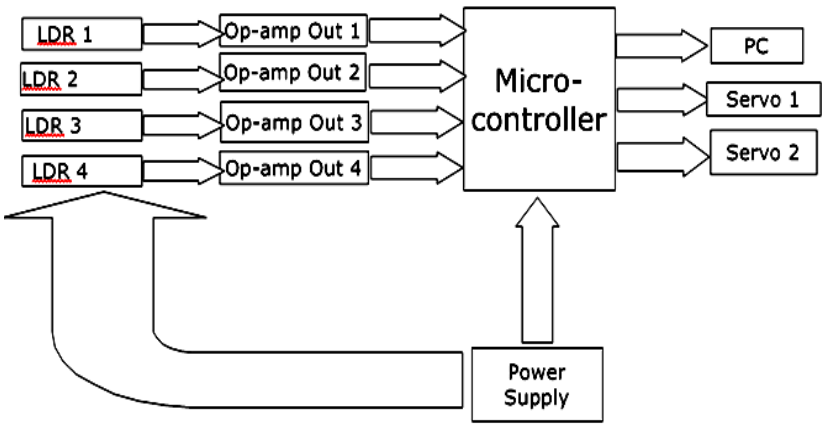

Figure 5 Schematic block diagram for the present tracking software

The RTDs signal pass through the OP AMP buffering circuits on their way to the analog input terminals of the arduino micro-controller. The tracking software, stored in the cash memory of the arduino, reads the light intensity signals. The control strategy of the software is processed by the arduino micro processor. Decided control actions commands, such that rotate with a specified angle increment or not, go to the servo motor actuators through the drivers, built in the arduino circuit. Connection with a personal computer is used to construct the control program and to load it in the arduino's memory.

3.1 The present Control software flow chart

Defining the following terms as:

θ:	Rotational angle around *x* axis	ϕ:	Rotational angle around *z* axis
UR:	For the up-right sensor reading.	UL:	For the up-left sensor reading.
DR:	For the down-right sensor reading.	DL:	For the down-left sensor reading.
U:	For UR + UL	D:	For DR + DL.
R:	For UR + DR	L:	For UL + DL.
UD:	UD = absolute (U – D).	RL:	RL = absolute (R – L).

The control target is to achieve both UD and RL equal to zero. But since noise is most probably affects the voltage readings so a dead band threshold is taken as 122 mV, equivalent to a binary corresponding value of 100. So if UD is greater than 100, digital, then if U > D, move the tracker to up, in counter clock wise, CCW, direction, and if D > U, move the tracker to down, in clock wise, CW, direction. Also, if RL is greater than 100, digital, then if R > L, move the tracker to right, in CW direction, and if L > R, move the tracker to left, in CCW direction. The flow chart of the soft ware is shown in Fig. 6.

IV. PRESENT EXPERIMENTAL RESULT

An experimental work was carried out in this study to evaluate the effectiveness of the present solar tracking model. The experiments were performed as follows:

4.1. Testing the control hard ware equipment

Basic control circuits were carried out to test the Arduino microcontroller using a number of buzzers and LED's in order to ensure that the microcontroller is operating as it should be.

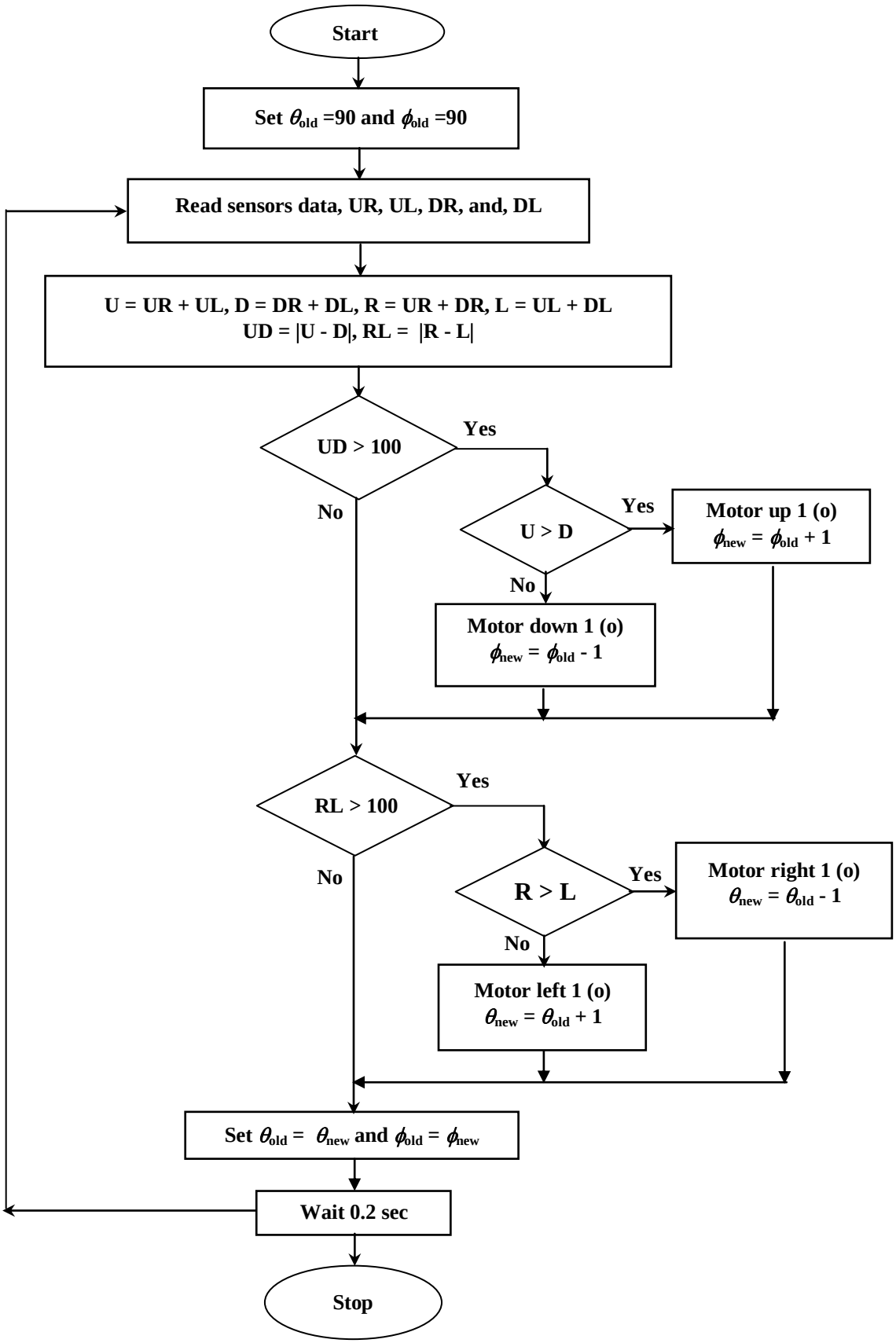

Figure 6 Flow chart of the present tracking control software

Commands for servo motors were written by the arduino software to ensure they are functioning properly under no load conditions. Servos motors are built in feedback controlled to reach a certain specified angle. They are initially set at 90 degrees. A command for increasing the motor angle above 90 (o) cause it to rotate in CCW direction and vice verse. The function "*write (angle value)"* gives a command to the servo motor to rotate to the given angle value, even it is large or less than its current angle. Testing the servos was crucial to ensure the absence of mechanical problems under no load conditions.

4.2. Light tracking experiment

The purpose of this experiment is to ensure that the tracker is functioning properly, attaching the PV cells on the tracker is not necessary in this step as the experiment was conducted in a room with low light intensity, dark conditions, to ensure reaching the light source the LDRs.

Controlling light sources that reaching LDRs is important to ensure that any output is due to light source acting as the sun in this simulation. In this case a torch was used to monitor the movements of the tracker corresponding to light variations.

Torch light was focused on the solar panel, on which the sensors are fixed, from various angles. Test results showed that the tracker successfully moves towards the direction of the torch light wherever it comes from.

4.3. PV voltage generation experiment

The experiment was conducted on two different days. First day, 5 readings were taken every one hour from 11:00 AM to 3:00 PM, representing the most effective daily sun power period. Solar PV cells panel was placed on the tracker, fixed without operating the tracking control system. Solar panel was fixed in the position recommended by the literature under the sun with no tracking occurred.

Second day, another 5 readings were taken at the same times as the previous day, but the tracking control was fully operated. Readings were taken for the panel output generated voltage measured by a voltmeter. The voltage reading is presented in Table 1 below. Experiment was conducted on the 11th and 12th of June 2014. Fig. 7 shows the distribution of the generated voltage for both the tracked and the un-tracked sun power collectors. Experiment data is presented in table 1.

Fig. 7 shows that, the voltage value produced at the noon time, 12 PM, is almost the same for both tracked and un-tracked panels. This result is expected since the fixed panel is already pre directed to be perpendicular to sun light rays at and near the noon time, as recommended by the literature.

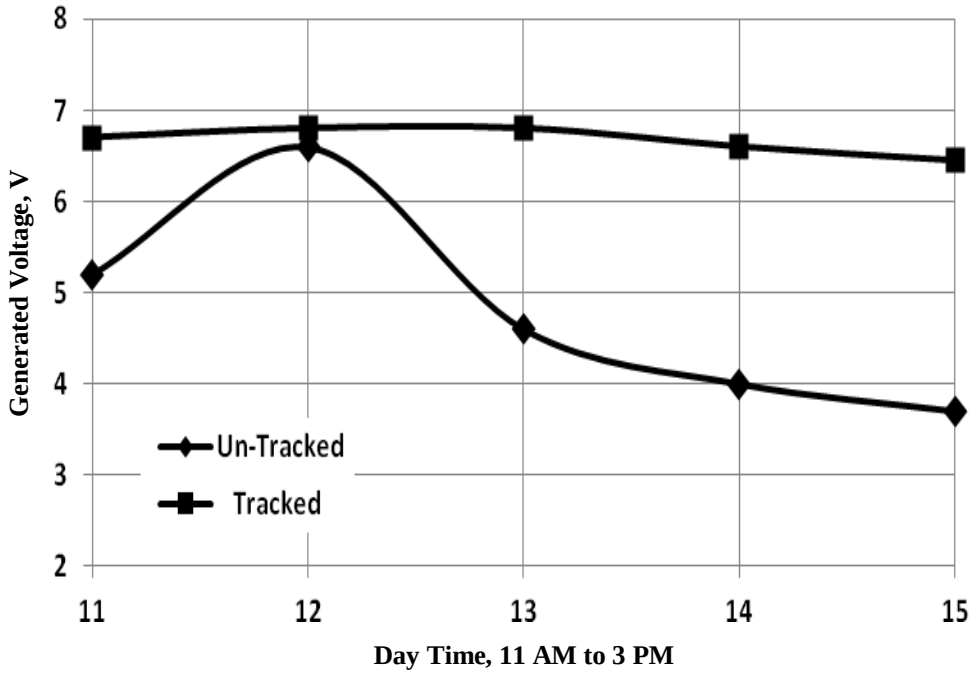

Figure 7 Daily time distribution of the generated voltage data for tracked and un-tracked solar collector systems

Table 1: Readings of the voltage generated experiment

Time	***Generated Voltage, V***	
	Tracked	***Un-Tracked***
11:00 AM	6.70	5.20
12:00 AM	6.80	6.60
1: 00 PM	6.80	4.60
2: 00 PM	6.60	4.00
3: 00 PM	6.45	3.70

Table 1 shows that the average generated voltage values are 6.67 V and 4.82 V for tracked and fixed panels respectively. This result shows that an improvement of 38.4% is gained, in the solar energy collecting efficiency, by using the present solar tracking system.

V. CONCLUSIONS

A dual axis solar control tracking system was designed and constructed in the present work. Two degrees of freedom small prototype was designed and constructed to simulate a tracking system of PV cells panels. A commercial arduino UNO R3 micro controller package was used to execute the present tracking control software. LDR light sensors were used to detect the intensity of the solar light incident on the PV cells panel. The control tracking software receives the light sensors data, according to which, it decides proper actions to actuate servo motor actuators so that change of sun location is compensated for to maximize the PV cells out electric power. Experiments to evaluate the present system tracking performance were carried out to check its light tracking process and the status of its output power along a period from 11 AM to 3 PM, representing the most effective daily sun power period.

Conclusions of the present study are summarized as follows:

1- The present tracking system successfully traced the light source even it is a small torch light, in a dark room, or it is the sun light rays.
2- The present system succeed in keeping the sun incident light rays perpendicular to the surface of the solar cells panel all the day light time.
3- A significant increase in output generated power of about 38% higher than of an equivalent fixed panel is concluded. The output power was measured as the average value of the panel produced voltage over the day light time.
4- The voltage value produced at the noon time, 12 PM, is almost the same for both tracked and un-tracked panels. This result is expected since the fixed panel is already pre directed to be perpendicular to sun light rays at and near the noon time.

ACKNOWLEDGEMENTS

The author would like to express his deep thanks to Mohamed Tarek and Mazen Emad, graduate students of the British University in Egypt, BUE, for their sincere help in constructing the tracker model and in carrying out the experiments.

REFERENCES

Journal Papers:

[1] E. Calabro, An algorithm to determine the optimum tilt angle of a solar panel from global horizontal solar radiation, *Journal of Renewable Energy, vol. 2013, Article ID307547*, 2013,12 pages.
[2] S. Seme, G. Stumberger, and J. Vorsic, Maximum efficiency trajectories of a two-axis sun tracking system determined considering tracking system consumption, *IEEE Transactions on Power Electronics, vol. 26, no. 4*, 2011, 1280–1290.
[3] C. Alexandru and I. N. Tatu, Optimal design of the solar tracker used for a photovoltaic string, *Journal of Renewable and Sustainable Energy, vol. 5, no. 2, Article ID023133*, 2013, 1–16.
[4] S. Seme and G. Stumberger, A novel prediction algorithm for solar angles using solar radiation and Differential Evolution for dual-axis sun tracking purposes, *Solar Energy, vol. 85, no. 11*, 2011, 2757–2770.
[5] Y. Oner, E. Cetin, H. K. Ozturk, and A. Yilanci, Design of a new three-degree of freedom spherical motor for photo voltaic tracking systems, *Renewable Energy, vol. 34, no. 12*, 2009, 2751–2756.
[6] I. Sefa, M. Demirtas, and I. C. olak, Application of one-axis sun tracking system, *Energy Conversion and Management, vol. 50, no. 11*, 2009, 2709–2718.

[7] K. K. Chong and C. W. Wong, General formula for on-axis sun-tracking system and its application in improving tracking accuracy of solar collector, *Solar Energy, vol. 83, no. 3*, 2009, 298–305.
[8] K. S. Karimov, M. A. Saqib, P. Akhter, M. M. Ahmed, J. A. Chattha, and S. A. Yousafzai, A simple photo-voltaic tracking system, *Solar Energy Materials and Solar Cells, vol. 87, no. 1–4*, 2005, 49–59.
[9] F. R. Rubio, M. G. Ortega, F. Gordillo, and M. Lopez-Martınez, Application of new control strategy for sun tracking, *Energy Conversion and Management, vol. 48, no. 7*, 2007, 2174–2184.
[10] S. Abdallah and S. Nijmeh, Two axes sun tracking system with PLC control, *Energy Conversion and Management, vol. 45, no. 11-12*, 2004, 1931–1939.
[11] M. Alata, M. A. Al-Nimr, and Y. Qaroush, Developing a multipurpose sun tracking system using fuzzy control, *Energy Conversion and Management, vol. 46, no. 7-8*, 2005, 1229–1245.
[12] B. Ai, H. Shen, Q. Ban, B. Ji, and X. Liao, Calculation of the hourly and daily radiation incident on three step tracking planes, *Energy Conversion and Management, vol. 44, no. 12*, 2003, 1999–2011.

Chapters in Books:
[13] R. Corio, M. Reed, and L. Fraas, Tracking the sun for more kilowatt hour and lower-cost solar electricity, in Solar Cells and Their Applications, (New York, NY, USA: John Wiley & Sons, 2010), 207–217.

Proceedings Papers:
[14] C. Alexandru and C. Pozna, Simulation of a dual-axis solar tracker for improving the performance of a photovoltaic panel, *Proceedings of the Institution of Mechanical Engineers A, vol. 224, no. 6*, 2010, 797–811.
[15] R. Sorichetti and O. Perpinan, PV solar tracking systems analysis, *in Proceedings of the 22nd European Photovoltaic Solar Energy Conference (EUPVSEC 07)*, 2007, 246–252.

Abbreviations

CCW: Counter clock wise.
CW: Clock wise.
IC: Integrated circuit.
LDR: Light dependent resistance.
new: The rotational angle value at the current control step.
old: The rotational angle value at the previous control step.
OP AMP: Operational amplifier.
θ: Tracker horizontal rotational angle around the *z* axis.
ϕ: Tracker vertical rotational angle around the *x* axis.
PV: Photovoltaic.

OPEN ACCESS

International
Journal
Of Modern Engineering Research (IJMER)

Punching Shear Strength of High Strength Fibre Reinforced Concrete Slabs

Dr. Abhijeet P. Wadekar[1], Prof. Rahul D. Pandit[2]
[1]*Principal of People's Education Society's, P. E. S. College of Engineering, Aurangabad, Maharashtra, India.*
[2]*Faculty of CSMSS's, Chh. Shahoo College of Engineering, Kanchanwadi, Aurangabd, Maharashtra, India*

Abstract: *The experimental study of punching shear behavior of High Strength fiber reinforced concrete slabs is carried out in the present work. Each of 24 square slabs was simply supported along four edges and loaded to failure under a concentrated load over a square area at the center. The test parameters were the effective span to depth aid ratio, volume fraction of 3 types of steel fibers, slab thickness h, concrete strength fck, and size of load-bearing plate r. Test results indicate that the load-deflection curve of slabs exhibits four distinct regions that may be characterized by first cracking, steel yielding, and ultimate load. Within the scope of the test program, an increase in the values of pf, h, or r was found to lead to an increase in both the punching shear strength and the ductility of the slab. The ultimate punching shear strength of the slabs was compared with the predictions of equations available in the literature and code equations for reinforced concrete.*

Key Words: *Steel Fibres, High Strength Fibre Reinforced Concrete, Punching shear strength, deflection.*

I. Introduction

High StrengthFibres Reinforced concrete (HSFRC) is being increasingly used in civil engineering construction due to its improved resistance to cracking, fatigue, abrasion, and impact and its greater durability, than conventional reinforced concrete (Vondran 1991). Some examples are its applications in shotcrete, precast concrete products, pavements, concrete floors, seismic structures, and structural repair.

HSFRC-slab applications are suited for bridge deck slabs, industrial floors or in flat-slab construction where, besides resistance to fatigue or damaging dynamic forces, additional reinforcement is required to avoid punching shear failure due to concentrated loads. Although much research has been carried out on HSFRC ("State" 1982), little attention has been focused on the punching shear behavior of HSFRC slabs. As a result, the full economical benefits of steel fibers in such applications may not be realized.

In this study, an investigation has been carried out on the punching shear behavior of HSFRC slabs. Each of 24 square slabs was prepared and tested under a concentrated load. The load-deflection characteristics and cracking pattern of the slabs were observed and compared. The ultimate punching shear strength of the slabs was compared to predictions made using the equations available in the literature as well as those given in building codes ("Building" 1989; "Code" 1972; "Model" 1978; "Structural" 1985; "Standard" 1986) for the punching shear strength of reinforced concrete slabs.

Objectives and Scope

The investigation is focused to study the effect of various types of fibres on punching shear strength of HSFRC slab.

The water to cementitious material ratio considered for the study of HSFRC of M70 grade was 0.27. The content of silica fume and fly ash in every mix was 5% and 10% by the weight of cementitious material. Three types of fibres considered for the study include, Hook Ended Steel Fibres (HESF), Flat Steel Fibres (FSF) and Waving Steel fibres (WSF). Dosage of fibre was varied from 0.5% to 4% at an interval of 0.5% by weight of cementitious material. Type of cement, fine aggregate, coarse aggregate, type of superplasticiser and its dosage are kept constant in every mix.

II. Test Program

Twenty fourHSFRC slabs were tested. The parameters investigated included the effective span to depth ratio, aid volume fraction of steel fiber p_f, thick-

Table 2.1: Schedule of Experimental Program

Sr. No.	Mix designation of M70 grade HSFRC	Fibre content (%)	No. of specimen (cubes, cylinders and prisms each) using types of Fibres		
			HESF	FSF	WSF
	M0	0.0	3		
	M1	1.0	3	3	3
	M2	2.0	3	3	3
	M3	3.5	3	3	3
	M4	4.0	3	3	3

2.1. Materials

Ordinary Portland Cement of 53 Grade conforming to IS: 12269-1987 was used in the investigation. The properties of cement are presented in Table 2.2.

Table 2.2: Physical Properties of Ordinary Portland Cement (OPC)

Sr. No.	Description of Test	Results
01	Fineness of cement (residue on IS sieve No. 9)	6.5%
02	Specific gravity	3.15
03	Standard Consistency of Cement	30
04	Soundness test of Cement (With Le-Chaterlier'sMould	1.5mm
05	Setting time of cement Initial setting time Final setting time	 40 minute 190 minute
06	Soundness test of cement (with Le-Chatelier'smould)	1mm
04	Compressive strength of cement (a) 3 days (b) 7 days (c) 28 days	 33.00N/mm^2 55.44N/mm^2 74.45N/mm^2

Crushed stone metal with a maximum size of 12.5 mm from a local conforming to the requirements of IS: 383-1970 was used. Locally available river sand passing through 4.75 mm IS sieve conforming to grading zone-II of IS: 383-1970 was used. The properties of aggregates are presented in Table 2.3

Table 2.3: Physical Properties of Fine and Course Aggregate

Sr. No	Property	Results	
		Fine Aggregate	Course aggregate
01	Particle Shape, Size	Rounded, 4.75 mm down	Angular, 10mm down
02	Fineness Modulus	3.20	7.79
03	Silt content	2%	-----
04	Specific Gravity	2.582	2.70
05	Bulking of sand	4.00%	0.4%
06	Bulk density	1850 kg/m^3	1603 kg/m^3
07	Surface moisture	Nil	1.03%

Sulphonated melamine based super plasticizer supplied by Roff. Chemicals India Pvt. Ltd. Mumbai is used as water reducing and self retarding admixture in the experimental work. The properties comply with the requirements of IS 9103-1999 (Amended 2003) as well as ASTM C 494-type F.

The fly ash are used which available from Nashik. The specific gravity of fly ash was 2.3. The properties of fly ash are presented in Table 2.4

2.4: Physical Properties of Fly Ash

Sr. No.	Description of Test	Results
01	Specific Gravity	2.3
02	Colour	Grayish white
03	Bulk Weight	Approx. 0.9 metric ton per cubic meter
04	Specific density	Approx. 2.3 metric ton per cubic meter
05	Average Particle size	0.14mm
06	Particle shape	Spherical

The properties of various types of fibres considered for the study are presented in Table 2.4

Table 2.4: Properties of Fibres used

Sr. No.	Property	Properties of various types of fibres		
		HESF	**FSF**	**WSF**
2	Length (mm)	30mm	30mm	30mm
3	Width (mm)	--	1mm	--
4	Diameter (mm)	0.5mm	--	0.25
6	Aspect Ratio	60	30	120
	Colour	White	Bright in clean wire	White
8	Specific Gravity	7.85	7.85	7.86
9	Density kg/m^3	1.36	1.36	1.36
10	Tensile strength MPa	1050	1050	1050
11	Melting point	$253^{\circ}C$	$253^{\circ}C$	$253^{\circ}C$
12	Young's modulus kN/mm^2	25.19	25.19	25.19
13	Water absorption	0.04%	0.04%	0.04%
14	Minimum elongation	8%	8%	8%
15	Resistance to alkali in high strength concrete	Excellent	Excellent	Excellent
16	% Elongation	8	8	8
17	Effective Diameter mm	0.476mm	1mm	0.25

2.2. Production of HSFRC Concrete

The high strength concrete of M70 grade was designed as per DOE method. Table 2.5 shows the weights of various constituents of HSFRC.

Table 2.5: Mix Proportion

Sr. No	Material	Weight of material in Mass kg/m^3
1	Ordinary Portland Cement (85 % of CM)	472
2	Silica fume (5 % of CM)	27.8
3	Fly Ash (10 % of CM)	55.6
4	Fine Aggregate	702
5	Coarse Aggregate	1042
6	Water	150
7	Superplasticizer	18 ml per kg of Cement
8	Water Binder Ratio	0.25

III. RESULT AND DISCUSSION

The Thickness of slab *h*,concrete strength*fck* and width of the loading platen *r*. The slabs were accordingly grouped into three for three different types of fibres.

For all the slabs, welded skeletal steel fabric with an average yield strength of 415MPa and a area of 500 mm 500mm was used as the main simply supports for testing. The total volume fraction of main reinforcement was 0.76 for each slab, and the reinforcement was placed longitudinal and lateral directions at 50mm c/c distance.

3.1. Central Deflection of Hooked End Steel Fibre High Strength Fibre Reinforce Slab.Variation of Central Deflection with Respect to Load for *a/d*= 1.25

Results ofcentral deflection of beams for *a/d*= 1, *a/d*= 1.25, *a/d*= 1.5,are obtained, and are presented in Table (4.1.3), (4.1.4), (4.1.5) respectively. Central Deflection with respect to Load is presented in Figure 3.1, 3.2 and 3.3 respectively.

	M_0		M_1		M_2		M_3		M_4	
Sr. No.	**Load (kN)**	**Deflection (mm)**	**Load (kN)**	**Deflection (mm)**	**Load (kN)**	**Deflection (mm)**	**Load (kN)**	**Deflection (mm)**	**Load (kN)**	**Deflection (mm)**
1	0	0.0000	0	0.0000	0	0.0000	0	0.0000	0	0.0000
2	25	0.0000	25	0.0000	25	0.0000	25	0.0000	25	0.0000
3	50	0.0000	50	0.0460	50	0.1060	50	0.1400	50	0.1900
4	75	0.0560	75	0.0760	75	0.1120	75	0.1720	75	0.2200
5	100	0.1460	100	0.1690	100	0.2100	100	0.2700	100	0.3200
6	125	0.2750	125	0.3460	125	0.3700	125	0.4100	125	0.5900
7	150	0.4120	150	0.4900	150	0.5400	150	0.6200	150	0.7400
8	175	0.5360	175	0.7400	175	0.7760	175	0.9600	175	1.0400
9	200	0.6920	200	0.9200	200	0.9600	200	1.0300	200	1.1700
10	225	0.7960	225	1.0200	225	1.0960	225	1.1400	225	1.3500
11	250	0.9200	250	1.1100	250	1.2200	250	1.3200	250	1.4900
12	275	1.1200	275	1.3200	275	1.3700	275	1.4700	275	1.5700
13	293	1.2700	300	1.4460	300	1.4900	300	1.6200	300	1.7960
14					322	1.5440	325	1.8700	325	1.9860
15							336	1.9340	349	2.0340

Table: 3.2 Central Deflection of Flat Steel Fibre High Strength Fibre Reinforce Slab. Variation of Central Deflection with Respect to Load for *a/d*= 1.25

	M_0		M_1		M_2		M_3		M_4	
Sr. No.	Load (kN)	Deflection (mm)	Load (kN)	Deflection (mm)	Load (kN)	Deflection (mm)	Load (kN)	Deflection (mm)	Load (kN)	Deflection (mm)
1	0	0.0000	0	0.0000	0	0.0000	0	0.0000	0	0.0000
2	25	0.0000	25	0.0000	25	0.0000	25	0.0000	25	0.0000
3	50	0.0000	50	0.0760	50	0.1460	50	0.2120	50	0.2760
4	75	0.1120	75	0.1460	75	0.2200	75	0.2900	75	0.3750
5	100	0.1560	100	0.2460	100	0.3270	100	0.4900	100	0.5120
6	125	0.3200	125	0.4560	125	0.5960	125	0.6760	125	0.7460
7	150	0.5700	150	0.6200	150	0.7460	150	0.9060	150	1.0220
8	175	0.7600	175	0.8400	175	0.9640	175	1.0760	175	1.1760
9	200	0.9560	200	1.0200	200	1.0760	200	1.1700	200	1.2760
10	225	1.0460	225	1.1960	225	1.2190	225	1.3960	225	1.5460
11	250	1.1700	250	1.2900	250	1.3960	250	1.5700	250	1.6960
12	275	1.2900	275	1.4300	275	1.4790	275	1.6740	275	1.8600
13	286	1.3460	298	1.5420	300	1.6940	300	1.8900	300	1.9670
14					314	1.7900	325	1.9760	325	2.1760
15							327	2.0460	338	2.2460

Table: 3.3 Central Deflection of Waving Steel Fibre High Strength Fibre Reinforce Slab. Variation of Central Deflection with Respect to Load for *a/d*= 1.25

	M_0		M_1		M_2		M_3		M_4	
Sr. No.	Load (kN)	Deflection (mm)	Load (kN)	Deflection (mm)	Load (kN)	Deflection (mm)	Load (kN)	Deflection (mm)	Load (kN)	Deflection (mm)
1	0	0.0000	0	0.0000	0	0.0000	0	0.0000	0	0.0000
2	25	0.0000	25	0.0000	25	0.0000	25	0.0000	25	0.0000
3	50	0.0960	50	0.1700	50	0.2660	50	0.3120	50	0.3760
4	75	0.1650	75	0.2200	75	0.2800	75	0.3300	75	0.4200
5	100	0.2400	100	0.3200	100	0.3920	100	0.4960	100	0.6220
6	125	0.3700	125	0.5760	125	0.7560	125	0.8760	125	0.9560
7	150	0.5940	150	0.7340	150	0.9640	150	1.0200	150	1.0490
8	175	0.7200	175	0.8960	175	1.0470	175	1.1740	175	1.2420
9	200	0.9760	200	1.0760	200	1.1760	200	1.2900	200	1.3760
10	225	1.0920	225	1.2340	225	1.3490	225	1.5200	225	1.6790
11	250	1.1940	250	1.3760	250	1.5230	250	1.7460	250	1.9460
12	275	1.3240	275	1.5200	275	1.6940	275	1.8450	275	2.0460
13	281	1.4560	291	1.6700	300	1.8950	300	1.9460	300	2.2450
14					307	1.9640	325	2.2400	325	2.4740
15							319	2.3240	331	2.5640

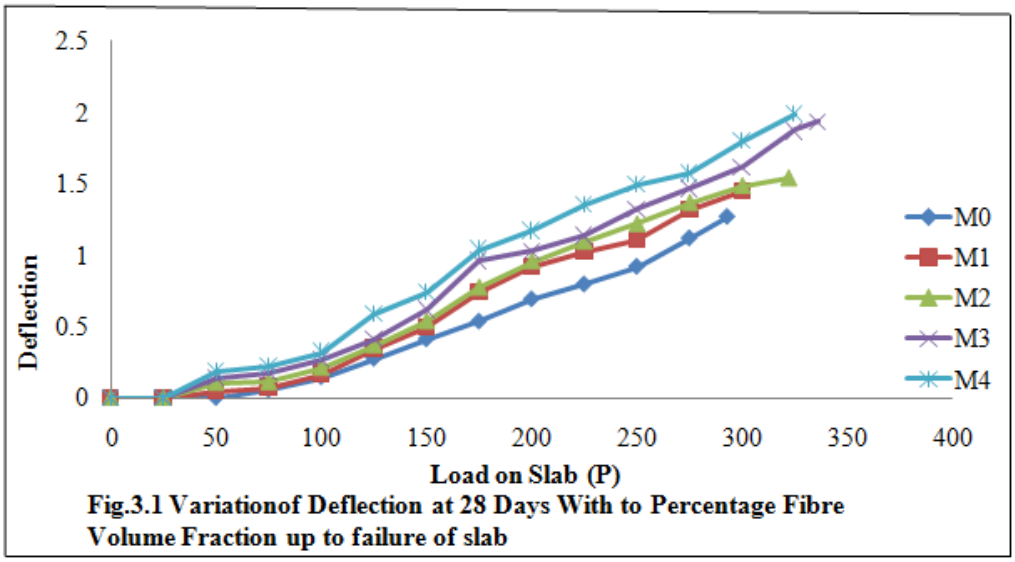

Fig.3.1 Variationof Deflection at 28 Days With to Percentage Fibre Volume Fraction up to failure of slab

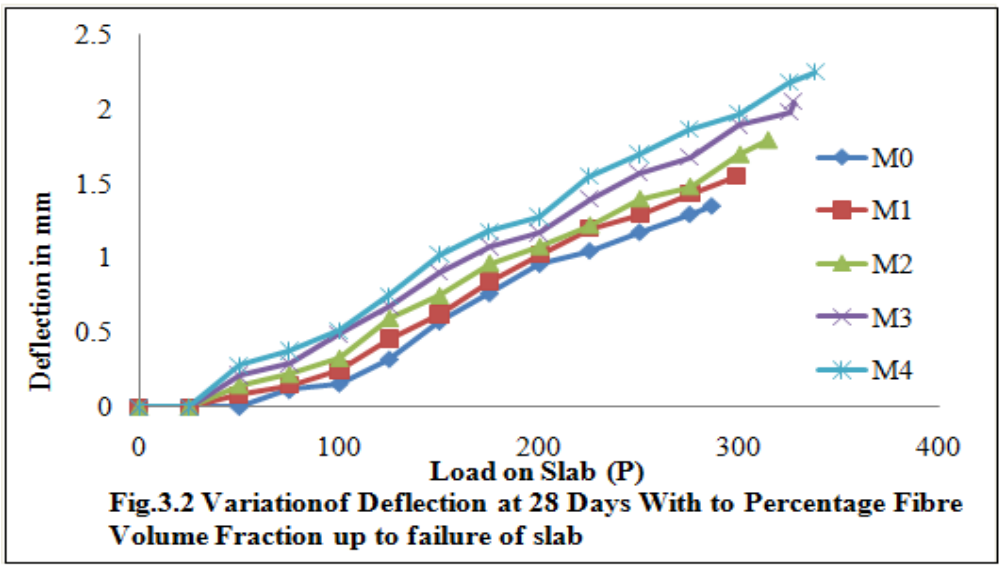

Fig.3.2 Variationof Deflection at 28 Days With to Percentage Fibre Volume Fraction up to failure of slab

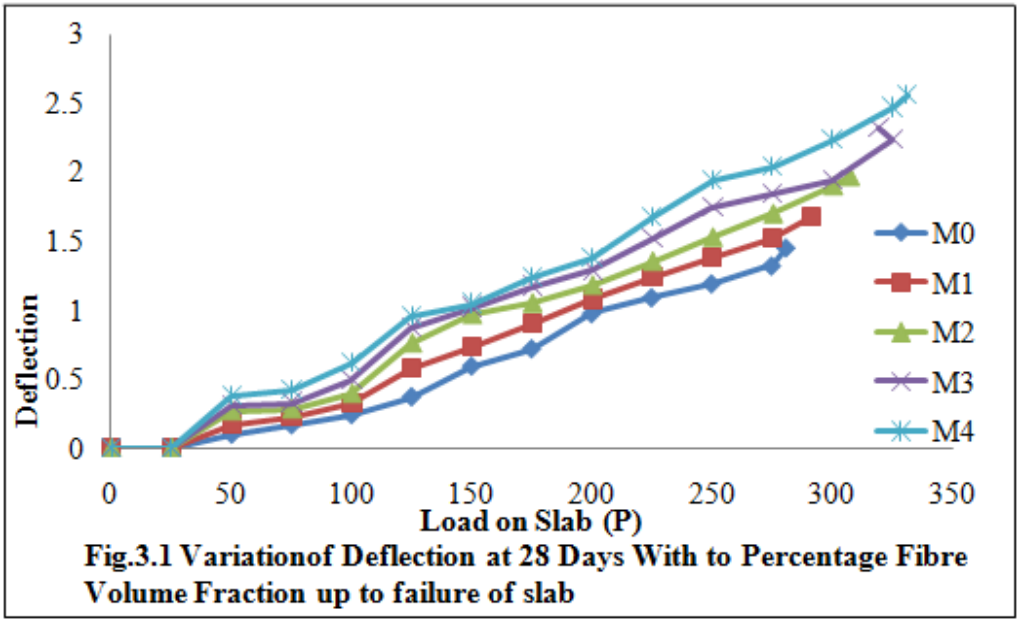

Fig.3.1 Variationof Deflection at 28 Days With to Percentage Fibre Volume Fraction up to failure of slab

3.4. Test Setup and Instrumentation

Slabs, a short platewas used for observed as the formation of cracks stabilized before the load picked up again. As the load further increased, more cracks appeared on the bottom of the slabs and were observed to propagate in a zigzag manner toward the edges of the slabs. Correspondingly, the steel strains increased rapidly, and eventually the yield strains were reached.

Further reduction in stiffness was observed as the applied load was increased and the yielding of steel reinforcement was deemed to have spread outwards to the edges of the slab. During this stage, the slab was observed to deflect excessively, and the increase in load was mainly due to membrane action of the slab. Near the ultimate load, the stiffness of the slab decreased rapidly and cracks started to appear on both the top and bottom surfaces of the slab in a circumferential direction around the loading plate. The loading plate began to punch through and finally, when the circumferential cracks became excessively wide, the load-carrying capacity of the slab dropped sharply.

The postpeak region indicated a further reduction in the load-carrying capacity of slabs. This reduction occurred in several steps, with spalling of the concrete from the bottom of the slab. Fig. 4.1 shows the crack patterns for some typical slabs after the tests.

For all slabs, the critical punching-shear perimeter was found to occur at some distance away from the loading plate. Measurements on both the top and bottom surfaces of the slabs indicated that the critical perimeter formed, on a

IV. Conclusions

Within the scope of the study, the following conclusions may be drawn. The load-deflection curve of HSFRC slabs under a concentrated load exhibits four distinct regions: (1) The initial elastic uncracked region; (2) the crack development region; (3) the post yielding region; and (4) the post peak region.

The critical perimeter for punching shear failure in HSFRC slabs forms at a distance of about 4.5 times the effective depth from the perimeter of the loading platen, with the shear plane inclined at 20^0-30^0 to the plane of the slab.

Punching shear failure in HSFRC slabs is preceded by yielding of steel reinforcement and is accompanied by cracks mainly in the radial direction and partly in the circumferential direction.

An increase in the volume fraction of steel fibers, slab thickness, compressive strength of fiber concrete, or the loaded area generally leads to an increase in the cracking load, yield load, ultimate load, and ductility of HSFRC slabs.

Fig 4.1 Yield line patterns are occurred in slab after application of punching shear.

REFERENCES

[1]. Building code requirements for reinforced concrete and commentary."(1989). ACI 318-89/ACI318R-89.American Concrete Institute, ACI, Detroit, Mich.

[2]. Code of practice for the structural use of concrete."(1972). CP110, Part 1, British Standards Institution, London, England.

[3]. Ito, K., Hirasawa, I., and Aichi, I. (1981)."Punching shear strength of steel fiber reinforced concrete slab."Trans., Japan Concrete Inst., Tokyo, Japan, 3, 267-272.

[4]. Model code for concrete structures."(1978). International System of Unified Standard Codes of Practice for Structures, Vol. II, Bull, *d'*Information No. 124/125-E, 3rd Ed., Comite Euro-International du Beton—Federation Internationale de la Precontrainte (CEB-FIP), London, England/Paris, France.

[5]. Narayanan, R., and Darwish, I. Y. S. (1987). "Punching shear tests on steel fibre reinforced micro concrete slabs." Magazine of Concr. Res., 39(138), 42-50.

[6]. Standard specifications for design and construction of concrete structures, part 1 (design)." (1986). Japan Society of Civil Engineers, Tokyo, Japan.

[7]. State-of-the-art report on fiber reinforced concrete." (1982). ACI544.IR-82, American Concrete Institute, ACI, Detroit, Mich.

[8]. Structural use of concrete; part 1, code of practice for design and construction."(1985). BS8110, British Standards Institution, London, England.

[9]. Swamy, R. N., and Ali, S. A. R. (1982). "Punching shear behavior of reinforced slab-column connection made with steel fiber concrete." J, ACI, 79(5), 392-406.

[10]. Vondran, G. L. (1991). "Applications of steel fiber reinforced concrete." Concr. Int.: Design & Constr., 13(11), 44-49.

[11]. Walraven, J., Pat, T., and Markov, I. (1986). "The punching shear resistance of fibre reinforced concrete slabs." 3rd Int. Symp. Developments in fibre reinforced cement and concrete, Vol. 2, Paper 8.9, RILEM Technical Committee TFR49, England, U.K.

OPEN ACCESS

International
Journal
Of Modern Engineering Research (IJMER)

Solar Chimney Power Plant-A Review

P. J. Bansod[1], S. B. Thakre[2], N. A Wankhade[3]

[1]*Research Scholar Department of Mechanical Engineering, PRMIT & R Badnera, Amravati University, India*
[2]*Professor Department of Mechanical Engineering, PRMIT & Badnera, Amravati University, India*
[3]*Associate Professor Department of Mechanical Engineering, PRMIT & Badnera, Amravati University, India*

Abstract: *Solar technology is the novel technology which uses the natural sunlight to produce electricity. It uses the combination of three simple technologies that is turbine, vertical chimney of some longer height and glass roof collector for absorbing the sun radiations. By proper utilization of this technology the electricity can be generated in abidance and continuously for twenty four hours throughout the year in county like India where there is sunlight almost for nine months in the major part of the country. Much advancement has taken place in this technology for last three decades but the full utilization of this technology has not taken place because of various aspects. This paper presents the critical review of this important technology in the form of the advancements and developments taken place in various parts of the world and analyzes its important aspects.*

Keywords: *chimney technology, greenhouse collector, power plant, Turbine, updraft.*

I. Introduction

The future of this earth and mankind substantially depends on our ability to slow down the population increase in the "Third World" by civilized means. The key is to increase the standard of living, to overcome the inhumane poverty and deprivation. Development requires mechanization and energy. Energy consumption increases proportionally to the gross national product or prosperity while simultaneously the population growth will decrease exponentially. Many developing countries possess hardly any energy sources and their population doubles every 15- 30 years. The result of which are commonly known that is civil wars and fundamentalism. If these developing countries are provided with only a humane and viable minimum of energy the global energy consumption will drastically increase. The sun is the only source which can supply such an enormous amount of energy without an ecological breakdown and without safety hazards and without a rapid depletion of natural resources at the expenses of future generations. Solar chimneys are such devices which can generate energy up to large extent by use of the simple device that is greenhouse collector, Vertical chimney and turbine and produce electricity continuously at minimum cost. It is very necessary to adopt this technology in every part of the world like other conventional sources which we are using regularly.

II. Solar Chimney

The solar chimney power plant combines three familiar components: A solar collector, a solar chimney and power conversion unit (Jorg Schlaich & Wolfgang Schiel, 2000) which include one or several turbine generators. The turbine is driven by air flow produced by buoyancy resulting from greenhouse effect inside the collector (Fig.1). The main function of solar chimney system is to convert solar energy into electrical energy. In the collector, the solar energy will transform into heat energy. The chimney converts the generated heat energy into kinetic energy, which will be transformed into electric energy by using a combination of a wind turbine and a generator. The collector in solar chimney system consists of support matrix, column structure and transparent roof. A large air collector is formed when a transparent glass or plastic roof supported above the ground by column structure and support matrix is stretched out horizontally many meters. The height of the roof slowly increases along a radius from the periphery to the center to guide inward airflow with minimum friction losses. This glass or plastic roof allows the transmission of the shorter wavelength solar radiation but blocks the longer wave length radiation emitted by the ground. As a result, the ground under the roof heats up which in turn heats the air flowing radially above it. The soil surface under the collector cover works as a storage medium, which saves a part of the incoming solar radiation during a day and releases it later during the night. This mechanism is capable of providing a continuous supply of power all year round.

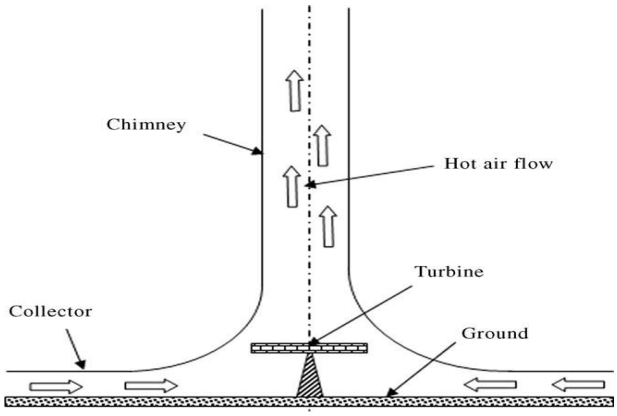

Fig. 1: Schematic illustration of a solar chimney power plant

The chimney situated in the collector center is the actual thermal engine of the solar chimney power plant. The up thrust of the air heated in the collector is proportional to the rise in air temperature flowing in the collector and its volumetric flow rate. Suitable turbines located at the base of chimney convert kinetic energy of the up flowing air inside chimney to mechanical power in the form of rotational energy. The typical solar chimney turbine is of the axial flow type. The principle of operation of these turbines is similar to the turbo generators used in hydroelectric power stations, where the static pressure is converted into mechanical work. The power output achieved is proportional to the product of the volume flow rate and the pressure drop across the turbine. The air flow through the turbine can be regulated by varying the turbine blades pitch angle. This mechanical energy can be converted into electric energy by coupling the turbine to the generator. Solar chimney does not necessarily need direct sunlight. They can exploit a component of the diffused radiation when the sky is cloudy. The lack of system dependence on the natural occurrence of wind, which is intermittent, makes it a very attractive development.

III. Project of Solar Chimney in Various Parts of the World.

3.1 Manzanares Prototype

Detailed theoretical preliminary research and a wide range of wind tunnel experiments led to the establishment of an experimental plant with a peak output of 50 kW on a site made available by the Spanish utility union Electrica Fenosa in Manzanaras about 150 km south of Madrid in 1981-82 (Jorg Schlaich & Wolfgang Schiel, 2000), with funds provided by the German Ministry of Research and Technology. The aim of this research project was to verify, through field measurements, the performance projected from calculations based on theory and to examine the influence of individual components on the plant's output and efficiency under realistic engineering and meteorological conditions. These results show that the components are highly dependable and that the plant as a whole is capable of highly reliable operation. This single global radiation is exploited and the thermodynamic inertia is a characteristic feature of the system. Continuous operation throughout the day is possible and even abrupt fluctuation in energy supply is effectively cushioned, the plant operated continuously even on cloudy days, albeit at reduced output.

Fig. 2. Prototype of Manzanares

3.2 Enviro Mission

Enviro mission is set to build the tallest structure of solar chimney power plant in North America (Reid smith and Lisa Cohn, 2012) with its innovative solar updraft tower design, which provides base load power. The solar updraft tower uses a solar energy collector canopy and a central tower to generate and updraft airflow that drives the rotation of pressure-staged turbines at the base of the tower and generates electricity. Enviro Mission plans to build its first commercial solar updraft tower on public lands in L Paz County, Arizona. If we imagine a sunny day in Arizona where the outside temperature would be 40degrees Celsius, the temperature under the collector would be 80 to 90 degrees Celsius and the temperature at the top of the tower would be 32 degree Celsius. This creates the ideal temperature differential that Enviro Mission desires.

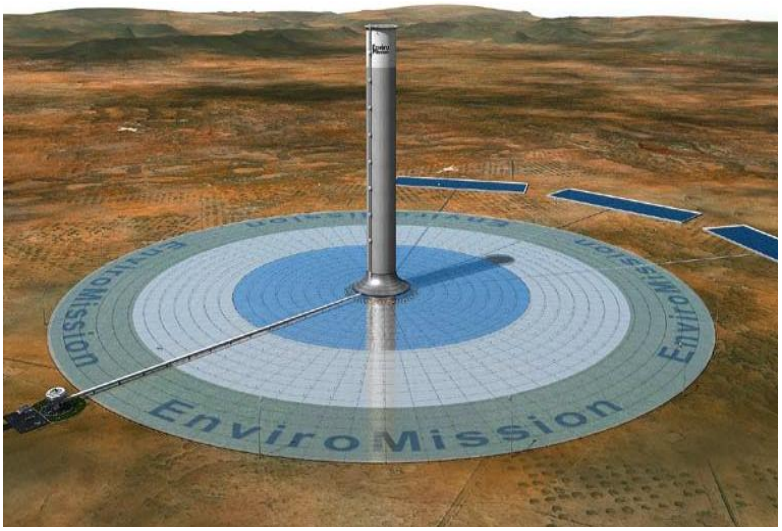

Fig.3 Enviro Mission Arizona USA

3.3 Solar Power Plant in Egypt

To evaluate the performance of solar chimney power plants in some locations in Egypt theoretically and to make an approximation of the quality of the generated electrical energy. A simple mathematical model (El-Haroun, 2012), based on the energy balance was developed to estimate the power output of solar chimneys as well as to observe the effect of various ambient conditions and structural dimensions on the power generation. It was found that the wind speed inside chimney reaches more than 7 times of the value of the free wind speed outside chimney. The solar chimney power plant with 500 m chimney height, 50 m chimney diameter and 3000 m collector diameter is capable of producing yearly between 1.6-1.7 x 10^8 kW hr. in the selected locations in Egypt. Therefore the use of solar chimney power plants in many locations in Egypt will be attractive. It can cover a considerable section of the increasing demand to energy. It can save the use of conventional sources of energy like oil and natural gas and consequently reduces the emissions of harmful gases.

3.4 Solar Technology Nigeria

Solar technology and its necessity in Nigeria were studied (Ngala & Suleiman, 2013). Nigeria which is located between longitude 3^0 and 14^0 East of Greenwich and latitude 4^0 and 14^0 north of equator has about 160 million people and a total land area of 923,768 km^2. Nigeria lies within a high sunshine belt and thus has enormous solar energy potentials. It also describes the economics of power generation by using solar chimney. During operating period the SCPP avoids the CO_2 emissions from coal-fired power plant, which typically emits 0.95 kg of CO_2 per kWh power output. Large amount of carbon credits was therefore obtained for SCPP. In this study the details of SC power technologies are described and the status and development of this technology reviewed including the experimental and theoretical study status, as well as the economics for SC power technology. There are also potentials of citing this technology in Nigeria especially in the semi-arid region with solar sunshine hours of up to 9 hours, solar radiation of 7kW/m^2/day and enormous flat land.

3.5 Solar Chimney in UAE

Analysis of a solar chimney power plant in the Arabian Gulf region of UAE was carried (Mohammad O. Hamdan, 2011). The developed analytical model was used to evaluate the effect of geometric parameters on the solar plant power generation. The analysis showed that chimney height and turbine pressure head are the most important physical variables for the solar chimney design. The study showed that second –law efficiency

has no monotonic relation with turbine pressure head. The model shows that second-law efficiency and power harvested increase with the increase of chimney height and/or diameter. The developed model is used to analyze the feasibility of solar chimney power plants for the UAE climate which possesses typical characteristics of the gulf climate. The solar characteristics of the UAE are shown along with characteristic metrological data. A solar chimney power plant with a chimney height of 500 m and a collector roof diameter of 1000 m would produce at least 8 MW of power.

3.6 Solar Chimney in Thailand

The experimental and numerical analysis for the utilization of cool ceiling with roof solar chimney in Thailand was carried out (Sudaporn Chungloo, 2009) to study the benefits of application of solar chimney on the south roof and cool metal ceiling on the north roof through the experiment in a detached building called a controlled cell, and the related numerical model constructed from a computational fluid dynamics (CFD) program. The experimental results are used for calculation on values of heat transfer coefficient of the cool ceiling and evaluation of the mean cooling potential of the combined passive cooling system. The two dimensional numerical models generated by the CFD program use the mean values of wall temperature in the application of solar chimney in the controlled cell as the boundary conditions. The effects of cool ceiling on the temperature, velocity and airflow rate in the controlled cell are investigated through the numerical model in which the north ceiling temperature is reduced by 2-4 ^{0}C from the measured value of 32.8 ^{0}C. The mean cooling potential of the application of combined system is found to be two times higher than the application of the solar chimney. Good agreements between the predicted and experimental results are obtained from the comparison of temperature and volume flow rate at the middle section of the controlled cell. The reduction of north ceiling temperature in the free-convection numerical model shows the decrease of air temperature in the upper region of the room by 0.5-0.7^{0}c from the original value of 33.3^0 C, and the increase of volume flow rate by 12%.

3.7 Solar Chimney Development In China

A heat transfer mode that is used to compare the performance of a conventional solar chimney power plant (CSCPP) and two sloped solar chimney power plant (SSCPPs) with the collector at 30^{0}c and 60^{0}c, respectively was developed in China (Fei Cao Liang Zhao, 2013). The power generation from SCPPs at different latitudes in China is also analyzed. Results indicate that the larger solar collector angle leads to improved performance in winter but results in lower performance in summer. It is found that the optimal collector angle to achieve the maximum power in Lanzhou, China, is around 60^{0}c. Main factors that influence the performance of SCPPs also include the system height and the air thermo physical characteristics. The ground energy loss, reflected solar radiation and kinetic loss at the chimney outlet are the main energy losses in SCPPs. The studies also show SSCPPs are more suitable for height latitude regions in Northwest China, but CSCPPs are suggested to be built in southeastern and eastern parts of China with the combination to the local agriculture.

3.8 Solar Chimney In Botswana

Import of huge proportion of electrical energy from the Southern African Power Pool, and the geographical location and population distribution of Botswana stimulated the need to consider renewable energy as an alternative to imported power. (Clever Ketlogtswe, 2008) a systematic experimental study on a mini-solar chimney system. Particular attention is given to measurements of air velocity, temperature and solar radiation. The result for the selected 5 and 6 clear days of October and November respectively are presented. These results enable the relationship between average insolation, temperature difference and velocity for selected clear days to be discussed.

3.9 Solar Technology in Algeria

The work presented by (Salah Larbi, Adel El Hella, 2013) is related to an energy system analysis based on passive cooling system for dwellings. It consists to solar chimney energy performances determination versus geometrical and environmental considerations. The site located in the southern region of Algeria is chosen for this study according to ambient temperature and solar irradiance technical data availability. The glazing temperature distributions, the chimney mass flow rate, the internal wall temperatures and the air room change per hour (ACH) parameter are presented and discussed. Obtained results show that the maximum of airflow velocity is obtained for small values of the width of the channel because for one fixed flow rate, the velocity increases when the section decreases. The influence of the incident solar radiation is important parameter on energy performances analysis of the chimney and an optimum design between the width of the chimney and the aperture of the absorber wall may exit for increasing ACH parameter. The air gap between the absorber and the glass cover plays an important role in the ventilation rate. The maximum of velocity is located near the main inlet air flow area. The sudden contraction increases the air velocity in this zone due to the vena-contracta effect.

IV. Recent Development In Solar Technologies

4.1 Sloped Solar Updraft Power Plant

A sloped solar updraft power plant was proposed (Shadi Kalasha, Wajih Naimeh, 2014). Designing a solar chimney collector system on sloped surface or suitable hills has two major advantages. First, if the collector slope is optimized, the solar radiation received by the collector system may be improved to a satisfactory level for a year round operation. Second, a slope surface constitutes a natural chimney; therefore the chimney height standing above the collector height may be reduced considerably, thus reducing civil engineering problems and cost. This new design is called the sloped solar updraft power plant (SSUPP). The monthly average values of the collector outlet, chimney inlet, ambient temperature and solar radiation were recorded and plotted to investigate the prototype performance a year round. The investigations show that the temperature difference between the ambient temperature and the chimney inlet temperature is almost the same in winter and summer. This result is due to optimizing the solar collector which was inclined in the same angle of the latitude in the prototype location. The results show a direct impact of both solar radiation and ambient temperature on the collector outlet air temperature.

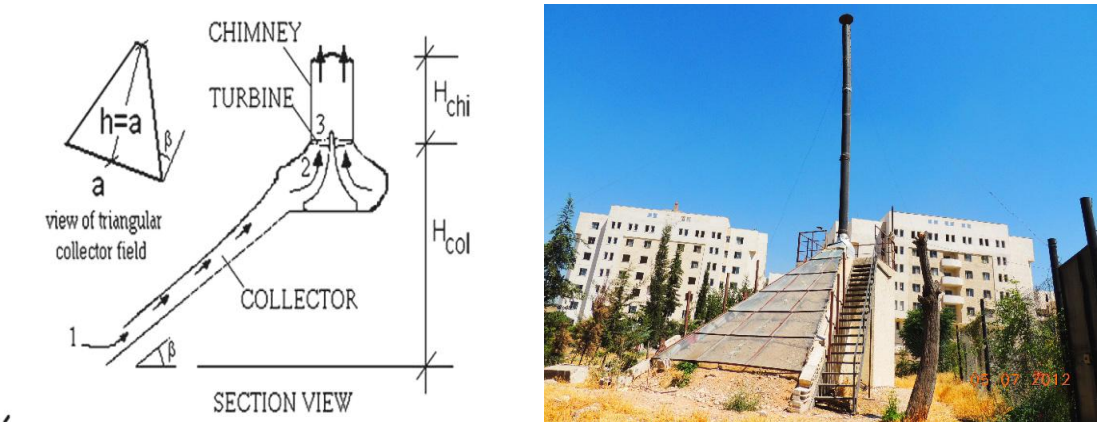

Fig.4 Systems in sloped surface at high latitudes

4.2 Counter Rotating Turbines

Two counter rotating turbines, one with inlet guide vanes, the other without, are compared to a single-runner system. The design and off-design performances are weighed against in three different solar chimney plant sizes. It was shown (Denantes, 2006) that the counter- rotating turbines without guide vanes have lower design efficiency and a higher off-design performance than a single-runner turbine. Based on the output torque versus power for various turbine layouts, advantageous operational conditions of counter rotating turbines are demonstrated. The counter-rotating turbines offer their best efficiency at higher load factors than the single-runner turbines. The main advantage of this turbine type in the solar chimney systems is its off-design performance. By considering that solar chimney power plant will be operated most of the time at a solar intensity of less than 800W/m^2, the counter rotating turbine systems will be advantageous with respect to single-runner systems from the efficiency point of view as well as annual electric energy production. One other advantage is the reduced torque on each axis compared to the single-runner turbine.

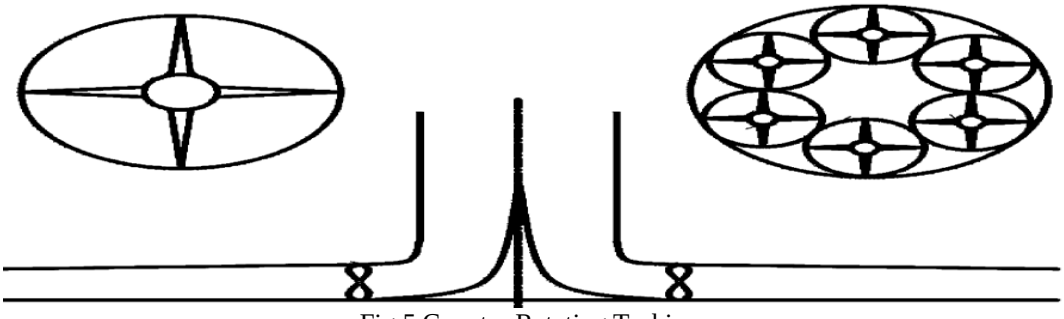

Fig.5 Counter Rotating Turbines

4.3 Asphalt Concrete Solar Collector

Asphalt concrete can absorb a considerable amount of the incident solar radiation. For this reason asphalt roads could be used as solar collector. There have been different attempts to achieve this goal. All of them have been done by integrating pipes conducting liquid, through the structure of the asphalt concrete. The

problem of this system is that all pipes need to be interconnected; if one is broken, the liquid will come out and damage the asphalt concrete. To overcome these limitations (Alvaro Garcia, 2014) an alternative has proposed that is parallel air conduits, where air can circulate will be integrated in the pavement structure. The idea is to connect these artificial pore volumes in the pavement to an updraft or to a downdraft chimney. Differences of temperature between the pavement and the environment can be used to create an air flow, which would allow wind turbines to produce an amount of energy and that would cool the pavement down in summer or even warm it up in winter. To demonstrate that this is possible, an asphalt concrete prototype has been created and basics calculations on the parameters affecting the system have been done. It has been found that different temperatures, volumes of air inside the asphalt and the difference of temperature between the asphalt concrete and the environment are critical to maximize the air flow through the pavement. Moreover, it has been found that this system can be also used to reduce the heat island effect.

4.4 Structural Stability of Concrete Wind Turbines and Solar Towers Exposed to Dynamic Wind Action

The solar chimney operates like a hydroelectric power plant, but instead of water, it uses a hot air. This is particularly useful in arid area, which is plentiful in Africa, even south of Sahara. It comprises a transparent roof collector, a central chimney tower and one or more turbo generators at the base. Beneath the collector, (Reinhard Hartea, 2007) a large, circular glass roof, air is heated. Through the coinciding change in air pressure, the air moves radially towards the centre, where it enters the tower, which creates an up-draught. By this suction effect, hot air is drawn in from the collector and as it rises up the chimney, it flows through one large turbine or numerous smaller turbines, the preferred option yet to be determined. These turbines are linked to conventional generators, whereby electricity is generated. The output of the solar chimney is proportional to its size. The scale of a 1000-1500m tall, 160m diameter chimney tower and a glass roof collector of diameter 4-7 km is proposed to produce an output of 200- 400MW.

4.5 Reinforce Concrete (RC) Chimneys With Fiberglass Reinforce Plastic(FRP)

A simple method to calculate fire duration and flue gas temperatures for reinforced concrete (RC) chimneys with fiberglass reinforced plastic (FRP) liners based on experimentally determined burning characteristics of the liner material was proposed (Artemis Agelaridou-Twohig, 2014). Implementation of the method to calculate fire durations and the transient heat transfer conditions is demonstrated for single and four liner chimney. A parametric study is carried out for chimney designs and geometries ranging from 100 m to 300 m in height and 7 m to 40m in diameter, with 1-4 liners and varying opening configuration. The results are used to identify a limited number of cases for which the RC chimney undergoes the most extreme reduction in its post-fire residual strength. Analytical estimations of the chimney residual strength after the fire are obtained using a method established based on the procedure outlined in the American Concrete Institute (ACI) 307 standard for chimney strength calculations. Calculations for a series of critical configuration of RC chimneys, with FRP liner geometries within the practical design limits detailed. This shows that the post-fire structural capacity of the chimney would not lead to catastrophic failures especially because the chimney is not expected to see other high design lateral loads such as wind or earthquake simultaneously.

4.6 Constructal Geometry of A Solar Chimney

The study to describe the constructal-theory search for the geometry of a solar chimney was conducted. The objective of (A.Koonsrisuk, S. lorente, 2010) was to increase the power production over the area occupied by the plant. The ratio height/radius, maximum mass flow rate and maximum power under the constraints of a fixed area and volume are determined. The power generated per unit of land area is proportional to the length scale of the power plant. The analysis is validated by a detailed mathematical model. Pressure losses are reported in terms of the dimensionless length scale of the system and are illustrated graphically. They indicate that the pressure drop at the collector inlet and at the transition section between the collector and chimney are negligible and the friction loss in the collector can be neglected when the svelteness of the entire flow architecture is greater than approximately 6.

4.7 Air Energy Available In Solar Chimney

Solar chimney is defined as low temperature solar thermal power plants, which use the atmospheric air as a working fluid, where only one part of the thermodynamic cycle within the plant is utilized. The available work potential that atmospheric air acquires while passing through the collector has been determined and analyzed. The dependence of the work potential on the air flowing into the air collector from the heat gained inside the collector, air humidity and atmospheric pressure as a function of elevation are determined. Various collector types using dry and humid air have been analyzed (N. Nini, 2006). The influence of various chimney heights on the air work potential was established. The possibly higher utilization factors of the available hot air work potential without the use of high solid chimneys are discussed. It has been shown that the vortex motion

flowing downstream of the turbine can be maintained under pressure and can possibly take over the role of the solid structure chimney. Thus a part of the available energy potential acquired in the collector would be used to maintain the vortex flow in the air column above the ground level turbine. Basic conditions for the maintenance of such a vortex flow are described and compared to the tornado phenomenon.

4.8 Turbine Layout of Solar Chimney Power Plant

The power conversion unit of a large solar chimney power plant converts the fluid power, first into mechanical power and then into electrical power (Thomas Peter Fluri, 2008). A tool is developed to determine the layout and the number of turbines of the solar chimney power conversion unit providing the lowest cost of electricity. An analytical turbine model is developed. Several modeling approaches and the performance of single rotor and counter rotating turbine layouts are compared. Preliminary turbine designs are investigated, experimentally and numerically. The main aim of the experimental investigation is to verify the applicability of the loss model used in the analytical turbine model. The aim of the numerical investigation is to evaluate a commercial software package as a tool in context with solar chimney turbines. For each component of the power conversion unit and analytical performance model is introduced. Using these models, the single vertical axis, multiple vertical axis and multiple horizontal axis turbine configurations are compared from an efficiency and energy yield point of view and the impact of the various losses on the overall performance is highlighted. A detailed cost model for the power conversion unit is also presented. To optimize for cost of electricity this cost model is then linked to the performance models and the resulting optimization scheme is applied to several plant configurations.

4.9 Solar Chimney and Linked Renewable Energy Conversion Devices

A solar tower constituted (Denis Bonnelle, 2004) from a wide circular glass collector and a1 km high chimney, where hot air flows upwards and drives some turbines; and a downwards tower where dry air is cooled down by the evaporation of sprayed water droplets. Each of both projects is born by a competent team, but their credibility is undermined by competitors, whose publication include serious basic errors. Some technical improvements are proposed for the solar tower, with the goal to be able to design a larger solar collector and a higher tower and boost the global efficiency. Possible effects on the global biosphere circulations are described, in order to find the most neutral or beneficent solution, e.g. a combination of energy towers and bigger towers having many common features with solar chimney.

4.10 Flows in Solar Chimney for an Optimal Design Purpose

Diversified approaches were used to find ways to improve the efficiency of a solar chimney (Atit Koonsrisuk, 2009). The approaches can be divided into categories of theoretical, experimental and numerical methodologies. He describes the objectives, the problem and rational and the methodology of the research. Dimensional analysis was used in to determine the scaling law for the flow in solar chimney systems and the results obtained were verified by using the computational Fluid Dynamics technique (CFD). Inspection of the mathematical model suggests the flow area ratio that can increase the plant performance. To support the idea, the mathematical analysis was carried out and then proved by CFD. The mathematical model of the system with a turbine was developed in to evaluate the plant performance. He shows the experimental performance of four small-scale physical models. Finally the method of constructal design was used to search for a better design of the flow system.

4.11 Control of Large-Scale Solar Chimney Power Plant

To control large scale solar power plant based on a reference location near Sishen in South Africa and a so called reference solar chimney power plant with a 5000 m collector diameter and a 1000 m high, 210 m diameter chimney. The numerical simulation model is refined and used to perform a sensitivity analysis (Johnnes Petrus, 2007) on the most prominent operating and technical plant specifications. Thermo-economically optimal plant configurations were established from simulation results and calculations according to an approximate plant cost model. The effects of ambient wind, temperature lapse rates and nocturnal temperature inversions on plant performance are examined. Various new technologies are investigated for the purpose of controlling plant output according to specific demand patterns. The incorporation of vegetation under the collector roof of the plant and the influence there of on plant performance is also explored.

Results indicate that, through the modification of the collector roof reflectance, collector roof emissivity, ground surface absortivity or ground surface emissivity; major improvements on plant performance are possible. Introducing thermal insulation or double glazing of the collector roof also facilitates substantial enhancements on plant yield. Simulations predict a notable sensitivity to the ground surface absortivity value, while variable atmospheric temperature lapse rates and windy ambient conditions may impair plant performance significantly. Furthermore, sand is found to be unsuitable as plant ground type and thermo economically optimal solar

chimney plant dimensions are determined to be generally larger than plant dimensions employed in previous studies. Good dynamics control of solar chimney power output is established, suggesting that a solar chimney power plant can be implemented as a base or peak load electricity generating facility.

4.12 Floating Solar Chimney Technology

Floating solar chimney (FSC) is a low cost alternative of the concrete solar chimney. The floating solar chimney, as a lighter than air structure, can be raised anywhere and its cost is as low as 2% of the cost of the respective concrete chimney. The approach (Papageogiou, 2011) includes a low cost greenhouse that can be used in FSC technology, which is also a low cost alternative to the usual glass roofed circular greenhouse related to the concrete chimney. This plastic covered low cost greenhouse could solve also the ingress of dust, which is a problem that could be a serious obstacle in desert installations of the FSC technology. Furthermore according to the construction cost and the electricity generation figures we present a scale analysis of the FSC technology. Even with moderate height FSC structures of 650m, is possible the direct production cost to be approximately 45USD /MWh. The unused mid-latitude desert or semi desert lands of high solar radiation in many countries in all continents can be used for large scale application of floating solar chimney technology securing sustainability and mitigating global warming effects.

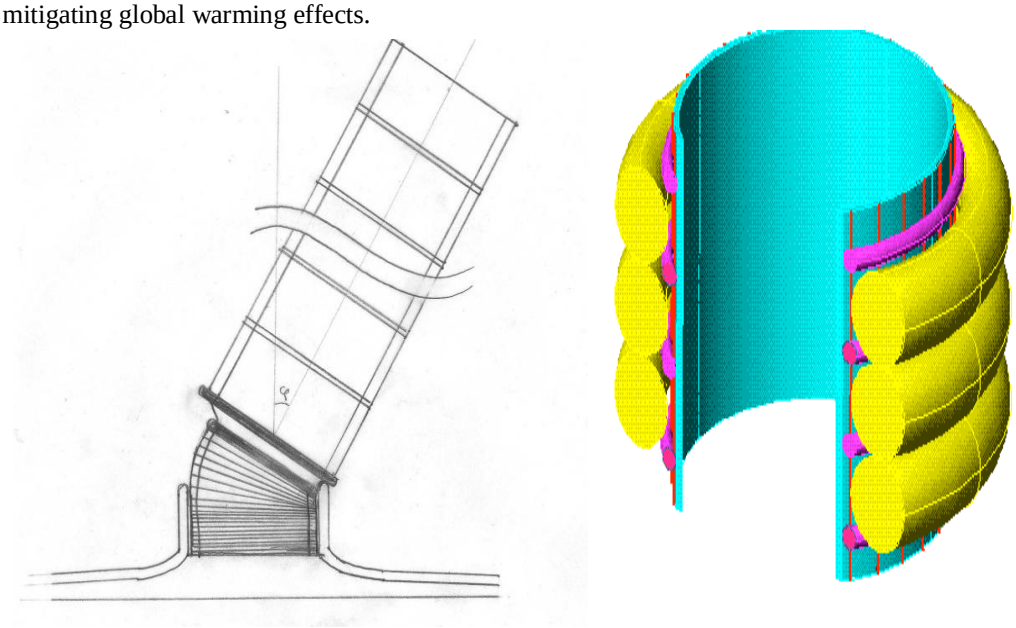

Fig.6- Floating Solar chimney Technology

V. Theoretical And Experimental Studies

Various theoretical and experimental studies are carried out after the successful testing of Manzanares France prototype in 1982. Size and configuration of solar chimney are different according to different regions. Few of these studies are stated as below.

5.1 Thermal and Technical Analyses of Solar Chimneys

An analysis for the solar chimney has been developed (Bernardes, 2003), aimed particularly at a comprehensive analytical and numerical model, which describes the performance of solar chimneys. This model was developed to estimate power output of solar chimney as well as to examine the effect of various ambient conditions and structural dimensions on the power output. Results from the mathematical model were compared with experimental results and the model was further used to predict the performance characteristics of large scale commercial solar chimneys. The results show that the height of chimney, factor of pressure drop at the turbine, the diameter and the optical properties of the collector are important parameters for the design of solar chimneys. The objective of this study was to evaluate the solar chimney performance theoretically. A mathematical model was developed to estimate the temperature and power output of solar chimney as well as to examine the effect of various construction conditions on the power output. The mathematical model was validated with the experimental data from the prototype in Manzanares. The power output can be increased by increasing the chimney height, collector area and the transmittance of the collector. The maximum power can be reached when the factor of pressure drop at the turbine is equal to approximately 0.97. Other parameters such as ground heat penetration coefficient distance between absorber and ground, double cover area, water-storage system area and thickness presented no significant variations on the energy output, but on power output vs. time.

5.2 Maximum Fluid Power Conditions in Solar Chimney Power Plant

The objective of the study (Von Theodor, W.Backstrom, Thomas P.fluri, 2006) was to investigate analytically the validity and applicability of the assumption that, for maximum fluid power, the optimum ratio of turbine pressure drop to pressure potential. The study developed two analyses for finding the optimal ratio of turbine pressure drop to available pressure drop in a solar chimney power plant for maximum fluid power. It was shown that the constant pressure potential assumption may lead to appreciable under estimation of the performance of a solar chimney power plant, when compared to the model using a basic model for the solar collector.

5.3 Mathematical Modeling of Solar Chimney Power Plant

A solar collector, chimney and turbine are modeled together theoretically (Atit Koonsrisuk, Tawit Chitsomboom, 2013) and the iteration techniques are carried out to solve the resulting mathematical model. Results are validated by measurements from an actual physical plant. Moreover the model is employed to predict the performance characteristics of large scale commercial solar chimney, indicating that the plant size, the factor of pressure drop at the turbine and solar heat flux are important parameters for performance enhancement. In addition the study proposes that the most suitable plant, affordable by local government standards to respond to the electricity demand of a typical village in Thailand, is the one with a collector radius and chimney height of 200 m and 400m, respectively. Furthermore, it is shown that the optimum ration between the turbine extraction pressure and the available driving pressure for the proposed plant is approximately 0.84. A simple method to evaluate the turbine power output for solar chimney systems is also proposed in the study using dimensional analysis.

5.4 Solar Updraft Power Plants: Engineering Structures for Sustainable Energy Generation

This present (Reinhard Harte, Tudiger Hoffer, Wilfried b. Kratzig, 2013), the working principles of solar updraft power plants; followed by explaining climatic and wind-technologic design assumptions. Then the central solar updraft chimney and the power tower are treated in more detail: a thin ring-stiffened RC shell of extreme height, forming the utmost structural challenge of such plants. This part is followed by technical requirements for the collector constructions, by far the largest glass-covered areas ever built, and of the wind loading on the glazing. Then, further design aspects are extracted by the durability requirements for at least 100 years of operation in extreme desert climates. The paper closes with some cost estimates for the generated electricity. This present manuscript has concentrated their own cost-estimations on optimized smaller plants with 500m and 750 m of chimney heights.

5.5 Solar Chimney Model with Uniform Wall Heat Flux

Experiments are carried out using an experimental solar chimney (Z.D. Chena, P.Bandopadhayay, J.Halldorsson, 2003) model with uniform heat flux on one chimney wall with a variable chimney gap-to-height ratio between 1:15 and 2:5 and different heat flux and inclination angles. Results showed that a maximum air flow rate was achieved at an inclination angle around 45^0 for a 200 mm gap and 1:5 m high chimney and the air flow rate is about 45% higher than that for a vertical chimney at otherwise identical conditions. It was found that the prediction method available in the literature can substantially over predict the airflow rate for the chimney geometry investigated in this work, especially for vertical chimneys with large gaps. The main reason for the over prediction of air flow rate was shown due to the underestimation of the pressure losses at the chimney outlet by using loss coefficients obtained for normal forced flows.

5.6 Behavior of the Airflow In A Solar Chimney

An analytical and numerical study of the unsteady airflow inside a solar chimney was performed by (Cristiana B. Maia, Andre G. Ferreira, Ramon M. Valle, 2009). The conservation and transport equations that describe the flow were modeled and solved numerically using the finite volumes technique in generalized coordinates. The numerical results were physically validated through comparison with the experimental data. The developed model was used for airflow simulation in solar chimneys with operational and geometric configurations different from those found in the experimental prototype. Analysis showed that the height and diameter of the tower are the most important physical variables for solar chimney design.

5.7 Enhanced Heat Transfer in Inclined Solar Chimneys

Numerical simulations are carried out to analyze the mechanism of natural convection inside the inclined solar Chimneys incorporating an electro hydrodynamic effect induced from wire electrodes (Nat Kasayapanand, 2007). The volume flow rate enhancement of fluid inside the solar chimney increases to the maximum point but reduces when the number of electrodes is sufficiently high due to pressure drop. The heat transfer enhancement decreases to the minimum point at the intermediate number of electrodes and significantly

increases at high number of electrodes. The inclined angle at 600 performs maximum volume flow rate and also heat transfer due to the highest temperature gradient along hot plate. Moreover, all chimney aspect ratios can be obtained by the optimization between augmented heat transfer and power consumption from a suitable electrode distance ratio. Thus, for high efficiency and economy design, it should be compromised among all concerning parameters.

5.8 Optimal Ratio of Pressure Drop Across the Turbine In Solar Chimney Power Plants

A simplified analytical approach for evaluating the factor of turbine pressure drop in solar chimney power plants is presented (S. Nizetic a, B. Klarin, 2010). This characteristic factor (or pressure drop ratio in turbines, according to the total pressure drop in the chimney) is important because it is related to the output power. The determined factor (or ratio) values of the turbine pressure drop are found to be within a value range consistent with other studies. It was concluded that for solar chimney power plants, turbine pressure drop factors are in the range of 0.8 -0.9. This simplified analytical approach is useful for preliminary analysis and fast evaluation of the potential of solar chimney power plants. In this work, a simplified analytical approach for the evaluation of the optimal pressure drop ratio in solar chimney power plants is presented. The approach is based on a simplified thermodynamic analysis of the overall SC cycle. It is estimated that the ratio depends on two parameters: the air flow velocity at the solar chimney inlet. It is also shown that changes in either parameters result in similar changes to the ratio, this ratio value is in accordance with values provided by other authors. Hence, this proposed simplified analytical approach demonstrates that in solar chimney power plants, the turbine pressure drop factor varies from 0.8 to 0.9. Therefore, it can be concluded that the proposed simplified approach is reliable and useful for a preliminary power estimation of solar chimney power plants for a given conditions.

5.9 Solar Chimney Simulation and Experiment

The use of solar chimneys in buildings is one way to increment natural ventilation and as a consequence, to improve indoor air quality (Clito Afonso, Armando Oliveira, 2000). They are similar to conventional chimneys except that the south wall is replaced by a glazing. In order to compare the behavior of a solar chimney with a conventional one, one of each was built in Porto. Results of measurements carried out in both chimneys are shown in this paper, as well as results of a thermal model specially developed for simulating solar chimneys, taking into account the wind effect. It was concluded that there is a significant increase in ventilation rate with solar chimneys and that the thermal model predicts with good accuracy the measurements carried out. Due to the variable nature of wind, the design of a solar chimney can be done without considering the wind effect, which will underestimate the real ventilation rates. In the design process, two parameters can be changed for satisfying the needed average flow rate: chimney section and chimney height; the average flow rate changes linearly with chimney section; for a given solar collection area, it is better to have a larger chimney width and a smaller height.

5.10 Solar Chimney Power Plant Systems Coupled with Turbine

Numerical simulations have been carried out on the solar chimney power plant systems coupled with turbine (Ming Tingzhena, Liu Weia, Xu Guolinga, Xiong Yanbin, 2008). The whole system has been divided into three regions : the collector, the chimney and the turbine and the mathematical models of heat transfer and flow have been set up for these regions. Using the Spanish prototype as practical example, numerical simulation results for the prototype with a 3-blade turbine show that the maximum power output of the system is a little higher than 50kW. Furthermore, the effect of the turbine rotational speed on the chimney outlet parameters has been analyzed which shows the validity of the numerical method advanced by the author. Thereafter, design and simulation of a MW-graded solar chimney power plant system with a 5-blade turbine have been presented and the numerical simulation results show that the power output and turbine efficiency are 10MW and 50%, respectively, which presents a reference to the design of the large-scale solar chimney power plant systems.

5.11 Solar Chimney and Building Ventilation

CFD was used to investigate the performance of a solar chimney. It was found that varying the slope of the chimney resulted in variations in performance, as measured by the airflow rate through the chimney (D.J. Harris, N.Helwig, 2007). The optimum slope –angle for maximum flow is 67.5m from the horizontal, giving an average benefit of 11% increase in flow rate in comparison with that for a vertical chimney. This gives an improved performance in cooling and ventilating the building and reduces the risk of overheating. Application of low-emissivity finishes to the wall offers an additional way of improving performance, giving approximately a further 10% improvement at that angle. The addition of double glazing gave a slight improvement in performance, but it was not significant enough to be cost effective. Although the effect of wind on the flow rates has not been investigated here, it would be an interesting avenue for future research. With roof angles less than

23^0 from the horizontal, the effect of wind always is to increase the stack suction pressure. With roof angles greater than this, wind direction plays a part in determining whether the stack pressure is increased or decreased.

5.12 A Comprehensive Approach to Design and Improve a Solar Chimney Power Plant

The objective of this paper was to present a comprehensive analysis including analytical and numerical models which were developed to predict the performance of a solar chimney power plant in Kerman, Iran. The numerical model results including air temperature, velocity and electrical power output were validated by comparing with experimental data of the Manzanares prototype power plant. Also the mathematical model was verified with the practical output of the Kerman pilot plant. Also in this paper novel approach to evaluate the influence of the site altitude on the potential of solar chimney power plants was presented and thereby a coefficient called altitude effectiveness was defined using Manzanares prototype geometrical parameters in different site altitudes. The development model was applied to improve the performance of a solar chimney pilot power plant built in Kerman, Iran. Based on an approximate cost model, the thermo-economic optimal configurations of the pilot power plant were illustrated; and also it was found that the chimney diameter was the most important structural dimension to improve the performance of this pilot power plant.

5.13 Simulating Home Cooling Load Reductions for a Novel Opaque Roof Solar Chimney Configuration

The roof solar chimney (RCS) is a low cost passive ventilation technique for reducing the energy consumption for cooling buildings (Justin DeBlois, Melossa Bilec, Laura Schaefer, 2013). This study examines the performance and level of energy savings by simulating a detached home in four climates with RSC, cross-ventilation and standard ventilation strategies. Each case was simulated in ESP –r for baseline and high efficiency construction, detached homes with a single story, three bedrooms a 189 m^2 floor plan and high thermal mass constructions. Photovoltaic panels were integrated into the surface of the solar chimney on the south-facing roof to improve the RSC performance with their absorptive properties, and provide cooling to the reverse of the panels with the ventilation airflow. To form the RSC, a gap under the external layer of the roof allowed air-flow from the interior of the house to a plenum in the peak of the attic with vents to the outside. Cross ventilation was aided with openings in the interior walls allowing flow between rooms. The ventilation gap was modeled by discretizing the RSC into 12 sections and calibrating the air-flow and convection coefficients with corresponding computational fluid dynamics models. The results indicate that the ventilated roof provides free cooling and natural ventilation in all climates and seasons tested. Flow was caused more by the stack effect rather than through natural convection and the solar chimney effect. Cross ventilation reduced cooling load by approximately 50% over the baseline and the ventilated roof by up to another 80%. Both advanced natural ventilation approach reduced cooling load by more than the green envelope and efficiency practices in three of the four climates. The natural ventilation techniques were proportionally as effective in reducing load in a high efficiency home as in the base case home.

5.14 Effects of Collector Radius and Chimney Height on Power Output of a Solar Chimney Power Plant with Turbines

A comprehensive theoretical model has been developed by (Jing-yin Li, Peng-hua Guo, 2012) taking account of the detailed thermal equilibrium equations in the collector, the system driving force and the flow losses based on existing experimental data or formulas. The theoretical model has been validated by the experimental data of the Spanish prototype. It concludes that the installation of the turbine in the SCPP system will considerably reduce the power output of the SCPP, compared with the unloaded condition. There exists a maximum power output for a given SCPP at a certain solar radiation. The operating points of the turbine and the SCPP system are recommended to be chosen on the left-hand-side of the maximum power line, to obtain a longer continuous power output. There is a limitation on the maximum collector radius, beyond which the attainable power output of the SCPP increases very slowly. On the contrary, no such limitation placed on the chimney height exists, in light of the current construction technology.

5.15 A Hybrid Cooling Tower and a Solar Chimney Concept

An innovative concept for recombining a thermal steam power plant dry cooling tower with a solar chimney is introduced (Arash Zandian, Mehdi Ashjaee, 2013). A model has been designed using the typical dimensions and properties of Shahid Rajaee 250 MW steam power plant and the Manzanaras solar chimney. A numerical simulation for the hybrid system including solar collectors, cooling tower radiators and wind turbine is then developed. The effects of environmental temperatures and solar irradiations on the generated turbine power have been illustrated. At the end, the effects of chimney diameter on the hybrid system (HCTSC) power output and the total fossil fuel power plant efficiency have been researched. The results indicate an over ten times increase in output power of the hybrid system compared to experimental results for the conventional solar chimney power plant prototype with similar geometrical dimensions in Manzanares, for the same environmental

conditions. In addition, with increase of chimney diameter the power generation can reach to MW-graded power output without the necessity of building huge individual solar chimney power plants. The results show a maximum of 3 MW power output from the HCTSC system that results in 0.37% increase in the thermal efficiency of the Shahid Rajaee 250 MW fossil fuel power plant, when the chimney diameter is 50 m.

5.16 Numerical Simulations of Solar Chimney Power Plant with Radiation Model

A three dimensional numerical approach incorporating the radiation, solar load and turbines models proposed, was first verified by the experimental data of the Spanish prototype (Jing-yin Li, Yuan Wang , 2014). It then was used to investigate the effects of solar radiation, turbine pressure drop and ambient temperature on system performance in detail. Simulation results reveal that the radiation model is essential in preventing the overestimation of energy absorbed by the solar chimney power plant. The predictions of the maximum turbine pressure drop with the radiation model are more consistent with the experimental data than those neglecting the radiation heat transfer inside the collector. In addition, the variation of ambient temperature has little impact on air temperature rise despite its effect on air velocity. The power output of the SCPP within the common diurnal temperature range was also found to be insensitive to ambient temperature. In simulating the performance of the SCPP system, the radiation, solar load and turbine models were incorporated into a 3-D numerical computation for the first time. The adopted numerical approach was first validated by the experimental data of the Spanish prototype and then was used to investigate the effects of solar radiation, turbine pressure drop and ambient temperature on system performance, the conclusions that can be drawn are that the radiation heat transfer is an important factor in the heat transfer process inside the SCPP and should be considered in the numerical simulation. Otherwise, heat losses would be dramatically underestimated. The effects of solar radiation and turbine pressure drop on SCPP performance are considerable. Furthermore the proposed numerical approach could provide a reasonable prediction of the maximum turbine pressure drop at a certain solar radiation, which is an important factor in the determination of turbine design point and operation range. The variation of ambient temperature has a negligible effect on air temperature rise, but has an evident effect on air velocity. The SCPP power output within the common diurnal temperature range is found to be insensitive to ambient temperature.

5.17 Performance of A Coupled Cooling System with Earth-To-Air Heat Exchanger and Solar Chimney

To utilize the solar energy and geothermal for free cooling (Haorong Li, Yuebin Yu, Fuxin Niu, Michel Shafik, 2014) devised a coupled passive energy system with a solar collector enhanced solar chimney and an earth-to-air heat exchanger. Research has been conducted on the coupled system at the solar energy research test facility to further investigate the performance of the coupled system. Experiments and analysis have been carried out in order to evaluate the cooling capacity that the coupled system can provide to the test room and the impact factor. In the test, the coupled system was operated in a natural passive mode. Without any mechanical component, the air was driven into the building by means of the passive solar energy and the stack effect. During the natural airflow test, the coupled system was able to maintain the indoor thermal environmental comfort conditions at a favourable range that complied with ASHRAE standard for thermal comfort. The indoor air temperature was maintained at a range of 21.3-25.1^{0}C, while the indoor humidity ratio was maintained at a range of 50-78%. The coupled system provided an acceptable amount of cooling capacity during the natural airflow test in 2008. The EAHE maximum cooling capacity during that test was 3308W. While the coupled system maximum cooling capacity was 2582 W, which almost covered the building design cooling load. During the natural airflow mode, it was found that the increase in the outdoor air temperature and solar radiation increases the solar chimney natural draft and the amount of airflow to the building, which in turn increase the amount of cooling capacity provided to the building.

5.18 Three-Dimensional CFD Analysis for Simulating the Greenhouse Effect in Solar Chimney Power Plan

The objective of this paper (Ehsan Gholamalizadeh, Man-Hoe Kim, 2014) was to analyse the buoyancy-driven flow field and heat transfer inside the solar chimney power plant, simulating the greenhouse effect. In this paper a three dimensional unsteady CFD model to analyze the solar chimney power plant system was developed. In order to simulate the turbulent flow inside the system the RNG ke-ε model was used. A two band model for short and long wavelength radiation was implemented to simulate the greenhouse effect in the system. In order to solve the radiative transfer equation the discrete ordinates method was used. To calculate radiation effects from the sun's rays, the solar load model's ray tracing algorithm was employed, which appears as a source term in the energy equation. The model provided good agreement with experimental measurements of the Manzanares power plant. The analysis showed that imulating the greenhouse effect through the collector has a significant effect on predicted characteristics of the flow and heat transfer in the system. Based on the results, the effects of solar insolation and pressure drop across the turbine on the distributions of the velocity and temperature were considered, using geometry parameters of the Manzanares power plant. Also, enthalpy rise

through the collector and energy loss from the chimney outlet for 1-band and two- band radiation model are compares in different solar insolations. Furthermore, temperature profile of the ground surface of the system is illustrated. It can be concluded that simulating the greenhouse effect has a significant effect to accurately describe all the phenomena occurring in SCPP systems.

5.19 Numerical Analysis on an Industrial-Scaled Solar Updraft Power Plant System with Ambient Crosswind

Existing research (Wenquing Shen, Tingzhen Ming, Tan Ding, Yongjia Wu, 2014) indicated that the ambient crosswind (ACW) has very complex influences on the SUPPS both through the chimney outlet and collector inlet and demonstrated by numerical analysis from the Spanish prototype. But what influence exert ACW through chimney outlet and collector inlet independently on the overall performance of SUPPS is still unclear. In this research, two geometrical models are instructed for numerical simulation on industrial-scale SUPPS in vicinity of 10 MW. In model 1, ACW acts on both chimney outlet and collector inlet; in model 2, ACW acts only on the chimney outlet. Fluid flow, heat transfer and power output performances of SUPPS are investigated and discussed. It is found that, the negative effect of ACW only occurs at the collector inlet, with cold ambient air into the collector resulting in changing of fluid distribution and deterioration of buoyant driving force, whereas the positive effect occurs at the chimney outlet, with strong ACW passing by the chimney outlet causing entrainment of buoyant airflow within the chimney outlet. To avoid deterioration and to improve the overall performance of SUPPS, effective measures can be taken to prevent ACW from entering the collector inlet and also to induce beneficial effects of high altitude strong ACW blowing across the chimney outlet.

5.20 Thermal Management of a Symmetrically Heated Channel Chimney System

A parametric study on a channel-chimney system was accomplished (Assunta Andrezzi, Bernardo Buonomo, Oronzio Manca, 2009). In this numerical investigation in order to evaluate some geometric optimal, configurations in terms of significant dimensionless geometric and thermal parameters. In the system, the channel walls are symmetrically heated at uniform heat flux. Temperature wall profiles, as a function of axial coordinate, suggested the evaluation of thermal performances of the channel-chimney system in terms of maximum wall temperatures for different expansion ratios, as a function of the chimney aspect ratio. For considered Rayleigh number values, the difference between the highest and the lowest maximum wall temperature increasing channel aspect ratio. This behavior was as greater as the extension ratio was. These differences decreased significantly for the highest Rayleigh number value. Correlations for dimensionless mass flow rate, maximum wall temperature and average Nusselt numbers, in terms of Rayleigh number and dimensionless geometrical parameters, were also proposed.

5.21 Study of the Natural Connection Phenomena inside a Wall Solar Chimney with One Wall Adiabatic and One Wall under a Heat

This work (Evangellos Bacharoudis, Michalis Gr. Vrachopoulos, Maria K. Koukou, 2007) focuses on the study of the thermo fluid phenomena occurring inside wall solar chimney that have been constructed and put at each wall and orientation of a small-scale test room. A numerical investigation of the buoyancy-driven flow field and heat transfer that take place inside the wall solar chimney is performed. The governing elliptic equations are solved in a two-dimensional domain using a control volume method. The procedure is general and can be applied for the simulation of solar chimneys of different aspects ratios and conditions. For the numerical simulation of the turbulent flow inside the wall solar chimney six turbulence models have been tested: the standard k-e model, the RNG k-e model, the realizable k-e model, the Reynolds stress model and two low-Reynolds models. It is concluded that the use of the k-e models and the use of the Abid Low-Re model assures the prediction of realistic velocity and temperature profiles as expected by theory. As the realizable k-e model is likely to provide superior performance for flows boundary layers under strong adverse pressure gradients, the later has been selected to be used in the simulations. Furthermore, this selection is confirmed from the comparison with the experimental results. Simulation results also show that the model predicts realistically the system behavior for various environmental conditions while they support the evaluation of the air mass flow rate that can be achieved through this system and the turbulence effects.

5.22 Analysis of Chimney Height for Solar Chimney Power Plant

Current in solar chimney power plant (xinping zhou, jiakuan yang, bo xiao, guoxiang hou, 2009) that drives turbine generators to generate electricity is driven by buoyancy resulting from the higher temperature than the surroundings at different heights. In this paper, the maximum chimney height for convection avoiding negative buoyancy at the later chimney and the optimal chimney height for maximum power output are presented and analyzed using a theoretical model validated with the measurements of the only one prototype in Manzanares. The result based on the Manzanares prototype show that as standard lapse rate of atmospheric

temperature is used, the maximum power output of 102.2 kW is obtained for the optimal chimney height of 615 m, which is lower than the maximum chimney height with a power output of 92.3 kW. Sensitivity analyses are also performed to examine the influence of various lapse rates of atmospheric temperatures and collector radii on maximum height of chimney. The results show that maximum height gradually increases with the lapse rate increasing and go to infinity at a value of around 0.0098 Km^{-1} and that the maximum height for convection and optimal height for maximum power output increase with large collector radius. In this paper, the maximum chimney height for convection and the optimal chimney height for maximum power output are presented and analyzed based on the Manzanares prototype using a theoretical model validated with the measurements of the only one prototype in Manzanares. With respect to a special collector, negative buoyancy at the latter chimney will occur it chimney height is more than the maximum height. The power plant would obtain the maximum energy conversion efficiency if chimney height is equal to the optimal height. To find out the optimal chimney height for a collector covered at finite ground is significant for the decision-making in determining the dimensions for construction.

5.23 Optimum Wall-To-Wall Spacing in Solar Chimney Shaped Channels in Natural Convection By Numerical Investigation

A numerical study on the laminar and turbulent flows was induced (B.zamora, A.S. Kaiser optimum, 2009) by natural convection in channels, with solar chimney configuration for a wide range of Rayleigh number, several values of the relative wall-to-wall spacing and different heating conditions has been performed. The low-Reynolds k-x turbulence model has been employed to simulate the turbulent cases. Numerical results for the average Nusselt number and the non-dimensional induced mass-flow rate have been obtained for values of Rayleigh number varying from 105 to 1012 for symmetrically, isothermal heating. For this heating condition, a correlation for the thermal optimum aspect ratio has been presented. The sudden change reached in the flow pattern for given conditions drives to obtain a different behavior of the optimum aspect ratio that maximizes the mass-flow rate with respect to the thermal optimum aspect ratio. Depending on the requirements of the real design, the correlations and the results proposed in this work let to optimize the inter-plate spacing that maximize the induced mass flow rate or the heat transfer within the chimney for a given conditions.

5.24 Experimental Study and Simulation of Airflow in Solar Chimney

A detailed mathematical simulation and experimental investigation of airflow in solar chimneys is studied in this paper (Nadia Saifia, Noureddine Settoua, Boubekaur Dokkara, 2012). Several experimental studies were carried out on the solar chimney; their choice depends on the parameter of the design and the thermal performances for different geometrical configurations. The experimental tests show that the field speeds in the chimney is influence by the width of the channel and also of the angle of inclination of the chimney. Therefore, investigations have been carried out to find the effect of inclination on the performance of solar chimney in Ouargla Province, Algeria. The simulation of this problem is implemented into the commercial CFD code Fluent 6.3.26. The conservation equations of mass continuity and energy are solved by the Finite Volume Method. The validation of the results is presented. A good agreement between the experimental results and simulation ones is observed. An experimental and numerical study is undertaken for a titled solar chimney. Experimental study under various chimney slopes (30^0 and 45^0) and air thickness located between absorber and pane (e=10cm, 20cm and 30cm), leads to the following conclusions: the variation in temperature between the absorber and the pane varies according to indent solar flow. Adopted design allows to obtain rather high air flow at chimney outlet, which is interesting to exploit them in natural ventilation Numerical simulation allows determining temperature contours and velocity profile inside solar chimney for various chimney inclination with Rayleigh number Ra=109. By using Boussinesq approximations, main results are summarized that the variation of air blade thickness plays a very important effect to increases significantly air flow. Optimal thermal pulling is reached at chimney inclination angle 45^0.

5.25 Numerical Study on the Thermal Environment of UFAD System with Solar Chimney for the Data Center

To improve the thermal environment in the data center, a solar chimney was integrated (Kai Zhang, Xiaosong Zhang, Shuhong Li, Geng Wang, 2014) with under-floor Air Distribution (UFAD) system in the computational Fluid Dynamics (CFD) software Airpak. By using the validated model, three types of solar chimney, such as solar chimney transversely over the hot and cold aisles, solar chimney lengthways above the cold or hot aisles, were simulated. The comparison between the model calculation result shows that all types of solar chimneys used in this paper has great potential in providing a better temperature and airflow distribution. Especially in the case of the solar chimney above the cold aisle, the temperature in upper zone of cold aisle can be decreased by 130^0C and the temperature field inside the rack is improved greatly without any additional power. Solar chimney is an ideal way to improve the thermal environment of the data center with UFAD

system. By using the validated model, three kinds of typical solar chimney were employed separately, which cannot only provide the power to exhaust air but also realize a more reasonable distribution of temperature and airflow in both the room and racks. The comparison between the model calculation result shows that the solar chimney installed above the cold aisle is more effective to this system, in which the temperature in upper zone of cold aisle can be decreased by 13^0 C, and the temperature field inside the rack is improved greatly without any addition power. The application of solar chimney in data center with (UFAD) system can acquire a better cooling effect by the way of improving the distribution of temperature and airflow rather than increasing cooling load, subsequently decreasing the waste of energy and the burden of power system.

5.26 Research for Ventilation Properties of Solar Chimney with Vertical Collector

Theoretical research and numerical simulation for ventilation properties of solar chimney with vertical collector are performed (Zhou Yan, Jing Guang-E, Liu Xiao0hue, Li Qing-Ling, 2011).They are compared with experimental results. Results show that: there are many factors to affect solar chimney ventilation that include heat collection height and weight, solar radiation intensity, inlet and outlet area ratio of chimney and air inlet velocity etc. When the collector height is increased, chimney ventilation is getting higher; but the ventilation increases slowly even decreases; the ventilation increases first and then decreases as growing of the air layer thickness under the same chimney height and width; there exists an optimal ratio between heat collector height and width which makes the ventilation largest; considering the urban architecture image and the influence of the air layer thickness on chimney ventilation, the best air layer thickness is between 0.2m and 0.4m. Besides the airflow temperature in solar chimney increases with chimney height in certain solar radiation intensity. It is consistent with the theoretical analysis and simulation results.

5.27 Solar Ventilation and Heating of Buildings in Sunny Winter Days Using Solar Chimney

The capability of solar chimney lonely to meet the required thermal and ventilation needs of individuals in winter days in investigated (A.P. Haghighi, M.Maerefat, 2014). In the analysis, the heat transfer by natural convection and surface radiation in a 2D vented room in contact with a cold external ambient is studied numerically. The dependence of the system performance on air gap depth of the solar chimney, size of openings, outdoor air temperature and solar radiation have been studied to determine the appropriate operation conditions, regarding thermal comfort criteria. The findings show that the system is capable of providing good indoor air condition at daytime in a room, even with poor solar intensity of 215 W/m^2 and low ambient temperature of 5^0C.

VI. Conclusion

Generation of electricity using solar energy is a feasible alternative for power generation over conventional power plants like thermal and hydraulic power plants. It is an ideal technology that can be adopted in the countries like India that have sunshine almost nine months in the year and lot of free space available for setting large amount of power plants. The only problem is awareness and initiative required and also some sound technical feasibility is required so that this technology can be adopted with ease. In this paper a detail literature review of this technology was performed. The review gives basic principle and operation of this system. It also gives the present status of this technology and various feature scope of this technology. This paper shows that lot of numerical and experimental studies are carried out by keeping Manzanares power plant as reference. It is concluded that such system should be constructed in a very large way to generate large amount of electricity. CFD methods are adopted by many researchers because of high constructional cost of these power plants.

REFERENCES

[1] Jorg Schlaich & Wolfgang Schiel, Solar Chimneys, Encyclopedia of Physical Science and Technology Third Edition, 2000.
[2] Reid Smith and Lisa Cohn, the 27 European Photovoltaic Solar energy conference and exhibition Messi Frankfurt Germany, 2012
[3] A.A. El-Haroun, Performance Evaluation of Solar Chimney Power Plants in Egypt, Int. J. Pure Appl. Sci. Techno., 13(2), 2012, 49-59.
[4] G.M.Ngala, A.T. Sulaiman, I. Garba, Review of Solar Chimney Power Technology and Its Potentials in Semi-Arid region of Nigeria, International Journal of Modern Engineering Research (IJMER) www.ijmer.com Vol.3, Issue.3,2013 283-1289
[5] Mohammad O. Hamden, Analysis of a solar chimney power plant in the Arabian Gulf region, Renewable Energy 36, 2011, 2593-2598.
[6] Sudaporn Chungloo, Bundit Limmeechokchai, Utilization of cool ceiling with roof solar chimney in Thailand: The experimental and numerical analysis, renewable energy 34, 2009, 623-633.

[7] Fei Cao Liang Zhao, Performance analysis of conventional and sloped power plants in China, Applied Thermal Engineering 50, 2013, 582-592.

[8] Clever Ketlogetswe, Jerze K. Fiszden, Solar chimney power generation project- the case for Botswana, Renewable and Sustainable Energy Reviews 12, 2008, 2005-2012.

[9] Salah Larbi, Adel El Hella, Thermo-fluid aspect analysis of passive cooling system case using solar chimney in the south regions of Algeria, Energy Procedia 36, 2013,628-637.

[10] Shadi Kalasha, Wajih Naimeh, Experimental Investigation of a pilot Sloped Solar Updraft Power Plant Prototype Performance Throughout a Year, Energy Procedia, 50,2014, 624-633.

[11] F. Denantes E. Bilgen, Counter-rotating turbines for solar chimney power plant, Renewable Energy, 31, 2006, 1873-1891.

[12] Alvaro Garcia, Manfred N.Partl, How to transform an asphalt concrete pavement into a solar turbine, Applied Energy, 119, 2014, 431-437.

[13] Reingard Hartea, Gideon P.A.G. Van Ziji, Structural stability of concrete wind turbines and solar chimney towers exposed to dynamic wind action, Journal of Wind Engineering and Industrial Aerodynamics, 95, 2007, 1079-1096.

[14] Artemis Agelaridou-Twohig, Franco Tamanini, Hosam Ali, Thermal Analysis of reinforced concrete chimneys with fiberglass plastic liners in uncontrolled fires, Engineering Structures 75, 2014, 87-98.

[15] A. Koonsrisuk, S.Lorente, A.Bejan, Constructal solar chimney configuration, International Journal of Heat and Mass transfer 53, 2010, 327-333.

[16] N.Ninic, Available energy of the air in solar chimney and the possibility of its ground-level concentration, Solar Energy 80,2006,804-811.

[17] Thomas Peter Fluri, Turbine Layout for and Optimization of solar chimney power plant, doctoral diss, University of Stellenbosch, South Africa, 2008.

[18] Denis Bonnelle, Solar Chimney, water spraying Energy Tower and Linked renewable energy conversion devices: presentation, criticism and proposals, doctoral diss, University Claude Bernard – Lyon1 – France, 2004.

[19] Atit Koonsrisuk, Analysis of flow in Solar Chimney for an Optimal Design Purpose, doctoral diss., Suranaree University of Technology Thailand, 2009.

[20] Johannes Petrus Pretorius, Control of a Large-Scale Solar Chimney Power Plant, Doctoral diss., University of Stellenbosch, Matieland, South Africa, 2007.

[21] Christos D. Papageorgiou, Floating Solar Chimney Technology Scale Analysis, Proc. IASTED Int. Conf. on Power and Energy Systems Crete, Greece 24,2011. 55-59.

[22] M.A. Dos S. Bernardes, A.Vob, G. Weinrebe, Thermal and technical analysis of solar chimney, Solar Energy, 75, 2003, 511-524.

[23] Von Theodor, W.Backstrom, Thomas P. Fluri, Maximum Fluid power condition in solar chimney power plants – An analytical approach, Solar Energy 80, 2006, 1417-1423.

[24] Atit Koonsrisuk, Tawit Chitsomboon, Mathematical modeling of solar chimney power plants, Energy 51, 2013, 314-322.

[25] Reinhard Harte, Rudiger Hoffer, Wilfried B. Kratzig, solar updraft power plants; Engineering Structures for sustainable energy generation, Engineering Structures, 56,2013, 1693-1706.

[26] Z.D. Chena, P. Bandopadhayay, J. Halldorsson, An experimental investigation of a solar chimney model with uniform wall heat flux, building and environment 38, 2003, 893-906.

[27] Cristiana B. Maia, Andre G.Ferreira, Ramon M. Valle, Theoretical evaluation of the influence of geometric parameters and materials on the behavior of the airflow in a solar chimney, Computers and Fluids 38, 2009, 625-636.

[28] Nat Kasayapanand, Enhanced heat transfer in inclined solar chimney by electro hydrodynamic technique, renewable energy, 33, 2008, 444-453.

[29] S. Nizetic a, B. Klarin, A simplified analytical approach for evaluation of the optimal ratio of pressure drop across the turbine in solar chimney power plants, Applied Energy , 87, 2010, 587-591.

[30] Clito Afonso, Armando Oliveria, Solar chimneys: simulation and experiment, Energy and Buildings, 32, 2000, 71-79.

[31] Ming Tingzhen, Liu Weia, Xu Guolinga, Xiong Yanbin, Numerical Simulation of the solar chimney power plant systems coupled with turbine, Renewable energy 33,2008, 897-905.

[32] D.J. Harris, N. Helwig, Solar chimney and building ventilation, applied Energy 84, 2007, 135- 146.

[33] E. Gholamelizadeh, S.H. Mansouri, A comprehensive approach to design and improve a solar chimney power plant: A special case – Kerman project, Applied Energy 102, 2013, 975-982.

[34] Justin DeBlois, Melissa Bilee, Laura Schaefer, Simulating home cooling load reductions for a opaque roof solar chimney configuration, Applied Energy 112, 2013, 142-151.

[35] Jing-yin Li, Peng-hua Guo, Yuan Wang, Effects of collector radius and chimney height on power output of a solar chimney power plant with turbines, Renewable Energy 47, 2012, 21-28.

[36] Arash Zandian, Mehdi Ashjace, the thermal efficiency improvement of a steam Rankine cycle by innovative design of a hybrid cooling tower and a solar chimney concept, Renewable Energy, 51, 2013, 465-473.

[37] Peng-hua Guo, Jing-yin Li, Yuan Wang, Numerical simulations of solar chimney power plant with radiation model, Renewable Energy 62,2014, 24-30.

[38] Haorong Li, Yuebin Yu, Fuxin Niu, Michel Shafik, Bing Chen, Performance of coupled cooling system with earth-to-air heat exchanger and solar chimney, Renewable Energy 62, 2014, 468-477.

[39] Ehsan Gholamalizadeh, Man-Hoe Kim, Three dimensional CFD Analyses for simulating the green house effect in solar chimney power plants using a two-band radiation model, Renewable Energy 63, 2014, 498-506.

[40] Wenquing Shen, Tingzhen Ming, Yan Ding, Yongjia Wu, Numerical analysis on an industrial- scaled solar updraft power plant system with ambient crosswind. Renewable Energy 68, 2014, 662-676.
[41] Assunta Anadreozzi Bernardo Buonomo, Oronzio Manca, Thermal management of a symmetrically heated channel chimney system, International Journal of Thermal Sciences 48, 2009, 475-487.
[42] Evangellos Bacharoudis, Michalis Gr. Vrachopoulos, Maria K. Koukou, Study of the natural convection phenomena inside a wall solar chimney with one wall adiabatic and one wall under a heat flux, Applied Thermal Engineering 27, 2007, 2266- 2275.
[43] Xinping Zhou a, Jiakuan Yang, Bo Xiao Guoxiang hou, Analysis of chimney height for solar chimney power plants, Applied thermal engineering 29, 2009, 178-185.
[44] Zamora, A.S. Kaiser Optimum, wall-to-wall spacing in solar chimney shaped channels in natural convection by numerical investigation, applied Thermal Engineering 29, 2009, 762-769.
[45] Nadia Saifia, Noureddine Settoua, Boubekeur Dokkara, Experimental study and simulation of airflow in solar chimney, Energy Procedia 118, 2012, 1289-1298.
[46] Kai Zhanga Xiaosong Zhang, Shuhong Li, Geng Wang, Numerical study on thermal environment of UFAD system with solar chimney for the data center, energy procedia 48, 2014, 1047-1054.
[47] Zhou Yan, Jing Guang-e, Liu Xiao-ling, Research for ventilation properties of solar chimney with vertical collector, Procedia Environment Sciences 11, 201, 1072-10 77.
[48] A.P. Haghighi, M.Macrefat, solar ventilation and heating of buildings in sunny winter days using solar chimney, sustainable cities and society , 10, 2014, 72-79.
[49] H.F. Nouanegue, E. Bilgen, Heat transfer by convection, conduction and radiation in solar chimney systems for ventilation of dwellings, International Journal of heat and fluid Flow 30, 2009, 15-157.
[50] Rakesh Khannal, Chengwang Lei, A scaling investigation of the laminar convective flow in a solar chimney for natural ventilation, International Journal of Heat and Fluid Flow 45, 2014, 98-108.
[51] Xinping Zhou, Bo Xiao, Wanchao Liu, Xianjun Guo, Comparison of classical solar chimney power system and combined solar chimney system for power generation and seawater desalination, desalination 250, 2010, 249-256.
[52] Lu Zuo, Yuan Zheng, Zhenjie Li, Yujun Sha, Solar Chimneys integrated with sea water desalination, Desalination 276, 2011, 207-213.
[53] Chi-Ming Chu, Md. Mizanur Rahman, Sivakumar Kumaresan, Effects of cold inflow on chimney height of natural draft cooling towers, Nuclear Engineering and Design 249, 2012, 125-131.
[54] Takahiko iyazakia , Atsushi Akisawaa, Isao Nikaib, The cooling performance of a building integrated evaporative cooling system driven by solar energy, Energy and building 43, 2011, 2211-2218.
[55] Amel Dhahri, Ahed Omri, A Review of solar chimney Power Generation Technology, International Journal of Engineering and Advanced Technology, 2013 Volume – 2, Issue-3.

OPEN ACCESS

International
Journal
Of Modern Engineering Research (IJMER)

Optimization of Tool Wear: A Review

Ramakant Rana[1], Kunal Rajput[2], Rohit Saini[3], Roop Lal[4]
[1]*Assistant Professor, Mechanical and Automation Engineering, Maharaja Agrasen Institute of Technology, Delhi, India*
[2,3]*Student, Mechanical and Automation Engineering, Maharaja Agrasen Institute of Technology, Delhi, India*
[4]*Assistant Professor, Mechanical Engineering, Delhi Technological University, Delhi, India*

Abstract: *The quality of the machined piece and tool life are greatly influenced by determination of maximum temperature of the cutting tool. Numerous researchers have approached to solve this problem with experimental, analytical and numerical analysis. There is hardly a consensus on the basics principles of the thermal problem in metal cutting, even though considerable research effort has been made on it. It is exceedingly difficult to predict in a precise manner the performance of tool for the machining process. This paper reviews work on the requirements for optimization of Tool wear so that its life could easily be predicted.*

Keywords: *Tool Wear, Taguchi, CNC, Optimization, Wear.*

I. INTRODUCTION

Research in metal cutting was started with Cocquilhat in 1851 which measured the work required to remove a given volume of material in drilling. The attempt made by Time led to the explanation of formation of chips in 1870 and further research was made by Tresca in 1873. Later in 1881, Mallock suggested that the cutting process was the shearing of workpiece to form the chip and emphasized the importance of the effect of friction occurring on the cutting tool face as the chip was removed. Further, Taylor investigated the effect of tool material and cutting conditions on tool life during rough operations. Latest fundamental work has been carried out by Ernst and Merchant in 1941 dealing with the mechanics of metal cutting process. The simplest and most widely used model for cutting was first by Ernest and Merchant (1941) and further contribution to study of Ernest and Merchant theory was done by Lee and Shaffer (1951), Kobayashi and Thomsen (1962). Large number of literature is available on the determination of chip-tool interface temperature, factors affecting the interface temperature and techniques of optimization of machining parameters including cutting speed, feed rate, cutting zone temperature, etc. Armerago (1969), Boothroyd (1981), Shaw (1984) and Trent (2000) wrote the most widely used text books. Kalpakjian, et al. (2006), and DeGarmo, et al. (1997) wrote books on more general introductory knowledge. The study machining process by experimental approach is expensive and time consuming peculiarly when a wide range of parameters is included like tool geometry, cutting conditions, and materials.

II. LITERATURE REVIEW

Jensen M.R. et al. [1] stated that an important problem in the machining of drawn parts is tool wear. They said that tool wear can be reduced by increasing the tool lifetime and by making more continuous production flow, by reducing the number of break-downs when the tools have to be re-polished. In their paper, an optimization of the shape of the draw-die profile with regard to wear was carried out using a conventional optimization method and explicit finite element. The optimized draw-die profile had almost twice the tool life compared to that of the initial circular draw-die, if the peak value of wear was used as the wear criteria. The relatively small resources used by them with their optimization approach made the tool wear design relevant for industrial use at the tool-design state.

Sullivan D.O' et al. [2] determined the temperature in a single point turning process. The total work done by a cutting tool in removing metal was determined from the force components on the cutting tool. Approximately, all of this work or energy is converted into heat which is dissipated into the chip, tool and workpiece material. The wear of the tool is related to the cutting forces. Initial experiments conducted involved the simultaneous measurement of forces and temperatures. These experiments focused on the use of embedded thermocouple (in the work piece) and using the infrared thermal camera to monitor the process. They concluded that in machining of aluminium Al 6082-T6 the decreased cutting tool forces and machined surface temperatures was resulted by increased cutting speed (V_C) and increased cutting tool forces and machined

surface temperature was resulted by tool wear. They left the examination of temperature distribution at the tool chip interface for the future work.

Abukhshim N.A. et al. [3] reviewed the previous research work. Research on heat generation and heat dissipation in the orthogonal machining process is critically studied. In addition, temperature measurement techniques applied in metal cutting were also reviewed. The emphasis was on the comparability of test results obtained by a thermal imaging camera in high speed cutting of high strength alloys. Finally, latest work on these topics in metal machining was also reviewed. They reviewed the methods of temperature measurement and the analytical and numerical models for the prediction of temperature and temperature distribution in metal cutting. In metal cutting the Prediction of cutting temperatures is a major challenge. They concluded that fiber-optic pyrometers and infrared thermography techniques for temperature measurement of the high speed cutting process are more promising as compared to other methods as these techniques can measure temperature, as well as, the cooling rate easily, accurately and with fast time response. They stated that technology for consideration of interactions at the tool/chip interface is mainly based on certain assumptions and not on a precise understanding of the underlying physics. They also stated that modeling and simulation of machining processes is mainly suffering from a lack of the fundamental input data.

Many researchers has been undertaking into measuring the temperatures generated during cutting operations. Investigators have attempted to measure these cutting temperatures with various techniques (see figure 1 based on [4])

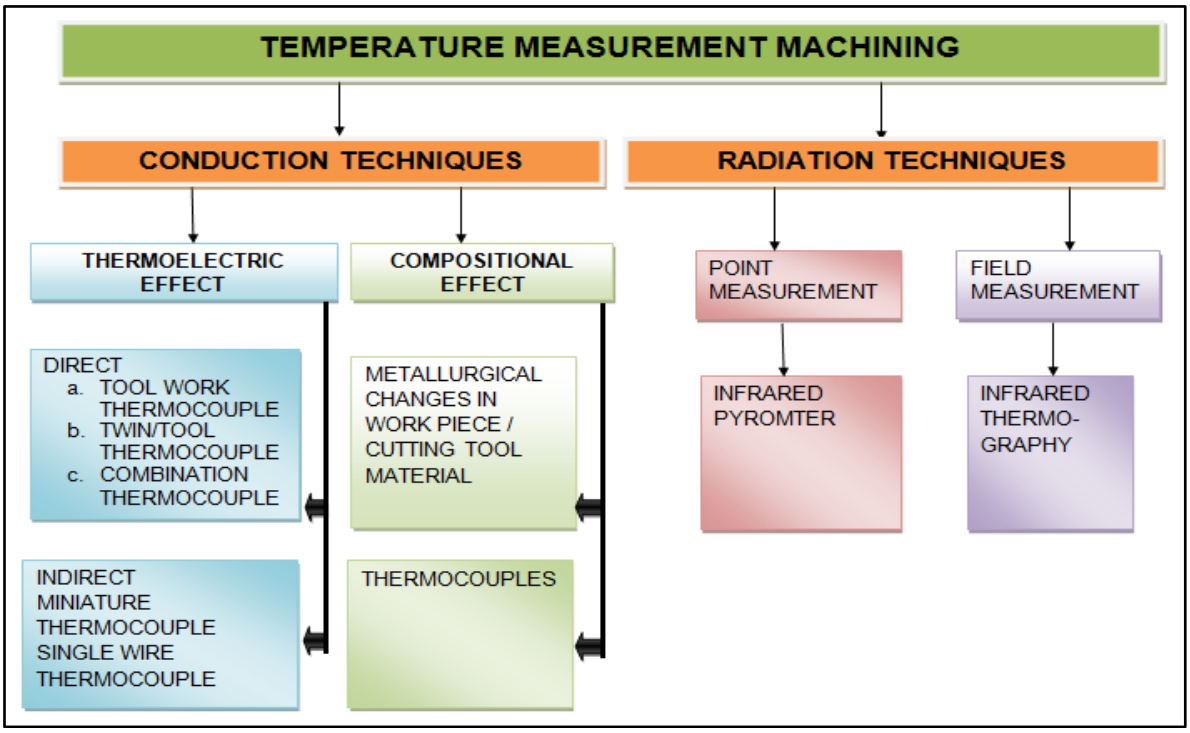

Figure 1: Temperature measurement in machining [4]

Lazoglu Ismail et al. [5] predicted the tool chip temperature in continuous and interrupted machining. They presented a numerical model based on the finite difference method to predict tool and chip temperature fields in continuous and interrupted machining and time varying milling processes. By modeling the heat transfer between the tool and chip at the tool-rake face contact zone Continuous or steady state machining operations like orthogonal cutting were studied. They determined Heat balance equations in partial differential equation forms for the chip and for the tool. The solutions of the steady-state tool and chip temperature fields were taken by finite difference method. The chip thickness was discretized along the time to determine the transient temperature variation in the case of interrupted machining.

Sutter G. et al. [6] presented an experimented setup for the measurement of temperature field in high speed machining. Their paper presented an experimental setup during an orthogonal machining operation with 42 CrMo 4 steel. The technique of temperature measurement was developed on the principle of pyrometer in the visible spectral range by using an intensified CCD camera with very short exposure time and interference filter at 0.8 micrometer. They obtained the temperature gradients in an area close to the cutting edge of the tool, along the secondary shear zone. It was established that their experimental arrangement shown in Figure 2 was quite

efficient and can provide fundamental data on the temperature field in material during orthogonal high speed machining. They showed experimentally that, for a cutting speed of 20 m/s a hot spot was located near the tool-chip interface at a distance of 300-350 μm of the tool tip. This value corresponds to about the two-thirds of the depth of cut. The reaching temperature is around 825°C. The temperature in the chip increases with increasing of the cutting speed. Their result showed that, with an increase of the cutting speed from 20–30 m/s the dependence of the temperature on the cutting speed was more noticeable. They even showed that, the temperature appeared to stabilize for the cutting speeds larger than 40 m/s. A similar tendency was observed with the increasing in the depth of cut and for a cutting speed fixed to 40 m/s by their experimental technique. The temperature in the chip was nearing a saturated value about of 840°C during the process of an un-deformed chip thickness larger than 0.5 mm.

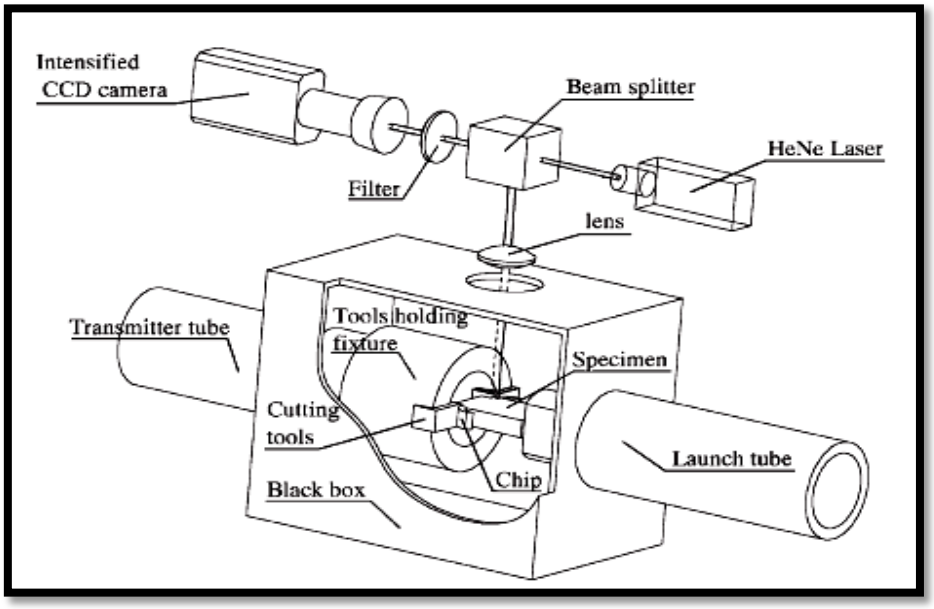

Figure 2: Experimental Apparatus's scheme used by **G. Sutter et al.** [6]

Dogu Yahya et al. [7] designed a numerical model to determine temperature distribution in orthogonal metal cutting. In their study, they developed a thermal analysis model to determine temperature distribution in orthogonal in metal cutting using FEM. Their model was used to calculate the temperature distribution as a function of heat function of heat generation. Assuming that all the work required for cutting is converted to the sensible heat energy the amount of heat generation was calculated by them. Accurate predictions of temperature field over the entire cutting zone were given by the developed model. It was also found that at the half of the contact length from cutting edge, the maximum temperatures for relatively smaller cutting speeds occurred for the analyzed cases. It was clear that the outer surface of the material will be subject to higher heat removal and sudden temperature drop.

Saglam Haci et al. [8] studied the effect of tool geometry and cutting speed on main cutting force and tool tip temperature. They investigated the temperature generated on the tip of the tool in turning and cutting speed on cutting force components and the effects of rake angle and entering angle in geometry of tool in their paper. The experiments were conducted on a CNC lathe to derive the data used for investigation. Each test was conducted with a sharp uncoated tool insert, while keeping the depth of cut and feed rate constant, during the tests. They found that the cutting speed was effective on the tool tip temperature, while the rake angle was effective on all the cutting force components. They found that, the deviation in temperature was 54%, while the average deviation between calculated and measured values of main cutting force was 0.26% in 64 numbers of experiments.

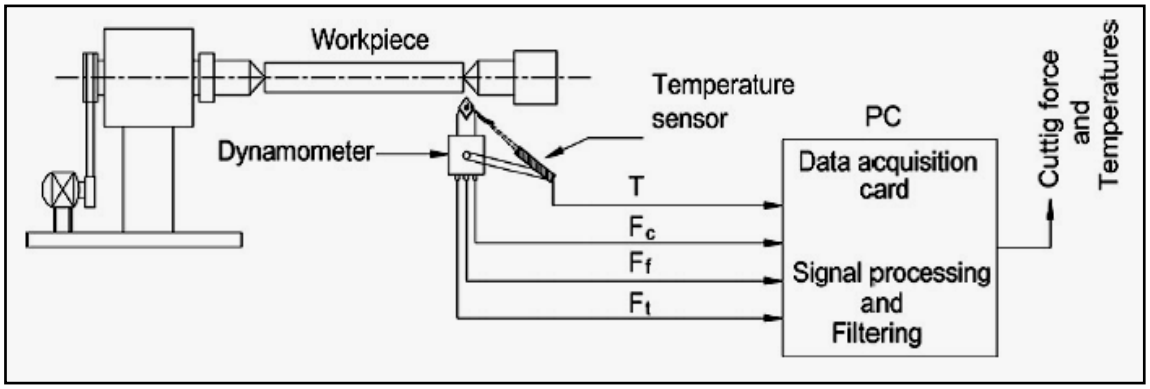

Figure 3: Experimental setup used by **Saglam et al.** [8].

They experimentally found that the main cutting edge subjected to maximum loading and unloading as it enters and leaves the cutting zone abruptly at 90^o of entering angle by using the experimental setup shown in Figure 3. They also found that the impact of load was not exerted on cutting tool when it has an entering angle different then 90^o, because the cutting edge enters and leaves the workpiece gradually. Hence, they concluded that at 60^o to 70^o the optimum entering angle was obtained. They showed that, the cutting forces were reduced and the temperature was increased when the cutting speed was raised. They also showed that, the cutting forces were decreased, for the increased positive rake angle. Their result of cutting forces and temperature evaluated together resulted that the optimum rake angle should be 12^o. Their results of analysis of variance evaluated, that the cutting speed was effective on tool tip temperature while, the rake angle had a significant effect on cutting forces components. They verified their conclusions by the correlation coefficients.

Ueda Takashi et al. [9] determined the temperature of a signal crystal diamond tool in turning. They in precision turning, investigated experimentally and theoretically the temperature on the rake face of a single crystal diamond tool. They used FEM to calculate the temperature distribution in the tool and in the work piece numerically. Two-color pyrometer with an optical fiber was used by them to measure the temperature on the rake face of a single crystal diamond tool in precision turning and then they calculated numerically using FEM. They showed that, regardless of the size of the object, the two-color pyrometer is capable of measuring the temperature when the temperature of the object is constant.

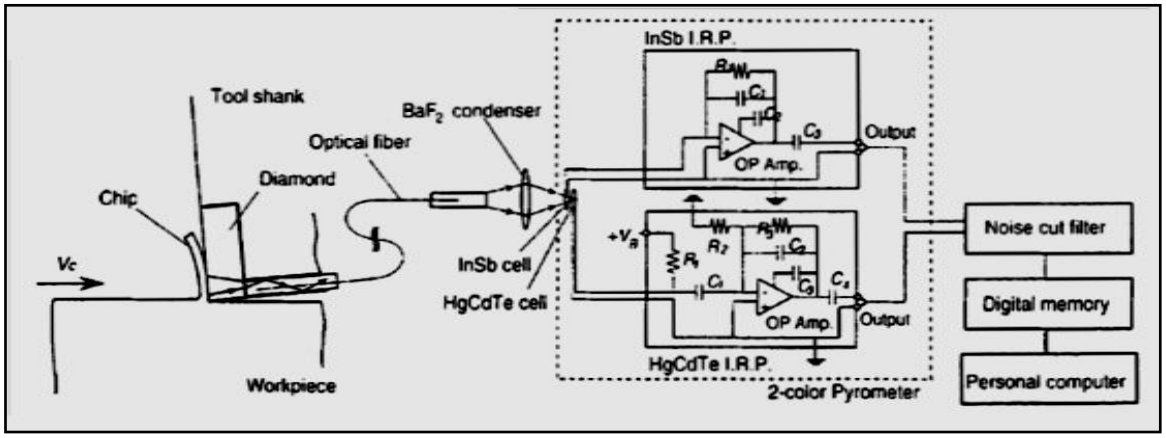

Figure 4: Experimental setup used by **Ueda Takashi et al.** [9]

They experimentally concluded that, it is possible to estimate the maximum temperature from the measured temperature, when the object has a surface of known temperature distribution. They also concluded that, when the object has a surface of known temperature distribution, it is possible to estimate the maximum temperature from the measured temperature and the increase in cutting speed increases the temperature on the rake face. Their measured values of temperatures in the experiment agreed well with their calculated results numerically using FEM.

Tanikic et al. [10] studied the metal cutting process parameters modeling using artificial neural network (ANN) and hybrid, adaptive neuro fuzzy systems. The main aim of their experiment was to conduct the qualitative analysis of metal cutting processes, and also identifying and resolving the frequently occurring problems, while improving the productivity of metal cutting by reducing the manufacturing costs. The infrared camera was used to measure and monitor the temperature at the chip tool interface. They also, modeled the

measured data by using ANN and neuro fuzzy system. Their work concluded that, the implementation of artificial intelligence based systems in metal cutting process is possible. In the end, they proposed the global system for predicting the state of cutting tool along with sub-systems for cutting temperature, cutting force and arithmetic mean deviation prediction.

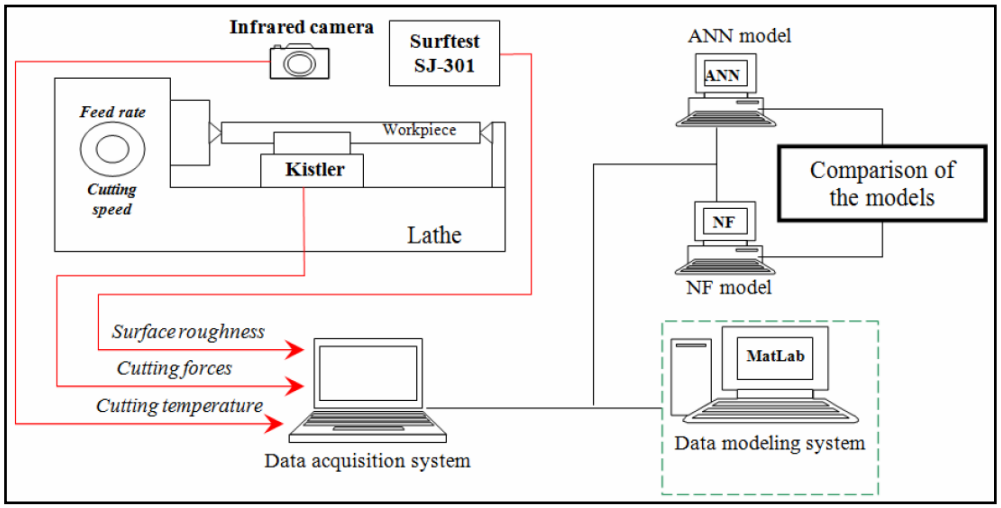

Figure 5: Component relations and information flow of material handling system

Fata [11] proposed the method of embedded thermocouple for temperature measurement along with infrared pyrometer. The experiments are conducted for dry and orthogonal machining condition with simultaneous measurement of temperature by embedded thermocouple and infrared pyrometer. With the help of these experiments a relation was established between tool temperature and cutting parameters such as cutting speed, feed rate and depth of cut. The results so obtained showed that if cutting speed, feed rate and depth of cut are increased then the tool temperature also increases which reduces the life of the cutting tool. These investigations revealed that the most effective cutting parameter in tool temperature rise is the cutting speed, especially at high range of cutting conditions. It also showed an increase in feed rate and depth of cut will lead to an almost straight line with low slope on the graph of tool temperature when plotted against them.

Adnan Jameel et al. [12] focused their study on the temperature generated at two heat zones namely primary heat zone (shear zone) and secondary heat zone (tool chip interface zone). They proposed two new objective functions for optimizing the cutting temperature problems and this system used particle swarm optimization (PSO) methodology to determine the optimal temperature. Their experiments showed that major amount of energy is converted into heat in the shear zone while the heat generated at the tool chip interface zone is due to the rubbing action at that interface. They concluded that heat distribution pattern is dependent on the size and thermal conductivity of the tool-work material and the cutting conditions. Specifically the results were obtained for mild steel work and carbide insert cutting tool in dry turning operation. Their study concluded that main cutting force, feed rate and depth of cut greatly influence the shear zone temperature while chip thickness and friction force have low effect. They also concluded that, the chip tool interface temperature increased with increase in feed rate and main cutting force while it decreased with increase in the depth of cut. Their whole study of paper concluded that feed rate has a huge effect on shear zone and chip tool interface zone temperature as compared to other parameters. Their study also concluded that till date the nearly all of optimization algorithms concentrated to optimize parameters are other than cutting temperature and according to their studies there are few papers focusing on the cutting temperature optimization.

Shirpurkar P.P. et al. [13] attempted to review the literature on optimization of machining parameters in turning processes by using different tool inserts. During their review of different conventional techniques employed for optimization of parameters were also studied by them. These techniques include geometric programming, geometric plus linear programming, non-linear programming, goal programming, sequential unconstrained minimization technique and dynamic programming. Later the latest optimization techniques were also discussed by them, specifically Taguchi technique, genetic algorithm, fuzzy logic and ant colony technique. These techniques were successfully applied in the industrial applications for optimal selection of process control variables. The paper concluded that Taguchi approach has the potential for savings in experimental time and cost on product or process, development and quality improvement and therefore is widely used in industries. According to their review, in most of the industries the skill, experience and mentality of the operators are the primary factors affecting the turning process parameters and surface roughness on the job/work piece. Therefore to attain minimum surface roughness it was very necessary to optimize the turning process parameters. Their

review concluded that the latest optimization techniques like Taguchi technique, genetic algorithm, Fuzzy logic and response surface methodology are being applied successfully in industrial applications for optimal selection of process variables in the area of machining.

Yen et al. [14] stated that the tool wear on the tool–workpiece and tool–chip interfaces in metal cutting (i.e. crater wear and flank wear) are strongly influenced by the relative sliding velocity and cutting temperature at the interface. Their study's overall objective was to develop a methodology to tool life in orthogonal cutting and predict the tool wear evolution using FEM simulations. To approach their goal, the methodology proposed by them had three different parts. In the first part, a tool wear model for the specified tool–workpiece pair was developed by them via a calibration set of tool wear cutting tests in conjunction with cutting simulations. In the second part, they modified the commercial FEM code, which was used to allow tool wear calculation and tool geometry updating. The last part was experimental validation of the developed methodology.

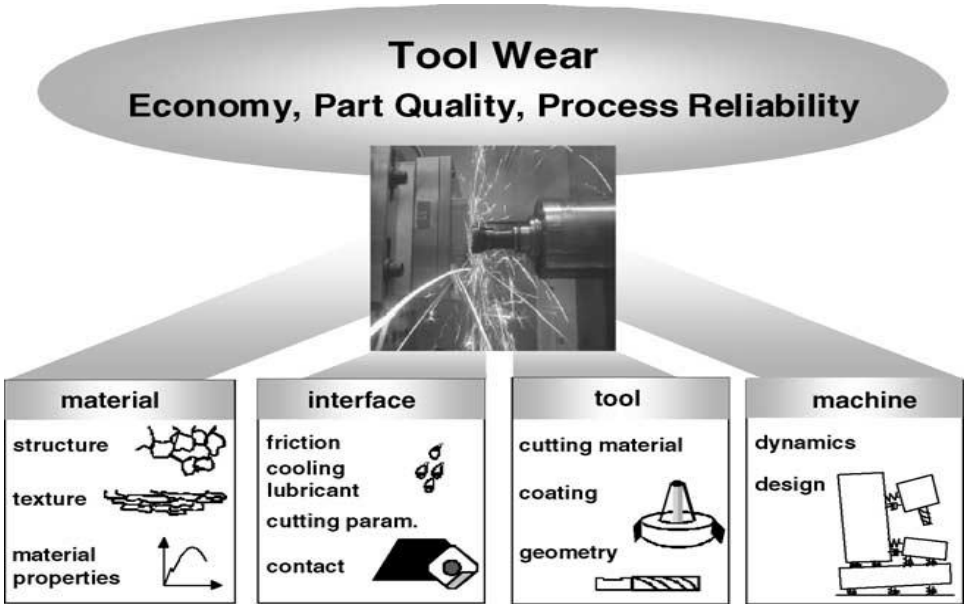

Figure 6: Four major functional elements influencing tool wear in machining processes. [14]

The maximum wear rate was clearly located on the tool rake face as shown in Figure 7. Nevertheless, they predicted small wear rates on the flank side of the tool edge radius, which were about one order of magnitude smaller than the rake face wear rates. They showed that the experimental results for uncoated carbide tools depicted that crater wear and flank wear on the tool face occur simultaneously at a similar wear rate [15].

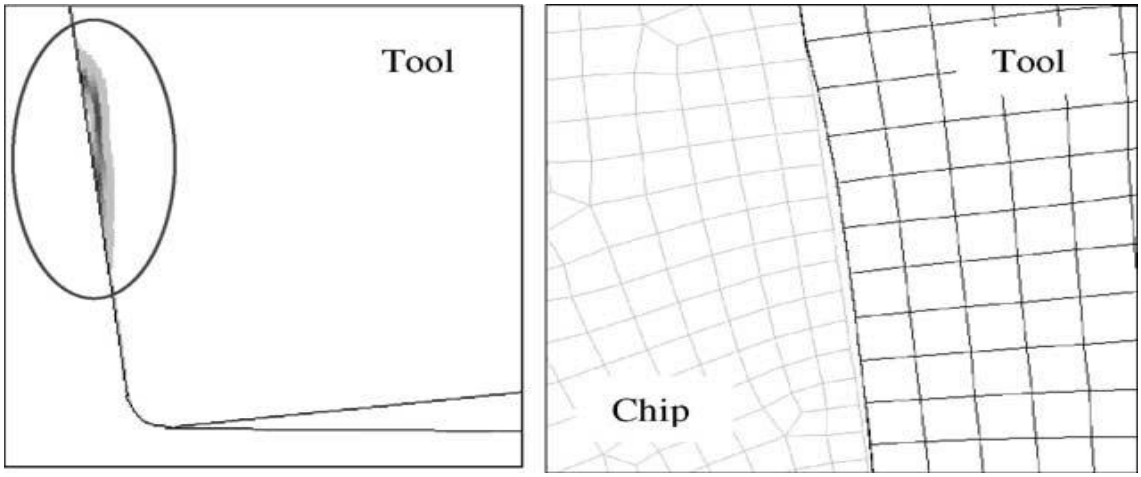

Figure 7: Result of wear rate (left) and updated rake face geometry (right) for an uncoated sharp tool. [14]

The initial results of tool wear simulations obtained by them using the developed method tend to underestimate the wear rates associated with the flank wear and crater wear, when the tool life was compared with the measured data obtained at the same conditions. They concluded that the reason to underestimate the

wear rates associated with the flank wear and crater wear may be partially due to the fact that the two wear constants in Usui's wear model were directly borrowed from the literature [16].

Thamizhmanii et al. [18] applied Taguchi method under optimum cutting condition for finding out the optimal value of surface roughness in turning SCM 440 alloy steel. They detected that the tool chattering and machine tool vibrations were the causes of poor surface finish whose effects were ignored by them for analysis. The authors concluded that that depth of cut of 1 to 1.5 mm can be used to get lowest surface roughness, and the only significant factor was depth of cut which, contributed to the surface roughness.

Kilickap [19] investigated the use of the Taguchi method and the Response Surface Methodologies (RSM) for minimizing the burr height and the surface roughness in drilling Al-7075. The optimization results showed that to minimize burr height, the combination of low cutting speed, low feed rate and high point angle were necessary. At the combination of lower cutting speed and feed rates and at higher point angles the lowest values of surface roughness were obtained. In his paper he presented an application of response surface methodology (RSM) and Taguchi method for selecting the optimum combination values of drilling parameters affecting the burr height and surface roughness in dry drilling of Al-7075. He also concluded that to perform trend analysis of the surface roughness and the burr height with respect to various combinations of drilling parameters Taguchi method is the most successful technique. The analysis of experiments perfumed by him has shown that Taguchi method can be successfully used to verify all the optimum cutting parameters.

III. SUMMARY

Experiments revealed that, the tool wear can be reduced by increasing the tool lifetime and by making more continuous production flow. The total work done by a cutting tool in removing metal was determined from the force components on the cutting tool. If cutting speed, feed rate and depth of cut are increased then the tool temperature also increases which reduces the life of the cutting tool. The chip tool interface temperature increased with increase in feed rate and main cutting force while it decreased with increase in the depth of cut. This review concluded that the decreased cutting tool forces and machined surface temperatures was resulted by increased cutting speed (V_C). It also revealed that, increased cutting tool forces and machined surface temperature was resulted by tool wear and the temperature in the chip increases with increasing of the cutting speed. Experiments also showed that, the temperature appeared to stabilize for the cutting speeds larger than 40 m/s and the temperature in the chip was nearing a saturated value during the process of an un-deformed chip thickness larger than 0.5 mm. It is now clear from the above that the outer surface of the material will be subject to higher heat removal and sudden temperature drop. The cutting forces were decreased, for the increased positive rake angle. The implementation of artificial intelligence based systems in metal cutting process is possible. The latest optimization techniques like Taguchi technique, genetic algorithm, Fuzzy logic and response surface methodology are being applied successfully in industrial applications for optimal selection of process variables in the area of machining. The maximum wear rate is located on the tool rake face. The crater wear and flank wear on the tool face occur simultaneously at a similar wear rate.

IV. FUTURE SCOPE

The future work may require validation of the proposed methodology [14] for selected cutting conditions, different from those in the calibration set by predicting tool wear curves, and comparing the results with the experiments. It may also require use of other wear rate models available in the literature (e.g. Takeyama and Murata's wear model [17]). From the above review one can optimize the turning process parameters like depth of cut, speed, feed, nose radius, material and type of tool, and even work piece material etc using Taguchi method for maximizing the tool life and minimizing the surface roughness by experimental setup. Taguchi technique will help to finalize the number of levels with orthogonal array and thus finalizing the number of experiments. Also the signal to noise ratio will help to observe the behavior of quality characteristics of work piece.

REFERENCES

[1] Jensen M.R., Damborg F.F., Nielsen K.B., Danckert J., "Optimization of the draw-die design in conventional deep-drawing in order to minimise tool wear", Journal of Materials Processing Technology 83 (1998) 106–114.

[2] Sullivan D. O' and Cotterell M., "Temperature measurement in single point turning". Cork Institute Technology. Vol. 118, 2001, pp. 301-308.

[3] Abukhshim N.A., Mativenga P.T., Sheikh M.A.,"Heat generation and temperature prediction in metal cutting: A review and implications for high speed machining", International Journal of Machine Tools & Manufacture xx (2005) 1–19.

[4] Byrne G., Thermoelectric signal characteristics and average interfacial temperature in the machining of metals under geometrically defined conditions, Int. J. Mach. Tools Manuf. 27 (2) (1987) 215-224.

[5] Lazoglu Ismail, Altintas Yusuf, "Prediction of tool and chip temperature in continuous and interrupted machining", International Journal of Machine Tools & Manufacture 42 (2002) 1011–1022.

[6] Sutter G., Faure L., Molinari A., Ranc N., Pina V., "An experimental technique for the measurement of temperature fields for the orthogonal cutting in high speed machining", International Journal of Machine Tools & Manufacture 43 (2003) 671–678.
[7] Dogu Yahya,Aslan Ersan, Camuscu Necip,"A numerical model to determine temperature distribution in orthogonal metal cutting", Journal of Materials Processing Technology 171 (2006) 1–9.
[8] Saglam Haci, Yaldiz Suleyman, Unsacar Faruk,"The effect of tool geometry and cutting speed on main cutting force and tool tip temperature", Materials and Design 28 (2007) 101–111.
[9] Ueda Takashi, Satoz Masahiko, Nakayama Kazuo,"TheTemperature of a Single Crystal Diamond Tool in Turning" Annals of the ClRP Vol. 47, issue 1, (1998) 41-44.
[10] Tanikic Dejan, Manic Miodrag, Radenkovic Goran, Mancic Dragan, "Metal cutting process parameters modeling: an artificial intelligence approach", Journal of Scientific & Industrial Research, Vol. 68, June 2009, pp. 530 – 539.
[11] Fata Ali,"Temperature Measurement During Machining Depending on Cutting Conditions", G. J. P&A Sc and Tech., 2011v01i2 (16-21) ISSN: 2249-7188.
[12] Jameel Adnan, Minhat Mohamad and Nizam Mohamad, "Optimal Parameters Selection to Reduce Cutting Temperature of Mild Steel Using Particle Swarm Optimization Intelligent Technique" Journal of Theoretical and Applied Information Technology, 31st July 2013. Vol. 53 No.3.
[13] Shirpurkar P.P., Bobde S.R., Patil V.V., Kale B.N., "Optimization of Turning Process Parameters by Using Tool Inserts- A Review", International Journal of Engineering and Innovative Technology (IJEIT) Volume 2, Issue 6, December 2012.
[14] Yen Yung-Chang, Söhner Jörg, Lilly Blaine, Altan Taylan, "Estimation of tool wear inorthogonal cutting using the finite element analysis", Journal of Materials Processing Technology 146 (2004) 82–91.
[15] Ivester R.W., Kennedy M., Davies M., Stevenson R., Assessment of Machining Models, Progress Report, Official contribution of NIST on the website http://www.nist.gov/amm/, 2001.
[16] Kitagawa T., Maekawa K., Shirakashi T., Usui E., Analytical prediction of flank wear of carbide tools in turning plain carbon steels. Part 2. Prediction of flank wear, Bull. Jpn. Soc. Precis. Eng. 23 (2) (1989) 126–134.
[17] Takeyama H., Murata T., Basic investigations on tool wear, Trans. ASME J. Eng. Ind. 85 (1963) 33–38.
[18] Thamizhmanii S., Saparudin S., Hasan S., "Analysis of surface roughness by using Taguchi method", Ach. Mater. Manuf. Eng. 20 (1–20) (2007) 503–505.
[19] Kilickap E., "Modeling and optimization of burr height in drilling of Al-7075 using Taguchi method and response surface methodology", Int. J. Adv Manuf. Technol. 49 (9–12) (2010) 911–923.

OPEN ACCESS

International
Journal
Of Modern Engineering Research (IJMER)

Tracking of Maximum Power from Wind Using Fuzzy Logic Controller Based On PMSG

Bipin Biharee Srivastava[1], Er. Sudhanshu Tripathi[2]
[1]*PG student, electrical Department SHIATS-DU,Allahabad-211007*
[2]*faculty, Electrical, Department SHIATS-DU Allahabad-211007*

Abstract: *Wind energy has gained a growing worldwide interest due to the nonstop rise in fuel cost. The main aim of the wind-energy system is to extract the maximum power present in the wind stream. In order to extract the highest power, the maximum power point tracking (MPPT) algorithm is used. This paper proposes the fuzzy logic MPPT controller to track the maximum power from the wind generation system. The maximum power is achieved based on the rotor speed of the wind system which consists of wind turbine and PMSG. The error and change in error is given as input to the fuzzy logic and its output is connected to the boost converter. The voltage from the dc link is controlled by the Voltage Source Inverter (VSI), and it is placed in grid side converter control. The proposed system is designed and evaluated in MATLAB/SIMULINK. Simulation results show the good dynamic performance of the proposed system.*

Index Terms*: Wind turbine, Permanent Magnet Synchronous Generator (PMSG), Maximum power point tracking (MPPT) and Fuzzy control.*

I. Introduction

Wind power is used to produce electricity or mechanical power and supplies it to homes, business, schools, etc. Wind turbine converts kinetic energy into mechanical energy and then the generator in the wind turbine converts this mechanical energy into electrical power. Wind turbine consists of rotor, generator, tower that supports rotor, gear box, electrical cables, etc. It is classified into two major types; Horizontal Axis wind turbine and Vertical Axis wind turbine. A Permanent Magnet Synchronous Generator (PMSG) is a generator contains the permanent magnet in the excitation field instead of coil. It is used to convert the mechanical power into electrical power and supply it to the grid. It consists of stator and rotor where stator is the armature and rotor contains the magnet.

Maximum Power Point Tracking (MPPT) is a technique which is used to track the maximum power from various devices especially photovoltaic systems. The capacity and higher value of current and voltage in the solar panel can make higher power. MPPT contains different algorithms such as Perturb and Observe, Incremental Conductance and Current Sweep Method. In wind turbine, the rotor speed continuously changes with changing the wind speed to get Maximum power. Therefore, the Maximum Power Point Tracking controller is presented in the wind energy conversion system to extract the maximum possible wind power [1-5].

MPPT is achieved by controlling the duty cycle of the dc-dc boost converter. When the boost converter is controlled, the rotor speed is also controlled to get the maximum power. Maximum power can also be tracked by maintaining the tip speed ratio (TSR) as optimal value [6]. Most of the authors [7-9] have proposed a various types of Fuzzy logic MPPT Controller for tracking maximum power from the wind turbine system. Two fuzzy logic controllers were used in the control scheme of wind energy conversion system [10]. In these papers, there is an impact of difference and uncertainty in the wind speed and the performance of the wind energy system is poor. In this paper, tracking of Maximum Power from the wind generation system by using the fuzzy logic MPPT controller is presented. An uncontrolled rectifier is employed to convert the ac power into dc power. The error between the actual rotor speed and the estimated speed is an input to the fuzzy logic controller. The change in error is another input to the fuzzy logic controller. The output of the fuzzy controller is given to the duty cycle of the boost converter. The maximum power is achieved by adjusting the duty cycle of the DC-DC boost converter. By adjusting the duty cycle, the rotor speed is controlled to get the maximum power from the wind. The boost converter increases the voltage and supply to the Voltage Source Inverter (VSI) which acts as an interface between the DC-DC boost converter and the grid.

The concept of this paper is organized as follows: In Section 2, the Literature review related to the proposed work is discussed. Section 3 provides the detailed explanation of the proposed work. In Section 4, the

various results for the proposed work obtained in the simulation are evaluated. Conclusions are summed up in Section 5.

II. Literature Review

T. Shanthi and A.S. Vanmukhil [8] have proposed the fuzzy logic controller to extract maximum power from the hybrid renewable energy system model. The proposed system includes both the photovoltaic (PV) and wind energy conversion system (WECS). Fuzzy logic controller was used to adjust the duty cycle of the switch converter to extract the maximum power from the PV array. The Voltage Source Inverter (VSI) was employed to control the voltage from the dc link and the output voltage of VSI was regulated by PI controller.

Huynh Quang Minh et.al [10] has proposed the control scheme of a wind energy conversion system using fuzzy logic. They have proposed two fuzzy controllers in the wind energy conversion system. The first fuzzy controller was used to track the maximum power from the wind turbine. The output of the fuzzy controller was given to the dc-dc converter to adjust the duty cycle. When adjusting the duty cycle, the rotor speed of PMSG was controlled to get the maximum power. The second one was used to maintain both the production and the storage of energy in respecting load demand for better performance of the system.

Wei Qiao et.al [11] have proposed the sensor less maximum wind power tracking controller based on the wind speed estimation. A Control algorithm was presented to control the wind turbine equipped with doubly fed induction generator (DFIG). The wind speed was estimated from the measured generator output power and the dynamics of the wind generator based on nonlinear mapping which was provided by a Gaussian radial basis function network (GRBFN). The estimated wind speed was used to find the optimal DFIG rotor speed for extraction of maximum wind power. The speed controller of DFIG was designed to damp low-frequency torsion oscillations.

M. Sarvi, Sh. and Abdi, S. Ahmadi [12] have proposed the maximum power point tracking control scheme based on particle swarm optimization _ fuzzy logic for wind turbine PMSG system. The maximum wind power was captured by adjusting the rotor speed of the PMSG. The rotor speed varies according to the wind speed and the wind turbine generator was operated by adjusting the duty cycle of the boost converter and increases the efficiency of wind energy conversion system.

Jogendra Singh Thongam and Mohand Ouhrouche [13] have proposed MPPT controllers to extract maximum power from the wind using various types of generators such as Permanent Magnet Synchronous Generator (PMSG), Squirrel Cage Induction Generator (SCIG) and Doubly Fed Induction Generator (DFIG). They have used three main control methods to track the maximum power namely tip speed ratio (TSR) control, Power signal feedback (PSF) control and hill-climb search control (HCS).

E. Koutroulis and K. Kalaitzakis [14] have proposed the Maximum power tracking system for wind energy conversion applications. The output voltage and current of the wind generator was determined to monitor the output power of wind generator. Based on the result of comparison between successive wind power values, the dc-dc boost converter was adjusted directly.

Y. Izumi et.al [15] has proposed a control method for tracking maximum power in a wind energy conversion system using online parameter identification. The wind turbine was connected with PMSG and transmits the power into AC grid through the converter. The generator side converter controls the torque of PMSG and the grid side inverter controls the voltage in the dc link and the grid for steady operation. The online parameter identification was used to determine the optimum torque of the PMSG and it varies due to wind turbulence, parameter error and other unexpected conditions. The parameter identification was achieved by the use of weighted least square method and it was appropriate for practical systems.

III. Proposed Work

System Description

Figure 1 shows the block diagram for the proposed wind generation system with fuzzy logic controller. The wind generation unit consists of PMSG and it is connected to uncontrolled rectifier which is used to convert the ac output voltage from the wind generation unit into dc voltage. The dc-dc boost converter is used to catch the maximum power from the wind, where a fuzzy logic MPPT controller is employed. In fuzzy logic controller two inputs are given, one is the error between the actual rotor speed and the estimated speed, another one is the derivative of this error. The output of the fuzzy controller is connected to the boost converter. The Voltage Source Inverter (VSI) is placed at the grid side converter control to control the dc link voltage. The proposed system is designed and simulated in the MATLAB/SIMULINK.

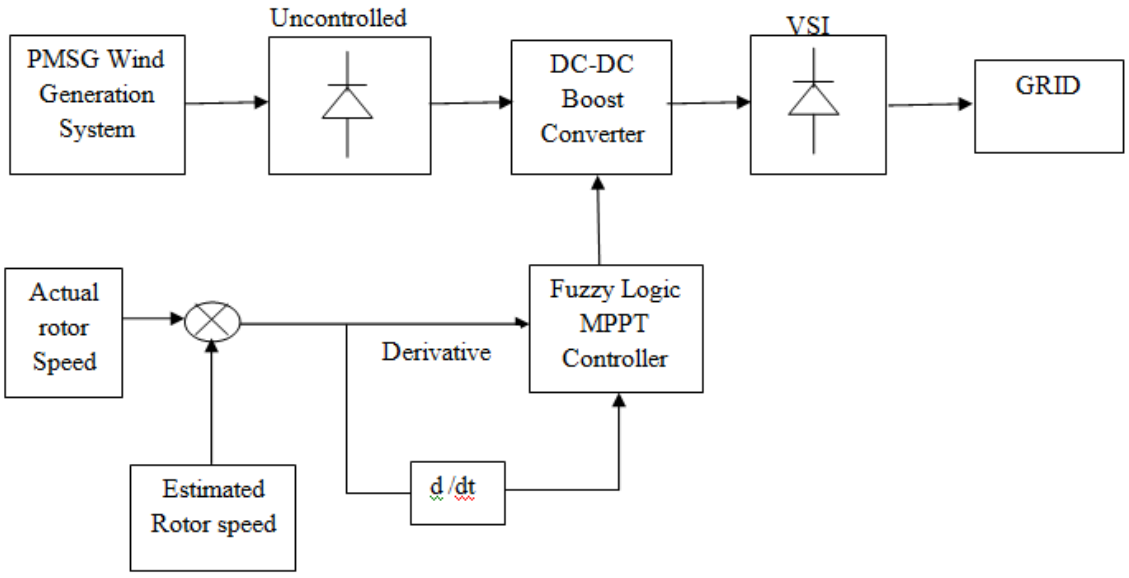

Figure 1: Block diagram of the proposed Wind generation system

Wind Energy Conversion System

The output mechanical power of the wind generation system is given by the following equation.

$$P_m = \frac{1}{2} C_p(\lambda, \beta) \rho A V_{wind}^3 \qquad (1)$$

where C_p is the power coefficient of the wind, ρ is the air density (kg/m^3), A is the swept area of the turbine (m^2), V_{wind} is the wind speed (m/s), λ is the tip speed ratio and β is the blade pitch angle (deg.).

Tip speed ratio (TSR) depends on the number of rotor blades of the wind turbine. If the number of rotor blade is less than the wind turbine rotates fast to get the maximum power from the wind. The equation of the TSR (λ) can be explained as follows,

$$\lambda = \frac{\omega_m R}{V_{wind}} \qquad (2)$$

Whereω_m, the rotor speed and R is the radius of the blade. The optimum value of TSR will be 8.1. The rotor speed can be estimated using the formula,

$$\omega_m = \frac{V_d + 2R_s I_d}{\frac{3\sqrt{3}}{\pi} K_m - \frac{P}{20} L_s I_d} \qquad (3)$$

Where V_d and I_d are the dc voltage and current respectively. The parameters of the wind generation system used in this paper are given in table 1.

Table 1: Parameters of the proposed system

Parameter Name	Value
Air density, ρ	1.225 kg/m^3
Rated Wind Speed	12 m/s
Pitch angle, β	0 deg.
Power coefficient, C_p	0.48
Stator Leakage Inductance, L_s	4.48 mH
Peak line-neutral back emf constant	1.4 V/rpm
Stator winding resistance, R_s	0.1764 ohm

Fuzzy logic MPPT controller

In this paper, the fuzzy logic controller is present to track the maximum power from the wind by using the rotor speed of the wind. Fuzzy logic is the best controller to track the maximum power point. The inputs of the fuzzy controller are the error between the actual rotor speed and the estimated rotor speed and change in this error. Output of the fuzzy controller is the duty cycle of the boost converter. By adjusting the duty cycle of the boost converter the maximum power will be achieved. The rotor speed is found out using the equation (3). At

first, the various terms are selected to form the fuzzy rules. Based on these terms, the different rules are formed. The linguistic terms used here are:

1. Error (Very Negative, Negative, Small Negative, Zero, Small Positive, Positive, Very Positive)
2. Derivative of error (Negative, Zero, Positive)

The seven various terms of error and three terms of change in error are shown in figure 2 (a) and (b) respectively. The output of fuzzy rule is shown in figure 3.

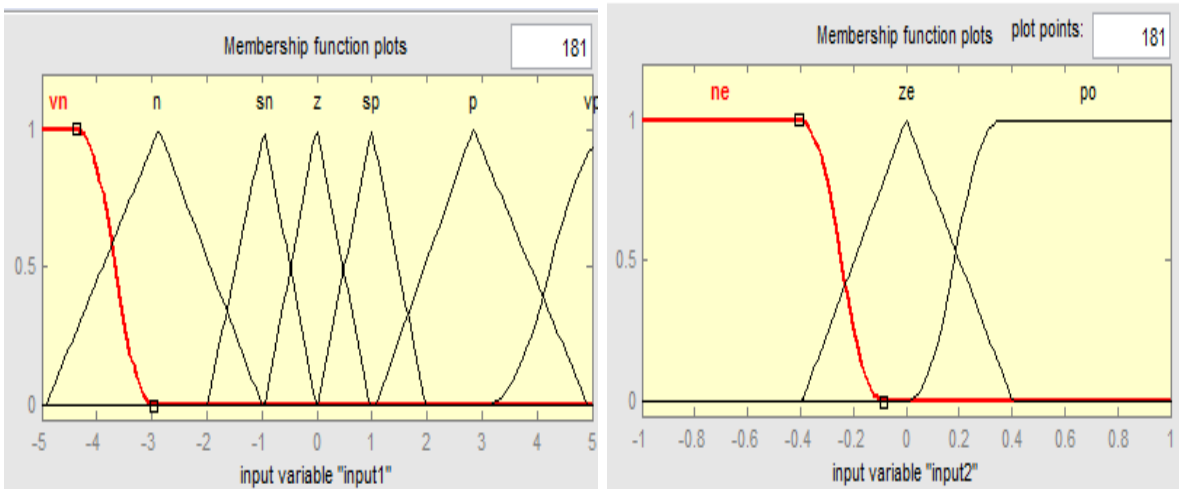

(a) (b)

Figure 2: (a) Variable terms of error, (b) Terms for change in error

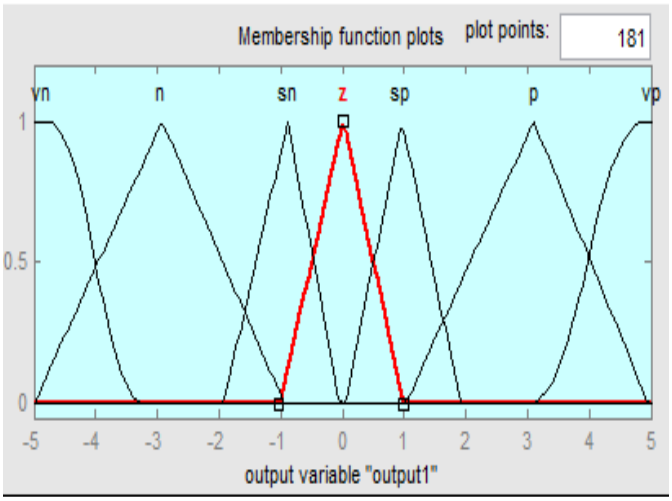

Figure 3: Output of fuzzy rules

Table 2: Various fuzzy rules for MPPT

D (%)		Derivative of error		
		Negative	**Zero**	**Positive**
Error	**VN**	VP	VP	VP
	N	SN	SN	VN
	SN	N	SN	VN
	Z	Z	Z	Z
	SP	SP	SP	P
	P	P	VP	VP
	VP	VP	VP	VP

In the proposed fuzzy controller, totally 21 rules are formed and it shown in table 2. For example, if the error is positive and change in error is negative then the duty cycle will be positive. The rules formed process is called as fuzzification. After the fuzzification process, the defuzzification is performed which converts the fuzzified value into defuzzified value. It gives the final output value. The defuzzification is shown in figure 4.

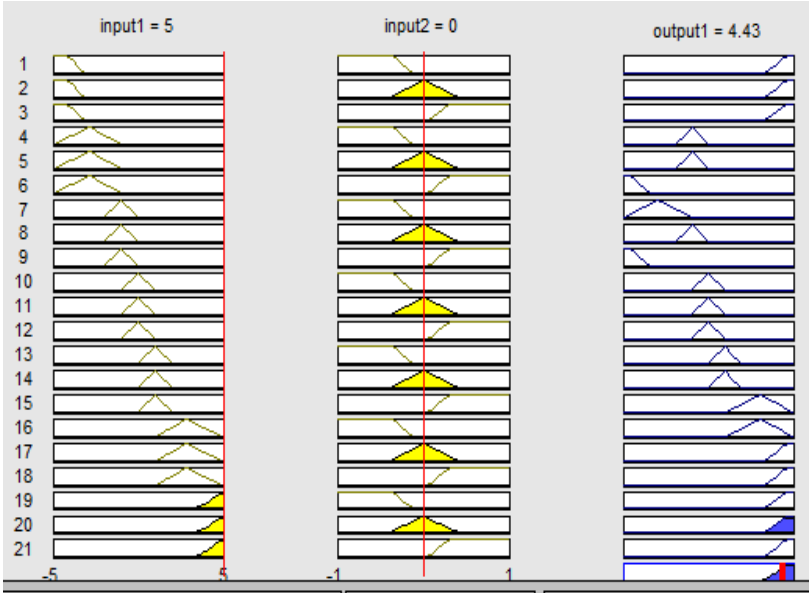

Figure 4: Defuzzification

IV. Simulation Results

The proposed work is implemented in MATLAB/SIMULINK and its simulation diagram is shown in figure 5. For tracking the maximum power from the wind, the fuzzy logic controller is presented. Fuzzy controller tracks the maximum power with respect to the speed of the wind generation system. The simulation diagram for the main wind generation system with PMSG is shown in figure 6. The diagram for the estimation of rotor speed is shown in figure 7.

The various results obtained from the simulation diagram are shown in figure 8. Figure 8(a) shows the output of wind speed, rotor speed, pitch angle and torque in the wind turbine model. The output from the PMSG is represented as generator terminal and generator terminal 2 and it is shown in figure 8(b) and 8(c) respectively. In figure 8(d), the overall output of the wind generation system is shown. Figure 8(e) shows the output voltage of uncontrolled rectifier and the voltage source inverter. The maximum power tracked from the wind using fuzzy controller is shown in figure 8(f). The maximum output power from the wind is 4.438 KW is evaluated using fuzzy logic controller.

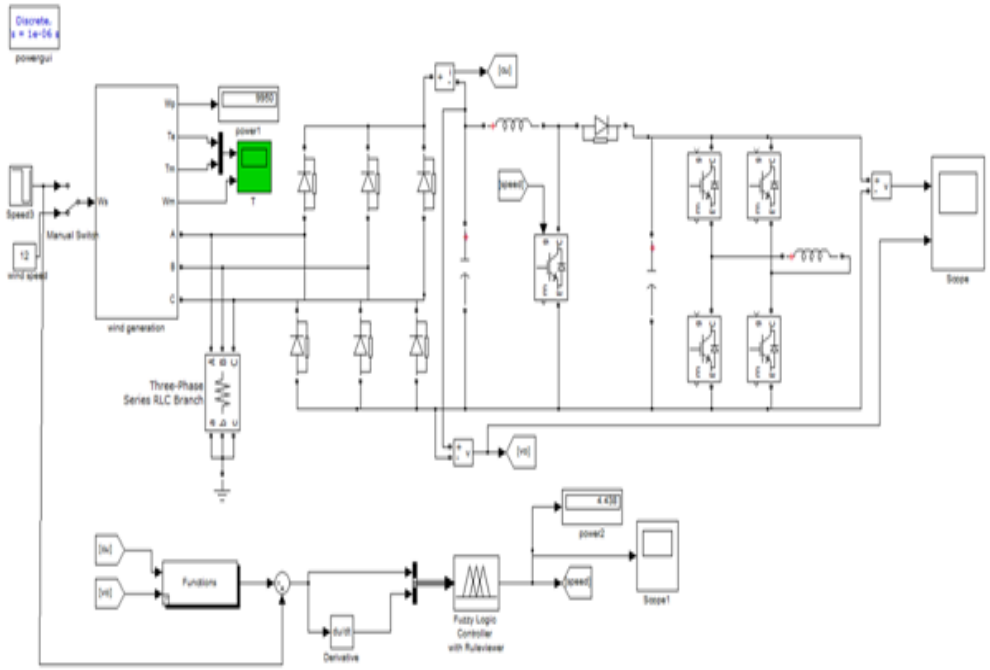

Figure 5: Simulation diagram for the proposed work

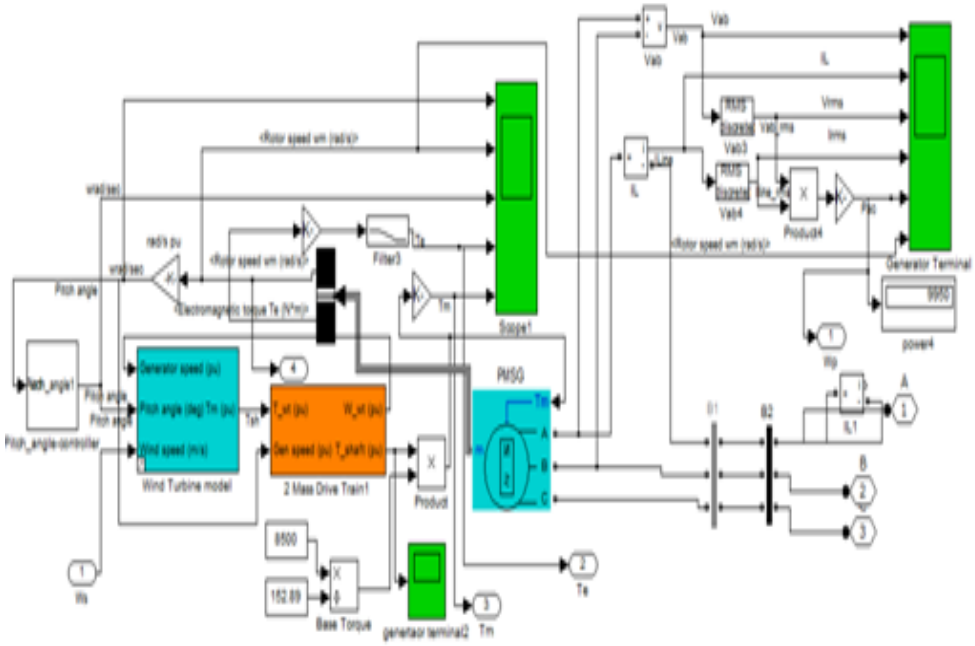

Figure 6: Simulation diagram for the wind generation system

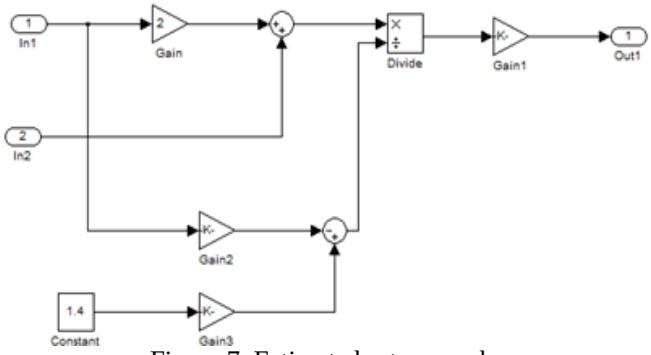

Figure 7: Estimated rotor speed

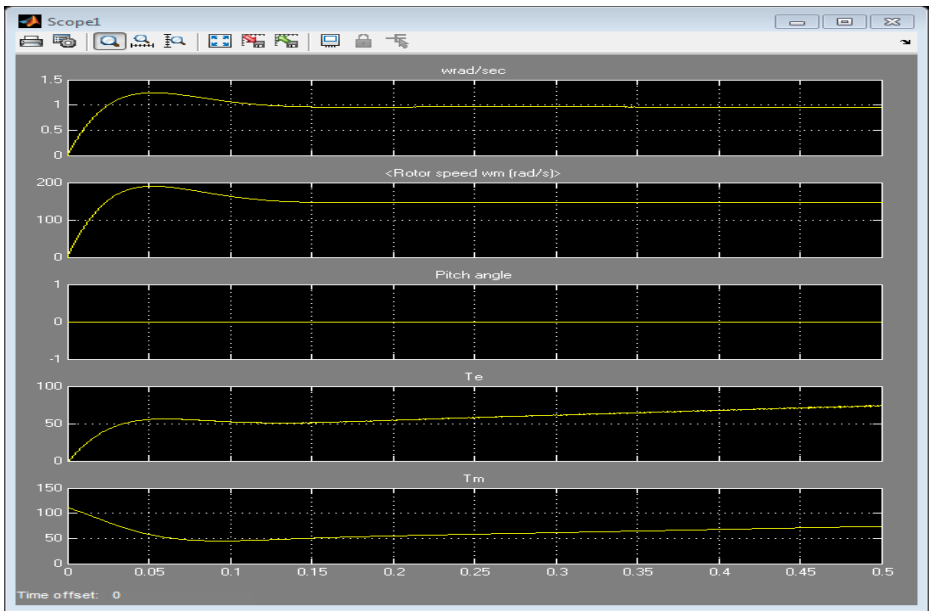

(a) Simulation results for wind speed, rotor speed, pitch angle and torque in wind turbine

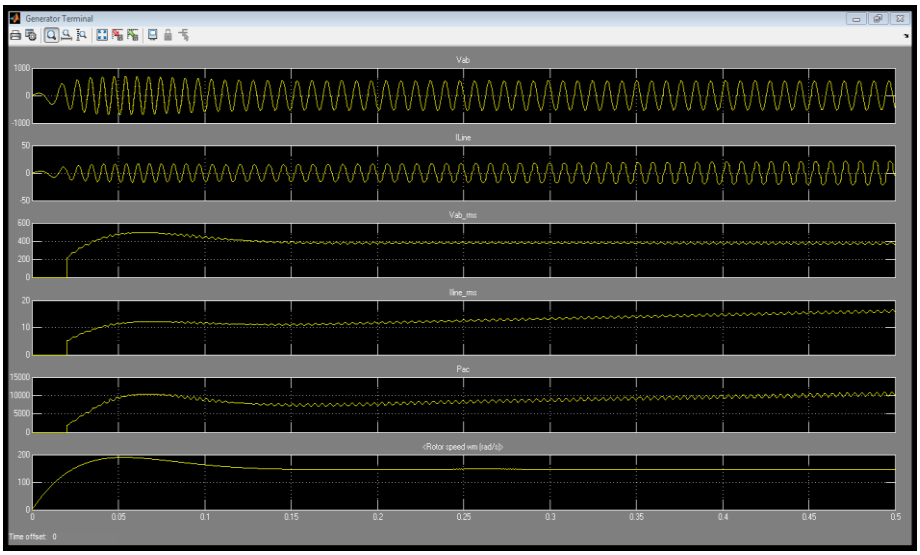

(b) Results for voltage, current, power and rotor speed in PMSG

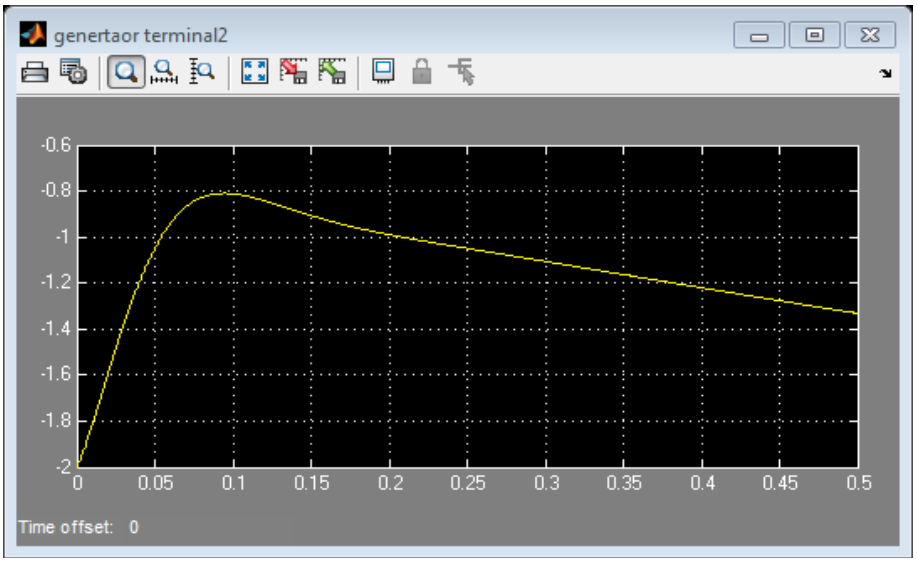

(c) Generator terminal 2

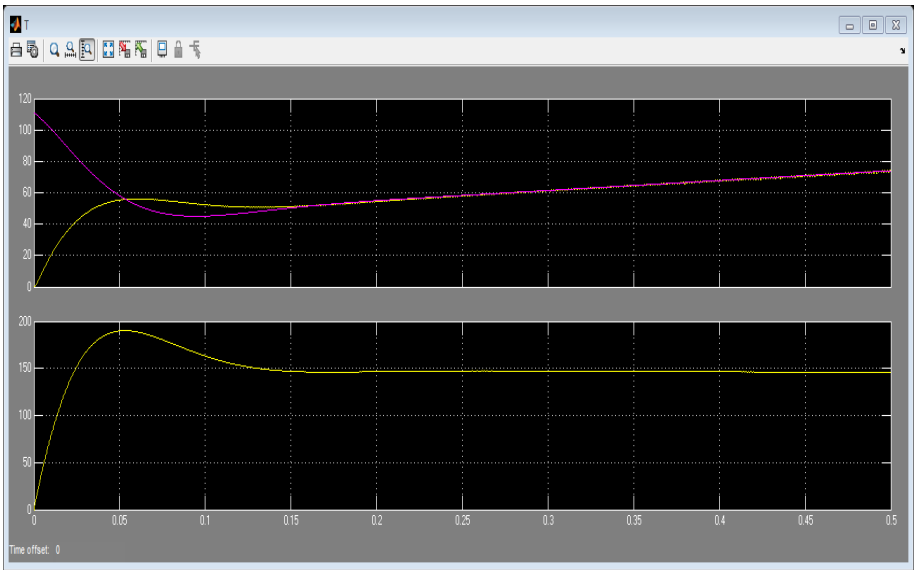

(d) Torque from wind generation system

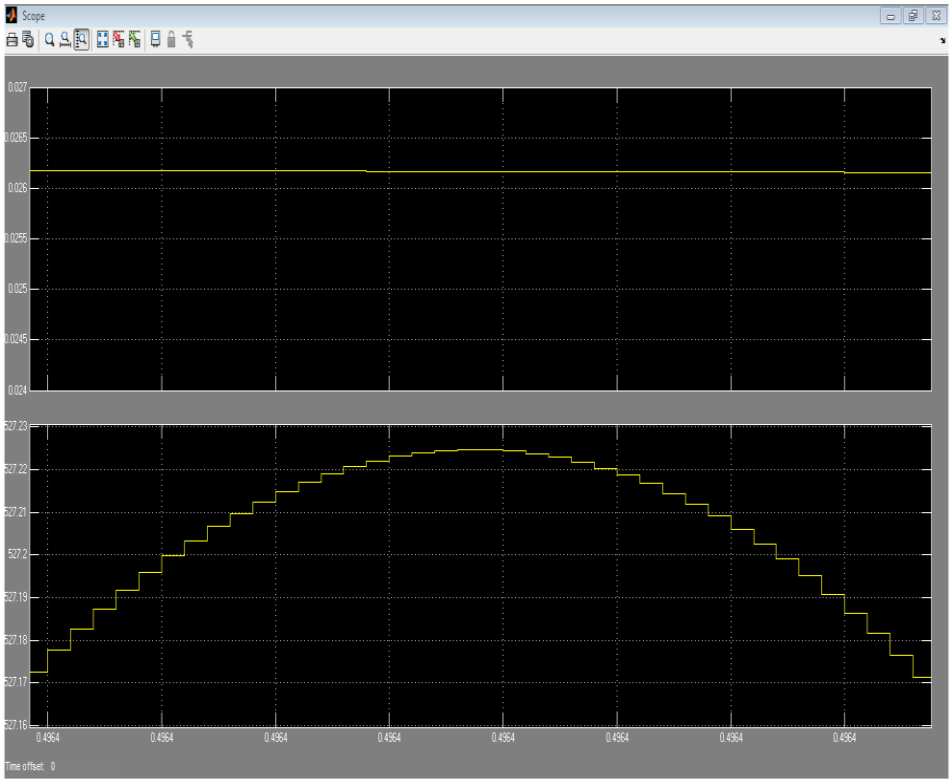

(e) Voltage from rectifier VSI

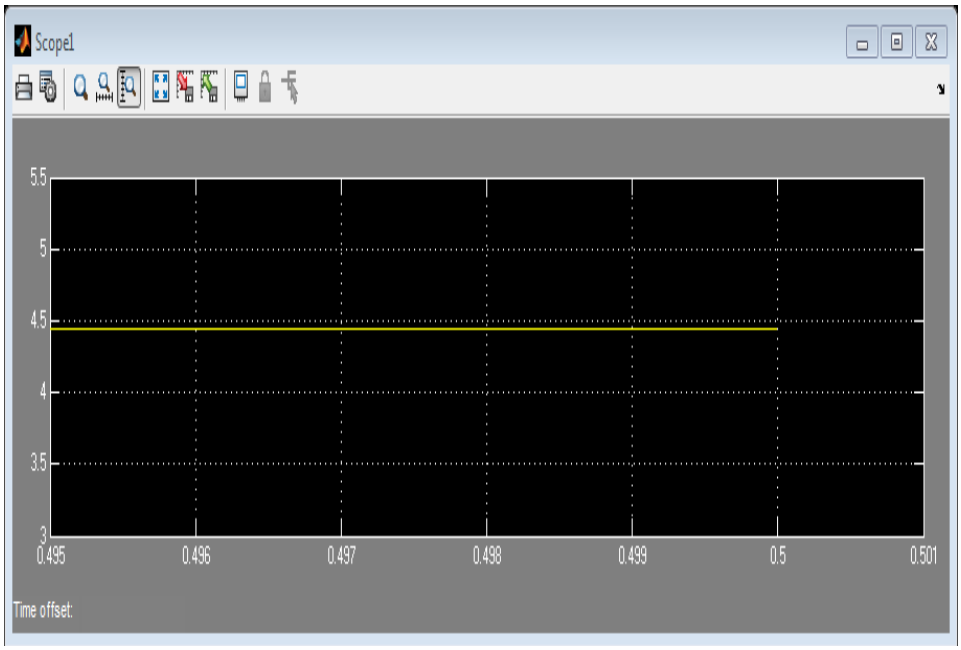

(f) Maximum output power from wind

Figure 8: The various simulation results for the proposed system

V. Conclusion

In this paper, maximum power point is tracked from the wind using fuzzy logic MPPT controller is presented. The maximum power is tracked based on the rotor speed of the wind generation system. The output of the fuzzy controller is connected to the boost converter to adjust the duty cycle. The maximum power is achieved by controlling the duty cycle of the boost converter. The system evaluations are performed in the MATLAB/SIMULINK. The simulation results represent that the proposed system shows the dynamic and steady state performances. Some advantages of using fuzzy controller are quick response, limit insensitivity and

universal control algorithm. The proposed wind generation system supplies maximum power to the grid with high efficiency and reliability.

REFERENCES

[1] M.E. Haque, Michael Negnevitsky and K. Muttaqi, "A novel control strategy for a variable speed wind turbine with permanent magnet synchronous generator", IEEE transactions on Industry Applications, vol. 46, Issue. 1, pp. 331-339, Jan-Feb 2010.

[2] Ahmed G. Abo-Khalil and Dong-Choon Lee, "MPPT control of Wind generation systems based on estimated wind speed using SVR", IEEE transactions on Industrial Electronics, vol. 55, no. 3, Mar. 2008.

[3] Agarwal .V, R.K. Aggarwal, P. Patidar, and C. Patki, "A Novel scheme for Rapid tracking of Maximum Power Point in Wind Energy Generation Systems", IEEE transactions on Energy Conversion, vol. 25, no. 1, pp. 228-236, Mar. 2010.

[4] N. Surekha, Dr. K. Ranjith Kumar, Dr. N. Deva Rajan, "Simulation of Soft Computing based maximum Power point tracking for PMSG Wind Generation System", International Journal of Advanced Technology and Engineering Research, pp. 107-115, 2014.

[5] Abdullah M.A., Yatim A.H.M., Tan C.W., Saidur R., "A Review of Maximum power point tracking algorithms for wind energy systems", Elsevier, Renewable and Sustainable Energy Reviews, vol. 16, no. 5, pp. 3220-3227, June 2012.

[6] M.M. Hussein, M. Orabi, M.E. Ahmed, M.A. Abd El-Wahab and M.M. Hamada, "Simple Direct Sensorless Control of Permanent Magnet Synchronous Generator Wind Turbine", Proceedings of the 14th International Middle Power Systems Conference (MEPCON '10), pp. 652-656, 2010.

[7] Chitesh Dubey, Yogesh Tiwari, Dr. Anup Mishra, "Maximum power point tracking of WECS using Fuzzy logic controller", International Journal of Emerging trends and technology in Computer Science, vol. 2, no. 2, Mar-April 2013.

[8] T. Shanthi and A.S. Vanmukhil, "Fuzzy logic based MPPT Control of Hybrid Power Generation System", International Journal of Computer Applications, vol. 86, no. 1, Jan. 2014.

[9] K. Sekhar, V. Durai Samy, "Fuzzy logic MPPT Controller with energy management system for solar wind battery diesel Hybrid power system", Journal of Theoretical and Applied Information Technology, vol. 59, no. 3, Jan. 2014.

[10] Huynh Quang Minh, Nollet Frederic, Essounbouli Najib, Hamzaoui Abdelaziz, "Control of Permanent Magnet Synchronous Generator wind turbine for stand-alone system using fuzzy logic", Advances in Intelligent Systems research, vol. 1, no. 1, pp. 720-727, July 2011.

[11] Wei Qiao, Wei Zhou, Jose M. Aller, and Ronald G. Harley, "Wind Speed estimation based sensor less output maximization control for a wind turbine driving a DFIG", IEEE transactions on Power Electronics, vol. 23, no. 3, pp. 1156-1169, May 2008.

[12] M. Sarvi, Sh. Abdi, S. Ahmadi, "A New method for Rapid Maximum power point tracking of PMSG Wind Generator using PSO _ Fuzzy Logic", Technical Journal of Engineering and Applied Sciences, vol. 3, no. 17, 2013.

[13] Jogendra Singh Thongam and Mohand Ouhrouche, "MPPT control methods in wind energy conversion systems", Fundamental and advanced Topics in Wind Power, pp. 339-361July 2011.

[14] E. Koutroulis and K. Kalaitzakis, "Design of Maximum power tracking system for wind-energy conversion applications", IEEE transactions on Industrial Electronics, vol. 53, no. 2, pp. 486-494, April 2006.

[15] Y. Izumi, A. Pratap, K. Uchida and K. Uehara, T. Senjyu, T. Yona and T. Funabashi, "A Control Method for Maximum power point tracking of a PMSG based WECS using Online parameter Identification of wind turbine", IEEE Ninth International Conference on Power Electronics and Drive systems, pp. 1125-1130, Dec. 2011.

OPEN ACCESS

International
Journal
Of Modern Engineering Research (IJMER)

Estimize Bull speed using Back propagation

A. NagaBhushana Rao[$1], K. Eswara Rao[$2]
[$1,$2]*Assistant Professor AITAM, Tekkali, Srikakulam, Andhra Pradesh.*

Abstract: *Now knowledge pre-processing, model and reasoning issues, power metrics, quality issues, post-processing of discovered structures, visualization, and on-line change is best challenge. In this paper Neural Network based forecasting of stock prices of selected sectors under Bombay Stock Exchange show that neural networks have the power to predict prices albeit the volatility in the markets[9]. The motivation for the development of neural network technology stemmed from the desire to develop an artificial system that could perform "intelligent" tasks similar to those performed by the human brain. Artificial Neural Networks are being counted as the wave of the future in computing. They are indeed self-learning mechanisms which don't require the traditional skills of a programmer. Back propagation is one of the approaches to implement concept of neural networks. Back propagation is a form of supervised learning for multi-layer nets. Error data at the output layer is back propagated to earlier ones, allowing incoming weights to these layers to be updated. It is most often used as training algorithm in current neural network applications. In this paper, we apply data mining technology to stock market in order to research the trend of price; it aims to predict the future trend of the stock market and the fluctuation of price. This paper points out the shortage that exists in current traditional statistical analysis in the stock, then makes use of BP neural network algorithm to predict the stock market by establishing a three-tier structure of the neural network, namely input layer, hidden layer and output layer. Finally, we get a better predictive model to improve forecast accuracy.*

Keywords: *Artificial Neural Network, Back propagation, Data mining*

I. Introduction

In recent years, monetary markets became additional reticular. The elemental factors have become additional essential for the analysis of monetary market. The analysis in recent past shows that the nonlinear domain with computing technologies may be sculptured additional exactly compared to single market and linear applied math strategies that are the mainstay for technical analysis for past decade.

Prediction of stock price level movement is thought to be a difficult task of monetary statistic prediction.

Associate degree correct prediction of stock worth movement might yield profits for investors. As a result of the quality of exchange information, development of Economical models for predicting is incredibly troublesome. Statistical strategies and neural networks are usually used for statistic prediction. Since stock markets are complicated, nonlinear, dynamic and chaotic.

Neural networks among varied computing tools are more and more accustomed the monetary prognostication as neural nets are found to be technologically versatile and powerful, ideally suited to perform monetary market research. Many studies have shown that artificial neural networks have the capability to be told the underlying mechanics of stock markets. In fact, artificial neural networks are wide used for prognostication monetary markets.

Artificial neural network is a mathematical model. It has capability to machine learning and pattern matching. Neuron is basic unit of nervous system such as brain. ANN is borrowed from central nervous system. It is inspired by biological technology. Biological neuron stores knowledge in memory bank, while in an artificial neuron the data or information is distributed through the network and stored in the form of weighted interconnection.

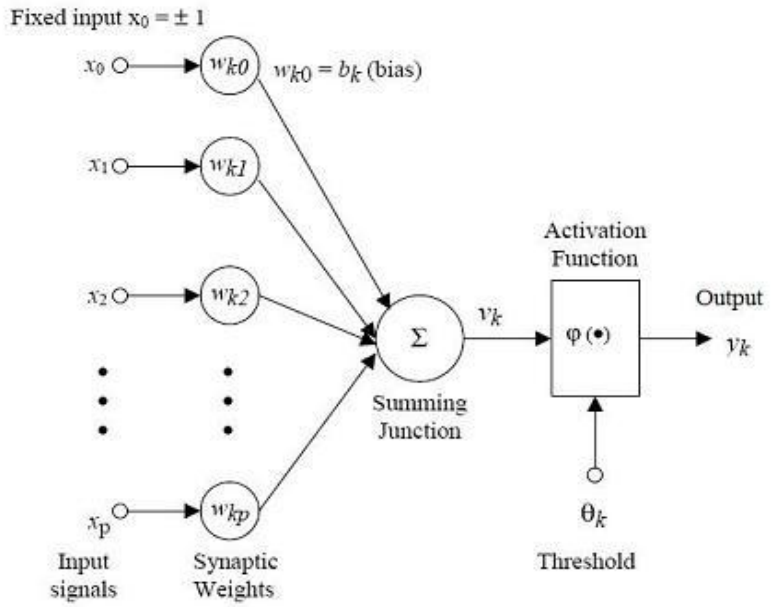

Figure 1: Graphical representation of artificial neurons

II. Literature Review

A share market could be a place of high interest to the investors because it presents them with a chance to learn financially by finance their resources on shares and derivatives of varied firms. it's a chaos system; that means the activity traits of share costs area unit unpredictable and unsure. to create some style of sense of this chaotic behavior, researchers were forced to search out a way which may estimate the result of this uncertainty to the flow of share costs. From the analyses of varied applied math models, Artificial Neural Networks area unit analogous to non-parametric, nonlinear, regression models.

So, Artificial Neural Networks (ANN) actually has the potential to tell apart unknown and hidden patterns in information which may be terribly effective for share market prediction. If successful, will this will this could this may} be useful for investors and finances which can completely contribute to the economy. There are unit totally different strategies that are applied so as to predict Share Market returns.

The securities market reflects the fluctuation of the economy, and receives 10 million investors' attention since its initial development. The securities market is characterized by bad, high-yield, thus investors are involved concerning the analysis of the securities market and making an attempt to forecast the trend of the securities market. However, securities market is wedged by the politics, economy and plenty of different factors, let alone the quality of its internal law, like value (stock index) changes within the non-linear, and shares knowledge with high noise characteristics, so the normal mathematical

Applied mathematics techniques to forecast the securities market has not yielded satisfactory results. Neural networks will approximate any advanced non-linear relations and has hardiness and fault-tolerant options. Therefore, it's terribly appropriate for the analysis of stock knowledge. In dozens of neural network models that were suggests, researchers usually use the hop garden network. hop garden network is that the commonest feedback network model, it's one among the models that almost typically studied currently. The hop garden network is that the mono layer recognized by an equivalent vegetative cell, and is additionally a symmetrically connected associative network while not learning operates.

III. Methods Used For Forecasting

Let us enumerate some available forecasting methods in predicting the stock prices.

A. Fundamental analysis

Fundamental analysis is a type of investment analysis adopted by investors for taking investment decisions an the investors who follow this approach are called 'fundamentalists'. They try to estimate the intrinsic worth of a company's share, by studying its sales, earnings, profits, dividends, management proficiency, and a host of other economic factors that have a bearing on the company's profitability and business prospects. The objective is to estimate what the price of a particular company's share out to be and consider this price to be its intrinsic or true value of the share as it reflects the inherent worth and value. With

the help of intrinsic price one can judge whether the shares are currently over-priced or under priced in the stock market. The fundamentalist makes his money by buying under priced shares and later selling them when they become over- priced. Fundamental analysis is more useful for long-term investors.

B. Technical analysis

The technical analysis is characterized by a large number of rules and indicators committed to identify and explain the regularity of historical price dynamics. Technical analysis uses patterns of the price history of a financial instrument in order to provide indications on the future behavior of prices [9]. Technical analysts argue that prices gradually adjust to new information. The Moving Average method (MA) is one of the most used methods of technical analysis. This method involves a comparison of the market prices or index with the long MA. The MA method is easy to use and apply in investment decision-making or empirical tests [10]. The research [11] showed that MA method can generate significant forecast value errors and deviations from real prices and is not successful in price movement trend generation.

Technical analysis is commonly used for taking 'buying' and 'selling' decisions in the stock market. This analysis attempts to predict the future price of a particular share on the basis of a study of its price movements in the past. Technical analysts are also called as 'chartists' as they use charts and graphs for keeping a record of share price movements. They believe that an elaborate study of share price charts and graphs will reveal regular and recurrent patterns of price behavior which are likely to be repeated in the future. Technical variables most frequently cited are shown [12]. They usually ignore all fundamental data like sales, earnings, profits, dividends, business prospects of the company, etc. and believe that these factors have already been taken into account by the market and are fully reflected in the current market price of a share. Technical analysis by the very nature of its approach is suitable for speculators and short-term traders in shares

IV. Proposed Solution

BP network is that the back-propagation network. It's a multi-layer forward network, learning by minimum mean sq. error. It may be employed in the sphere of language integration, identification and adaptation management, etc. BP network is semi supervised learning. Initial of all, artificial neural network has to learn an exact learning criteria, so it will work. Tips for e-learning (Electronic Learning) may be listed as below. If the result yielded by network is wrong, then the network ought to scale back the chance of creating identical mistake next time through learning. This project uses data processing technique to check historical information concerning share market in order that it will predict the desired values a lot of accurately.

Algorithm:-

1. Accept input sample
2. Perform its weighted summation.
3. Apply it to input layer neurons.
4. Process all inputs at each neuron by transfer function to get individual.
5. Hidden layer and repeat 1,2,3,4 steps pass it as an input to all neurons of for hidden layer neurons.
6. Pass output of hidden layer neurons to all output layers and repeat 1,2,3,4 steps to get final output.
7. Display the final output.

V. Mathematical Model

Error calculation

Calculating Root Mean Square, Let RMS is denoted as Root Mean Square, E is denoted as Error of difference between actual value and predicted value GE means Global Error.

Root mean square error (RMSE)

The Root Mean Square Error (**RMSE**) (also called the root mean square deviation, RMSD) is a frequently used measure of the difference between values predicted by a model and the values actually observed from the environment that is being modelled. These individual differences are also called residuals, and the RMSE serves to aggregate them into a single measure of predictive power. The RMSE of a model prediction with respect to the estimated variable X_{model} is defined as the square root of the mean squared error:

$$RMSE = \sqrt{\frac{\sum_{i=1}^{n} (X_{obsi} - X_{model,i})^2}{n}}$$

where X_{obs} is observed values and X_{model} is modelled values at time/place *i*.

The calculated RMSE values will have units, and RMSE for phosphorus concentrations can for this reason not be directly compared to RMSE values for chlorophyll *a* concentrations etc. However, the RMSE values can be used to distinguish model performance in a calibration period with that of a validation period as well as to compare the individual model performance to that of other predictive models.

Normalized root mean square error (NRMSE)

Non-dimensional forms of the RMSE are useful because often one wants to compare RMSE with different units. There are two approaches: normalize the RMSE to the range of the observed data, or normalize to the mean of the observed data.

1: $$NRMSE = \frac{RMSE}{X_{obs,\max} - X_{obs,\min}}$$

2: $$NRMSE = \frac{RMSE}{\overline{X_{obs}}}$$

(the latter one is also called C_V,RMSE for the resemblance with calculating the coefficient of variance).

Pearson correlation coefficient (r)

Correlation – often measured as a correlation coefficient – indicates the strength and direction of a linear relationship between two variables (for example model output and observed values). A number of different coefficients are used for different situations. The best known is the Pearson product-moment correlation coefficient (also called Pearson correlation coefficient or the sample correlation coefficient), which is obtained by dividing the covariance of the two variables by the product of their standard deviations. If we have a series n observations and n model values, then the Pearson product-moment correlation coefficient can be used to estimate the correlation between model and observations.

$$r = \frac{\sum_{i=1}^{n}(x_i - \overline{x}) \cdot (y_i - \overline{y})}{\sqrt{\sum_{i=1}^{n}(x_i - \overline{x})^2 \cdot \sum_{i=1}^{n}(y_i - \overline{y})^2}}$$ The correlation is +1 in the case of a perfect increasing linear relationship, and -1 in case of a decreasing linear relationship, and the values in between indicates the degree of linear relationship between for example model and observations. A correlation coefficient of 0 means the there is no linear relationship between the variables.

The square of the Pearson correlation coefficient ($\mathbf{r^2}$), known as the coefficient of determination, describes how much of the variance between the two variables is described by the linear fit.

Nash-Sutcliffe coefficient (E)

The Nash-Sutcliffe model efficiency coefficient (E) is commonly used to assess the predictive power of hydrological discharge models. However, it can also be used to quantitatively describe the accuracy of model outputs for other things than discharge (such as nutrient loadings, temperature, concentrations etc.). It is defined as:

$$E = 1 - \frac{\sum_{i=1}^{n}(X_{obs,i} - X_{model})^2}{\sum_{i=1}^{n}(X_{obs,i} - \overline{X_{obs}})^2}$$

where X_{obs} is observed values and X_{model} is modeled values at time/place *i*.

Nash-Sutcliffe efficiencies can range from -∞ to 1. An efficiency of 1 (E = 1) corresponds to a perfect match between model and observations. An efficiency of 0 indicates that the model predictions are as accurate as the mean of the observed data, whereas an efficiency less than zero (-∞ < E < 0) occurs when the observed mean is a better predictor than the model. Essentially, the closer the model efficiency is to 1, the more accurate the model is.

VI. Artificial Neural Networks

An important application of neural networks is pattern recognition. Pattern recognition can be implemented by using a feed-forward neural network that has been trained accordingly. During training, the network is trained to associate outputs with input patterns. When the network is used, it identifies the input pattern and tries to output the associated output pattern. The power of neural networks comes to life when a pattern that has no output associated with it, is given as an input. In this case, the network gives the output that corresponds to a taught input pattern that is least different from the given pattern.

The study of artificial neural networks has been inspired by the biological learning systems [13] which consist of very complex webs of interconnected neurons. ANNs are built out of densely interconnected units (neurons) where each unit takes a number of real-valued inputs which produces a single real-valued output that may in turn be an input to other units. ANNs have the ability to learn and thereby acquire knowledge and make it available for use. ANNs are among the most effective learning methods to learn and interpret complex real-world sensor data [14].We just recall the notion of neural network called the Weighted Multi Expert Neural Network (Wt.M.E.N.N) constructed using the fuzzy neural networks. This Wt.M.E.N.N. Guarantees equal representation of opinion of each expert; hence this method has an advantage over the Fuzzy Neural Networks. Neural Network learning can be either supervised one or an unsupervised one. In a supervised learning algorithm, learning is guided by specifying, for each training input pattern the class to which the pattern is supposed to belong. In an unsupervised one, the network forms its own classification of patterns. The classification is based on commonalties in certain features of input pattern. Since the data is an unsupervised one,we make use of Wt.M.E.N.N. In any supervised learning, a training set of correct input-output pairs is given so as to minimize the error, but in an unsupervised one the output is purely based on the input data. We just recall the definition of Neural Network.

VII. Result

Testing was performed on different companies and results obtained were quite satisfactory. We are showing the Table of actual and predicted price of companies. From the table prediction accuracy is good.

Previous Results:

Date	Forecast				Actual			
	Open	High	Low	Close	Open	High	Low	Close
2012-12-07	1,413.93	1,420.53	1,407.21	1,414.65	1,413.95	1,420.34	1,410.90	1,418.07
2012-12-06	1,409.27	1,417.30	1,402.61	1,410.59	1,409.43	1,413.95	1,405.93	1,413.94
2012-12-05	1,407.05	1,413.65	1,400.23	1,407.67	1,407.05	1,415.56	1,398.23	1,409.28
2012-12-04	1,409.45	1,416.05	1,402.05	1,408.67	1,409.46	1,413.14	1,403.65	1,407.05
2012-12-03	1,416.18	1,422.19	1,408.98	1,415.61	1,416.34	1,423.73	1,408.46	1,409.46

Showing the past stock price

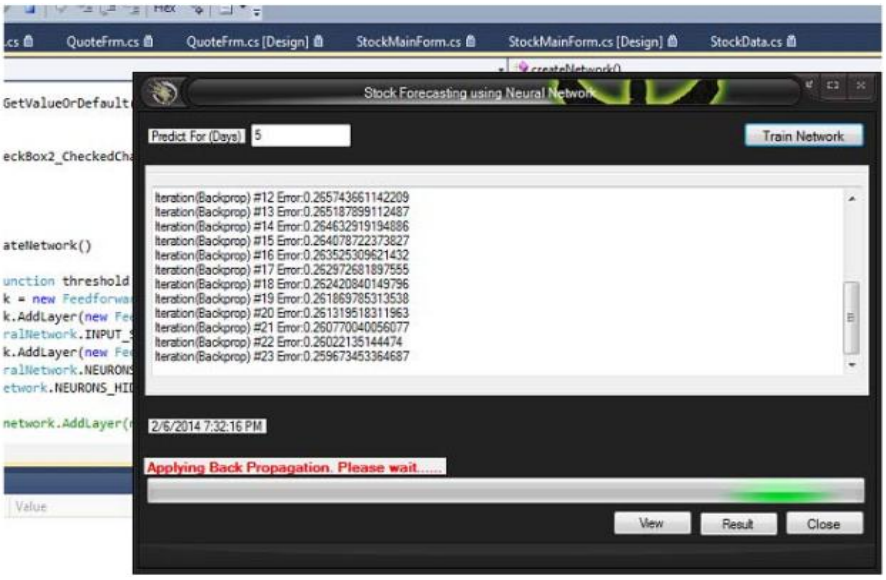

Showing the process of a algorithm

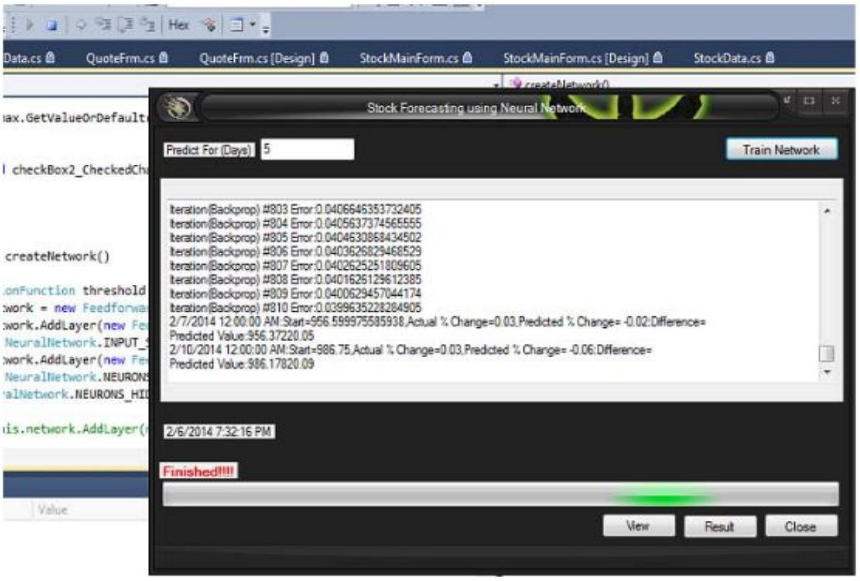

Showing the actual price and predicted price

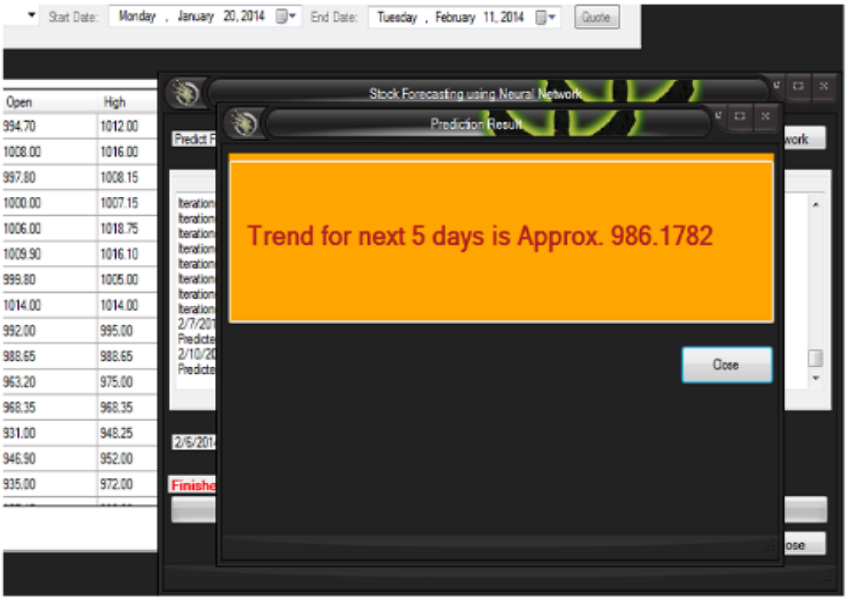

Showing the actual prediction result of next 5 days

VIII. Conclusion

In this paper, we tried to sum up the application of Artificial Neural Networks (ANN) for predicting stock market. ANN have shown to be an effective, general purpose approach for pattern recognition, classification, clustering and especially time series prediction with a great degree of accuracy. Nevertheless, their performance is not always satisfactory. Back propagation algorithm is the best algorithm to be used in Feed forward neural network because it reduces an error between the actual output and desired output in a gradient descent manner.

REFERENCES

[1] Prakash Ramani, Dr.P.D.Murarka,"Stock market Prediction Using Artificial Neural Network", International Journal of Advanced Research in Computer Science and Software Engineering, volume 3 issue 4, April 2013.

[2] Neelama Budhani, Dr.C.K.Jha, Sandeep K. Budhani "Application Of Neural Network In Analysis Of Stock Market Prediction", International Journal Of Computer science And Engineering Technology, volume 3 no.4 April 2012.

[3] Zhou Yixin Jie Zhang, Stock data analysis based on BP neural network,2010 second international conference on communication Software and Network.

[4] Zabir Haider khan, Tasnim Sharmin Alin md. Akter Hussain,price prediction of share market using Artificial Neural Network(ANN), International Journal of computer application(09758887) volume 22 no.2, May 2011.

[5] K. K. Sureshkumar, Dr. N. M. Elango, Performance analysis of Stock price prediction using Artificial neural Networks, Global journal of computer science and Technology, volume 2 issue 1 version 1.0 January 2012.
[6] B. Manjula, S.S.V.N. Sharma, R.Lakshman Naik, G. Shruthi, Stock Prediction using Neural Network, International journal of advantage engineering sciences and technologies vol.no 10,issue no 1,013018.
[7] K. K. Sureshkumar, Dr. N. M. Elango ,An Efficient Approach to forecast Indian Stock Market Price and their Performance analysis,International journal of computer application (09758887) volume 34, no 5, November 2011.
[8] Md. Syedul Amin,Md. Mamun, Fazida Hanim Hashim,Jubayer Jalil and HazahHusain,Design and Implementation of Novel Artificial Neural Network Based StockMarket Forecasting System on Field-Programmable Gate Arrays, American Journalof Applied Sciences 8 (10): 1054-1060, 2011 ISSN 1546-9239
[9] A. Victor Devadoss, T. Antony Alphonnse Ligori "Forecasting of Stock Prices Using Multi Layer Perceptron " Volume: 02, December 2013, Pages: 440-449 International Journal of Computing Algorithm
[10] U. BenZion, P. Klein, Y. Shachmurove and J. Yagil, "Efficiency Differences Between the S&P 500 and the Tel-Aviv 25 indices: A Moving Average Comparison". International Journal of Business, Vol. 8, No.3, pp. 267-284, 2003. [11] A. Dzikevicius, S. Saranda, and A. Kravcionok, "The Accuracy of Simple Trading Rules in Stock Markets", Economic and Management, No.15, pp. 910-916, 2010.
[11] Chang, Shih-Fu. "How far we've come: Impact of 20 years of multimedia information retrieval." *ACM Transactions on Multimedia Computing, Communications, and Applications (TOMCCAP)* 9.1s (2013): 42.
[12] B. Vanstone and G. Finnie, "Combining Technical Analysis and Neural Networks in the Australian Stockmarket". Bond University ePublications@bond. Information technology papers, 2006
[13] Rao, K. Eswara, et al. "AN APPROACH FOR CBIR SYSTEM THROUGH ADAPTIVE RESONANCE THEORY (ART1)." *International Journal of Engineering Science* (2010).
[14] T. Mitchell, "Artificial Neural Networks: Based on Machine Learning", Mc Graw Hill, 1994.

OPEN ACCESS

International
Journal
Of Modern Engineering Research (IJMER)

Comparison of Spatial Interpolation Techniques - A Case Study of Anantnag District J&K, India

Muzaffar A. Malla[1], Manzoor A. Rather[2], Muzafar N. Teli[3], Nisar A. Kuchhay[4]
[1,2,3,4,] *State Remote Sensing Centre J&K Government*

Abstract: *Groundwater is used for a variety of purposes, including irrigation, industrial, drinking, and manufacturing. Assessment and mapping of quality of groundwater is an important because the physical and chemical characteristics of groundwater determine its suitability for agricultural, industrial and domestic usages. The present study area i.e, District Anantnag lies in southern part of Jammu and Kashmir and is characterized by undulating topography, rugged mountains. The habitants of the study area mainly depend on ground water resources viz; springs and tube wells. The present study attempts to explore the best spatial interpolation technique that will best represent the actual ground water quality of district anantnag. In the present study various maps representing various physio-chemcial properties of ground water quality were generated using spatial interpolation techniques viz; Inverse Distance Weighted (IDW) and Nearest Neighbor (NN). Out of total 92 ground water samples, 8 points were preserved for cross validation between the two interpolation techniques using Root Mean Square Error (RMSE) test. Finally it can be conclude that IDW is the most preferable technique for spatial interpolation measurement of ground water quality data.*

Keywords*: Root mean Square error, IDW interpolation, NN interpolation, Anantnag,*

I. Introduction

The continuous circulation of water between ocean, atmosphere, and land is called the hydrologic cycle The hydrologic cycle can be viewed as a major machine on the planet, controlling distribution of water on the earth. Groundwater is one of the major links in the hydrologic cycle. Groundwater forms the invisible, subsurface part of natural hydrological cycle. Inflow to the hydrologic system arrives as precipitation, in the form of rainfall or snowmelt. Outflow takes place as stream flow or runoff and as evapo-transpiration, a combination of evaporation from bodies of water, evaporation from soil surfaces, and transpiration is delivered to streams both on the land surface, as overland flow tributary channels; and by subsurface flow routes, as inter flow and base flow following infiltration into the soil (Freeze & Cherry, 1979). Excluding the freshwater that is locked up in the form of polar ice caps and glaciers, about 97 percent of the worlds freshwater exist in aquifers. The present study has been carried out in district Anantnag of Jammu & Kashmir state. In the present study the available physio-chemical data of 92 locations of the various tehsils of district Anantnag, was used, the data was obtained from PHE and Central ground water authorities of concerned districts. The physio-chemical data contained the information about various water quality determining factors. The data was digitized and put up in Arcgis Software for Spatial Interpolation and based on previous experience most commonly used interpolation methods viz; Inverse Distance Weighted (IDW) and nearest Neighbor were applied to the above data for generation of continuous raster surface for studying the influence of each interpolation technique and best judging which interpolation technique is best. Finally the results obtained were Cross Validated for RMSE Error, as this error test is used to know which Spatial interpolation technique is best based on the value of RMSE Error. This was achieved by keeping 12 points reserved from total 92 sample points and later was used to study deviation if any. Finally the interpolation technique which showed the lowest value for RMSE error was found to be IDW interpolation method. Through this study it is hoped that basic Interpolation method needed to study the water quality of this area further in future has been generated.

II. Study Area

Anantnag district is southernmost district of Kashmir valley separated from the Jammu Province by the mighty Pir- Panjal Range & connects both the regions by the famous Jawahar Tunnel. The districtwith its headquarters at Anantnag forms the southern part of Kashmir valley and is located between $33^0$17'20" and 34^o15'30" North latitude and between 74^o30'15" and 74^o35'00" East longitude and is covered by SOI Degree sheet no. 43 K, N, O. The district is bounded by Poonch district in the west, Srinagar district in the North & Kargil district in the North East and Doda district in the East, by Pulwama district in the North West and Rajouri & Udhampur districts in the South & South East. The district is approachable NH IA and is

interconnected by metalled roads from all parts of the Valley. The district is also famous for Holy Amarnath Cave situated in Pahalgam tehsil where Lacs of pilgrims visit every year from all over the country. The district has a total geographical area of 3,984 sq km, comprising of 605 villages (605 inhabited). Administratively, the district is divided into 05 tehsils (Anantnag, Kulgam, Bijbehra, Pahalgam & Dooru) and 12 blocks (Achabal, Breng, Dachnipora, D. H. Pora, Kulgam, Khovripora, Qazigund, Qaimoh, Shahabad, Shangus, Devsar & Pahloo). Hydro-geologically, the district is divided into two distinct and well-defined aquifer systems, viz., hard rock or fissured aquifer constituted mainly by semi-consolidated to consolidated rock units and soft sedimentary or porous aquifer constituted mainly by unconsolidated sediments. The study site location is shown in Figure 1 below.

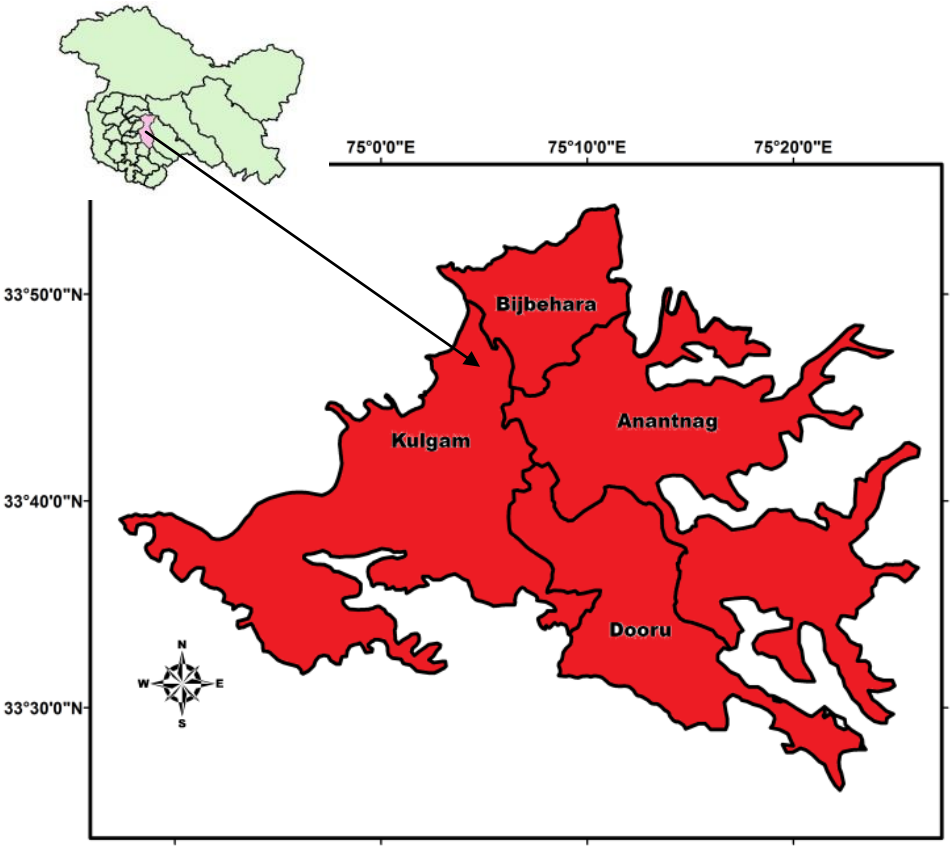

Figure 1: Location of Study Area

III. METHODOLOGY

In order to carry out the research the 92 groundwater quality samples were collected and out of these 12 sample points were kept reserved for cross validation in order to explore which interpolation is best. Ancillary data containing various water quality parameters such as pH, and other physio-chemical parameters like concentration of Na, Fe, SO_4, NO_3etc were collected from the department of the Public Health Engineering Srinagar and central groundwater board Jammu. Later field work to various locations was organized to collect the co-ordinates (lat/long) of the locations of the ancillary data, with the help of Global Positioning System (GPS) pertaining to the water quality parameters collected from the two respective departments. Figure 2 below shows the methodology in flowchart below. Physio-Chemcial Data of water Quality Determining factors obtained from J&K PHE department and Central Ground water Board. IRS-LISS image of October 2005. For ground truthing Trimble GPS was used for validating and locating the various water resources sites of the study area. The further step was to digitize groundwater ancillary data using the MS Excel and assigning of GPS locations to each points which was otherwise without locations for the creation of the database Then the groundwater ancillary data and the spatial data (co-ordinates) which were collected with the help of GPS were joined in the ArcGIS 9.2 software.

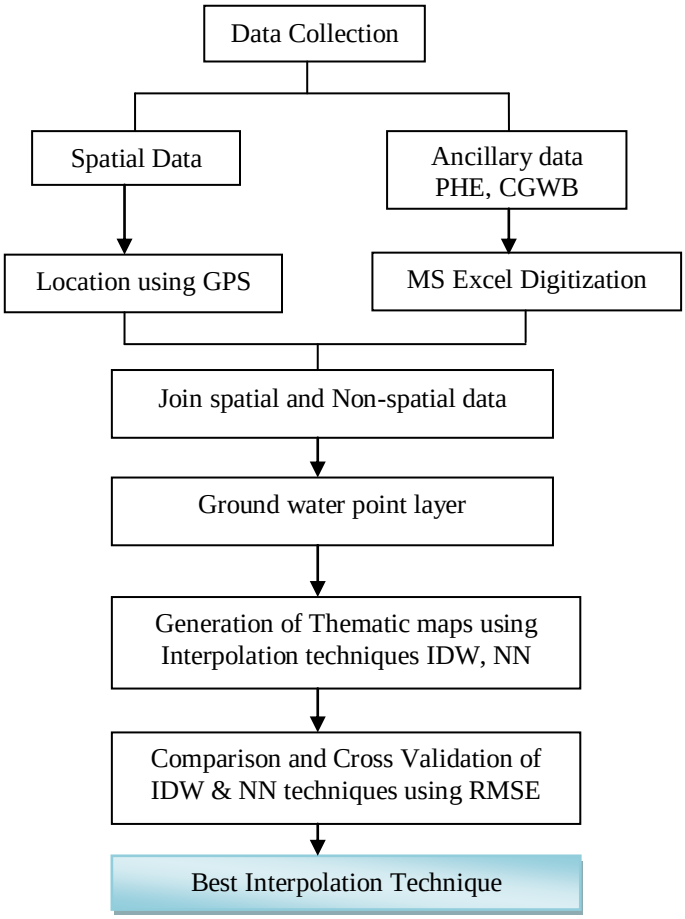

Figure 2.Overall Methodology Adopted

After linking the spatial and non-spatial data the groundwater quality point layer was generated for further analysis. Later on the other analysis was carried out using the IDW (Inverse Distance Weighted) Interpolation and Nearest Neighbor (NN) in Geographic information system environment using the Arc Map software. Interpolation creates a continuous (or prediction) surface from sampled point values. The continuous surface representation of a raster dataset represents height, concentration, or magnitude—for example, elevation, pollution, or noise. Interpolation makes predictions from sample measurements for all locations in a raster dataset whether or not a measurement has been taken at the location. In the present data analysis we used IDW (Inverse distance weighted) interpolation technique and nearest neighbor. Later on Root mean square error and absolute error was used to cross validate the two different interpolation techniques and select the best interpolation techniques.

IV. RESULTS & DISCUSSIONS

Two interpolation methods were implemented in this study Inverse Distance Weighted (IDW) and Nearest Neighbor (NN). These interpolation techniques were compared to get the best interpolation techniques i.e., to see which of the interpolation technique gives the result which is more acceptable. The interpolation results are presented in a tabular form below in table 1. The table shows different water quality determining factors which are acceptable with the regulating agencies like Bureau of Indian Standards (BIS), Indian Council of Medical Research (ICMR) and World Health Organization (WHO). The results are given with the ranges of values for two interpolation techniques. From the table it is apparent that some parameters show increase in value and some show decrease. The values are inferred using Bureau of Indian standards as Desirable, Permissible Limit and Non-potable. In addition to this various thematic layers of interpolation have been generated using the above parameters as input to Arcgis spatial analyst module for interpolation. The interpolation maps generated shows the influence of each water quality factor in the study district. Water quality interpolation results are generated for various layers like hardness, pH, Nitrates, sulphates, iron calcium, fluorides, sodium, chlorine and magnesium. The interpolation maps generated have been shown from Figure 3-14 below.

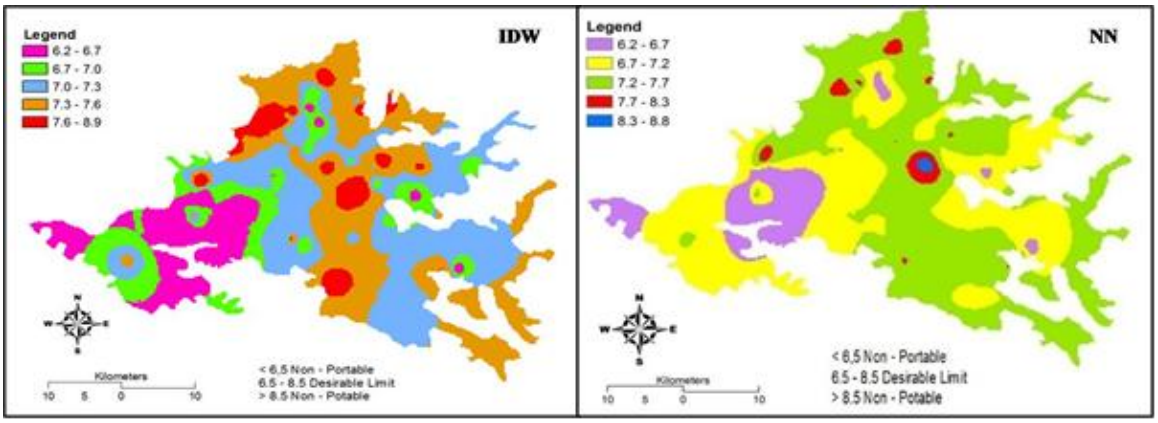

FIGURE 3**:** Interpolation Results for pH

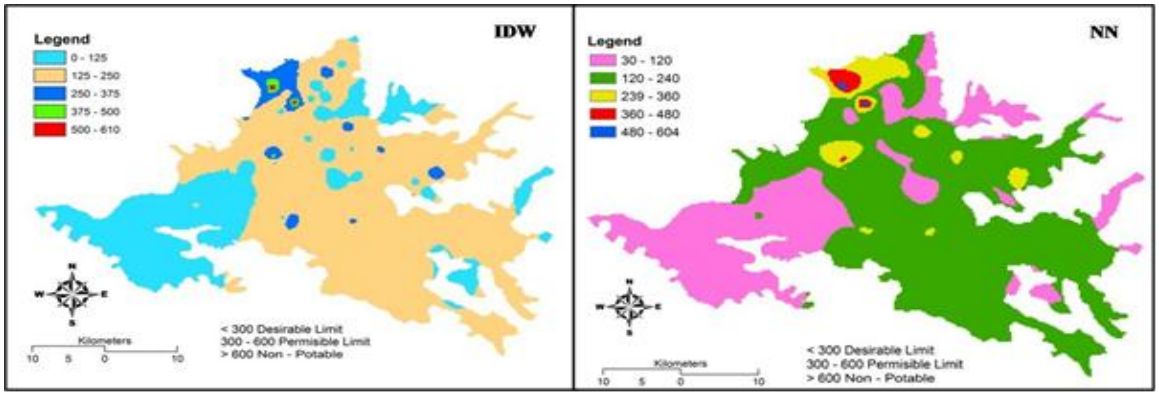

FIGURE 4: Interpolation Results for Total Hardness

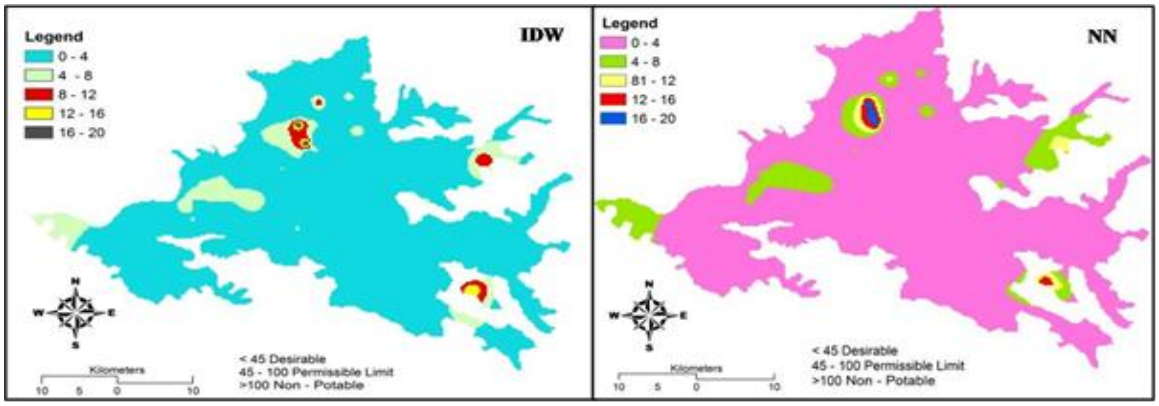

FIGURE 5: Interpolation Results for Nitrates

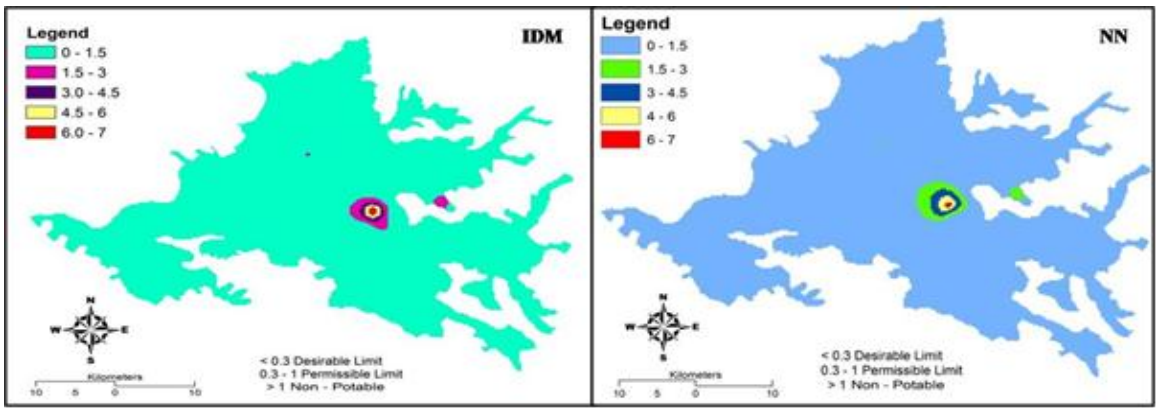

FIGURE 6: Interpolation Results for Iron

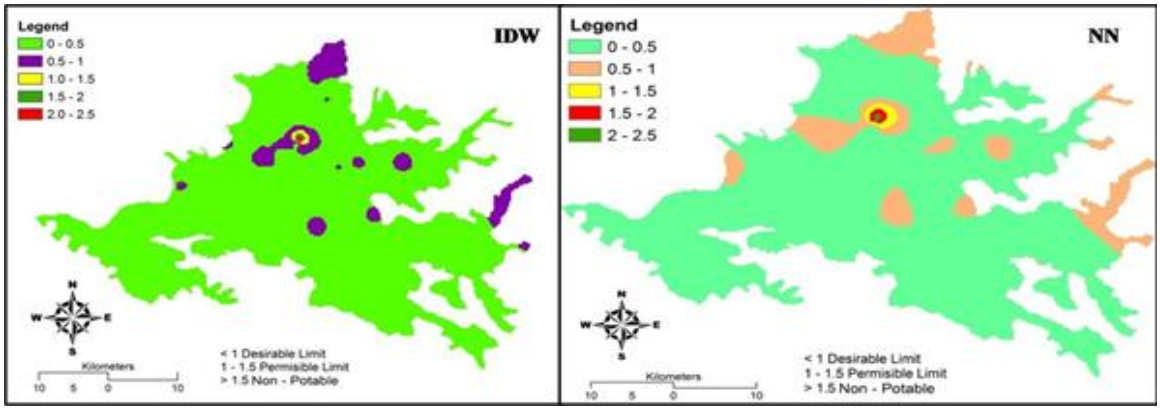

FIGURE 7: Interpolation Results for Fluorides

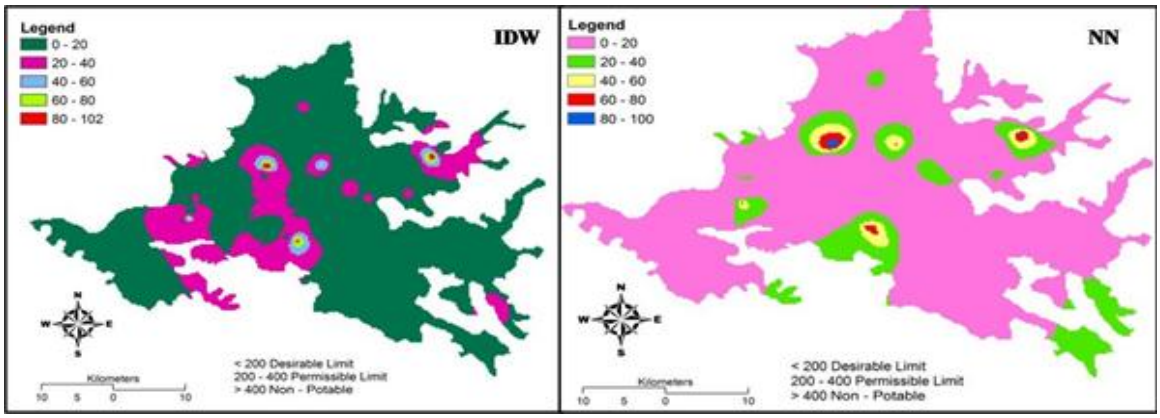

FIGURE 8: Interpolation Results for Sulphates

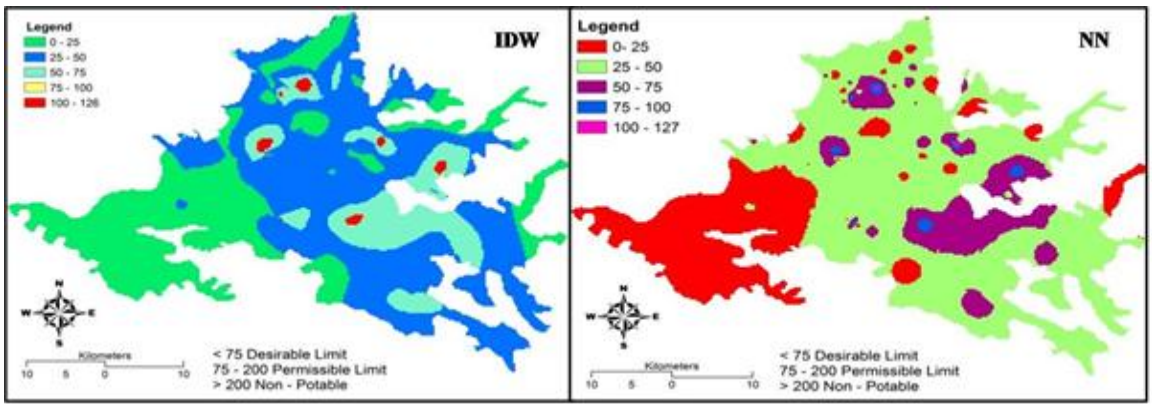

FIGURE 9: Interpolation Results for Calcium

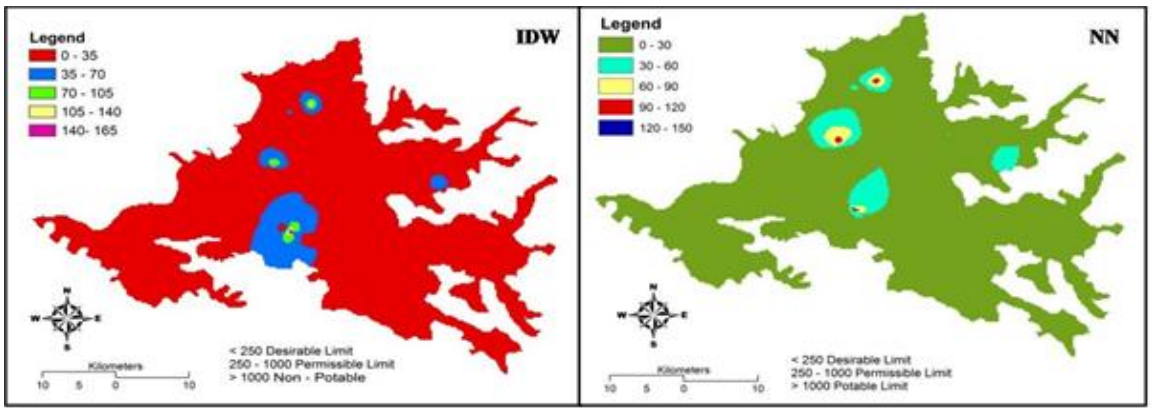

Figure 10: Interpolation Results for Chlorides

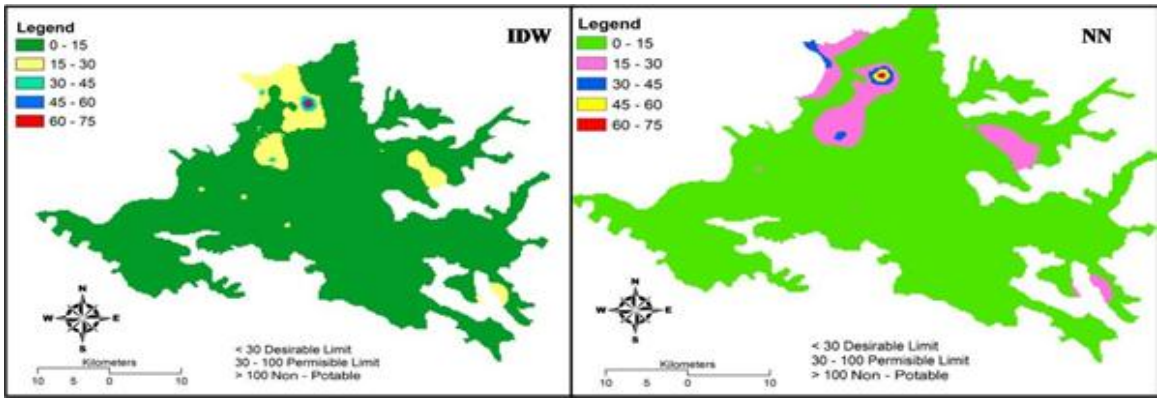

Figure 11: Interpolation Results for Magnesium

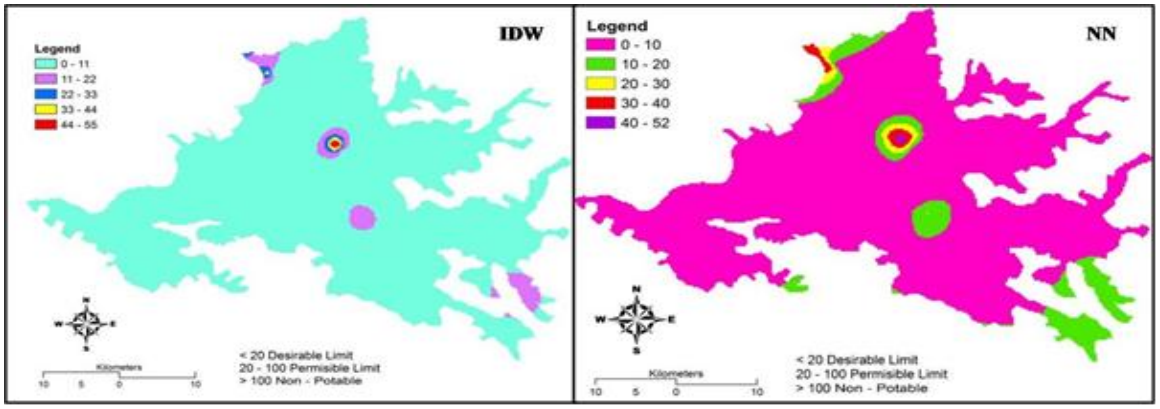

Figure 12**:** Interpolation Results for Sodium

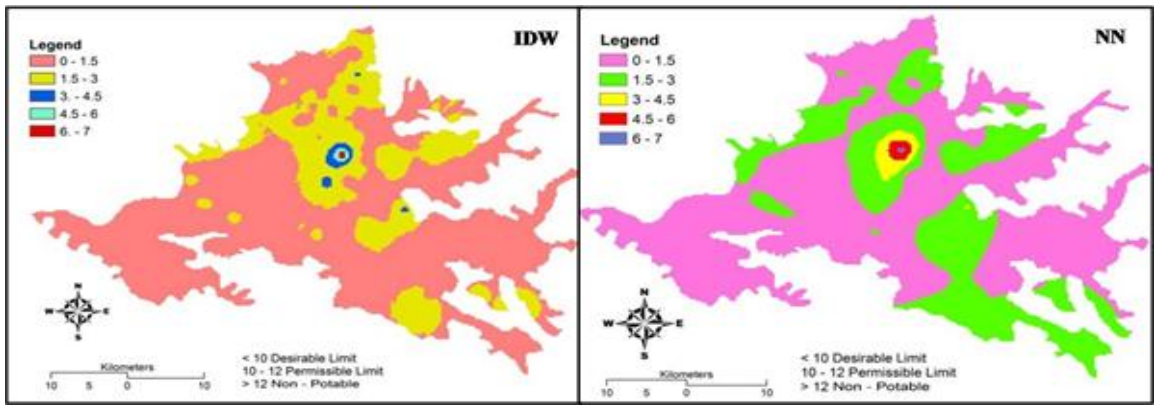

Figure13: Interpolation Results for Potassium

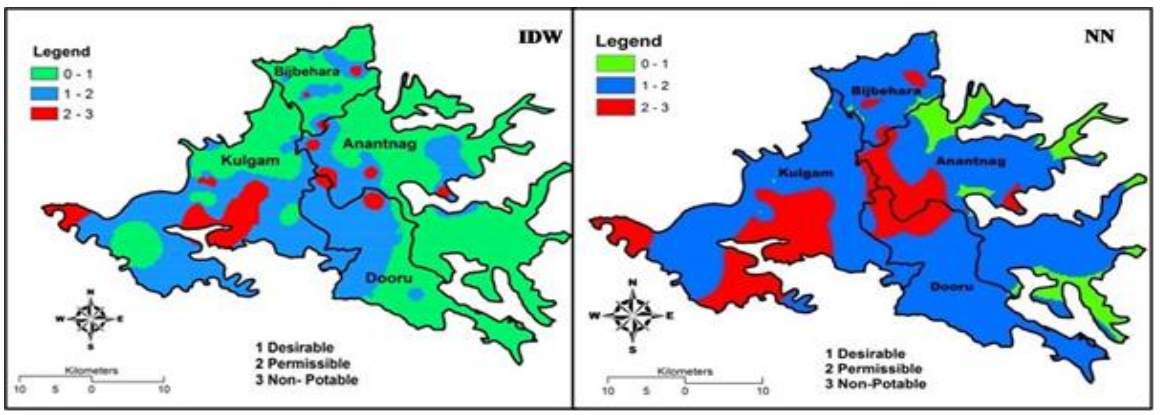

Figure 14: Interpolation Results for Ground Water Quality Map

Table 1: The Overall Water Quality (Element Wise) Obtained Using Two Different Interpolation Techniques.

S.NO	Element	IDW-Interpolation	Results IDW	NN-Interpolation	Results NN	BIS Standards
1	pH	6.2-8.9	High for Sond village	6.19-8.183	8.83 at Sond village	<6.5 NP 6.5-8.5D >8.5 NP
2	TH	14-610	High at Kareiteng	331-603.47	Kraiteng	<300 D 300-600 P >600 NP
3	Nitrates	0.1-20	-	0.001-19.34	-	<45 D 45-100 P >100 NP
4	Iron	0.001-7	Exceed at Damhal, Nowshera, Kareiteng,Tokerpura	0.001-6.74	Damhal	<0.3 D 0.3-1 P >1 P
5	Fluorides	0.002-2.5	Tokerpura	0.002-2.39	Tokerpura	<1 D 1-1.5 P >1.5 P
6	Sulphates	0.01-104	Botachloo	0.09-99.30	Botachloo	<200 D 200-400 P >400 NP
7	Calcium	0.1-127	Rembalpura	0.22-125.099	Rembalpura	<75 D 75-200 P >200 NP
8	Chlorides	0.03-184.3	Supat	0.18-149.35	Supat	<250 D 250-100 P >1000NP
9	Magnesium	0.1-75	Wupzan,Botathchloo	0.0047-71.75	Wupzan	<30 DL 30-100 P >100 NP
10	Sodium	0.001-53.6	Maliknag	0.085-51.56	Maliknag	<20 D 20-100PL >100 NP
11	Potassium	0.0015-68	-	0.0023-6.63	Maliknag	<10 D 10-12 PL >12 NP

*****D= Desirable Limit, P = Potable, PL = Permissible Limits, NP = Non Potable

Also for two interpolation technique viz; IDW and NN, the RMSE error test was applied to see which interpolation technique best suits and is more efficient. Evaluation of the accuracy of spatial interpolation techniques. The cross-validation technique was achieved by removing data from one observation point at a time (j), taken from all of the available observation points in the data set and then estimating the value of the removed observation point data using the data from the remaining (n − 1) observation points. This technique is used to evaluate how well the neighboring stations estimate the missing value. The accuracy of spatial interpolation techniques was evaluated by using the following two statistical indicators. Several researchers (e.g. Chang 2004; Kane ski & Malignant 2004; Ahrens 2006) have recommended these two measures for comparison of spatial predictions of interpolation models for testing data. Formula of RMSE is given bellow.

$$RMSE = \frac{\sqrt{\sum_{j=1}^{n}(y_j - \hat{y_j})^2}}{n}$$

Where, y_j is the measured value
$\hat{y_j}$ is the estimated value of the dependent variable,
n is the number of observations.

From the results obtained from Root mean square error (RMSE). The root mean square error for IDW is 0.011while as Root mean square Error (RMSE) for Nearest Neighbor analysis comes out to be 0.172 thus it is

quite evident that IDW inverse Distance weighted interpolation is the best interpolation technique than Nearest Neighbor analysis. The value Lower RMSE values indicate greater central tendencies and generally smaller extreme errors. In this comparative study the best suitable spatial interpolation techniques were determined based on Root Mean Square error.it is hoped that through this study basic data and technique needed for studying the water quality of the study district in great detail in future has been generated.

V. Conclusions

From the current study it has been found that Inverse distance weighted interpolation techniqueis the best way of determining the water quality, As in this technique the chances of error are minimized to a great extent and chances of deviation of original value are extremely low.

Acknowledgment

The Authors are highly thankful to the Department of Earth Sciences University of Kashmir for support, guidance and help during this study. We are also thankful to Government agencies for providing data necessary for this study, and above all thanks to authors, publishers and reviewers for their support in various forms.

REFERENCES

[1] Stefanoni LH, Hernandez RP, "Mapping the spatial variability of plant diversity in a tropical forest: Comparison of spatial interpolation methods", Environmental Monitoring and Assessment Vol. 117, pp. 307-334, 2006.

[2] Aghazadeh N, Mogaddam AA, "Assessment of groundwater Quality and its Suitability for Drinking and Agricultural Uses in the Oshnavieh Area, Northwest of Iran", Journal of Environmental Protection Vol. 1, pp. 30-40, 2010.

[3] Shomar B, Fakher S. A, Yahya1 A "Assessment of Groundwater Quality in the Gaza Strip, Palestine Using GIS Mapping". Journal Water Resource and Protection Vol. 2, pp. 93-104, 2010.

[4] Lam NS, "Spatial Interpolation Methods: A Review", The American Cartographer Vol. 10, pp. 129-149, 1983.

[5] Gyananath G, Islam SR, Shewdikar SV, "Assessment of Environmental Parameter on ground water quality". Indian Journal of Environmental Protection Vol. 21, pp. 289-294, 2001 .

[6] Taesombat Wisuwat, Sriwongsitanon Nutchanart, "Thailand Areal rainfall estimation using spatial interpolation techniques". Science Asia, pp. 268–275, 2009.

[7] Hong Yan, Nix A. Henry, Hutchinson F. Mike and Booth H. Trevor., "Spatial interpolation of monthly mean climate data for china". International Journal of Climatology Vol. 25, pp. 1369-1379, 2005.

[8] JantakatYaowaret and Ongsomwang Suwit, "Assessing the effect of incorporating topographical data with geostatistical interpolation for monthly rainfall and temperature in ping basin, Thailand", Strategic Integration of Surveying Services, pp.13-17, 2009.

[9] Naoum S., Tsanis I.K., (2004), "Ranking spatial interpolation techniques using a GIS based DSS". Global Nest: the Int. J. Vol 6, No 1, pp. 1-20, 2004.

[10] R.Anis , F. Saeed , R. Aslam. "Comparison of different interpolation methods for temperature mapping of Pakistan". Water resource and arid environment, 2006.

[11] W. Luo, M. C. Taylor and S. R. Parker, "A comparison of spatial interpolation methods to estimate continuous wind speed surfaces using irregularly distributed data from England and Wales," International Journal of Climatology, Vol. 28, pp. 947–959, 2008.

[12] Weekly Rainfall Probability for Selected Stations of India, IMD (Division of Agricultural Meteorology, Pune), Vol. 2, Edition- I, 1995.

[13] McCuen, R.H. "Hydrologic Analysis and Design", N.J Prentice Hall, 1998.

[14] Ducci D, "GIS techniques for mapping groundwater contamination risk", Natural Hazards, Vol. 20 pp. 279-294, 1999.

[15] Busuioc A, Chen D, Hellström C, "Performance of statistical downscaling models in GCM validation and regional climate change estimates: application for Swedish precipitation", International Journal of Climatology, Vol. 21, pp. 557–578, 2001.

[16] Gupta MD,Purohit A, Datta KMJ, "Assessment of drinking water quality of river Brahmani", Indian Journal of Environmental Protection Vol 8, Edition 3, pp. 285-291, 2001.

[17] Chatterjee R, Tarafder G, Paul S, "Groundwater quality assessment of Dhanbad district, Jharkhand, India", Bulletin of Engineering Geology and Environment, Vol. 69, Edition 1, pp. 137-141, 2010.

[18] Yammani S, "Groundwater quality suitable zones identification: application of GIS, Chittoor area, Andhra Pradesh, India", Environmental Geology Vol. 53, Edition 1, pp. 201–210, 2007.

[19] Babiker IS, Mohamed AM, Hiyama T, "Assessing groundwater quality using GIS", Water Resource Management, Vol. 21, Edition 4, pp. 699 –715, 2007.

[20] Ducci D, "GIS techniques for mapping groundwater contamination risk", Natural Hazards Vol. 20, pp. 279-294, 1999.

[21] Isaaks EH, Srivastava RM, "An Introduction to Applied Geostatistics", Oxford University Press, 1989.

[22] Sibson R, "A brief description of Natural Neighbor interpolation", In V. Barnett, editor, Interpreting Multivariate Data, Wiley, New York, USA, 1981.
[23] Watson D F, "Contouring: A Guide to the Analysis and Display of Spatial Data", Pergamon Press, Oxford, UK, 1992.
[24] Gold Cm, "Surface interpolation, spatial adjacency and GIS", In J. Raper, editor, Three Dimensional Applications in Geographic Information Systems, Taylor & Francis, 1989.
[25] Tobler W R, Kennedy S, "Smooth multi-dimensional interpolation", Geographical Analysis, Vol. 17, pp. 251–257, 1985.
[26] Watson DF, Philip GM, "A Refinement of Inverse Distance Weighted Interpolation", Geo-Processing Vol. 2, pp. 315-327, 1985.
[27] Hong, I. A, Chon. H T, "Assessment of groundwater contamination using geographic information systems", Environmental Geochemistry and Health, Vol. 21, Edition 3, pp. 273-289, 1999.

.

OPEN ACCESS

International
Journal
Of Modern Engineering Research (IJMER)

PV/Diesel Hybrid System for Fuel Production from Waste Plastics Recycling

Faten Hosney Fahmy[1], Ninet Mohamed Ahmed[2], Hanaa Mohamed Farghally[3],
Photovoltaic Department, Electronics Research Institute, Giza, Egypt.

Abstract: *The treatment of wastes has become one of the most important concerns of modern society. Converting waste plastic into gasoline and diesel fuel through a highly effective low-cost pyrolysis process is a promising technology. In this paper PV/Diesel/Battery hybrid system is suggested to fulfill the load demand of waste plastic recycling pyrolysis process. A Mathematical and simulation models using MATLAB/ SIMULINK software for the hybrid PV/Diesel/Battery system components have been developed. Also, this paper presents a control strategy using Artificial Neural Network Controller (NNC) technique for coordinating the power flow among the different components of the PV/Diesel/Battery hybrid system. The results indicate that the proposed control unit using NNC can be successfully used for controlling the power system for the waste plastic recycling pyrolysis process.*

Keywords*- Battery, Diesel generator, Matlab/Simulink, NNC, Photovoltaic, Waste plastic recycling.*

I. Introduction

Increased population growth and economic development are accelerating the rate at which energy, and in particular electrical energy is being demanded. The use of fossil fuels is now widely accepted as unsustainable due to depleting resources and the subsequent increase in price and the accumulation of greenhouse gases in the environment that have already exceeded. All methods of electricity generation have consequences for the environment, so meeting this growth in demand, while safeguarding the environment poses a growing challenge [1-3]. After food waste and paper waste, waste plastic is the major constitute of municipal and industrial waste in cities. The global production of plastics has seen an increase from around 1.3 million tons in 1950 to 245 MT in 2006 [4]. Worldwide consumption of plastic is expected to touch 297 million tons by 2015. Hence, waste plastics pose a very serious environmental challenge because of their huge quantity and disposal problem as thermoplastics do not biodegrade for a very long time. Thus mankind has to rely on the alternate/renewable energy sources like biomass, hydropower, geothermal energy, wind energy, solar energy, nuclear energy, etc. [5]. Among all the renewable energy resources the solar and wind energies have the great potential as a power generating energy source, because of their many advantage like low or zero emission of pollutant gases, low cost, inexhaustible sources and easy availability of these energy sources [6 -7]. In addition to, waste plastic to liquid fuel is also an alternate energy source path, which can contribute to depletion of fossil fuel as in this process. Pyrolysis process appears to be a technique that is able to reduce a bulky, high polluting industrial waste, while producing energy and/or valuable chemical compounds. Liquid fuel with similar fuel properties as that of petro fuels is obtained [4].

Hybrid renewable energy sources can ensure sustainable, efficient utilization and electric AC-DC supply_security [8]. It can raise power supply reliability and reduce the system cost according to local environmental condition and load characteristics. The choice of renewable power options is partly determined by the region in which the facility is located [9 -10].

One of the most promising renewable energy technologies is photovoltaic (PV) technology since it offers many advantages such as incurring no fuel costs, not being polluting, requiring little maintenance , and emitting no noise, The performance of the PV system depends upon several factors, especially the meteorological conditions such as solar radiation, ambient temperature and wind speed [11].

The use of diesel generators to ensure continuous power supply has the disadvantage of increasing the greenhouse gas emission which has a negative impact on the environment. Incorporating battery storage and a renewable energy source, to form a hybrid power supply system, can alleviate most of the problems mentioned for the diesel-only power system. The combinations of PV locally available solar energy systems with the continuously available diesel power plants is being disseminated worldwide to reduce diesel fuel consumption and to minimize atmospheric pollution [12-14].

Utilization of renewable energy sources for producing liquid fuel from recycling of waste plastics by a cost effective pyrolysis method will contribute on both solving the problem of plastic disposal to a great extent and consequently solving the environment problem. In addition to, adding one source of energy [4].

This paper presents the use of PV/Diesel/Battery hybrid energy system for supplying the electrical power to meet the load requirement for household waste plastics recycling system for liquid fuel production. A simulation of hybrid PV/Diesel/Battery system using MATLAB/ SIMULINK software has been performed. The simulation has been done to assure that the PV/Diesel/Battery system is suitable for recycling process operation. Artificial Neural Network Controller (NNC) model was developed to simulate the performance of PV/Diesel/Battery power system.

II. Location

Cairo is chosen as the site under consideration. The specific geographical location of Cairo city is at a location of 30° 05' N latitude, 31° 17' E longitude and elevation 34.4 m with annual average solar radiation of 5.21 kWh/m²/d and clearness index of 0.597. Solar radiation, ambient temperature and the specific geographical location data for this city were obtained from Egyptian solar radiation atlas [15].

III. PV/Diesel/Battery Waste Plastic Recycling System Description

Figure1 illustrates the proposed PV/Diesel/Battery waste recycling system. It contains power sources which are PV array, diesel generator engine system, storage battery bank, inverter, NN controller unit and AC load (M_1, M2, M3, P1, P2, P3 and pyrolysis reactor).

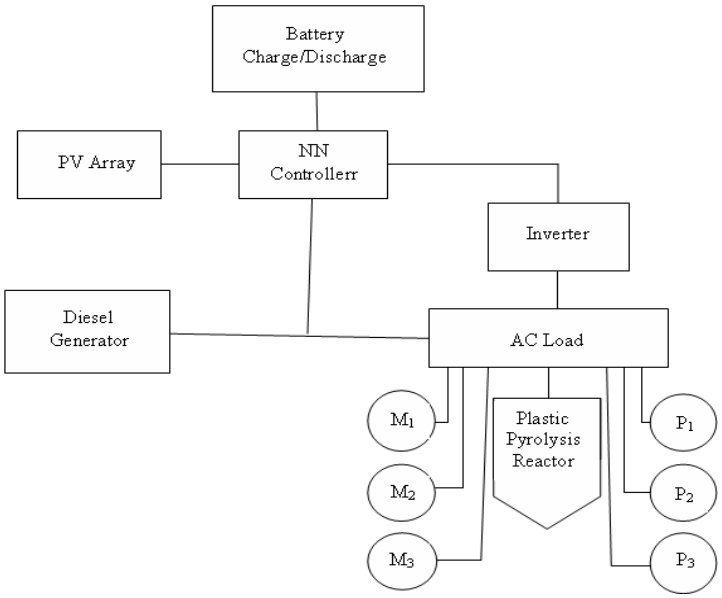

Fig.1 The proposed PV/Diesel/Battery waste recycling system configuration

IV. Load Estimation

Table I illustrates the main electrical equipments for waste plastic recycling system. The waste recycling system is assumed to operate for 10 hours from 8:00 to 18:00 o'clock with a peak load of 21.5 kW in addition to 1 hour before 8:00 o'clock and 1 hour after 18:00 o'clock of 1 kW for preparation and closing as shown in Fig. 2. The electrical daily load curve during two days in the year, one in winter and the other in summer is the same since the electrical load is the same for summer and winter seasons. Figure 2 illustrates the hourly daily electrical load of the waste recycling system. This figure indicates that, the peak load occurs during the period between 12:00 and 16:00 o'clock.

Table I: The hourly load demand for household waste plastic recycling system

Symbol	Equipment	Power (KW)
M1	Crusher motor	2.5
M2	Feeder motor	2.5
M3	Reactor motor	1.5
P1	Receiver tank pump motor	1.5
P2	Storage tank pump motor	1.5
P3	Heavy oil tank pump motor	1.5
I H	Waste plastic recycling induction heater	15

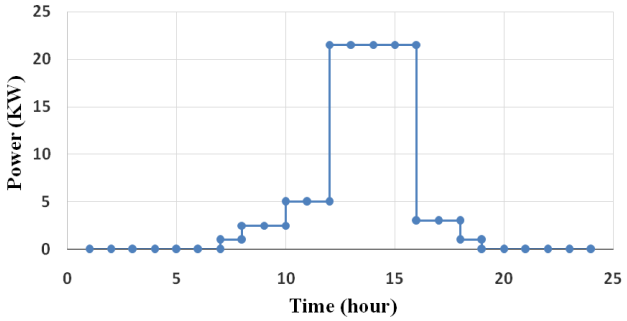

Fig.2 Electrical hourly load curve of waste plastic recycling system

V. Weather Data

The inputs to PV system are the solar radiation and the air temperature. Figure 3 shows the hourly solar irradiance data for Cairo city which is collected for a typical summer and winter days. By comparing the winter & summer solar data which is shown in Fig. 3, it is noticed that the time frame when solar energy is available (the solar insolation duration) is wider in the summer than in the winter. Also, for a typical summer day, the peak radiation of about 926 W/m^2 is estimated, while for a typical winter day a peak of about 780 W/m^2 is estimated.

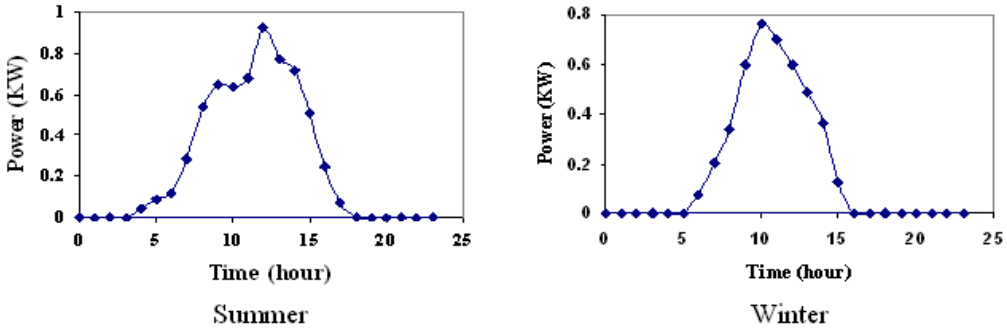

Fig.3 Global solar irradiance of Cairo city for a typical two days in summer and winter

Figure 4 shows the hourly air temperature of Cairo city for a typical two days in winter and summer. It is observed that, the air temperature in summer season is much higher than that in winter.

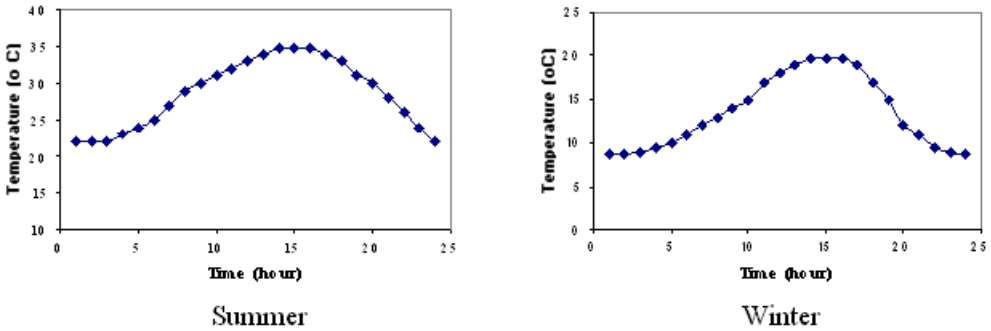

Fig. 4 Air temperature of Cairo city for a typical two days in summer and winter

VI. Commercial Waste Pyrolysis System

The waste plastic pyrolysis process to produce oil for using as liquid fuel or chemical feedstock is common at the commercial scale in Japan. At the small scale, there are many companies manufacturing 1 ton /day batch pyrolysis units, using plastics derived from household waste. For example, the MCC Yukaki Ltd. company in Japan operates a plastic pyrolysis plant that typically processes one tone per day of plastics, producing medium and light oil is shown in Fig.5 [16-18].The oil is combusted to provide the energy

requirements of the pyrolysis system and exported for combustion to raise steam for both thermal and electrical power generation.

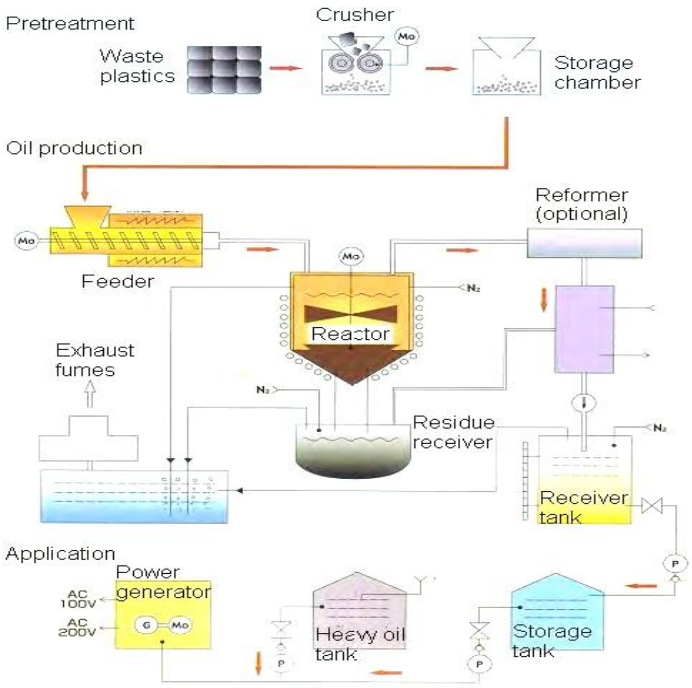

Fig.5 Schematic diagram of the MCC Yukaki Ltd. 1 ton per day plastics pyrolysis system

The process of conversion waste plastic to liquid fuel consists of three main stages; pretreatment, generation and application which is indicated in Fig.5 and can be described as follow:

***Pretreatment stage*:** The pretreatment stage includes sorting for the removal of unsuitable materials from incoming waste plastic, crushing and storing the crushed plastic in the storage chamber.

***Generation stage**:* The generation process takes place in a stainless steel cylindrical reactor with an opening at each end of its upper section: one opening for raw material feeding and the other for waste removal. It is operated in ambient pressure at temperatures lower than 500 degrees Celsius. There are also different types of reactors and heating equipment. Both kiln-type and screw-type reactors have been proposed, while induction heating by electric power has been developed as an alternative to using a burner. The output of the reactor is stored in the reservoir tank and the residue outs from the bottom of the reactor to the residue receiver.

Application stage: In this stage the generated oil is pumped to the storage tank from which it also pumped to the heavy oil tank and to the power generation unit.

VII. Hybrid System Components

7.1 Photovoltaic Array

Photovoltaic (PV) Solar energy is used as the base-load power source. PV array size is dependent on the load profile, solar radiation, and renewable fraction. The PV modules used were Polycrystalline silicon with 130W Maximum Power. The details of solar module properties are shown in Table II [19].

Table II: Specifications of PV module

Parameter	Value
Maximum power (P_{max})	130 Wp
Open circuit voltage (V_{oc})	21.5 V
Maximum power point voltage(V_{mpp})	17.4 V
Short circuit current (I_{sc})	7.99 A
Maximum power point current (I_{mpp})	7.49 A

7.2 Diesel Generator (DG)

Diesel generator (DG) technology is widespread and the development of the power plant is relatively easy. A diesel generator is in service at times when the PV array fails to meet the load. Due to few inherent advantages of diesel generator listed below, it is used as a backup source of power generation [20-21].

a) It attains full load operating condition very quickly.
b) Highly qualified people are not required to operate this generator because of simplicity of application.
c) In a few seconds it can be started and it can gain rated speed.
d) Under varying load condition stability is maintained.
e) Installation requires smaller place compare to other generating systems.

Diesel generator is a combination of a diesel engine with an electric generator (alternator) to generate electrical energy. The diesel generator comprises a speed governor, a diesel engine, an excitation system and a synchronous generator.

The governor and the diesel engine system control the generator speed and provide mechanical power to the generator. A speed regulator and an actuator are the main components of this system. A 25 kW KOBOTA diesel generator is chosen in this study.

7.3 Battery

Battery is used as a storage device which has two operation modes: charging and discharging. Excess electricity from PV and diesel can be stored in the battery. The purpose of the battery is to alleviate the mismatch between the load demand and electricity generation. The storage batteries are a key factor in a hybrid system of renewable energy; it allows to minimize the number of starting/stopping cycle of the diesel generator which reduces the problem of its premature wear, and to satisfy the request of the load in spite of solar source fluctuations.

The battery type chosen is Trojan Battery. It is a 6 volt, 225 AH Flooded Lead Acid Battery T-105, which is perfectly suited for use in renewable energy systems where lowest life-cycle cost is the key consideration [22].

7.4 Inverter

The inverter is used to interface the DC voltage to the consumer load AC requirements. The PV arrays produce direct current (DC) at a voltage that depends on the design and the solar radiation. The DC power then runs to an inverter, which converts it into AC voltage. The inverter size is rated based on the selected PV size, in order to maximize the quantity of energy which is harvested from the PV arrays. A 25 KW inverter is used in this study.

VIII. Power System Mathematical Model

The development of the mathematical model of the hybrid power system sources which are used for supplying the electrical system of waste plastic recycling process is described in this section.

8.1 Modeling of Diesel Engine

The diesel engine is a combination of an internal combustion (IC) engine and governor. The governor comprises speed controller and actuator. The governor of a diesel engine maintains the constant speed throughout the operation of diesel engine. The regulator and the actuator transfer functions can be expressed by Eq. (1) and Eq. (2) as follow [21]:

$$H_r = \frac{k_r(1+T_{ra}s)}{(1+T_{r1}s+T_{r2}s^2)} \qquad (1)$$

$$H_a = \frac{(1+T_{a1}s)}{s(1+T_{a2}s)+(1+T_{a3}s)} \qquad (2)$$

Where, k_r is the regulator gain, T_{r1}, T_{r2} *and* T_{r3} are the regulator time constants, T_{a1}, T_{a2} *and* T_{a3} are the actuator time constants. The differential equations describing the diesel engine and speed regulation are given by Eq. (3) and Eq. (4) [21]:

$$\frac{dP_c}{dt} = -\frac{k_1}{\omega_{ref}}\Delta\omega \quad (3)$$

$$\frac{dm_B}{dt} = \frac{1}{\tau_2}(k_2 P_C - \frac{k_2}{\omega_{ref} R}\Delta\omega - m_B) \quad (4)$$

Where,
P_c is the compression ratio*;* m_B is the diesel engine fuel consumption rate (kg/sec),
K_1 is the governor summing loop amplification factor,
R is the diesel engine permanent speed droop,
ω_{ref} is the reference speed of engine in rad/sec,
The engine is represented by a gain K_2 and a dead time τ_2,
The dead time can be expressed as [21]:

$$\tau_2 = \frac{60 s_t}{2Nn} + \frac{60}{4N} \quad (5)$$

Where, s_t =4 for four stroke engine, N is the speed in rpm, and n is the number of cylinders.
The mechanical power (P_m) output produced as a result of combustion is [21]:

$$P_m = C_1 m_B \eta \quad (6)$$

Where, C_1 is proportionality constant, η is the efficiency. The numerical values of these constant parameters are listed in Table III [21].

Table III: Values of constant parameters of the diesel model

Constants Parameter	**Numeric values**
T_{r1}, T_{r2} and T_{r3}	0.01, 0.001 and 0.2
T_{a1}, T_{a2} and T_{a3}	0.25, 0.009 and 0.0384
K_r	40
Engine Time Delay	0.24

8.2 Modeling of PV Array

PV array consists of many modules connected in series and parallel to provide the desired output terminal voltage, current and power. The output current (I) from the PV cell is found by applying the Kirchhoff's current law (KCL) [3].

$$I - I_{SC} - I_d \quad (7)$$

Where, I_{sc} is the short-circuit current that is equal to the photon generated current, and I_d is the current shunted through the intrinsic diode. The diode current I_d is given by the Shockley's diode equation [3]:

$$I_d = I_o(e^{\frac{qV}{kT}} - 1) \quad (8)$$

Where: I_o is the reverse saturation current of diode (A), q is the electron charge (1.602×10^{-19} C), V is the voltage across the diode (V), k is the Boltzmann's constant (1.381×10^{-23} J/K), T is the junction temperature in Kelvin (K). Replacing I_d of Eq. (7) by Eq. (8) gives the current-voltage relationship of the PV cell.

$$I = I_{SC} - I_o(e^{\frac{qV}{kT}} - 1) \quad (9)$$

The reverse saturation current of diode (I_o) is constant under the constant temperature and found by setting the open circuit condition. Using Eq. (9) let I = 0 (no output current) and solve for I_o.

$$0 = I_{SC} - I_o(e^{\frac{qV}{kT}} - 1) \quad (10)$$

$$I_{SC} = I_o(^{\frac{qV}{kT}} - 1) \quad (11)$$

8.3 Battery Model

The battery model describing the relationship between the voltage, current and the state of charge can be found in [23]. The terminal voltage of a battery can be expressed in terms of its open circuit voltage and the voltage drop across the internal resistance of the battery as given in the following equation [23]:

$$V_B = E_{oc} + I_B R_B \quad (12)$$

Where V_B is battery terminal voltage (V), E_{OC} is battery open circuit voltage (V), I_B is battery current (A) (positive when charging and negative when discharging), R_B is internal resistance of the battery (ohms). The open circuit voltage, E_{OC}, is expressed as a logarithmic function of the state of charge of the battery using the flowing formula [23]:

$$E_{oc} = VF + b\log(SOC) \quad (13)$$

Where *VF* is a full charge rest voltage (V), b is an empirical constant, and *SOC* is battery state of charge. The battery state of charge is the instantaneous ratio of the actual amount of charge stored in the battery and the total charge capacity of the battery at a certain battery current. In the model, it is estimated as [23]:

$$SOC = SOC_0 + (\frac{Q}{BC}) \quad (14)$$

Where SOC_0 is the previous *SOC*, *Q* is amount of exchanged charge from the previous time to the time of interest (C), and *BC* is battery capacity (C). The exchanged charge, *Q*, in Eq. (14) can be determined by summing up the charge flowing over the period of interest which is expressed as [23]:

$$Q = \int_0^t I_B dt \quad (15)$$

Where I_B is battery current (A), the value of I_B can be positive or negative depending on whether the battery is charging or discharging. The positive or negative value therefore represents the direction of the charge that flows into or out of the battery, respectively. The variation of the internal resistance of battery, R_B, is mainly due to two components; namely, the resistance of the electrode, $R_{electrode}$, and the resistance of the electrolyte, $R_{electrolyte}$ as indicated by the following equation [23]:

$$R_B = R_{electrode} + R_{electrolyte} \quad (16)$$

$R_{electrode}$ and $R_{electrolyte}$ are a function of *SOC*, which can be expressed as:

$$R_{electrode} = r_1 + r_2(SOC) \quad (17)$$

$$R_{electrolyte} = [r_3 - -r_4(SOC)]^{-1} \quad (18)$$

Where, r_1, r_2, r_3 and r_4 are empirical constants. It is noted that as these constants have different values for charging and discharging modes, the values of $R_{electrode}$ and $R_{electrolyte}$ are therefore different in those modes as well. Table IV indicates the values of various parameters for the battery model in this study.

Table IV: Values of various parameters for the battery model in this study [23]

Parameter	Charging Mode	Discharging Mode
For open circuit voltage (E_{oc})		
VF	*13.250V*	*12.662V*
B	*0.810*	*0.724*
For internal resistance (R_B)	*0.062 ohms*	*0.055 ohms*
r_1	*0.046 ohms*	*–0.010 ohms*
r_2	*95.638 ohms^{-1}*	*4.270 ohms^{-1}*
r_3	*52.671 ohms^{-1}*	*–100.730 ohms^{-1}*
r_4		

IX. System Controller

Artificial intelligence (AI) techniques are becoming useful as alternate approaches to conventional techniques or as components of integrated systems. They have been used to solve complicated practical problems in various areas and are becoming more and more popular nowadays. Neural Network controller (NNC) is a computational structure where many simple computational elements, called artificial neurons, perform a nonlinear function of their inputs. Such computational units are massively interconnected and are able to model a system by means of a training algorithm. This algorithm attempts to minimize an error measure that is computed in different ways depending on the specific technique used to adjust the connections (i.e., the learning algorithm) [24].

Neural networks have the potential to provide some of the human characteristics of problem solving that are difficult to simulate using the logical, analytical techniques of expert system or standard software technologies. A control system, which includes the NNC, is developed for achieving the coordination between the components of a PV/Diesel/Battery hybrid system as well as control the energy flow.

The purpose of the controller in this work is to ensure that the demand is supplied at all times. The control unit controls the system under weather fluctuation conditions by comparing the summation of PV generator power, diesel generated power and battery power with the reference load power. The difference between them is the error of power which is fed as input to the controller which attempts to reduce the difference between the actual power and the reference load power.

The developed NNC which is shown in Fig. 6 is employed a 2-neuron input layer, an 8-neuron hidden layer and 1-neuron output layer. The input parameters to the NNC are; the reference load power (P_{Lref}) and the error signal (difference between the reference load power and the total output generated power). The output of the NNC is the variation of the battery power $\Delta P_{Battery}$.

Control Strategy of the System

A power management controller is designed for the system to coordinate the power flows among the different power sources. The block diagram of the PV/ Diesel/ Battery hybrid energy system with the associated NNC is shown in Fig.7. During the operation of the hybrid PV/ Diesel/ Battery system, different situations may appear: The input to the controller is the reference load power and the error signal (E) which is the difference between the reference load power (P_{Lref}) and the total system power (P_{PV}, P_{DG}, P_B). The suggested power management strategy can be described by the following three situations shown in Table V.

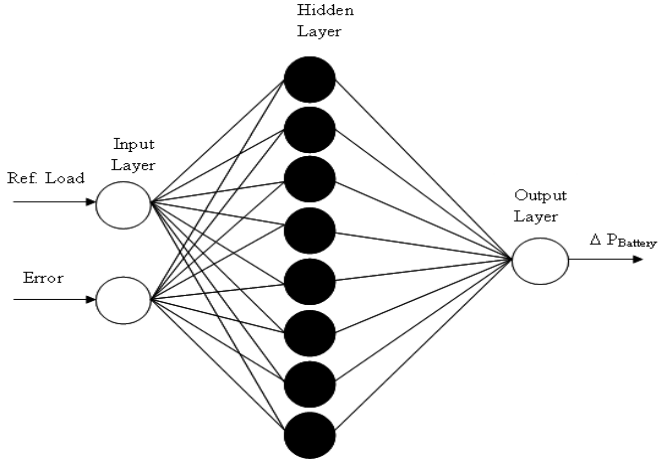

Fig. 6 NNC architecture used for controlling the operation of the PV/ Diesel/Battery system

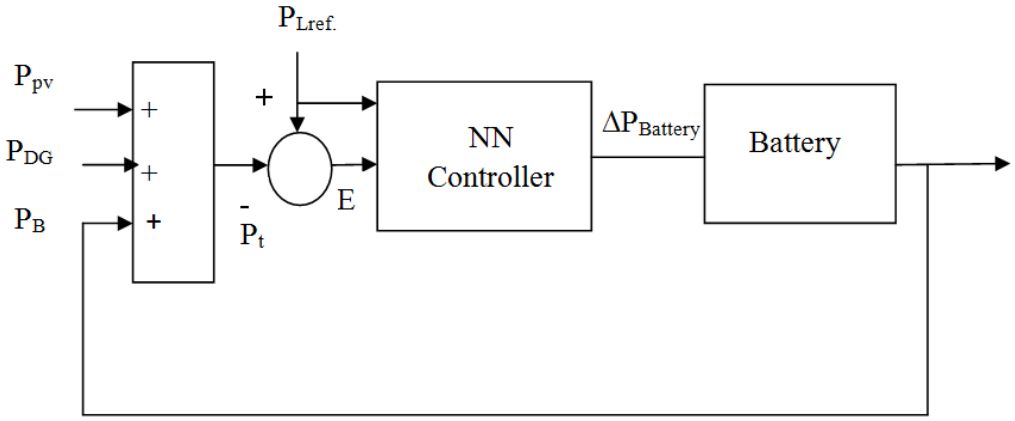

Fig.**7** The block diagram of the PV/ Diesel / Battery power system with NNC

Table V**:** Different situations of controller action for the PV /Diesel/Battery system

Situation	Power Situation	Controller Action
1	$P_t > P_L$	The controller puts the battery in charge condition. When the battery capacity reaches a maximum value, the control system stops the charging process.
2	$P_t < P_L$	The controller puts the battery in the discharge condition. If the battery capacity decreases to its minimum level, C_{batmin}, the control system disconnects the load.
3	$P_t = P_L$	The storage capacity remains unchanged.

X. System Simulation

In this section, the SIMULINK model of hybrid power system based on PV array and diesel generator set is briefly described. MATLAB/ SIMULINK software is used to model the proposed hybrid system. Figure 8 shows the MATLAB/ SIMULINK diagram of the hybrid power system. The system consists of a number of units which are PV array, diesel generator, storage battery bank, load and NNC unit.

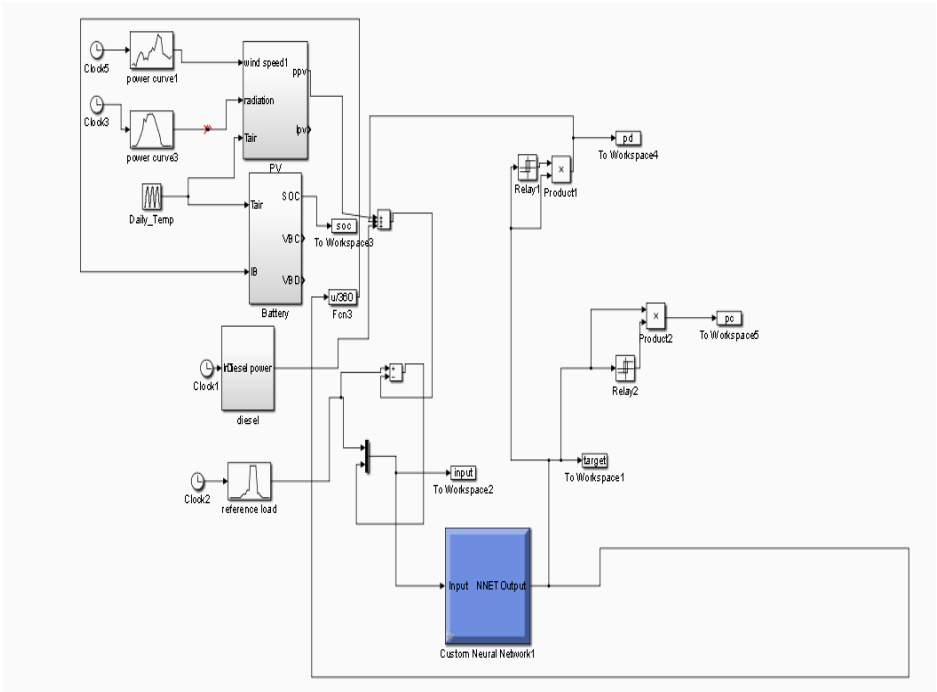

Fig. 8 MATLAB/ SIMULINK block diagram of the PV/ Diesel/Battery with NNC

XI. Result and Discussion

In this section the performance of the PV/ Diesel/Battery power system is evaluated and compared, for two different days (one day in winter and the other in summer). The simulation results of PV/ Diesel /Battery system are reported to verify the effectiveness of the proposed controller under variable weather conditions. Although, the PV generator is the base power source, supplying its maximum output depending on solar radiation levels, the diesel generator and battery bank contribution depending on the load demand.

The power generation of the hybrid power system components such as PV generated power, diesel power and battery power for a typical two days in summer and winter are investigated**.** Figure 9 shows the typical power profile generated by a PV generator for two days in the year, one in winter and the other in summer. A PV generator offers power production during the day's hours between 3:00-18:30 o'clock in summer day, and during winter day between 5:00-15:30 o'clock. The variations of PV output power have the same tendency as the solar insolation.

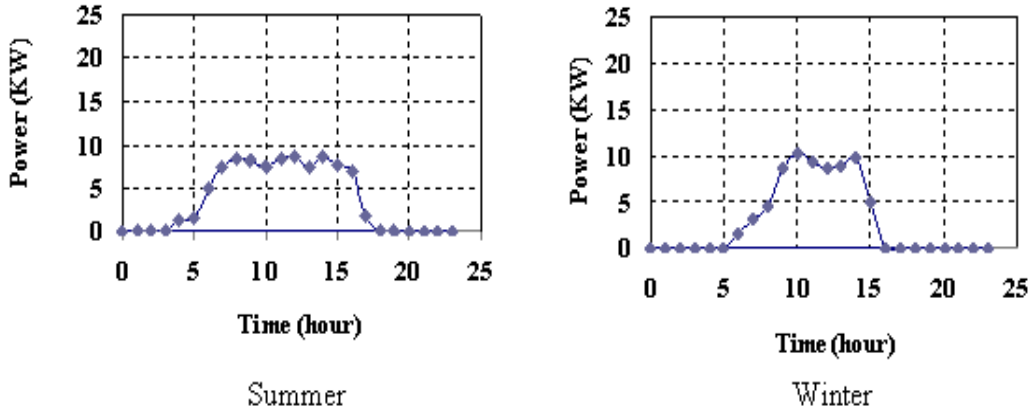

Fig.9 The l power profile generated by a PV generator for two days

Figure 10 shows the typical power profile generated by a diesel generator in two days in the year, one in summer and another in winter. The diesel generator is shown to operate only to supply the deficit in peak load power in conjunction with the battery bank. It is observed that, the diesel generated power in winter is larger than that produced in summer.

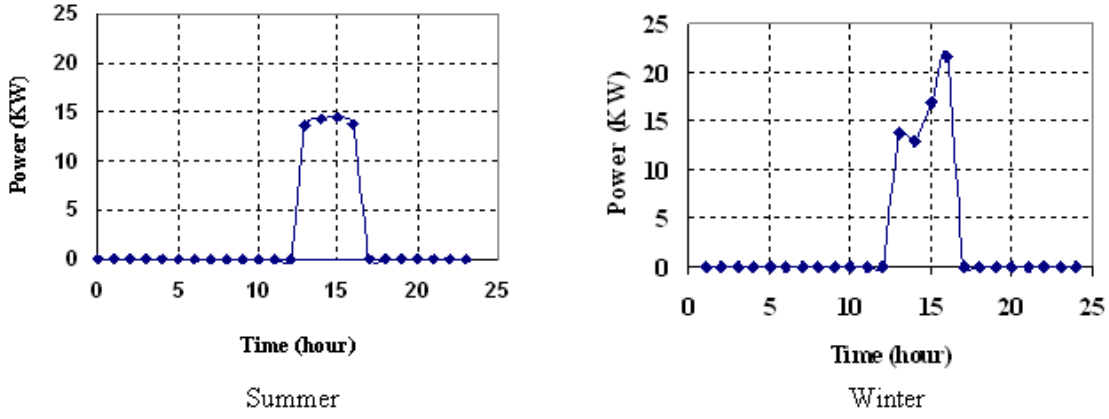

Fig.10 The power profile generated by a diesel generator in two days

The power profile of battery in two days in the year, one in winter and the other in summer is indicated in Fig. 11. When the generated electrical power from both the PV and diesel generator is greater than the power needed by the load, the energy surplus is stored in the battery and the battery is in charge state and the battery power is positive. So it could be clear from Fig. 11 that, when the generated power is more than the required load power, the controller is able to charge the battery bank, and when the required load power is more than generated power of the hybrid system then the controller is able to discharge the battery bank. Power from the battery bank changes (discharge/charge) to maintain the power stability of the system. Figure 12 indicates the NNC output through 24 hours, the error resulting with NNC is approximately zero during the whole day. Thus, it is clear that whatever the day is in summer or in winter the load is completely covered, and this is achieved by

adjusting the battery and/or the diesel to supply the complementary power when there is a deficit on the PV power noitareneg, which is shown to be variable according to the incident solar insolation level for the summer and winter days.

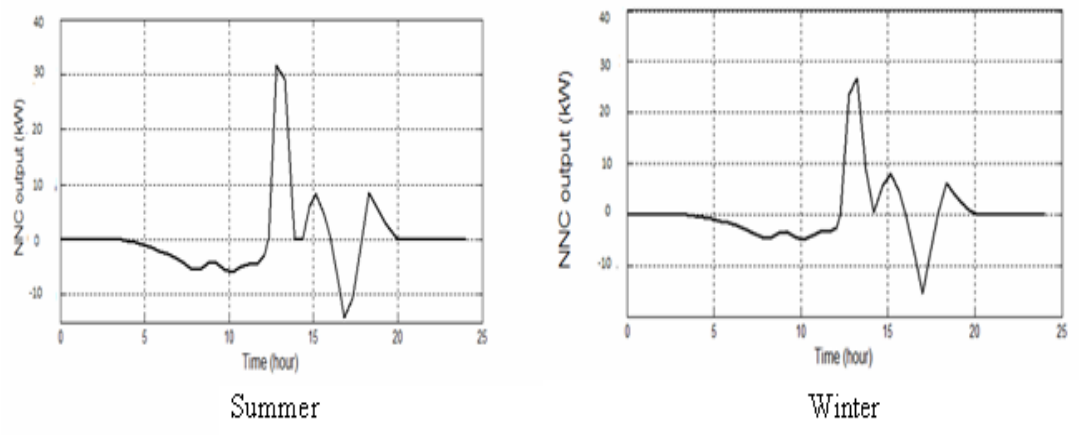

Fig. 11 The power profile of battery in two days in the year

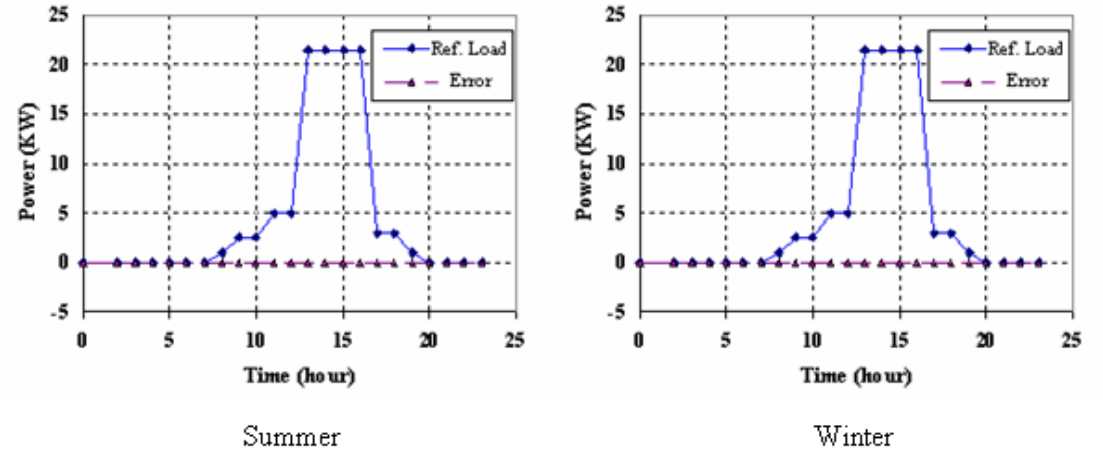

Fig. 12 NNC output through 24 hours in two days in the year

XII. Conclusion

In this paper, a hybrid PV/Diesel/Battery system with appropriate power flow controller was designed and modeled for powering the waste plastic recycling process. A simulation of hybrid PV/Diesel/Battery system using MATLAB/ SIMULINK software was performed. Artificial Neural Network Controller model was developed to simulate the performance of PV/Diesel/Battery power system. The simulation results showed that the performance of the suggested hybrid power system is satisfactory under transient solar and load power conditions. Also the developed NNC can successfully regulate the power flow through the system components and the load. The produced liquid fuel from the waste plastic recycling process is considered as a source of power which can be used as a fuel for the diesel generator power source.

REFERENCE

[1] Anke Brems, Jan Baeyens, and Raf Dewil , Recycling and recovery of post-consumer plastic solid waste in a European context, thermal science, 16(3) , 2011, 669-685.

[2] Ayhan Demirbas, M. Fatih Demirbas, Green energy and technology algae energy, algae as new source of biodiesel (Dordrecht Heidelberg New York, Springer Verlag London Limited, 2010).

[3] Jitendra Kasera, Ankit Chaplot, Jai Kumar Maherchandani, Modeling and simulation of wind-PV hybrid Power system using MATLAB/Simulink, IEEE Students' Conference on Electrical, Electronics and Computer Science, 2012, pp. 1-4.

[4] Lekhasri Samantsinghar & D K Behera, Energy recovery through depolymerisation of plastic reclaimed from MSW-a feasibility study for Bhubaneswar, International Journal of Sustainable Development And Green Economics (IJSDGE), 1 (1), 2012, 14-19.

[5] Achyut Kumar Panda, Studies on process optimization for production of liquid fuels from waste plastics, Ph. D, Chemical Engineering Department, National Institute of Technology, Rourkela, 2011.
[6] Ani Vincent Anayochukwu, Nzeako Anthony Ndubueze, Potentials of optimized hybrid system in powering off-Grid macro base transmitter station site, International Journal of Renewable Energy Research, 3(4), 2013, 861-862.
[7] Aparna Pachori and Payal Suhane, Modeling and simulation of photovoltaic/wind/diesel/battery hybrid power generation system, International Journal of Electrical, Electronics and Computer Engineering 3(1), 2014, 122-125.
[8] Abdelrahman Atallah Z. Saleh, Loai S. Nasrat, Barakat M. Hasaneen, Ahmed F. M. A. Elbendary, Simulations of hybrid renewable energy systems and environmental impact for Qena Al-Gadida City", International Journal of Recent Development in Engineering and Technology, 2(6), 2014, 1-8.
[9] Abd El-Shafy A. Nafeh, Fuzzy Logic Operation Control for PV-diesel-battery hybrid energy, The Open Renewable Energy Journal, 2, 2009, 70-78.
[10] Tiberiu Tudorache, Cristian Roman, The numerical modeling of transient regimes of diesel generator sets, Acta Polytechnica Hungarica 7(2), 2010, 39-53.
[11] Sonam Mishra, Manju Gupta, Modeling & simulation of a photovoltaic energy system, International Journal of Electrical and Electronics Engineering Research (IJEEER), 3(1), 2013, 61-66.
[12] P. Balamurugan, S. Kumaravel, and S. Ashok, Optimal operation of biomass gasifier based hybrid energy system, International Scholarly Research Network, ISRN Renewable Energy, Article ID 3956957, 2011, 1-7.
[13] Hussein A. Kazem and Tamer Khatib, A novel numerical algorithm for optimal sizing of a photovoltaic/wind/diesel generator/battery microgrid using loss of load probability index, International Journal of Photoenergy, Article ID 718596, 2013, 1-8.
[14] Abdulqadiri Bello Abdulqadiri, Elwan Abubakar Ahmed, Comparative techno-economic analysis of hybrid PV/diesel and hybrid wind/diesel energy generation for commercial farm land in Nigeria, International Journal of Engineering and Advanced Technology (IJEAT), 2(1), 2012, 102-106.
[15] New and Renewable Energy Authority, Ministry of Electricity and Energy, Egyptain solar radiation atlas, Cairo, Egypt, 1998.
[16] Waste Plastic to Fuel Zero Pollution Conversion Technology, Plastic Advanced Recycling Corp, www.plastic2x.com/parccontactus/eBrochure.pdf..
[17] "Fuels, chemicals and materials from waste" Royal Society of Chemistry-Environmental Chemistry Group Bulletin, 1-28, www.rsc.org/ecg.
[18] Converting Waste Plastics Into a Resource, United Nations Environmental Programme, Division of Technology, Industry and Economics, International Environmental Technology Centre, Osaka/Shiga, Japan, 2009,www.unep.or.jp/Ietc/.../spc/WastePlasticsEST_Compendium.pdf.
[19] PV Module Product datasheet, Candian solar Inc., www.CandianSolar.com.
[20] Raja Sekhar Gorthi, K. Giri Babu, Dr. S. Shiv Prasad, Simulink model for cost-effective analysis of hybrid system, International Journal of Modern Engineering Research (IJMER), 4(2), 2014, 63-71.
[21] Amit Kumar Singh, Modeling and simulation of micro hydro-diesel hybrid power system for localized power requirement using MATLAB/Simulink, Master of Power Engineering, Jadavpur University, 2013.
[22] T-105 Battery Data Sheet, www.Trojan-battery.com.
[23] Y. Sukamongkol, S. Chungpaibulpatana, W. Ongsakul , A simulation model for predicting the performance of a solar photovoltaic system with alternating current loads, Renewable Energy, 27, 2002, 237–258.
[24] A. Mellit, S.A. Kalogirou, L. Hontoria, S. Shaari , Artificial intelligence techniques for sizing photovoltaic systems: A review, Renewable and Sustainable Energy Reviews 13, (2009), 406–419.

OPEN ACCESS

International
Journal
Of Modern Engineering Research (IJMER)

Strehl Ratio with Higher-Order Parabolic Filter

P Thirupathi[1], T Ramakrishna Goud[2]

[1]*Department of Mathematics, University College of Engineering, Osmania University, Hyderabad, Telangana, India*

[2]*Department of Mathematics, University College of Science Saifabad, Osmania University, Hyderabad, Telangana, India*

Abstract: *In all the branches of science, engineering and technology, it is known that the output due to an input impulse function, spatial or temporal, is never an impulse. There is a spread of the input impulse function in the output due to the noise introduced by the physical device. It was Strehl who first introduced the important image-quality assessment parameter* ***"Definitionshelligkeit"*** *or simply known as the Strehl Ratio (SR) after his name. In this paper, we have studied this parameter for an optical system apodised with the higher-order super-resolving parabolic filters. The results obtained have been discussed graphically.*

Key-words: *Mathematical Optics, Higher order Parabolic Filters, Fourier Optics, Strehl Ratio ..... etc.*

I. Introduction

It is well-known that the image of a point object obtained even with a diffraction limited system is not a point. There is a spread of light flux over a considerable region of space in the focus of the image plane, the actual nature of the spread, known as the Point Spread Function is controlled by the size and shape of the aperture and the type of the non-uniformity of transmission. The importance of this was first realized by LOMMEL [1] and he developed the theory of the distribution of light at and near the focus of an optical system with a circular aperture. In the present paper, we shall present the results of our studies on one of the most important image-quality assessment parameters, the Strehl ratio which is based on the point-spread function of the optical system and is apodised with higher-order parabolic filters. Initially, the Strehl ratio was introduced as **"Definitionshelligkeit"** by its originator Strehl himself. In its original nomenclature, the term **"definition"** was used to mean **"distinctness"** of an outline or **detail** in the image.

II. Previous Studies on Strehl-Ratio

Strehl ratio[2,3] is an important quality assessment parameter for imaging systems and its maximization by the use of amplitude filters has been attempted by several workers. BARAKAT [4], in his study on solutions to Lunenburg's apodization problems, investigated the Strehl ratio for both circular and slit apertures. It is not a physically measurable quantity in the strict sense of the word but nevertheless is a common measure of theoretical performance of the system. WILKINS [5], while solving the modified Lunenburg apodization problems discussed the Strehl ratio. BARAKAT and HOUSTON [6] computed Strehl ratio for an annular aperture possessing third-order and fifth- order spherical aberration. They have adopted the approach of MARECHAL [7] to minimize the mean square deviation of the wave front and hence maximize the Strehl ratio.

DEVELIS [8], in his study of comparisons of methods of evaluation, discussed the Strehl ratio and its relation to Marechal tolerance. HOPKINS [9] stated that for highly corrected optical systems, that is those substantially satisfying the Rayleigh quarter-wave criterion, the Strehl ratio may be used as diffraction based criterion of image quality. Strehl ratio, for circular apertures with a ring- shaped π - phase change, has been investigated by ASAKURA and MISHINA [10]. This work has been extended by ASAKURA and NAGAI [11] to modify annular and annulus apertures. It has been found that the Strehl ratio is always reduced in comparison with that of a clear aperture as long as the semi-transparent and phase annulus aperture is used.

KUSAKAWA [12] has studied the problem of finding the pupil function which minimizes the **dispersion factor** (Excluded energy), subject to the condition that the Strehl ratio, must have a certain prespecified value. The relation between the minimum obtainable **second order-moment** and the prespecified Strehl ratio has been discussed by them. HAZRA [13] studied the problem of maximization of Strehl ratio for the more general case of partially space-coherent illumination. Hazra restated the criterion of "**maximization of Strehl ratios"** as the criterion of **"maximization of effective central illumination within a circle of infinitesimally small radius around the centre of the diffraction pattern"**. The apodization problem of

finding the diffraction pattern has specified Sparrow limit of resolution and the maximum possible Strehl criterion has been solved by PENG and WILKINS [14], for both incoherent and coherent illumination, respectively. MAHAJAN [15] calculated the Strehl ratio, quite accurately from the phase aberration variance. KIBE and WILLIAMS [16] have studied Strehl ratio for a specified Rayleigh limit and for maximum central irradiance. McCUTCHEN'S theorem has been used by LOHMANN and OJEDA CASTANEDA [17], to derive the condition for axial symmetry and periodicity of Strehl ratio, which may serve as a focus criterion.

Formulae for estimating the Strehl, coefficient in the presence of third and Fifth-order aberrations as well as defocusing have been obtained by GRAMMATIN and OKISHEVA [18]. RAMNATHAN [19] examined the effect of Kaiser Pupils on the Strehl ratio. MURTY [20], used co-sinusoidal filters and investigated the influence of apodization and defocusing, with both circular and annular apertures on Strehl ratio. SURENDAR [21] has evaluated the Strehl ratio for apodised optical systems, circular and annular, using Lanczo's filters and determined that apodisations in combination with obscuration further lowers the Strehl ratio. KARUNASAGAR [22] has evaluated the Strehl ratio for both circular and annular apertures apodised with generalized Hanning filters for the first, second, third and the fourth orders of the filter considered. A good account and a comprehensive review on Strehl ratio can be found in the reference [23].

III. Definition of Strehl ratio

STREHL suggested the use of the **relative intensity** of the diffraction as a measure of the image quality. **The strehl ratio (SR)** is defined as the ratio of the central intensity of the PSF of the system and that of the uniform pupil function for diffraction limited system.

$$SR = \frac{I_p(0,0)}{I_A(0,0)} \quad \ldots\ldots\ldots\ldots (1)$$

Where the subscripts P and A referred to the parabolic and Airy pupils respectively. $I_p(0,0)$ represent the intensity point spread function at centre (0,0) of the diffraction pattern due to the optical system used and $I_A(0,0)$ represent the same for the diffraction-limited perfect system. According to the above expression for SR can be written in terms of respective pupil function as follows. Therefore,

$$SR = \frac{\left|G_p(0,0)\right|^2}{\left|G_A(0,0)\right|^2} \quad \ldots\ldots\ldots\ldots (2)$$

Where the symbol G_P and G_A stand for the point spread function for the actual optical system used and the perfect system respectively, thus,

$$SR = 4\left[\int_0^1 f(r)\,r\,dr\right]^2 \quad \ldots\ldots\ldots\ldots (3)$$

Where f(r)= $(\alpha + \beta r^2)^N$ where N=2,3,4&5.

Thus finally,

$$SR = 4\left[\int_0^1 (\alpha + \beta r^2)^N\, r\,dr\right]^2 \quad \ldots\ldots\ldots\ldots (4)$$

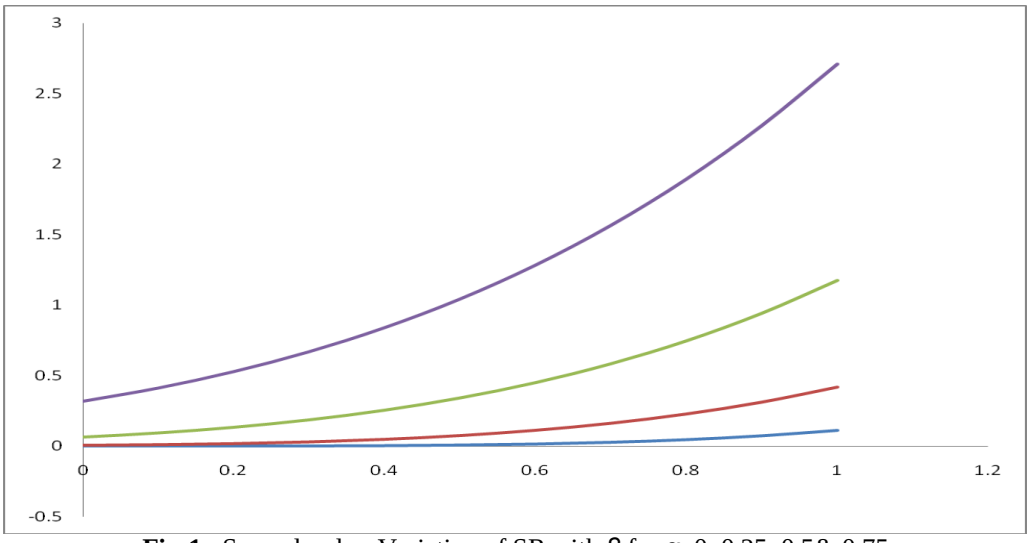

Fig:1 Second order: Variation of SR with β for α=0, 0.25, 0.5& 0.75

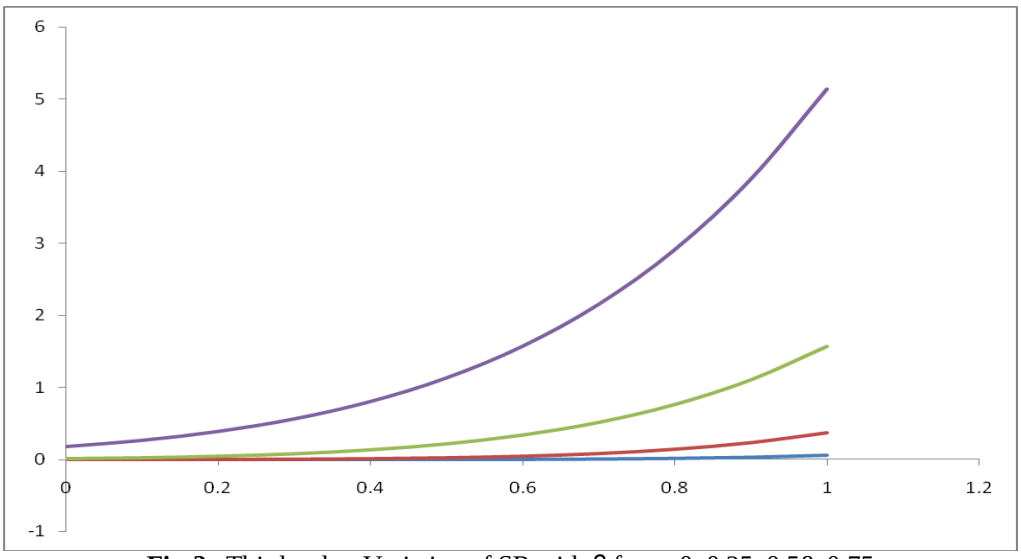

Fig:2 Third order: Variation of SR with β for α=0, 0.25, 0.5& 0.75

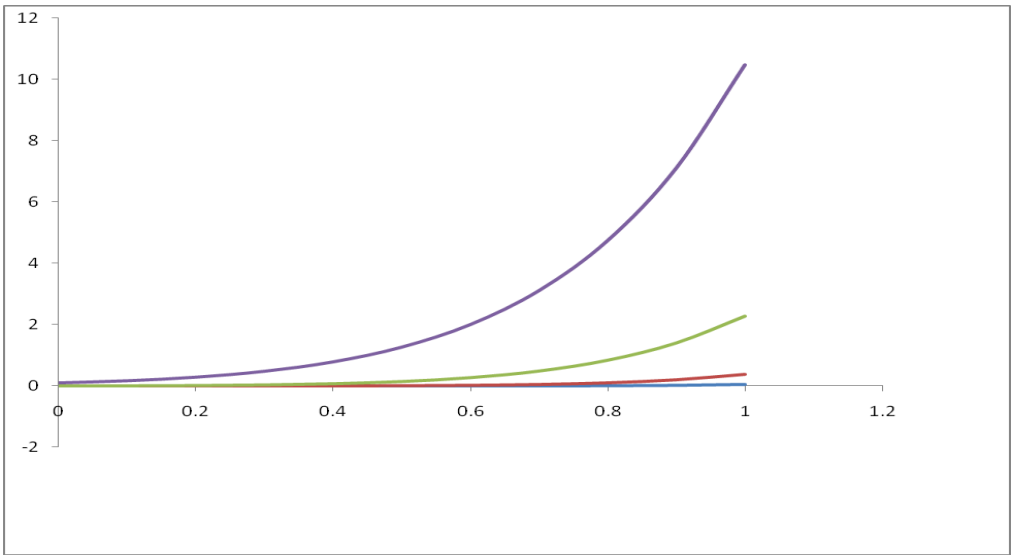

Fig:3 Fourth order: Variation of SR with β for α=0, 0.25, 0.5& 0.75

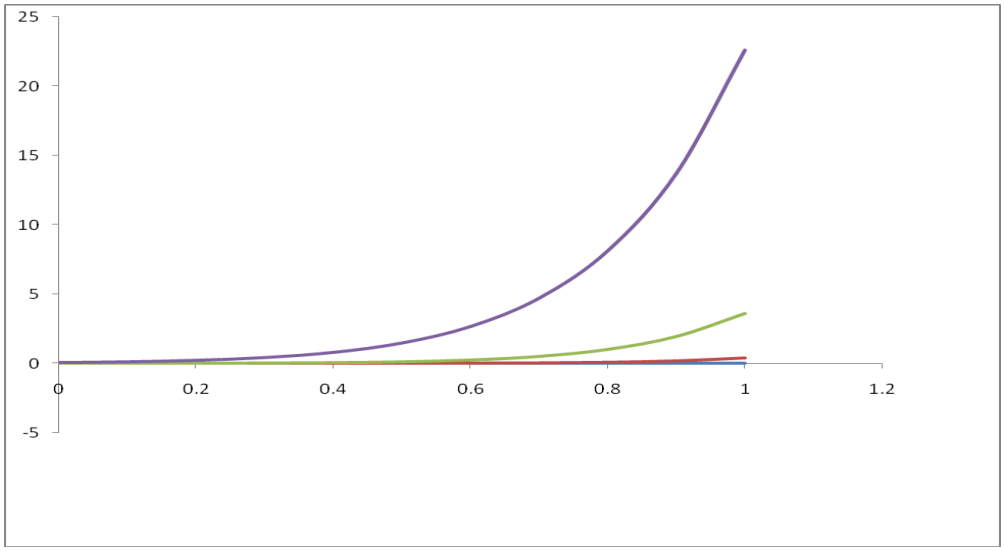

Fig:4 Fifth order: Variation of SR with β for α=0, 0.25, 0.5& 0.75

IV. Results and Discussions

Fig 1 to 4 represents the SR curves for values of $\alpha = 0, 0.25.0.5 \& 0.75$ with β=0 to 1 with deference 0.1. It is observed from the figures that for all the values of α, as the values of β are increased, over all curves increases, maintaining of course, their super-resolving parabolic shape. The most important feature to be observed in this figure is that the order increasing then all the curves starts from origin i.e. for second order the curves start from deferent values and the fourth and fifth order the curves start from origin. If the order increasing the α =0 curve coincide with the β -axis.

In the figure 1,,2,3&4 we have shown variation of Strehl ratio with various values of apodisations parameter and for various values of the D.C.bias α =0,0.25,0.5,0.75 it is observed from the figures that the various SR curves for all the values of α are parabola curves. These curves can therefore, be mathematically represented by the following equation.

$$\text{SR} = \alpha + \beta r^2 \quad \ldots\ldots\ldots (5)$$

Where m is the slope of SR curve and α is its intercept on the SR-axis. The important point to be mentioned here is that the effect of β on the SR values is quantitatively different. Quantitatively, however, the SR values depend prominently on the α values. Because, higher is the value of α the Strehl ratio values are quantitatively higher than those for lower values of α. However, it must be pointed out that we can not increase the value of α indefinitely in order to keep the over-all value of f(r) ≤ 1, in order to satisfy the fundamental passivity condition of an optical system.

REFERENCES

[1]. LOMMEL, E., Abh.Bayer Akad., vol.15, Abth.2, 1885
[2]. STREHL, K., (1895), Z.f Instrummkede, 15, 364
[3]. STREHL, K., (1902), Z., f Instrumkde, 22, 213
[4]. BARAKAT, R. (1962), J. Opt, Soc. Am., 52, 264, 276 & 985.
[5]. WILKINS, J. E., Jr., (1963), J, Opt, Soc, Am., 53, 420.
[6]. BARAKAT, R. and HOUSTON, A., (1963), J. Opt. Soc. Am., 53, 1244.
[7]. MARECHAL, A., (1947), Rev, Opt., 26, 257
[8]. DEVELIS, J.B., (1965), J. Opt. Soc. Am., 55,165
[9]. HOPKINS, H. H., (1966), Opt, Acta. 13, 343.
[10]. ASAKURA, T., MISHINA, H., (1970), Jap. J. Appl. Phys., 9,195
[11]. ASAKURA, T., NAGAI, S., (1971), J, Appl, Phys., (Japon), 10,879.
[12]. KUSAKAWA, T., (1972), Jap, J, Appl, Phys., 11,1632.
[13]. HAZRA, L.N., (1975), j.Opt, (India), 4, 51.
[14]. PENG, W. P., WILKINS, J.E., Jr, (1975), J, Opt, Sci, Am., 65, 1292
[15]. MAHAJAN, V.N., (1983), Appl, Opt., 22 3035

[16]. KIBE, J.N., WILKINS, J.E., Jr., (1984), J, Opt, Soc, Am, A., 1,337.
[17]. LOHMANN, A.W., OJEDA-CASTNEDA, J, (1984), Opt, Acta, 31, 603
[18]. GRAMMATIN, A.P., OKISHEVA, E.V., (1986), Sov, J, Opt, Techno (USA), 53,460
[19]. RAMANATHAN, S., (1986), Ph.D, Thesis, p, 41. Osmania Univ, Hyderabad.
[20]. MURTY, P.V.V.S., (1992), p.32, in Thesis entitled " Studies on Diffracted Field and Imaging Characteristics of Optical Systems with Co sinusoidal Apodisations Filters", presented to Osmania University, for Ph.D.
[21]. SURENDAR, K., (1993), P, 69, Ph.D Thesis, "Studies on Diffracted Field and Image Characteristics of Optical Systems Apodised with Lanczo Filters" SURENDAR, K., GOUD, S, L., MONDAL, P.K., (1992), Acta ,Cienca Indica 18, P, 6134
[22]. KARUNASAGAR, D., (2003), p, 62, Ph.D Thesis: "Studies on the Performance of Optical Systems Apodised with Generalized Hanning amplitude Filters"
[23]. RATHNAM, C., "Fourier Analytical Investigations on the performance of multiple-Annuli coded Aperture in multiplexed Tomography", Ph.D thesis, Osmania University, Hyderabad, A.P, India, 2005.
[24] **P Thirupathi 1** , Sreehari Pagidipally 2 "Strehl Ratio of Point Spread Function with First-Order Parabolic Filter" International Journal of Engineering Research & Technology (IJERT) ISSN: 2278-0181 Vol. 3 Issue 3, March – 2014.

OPEN ACCESS

International
Journal
Of Modern Engineering Research (IJMER)

Effect of Subzero Treatment on Microstructure and Material Properties of EN24 Steel

K. M. B. Karthikeyan[1], R. Gowtham Raj[2], K. Dinesh[3], K. Aravind Kumar[4]
[1]*Assistant Professor,* [2, 3, 4] *B. E students, Department of Mechanical Engineering,*
St. Joseph's College of engineering, OMR, Chennai, Tamilnadu, India

Abstract: *Cryogenic treatment of steels has been widely used for enhancing mechanical properties like hardness, toughness and stable metallurgical structure. Application such as gears, kicker rods, bolts are made of medium carbon alloy steels like EN-24 steel. In these applications, percentage of retained austenite has considerable effects on the life of the material. A comparative study on conventionally heat-treated (CHT) and shallow cryogenic treated (SCT) EN-24 steel was done to evaluate the effect of shallow cryogenic treatment (SCT) on hardness, toughness and the amount of retained austenite present in the structure of EN24 steel. The microscopic structure of cryogenic treated EN24 steel revealed the formation of carbides, both primary and secondary carbides. An estimated amount of 15% retained austenite after CHT tempered condition was less than 2% after SCT tempered condition. Tensile test fractography of subzero treated (SCT) specimen revealed ductile fracture. The maximum hardness observed in case of SCT tempered samples was 415BHN, 15% increase from CHT tempered samples. The maximum impact strength observed in case of SCT tempered samples was 240kJ/m2, 11% increase from CHT tempered samples. Further SCT tempered samples, tempered at 650°C resulted in ductility increase by 55% as compared to CHT tempered samples without sacrificing hardness.*

Index Terms: *EN24 Steel, hardness, shallow cryogenic treatment, retained austenite, tensile test fractography.*

I. INTRODUCTION

Cryogenic treatment is an added heat treatment technique over conventionally heat-treated materials. It is an effective method to improve the engineering performance of steels [1] - [2]-[3]-[4]. Cryogenic treatments are carried out in two aspect, the shallow cryogenic treatment (SCT) conducted at temperature between -75°C (198°K) and -90°C (183°K), the deep cryogenic treatment (DCT) conducted at temperatures below -195°C [8]. The commonly used cryogenics are liquid nitrogen (-195.8°C), liquid helium (-269°C), liquid hydrogen (-252.9°C), methane (-161.5°C) and solid carbon dioxide (-78°C). Cryogenic treatment increases the mechanical properties of cutting tool materials, die materials and bearing materials such as hardness, toughness, tensile strength, wear resistance and corrosion resistance [3]-[7]. The lifetime of material under mechanical wear, get affected by the retained austenite present in it [1]-[7]. In working conditions there may be chances for micro structural transformations of retained austenite into martensitic structure which causes parts to break due to sudden brittleness. This investigation revealed the fact that the retained austenite present after conventional heat treatment is reduced substantially by lowering the quenching temperature up to subzero temperature without sacrificing hardness and toughness of the heat treated material.

II. LITERATURE REVIEW

Cryogenic treatment reduces percentage of retained austenite into tempered martensitic structure thereby increasing material resistance to wear [2]-[7]. Cryogenic treatment not only helps in microstructural transformations (retained austenite to martensite) but also helps in improving the metallurgical structure [5]-[7]. For high carbon steels the retained austenite transformation to martensite structure, require deep cryogenic treatment [1]-[2]-[7]. In this investigation, the shallow cryogenic treatment (SCT) on EN24 medium carbon steel was conducted and the effect of SCT on material hardness and toughness was investigated. EN24

(817M40T–Molybdenum steel) is a high tensile alloy steel known for its wear resistance and used for high strength applications. EN24 steel is surface-hardened to enhance wear resistance by induction hardening or nitriding processing. Application includes propeller or gear shafts; connecting rods; aircraft landing gear components etc.

The EN24 specimens are kept in a sealed insulated container containing solid carbon dioxide known as dry ice for a period of 24 hours. The temperature was maintained at -76°C (197°K). The directions followed during the investigation are ***a)*** retained austenite during conventional heat treatment (CHT) process transforms to martensitic structure after shallow cryogenic treatment (SCT) and ***b)*** increase in material hardness as an effect of martensitic transformation imparted into the material due to cryogenic treatment.

III. PROCESS METHODOLOGY

A. Specimen preparation

Specimens were prepared as per ASTM standards from annealed EN24 alloy steel bar with nominal material composition of C-0.35%, Mn-0.45%, Si-0.11%, Cr-0.91%, Ni-1.31%, Mo-0.21%. For comparative study, two sets (CHT and SCT) of specimens with four samples under each treatment were prepared for standard laboratory tests.

B. Conventional heat treatment

The specimens are first austenized at a temperature of 850°C and quenched in a gas-carburizing furnace with neutral proportions of one-inch one hour soak condition. The specimens treated are free of quench cracks imply a little or nil residual stress. After confirming, the as quenched hardness, specimens are either double tempered (2T) or triple tempered (3T). The specimens are soaked for 90 minutes duration at temperatures of 450°C and 650°C followed by air-cooling at room temperature as shown in Fig. 1.

C. Shallow Cryogenic treatment

Shallow Cryogenic treatment is a supplement treatment to conventional heat treatment and it involves three stages. *Stage-1*: Conventional heat treatment (CHT) and quenched, *Stage-2*: Subzero treatment (SCT at -78°C) and *Stage-3*: Subzero treatment (SCT) followed by double or triple tempering process at temperatures 450°C and 650°C and cooled down at room temperature. Subzero treatment is carried in an insulated container with solid CO_2 at a temperature of -78°C and then bringing it to room temperature followed by tempering as shown in Fig. 1.

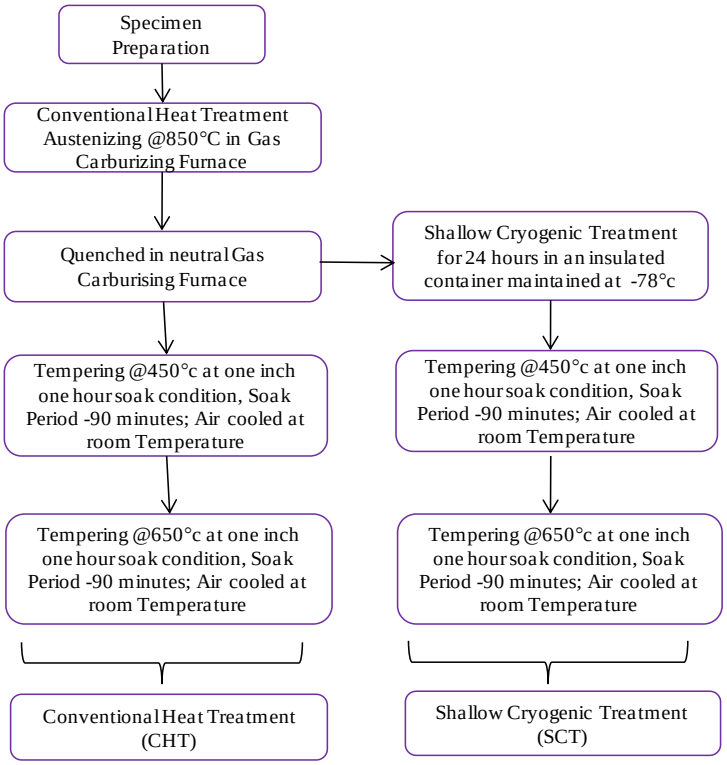

Fig. 1. Process flow chart

IV. RESULTS AND ANALYSIS

A. Hardness Test

Hardness testing is widely used for material evaluation due to its simplicity and low cost relative to direct measurement of many properties [9]. Hardness testing does not give a direct measurement of any performance properties, hardness correlates with material strength, wear resistance and other mechanical properties [9]. The annealed EN24 Steel sample has an equivalent hardness of 217BHN and the average hardness of the CHT quenched samples was 363BHN. The maximum hardness observed in case of SCT tempered samples were 415BHN. There is a considerable increase in the hardness value of the subzero treated samples as compared to conventionally heat treated and annealed EN24 Steel. The average value of hardness is tabulated for reference in Table 1.

Table 1. Hardness test Results

Sl. No	Specimen	Hardness (BHN)	Micro Vickers hardness (HRC)
1	Annealed	217	239
2	CHT Tempered	363	388
3	SCT Tempered	415	465

B. Impact Test

The impact test was performed as per ASTM A370 (standard test method and definitions for mechanical testing of steel products) to study the effect of cryogenic treatment on the toughness of EN-24 steel. The most common test is the Charpy V-notch impact test, in which the standard specimen is struck opposite the notch by a heavy falling pendulum. The toughness is expressed in terms of the kinetic energy absorbed by the fracture. The result of tests revealed that conventional heat treated and quenched samples absorbed 17.5 joules of energy whereas subzero tempered samples absorbed 24 joules. The average value of toughness is tabulated for reference in Table 2.

Table 2. Toughness test Results

Sl. No	Description of samples	Impact value (Joules)	Impact Strength (KJ/m2)
1	CHT and quenched	17.5	175
2	CHT and tempered	21.50	215
3	SCT and tempered	24.00	245

C. Tensile test

Tensile test was performed on six different samples of EN24 steel. The test was done on annealed, CHT quenched, CHT tempered at 450°C, SCT quenched, SCT tempered at 450°C and SCT tempered at 650°C. The SCT samples are tempered under two different temperatures, 450°C and 650°C to understand its elastic and elasto-plastic elongation. The tensile test was carried out according to ASTM A370-05. The test specimen dimensions are presented in Fig. 2.

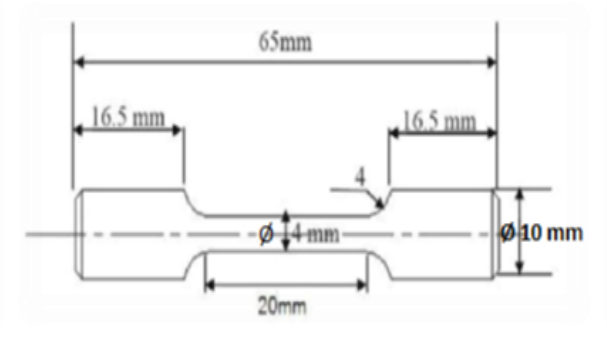

Fig. 2 Tensile Test Specimen

From Table 3 it has been observed that the tensile strength of subzero treated samples is more than that of the conventionally quenched and annealed samples. Tempering after subzero treatment at 450°C has lesser elongation, greater ultimate strength, greater yield strength than tempering at 650°C. The experimental results reveal that it is optimum to use tempering temperature scale at 450°C.

Table 3. Tensile Test Results

Sl. No	Specimen	Tensile Strength (MPa)	Yield Strength (MPa)	Elongation (%)	Reduction (%)
1	Annealed specimen	849.95	759.04	15.60	59.04
2	CHT Quenched	2177.99	2095.58	10.00	39.88
3	CHT Tempered @450°C	1580.16	1517.81	7.20	21.36
4	Subzero Quenched	2248.55	2158.45	10.40	37.83
5	Subzero Tempered @450°C	1587.31	1550.29	4.80	23.44
6	Subzero Tempered @650°C	1184.33	1098.79	11.20	29.56

D. Graphical Analysis

Percent elongation is the ability of the material to flow plastically before facture. Even though there is no proportional relationship between ductility and load carrying capacity of the material under elasto-plastic region, yet the material of low percent elongation can withstand greater loads. From Table 3, SCT tempered EN24 steel has least percent elongation in elasto- plastic region; it means that it can withstand greater loads compared to CHT tempered EN24 steel. SCT tempered EN24 steel, tempered at 450°C has lesser elongation, greater ultimate strength, greater yield strength and high ductility when compared to CHT tempered EN24 steel. The stress strain curve for different material treatment condition is presented in Fig. 3.

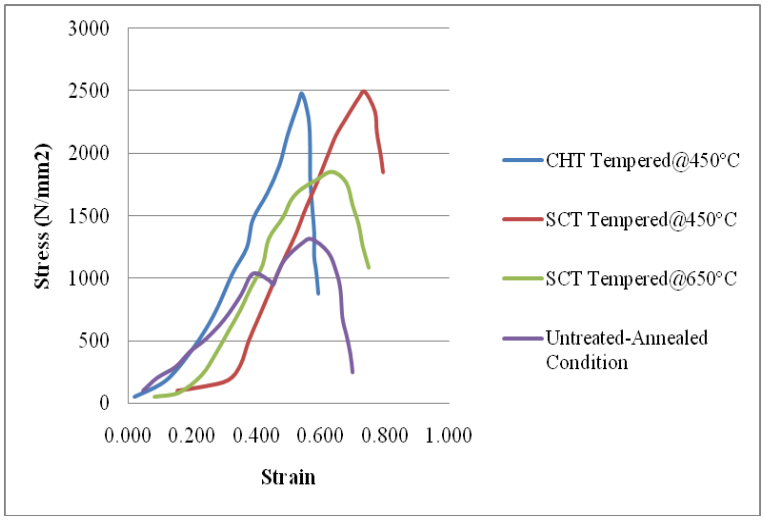

Fig. 3. Stress strain curves –Comparative Trend

E. Tensile Test Fractography analysis using SEM

Broken tensile test samples were tested for fractography analysis. Test Sample made with cut section diameter of 10 mm and length 20 mm molded using Bakelite. The specimen are ground progressively with finer SiC water proof papers from 120 to 1000 grit to produce polished flat surface. The surface was etched using 2% Nital and cleansed using alcohol. In CHT quenched specimen presences of voids are visualized. More over the grain refinement is very small it means that the particles are coarse and load withstanding capacity will be less.

Fractography test of Annealed EN24 material as shown in Fig. 5, exhibits ductile fracture mode with cracks and micro voids. The annealed material under heavy loads develops voids in the structure that prolongs and collapse.

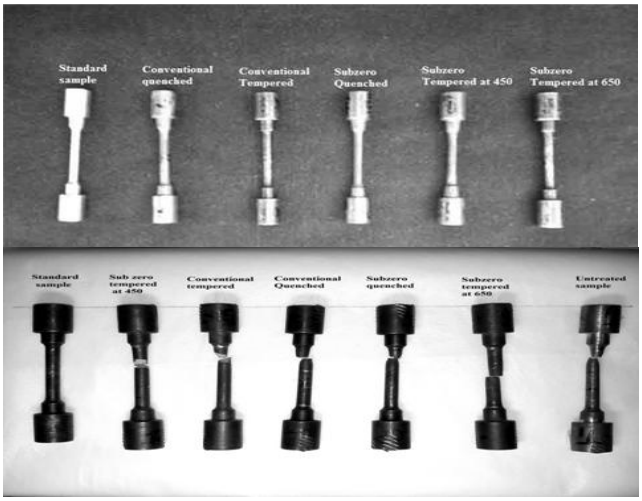

Fig. 4. Specimens before and after tensile testing

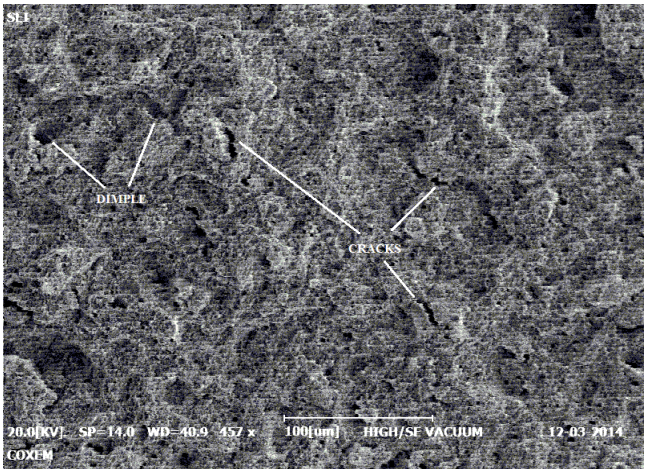

Fig. 5. SEM Fractography of Annealed EN24 material.

Fractography test for CHT tempered material as shown in Fig. 6, exhibits ductile fracture mode. It means that due to elongation the material reduces its diameter and after yielding failure takes place. Dimples and hot tear phenomenon are clearly seen in the surface, observed uneven breakage due to unevenly scattered carbides.

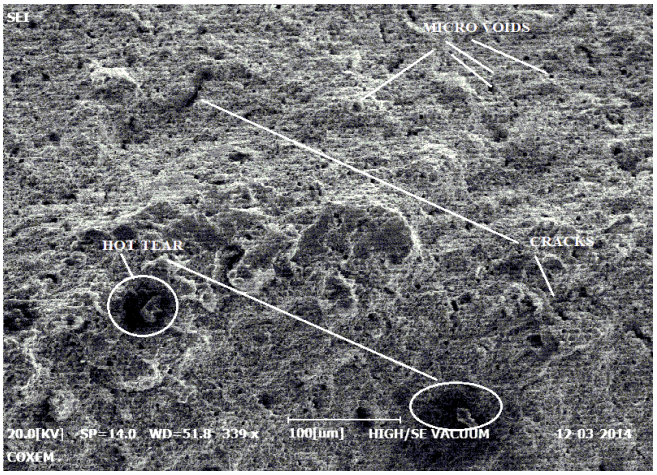

Fig. 6 SEM Fractography of CHT Tempered EN24 material

Fractography test of SCT Tempered EN24 material as shown in Fig. 7, exhibits micro cracks, small in size when compared to CHT quenched samples. The presence of dimples are negligible hence even fracture is visible in the picture. Plastic flow prior to fracture was observed as shown in Fig.8. The secondary carbides observed in the microstructure of SCT Tempered at 450°C as shown in Fig.11, increases the wear resistant property of the material.

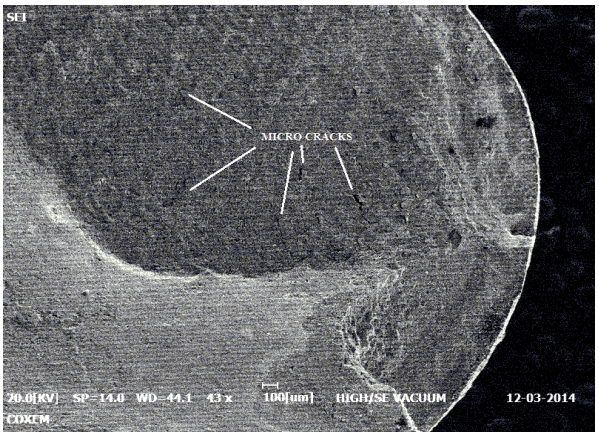

Fig 7. SEM Fractography of SCT Tempered EN24 material

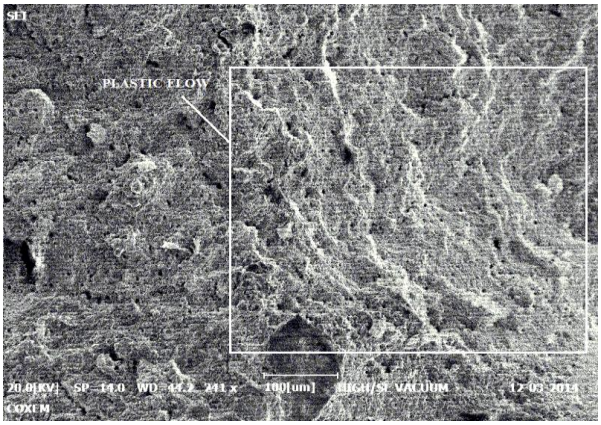

Fig 8. SEM Fractography of SCT Tempered EN24 material Showing Plastic Flow behavior before fracture

F. Microscopic study

The test samples for micro examination grounded using different grades of emery papers (200, 400, 800, and 1200) then polished using diamond paste. It is cleansed using etchant Nital 2% and allowed to dry. The microstructure was examined using Optical Microscope. Fig.9 shows the microstructure of annealed EN24 Steel revealing fine pearlite matrix structure.

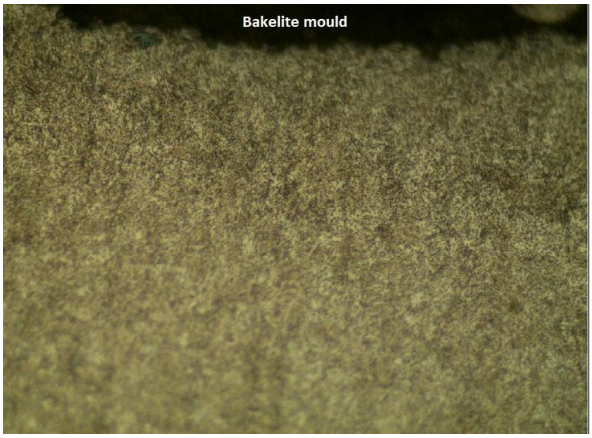

Fig 9. Microstructure of annealed En-24 steel, Mag: 500X

The microstructure of steel at conventionally heat treated condition as shown in Fig.10 reveals an estimated amount of the retained austenite was 15%. The microstructure in Fig.10 where more of white spots (retained austenite) present is responsible for the decrease in the hardness value of the specimen.

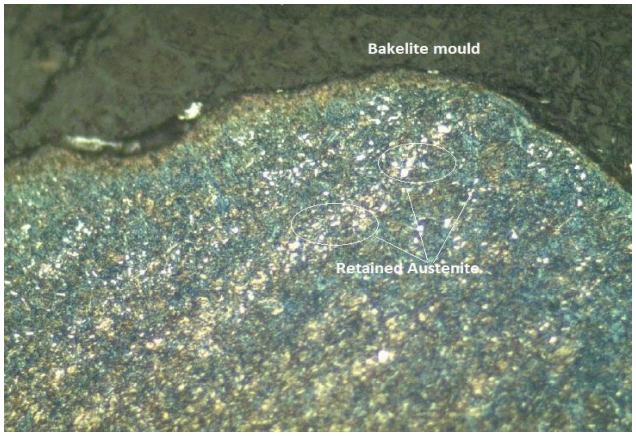

Fig 10. Microstructure of CHT and quenched En-24 steel

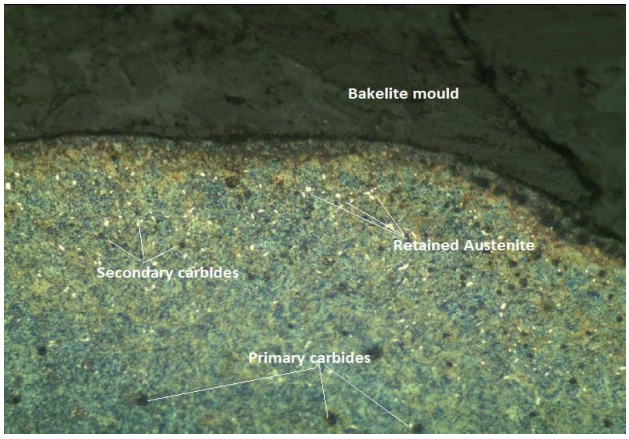

Fig 11. Microstructure of SCT Tempered at 450°C

For subzero treated sample the retained austenite present was observed to be less than 2%. The retained austenite found as shown in Fig.11 are scattered and the presence of secondary carbides on the surface are evident. Secondary carbides formed mainly due to transformation of retained austenite particles to temper martensitic.

V. CONCLUSIONS

The comparative study made on the effect of cryogenic treatment on EN-24 steel revealed the following:

- A substantial improvement in hardness from 363BHN for conventionally heat treated (CHT) material to 415BHN for subzero treated (SCT) material.
- A substantial improvement in toughness of material from 17.5 Joules in case of annealed sample to 24 Joules in case of SCT sample.
- A substantial improvement in ultimate tensile strength in case of SCT EN24 steel with decrease in percentage elongation. The tensile strength and yield strength of SCT tempered samples depicted marginal improvement than CHT tempered samples, tempered at 450°C, but percentage elongation for SCT tempered samples reduced by 50% compared to CHT tempered samples.
- The Tensile test fractography study indicates the mode of failure was ductile in each case.
- Presence of retained austenite from 15% in case of conventionally heat treated condition has been reduced to less than 2% in case of subzero treatment.

The mechanical testing of shallow cryogenically treated EN24 carbon steel material exhibited increase in mechanical properties like hardness, toughness and substantial reduction in percentage of retained austenite.

VI. ACKNOWLEDGEMENT

The authors acknowledge the services M/s.Micro- Hard Processing-Heat Treatment, Ambattur, M/s.Microlab, Ambattur Industrial Estate, and St. Joseph's College of Engineering, OMR, Chennai, Tamilnadu, to encourage us to carry out a part of this research.

REFERENCES

[1] Lukwinder Pal Singh, Jagtar Singh, "Effects of Cryogenic Treatment on High Speed Steel Tools," Journal of Engineering and Technology, vol. 14, issue 2, pp.88-93, July –December 2011.

[2] P. I. Patel, R. G. Tated, "Comparison of Effects of Cryogenic Treatment on Different Types of Steels: A Review", International Conference in Computational Intelligence (ICCIA) 2012, Published by IJCA Journal, ICCIA- Number 9, March 2012

[3] Harpreet Singh, Er.B.S.Ubhi and Er. Harvinder Lal, "Improvement in the Corrosion Rate and Mechanical Properties of Low Carbon Steel through Deep Cryogenic Treatment", International Journal of Scientific and Technology Research, volume 2, issue 6, pp.10-29, June 2013

[4] Ajit Behera, S.C. Mishra, "Comparitive Study of Cryo-Treated Steel", International Journal of Scientific and Technology Research, volume 1, issue 7, pp.46-48, August 2012

[5] Kamran Amini, Said Nategh, Ali Shafiey and Mohhamad Ali Solanty, "To Study the Effect of Cryogenic Heat Treatment on Hardness and the amount of Residual Austenite in 1/2304 Steel", Metal, volume 13, pp.1-7, May 2008

[6] D.Candane, N.Alagumurthi and K.Palaniradja, "Tribological Studies on Deep Cryogenic Treated AISI T42 High Speed Steel using Response Surface Methodology", Advances in Materials, volume 2(2), pp.12-22, April 2013

[7] D. Candane, N.Alagumurthi and K.Palaniradja, "Effect of Cryogenic Treatment on Microstructure and Wear Characetristics of AISI M35 HSS", International Journal of Materials Science and Applications, volume 2(2), pp.56-65, March 2013

[8] Dr.Abbas A Hussein, Murtadha Qasim Idan Alkinani, "Effect of Cryogenic Treatment on the Properties of Low Carbon A858 Steel, Journal of Engineering, pp.837-843, volume 18, July 2012

[9] Handbook of Analytical Methods for Materials, Materials Evaluation and Engineering, Inc, pp.35. http://mee-inc.com/

International Journal of Modern Engineering Research (IJMER)

Volume : 4 Issue : 11 (Version-2) ISSN : 2249-6645 November- 2014

Contents :

OPEN ACCESS

International
Journal
Of Modern Engineering Research (IJMER)

GPS cycle slips detection and repair through various signal combinations

M. E. El-Tokhey[1], T. F. Sorour [2], A. E. Ragheb[3], M. O. Moursy[4]

[1]*Professor of surveying and geodesy, Public Works department, Faculty of Engineering, Ain Shams University, Egypt*

[2]*Associate Professor of surveying and geodesy, Public Works department, Faculty of Engineering, Ain Shams University, Egypt*

[3]*Assistant Professor of surveying and geodesy, Public Works department, Faculty of Engineering, Ain Shams University, Egypt*

[4]*Instructor of surveying and geodesy, Public Works department, Faculty of Engineering, Ain Shams University, Egypt*

Abstract: *GPS Cycle slips affect the measured spatial distance between the satellite and the receiver, thus affecting the accuracy of the derived 3D coordinates of any ground station. Therefore, cycle slips must be detected and repaired before performing any data processing. The objectives of this research are to detect the Cycle slips by using various types of GPS signal combinations with graphical and statistical tests techniques, and to repair cycle slips by using average and time difference geometry techniques. Results of detection process show that the graphical detection can be used as a primary detection technique whereas the statistical approaches of detection are proved to be superior. On the other hand, results of repairing process show that any trial can be used for such process except for the 1st and 2nd time differences averaging all data as they give very low accuracy of the cycle slip fixation.*

Key Words: *Cycle slips detection and repair, Quartiles, Time difference, Z-score.*

I. Introduction

It is well known that there are two fundamental types of GPS observations which are the pseudo-range (code) observations and the carrier phase observations **[1]**. The pseudo-range observations are immune against cycle slips. On the other hand, carrier phase measurements are much more accurate than pseudo-range observations. The accuracy of pseudo-range measurement is in the meter (or sub-meter) level, whereas in the centimeter level for carrier phase measurements. So, cycle slips must be detected and then repaired for the carrier phase observations to determine accurate position **[2]**.

Cycle slips detection is the process of checking the occurrence of the cycle slips and then discovering the specific epoch which the slipped cycles took place. Cycle slips repair process takes place after detecting the time of occurrence when the cycle slips took place at a certain epoch **[3]**. Cycle slip repair involves the determination of the integer number of slipped cycles, and then removing these slipped cycles from the data (i.e.; correcting all subsequent phase observations for this satellite and this carrier by a fixed amount which is the slipped cycles **[4]**.

Many researches were concerned with the handling of cycle slips, leading to many different techniques. Such developed techniques are different in their mathematical basis, required pre-requisite data, type of used GPS receiver and possibility of application in real-time. In this paper, many different techniques of cycle slip detection and repairing are tested. Such techniques are different in the nature of the used data and the used test quantity. Also, some new approaches will be tried to increase the quality of the detection and repairing processes.

II. Different used test quantities in detecting and repairing GPS cycle slips

Single series of phase observations cannot detect and repair cycle slips alone, but they should be combined with other quantities and the behavior of this combination should be analyzed. This combination is called test quantity which should have a smooth behavior **[5]**. In other words, when plotting the test quantity versus time, a smooth curve is created. If a sudden jump (discontinuity) appears in that curve, this will indicate a cycle slip at this epoch. There are some factors should be taken into consideration when choosing the test quantity, which are **[6]**:

1. Type of receiver used (single or dual frequency)
2. Kind of observation mode (static or kinematic)

3. Type of positioning mode (single point or relative positioning)
4. The availability of some information such as satellite and station coordinates

On the other hand, different types of test quantities are available based on:

- Linear combinations between carrier phase observations (L_1) and (L_2) which are used in case of dual frequency receivers
- Combination between carrier phase and pseudo-range observations in case of both single or dual frequency receivers
- Differencing between the carrier observations or any of the previous combinations between two successive epochs in case of both single or dual frequency receivers.

The main aim of using combining different types of GPS observables to reduce or to eliminate most of the GPS errors except some random errors such as the receiver noise for improving the quality of the detection process. Table (1) summarizes the main characteristics of the used linear combination in this paper according to Zhen **[7]**, Abdel Maged **[8]** and Yongin Moon **[9]**; such listed linear combinations will be used informing the different applied test quantities

Table 1: Different types of linear combinations (Φ: Phase range, λ: wave length of the carrier, $\emptyset$: Phase measurement, P: measured code pseudorange, t: time, f: wave frequency)

Linear combination	Equation	Advantages	Disadvantages
Time differences between observations	$\Delta\Phi(t_2 - t_1) = \lambda\Delta\emptyset(t_2 - t_1)$	Ionospheric and troposheric effect for small sampling rate data are highly reduced	multipath and noise still remain
Carrier phase and Code combination	$\Phi - P = \lambda\emptyset - P$	Satellite and receiver clock error, tropospheric delay and the geometric range are eliminated	Ionospheric delay is doubled, while multipath and noise still remain
Ionospheric free combination (L3)	$\emptyset_{L3} = \emptyset_{L1} - \frac{f_{L2}}{f_{L1}} * \emptyset_{L2}$	Ionospheric delay is eliminated	The noise level increases and it reaches about twice the noise affecting L1 carrier
Geometric free combination (Lgf)	$\Phi_{gf} = \Phi_{L1} - \Phi_{L2} = \lambda_{L1}\emptyset_{L1} - \lambda_{L2}\emptyset_{L2}$	Satellite and receiver clock error, tropospheric delay and the geometric range are eliminated	Ionospheric delay, multipath and noise still remain
Wide lane combination (Lwl)	$\emptyset_{wl} = \emptyset_{L1} - \emptyset_{L2}$	longer wavelength is useful for cycle-slips detection and ambiguity resolution	noise is much greater than the original signals
Narrow lane combination (Lnl)	$\emptyset_{nl} = \emptyset_{L1} + \emptyset_{L2}$	Noise decreases	Ionospheric delay increases
Ionospheric residual (IR)	$\emptyset_{IR} = \emptyset_{L1} - \frac{f_{L1}}{f_{L2}} * \emptyset_{L2}$	Satellite and receiver clock error, satellite orbital error, tropospheric delay and the geometric range are eliminated	Ionospheric delay still remains

III. Methodology of application

The used data series collected from a (LEICA GX-1230) dual frequency GPS receiver of sampling rate 15 seconds with time span 3 hours in a static mode in RINEX format.

For the detection process, (36) test quantities are used, with variable time differences namely (1^{st}, 2^{nd}, $3^{rd}$and 4^{th} time differences) in terms of: (L1) and (L2) carrier phases, (L3) ionospheric free linear combination, (Lwl) wide lane linear combination, (Lnl) narrow lane linear combination, (Lgf) geometric free linear combination, (IR) Ionospheric Residual combination, combination of (L1) carrier and (C/A) code, and

combination of (L2) carrier and (P) code. But for the repair process, the time differences of the original signal (L1) or (L2) carrier phase are studied as it is known that cycle slips may occur in any or both carriers, thus number of slipped cycles are required to be determined separately for each original signal. Computer programs and codes for the detection and the repair process were established using MATLAB package which deal with RINEX format.

To illustrate the effect of cycle slips at different test quantities, simulated slipped cycles with different values were applied at different observation time. Simulated slipped cycles are applied once on L1 and once on L2 carrier phase and on both L1 and L2 at the same time, with 5 different simulated values (1, 5, 10, 100 and 100 000 slipped cycles) at a specific epoch. This is done to have the ability of assessing the reliability of all the used techniques of detecting and repairing GPS cycle slips.

IV. GPS cycle slips detection

Cycle slips detection is the process of checking the occurrence of the cycle slips and then discovering the specific epoch which the slipped cycles took place. The detection process depends mainly on the studying of the effect of the slipped cycles on the various types of test quantities that are mentioned before.

Cycle slips can be detected by two main techniques through different test quantities used mainly; graphical detection and statistical tests.

4.1 Graphical detection

Cycle slips can be detected graphically (visual inspection), when a test quantity or its time difference is plotted against time and thus the occurrence of any spike in the plot represents a cycle slip at this epoch.

Graphical detection for the used data series can be interpreted visually for (36) test quantities for the dual frequency receiver's data series. X-axis represents the observations time, while the Y-axis represents the different test quantities along with their time differences and their units are cycles for all linear phase combinations and their time differences. For the phase and code combinations and their time differences, their units are in meters. A sample of the graphical detection for the 4 time differences of the L1 carrier phase is shown at Figure (1) and Figure (2).

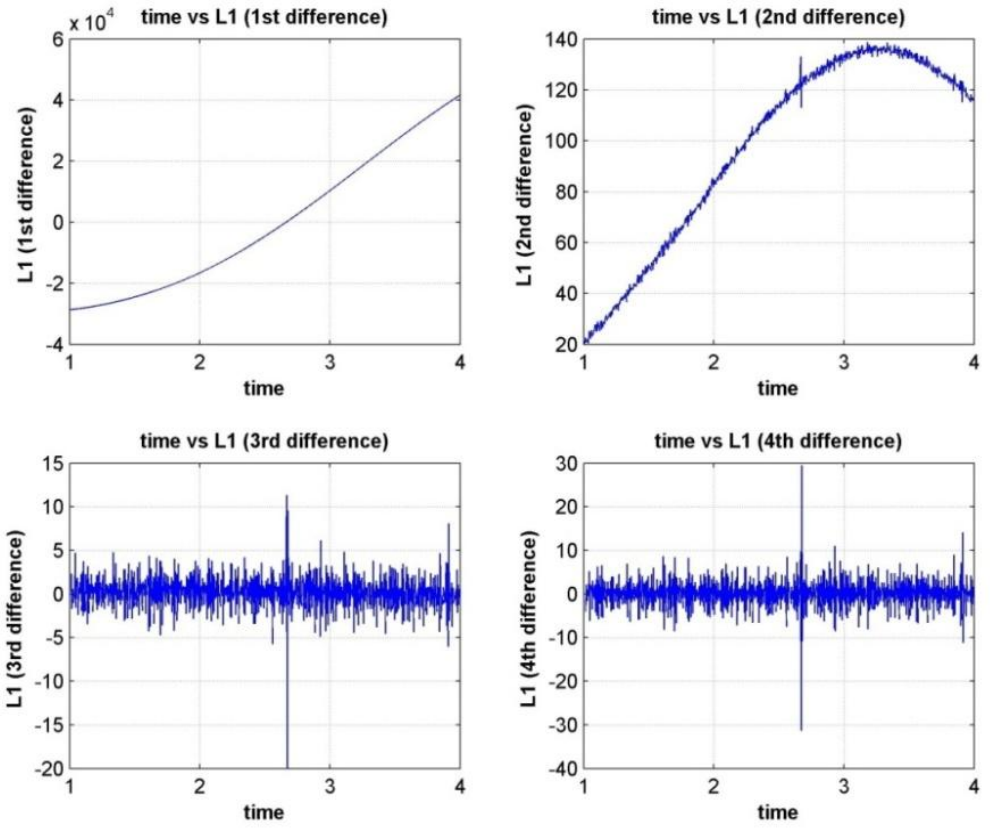

Figure 1: Effect of 10 simulated slipped cycles on time differences of L1 carrier (in cycles)

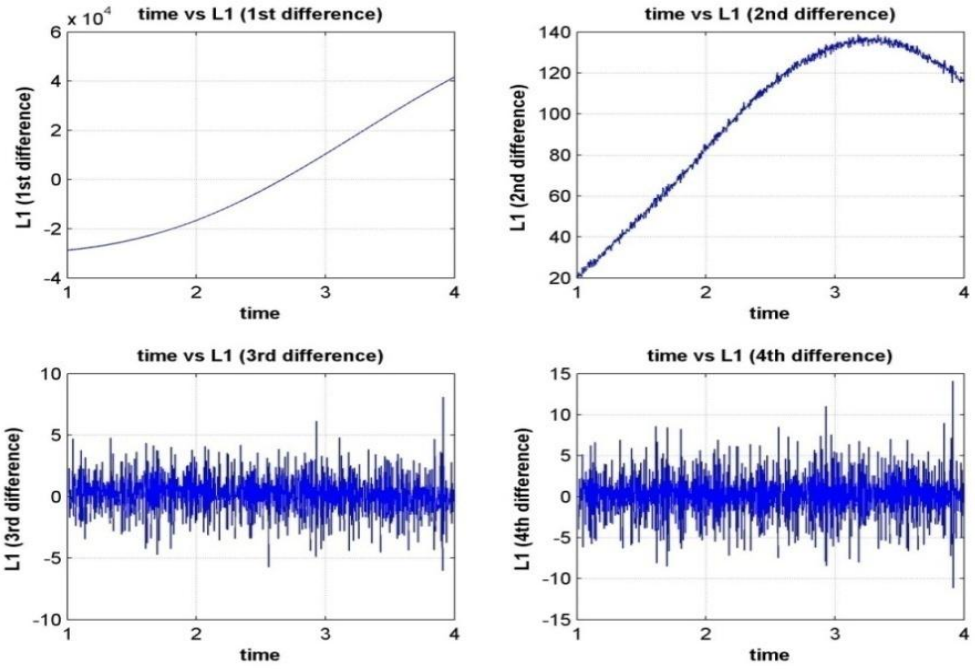

Figure 2: Effect of one simulated slipped cycle on time differences of L1 carrier (in cycles)

It is very obvious that 1 cycle slip can't be inspected graphically for any of the time differences of L1 carrier phase, while the 10 cycles can be observed graphically for the 2nd, 3rd, and 4th time differences. As a closing remark, all the tested test quantities and different values of simulated slipped cycles are summarized in Table (2) and Table (3):

Table 2: Graphical detection of cycle slips of various test quantities and their time differences (D: slipped cycles are Detected, N: slipped cycles are Not detected)

Test quantity	Time diff.	Simulated slipped cycles				
		1	5	**10**	100	100000
L1 or L2	1st	**N**	N	**N**	N	D
	2nd	**N**	N	**D**	D	D
	3rd	**N**	D	**D**	D	D
	4th	**N**	D	**D**	D	D
L3	1st	N	N	N	N	D
	2nd	N	D	D	D	D
	3rd	N	D	D	D	D
	4th	N	D	D	D	D
Lwl	1st	D	D	D	D	D
	2nd	D	D	D	D	D
	3rd	D	D	D	D	D
	4th	D	D	D	D	D
Lnl	1st	N	N	N	N	D
	2nd	N	N	D	D	D
	3rd	N	N	D	D	D
	4th	N	N	D	D	D
Lgf	1st	D	D	D	D	D
	2nd	D	D	D	D	D
	3rd	D	D	D	D	D
	4th	D	D	D	D	D
IR	1st	D	D	D	D	D
	2nd	D	D	D	D	D
	3rd	D	D	D	D	D
	4th	D	D	D	D	D

Table 3: Graphical detection of cycle slips of various test quantities and their time differences (D: slipped cycles are Detected, N: slipped cycles are Not detected)

Test quantity	Time diff.	Simulated slipped cycles				
		1	5	10	100	100000
L1 & C/A	1st	N	N	D	D	D
	2nd	N	N	D	D	D
	3rd	N	N	D	D	D
	4th	N	N	D	D	D
L2 & P	1st	N	N	D	D	D
	2nd	N	N	D	D	D
	3rd	N	N	D	D	D
	4th	N	N	D	D	D

As a closing remark, it is obvious that not all cycle slips can be detected graphically especially that slips which have small values, thus another approach should be followed in detecting cycle slips which are the statistical approach.

4.2 Statistical tests for outlier (cycle slips) detection

Cycle slip could be considered to be an outlier in any data series **[10]**. Outlier is defined as "an observation (or subset of observations) which appears to be inconsistent with the remainder of that set of data". However, the identification of outliers in data sets is far from clear given that suspicious observations may arise from low probability values from the same distribution or perfectly valid extreme values for example**.** There are many methods to reduce the effect of outliers; one of the most used alternatives is the robust statistics which solves the problem of removing and modifying the observations that appear to be suspicious. In some situations robust statistics are not practical, thus it is important to investigate the causes of the possible outliers, and then remove only the data points clearly identified as outliers.

There are many statistical tests for outlier detection, here the most two famous ones are used and will be illustrated in the next subsection namely Z-score and lower and upper quartiles

4.2.1 Z-score

A Z- scores outlier detector is used to identify any outlier in the data set. Z scores are based on the property of the normal distribution **[10]**

$$Zscores = \frac{x_i - \bar{x}}{s} \quad (1)$$

Where $s = \sqrt{\frac{\sum_{i=1}^{n}(x_i - \bar{x})^2}{n-1}}$

Wherex_i: is a data sample, $\bar{x}$: is the mean value, s: is the standard deviation, n: is the number of the data set

A common rule considers observations with |Z scores| greater than 3 as outliers. This method has a main disadvantage which is both the mean value and the standard deviation is greatly affected by the outliers **[10].**

4.2.2Lower and upper quartile

Lower and upper quartile method is considered a good outlier detector. The main idea of this statistical test is creating lower and upper limits (fences) for the observations, while these fences depend on three main elements. The first element is called the first quartile (Q1) which is the middle number between the smallest number and the median of the data set, while the second quartile (Q2) is the median of the data and the third quartile (Q3) is the middle value between the median and the highest value of the data set, see Equations (2) and (3):

$$Lower\ fence = Q1 - 1.5 * (IQR) \quad (2)$$

$$upper\ fence = Q3 + 1.5 * (IQR) \quad (3)$$

Where IQR is called inter-quartile range which is measure of statistical dispersion and is equal to the difference between the third quartile (Q3) and the first quartile (Q1) as shown in equation (4):

$$IQR = Q3 - Q1 \quad (4)$$

Any data lying outside the defined boundary can be considered an outlier (i.e. any data below the lower fence or above the upper fence can be considered as an outlier).The sensitivity of each test quantity is studied to determine the most suitable and sensitive test quantity for cycle slip detection. Sensitivity is defined as the number of slipped cycles which can be detected at a test quantity by using any statistical tests for outliers' detection.

The sensitivity of each test quantity at three different times (1:30:00 AM, 2:40:00 AM and 3:30:00 AM) for each data series, are determined from Z score and lower and upper quartiles tests as shown in Figures (3) and (4) respectively. X-axis represent the different test quantities, where (1): L1, (2): L2, (3): L3, (4): Lwl, (5): Lnl, (6): Lgf, (7): IR, (8): L1 & C/A and (9): L2 & P, while Y-axis represent the sensitivity in unit of cycles. Three bars of each test quantities represent the sensitivity at three different times which are mentioned before. This is to study the effect of the time of GPS data acquisition process on the resulted sensitivity.

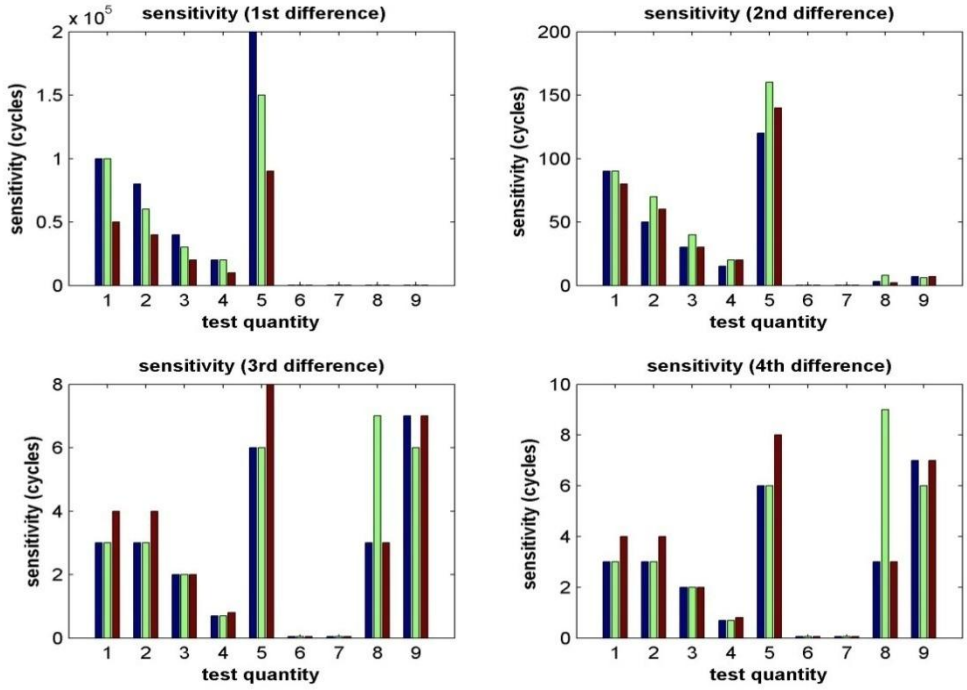

Figure3: Sensitivity of different test quantities for three different epochs by using Z-score test

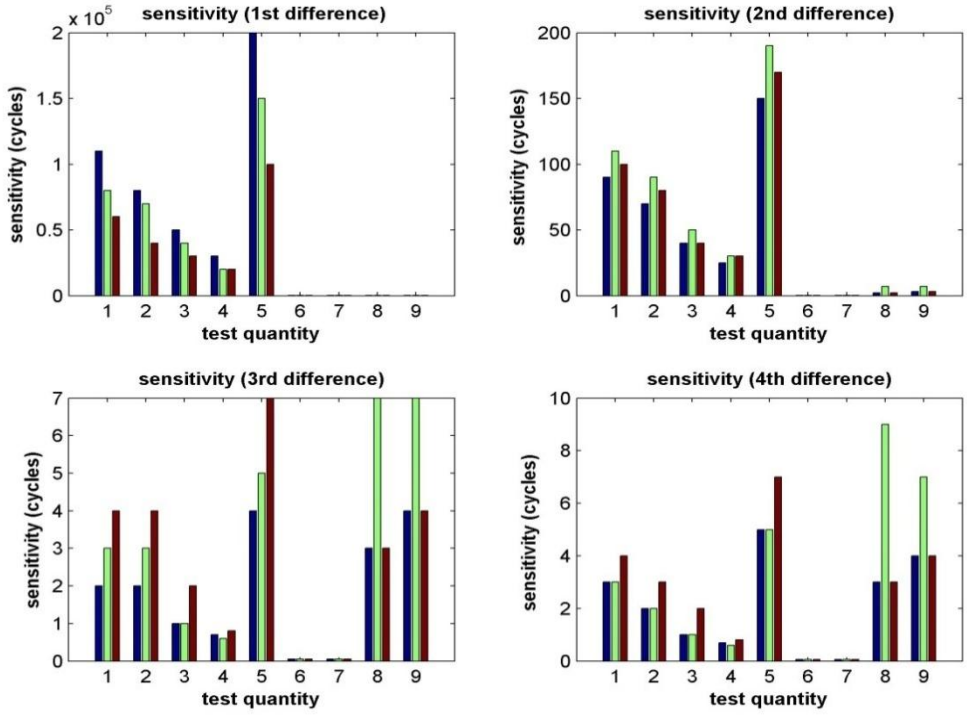

Figure 4: Sensitivity of different test quantities for three different epochs by using Quartile test

It is very obvious that the sensitivity improved when the time differences increase for different test quantities, (i.e. the sensitivity of the 4th time difference is much more better than the sensitivity of the 1st time difference for any test quantity except for (L1) & C/A and (L2) & P combinations)

For anytime difference, the Lgf and IR are the most sensitive test quantities as the sensitivity of both reach to less than one cycle, while the sensitivity of (L1) & C/A and (L2) & P combinations ranges between 3 to 8 cycles, while the Lnl considered to be the worst test quantity. It is concluded that the sensitivity differ from time to another for the same data series; as it is function in the error budget of the received signal in different times.

V. Repair of GPS cycle slips

Cycle slip repair process takes place after detecting the time of occurrence of cycle slips at a certain epoch. L1 and L2 carrier phase along with their time differences are used in the repairing process. There are two different methods used here in this research for the purpose of repair cycle slips: Cycle slips repair using average method and time difference geometry.

5.1Cycle slips repair using average method

The main idea of the average method for cycle slips repair depends on after detecting the epoch at which the slipped cycles occur, the values of L1 or L2 time differences at this epoch will be removed, and then replace these contaminated values with the average values of the time differences of L1 or L2, then the values of the slipped cycles can be obtained by subtracting the contaminated values from the average values. The average values can be obtained through two main trials:

1. Taking the average values for the 2 epochs just after and just before the contaminated epochs.
2. Taking the average values for all the epochs excluding the contaminated epochs (i.e. the average for all the data except the biased epochs).

5.2 Cycle slips repair using time difference geometry method

The main idea of this method depends on the scheme of time difference of the effect of the cycle slips on the L1 or L2 carrier phase time differences as shown in Table (4). It is very obvious from the scheme of time difference, that the 1st time difference is affected by the slipped cycles at an epoch with value of these slipped cycles; while the 2nd time difference is affected by the cycle slips at a zone of 2 successive epochs with the values of these slipped cycles; but for the 3rd time differences, it is contaminated at a zone of 3 epochs and finally the 4th time difference is affected by the slipped cycles at a zone of 4 epochs. The number of slipped cycles can be directly obtained from the 3rd and 4th time differences using all possible combinations of resulted differences

Table 4: represents the effect of cycle slips of value Є on the scheme of time differences of carrier phase observations (y: represent various time differences)

Ti	y(ti)	y1	y2	y3	y4
t1	0				
		0			
t2	0		0		
		0		0	
t3	0		0		0
		0		0	
t4	0		0		Є
		0		Є	
t5	0		Є		-3Є
		Є		-2Є	
t6	Є		-Є		3Є
		0		Є	
t7	Є		0		-Є
		0		0	
t8	Є		0		0
		0		0	
t9	Є		0		
		0			
t10	Є				

The uncertainty of each time difference for both L1 and L2 carrier phase and its time differences are studied, which is the accuracy of obtaining the integer number of the slipped cycles. In the repairing process, the

uncertainty of each method is studied as shown in Tables (5), (6) and (7). Three columns express the uncertainty of each time difference for all data for each table of different data:

1. The first column expresses the uncertainty in units of cycles, fraction of cycles are used.
2. The second one represents the uncertainty in units of cycles; integer numbers of cycles are used.
3. The third column expresses the uncertainty in units of meters, to show the effect of the slipped cycles on the distance between the receiver and the satellites.

Table 5: Uncertainty using average method of satellite at three different times

Carrier	Time	Time diff	Average between the biased epochs			Average for all data		
			Cycles	Integer cycles	m	Cycles	Integer cycles	m
L1	1:30:00	1st	0.662	1	0.126	24038	24038	4574.2
		2nd	0.609	1	0.116	46.733	47	8.893
		3rd	1.434	1	0.273	0.094	0	0.018
		4th	3.654	4	0.695	2.517	3	0.479
L2		1st	0.52	1	0.127	18731	18731	4574.2
		2nd	0.477	0	0.116	36.411	36	8.892
		3rd	1.104	1	0.27	0.066	0	0.016
		4th	2.871	3	0.701	1.96	2	0.479
L1	2:40:00	1st	0.028	0	0.005	13462	13462	2561.8
		2nd	0.86	1	0.164	1.124	1	0.214
		3rd	1.175	1	0.224	1.087	1	0.207
		4th	2.204	2	0.419	0.621	1	0.118
L2		1st	0.018	0	0.004	10490	10490	2561.8
		2nd	0.67	1	0.164	1.964	2	0.48
		3rd	0.926	1	0.226	1.079	1	0.264
		4th	1.708	2	0.417	4.018	4	0.981
L1	3:30:00	1st	1.376	1	0.262	254.46	254	48.422
		2nd	0.036	0	0.007	3.06	3	0.582
		3rd	1.67	2	0.318	0.327	0	0.062
		4th	7.94	8	1.511	2.894	3	0.551
L2		1st	1.069	1	0.261	198.15	198	48.389
		2nd	0.032	0	0.008	0.385	0	0.094
		3rd	1.304	1	0.319	3.3	3	0.806
		4th	6.194	6	1.513	4.297	4	1.049

Table 6: Uncertainty of the 7 trials of 3rd time difference using time diff. geometric method

Trials	L1			L2		
	Cycles	m	Nearest cycle	Cycles	m	Nearest cycle
(ξ)	0.041	0.008	0	0.039	0.01	0
(-2ξ)	0.662	0.126	1	0.52	0.127	1
(ξ)	0.147	0.028	0	0.126	0.031	0
(ξ,-2ξ)	0.455	0.087	0	0.36	0.088	0
(ξ,ξ)	0.094	0.018	0	0.082	0.02	0
(-2ξ,ξ)	0.491	0.093	0	0.389	0.095	0
(ξ,-2ξ,ξ)	0.378	0.072	0	0.301	0.074	0

Table 7: Uncertainty of the 15 trials of 4thtime difference using time diff. geometric method

Trials	L1			L2		
	Cycles	m	Nearest cycle	Cycles	m	Nearest cycle
(ξ)	2.519	0.479	3	1.961	0.479	2
(-3ξ)	0.455	0.087	0	0.36	0.088	0
(3ξ)	0.491	0.093	0	0.389	0.095	0
(-ξ)	0.242	0.046	0	0.16	0.039	0
(ξ,-3ξ)	0.288	0.055	0	0.22	0.054	0
(ξ,3ξ)	0.262	0.05	0	0.199	0.048	0
(ξ,-ξ)	1.381	0.263	1	1.061	0.259	1
(-3ξ,3ξ)	0.473	0.09	0	0.374	0.091	0
(-3ξ,-ξ)	0.281	0.053	0	0.23	0.056	0
(3ξ,-ξ)	0.307	0.059	0	0.252	0.061	0
(ξ,-3ξ,3ξ)	0.046	0.009	0	0.041	0.01	0
(ξ,-3ξ,-ξ)	0.279	0.053	0	0.208	0.051	0
(-3ξ,3ξ,-ξ)	0.371	0.071	0	0.298	0.073	0
(ξ,3ξ,-ξ)	0.258	0.049	0	0.191	0.036	0
(ξ,-3ξ,3ξ,-ξ)	0.01	0.002	0	0.016	0.004	0

It is found from the uncertainty of the 1stand 2nd time differences for the average of all data considered to be the worst fixation methods, while the uncertainty of the 4th time difference for both trials range between 2 and 8 cycles which can be considered to be unpleasant fixation method, while the uncertainty of the other trials range between 0 and 3 cycles which is reasonable for the fixation procedure.

Any of these trials can be used in the fixation process (7 trials for the 3rd time difference or 15 trials for the 4th time difference) as they range from 0 to 1 cycle for the majority of all trials.

VI. Conclusion

Based on the used data and the obtained results, many important conclusions are extracted from this paper, these conclusions are going to be categorized according to the detection and repair methods at first, followed by a summary of obtained conclusions:

6.1 Graphical detection

All the test quantities are graphically interpreted when there are very large numbers of slipped cycles (100000 cycles) at a certain epoch.IR and Lgf along with their time differences are considered to be the most sensitive test quantities as they are affected by very small values of cycle slips reach to 1 cycle or less.

6.2 Detection by (Z score) and (Quartiles)

1. 3rd and 4th time differences are more sensitive than 1st and 2nd time differences for test quantities L1, L2, L3, Lwl, Lnl.
2. 2nd time difference is more sensitive than 1st time differences for all test quantities except L1&C/A combinations, L2&P combinations, Lgf, and IR.
3. 3rd and 4th time differences gives almost the same sensitivity for all test quantities, however they may vary in 1 cycle in some test quantities.
4. For test quantities L1&C/A combinations and L2&P combinations: the 1st time difference is more sensitive than 2nd, 3rd and 4th time differences, the same for Lfg and IR
5. L3 for all time differences are more sensitive than L1 and L2 for all time differences.
6. Lwl for all time differences are more sensitive than L1, L2, and L3 for all time differences.
7. Lnl for all time differences are the worst sensitive test quantities.
8. Lgf& IR for all time differences are the most sensitive test quantities.

6.3 Comparing between sensitivity by using (Z score) and (Quartiles)

1. Z score is better than quartiles in sensitivity for both 1stand 2ndtime differences for all test quantities.
2. Quartile is better than Z score for both 3rdand 4thtime differences for all test quantities.
3. Quartile has the advantage; that it can detect both very small and very large slipped cycles at the same data series without needing to make a loop conditions at formulated programs.

6.4 Repair by average method

1. For 1st and 2nd time differences: average between biased epochs is better than average for all data
2. For 3rdand 4th time differences: average between biased epochs is less than average for all data
3. 1st time difference average for all data is the worst repair method.

6.5 Repair by geometric method

For all data series, any of these trials can be used (7 trials for the 3rd time difference or 15 trials for the 4th time difference) as it ranges for 1 cycle only for the majority of all trials.

6.6 Overall Summary

Graphical detection method can be considered as a primary stage for cycle slips detection, while the statistical tests (Z-score or quartiles) for cycle slips detection are considered to be more reliable than graphical detection thus they identify the occurrence of the cycle slips at specific epochs. In case of using dual frequency receivers data series any time difference for Lgf or IR can be used as test quantities for the cycle slip detection by any statistical tests, while in case of using single frequency receivers data series, 1st time difference of L1 and C/A combination can be used as test quantity for the cycle slip detection by any statistical tests.

There are many factors affect the sensitivity of the detection procedure which are: the time span of the observations, type of the used receiver (single or dual), the type of used antenna, the type of test quantity, type of the used statistical test, and the existence of large signal noise, ionospheric effect, multipath, and other biases. There are many factors affect the uncertainty of the repair procedure which are: the time span of the observations, and the existence of large signal noise, ionospheric effect, multipath, and other biases. Any trial can be used for the cycle slips repair by geometric method and average method except for the 1st and 2nd time differences for the average for all data as they give very low accuracy of the cycle slip fixation.

REFERENCES

[1] El-Rabbany, A., 2002, "Introduction to Global Positioning System (GPS)", ArtechHousemobile communication series, Boston, London.

[2] Sorour, T.F., 2004, "Accuacy study of GPS surveying operations involving long baselines", Ph.D. Thesis, Department of public works department, Faculty of Engineering, Ain Shams University, Cairo, Egypt.

[3] Liu, Z., 2011, "A new automated cycle slip detection and repair method for a single dual-frequency GPS receiver", Journal of Geodesy, 85(3), 171-183.

[4] Hofmann Wellenhof, B., H. Lichtenegger and J. Collins, 2001, "Global Positioning System- theory and practice 5th edition", Springer, Verlag, New York, USA.

[5] Sorour, T.F., 2010, "A new approach for cycle slips repairing using GPS single frequency Data",World Applied Sciences Journal 8(3): 315-325, 2010. ISSN: 1818-4952.

[6] Seeber,G., 2003, "Satellite Geodesy: Foundation, Methods and Applications", Walter de Gruyter, Berlin, New York.

[7] Zhen, D., 2012, "MATLAB software for GPS cycle slips processing", GPS Solut.(2012) 16:267-272, Springer, Verlag, New York, USA.

[8] Abdel Mageed, K.M., 2006, "Towards improving the accuracy of GPS single point positioning", Ph.D. Thesis, Department of public works department, Faculty of Engineering, Ain Shams University, Cairo, Egypt.

[9] Yongin Moon, 2004, "Evaluation of 2-Dimensional Ionosphere Models for National and Regional GPS Networks in Canada", Msc, department of GeomaticsEngineering, Calgary, Alberta, Canada.

[10] Garcia,FAA, 2012, "Tests to identify outliers in data series", Pontifical Catholic University of Rio de Janeiro-habcam.whoi.edu.

OPEN ACCESS

International
Journal
Of Modern Engineering Research (IJMER)

A Review on Implementation of TPM in Manufacturing Industry

Suchisnata Pradhani[1], Prof. Ajit Senapati[2]
[1]*Department of Mechanical Engineering, Biju Patnaik university of Technology, India*
[2]*Department of Mechanical Engineering, Biju Patnaik university of Technology, India*

Abstract: *The intent of the study is to appraise the challenges faced by manufacturing industries to implement Total Productive Maintenance (TPM). The scheme of this research is to critically analyze the factors influencing TPM implementation in manufacturing organizations, and to formulate comprehensive strategy for overcoming impediments to successful TPM implementation . The introduction of several philosophies such as Corrective Maintenance (CM), Preventive Maintenance (PM) or Total Productive Maintenance (TPM) have allowed extra solutions to a process planning problem faced by company in comparison to the conventional fire-fighting syndrome. This main purpose of this study was to focus on developing a framework of maintenance strategy TPM initiatives to confront exponential global challenges.*

Keywords: *Total productive maintenance (TPM), manufacturing organizations, TPM implementation, Manufacturing performance. Maintenance management system framework*

I. INTRODUCTION

Globalization and economic turbulence is the hallmark of contemporary business environment. The manufacturing sector over the past three decades has experienced an unprecedented degree of change embracing radical changes in management approaches, product and process technologies, customer expectancies, supplier attitudes as well as competitive behavior [1]. The dynamic business environment turns out to be highly exigent and manufacturing industries are finding it acutely difficult to endure the competition and customer expectations. The global marketplace has witnessed an exponential upsurge in pressure from consumers and competitors for increased value from their purchase in terms of quality, faster delivery, and lower cost not only in manufacturing but also in the service sector [2], [3]. At present, manufacturing organizations compete on various factors such as technology, time, cost, quality, reliability, innovation, and knowledge management. There is a colossal emphasis upon manufacturing organizations to adapt Total Quality Management (TQM), lean and six sigma principles, and business process improvement strategies for achieving remarkable results in quality, cost, and delivery by focusing on process performance [4]. Rapidly changing requisites of novel manufacturing and aggrandizing global competition has stressed upon the review of the aspect of a maintenance management system towards enhancing organizational competitiveness [5].

Manufacturing organizations perceived and approbated that the equipment maintenance and its reliability are important strategies that can significantly influence the organization's dexterity to compete efficiently [6]. The maintenance processes can be streamlined to eliminate wastes thereby resulting an upswing of performance in areas valued by customers [7]. This has stimulated the manufacturing organizations to adapt Total Productive Maintenance (TPM) as a substantial process improvement and problem solving methodology for enhancing the organization's responsiveness to satiate customer needs and influencing cost optimization as part of management strategy to increase the market share and maximize profit. TPM has been acknowledged as the most propitious strategy for improving maintenance performance in order to succeed in an exceedingly demanding market arena [8]. The TPM implementation that has emerged as an operational strategy renders organizations with a guide to fundamentally transform their shop floor by integrating processes, culture, and technology [9].

II. BASIC ELEMENTS OF TOTAL PRODUCTIVE MAINTENANCE

TPM is an important world-class manufacturing program introduced during the quality revolution. TPM seeks to maximize equipment effectiveness throughout the lifetime of equipment. It strives to maintain equipment in optimum condition in order to prevent unexpected breakdowns, speed losses and quality defects occurring from process activities. There are three ultimate goals of TPM: zero defects, zero accident, and zero breakdowns. Nakajima (1988) [10] suggests that equipments should be operated at 100% capacity 100% of the

time. The benefits arising from TPM can be classified in six categories including productivity (P), quality (Q), cost (C), delivery (D), safety (S) and morale (M). TPM has been envisioned as a comprehensive manufacturing strategy to improve equipment productivity. Benchmarking on OEE, P, Q, C, D, S and M can enable an organization to realize zero breakdown, defect, machine stoppage, accidents, and pollution, which serve as an ultimate objective of TPM. The strategic elements of TPM include cross-functional teams to eliminate barriers to machine uptime, rigorous preventive maintenance programs, improved maintenance operations management efficiency, equipment maintenance training to the lowest level, and information systems to support the development of imported equipment with lower cost and higher reliability. Similar to TQM, TPM is focused on improving all the big picture indicators of manufacturing success. TPM implementation requires a long-term commitment to achieve the benefit of improved OEE through training, management support and teamwork.

Figure1 shows the framework of TPM implementation and depicts tools used in TPM implementation program with potential benefits accrued and targets sought. TPM initiatives as suggested by Japan Institute of Plant Maintenance (JIPM) involve an eight pillar implementation plan that results in substantial increase in labor productivity through controlled maintenance, reduction in maintenance costs, and reduced setup and downtimes. The basic principles of TPM are often called the pillars or elements of TPM. The entire edifice of TPM is built and stands on eight pillars. TPM paves the way for excellent planning, organizing, monitoring, and controlling practices through its unique eight pillar methodology involving: autonomous maintenance; focused improvement; planned maintenance; quality maintenance; education and training; safety, health and environment; office TPM; and development management (Rodrigues and Hatakeyama, 2006) [11]. The eight pillar Nakajima model of TPM implementation has been depicted in Figure .2 (Ahuja and Khamba, 2007)[1].

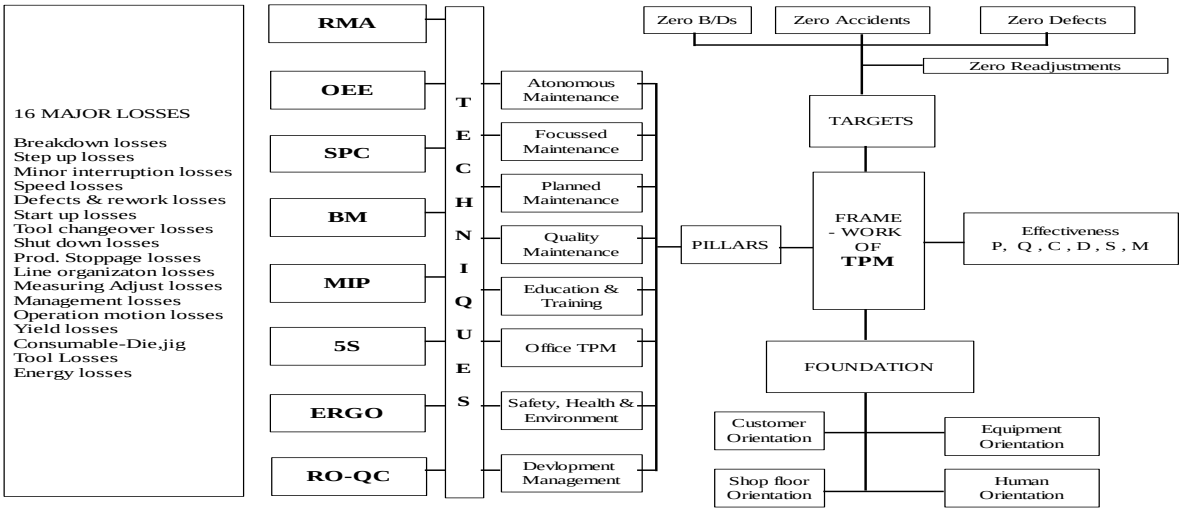

Figure1. Framework of total productive maintenance

Figure1. Framework of total productive maintenance TPM initiatives aim at achieving enhanced safety, asset utilization, production capacity without additional investments in new equipment, human resources and continuing to lower the cost of equipment maintenance and improving machine uptime. It provides an effective way of deploying activities through its TPM promotion organization involving 100% of employees on a continuous basis. The main goal of an effective TPM program is to bring critical maintenance skilled trades and production workers together. Total employee involvement, autonomous maintenance by operators, small group activities to improve equipment reliability, maintainability, productivity, and continuous improvement (Kaizen) are the principles embraced by TPM. There are a variety of tools that are traditionally used for quality improvement. TPM uses the following tools among others to analyze and solve the equipment and process related problems: pareto analysis; statistical process control (SPC - control charts); problem solving techniques (brainstorming, cause-effect diagrams, and 5-M approach); team based problem solving; poka-yoke systems (mistake proofing); autonomous maintenance; continuous improvement; 5S; setup time reduction (SMED); waste minimization; benchmarking; bottleneck analysis; reliability, maintainability and availability (RMA) analysis; recognition and reward programs; and system simulation. TPM provides a comprehensive, life cycle approach to equipment management that minimizes equipment failures, production defects, and accidents. The objective is to improve continuously production system availability and prevent

degradation of equipment to realize maximum effectiveness. These objectives require strong management support as well as continuous use of work teams and small group activities to achieve incremental improvements.

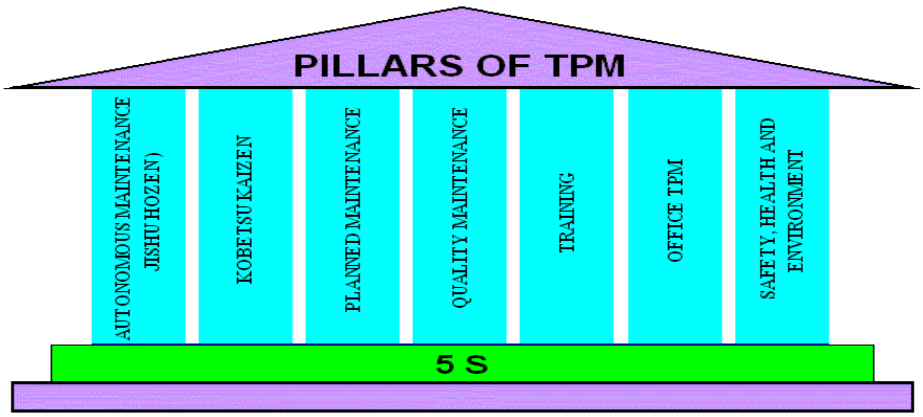

Figure 2. Eight pillar approach for TPM implementation (suggested by JIPM)

TPM employs OEE as the core quantitative metric for measuring the performance of a productive system. OEE has been widely accepted as an essential quantitative tool for measurement of productivity of manufacturing operations. The role of OEE goes far beyond the task of just monitoring and controlling. OEE measure is central to the formulation and execution of a TPM improvement strategy. It provides a systematic method for establishing production targets and incorporates practical management tools and techniques in order to achieve a balanced view of process availability, performance rate, and quality. OEE has been used as an impartial daily snapshot of the equipment and promotes openness in information sharing and a no-blame approach in handling equipment related issues. OEE is the measure of contribution of current equipment to the added value generation time, based on overall consideration of time, speed performance, and non-defective ratio of the equipment. The improvement of OEE is essential to drive a lean production system and is calculated by multiplying availability of equipment, performance efficiency of process and rate of quality products (Gregory, 2006).[12]

With equipment availability, utilization and reliability becoming critical issues in capital-intensive operations, TPM evolves to be strategically imperative in such businesses. The inception of TPM is destined to actualize collaboration between production and maintenance functions by an amalgamation of team working, continuous improvement, and good working practices [13].

The philosophy of TPM shifts the paradigm of an organization's conventional maintenance system from being reactive to being more proactive by maintaining the equipment in optimum condition at all times. TPM methodology embraces an array of techniques that assures each piece of equipment in a production process is always able to perform its required task. It also articulates all other maintenance and reliability processes and methodologies together for a new business strategy that focuses on results and changes the work culture along the line. TPM promotes the participation of all employees to I improve production equipment's availability, performance, quality, safety, and reliability. TPM is a long-term program that strives to tap the "hidden capacity" of unreliable and inefficient equipment. It capitalizes on proactive and progressive maintenance strategies and calls for the knowledge and collaboration of operators, maintenance technicians, equipment suppliers, engineering, and support personnel to optimize equipment performance, thereby resulting in elimination of breakdowns, reduction of unscheduled and scheduled downtime, improved utilization hence productivity and enhanced product quality. The bottom-line accomplishment of a successful TPM implementation in an organization embodies lower operational costs, prolonged equipment life span and lower overall maintenance expenditure [14].

III. REVIEW ON IMPLEMENTATION OF TPM IN MANUFACTURING INDUSTRY

1. Hurdle to TPM implementation: A review

Literature states that TPM implementation is not an effortless task by any means. The failure of TPM implementation is primarily due to the lack of a support system to facilitate learning and transform the same into effective TPM practices followed by its diffusion. Many organizations that attempted to implement TPM initiatives experienced difficulties and are unable to gain the anticipated benefits. The failure of an

organization to successfully implement TPM philosophy has been attributed to various barriers including lack of management commitment and understanding, lack of adequate training, failure to allow adequate time for its evolution [15]. Some of the conspicuous hurdles in TPM implementation includes partial implementation of TPM, inordinate expectations, lack of a systematic approach for achieving the objectives of implementation, cultural resistance to change, inadequate training and education, lack of organizational communication, and implementation to conform to societal norms rather than for its instrumentality to achieve world class manufacturing [16].

A further cogent influencing factor for failure of TPM implementation program is the organization's ineffectualness to obviate resistance to change. There are different dimensions of resistance to change such as, individual's reluctance to change roles [5], [13], inability to change organizational roles and culture [17], [18] and inability to create dissatisfaction with the current situation [19], [20]. Bamber et al. [21] has carried out a study intended to reveal the factors affecting the successful implementation of TPM in UK small-to-medium size enterprises (SME). Davis [22] has epitomized a range of reasons for the failure of TPM within UK manufacturing organizations including lack of top management support and commitment, use of inexperienced consultants, failure to implement change on the shop floor, inadequate training and education for employees, lack of structured approach to support TPM initiatives and lack of employee involvement. According to Cooke [13], the failure of TPM implementation program is prominently due to the inability of management to holistically implement the TPM practices at the workplace. He also emphasize that considerable deviations have been observed between the official TPM policies and the actual practices deployed at workplace. McAdam and Duffner [23] have outlined that copious issues arise while trying to implement TPM in a union environment. Workers perceive that the TPM mainly strives to improve production efficiency, reduce labor, and increase employee workload. Some operators are not keen for additional responsibilities and are satisfied with the current situation. Furthermore, the skilled trades like maintenance technicians enjoy feeling indispensable and believe that the autonomous maintenance approach is posing a threat to their jobs

2. Success factors for TPM implementation: A review

Several generic success criteria for TPM implementation is presented in the TPM literature. For an organization to realize the true potential of TPM philosophy and ensure successful TPM implementation, the goals and objectives of TPM need to be integrated into its overall business strategy because TPM influences the whole organization, not just production. Lycke and Akersten [24] have recommended that cautious, thorough planning and preparation are indispensable for a successful company-wide TPM implementation and so is top management's belief and understanding in the philosophy. For TPM to be successful, the improvement processes need to be re- marked as availing not only to the organization but also to the employees [25]. Groote [26] suggests an approach to evaluate maintenance performance based on quality audit and quantifiable maintenance performance indicators. He proposes that the effectiveness of maintenance functions ought to be defined through relative economic and technical ratios, to allow the management to track the evolution of its performance and to make crucial decisions for improved maintenance management. Bohoris et al. [27] enunciates, significance of inducing a change in the management structure, managing synergy between production and maintenance functions, concentrating on continuous production system improvements, use of efficient computerized maintenance management system (CMMS) and gradual TPM implementation as a pilot project on a few machines at a prescribed time acts as catalysts for successful TPM implementation. A typical TPM development program should emphasize the need for top management's initiative in launching and implementing TPM, formulation of TPM policies, goals and concepts and its effective communication within the organization and frame a system for training and employee involvement [28]. Building of teams, inducing synergy, recognizing them and enabling them to display their efforts supports TPM's success [29]. Top management's support and commitment in fortifying a suitable environment for the introduction of TPM in conjunction with its planning and co-ordination is regarded as a key success factor. Hansson et al. [30] have emphasized upon effective management of organizational change in pursuance of an improved organization's performance for strategic survival in the competitive environment.

Blanchard [31] proposes a provision of suitable training to the employees at an early phase of TPM implementation in order to obtain shop floor's buy in. Hence, the whole of shop floor should receive a comprehensive suite of new skills, new knowledge and new abilities apropos to TPM even before the pilot implementation program embarks. Davis [22] strongly suggested to approach TPM realistically and to establish a practical and comprehensive training program for all employees. Furthermore, he propose to accept that the TPM program will take a long time to be diffused across the organization. Davis [22] stated

that the success factors for TPM implementation include refinement of maintenance systems and culture, and developing a network of TPM coordinators thereby promoting and supporting TPM activities. Developing impeccable performance measures, continuous monitoring of its progress and frequent publishing of the benefits in terms of financial gains caused by TPM fosters the success and sustainability of TPM implementation. The TPM methodology also accentuates the importance of conducting audits and benchmarking activities that cater cardinal measures for invigorating maintenance productivity to achieve world-class competitiveness [32]. Nevertheless, there has not been any reference to the challenges faced, lessons learnt and strategies for overcoming impediments to successful implementation of TPM from an industrial frame of reference. Along these lines, the present study assumes significance as it emphasize upon formulation of critical success factors to overcome the barriers to implement TPM in manufacturing organizations.

IV. CONCLUSION

TPM is not a quick solution. It necessitates a change in both the company's and employee's attitude, and their values, which takes time to bring about. Hence, it entails long-term planning. Rapid and organization wide benefits should not be stressed during the initial phases of implementation. Holistic TPM implementation can lead to the establishment of strategic proactive maintenance practices in the organization for avoiding future system and equipment related losses and marshal the organizations towards capability building for sustained competitiveness. TPM is not a radically new idea; it is simply the next step in the evolution of good maintenance practices. TPM is indispensable to sustain just-in-time operations. TPM facilitates immensely the organizations in improving the synergy between maintenance department and rest of the production functions, resulting in eliminating defects, improving manufacturing process reliability, improving overall equipment effectiveness, and reducing costs, thereby affecting sustainability efforts of the organization to meet cut-throat global Competition for business excellence. TPM has proved to be a means to supplement the concerted improvement efforts by addressing equipment and other related problems that adversely affect the performance of the manufacturing system. Thus, in a highly competitive scenario, TPM can prove to be the best proactive strategic initiative that can lead organizations to scale new levels of achievements and could really make the difference between success and failure of organizations .The research has critically evaluated various barriers and challenges that influence the successful implementation of TPM in manufacturing industries.

REFERENCES

[1] I.P.S. Ahuja, J.S. Khamba and R. Choudhary, Improved organizational behavior through strategic total productive maintenance implementation, (Proc. International Mechanical Engineering Congress and Exposition (IMECE), November. 2006.), 1-8,

[2] R. Basu, Six Sigma to fit Sigma,(IIE Solutions, vol. 33, no. 7, , 2001) , 28 -33.

[3] M. George, Lean Six Sigma: Combining Six Sigma Quality with Lean Speed,(New York ,McGraw-Hill, 2002).

[4] M. Kumar, J. Antony, R.K. Singh, M.K. Tiwari and D. Perry, Implementing the Lean Sigma framework in an Indian SME: A case study, 17(4) (Production Planning and Control, 2006),407-23.

[5] J. Riis, J. Luxhoj andU. Thorsteinsson, A situational maintenance model, International Journal of Quality & Reliability Management, vol. 14(4), 1997, 349-366,.

[6] C.N. Madu, Competing through maintenance strategies, International Journal of Quality & Reliability Management, vol. 17(9), 2000, 937-949,

[7] M. Hammer and J. Champy, Reengineering the Organization,(New York: Harper Business , 1993).

[8] S. Nakajima, Introduction to Total Productive Maintenance (TPM),(Portland :Productivity Press, 1988).

[9] R. Moore, Combining TPM and reliability-focused maintenance, Plant Engineering, 51(6),1997, 88-90.

[10] Nakajima S , Introduction to TPM(Cambridge :Productivity Press In,1988).

[11] Rodrigues M and Hatakeyama K, Analysis of the fall of TPM in companies (J of Mate Process Techno,2006), 276–279.

[12] Gregory, A Number cruncher – overall equipment effectiveness and total productive maintenance,59(7)(Work Manage, ,2006), 18–20.

[13] F.L. Cooke, Implementing TPM in plant maintenance: some organizational barriers, International Journal of Quality & Reliability Management, 17(9), 2000, 1003 -1016.

[14] I.P.S. Ahuja and J.S. Khamba, Strategies and Success Factors for Overcoming Challenges in TPM Implementation in Indian Manufacturing Industry, Journal of Quality in Maintenance Engineering, 14, 2008, 123-147.

[15] R. Bakerjan, Tool and Manufacturing Engineers' Handbook, 7(4)(ASME: Fairfield, 1994).

[16] K.M. Crawford, J.H. Jr Blackstone and J.F. Cox, A study of JIT implementation and operating problems, International Journal of Production Research, 26(9), 1988,1561 -1568.
[17] J.W. Patterson, W.J. Kennedy and L.D. Fredendall, Total productive maintenance is not for this company, Production and Inventory Management Journal, 36(2), 1995, 61-64.
[18] J.J. Lawrence, Use mathematical modeling to give your TPM I implementation effort an extra boost, Journal of Quality in Maintenance Engineering,5(1), 1999, 62-69.
[19] B.N. Maggard and D.M. Rhyne, Total productive maintenance: a timely integration of production and maintenance, Production and Inventory Management Journal, 33(4), 1992, 6-10.
[20] F. Ireland and B.G. Dale, A study of total productive maintenance implementation, Journal of Quality in Maintenance Engineering , 7(3), 2001, 183-192.
[21] C.J. Bamber, J.M. Sharp and M. Hides, Factors affecting successful implementation of total productive maintenance: a UK manufacturing case study perspective, Journal of Quality in Maintenance Engineering, 5(3), 1999, 162-181.
[22] R. Davis, Productivity Improvements through TPM (Englewood Cliffs: Prentice-Hall, 1995).
[23] R. McAdam and A.M. Duffner, Implementation of total productive maintenance in support of an established total quality programme,7(6)(Total Quality Management, 1996), 613-630.
[24] L. Lycke and P.A. Akersten, Experiences of implementing TPM in Swedish industries, International Journal of Reliability and Application , 1(1), 2000, 1-14.
[25] C.J. Robinson and A.P. Ginder, The North American Experience (Portland: Productivity Press, 1995).
[26] P.D. Groote, Maintenance performance analysis: a practical approach , Journal of Quality in Maintenance Engineering , 1 (2), 1995, 4-24.
[27] G.A. Bohoris, C. Vamvalis, W. Tracey and K. Ignatiadou, TPM implementation in Land-Rover with assistance of a CMMS, Journal of Quality in Maintenance Engineering, 1(4),1995, 3-16.
[28] L.D. Fredendall, J.W. Patterson, W.J. Kennedy and T. Griffin, Maintenance modelling, its strategic impact, Journal of Managerial Issues , 9(4), 1997, 440-453.
[29] D. Hutchins, Introducing TPM, 77(1)(Manufacturing Engineer, 1998) ,34-37.
[30] J. Hansson, F. Backlund and L. Lycke, Managing commitment: increasing the odds for successful implementation of TQM, TPM or RCM, International Journal of Quality & Reliability Management , 20(9), 2003, 993-1008.
[31] B.S. Blanchard, An Advance Approach for Implementing TPM in Manufacturing Environment, Journal of Quality in Maintenance Engineering, 5, 1997, 162-181.
[32] M. Ben-Daya and S.O. Duffuaa, Maintenance and Quality: The Missing Link, Journal of Quality in Maintenance Engineering,1,1995, 20-26.

OPEN ACCESS

International
Journal
Of Modern Engineering Research (IJMER)

Multiexposure Image Fusion

Suhaina J[1], Bindu K. R[2]

[1]*Department of Electronics and Communication Engineering, FISAT/ Mahatma Gandhi University, India*
[2]*Department of Electronics and Communication Engineering, FISAT/ Mahatma Gandhi University, India*

Abstract: *Many applications such as robot navigation, defense, medical and remote sensing perform various processing tasks, which can be performed more easily when all objects in different images of the same scene are combined into a single fused image. In this paper, we propose a fast and effective method for image fusion. The proposed method derives the intensity based variations that is large and small scale, from the source images. In this approach, guided filtering is employed for this extraction. Gaussian and Laplacian pyramidal approach is then used to fuse the different layers obtained. Experimental results demonstrate that the proposed method can obtain better performance for fusion of all sets of images. The results clearly indicate the feasibility of the proposed approach.*

Keywords: *Gaussian Pyramid, Guided Filter, Image Fusion, Laplacian Pyramid, Multi-exposure images*

I. INTRODUCTION

Often a single sensor cannot produce a complete representation of a scene. Visible images provide spectral and spatial details, and if a target has the same color and spatial characteristics as its background, it cannot be distinguished from the background. Image fusion is the process of combining information from two or more images of a scene into a single composite image that is more informative and is more suitable for visual perception or computer processing. The objective in image fusion is to reduce uncertainty and minimize redundancy in the output while maximizing relevant information particular to an application or task. Given the same set of input images, different fused images may be created depending on the specific application and what is considered relevant information. There are several benefits in using image fusion: wider spatial and temporal coverage, decreased uncertainty, improved reliability, and increased robustness of system performance.

A large number of image fusion methods [1]–[4] have been proposed in literature. Among these methods, multiscale image fusion [2] and data-driven image fusion [3] are very successful methods. They focus on different data representations, e.g., multi-scale coefficients [5], [6], or data driven decomposition coefficients [3], [7] and different image fusion rules to guide the fusion of coefficients. The major advantage of these methods is that they can well preserve the details of different source images. However, these kinds of methods may produce brightness and color distortions since spatial consistency is not well considered in the fusion process. Spatial consistency means that if two adjacent pixels have similar brightness or color, they will tend to have similar weights. A popular spatial consistency based fusion approach is formulating an energy function, where the pixel saliencies are encoded in the function and edge aligned weights are enforced by regularization terms, e.g., a smoothness term. This energy function can be then minimized globally to obtain the desired weight maps. To make full use of spatial context, optimization based image fusion approaches, e.g., generalized random walks [8], and Markov random fields [9] based methods have been proposed. These methods focus on estimating spatially smooth and edge aligned weights by solving an energy function and then fusing the source images by weighted average of pixel values. However, optimization based methods have a common limitation, i.e., inefficiency, since they require multiple iterations to find the global optimal solution. Moreover, another drawback is that global optimization based methods may over-smooth the resulting weights, which is not good for fusion. An interesting alternative to optimization based method is guided image filtering [10]. The proposed method employs guided filtering for layer extraction. The extracted layers are then fused separately.

The remainder of this paper is organized as follows. In Section II, the guided image filtering algorithm is reviewed. Section III describes the proposed image fusion algorithm. The experimental results and discussions are presented in Section IV. Finally, Section V concludes the paper.

II. GUIDED IMAGE FILTERING

Guided filter is an image filter derived from a local linear model. It computes the filtering output by considering the content of a guidance image, which can be the input image itself or another different image. The guided filter can be used as an edge-preserving smoothing operator like the popular bilateral filter, but it has better behaviors near edges. The guided filter is also a more generic concept beyond smoothing: It can transfer the structures of the guidance image to the filtering output, enabling new filtering applications like dehazing and guided feathering. Moreover, the guided filter naturally has a fast and nonapproximate linear time algorithm, regardless of the kernel size and the intensity range. Currently, it is one of the fastest edge-preserving filters. Guided filter is both effective and efficient in a great variety of computer vision and computer graphics applications, including edge-aware smoothing, detail enhancement, HDR compression, image matting/feathering, dehazing, joint upsampling, etc.

The filtering output is locally a linear transform of the guidance image. On one hand, the guided filter has good edge-preserving smoothing properties like the bilateral filter, but it does not suffer from the gradient reversal artifacts. On the other hand, the guided filter can be used beyond smoothing: With the help of the guidance image, it can make the filtering output more structured and less smoothed than the input. Moreover, the guided filter naturally has an O(N) time (in the number of pixels N) nonapproximate algorithm for both gray-scale and high-dimensional images, regardless of the kernel size and the intensity range. Typically, the CPU implementation achieves 40 ms per mega-pixel performing gray-scale filtering. It has great potential in computer vision and graphics, given its simplicity, efficiency, and high-quality.

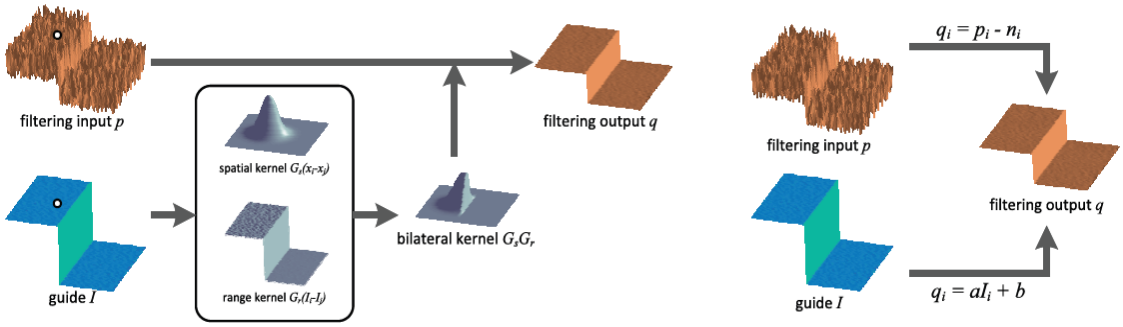

Fig. 2.1. Illustrations of the bilateral filtering process (left) and the guided filtering process (right)

2.1 Guided filter

A general linear translation-variant filtering process is defined, which involves a guidance image I, an filtering input image p, and an output image q. Both I and p are given beforehand according to the application, and they can be identical. The filtering output at a pixel i is expressed as a weighted average:

$$q_i = \sum_j W_{ij}(I)\, p_j \tag{1}$$

where i and j are pixel indexes. The filter kernel W_{ij} is a function of the guidance image I and independent of p. This filter is linear with respect to p. An example of such a filter is the joint bilateral filter (Fig. 2.1 (left)). The bilateral filtering kernel W_{bf} is given by :

$$W_{ij}^{bf}(I) = \frac{1}{K_i} exp\left(-\frac{||x_i - x_j||^2}{\sigma_s^2}\right) exp\left(-\frac{||I_i - I_j||^2}{\sigma_r^2}\right) \tag{2}$$

where x is the pixel coordinate and K_i is a normalizing parameter to ensure $\sum_j W_{ij}^{bf} = 1$. The parameters σ_s and σ_r adjust the sensitivity of the spatial similarity and the range (intensity/color) similarity, respectively. The joint bilateral filter degrades to the original bilateral filter when I and p are identical. The implicit weighted-average filters optimize a quadratic function and solve a linear system in this form:

$$Aq = p \tag{3}$$

where q and p are N-by-1 vectors concatenating $\{q_i\}$ and $\{p_i\}$, respectively, and A is an N-by-N matrix only depends on I. The solution to (3), i.e., $q = A^{-1}p$, has the same form as (1), with $W_{ij} = (A^{-1})_{ij}$.

The key assumption of the guided filter is a local linear model between the guidance I and the filtering output q. We assume that q is a linear transform of I in a window w_k centered at the pixel k:

$$q_i = a_k I_i + b_k \,, \forall i \epsilon w_k \tag{4}$$

where (a_k, b_k) are some linear coefficients assumed to be constant in w_k. We use a square window of radius r. This local linear model ensures that q has an edge only if I has an edge, because $\nabla q = a\nabla I$. This model has been proven useful in image super-resolution, image matting and dehazing.

To determine the linear coefficients {a_k, b_k}, we need constraints from the filtering input p. We model the output q as the input p subtracting some unwanted components n like noise/textures:

$$q_i = p_i - n_i \tag{5}$$

A solution that minimizes the difference between q and p while maintaining the linear model (4) is suggested. Specifically, the following cost function in the window w_k is minimized :

$$E(a_k, b_k) = \sum_{i \in w_k}((a_k I_i + b_k - p_i)^2 + \epsilon a_k^2) \tag{6}$$

Here, ϵ is a regularization parameter penalizing large a_k.

Equation (6) is the linear ridge regression model [11] and its solution is given by :

$$a_k = \frac{\frac{1}{|w|}\sum_{i \in w_k} I_i p_i - \mu_k \bar{p}_k}{\sigma_k^2 + \epsilon} \tag{7}$$

$$b_k = \bar{p}_k - a_k \mu_k \tag{8}$$

Here, μ_k and σ_k^2 are mean and variance of I in w_k, |w| is the number of pixels in w_k, and $\bar{p}_k = \frac{1}{|w|}\sum_{i \in w_k} p_i$ is the mean of p in w_k. Having obtained the linear coefficients {a_k, b_k}, we can compute the filtering output q_i by (4). Fig.2.1 (right) shows an illustration of the guided filtering process.

However, a pixel i is involved in all the overlapping windows w_k that covers i, so the value of q_i in (4) is not identical when it is computed in different windows. A simple strategy is to average all the possible values of q_i. So after computing (a_k, b_k) for all windows w_k in the image, we compute the filtering output by :

$$q_i = \frac{1}{|w|}\sum_{k|i \in w_k}(a_k I_i + b_k) \tag{9}$$

Noticing that $\sum_{k|i \in w_k} a_k = \sum_{k \in w_i} a_k$ due to the symmetry of the box window, (9) is rewritten as :

$$q_i = \bar{a}_i I_i + \bar{b}_i \tag{10}$$

where $\bar{a}_i = \frac{1}{|w|}\sum_{k \in w_i} a_k$ and $\bar{b}_i = \frac{1}{|w|}\sum_{k \in w_i} b_k$ are the average coefficients of all windows overlapping i. The averaging strategy of overlapping windows is popular in image denoising.

With the modification in (10), ∇q is no longer scaling of ∇I because the linear coefficients $(\bar{a}_i, \bar{b}_i)$ vary spatially. But as $(\bar{a}_i, \bar{b}_i)$ are the output of a mean filter, their gradients can be expected to be much smaller than that of I near strong edges. In short, abrupt intensity changes in I can be mostly preserved in q.

Equations (7), (8), and (10) are the definition of the guided filter. A pseudocode is in Algorithm 1. In this algorithm, f_{mean} is a mean filter with a window radius r. The abbreviations of correlation (corr), variance (var), and covariance (cov) indicate the intuitive meaning of these variables.

Algorithm 1. Guided Filter.

Input: filtering input image p, guidance image I, radius r, regularization ϵ

Output: filtering output q.

1: $mean_I = f_{mean}(I)$
   $mean_p = f_{mean}(p)$
   $corr_I = f_{mean}(I.*I)$
   $corr_{Ip} = f_{mean}(I.*p)$
2: $var_I = corr_I - mean_I .* mean_I$
   $cov_{Ip} = corr_{Ip} - mean_I .* mean_p$
3: $a = cov_{Ip} ./(var_I + \epsilon)$
   $b = mean_p - a.* mean_I$
4: $mean_a = f_{mean}(a)$
   $mean_b = f_{mean}(b)$
5: $q = mean_a .* I + mean_b$

III. OVERALL APPROACH

The flowchart of the proposed image fusion method is shown in Fig. 3.1. We first employ guided filtering for the extraction of base layers and detail layers from the input images. qi computed in (9) preserves the strongest edges in I while smoothing small changes in intensity. Let $b_K(i',j')$ be the base layer computed from (9) (i.e.,$b_K(i',j') = qi$ and $1 \leq K \leq N$) for K^{th} input image denoted by $I_K(i',j')$. The detail layer is defined as the difference between the guided filter output and the input image, which is defined as

$$d_K(i',j') = I_K(i',j') - b_K(i',j') \quad (11)$$

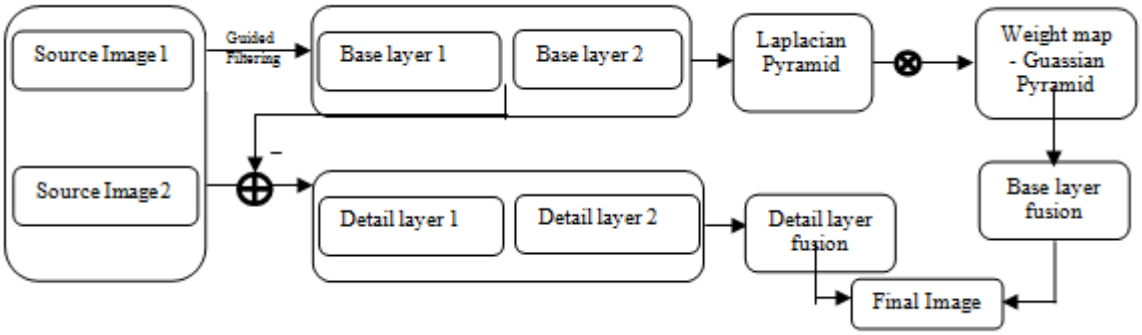

Fig 3.1. Flowchart of the proposed method

3.1 Base Layer Fusion

The pyramid representation expresses an image as a sum of spatially band-passed images while retaining local spatial information in each band. A pyramid is created by lowpass filtering an image $G0$ with a compact two-dimensional filter. The filtered image is then subsampled by removing every other pixel and every other row to obtain a reduced image $G1$.This process is repeated to form a Gaussian pyramid $G0$, $G1$, $G2$, $G3$, . . . , Gd. Expanding $G1$ to the same size as $G0$ and subtracting yields the band-passed image $L0$. A Laplacian pyramid $L0$, $L1$, $L2$, . . . , $Ld-1$, can be built containing band-passed images of decreasing size and spatial frequency.

$$L_l = G_l - G_{l+1}, \qquad l = 1, \ldots\ldots, d-1 \quad (12)$$

where l refers to the number of levels in the pyramid.

The original image can be reconstructed from the expanded band-pass images:

$$G0 = L0 + L1 + L2 + \cdots + Ld - 1 + Gd \quad (13)$$

The Gaussian pyramid contains low-passed versions of the original $G0$, at progressively lower spatial frequencies. This effect is clearly seen when the Gaussian pyramid levels are expanded to the same size as $G0$. The Laplacian pyramid consists of band-passed copies of $G0$. Each Laplacian level contains the edges of a certain size and spans approximately an octave in spatial frequency.

(a) Quality measures

Many images in the stack contain flat, colorless regions due to under- and overexposure. Such regions should receive less weight, while interesting areas containing bright colors and details should be preserved. The following measures are used to achieve this:

• Contrast: Contrast is created by the difference in luminance reflected from two adjacent surfaces. In other words, contrast is the difference in visual properties that makes an object distinguishable from other object and the background. In visual perception contrast is determined by the difference in color and brightness of the object with other object. It is the difference between the darker and the lighter pixel of the image, if it is big the image will have high contrast and in the other case the image will have low contrast.

A Laplacian filter is applied to the grayscale version of each image, and take the absolute value of the filter response. This yields a simple indicator C for contrast. It tends to assign a high weight to important elements such as edges and texture.

• Saturation: As a photograph undergoes a longer exposure, the resulting colors become desaturated and eventually clipped. The saturation of a color is determined by a combination of light intensity and how much it is distributed across the spectrum of different wavelengths. The purest (most saturated) color is achieved by using just one wavelength at a high intensity, such as in laser light. If the intensity drops, then as a result the saturation drops. Saturated colors are desirable and make the image look vivid. A saturation measure S is included which is computed as the standard deviation within the R, G and B channel, at each pixel.

• Exposure: Exposure is a term that refers to two aspects of photography – it is referring to how to control the lightness and the darkness of the image. In photography, exposure is the amount of light per unit area reaching a photographic film. A photograph may be described as overexposed when it has a loss of highlight detail, that is, when important bright parts of an image are washed out or effectively all white, known as blown out highlights or clipped whites. A photograph may be described as underexposed when it has a loss of shadow detail, that is, when important dark areas are muddy or indistinguishable from black, known as blocked up shadows. Looking at just the raw intensities within a channel, reveals how well a pixel is exposed. We want to

keep intensities that are not near zero (underexposed) or one (overexposed). We weight each intensity i based on how close it is to 0.5 using a Gauss curve:

$$exp\left(-\frac{(i-0.5)^2}{2\sigma^2}\right) \quad (14)$$

To account for multiple color channels, we apply the Gauss curve to each channel separately, and multiply the results, yielding the measure E.

The fused base layer $bf(i',j')$ is computed as the weighted sum of the base layers $b1(i',j'), b2(i',j'), \ldots, bN(i',j')$ obtained across N input exposures. Pyramidal approach is used to generate Laplacian pyramid of the base layers $L\{b_K(i',j')\}^l$ and Gaussian pyramid of weight map functions $G\{W_K(i',j')\}^l$ estimated from three quality measures (i.e., saturation $S_K(i',j')$, contrast $C_K(i',j')$, and exposure $E_K(i',j')$). Here, l ($0 < l < d$) refers to the number of levels in the pyramid and K ($1 < K < N$) refers to the number of input images. The weight map is computed as the product of these three quality metrics (i.e. $W_K(i',j') = S_K(i',j') \cdot C_K(i',j') \cdot E_K(i',j')$). The $L\{b_K(i',j')\}^l$ multiplied with the corresponding $G\{W_K(i', j')\}^l$ and summing over K yield modified Laplacian pyramid $L^l(i', j')$ as follows:

$$L^l(i',j') = \sum_{K=1}^{N} L\{b_K^l(i',j')\}\, G\{W_K^l(i',j')\} \quad (15)$$

The $b_f(i',j')$ that contains well exposed pixels is reconstructed by expanding each level and then summing all the levels of the Laplacian pyramid:

$$b_f(i',j') = \sum_{l=0}^{d} L^l(i',j') \quad (16)$$

3.2 Detail Layer Fusion

The detail layers computed in (11) across all the input exposures are linearly combined to produce fused detail layer $df(i',j')$ that yields combined texture information as follows:

$$d_f(i',j') = \frac{\sum_{K=0}^{N} \gamma(d_K(i',j'))}{N} \quad (17)$$

where γ is the user defined parameter to control amplification of texture details (typically set to 5).

Finally, the detail enhanced fused image $g(i',j')$ is easily computed by simply adding up the fused base layer $b_f(i',j')$ computed in (16) and the manipulated fused detail layer $df(i',j')$ in (17) as follows:

$$g(i',j') = d_f(i',j') + b_f(i',j') \quad (18)$$

3.3 Numerical Analysis

Numerical analysis is the process of evaluating a technique via some objective metrics. For this purpose, two fusion quality metrics [12], i.e., information theory based metric (Q_{MI}) [13] and structure based metrics (Qc) [14] are adopted. In order to assess the fusion performance, fusion quality metric is used.

(a) Normalized mutual information (Q_{MI})

Normalized mutual information, Q_{MI} is an information theory based metric. Mutual information improves image fusion quality assessments. One problem with traditional mutual information metric is that it is unstable and may bias the measure towards the source image with the highest entropy.

The size of the overlapping part of the images influences the mutual information measure in two ways. First of all, a decrease in overlap decreases the number of samples, which reduces the statistical power of the probability distribution estimation. Secondly, with increasing misregistration (which usually coincides with decreasing overlap) the mutual information measure may actually increase. This can occur when the relative areas of object and background even out and the sum of the marginal entropies increases, faster than the joint entropy. Normalized measure of mutual information is less sensitive to changes in overlap. Hossny *et al.* modified it to the normalized mutual information [13]. Here, Hossny *et al.*'s definition is adopted.

$$Q_{MI} = 2\left[\frac{MI(A,F)}{H(A)+H(F)} + \frac{MI(B,F)}{H(B)+H(F)}\right] \quad (19)$$

where $H(A)$, $H(B)$ and $H(F)$ are the marginal entropy of A, B and F, and $MI(A, F)$is the mutual information between the source image A and the fused image F.

$$MI(A,F) = H(A) + H(F) - H(A,F) \quad (20)$$

where $H(A, F)$ is the joint entropy between A and F, $H(A)$ and $H(F)$ are the marginal entropy of A and F, respectively, and $MI(B,F)$ is similar to $MI(A, F)$. The quality metric Q_{MI} measures how well the original information from source images is preserved in the fused image.

(b) Cvejic et al.'s metric (Qc)

Cvejic et al.'s metric, Qc is a structure based metric. It is calculated as follows :

$$Q_C = \mu(A_w, B_w.F_w)UIQI(A_w, F_w) + (1 - \mu(A_w, B_w, F_w))UIQI(B_w, F_w) \quad (21)$$

where $\mu(A_w, B_w.F_w)$ is calculated as follows :

$$\mu(A_w, B_w, F_w) = \begin{cases} 0, & if \frac{\sigma_{AF}}{\sigma_{AF}+\sigma_{BF}} < 0 \\ \frac{\sigma_{AF}}{\sigma_{AF}+\sigma_{BF}}, & if\ 0 \leq \frac{\sigma_{AF}}{\sigma_{AF}+\sigma_{BF}} < 1 \\ 1, & if \frac{\sigma_{AF}}{\sigma_{AF}+\sigma_{BF}} > 1 \end{cases} \quad (22)$$

σ_{AF} and σ_{BF} are the covariance between A,B and F, UIQI refers to the universal image quality index. The Qc quality metric estimates how well the important information in the source images is preserved in the fused image, while minimizing the amount of distortion that could interfere with interpretation.

IV. Results And Discussion

The system described above is implemented using Matlab and the result was successfully obtained. In this section, the obtained results are provided. Figure 4.1 shows the base and detail layers.

Figure 4.2: Base layers and Detail layers

Pyramidal approach is used for fusing base layers. Quality measures of images are considered to compute the weight map. Weight map is the combination of contrast, saturation and exposure. Figure 4.3 shows the gaussian pyramid of weight map function.

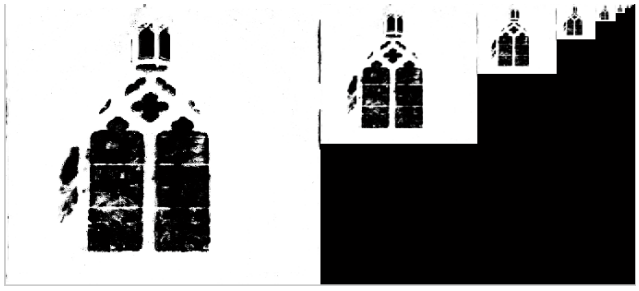

Figure 4.3: Gaussian pyramid

Laplacian pyramid of the base layers are generated. Thus obtained laplacian pyramid is shown in figure 4.4.

Figure 4.4: Laplacian pyramid

Fused pyramid is obtained by combining the Gaussian pyramid of weight map functions and Laplacian pyramid of base layers. Figure 4.5 shows the fused pyramid.

Figure 4.5: Fused pyramid

Fused base layer is the weighted sum of base layers. The detail layers obtained are boosted and fused. Figure 4.6 shows the fused base and detail layers.

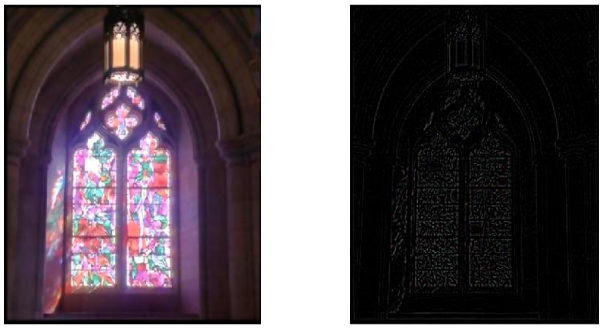

Figure 4.6: Fused base layer and detail layer

Finally, the fused image is obtained by combining the obtained fused base and fused detail layers. The fused image is shown in figure 4.7. Numerical analysis is performed on the obtained results.

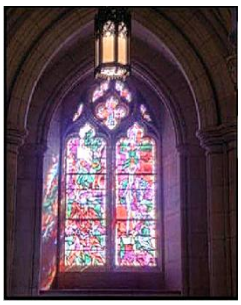

Figure 4.7: Fused image

The following shows the results obtained for some of the other source images.

(a) (b)

Figure 4.8: (a) Source Images (b) Fused Image

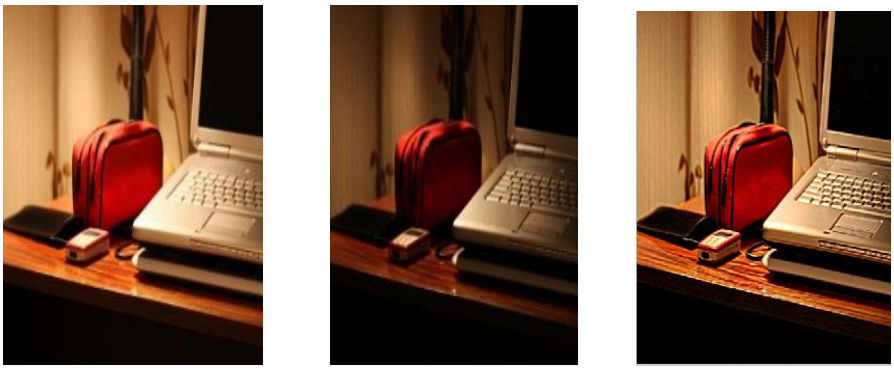

(a) (b)

Figure 4.9: (a) Source Images (b) Fused Image

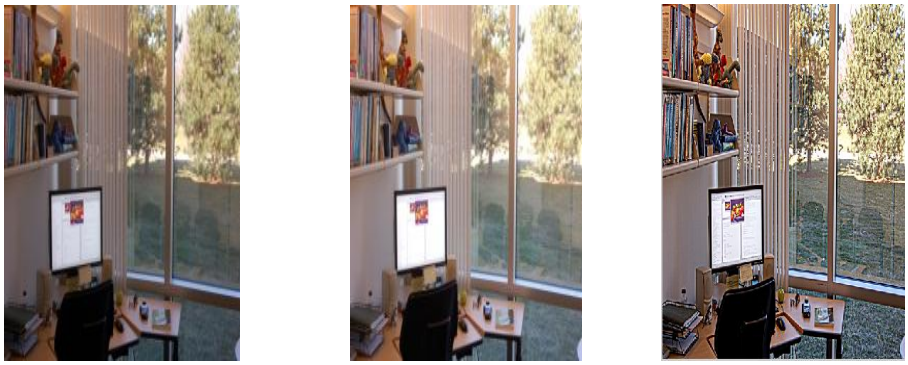

(a) (b)

Figure 4.10: (a) Source Images (b) Fused Image

V. Conclusion

We proposed a technique for fusing multiexposure input images. The proposed method constructs a detail enhanced image from a set of multiexposure images by using a multiresolution decomposition technique. When compared with the existing techniques which use multiresolution and single resolution analysis for exposure fusion, the current proposed method performs better in terms of enhancement of texture details in the fused image. The framework is inspired by the edge preserving property of guided filter that has better response near strong edges. Experiments show that the proposed method can well preserve the original and complementary information of multiple input images.

REFERENCES

[1] S. Li, J. Kwok, I. Tsang, and Y. Wang, "Fusing images with different focuses using support vector machines," *IEEE Trans. Neural Netw.*, vol. 15, no. 6, pp. 1555–1561, Nov. 2004.

[2] G. Pajares and J. M. de la Cruz, "A wavelet-based image fusion tutorial," *Pattern Recognit.*, vol. 37, no. 9, pp. 1855–1872, Sep. 2004.

[3] D. Looney and D. Mandic, "Multiscale image fusion using complex extensions of EMD," *IEEE Trans. Signal Process.*, vol. 57, no. 4, pp. 1626–1630, Apr. 2009.

[4] M. Kumar and S. Dass, "A total variation-based algorithm for pixellevel image fusion," *IEEE Trans. Image Process.*, vol. 18, no. 9, pp. 2137–2143, Sep. 2009.

[5] P. Burt and E. Adelson, "The laplacian pyramid as a compact image code," *IEEE Trans. Commun.*, vol. 31, no. 4, pp. 532–540, Apr. 1983.

[6] O. Rockinger, "Image sequence fusion using a shift-invariant wavelet transform," in *Proc. Int. Conf. Image Process.*, vol. 3, Washington, DC, USA, Oct. 1997, pp. 288–291.

[7] J. Liang, Y. He, D. Liu, and X. Zeng, "Image fusion using higher order singular value decomposition," *IEEE Trans. Image Process.*, vol. 21, no. 5, pp. 2898–2909, May 2012.

[8] R. Shen, I. Cheng, J. Shi, and A. Basu, "Generalized random walks for fusion of multi-exposure images," *IEEE Trans. Image Process.*, vol. 20, no. 12, pp. 3634–3646, Dec. 2011.

[9] M. Xu, H. Chen, and P. Varshney, "An image fusion approach based on markov random fields," *IEEE Trans. Geosci. Remote Sens.*, vol. 49, no. 12, pp. 5116–5127, Dec. 2011.
[10] K. He, J. Sun, and X. Tang, "Guided image filtering," in *Proc. Eur. Conf. Comput. Vis.*, Heraklion, Greece, Sep. 2010, pp. 1–14.
[11] N. Draper and H. Smith, *Applied Regression Analysis*. New York, USA: Wiley, 1981.
[12] Z. Liu, E. Blasch, Z. Xue, J. Zhao, R. Laganiere, and W. Wu,"Objective assessment of multiresolution image fusion algorithms for context enhancement in night vision: A comparative study," *IEEE Trans. Pattern Anal. Mach. Intell.*, vol. 34, no. 1, pp. 94–109, Jan. 2012.
[13] M. Hossny, S. Nahavandi, and D. Creighton, "Comments on 'information measure for performance of image fusion'," *Electron. Lett.*, vol. 44, no. 18, pp. 1066–1067, Aug. 2008.
[14] N. Cvejic, A. Loza, D. Bull, and N. Canagarajah, "A similarity metric for assessment of image fusion algorithms," *Int. J. Signal Process.*, vol. 2, no. 3, pp. 178–182, Apr. 2005.

OPEN ACCESS

International
Journal
Of Modern Engineering Research (IJMER)

Driver Fatigue Monitoring System Using Eye Closure

Miss.G.Victoreia[1], Miss.D.Yazhini[2], Miss.G.Parameswari[3], Mr. E.Gurumoorthi[4], Mrs. G.Vijayabarathy[5]

[1,2,3]*MCA student, Sri Manakula Vinayagar Engineering College, Puducherry*
[4]*Assistant Professor, Sri Manakula Vinayagar Engineering College, Pondicherry*
[5]*Assistant Professor, Perunthalaivar kamarajar arts college, Puducherry*

Abstract: *Now-a-days so many road accidents occur due to driver distraction while he is driving. Those accidents are broadly depends upon wide range of driver state such as drowsy state, alcoholic state, depressed state etc. Even driver distraction and conversation with passengers during driving can lead in major problems. To address the problem we propose a Driver fatigue Monitoring and warning system based on eye-tracking, which is consider as active safety system. This system is useful and helpful for drivers to be alert while driving. Eye tracking is one of the major technologies for future driver system since human eyes contains much information. Sleepiness reduces reaction time of safe driving. The driver distraction is measured by the person eye closure rate for certain period while driving. It is implemented by comparing the image extracted from video and the video that is currently performing. The percentage of eyes is compared from both the frames, if the driver is suspected to be sleeping then a warning alarm is given to alert the driver.*

Keywords: *Driver fatigue, Eye Tracking, Drowsiness detection.*

I. INTRODUCTION

Now-a-days the society faces more number of accident rates. The Driver fatigue problems have become important factors for causing road accidents. Driver fatigue is a major cause for four wheeler accidents since the drivers are unable to take sudden decision while they are sleepy. This kind of accident can be predicted and given solutions. The fatigue behaviors are predicted whether the drivers stay awake or not and make a warning when they begin to fall asleep. The system can detect the changes in eyes by measuring closed/opened eye state. This technology is used to track the eyes of the driver and alert them.

This system capture the eye sight from the face and it measures the eye rate by closed/opened state. In addition to detect the drowsiness of the driver, if the eyelid is closed for more than 8-10 seconds then it is the indicator of fatigue state and by that time the system alerts the driver. The system detects driver fatigue status by measuring the proportion of eyes closed in a certain period of time and the continued closure time.

The Algorithm is used to detect the drowsiness of the driver is PERCLOS. It is abbreviated as (PERcentage ClOSure) is a measure of driver alertness. This algorithm is helpful in measuring the person eyelid closure. It measures the slow eyelid closures rather than blinks, and is the measurement of choice for drowsiness detection. This Algorithm is been considered as the Standard for drowsiness detection. In this it measures the percentage of eyelid closure over the pupil and reflects the slow eyelid closure with the movement of eye blinking.

PERCLOS is the Real-Time measures of alertness for drowsiness detecting system. It measure by capturing the face and focused on the eyes and detects the pupil from the eyes. Eyes has the various parameters of measures and colors the white area will not be detected, the Retina of the eyes will detected from the whole eyes and it has a various point and individual color to be measured from the retina.

In this system the face and the eyes are localized by comparing the image and the video input, but the camera will be focused on the eyes. When the camera first detects the face, the image is saved to a file for the usage of comparing. The points determine whether the person is feeling sleepy or not. Once the person closed his eyes or moves outside of the frame, the warning system alert the driver from drowsiness or distraction or it is helpful to other passengers to be alert and wake the driver from fast asleep.

II. EXISTING SYSTEM

The existing system evaluate whether changes in the eye-steering correlation that can indicate distraction. The auto-correlation and cross-correlation of horizontal eye position and steering wheel angle show that eye movements associated with road scanning procedure a low eye steering correlation. The eye steering correlation will control the relationship on a straight road. The straight road led to a low correlation between the steering movement and eye glances. In this system it is aim to detect the driver distraction based on visual behavior or the performance of the driver so for this purpose it is used to define the relationship between the visual behavior and the vehicle control.

This system evaluates the eye-steering correlation associated with the straight road with the assumption that it might show a qualitatively and quantitatively different relationship compared with curvy road and that it might be sensitive to distraction. Here in the visual behavior and vehicle control relationship reflects a fundamental perception-control mechanism which plays a major role in driving and a strong eye-steering correlation associated with this process has been observed on curvy roads.

1. Driver Distraction Detection Algorithm

Driver Distraction Detection Algorithm is used in earlier system which is the combination of glance behavior and vehicle control. Two types of distraction are focused:

a) Cognitive b) Visual

Cognitive described as "Mind-off-road" and Visual has been described as "Eye-off-road". Cognitive tasks tend to reduce the lane position variance and visual tasks tend to increase the variance. Although both can determine the driving performance, their effects are different.

2. Disadvantage in Cognitive distraction detection

Although it improves drive performance it degrades. Longitudinal control with hazards perception. It is complex because the mechanism involved in cognitive distraction has not been precisely described.

There are two approach has given in distraction detection algorithm. First approach focuses distraction detection systems on visual behavior and another approach focuses on driver behavior such as speed, lane position and steering. Considering a combination of both glance behavior and vehicle control might increase algorithm sensitivity to detecting different types of inattention.

This paper presents a new approach to algorithm design that focuses on the relationship between the eye movement and steering wheel movement.

3. Eye-steering coordination

Two modeling approaches are there to describe and predict the allocation of driver's visual attention. They are:

a) Models of visual search:

This model describes how people locate targets in the environment to complete the task.

b) Models of visual sampling:

This model describes a scanning pattern of particular areas to find relevant information

4. Problems related with existing system

- For identifying the driver's fatigue level, detecting the eye state is important more than detecting the eye-steering correlation.
- Correlation between the eye-steering is complex and might produce wrong results undetermined cases.
- Steering movements consists of large calculations and graphs and it is difficult to merge with eye movements in all type of roads. Lane determination is not necessary for driver distraction.

III. PROPOSED SYSTEM

In the proposed system, the driver fatigue and distraction is detected only by processing of eye region. The main symptoms of driver fatigue and distraction appear in the driver's eyes because of sleeping while driving. Nowadays, there are many fatigue detection methods and the best is capturing the eyes in real time using web camera to detect the physical responses in eyes. Moreover, the processing of the eye region instead of the processing of the face region has less computational complexity.

3.1. Researches and Statistics

India has the highest proportion of deaths due to road traffic accidents in South East Asia. India accounts for as high as 6 per cent of the world's RTAs, although it has 1 per cent of the world's vehicles. The RTA (Road Traffic Accident) rate of 35 per 1,000 vehicles in India is one of the highest in the world and so is the RTA fatality rate of 25.3 per 10,000 vehicles.

Recent years have been witnessing an increasing amount of traffic on the roads leading to increased risks for road traffic accidents to occur. Evidence from developed and especially developing countries indicates that road traffic accidents are on the rise and are found to be fifth among important causes of deaths globally, leading to a significant proportion of injuries, deaths and disabilities in the population.

3.2. Process of proposed system

In the existing system, it detects the driver's fatigue using eye-steering correlation monitoring. Thus it uses the "Driver distraction detection algorithm" which concentrates on both visual and cognitive behaviors. We consider that for detecting the fatigue of the driver only eye state or behavior is sufficient and provides a easy way to use in all the vehicles.

The detection of cognitive method is tedious and it may go wrong sometimes which may provide wrong results. The steering movement consists of large calculations and graphs and it is difficult to merge with eye movements in all type of roads.

So in the proposed system we detect only the eye region and monitor the eyelid closure using PRECLOS (PERcentage CLOSure). A commonly used measure of eye closure duration is 'PERCLOS' – percentage of time a person's eyes are 80-100% closed over a period of time. When the eye is not detected the person is considered to be distracted or in the sleepy state.

Fig 1: Overall process of Proposed approach

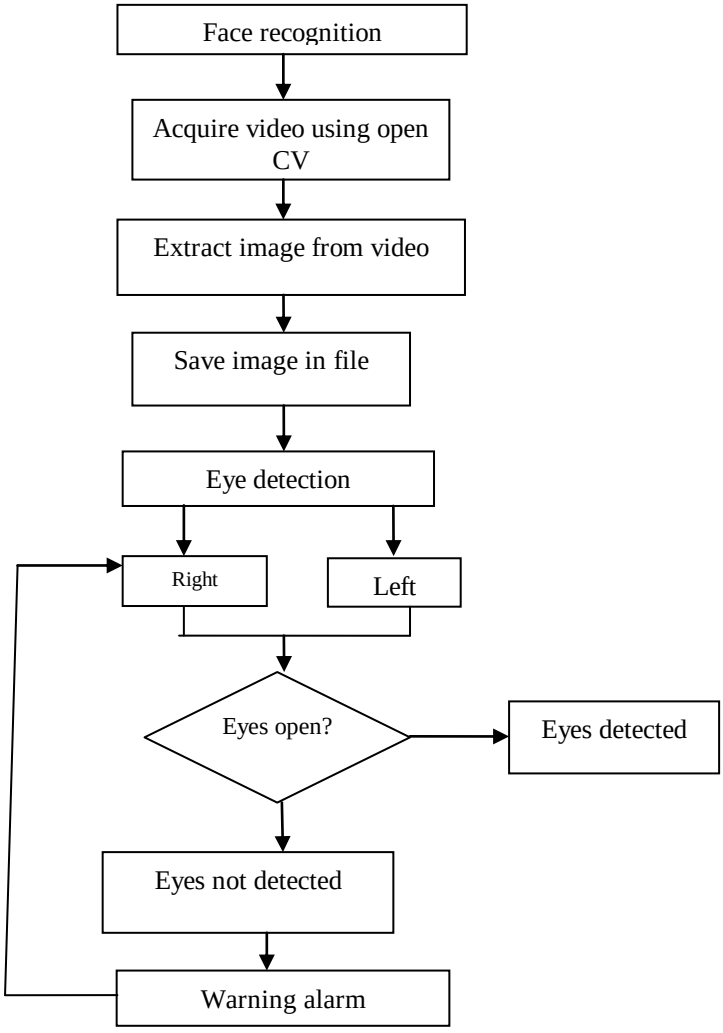

3.3 PERCLOS algorithm

A real time driver attention monitoring system is proposed using PERCLOS algorithm which is said to be the estimator of fatigue level. The main purpose of this algorithm is eye detection for a general driver under varying illumination conditions and finding class of the detected eye.

When the driver sits in the driver seat and start the vehicle, the webcam started to detect the face automatically refer figure 1.1. Unless the web camera is on, the vehicle cannot be started.

Fig 1.1: Face detection and extraction of eyes

When the eye region is detected from the video a photograph is taken and stored in the file to identify the person's eye as shown in the figure 1.2. Then video is captured throughout the journey and detects the eye movements to find the state of eyes.

Fig 1.2: Add face module

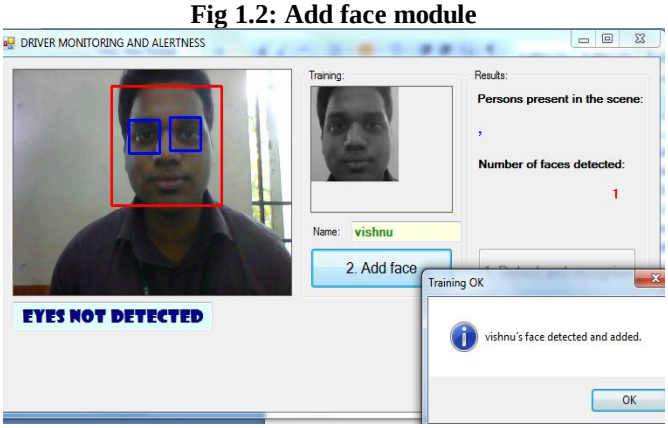

The driver's eye in the video is compared with the stored image and when the driver's eye is located in the video as detected, the eyes is said to be in active state (refer figure 1.3).

Fig 1.3: Eyes detected

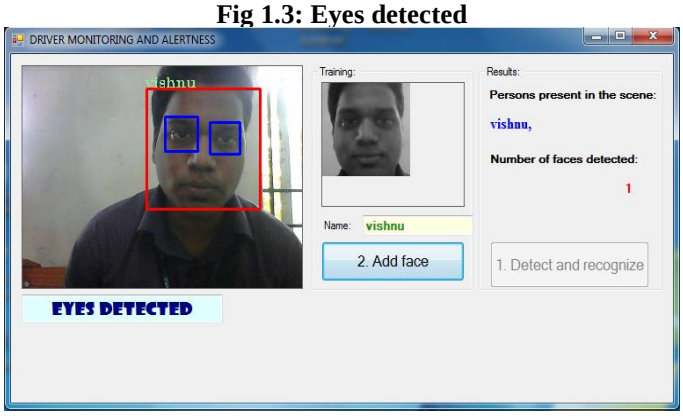

The driver's eye in the video is compared with the stored image and when the driver's eye is not located in the video then he is said to be distracted and a message is given as shown in figure 1.4. When the eye's is found to be in the closed state automatically an alarm signal is given to awaken the driver. This system not only detects the drowsiness of the driver it also detects the driver distraction such as moving, looking around etc. The timely warning alerts the driver as well as the passengers to be aware of the happening.

Fig 1.4: Eyes not detected

3.4 Advantages

- Accidents can be avoided by alerting the driver's distraction and drowsiness using warning signals.
- Comparing to the driver detection algorithm this PERCLOS system reduces the time complexity.
- It is used to track the alertness of the driver throughout the journey.
- The warning alarm alerts the driver as well as the passengers to be conscious about the driver's behavior.
- This system typically behaves as a user-friendly application.

IV. CONCLUSION

This system will analyze the state of driver's eye state whether it is closed or opened. If it is closed then produce the warning alarm to awaken the driver and prevent the vehicle from accident. By monitoring the driver's eye state using the PRECLOS algorithm by web camera the system can detect symptoms of driver fatigue early enough to avoid an accident and save people life by detecting the distraction an drowsiness. So this project is useful and easy to detect the driver's fatigue level and give the warning output in the form of sound to alert the driver as well as the passengers.

REFERENCES

Journal Papers:

[1] Lora yekhshatyan, John D.Lee, " *Changes in correlation between eye and sterring movements indicate driver distraction" IEEE trans. Intell. Transp*. Syst.,vol .14, no.1,pp. 136-145,Mar 2013.

[2] Mohamad-Hoseyn Sigari, Mahmood Fathy, Mohsen Soryani, **"A Driver** *Face Monitoring System for Fatigue and Distraction Detection"* International Journal of Vehicular Technology, Volume 2013 (2013), Article ID 263983.

[3] Boon-Giin Lee , Wan-Young Chung, *"Driver Alertness Monitoring Using Fusion of Facial Features and Bio-Signals"* IEEE sensor journal., vol. 12, no. 7, pp. 2416-2422, july. 2012.

[4] Yanchao Dong, Zhencheng Hu ,Uchimura K, Murayama. N *"Driver Inattention Monitoring system for Intelligent Vehicles" IEEE trans. Intell.Transp*. Syst., vol .12, Issue . 2, no.1,pp. 596-614, 2011.

[5] M.Omidyeganesh,Javadtalab.A,Shirmohammadhi.S *"Intelligent driver drowsiness detection through fusion of yawning and eye closure"* Virtual Environments Human-Computer Interfaces and Measurement Systems (VECIMS), 2011 IEEE International Conference on Sep-2011

[6] I.Daza, N. Hernandez, L. Bergasa, I. Parra, J. Yebes, M. Gavilan, R. Quintero, D. Llorca, and M. Sotelo, *"Drowsiness monitoring based on driver and driving data fusion"* in Intelligent Transportation Systems (ITSC), 2011 14th International IEEE Conference on, oct. 2011, pp. 1199-1204.

[7] M.Wollmer, C.Blaschke, T.Schindl, B.Schuller, B.farber, S.Mayer, and B.Treffich. *"Online Driver Distraction Detection using short-term Memory" IEEE trans.intell*. transp.syst., vol.12, no.2, pp.574-582, jun 2011.

[8] Hardeep Singh, J,S Bhatia, Jasbir Kaur, *"Eye Tracking based driver fatigue monitoring and Warning System"* Power electronics (IICPE),2010 India International Conference on Jan-2011, ISBN:978-1-4244-7883-5, INSPEC Accession no: 11873780, publisher: IEEE.

[9] Marco Javier Flores, Jose Maria Armingol, Arturo de la Escalera, *"Real Time Warning System for Driver Drowsiness Detection Using Visual Information"* Vol. 59, Issue. 2, pp. 103-125, August 2010.

[10] L. Yunqi, Y. Meiling, S. Xiaobing, L.Xiuxia, O. Jiangfan, *"Recognition Of Eye States in Real Time Video"* in Proceedings of the International Conference on Computer Engineering and Technology, IEEE Computer Society, Vol. 10, No.105, 2009, pp. 554-559.

[11] M. Wilson, M. Chattington, and D. E. Marple-Horvat, *"Eye movements drive steering: Reduced eye movement distribution impairs steering and driving performance" J. Motor Behav.*, vol. 40, no. 3, pp. 190–202, May 2008.

[12] E. Rogado, J.L. García, R. Barea, L.M. Bergasa, E. López, *"Driver Fatigue Detection System"* in the Proceedings of the IEEE International Conference on Robotics and Biomimetics Bangkok, Thailand, 2009, pp.1105-1110.

[13] M.H Sigari, *"Driver Hypo-Vigilance Detection based on Eyelid Behavior"* in Proceedings of the Seventh International Conference on Advances in Pattern Recognition, IEEE Computer Society, 2009. pp. 426-429.

[14] Dr. P.R Bajaj, M.S Devi, *"Driver Fatigue Detection Based on Eye Tracking"* in Proceedings of the First International Conference on Emerging Trends in Engineering and Technology, IEEE Computer Society, 2008, pp. 649-652.

[15] Branzan, A., Widsten, B., Wang, T., Lan, J., Mah, J. *"A computer vision-based system for real-time detection of sleep onset in fatigued drivers"* In: IEEE Intelligent Vehicles Symposium, pp. 25–30 (2008).

OPEN ACCESS

International
Journal
Of Modern Engineering Research (IJMER)

$\hat{g}^*$S-closed sets in topological spaces

S. Pious Missier[1], M. Anto[2]

[1]*Associate Professor, PG and Research Department of Mathematics, V.O.Chidambaram College of Arts and Sciences, Thoothukudi 628008, India.*

[2]*Associate Professor, Department of Mathematics, Annai Velankanni College, Tholayavattam 629157, India*

Abstract: *In this paper, we define and study about a new type of generalized closed set called, $\hat{g}^*$s-closed set.Its relationship with already defined generalized closed sets are also studied.*

Keywords: *$\hat{g}^*$s-closed sets, S$\hat{g}$ space*

2010 AMS Classification: 54A05

I. Introduction

Norman Levine introduced the notion of semi open sets[8] and generalized closed(briefly,g-closed) sets[7] in a topological space (X,τ) in 1963 and 1970 respectively. The initiation of the study of generalized closed sets was done by Aull[3] in 1968 as he considered sets whose closure is contained in every open super set. Since then extensive research on generalization of closed sets has been going on. The notion of 'generalized semi closed sets' was introduced by Arya and Nour[2] in 1990.In 1987,Bhattacharya and Lahiri[14] defined and studied the concept of 'semi gen eralised closed sets' via the notion of semi closed sets. In 2009, A.I.El.Maghrabi and A.A.Nasef introduced and studied a new class of sets, namely g^*s-closed sets[6], which is properly placed between the class of all semi closed sets and the class of all gs-closed sets. The authors introduce the class of $\hat{g}^*$s-closed sets which happen to lie between the class of all g^*s-closed sets and the class of all gs-closed sets.

Throughout this paper, (X,τ) denotes a topological space in which no separation axiom is assumed unless explicitely stated.

II. Prelimineries

Definition 2.1: A subset A of a topological space (X,τ) is called

(i) semi-open[8] if $A \subseteq cl(int(A))$ and semi-closed if $int(cl(A)) \subseteq A$,

(ii) pre-open[11] if $A \subseteq int(cl(A))$ and pre-closed if $cl(int(A)) \subseteq A$,

(iii) α-open[12] if $A \subseteq int(cl(int(A)))$ and α-closed if $cl(int(cl(A))) \subseteq A$,

(iv) Semi pre open or β-open[1] if $A \subseteq cl(int(cl(A)))$ and semi pre-closed β-closed if $int(cl(int(A))) \subseteq A$.

The semi closure (respectively, pre-closure, α-closure and semi pre closure) of a subset A of a space (X,τ) is the intersection of all semi-closed sets(respectively, pre-closed, α-closed and semi pre closed) sets containing A and is denoted by scl(A) (respectively, p- cl(A), α- cl(A) and sp cl(A)).

The semi interior (respectively, pre-interior) of a subset A of a space (X,τ) is the union of all semi open(respectively, pre-open) sets contained in A and is denoted by sint(A) (respectively, pint(A)).

Definition 2.2 [20]: A subset A of a topological space (X,τ) is called $\hat{g}$-closed if $cl(A) \subseteq U$ whenever $A \subseteq U$ and U is semi-open in (X,τ).

Remark 2.3: Note that $\hat{g}$-closed sets are called ω-closed sets by P.Sundaram and M.Sheik John[15] in 1995 and s^*g-closed sets[4] by K.Chandrasekara Rao and K.Joseph in 2000.

Definition 2.4 [7]: A subset A of a topological space (X,τ) is called a g-closed if $cl(A) \subseteq U$ whenever $A \subseteq U$ and U is open in (X,τ).

Definition 2.5 [14]: A subset A of a topological space (X,τ) is called a sg-closed if $scl(A) \subseteq U$ whenever $A \subseteq U$ and U is semi-open in (X,τ).

Definition 2.6 [18]: A subset A of a topological space (X,τ) is called a g^*-closed if cl(A) $\subseteq U$ whenever A $\subseteq$ U and U is g-open in (X,τ).

Definition 2.7 [6]: A subset A of a topological space (X,τ) is called a g^*s-closed if scl(A) $\subseteq U$ whenever A $\subseteq$ U and U is g-open in (X,τ).

Definition 2.8 [2]: A subset A of a topological space (X,τ) is called a gs-closed if scl(A) $\subseteq U$ whenever A $\subseteq$ U and U is open in (X,τ).

Definition 2.9 [19]: A subset A of a topological space (X,τ) is called a $\hat{g}^*$-closed if cl(A) $\subseteq U$ whenever A $\subseteq$ U and U is $\hat{g}$-open in (X,τ).

Definition 2.10 [16]: A subset A of a topological space (X,τ) is called a $\hat{g}^*\alpha$-closed if αcl(A) $\subseteq U$ whenever A $\subseteq$ U and U is $\hat{g}$-open in (X,τ).

Definition 2.11 [9]: A subset A of a topological space (X,τ) is called a $g\alpha$-closed if αcl(A) $\subseteq U$ whenever A $\subseteq$ U and U is α-open in (X,τ).

Definition 2.12 [10]: A subset A of a topological space (X,τ) is called a αg-closed if αcl(A) $\subseteq U$ whenever A $\subseteq$ U and U is open in (X,τ).

Definition 2.13 [5]: A subset A of a topological space (X,τ) is called a generalized semi pre closed set(briefly,gsp-closed), if spcl(A) $\subseteq U$ whenever A $\subseteq$ U and U is open in (X,τ).

Definition 2.14 [13]: A subset A of a topological space (X,τ) is called a $\hat{\eta}^*$-closed set if spcl(A) $\subseteq U$ whenever A $\subseteq$ U and U is ω-open in (X,τ).

Definition 2.15 [21]: A subset A of a topological space (X,τ) is called a pre semi closed set if spcl(A) $\subseteq U$ whenever A $\subseteq$ U and U is g-open in (X,τ).

Definition 2.16 [17]: A subset A of a topological space (X,τ) is called a ψ-closed set if $s$cl(A) $\subseteq U$ whenever A $\subseteq$ U and U is sg-open in (X,τ).

Notations Used:

(i) $\hat{g}^*$sC(X,τ) denotes the class of all $\hat{g}^*$s-closed sets in (X,τ).
(ii) $\hat{g}^*$sO(X,τ) denotes the class of all $\hat{g}^*$s-open sets in (X,τ).
(iii) SC(X,τ) denotes the class of all semi-closed sets in (X,τ).
(iv) SO(X,τ) denotes the class of all semi-open sets in (X,τ).
(v) gC(X,τ) denotes the class of all g-closed sets in (X,τ).
(vi) gO(X,τ) denotes the class of all g-open sets in (X,τ).
(vii) $\hat{g}^*$C(X,τ) denotes the class of all $\hat{g}^*$ -closed sets in (X,τ).
(viii) $\hat{g}^*\alpha$C(X,τ) denotes the class of all $\hat{g}^*\alpha$ -closed sets in (X,τ).
(ix) g^*s C(X,τ) denotes the class of all g^*s -closed sets in (X,τ).
(x) ψ C(X,τ) denotes the class of all ψ-closed sets in (X,τ).
(xi) sgC(X,τ) denotes the class of all sg-closed sets in (X,τ).
(xii) gsC(X,τ) denotes the class of all gs-closed sets in (X,τ).
(xiii) SPC(X,τ) denotes the class of all semi pre-closed sets in (X,τ).
(xiv) $\hat{\eta}^*$C(X,τ) denotes the class of all $\hat{\eta}^*$-closed sets in (X,τ).
(xv) $\hat{g}$C(X,τ) denotes the class of all $\hat{g}$-closed sets in (X,τ).
(xvi) $\hat{g}$cl(A) denotes the $\hat{g}$-closure of A in (X,τ).
(xvii) A^c or X-A denotes the complement of A in (X,τ).
(xviii) P(X) denotes the power set of X.

III. $\hat{g}^*$s-closed sets

Definition 3.1: A subset A of a topological space (X,τ) is called a $\hat{g}^*$s-closed set if $scl(A) \subseteq U$ whenever $A \subseteq U$ and U is $\hat{g}$-open.

Example 3.2: :Let (X,τ) be a topological space where X = {a,b,c,d} with τ = {∅, X. {a}, {b}, {a,b}}.Then $\hat{g}^*sC(X,\tau)$ = { φ, X. {b,c,d}, {a,c,d},{a,b,d}, {a,b,c},{c,d}, {b,d},{b,c}, {a,d},{a,c}, {d},{c}, {b},{a}}.

Example 3.3: Let (X,τ) be a topological space where X = {1,2,3,4,……} with τ = {∅, X,{1}, {1,2}, {1,2,3}, {1,2,3,4},……}.

We can easily find out that $\hat{g}^*sC(X,\tau)$ = { ∅, X, {2,3,4,……}, {1,3,4,……}, {1,2,4,……}, {1,2,3,5,6,,……},……., {3,4,5,……}, {2, 4,5,……}, {2,3,5,6,……}, {2,3,4,6,7,……},……., {1, 4,5,……}, {1,3,5,……}, {1, 3,4,6,……},……., {1,5,6,7,……}, {1, 4,6,7,……}, {1, 4,5,7……},……}.

Remark 3.4: The following example shows that the intersection of two $\hat{g}^*$s-closed sets need not be a $\hat{g}^*$s-closed set.

Example 3.5: Let (X,τ) be a topological space where X = {a,b,c,d} with τ = {∅, X. {a}, {b}, {a,b}}.Here A = {a,b,d} and B = {a,b,c} are $\hat{g}^*$s-closed sets. But A∩B = {a,b} is not a $\hat{g}^*$s-closed set.

Remark 3.6: The following example shows that the union of two $\hat{g}^*$s-closed sets need not be a $\hat{g}^*$s-closed set.

Example 3.7: Let (X,τ) be a topological space where X = {a,b,c,d} with τ = {∅, X. {a}, {b}, {a,b}}.Here A = {a } and B = {b} are $\hat{g}^*$s-closed sets. But A∪B = {a,b} is not a $\hat{g}^*$s-closed set.

Proposition 3.8: Every semi closed set in a topological space X is $\hat{g}^*$s-closed in X.

Remark 3.9: The following example shows that the converse of the above proposition is not true.

Example 3.10: Let (X,τ) be a topological space where X = {a,b,c,d} with τ = {∅, X. {a}, {b}, {a,b}}.Here {a,b,d} is $\hat{g}^*$s-closed but not semi closed.

Proposition 3.11: Let A be a $\hat{g}^*$s-closed subset of X. Then scl(A) – A contains no nonempty $\hat{g}$-closed subset.

Proof: Let F be a $\hat{g}$-closed subset of scl(A) – A. Now $F \subseteq$ scl(A) – A and $A \subseteq X - F$ where A is $\hat{g}^*$s-closed and X – F is $\hat{g}$-open. Thus $scl(A) \subseteq X - F$ or equivalently $F \subseteq X - scl(A)$. But $F \subseteq$ scl(A). Therefore $F \subseteq [X - scl(A)] \cap [scl(A)]$.i.e., $F = \emptyset$.Hence the proof.

Corollary 3.12: If A is $\hat{g}^*$s-closed in (X,τ), then A is semi closed iff scl(A) – A is $\hat{g}$-closed in X.

Proof:

NECESSISITY

If A is semi closed,then scl(A) – A = ∅ and hence scl(A) – A is $\hat{g}$-closed in X.

SUFFICIENCY

Let scl(A) – A be $\hat{g}$-closed in X. By Proposition 3.11, scl(A) – A contains no nonempty $\hat{g}$-closed subset in X.Then scl(A) – A = ∅ and hence A is semi closed.

Remark 3.13: The following example shows that the converse of the Proposition 3.11 is not true.

Example 3.14: Let (X,τ) be a topological space where X = {a,b,c,d} with τ = {∅, X. {a}, {a, b}, {a, b, c}}. Then $SC(X,\tau)$ = { ∅, X. {b, c, d},{c, d}, {b, d},{b, c},}, {d},{c}, {b}};$\hat{g}c(X,\tau)$ = {∅, X. {b,c,d},{c,d}, {d}}; $\hat{g}^*sC(X,\tau)$ = {∅, X. {b,c,d}, {a,c,d},{a,b,d}, {c,d}, {b,d},{b,c}, {a,d}, {d},{c}, {b}}. Consider A = {*a,c*}.It is clear that scl(A) – A = {b,d} contains no nonempty $\hat{g}$-closed subset in X. But A = {*a,c*} is not $\hat{g}^*$s-closed.

Proposition 3.15: In a topological space (X,τ),for each $x \in X$, {x} is $\hat{g}$-closed in X or $\{x\}^c$ is $\hat{g}^*$s-closed in X.

Proof: If {x} is not $\hat{g}$-closed in X, then the only $\hat{g}$-open set containing X – {x} is X. Then scl(X – {x}) ⊆ X. Therefore, X – {x} is $\hat{g}^*$s-closed.

Proposition 3.16: In a topological space (X,τ), every $\hat{g}$-open set is semi closed iff every subset of X is $\hat{g}^*$s-closed.

Proof:

NECESSISITY

Suppose that every $\hat{g}$-open set is semi closed. Let A be a subset of X such that A ⊆ U whenever U is $\hat{g}$-open.But scl(A) ⊆ scl(U) = U. Therefore A is $\hat{g}^*$s-closed.

SUFFICIENCY

Suppose that every subset of X is $\hat{g}^*$s-closed.Let U be $\hat{g}$-open. Since U is $\hat{g}^*$s-closed, we have scl(U) ⊆ U. Therefore, scl(U) = U. Hence the proof.

Proposition 3.17: If A is both $\hat{g}$-open and $\hat{g}^*s$-closed, then A is semi closed.

Proof:

Let A ⊆A and A is both $\hat{g}$-open.Since A is $\hat{g}^*$-closed, scl(A) ⊆ A. Therefore, scl(A) = A and hence, A is semi closed.

Proposition 3.18: Every $\hat{g}^*$-closed set is $\hat{g}^*$s-closed.

Remark 3.19: The following example shows that the converse of the Proposition 3.18 is not true.

Example 3.20: Let (X,τ) be a topological space where X = {a,b,c,d} with τ = {∅, X. {a}, {a,b,c} }. Then $\hat{g}^*$C(X,τ) = { φ, X. {b,c,d}, {a,c,d},{a,b,d}, {c,d}, {b,d}, {a,d}, {d}};$\hat{g}^*$sC(X,τ) = { φ, X. {b,c,d}, {a,b,d}, {a, c, d},{c,d}, {b,d},{b,c}, {a,d}, {d},{c}, {b}}.Here {b} is $\hat{g}^*$s-closed but not $\hat{g}^*$-closed.

Proposition 3.21: Every g^*s -closed set is $\hat{g}^*$s-closed.

Remark 3.22: The following example shows that the converse of the Proposition 3.21 is not true.

Example 3.23: Let (X,τ) be a topological space where X = {a,b,c,d} with τ = {∅, X. {a}, {a,b,c} },{a,d}}. Then g^*s C(X,τ) = { φ, X. {b,c,d}, {c,d}, {b,d},{b,c}, {d},{c}, {b}};$\hat{g}^*$sC(X,τ) = { φ, X. {b,c,d}, {a,b,d}, {a, c, d},{c,d}, {b,d},{b,c}, {d},{c}, {b}}.Here {a,b,d} is $\hat{g}^*$s-closed but not g^*s -closed.

Proposition 3.24: Every ψ-closed set is $\hat{g}^*$s-closed.

Remark 3.25: The following example shows that the converse of the Proposition 3.24 is not true.

Example 3.26: Let (X,τ) be a topological space where X = {a,b,c,d} with τ = {∅, X. {a}, {a,b,c} }}. Then ψC(X,τ) = { φ, X. {b,c,d}, {c,d}, {b,d},{b,c}, {d},{c}, {b}};$\hat{g}^*$sC(X,τ) = { φ, X. {b,c,d}, {a,b,d}, {a, c, d},{c,d}, {b,d},{b,c}, {a,d},{d},{c}, {b}}.Here {a,b,d} is $\hat{g}^*$s-closed but not ψ-closed.

Proposition 3.27: Every $\hat{g}^*$s-closed set is $\hat{\eta}^*$- closed.

Remark 3.28: The following example shows that the converse of the Proposition 3.27 is not true.

Example 3.29: Let (X,τ) be a topological space where X = {a, b, c, d} with τ = {∅, X. {a,b}, {a,b,c}, {a,b,d} }}. Then $\hat{\eta}^*$C(X,τ) = { φ, X,{b,c,d},{a,c,d}, {c,d}, {b,d},{b,c},{a,d}, {a,c}, {d},{c}, {b},{a}};$\hat{g}^*$sC(X,τ) = { φ, X. {b,c,d}, {a, c, d},{c,d},{d},{c} }. Here {a} is $\hat{\eta}^*$-closed but not $\hat{g}^*$s -closed.

Proposition 3.30: Every $\hat{g}^*$s-closed set is gs- closed.

Remark 3.31: The following example shows that the converse of the Proposition 3.30 is not true.

Example 3.32: Let (X,τ) be a topological space where X = {a, b, c } with τ = {∅, X. {a}, {b,c}}}. Then gsC(X,τ) = { φ, X,{b,c },{a,c }, {a,b},{c}, {b},{a}}; $\hat{g}^*$sC(X,τ) = { φ, X. {b,c }, {a} }. Here {a,c} is gs-closed but not $\hat{g}^*$s -closed.

Proposition 3.33: Every $\hat{g}^*\alpha$-closed set is $\hat{g}^*$s-closed.

Remark 3.34: The following example shows that the converse of the Proposition 3.33 is not true.

Example 3.35: Let (X,τ) be a topological space where X = {a,b,c,d} with τ = {∅, X. {a}, {b},{a,b} }}. Then $\hat{g}^*\alpha$ C(X,τ) = { φ, X. {b,c,d},{a,b,d}, {a, c, d},{a,b,c}, {c,d}, {b,d},{b,c}, {a,d},{*a,c*}, {d},{c}}; $\hat{g}^*$sC(X,τ) = { φ, X. {b,c,d}, {a,b,d}, {a, c, d},{a,b,c},{c,d}, {b,d},{b,c}, {a,d},{*a,c*}, {d},{c}, {b},{a}}.Here {a} is $\hat{g}^*$s-closed but not ψ-closed.

Remark 3.36: The following two examples show that g-closedness and $\hat{g}^*$s-closedness are independent of each other.

Example 3.37: Let (X,τ) be a topological space where X = {a,b,c,d} with τ = { φ, X,{a},{a,b,c}}.Then gC(X,τ) = { φ, X,{b,c,d}, {a,c,d},{a,b,d}, {c,d}, {b,d}, {a,d},{d}}; $\hat{g}^*$sC(X,τ) = { φ, X,{b,c,d}, {a,c,d},{a,b,d},{c,d}, {b,d},{b,c}, {a,d}, {d},{c}, {b}}.Here {c} is $\hat{g}^*$s-closed but not g-closed.

Example 3.38: Let (X,τ) be a topological space where X = {a,b,c} with τ = { φ, X,{a},{ b,c}}.Then $\hat{g}^*$sC(X,τ) = { φ, X,{b,c}, {a}}; gC(X,τ) =P(X).Here {b} is g-closed but not $\hat{g}^*$s-closed.

Remark 3.39: The following two examples show that sg-closedness and $\hat{g}^*$s-closedness are independent of each other.

Example 3.40: Let (X,τ) be a topological space where X = {a,b,c,d} with τ = { φ, X,{a,b},{ c,d}}.Then sgC(X,τ) = P(X); $\hat{g}^*$sC(X,τ) = { φ, X, ,{a,b},{ c,d}}.Here {a} is sg-closed but not $\hat{g}^*$s-closed.

Example 3.41: Let (X,τ) be a topological space where X = {a,b,c,d} with τ = { φ, X,{a}}.Then sgC(X,τ) = { φ, X,{b,c,d}},{c,d}, {b,d},{b,c},{d},{c}, {b}} ; $\hat{g}^*$sC(X,τ) = { φ, X,{b,c,d}, {a,c,d},{a,b,d}, {a,b,c},{c,d}, {b,d},{b,c}, {a,d},{a,c},{a,b} , {d},{c}, {b}}. Here {a,b} is $\hat{g}^*$s -closed but not sg-closed.

Remark 3.42: The following two examples show that $\hat{g}$-closedness and $\hat{g}^*$s-closedness are independent of each other.

Example 3.43: Let (X,τ) be a topological space where X = {a,b,c,d} with τ = { φ, X,{a},{ a,b,c }}.Then $\hat{g}$C(X,τ) = { φ, X,{b,c,d},{ d }}; $\hat{g}^*$sC(X,τ) = { φ, X,{b,c,d}, {a,c,d},{a,b,d}, {c,d}, {b,d},{b,c}, {a,d}, {d},{c}, {b}}.Here {c} is $\hat{g}^*$s-closed but not $\hat{g}$-closed.

Example 3.44: Let (X,τ) be a topological space where X = {a,b,c} with τ = { φ, X,{a},{b,c}}.Then $\hat{g}$C(X,τ) = P(X) ; $\hat{g}^*$sC(X,τ) = { φ, X,{b,c}, {a,}}. Here { b} is $\hat{g}$-closed but not $\hat{g}^*$s-closed.

Remark 3.45: From the above Propositions and Remarks, we obtain the following diagram.

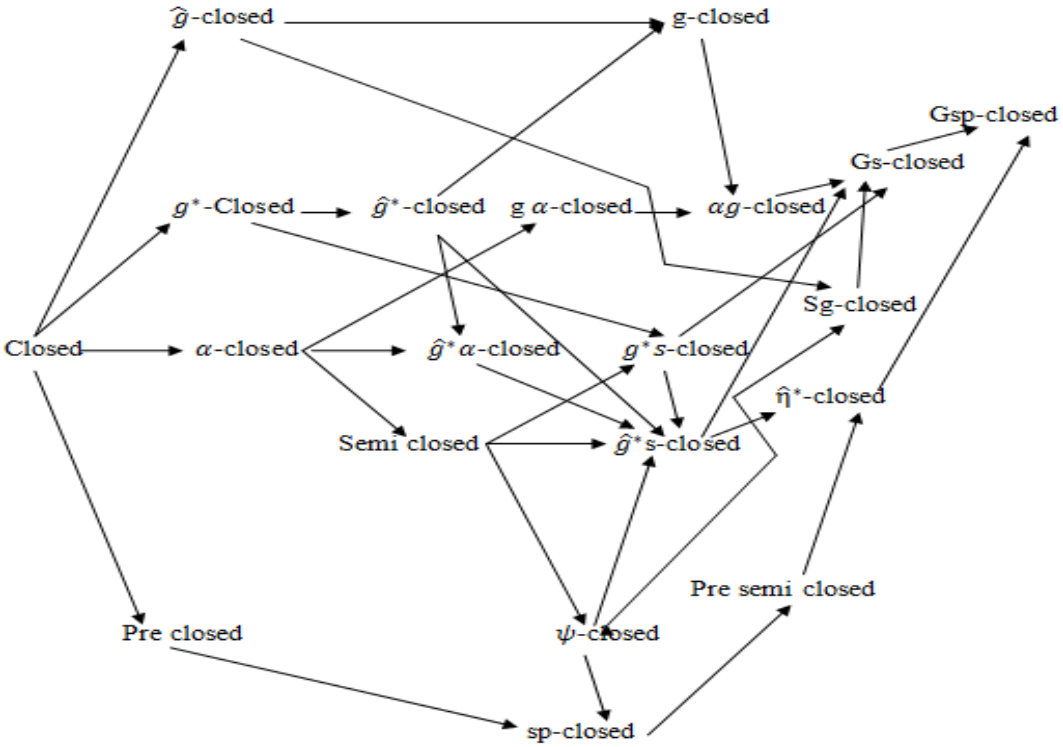

Definition3.46: A topological space (X,τ) is called a S$\hat{g}$ space if the intersection of a semi closed set with a $\hat{g}$-closed set in it is $\hat{g}$-closed.

Example 3.47: Let (X,τ) be a topological space where X = {a,b,c,d} with τ = {∅, X. {a,b}, {a, b,c}, {a, b, d}}. Then SC(X,τ) = { ∅, X. { c, d},{ d}, {c}}; $\hat{g}$c(X,τ) = {∅, X, {b,c,d},{a,c,d},{c,d}, {d},{c}}.As the intersection of a semi closed set with a $\hat{g}$-closed set is $\hat{g}$-closed, the above topological space (X,τ) is a S$\hat{g}$ space.

Proposition 3.48: For a subset A of a S$\hat{g}$ space (X,τ), the following are equivalent.

(i) A is $\hat{g}^*$s-closed.

(ii) $\hat{g}$cl({ x}) ∩ A ≠ ∅ for each x ∈ scl(A).

(iii) scl(A) – A contains no nonempty $\hat{g}$-closed set.

Proof: (i) ⟹ (ii)

Let x ∈ scl(A).Suppose $\hat{g}$cl({ x}) ∩ A = ∅. Then A ⊆ (X – $\hat{g}$cl({ x})).Since A is $\hat{g}^*$s-closed, scl(A) ⊆ (X – $\hat{g}$cl({ x})) which is a contradiction to x ∈ scl(A).Therefore $\hat{g}$cl({ x}) ∩ A ≠ ∅.

(ii) ⟹ (iii)

Let F be a $\hat{g}$-closed set such that F ⊆ scl(A) – A. Suppose F ≠ ∅. Let x ∈ F. Then $\hat{g}$cl({ x}) ⊆ F. Therefore, by (ii), ∅ ≠ $\hat{g}$cl({ x}) ∩ A ⊆ F ∩ A ⊆ (scl(A) – A) ∩ A = ∅ which is a contradiction. Therefore, F = ∅.

(iii) ⟹ (i)

Let A ⊆ G and G be $\hat{g}$-open in X.Suppose scl(A) is not a subset of G.Then scl(A) ∩ (X – G) is nonempty $\hat{g}$-closed subset of scl(A) – A which is a contradiction. Therefore scl(A) ⊆ G and hence A is $\hat{g}^*$s-closed.

Proposition 3.49: In a S$\hat{g}$ space (X,τ), the converse of Proposition 3.11holds.

Proof: (iii) ⟹ (i) of Proposition3.48.

Definition 3.50: Let A be subset of a topological space (X,τ).We define $\Lambda_{\hat{g}}(A)$ as follows. $\Lambda_{\hat{g}}(A) = \cap\{ U : : U \supseteq A, U \in \mathcal{g}O(X,\tau)\}$, where $\mathcal{g}O(X,\tau)$ denotes the collection all $\mathcal{g}$-open sets in (X,τ).

Proposition 3.51: A subset A of a topological space (X,τ) is $\hat{g}^*$s-closed iff $scl(A) \subseteq \Lambda_{\hat{g}}(A)$.

Proof:

NECESSISITY

Since A is $\hat{g}^*$s-closed, $scl(A) \subseteq U$ whenever $A \subseteq U$ and U is $\hat{g}$-open. Therefore $scl(A) \subseteq \Lambda_{\hat{g}}(A)$.

SUFFICIENCY

Let U be $\hat{g}$-open such that $A \subseteq U$.By assumption, $scl(A) \subseteq \Lambda_{\hat{g}}(A) \subseteq U$. Therefore A is $\hat{g}^*$s-closed.

REFERENCES

[1] D.Andrijeyic, Semi pre open sets, Mat. Vesnik 38 (1986), No.1,24-32.
[2] S.P.Arya and T.Nour, Characterizations of S-normal spaces, Indian J. Pure Appl. Math.,21(1990),717-719.
[3] C. E. Aull, Para compact and countably para compact spaces, General topology and its relation to modern Analysis and Algebra, Proc.Kanpur Topological Con.,(1968), 49-53.
[4] K.Chandrasekhara Rao and K.Joseph, Semi star generalized closed sets, Bulletin of Pure and Applied Sciences, I9E(No.2) 2000, 281-290.
[5] J.Dontchev, On generalizing semi pre open sets, Mem. Fac. Sci, Kochi Univ., Ser.A.Math. 16(1995), 35-48.
[6] A.I.El.Maghrabi and A.A.Nasaf, Between semi closed and gs closed sets,Journal of Taibah University for Science 2: 78-87(2009).
[7] N.Levine, Generalised closed sets in topology, Rend.Circ.Mat.Palermo.19(2)(1970), 89-96.
[8] N.Levine, Semi open sets and semi continuity in topological spaces, Amer. Math. Monthly 70(1963) 36-41.
[9] H.Maki, R.Devi and K.Balachandran, Generalized α-closed sets in topology, Bull.Fukuoka Univ. Ed.Part III, 42(1993), 13-21.
[10] H.Maki, R.Devi and K.Balachandran, Associated topologies of generalized α-closed sets α- generalized closed sets, Mem. Fac. Sci, Kochi Univ., Ser.A.Math. 15(1994), 51-63.
[11] A.S. Mashhour, M.E.Abd.El-Monsef and S.N.El.Deeb, On pre continuous and weak pre continuous mappings, Proc.Math.and Phys. Soc. Egypt.53(1982),47-53.
[12] O.Njastad, On some classes of nearly open sets, Pacific J. Math.15(1965),961-970.
[13] N.Palaniappan, J.Antony Rex Rodrigo and S.Pious Missier,On $\hat{\eta}^*$-closed sets in topological spaces(accepted).
[14] Paritosh Bhattacharya and B.K Lahiri, Semi generalized closed sets, Indian J of Mathematics, Vol.29, No.3, 1987, 375-382.
[15] P.Sundaram and M.Sheik John, Weakly closed sets and weak continuous maps in topological spaces, Proc., 82nd Indian Sci.Cong.,Calcutta, (1995), 49.
[16] M.K.R.S.Veerakumar, μ-closed sets in topological spaces, Antartica J. Math., 2(1)(2005), 1-18.
[17] M.K.R.S.Veerakumar, Between semi closed sets and semi pre closed sets, Rend.Istit.Mat. Univ. Trieste, Vol.XXXI,25-41(2000).
[18] M.K.R.S.Veerakumar, Between closed sets and g closed sets, Mem. Fac. Sci, Kochi Univ., Ser.A.Math., 21(2000), 1-19.
[19] M.K.R.S.Veerakumar, Between g^* closed sets and g closed sets, Antartica J. Math., 3(1)(2006), 43-65.
[20] M.K.R.S.Veerakumar, On $\hat{g}$-locally closed sets and $\hat{g}$LC-functions, Indian Journal of Mathematics, Vol.43, No.2,2001,231-247.
[21] M.K.R.S.Veerakumar, Pre Semi Closed Sets, Indian Journal of Mathematics, , Vol.44, No.2,2002,165-187.

OPEN ACCESS

International
Journal
Of Modern Engineering Research (IJMER)

Mechanical Characterization of Biodegradable Linen Fiber Composites

I. Keerthi[1], V. Devender[2], V. Mahesh[3]
[1]*PG Scholar, Department of Mechanical Engineering, SREC, Warangal, India*
[2]*Asst. Professor, Department of Mechanical Engineering, SREC, Warangal, India*
[3]*Professor, Department of Mechanical Engineering, SREC, Warangal, India*

***Abstract**: The conventional materials like iron, mild steel, cast iron etc are having good mechanical properties. Hence they are widely used in structural engineering applications. These conventional materials have some defects like formation of rust, low weight to strength ratio, high production cost. To overcome these defects, engineers started fabricating composite materials. Composites exhibit peculiar properties like different strengths in different directions, rust resistant, high strength to weight ratio, but they pollute the environment. Now the natural fibre composites are widely used in automobile industry. The natural fibres and resins are used to fabricate an eco friendly composite material. Lack of resources and increasing environmental pollution has evoked great interest in the research of materials that are friendly to our health and environment. Bio polymer composites fabricated from natural fibres is currently the most promising area in polymer sciences. This is designed to assess the possibility of fibre as reinforcing material in composites. Epoxy resin was made a stiffened panel to conduct tensile test. In this paper it is aimed to explain all possible ways to use natural composites in automobile components. The main advantages of using natural fibers are their degradability and light weight. They are environment friendly and also increase the fuel economy.*

***Keywords:** Natural fibers, Natural composites, automobile parts, biodegradable.*

I. Introduction

With the development of new high performance fibres, composites began to compete with metals, and replace them, in myriad application. Fibre reinforced composites ventured into areas which were unthinkable few decades ago, making the products light weight, improving the performance of the product and in some cases improving the life time too. Better mechanical properties of these composites are due to excellent interfacial adhesion between fibre and matrix, in addition to good mechanical properties of fibres. However the good interfacial adhesion between fibre and matrix, which is beneficial in the product, is a significant disadvantage in the products "afterlife" since the fibres and matrix cannot be separated easily. This impairs the recycling of either or both. Also these fibres are not easily compostable; hence the composite cannot be used to recover energy. Within today's climate of growing environmental awareness and with depleting natural resources, people have resorted back to using natural fibres in lieu of polymeric fibres wherever possible.

Based on the objectives of the present work a close review has been carried out of the following topics to understand and assess the current status. With the strong emphasis on environmental awareness, much attention has been brought into the development of recyclable and environmentally sustainable literature composite materials since the last decade. Environmental legislation as well as consumer demand in many countries is imposing higher pressure on manufacturers of materials and end products. They have to consider the environmental impact of their products at all stages of their life cycle, including recycling and ultimate disposal. These environmental issues have recently generated considerable interest in the development of recyclable and biodegradable composite materials. Therefore, research in the field of using natural fibres has attracted much attention in the material science and engineering discipline. Natural fibre is certainly a renewable resource that can be grown and made within a short period of time, in which the supply can be unlimited when compared with traditional glass and carbon fibre for making advanced composites. This natural fibre mixing with polymers can produce new class of materials in bio-medical application and lightweight structural application.

The variation in mechanical properties of natural fibres is due to the conditions during growth. Depending on the extraction process, the chemical composition, fibre shape, fibre strength, flexibility, and ability to adhere to other fibres or matrix differ widely between different types of woods. This makes it difficult to predict the mechanical properties of the natural fibre reinforced composites, studied comparative life cycle assessment of natural fibre and glass fibre composites. Natural fibre is emerging as low cost, lightweight and apparently environmentally superior alternatives to glass fibres in composites. Natural fibre composites are

likely to be environmentally superior to glass fibre composites in most cases for instance, the natural fibre production has lower environmental impacts compared to glass fibre production and end of life incineration of natural fibres results in recovered energy and carbon credits. Plant based composites may in future, become materials to replace polymer based composites and wood in terms of their attractive specific properties, lower cost, simple processing technologies, eco friendliness, and ability to be recycled after use [2]. The quality and performance of plant-based composites can further be improved by adopting appropriate engineering techniques.

Research on natural fibre composite is still relatively new. It is clear that improvements must be made if natural fibres are to compete with synthetic fibres on the composite market. The adhesion between the fibre and the matrix, the processing of the fibres and the structure of the fibres are examples of areas that need to be studied in more detail. The adhesion between the fibres and the matrix is crucial to all fibre composite materials. If the adhesion is good, stress is transferred between the load carrying fibres over the matrix, which makes the material strong and stiff. A directly proportional relationship was discovered between interphase thickness and adhesion. This, we believe, is a consequence of entanglements formed in an inter diffusion process at the fiber/matrix interface [1].

1.1 Two main reasons for the interest in biodegradable materials are:

1. The growing problem of waste thereby resulting general shortage of landfill availability, and 2. The need for environmentally responsible use of resources, together with the carbon dioxide neutrality aspect. Bio-composites or more specifically the "green composites," consists of bio-fibre and bio-plastic from renewable resources and thus are expected to be biodegradable. Biodegradable polymers may be defined as those that undergo microbially induced chain scission, leading to mineralization, photo degradation, oxidation, and hydrolysis, which can alter a polymer during the degradation process.

II. Materials And Procedure To Prepare Laminate

2.1. Lenin Fibre

Linen is made from the fibres of the flax plant, *Linum usitatissimum*. Linen is labour-intensive to manufacture but when it is made into garments, it is valued for its exceptional coolness and freshness in hot weather.

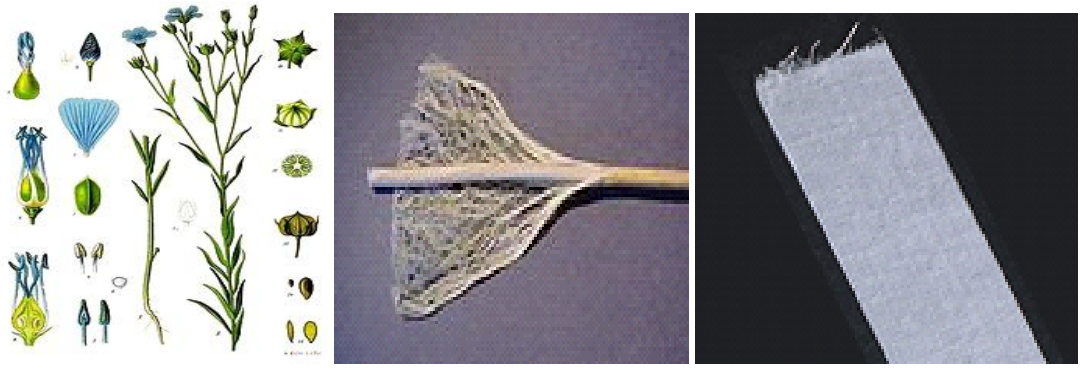

Figure 1: Preparation of Linen fibre from flax plant

2.2 Properties of Linen

- Linen is renowned for its spectacular durability and long life. The tensile strength of linen thread is twice as high as that of cotton and three times that of wool.
- Flax cell is highly compatible with the human cell thereby producing a benevolent effect on the human organism.
- Used as bed linen as it reduces fatigue and lifts spirits.
- Flax fabric is an excellent filter protecting against a chemically aggressive medium, noise and dust.
- Linen reduces gamma radiation nearly by half and protects the human organism against solar radiation. Flax fibre from contaminated soils appears not to exhibit even traces of radiation.
- Linen underwear possesses rare bacteriological properties. Resistant to fungus and bacteria, it is found to be an effective barrier to some diseases. According to medical studies conducted by Japanese researchers, bed-ridden patients do not develop bedsores where linen bed sheets are used. Wearing linen clothes helps to get rid of some skin diseases - from common rash to chronic eczemas.
- Linen does not cause allergic reactions and is helpful in treating a number of allergic disorders.

- Linen is effective in dealing with inflammatory conditions, reducing fever and regulating air ventilation, and is also helpful in the treatment of some neurological ailments;
- Linen cloth does not accumulate static electricity - even a small addition of flax fibres (up to 10%) to a cloth is enough to eliminate the static electricity effect.
- Linen is highly hygroscopic as it is capable to rapidly absorb and yield moisture. [3]It evaporates water as quickly as the pond surface. It has been established that before giving a feeling of being wet, linen cloth can absorb as much as 20% of its dry weight. That explains why linen cloth always feels fresh and cool.
- Linen possesses high air permeability and heat conductivity properties. Heat conductivity of linen is five times as high as that of wool and 19 times as that of silk. In hot weather those dressed in linen clothes are found to show the skin temperature 3°-4°C below that of their silk or cotton-wearing friends. According to some
- Studies, a person wearing linen clothes perspires 1.5 times less than when dressed in cotton clothes and twice less than when dressed in viscose clothes. Meanwhile in cold weather linen is an ideal warmth-keeper.
- Silica present in the flax fibre protects linen against rotting - the mummies of Egyptian Pharaohs preserved to the present day are wrapped in the finest linen cloth.
- Linen rejects dirt and does not get teaselled.
- Linen and Linen-containing articles are easily laundered in hot water, may be boiled and dried in the sun, besides they may be hot-ironed thereby ensuring maximum sterilization.
- The more Linen is washed the softer and smoother it becomes.
- Linen underscores naturalness, softness and relief increasing is yet another precious property possessed by Linen.

The main drawback of natural fibers is their hydrophilic nature that lowers their compatibility with comparatively hydrophobic polymer matrix. The surface chemical modifications of natural fibers like dewaxing, alkali treatment, vinyl grafting, cyanoethylation, acetylation, bleaching, peroxide treatment, sizing with polymeric Iso cyanides, treatment with saline and other coupling agents have achieved various levels of success in improving fiber-matrix adhesion in natural fiber composites [7]

2.3 Matrix (Resin)

Araldite sets by the interaction of a resin with a hardener. Heat is not necessary although warming will reduce the curing time and improve the strength of the bond. After curing, the joint is claimed to be impervious to boiling water and all common organic solvents. It is available in many different types of packs, the most common containing two different tubes, one each for the resin and the hardener. Other variations include double syringe-type packages which automatically measure equal parts.

Interior parts from natural fiber and polypropylene (PP),exterior parts from natural fiber - polyester resins are already in use[5].Ford has a long history of R&D on new materials[6]. He performed a durability test with a fire axe on prototype car made of plastics derived from soybeans

Araldite (Resin/ Hardener) is an epoxy adhesive used for multi-purpose, viscous material that is suitable for bonding a variety of materials including metal, Ceramic and wood. The various applications, advantages and properties of Resin are shown in Table 1. The electrically insulating adhesive is easy to apply either manually by spatula and stiff brush or mechanically with meter/mix and coating Equipment. Araldite resin/Hardener an epoxy adhesive cures at temperatures from 68ºF (20ºC) to 356ºF (180ºC) with no release of volatile constituents. Unlike other biopolymers, cellulosic plastic shows better compatibility with lingo-cellulosic bio-fibers [4]

Table 1: Applications, Advantages and Properties of Resin

Applications of Resin in other materials	***Advantages***	***Key Properties***
• Metal • Ceramics • Wood • Vulcanized Rubber • Foams • Plastics	• Long open time • High shear and peel strength • Easy to apply • Good resistance to static and dynamic loads • Electrically insulating	• Easy to mix and apply • Gap filling • Excellent resistance to chemicals • Solvent free • Heat resistance up to 120°C • Cures @5^0-100°C

2.4 Preparation of Laminate

Step-1: Remove every alternate string from the Lenin cloth horizontally and vertically in such a manner that it Looks like a band aid cloth, leaving gaps such that resin can be uniformly filled.

Step-2: Take a single layer of PVC sheet and apply grease on it.

Step-3: Take equal proportions of Hardener and Resin forms of Araldite in a bowl and mix properly to get a uniform mixture.

Step-4: Apply this mixture uniformly on the PVC sheet.

Step-5: Place a woven linen fibre of two folds on the PVC sheet and coat on the fibre uniformly with brush . Place it in open air for curing, formed a laminate as **sample-I**.

Step-6: Again repeat steps 4 and 5 to obtain Three layered laminate by keeping three layers on PVC sheet and Considered as **sample-II**.

Step-8: Make four such layers and consider it as **Sample-III.**

Step-9: Now repeat steps 2-4 to get a sample and individual strings removed from the original Linen fibre. Finally apply Araldite mixture uniformly on the sample obtained, which will be considered as **Sample-IV**. Table-2 shows different samples and their individual weights of all the four samples were taken after curing for 24 hours and tabulated as below:

Table-2: Different samples and their individual weights of all the four samples

S. No	*Sample No*	*Total Weight (g) after curing*
1	Sample-I	70.2
2	Sample-II	54.2
3	Sample-III	41.6
4	Sample-IV	36.6

Figure 2: Four layered sample-III

Figure 3: Three Layered sample-II

Figure-4: Two Layered sample-II

Figure-5: Individual fibre sample-I

Table 3: Calculation for weight of resin used in different samples

Sample No	*Total weight of sample (g)*	*Weight of Linen used (g)*	*Weight of Resin (g)*
Sample-I	70.2	3.4×4= 13.6	56.6
Sample-II	54.2	3.4×3= 10.2	43.0
Sample-III	41.6	3.4×2= 6.8	34.6
Sample-IV	36.6	4	32.6

Figure-6: Samples after curing

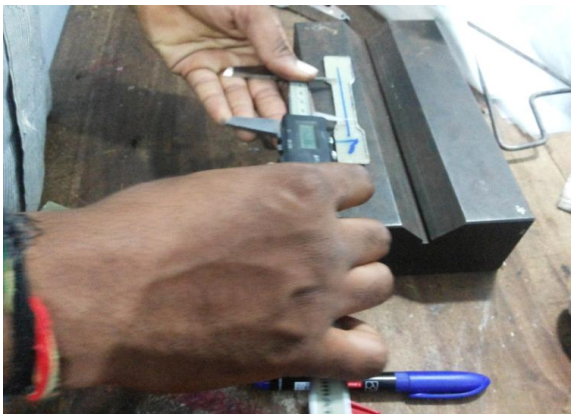

Figure-7: Sample Measurement

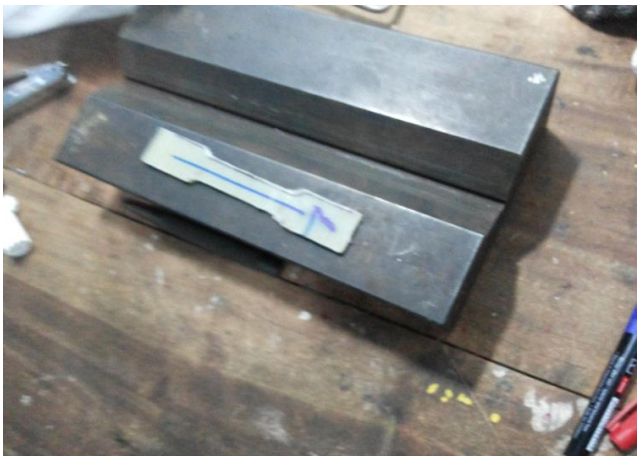

Figure 8: Test sample

III. Results Of Tensile Test Conducted On Samples

3.1 Sample-I

Table 4: Results of the tensile test conducted on sample containing 4 layers

Input			*Output*		
Specimen shape	=	Flat	Load at yield	=	0.63 KN
Specimen width	=	13.34 mm	Elongation at yield	=	2.790 mm
Specimen thickness	=	2.98 mm	Yield stress	=	15,848 N/mm2
Gauge length	=	50 mm	Load at peak	=	0.78 KN
Pre load value	=	0 KN	Elongation at peak	=	4.07 mm
Max.load	=	600 KN	Ultimate strength	=	19.621 N/mm2
Max.Elongation	=	250 mm	Load at break	=	0.78 KN
Cross section area	=	39.75 mm^2	Elongation at break	=	4.02 mm
Final gauge length	=	50.36 mm	% elongation	=	0.72 %

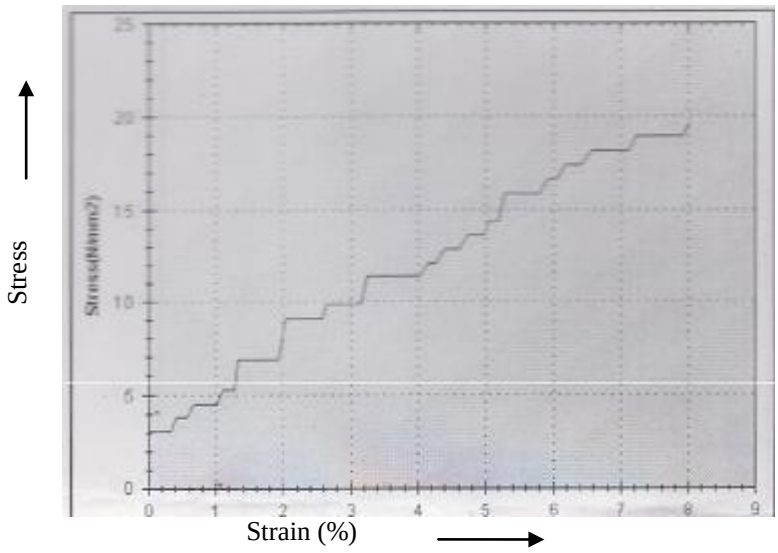

Figure 9: Stress Vs Strain

3.2 Sample-II

Table 5: Results obtained for sample containing 3 layers.

Input			***Output***		
Specimen shape	=	Flat	Load at yield	=	0.57 KN
Specimen width	=	13.77 mm	Elongation at yield	=	4.73 mm
Specimen thickness	=	2.55 mm	Yield stress	=	16.234 N/mm^2
Gauge length	=	50 mm	Load at peak	=	0.72 KN
Pre load value	=	0 KN	Elongation at peak	=	6.04 mm
Max.load	=	600 KN	Ultimate strength	=	20.506 N/mm^2
Max.Elongation	=	250 mm	Load at break	=	0.69 KN
Cross section area	=	35.11 mm^2	Elongation at break	=	6.14 mm
Final gauge length	=	50.44 mm	% elongation	=	0.88

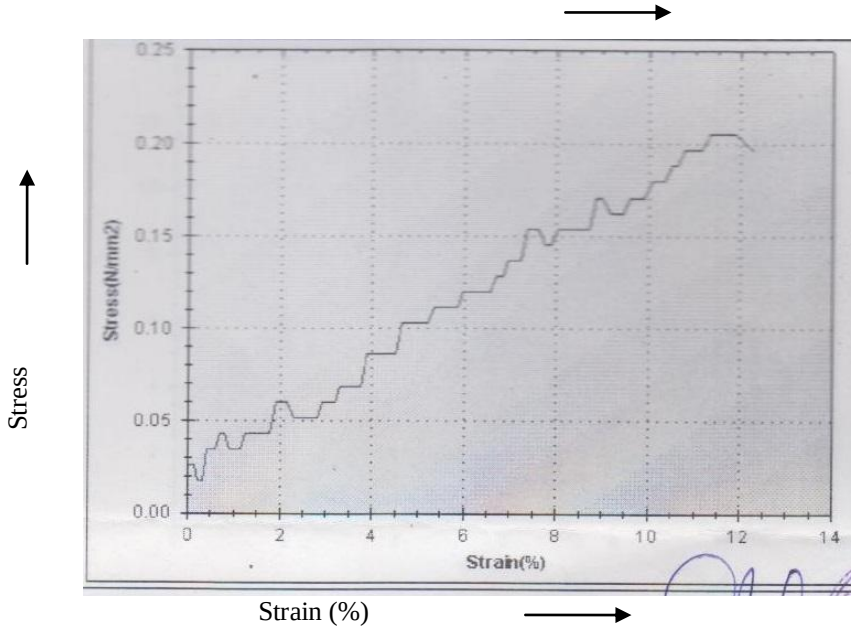

Figure 10: Stress Vs Strain

3.3 Sample-III

Table 6: Results obtained for sample containing 2 layers.

Input			*Output*		
Specimen shape	=	Flat	Load at yield	=	0.21 KN
Specimen width	=	14.34 mm	Elongation at yield	=	3.970 mm
Specimen thickness	=	1.74 mm	Yield stress	=	8.434 N/mm2
Gauge length	=	50 mm	Load at peak	=	0.3 KN
Pre load value	=	0 KN	Elongation at peak	=	5.27 mm
Max.load	=	600 KN	Ultimate strength	=	12.048 N/mm2
Max.Elongation	=	250 mm	Load at break	=	0.27 KN
Cross section area	=	24.9 mm2	Elongation at break	=	5.36 mm
Final gauge length	=	50.21 mm	% elongation	=	0.42

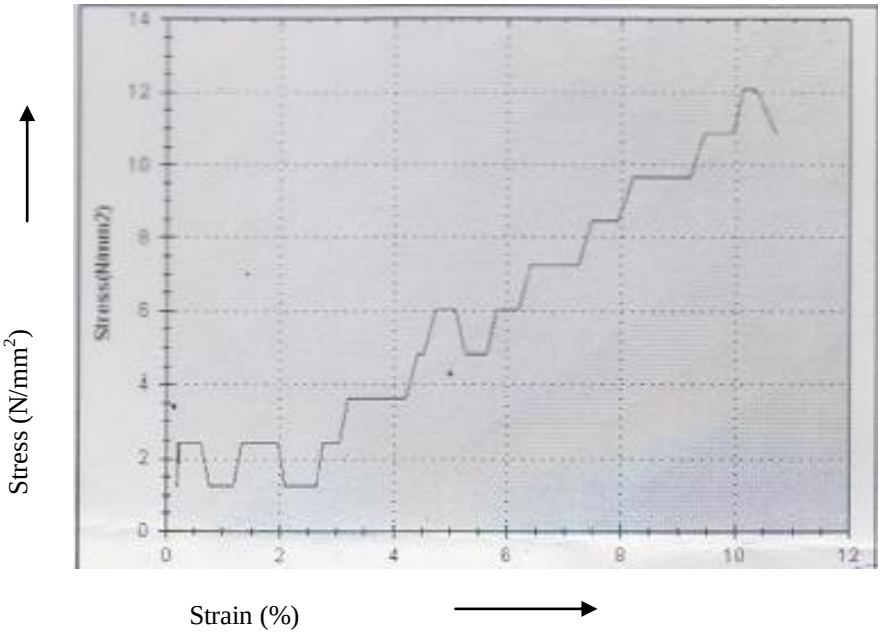

Figure 11: Stress Vs Strain

3.4 Sample-IV

Table 7: Results obtained for sample containing Individual fibres.

INPUT			*OUTPUT*		
Specimen shape	=	Flat	Load at yield	=	0.96 KN
Specimen width	=	13.33 mm	Elongation at yield	=	7.4 mm
Specimen thickness	=	3.13 mm	Yield stress	=	23.009 N/mm^2
Gauge length	=	50 mm	Load at peak	=	1.2 KN
Pre load value	=	0 KN	Elongation at peak	=	8.9 mm
Max.load	=	600 KN	Ultimate strength	=	28.761 N/mm2
Max.Elongation	=	250 mm	Load at break	=	1.2 KN
Cross section area	=	41.72 mm^2	Elongation at break	=	8.81 mm
Final gauge length	=	50.12 mm	% elongation	=	0.24

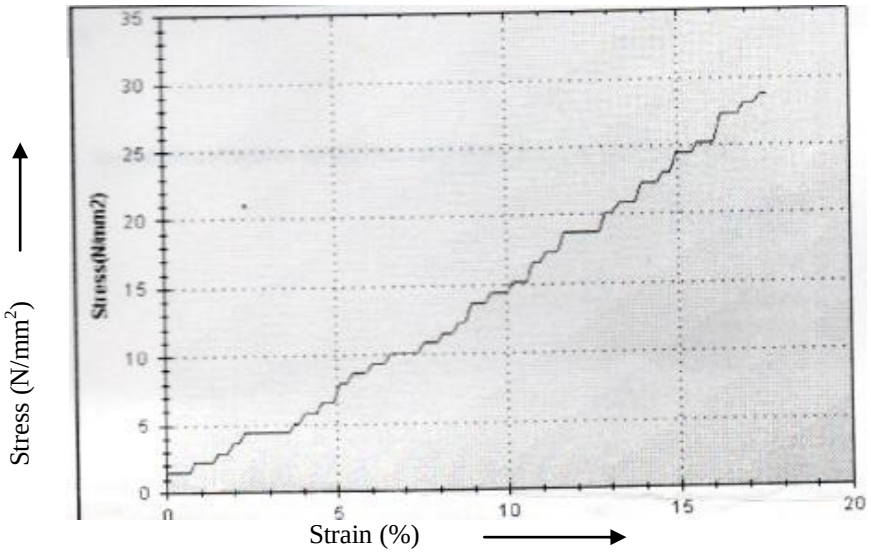

Figure 12: Stress Vs Strain

IV. Conclusion

After decades of high- tech developments of artificial fibers like aramid, carbon and glass it is remarkable that natural fibers have gained a renewed interest, especially as a glass fiber substitute in automotive industries.

Pure woven linen fibre-Araldite resin laminate has more strength than loose fibre –Araldite resin laminate. Both the laminates are very economical and pure plant fibres. Biodegradability of linen fibre is high and absolutely pollution free. Again renewable resource based bio-plastics are currently being developed and need to be researched more to overcome the performance limitations. The main advantage of using renewable materials is that the global CO_2 balance is kept at a stable level.

REFERENCES

[1] J.M. Felix and P. Gatenholm, , Interphase Design in Cellulose Fiber/Polypropylene Composites, Springer link(1993)
[2] Bwire S. Ndazi, Christian Nyahumwa, Joseph Tesha, Chemical and Thermal stability of rice husks against alkali , www.biosources.com(2007)
[3] Gassan and A.K. Bledski, Angew. Makromol. Chemie, "Wood filled thermoplastic composites" Springer link (1998)
[4] D. Hokens, A. K. Mohanty, M. Misra, L. T. Drzal, Polymer Preprint, Polym. Chem. ACS Chicago, Fall 2001.
[5] DaimlerChrysler "Grown to Fit the Part", High Tech. Report 1999, p. 82-85
[6] William F. Powers, "Automotive Materials in the 21st Century", Adv. Mater. Process, May 2000, p. 38-41.
[7] A. K. Mohanty, M. Misra, L. T. Drzal, "Surface modifications of natural fibers and performance of resulting bio-composites –An overview", Composite Interf. Accepted January 2001.

OPEN ACCESS

International
Journal
Of Modern Engineering Research (IJMER)

The Effect of insertion of different geometries on heat transfer performance in circular pipe- A review

Amol P. Yadav[1], Pranit M. Patil[2,] Dr. P. A. Patil[3]
[1]*P.G. Student, M.E. Heat Power, J.S.C.O.E, Hadapsar, Pune(M.S.) India*
[2]*Assistant Professor, Department of Mechanical Engineering, G.I.T, Lavel, Khed (M.S.) India*
[3]*Professor, Department of Mechanical Engineering, J.S.C.O.E, Hadapsar, Pune (M.S.) India*

Abstract: *Under turbulent flow conditions, the increase in heat transfer rate is more significant than that under laminar flow conditions. The turbulent effects become a dominant factor over secondary flow at higher Reynolds number. The turbulent flow can be produced by inserting different geometries in the circular pipe. This study focuses on the various methods or geometries used to produce turbulent geometries and its effect on the heat transfer. The turbulent generators with different geometrical configurations have been used as one of the passive heat transfer enhancement techniques and are the most widely used in tubes in several heat transfer applications. Insertion of such geometries may lead to increase the friction factor and pressure drop which directly enhances the heat transfer characteristics.*
Keywords: *Heat transfer characteristics, Turbulent flow, Reynolds number, Friction factor.*

I. INTRODUCTION

When turbulent flow is considered, many techniques were investigated for augmentation of heat transfer rates inside circular tubes using wide range of inserts. The inserts studied included coil wire inserts, brush inserts, mesh inserts, strip inserts, twisted tape inserts etc. Heat exchangers have many industrial applications for example, heat recovery processes, air conditioning and refrigeration systems, chemical reactors, and food and dairy processes. For better performance and economic aspects of the equipment, the design of heat exchanger needs exact analysis of heat transfer rate and pressure drop. Garc et al. [1] investigated the laminar–transition–turbulent heat transfer enhancement and flow patterns in the tube with wire coil inserts. Hsieh et al. [2] experimentally studied the turbulent heat transfer and flow characteristics in a horizontal circular tube with strip-type inserts. Bhuiya et al. [3] studied the heat transfer performance and friction factor characteristics in a circular tube fitted with twisted wire brush inserts were investigated experimentally. Halit bas [4] Flow friction and heat transfer behavior in a twisted tape swirl generator inserted tube are investigated experimentally Bhuiya et al. [5] have done the experimental investigation on Nusselt number, friction factor and thermal performance factor in a circular tube equipped with perforated twisted tape inserts with four different porosities of Rp = 1.6, 4.5, 8.9 and 14.7%. M.M.K. Bhuiya [6] explored the effects of the double counter twisted tapes on heat transfer and fluid friction characteristics in a heat exchanger tube. The double counter twisted tapes used as counter-swirl flow generators in the test section. Pankaj N. Shrirao et.al [7] Experimental investigation of heat transfer and friction factor characteristics of horizontal circular pipe using internal threads of pitch 100mm, 120mm and 160mm with air as the working fluid. Bodius Salam et.al [8] have carried an experimental investigation for measuring tube-side heat transfer coefficient, friction factor, heat transfer enhancement efficiency of water for turbulent flow in a circular tube fitted with rectangular-cut twisted tape insert.

In the above literature review, the numerous research articles were reported on heat transfer enhancement and pressure drop characteristics in tubes with various geometrical configurations of turbulence creator. Hence this study gives the overview of different techniques to enhance the heat transfer characteristics by producing turbulent flow in circular pipe with insertions of different types of inserts or geometries.

1. Twisted wire brush inserts
2. Twisted tape
3. Perforated twisted tapes
4. Double counter twisted tapes
5. Pipe with internal threads.

C_p	specific heat at constant pressure [J/(kgK)]	k	thermal conductivity [W/(m K)]
d	core-rod diameter [m]	L	tube length [m]
Di	tube inside diameter [m]	η	thermal performance factor, dimensionless
Do	tube outer diameter [m]	ηp	predicted thermal performance factor, dimensionless
d_w	wire diameter [m]		
f	friction factor, dimensionless	Re	Reynolds number, dimensionless
fp	predicted friction factor, dimensionless	Nu	Nusselt number, dimensionless

II. WIRE BRUSH INSERTS

Bhuiya et al. [3] the twisted wire brush inserts fabricated with four different twisted wire densities of 100, 150, 200, and 250 wires per centimeter by winding a 1 mm diameter of the copper wire over a 5 mm diameter of two twisted iron core-rods used for experimentation as shown in figure 1.

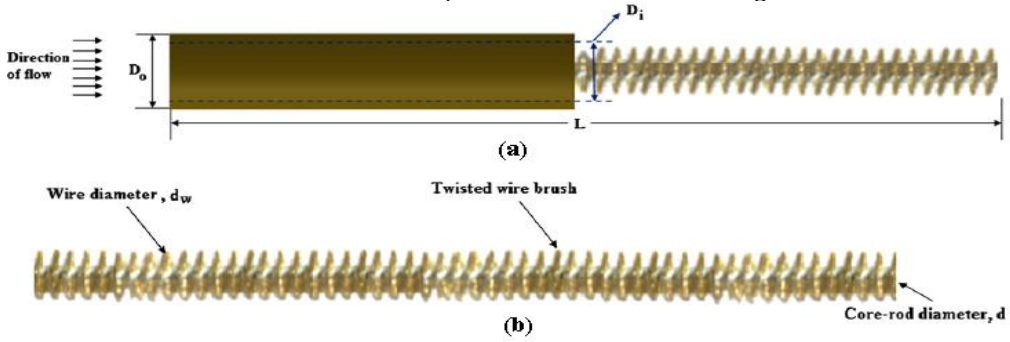

Figure 1. (a) Geometry of the test section fitted with the twisted wire brush insert. (b) Geometric parameters of the twisted wire brush insert.

By examining heat transfer and friction factor data in tubes for Reynolds number ranging from 7,200 to 50,200, it is found that the heat transfer performance and friction factor characteristics for turbulent flow through a tube are affected by means of twisted wire brush inserts. The twisted wire brush inserts provided significant enhancement of heat transfer with the corresponding increase in friction factor. The friction factor achieved for the tube with twisted wire brush inserts varied from 1.35 to 2.0 times than those of the plain tube values at the comparable Reynolds number. It was found that the Nusselt number, friction factor, and thermal performance factor increased with the increase of twisted wire densities. The thermal performance factor (η) obtained for the tube with twisted wire brush inserts varied from 1.1 to 1.85 times than those of the plain tube values at constant blower power as shown in Figure 2.

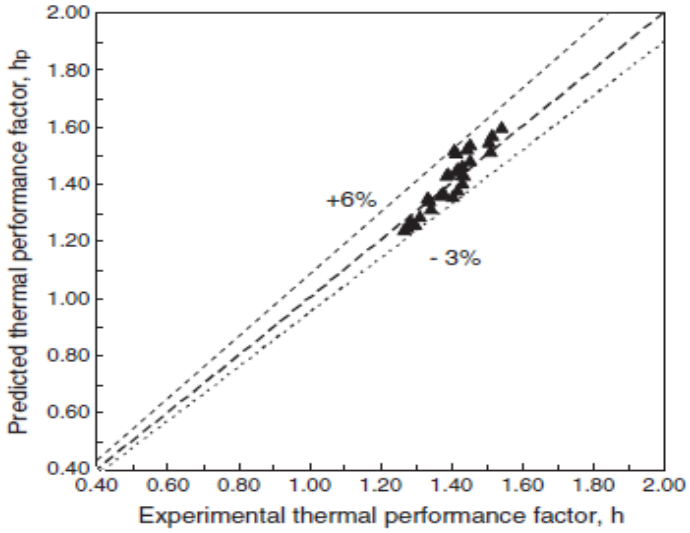

Figure 2. Comparison between the predicted and experimental thermal performance factor, η_p and experimental thermal performance factor η. [3]

III. TWISTED TAPE

The Use of twisted tape swirl generator in tube is one of the technique to enhance flow friction and heat transfer behavior. The twisted tapes are inserted separately from the tube wall. The effects of twist ratios (y/D = 2, 2.5, 3, 3.5 and 4) and clearance ratios (c/D = 0.0178 and 0.0357) are discussed in the range of Reynolds number from 5132 to 24,989, and the typical one (c/D = 0) is also tested for comparison by Halit bas [4]. He used SS304 seamless steel test and calming tube with 56 mm inner diameter (D1), 60 mm outer diameter (D2), and 2 mm thickness (t). The twisted tapes tested in experiments, with five different twist ratios (y/D = 2.0, 2.5, 3.0, 3.5 and 4.0) and two different clearance ratios (c/D = 0.0178 and 0.0357) are considered in this experimental study, are fabricated from steel. The schematic figure of the test tube with twisted tape insert is given in Figure 3.

Figure 3. Schematic view of the twisted tape inserted tube separated from the tube inner surface with teflon rings.

The twisted tapes are placed separately from the tube wall to obtain only heat transfer increase depending on laminar sub layer destruction near the tube wall. So, the effect of increased heat transfer surface area is eliminated. It is showed that the twist ratio (y/D) has major effect when compared with the clearance ratio (c/D) on heat transfer in twisted tape inserted tube. The heat transfer enhancement decreases, while Reynolds number increases and it is nearly constant at Reynolds number is higher than 15,000 and twist ratios are lower than 3. The highest heat transfer enhancements are obtained as 1.756 for c/D = 0.0178, as 1.744 for c/D = 0.0357 and as 1.789 for the typical twisted tape (c/D = 0) at y/D = 2 of all twist ratios. Heat transfer enhancement is higher in the tube with twisted tape inserted which has c/D = 0.0178 than c/D = 0.0357 for all cases as shown in figure 4 and 5.

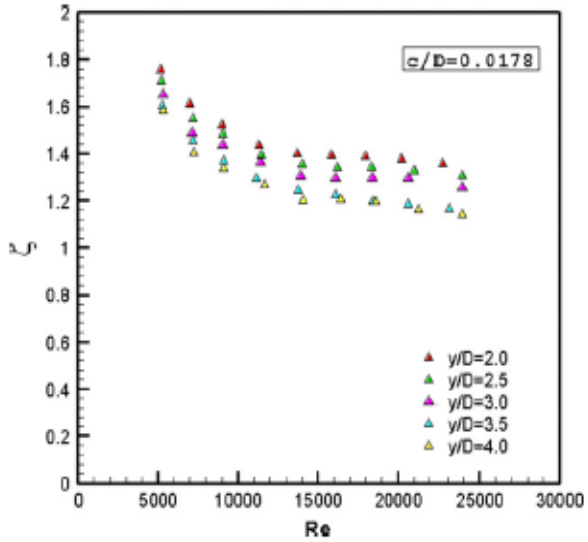

Figure 4. Variation of heat transfer enhancement with Reynolds number for different y/D ratios (c/D = 0.0178).

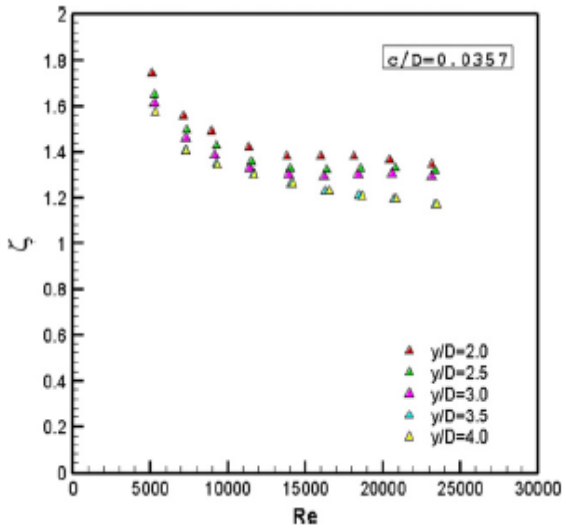

Fig. 5. Variation of heat transfer enhancement with Reynolds number for different y/D ratios (c/D = 0.0357).

IV. PERFORATED TWISTED TAPE

To obtain better heat transfer perforated twisted tapes are also used. Bhuiya [5] worked on Nusselt number, friction factor and thermal performance factor in a circular tube equipped with perforated twisted tape inserts with four different porosities of Rp = 1.6, 4.5, 8.9 and 14.7%. He conducted experiments in a turbulent flow regime with Reynolds number ranging from 7200 to 49,800 using air as the working fluid under uniform wall heat flux boundary condition.

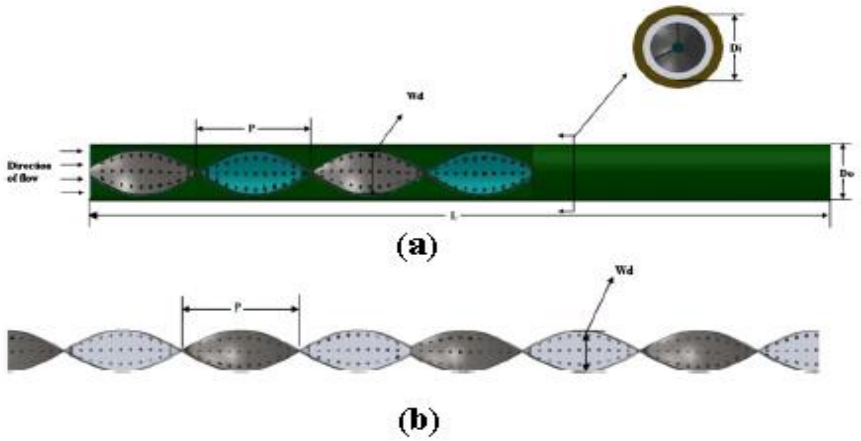

Figure 6. Geometry of test section fitted with perforated twisted tape insert; (b) Geometric parameters of the perforated twisted tape insert

The perforated twisted tape offered a higher heat transfer rate, friction factor and thermal performance factor compared to that of the plain tube. The Nusselt number (shown in Figure 8) friction factor and thermal performance factor obtained from the tube with perforated twisted tape inserts was 340%, 360% and 59% higher than those of the plain tube values, respectively. In addition, the influence of porosity 4.5% was more dominant than that of the other porosities of 1.6, 8.9 and 14.7% for all the Reynolds number. Figure 7 shows the performance factors for all twisted tapes tended to decrease with increasing Reynolds number. The thermal performance factors for all the cases were more than one indicated that the effect of heat transfer enhancement due to the enhancing tool was more dominant than the effect of the rising friction factor and vice versa as shown in figure 9.

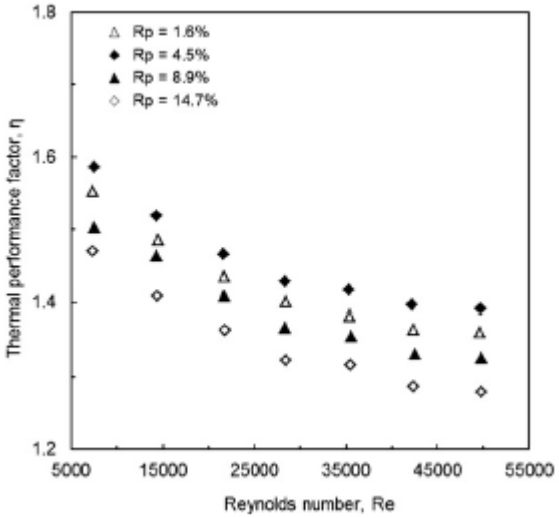

Fig 7 Relationship between the thermal performance factor and Reynolds number

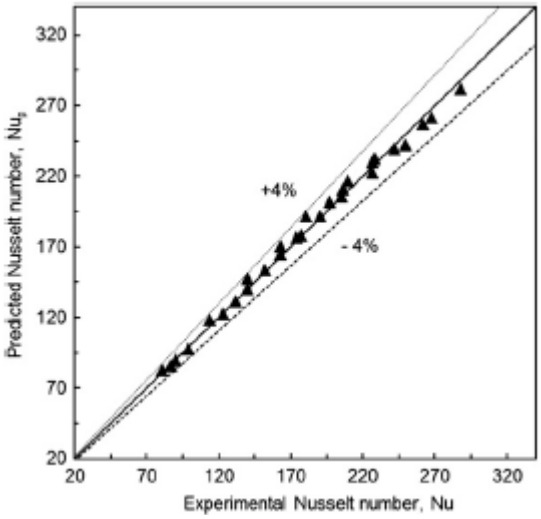

Fig 8 Comparison between the predicted and experimental Nusselt number.

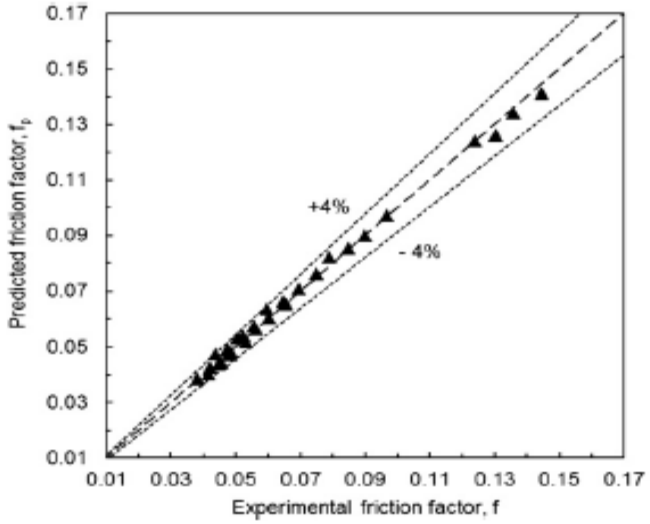

Fig. 9 Comparison between the predicted and experimental friction factor

V. DOUBLE COUNTER TWISTED TAPE

The double counter twisted tapes can be used as counter-swirl flow generators as shown in figure 10. M.M.K. Bhuiya [6] performed experiments with double counter twisted tapes of four different twist ratios (y = 1.95, 3.85, 5.92 and 7.75) using air as the testing fluid in a circular tube turbulent flow regime where the Reynolds number was varied from 6950 to 50,050. The experimental results demonstrated that the Nusselt number, friction factor and thermal enhancement efficiency were increased with decreasing twist ratio. The heat transfer rate in the tube fitted with double counter twisted tape was significantly increased with corresponding increase in pressure drop.

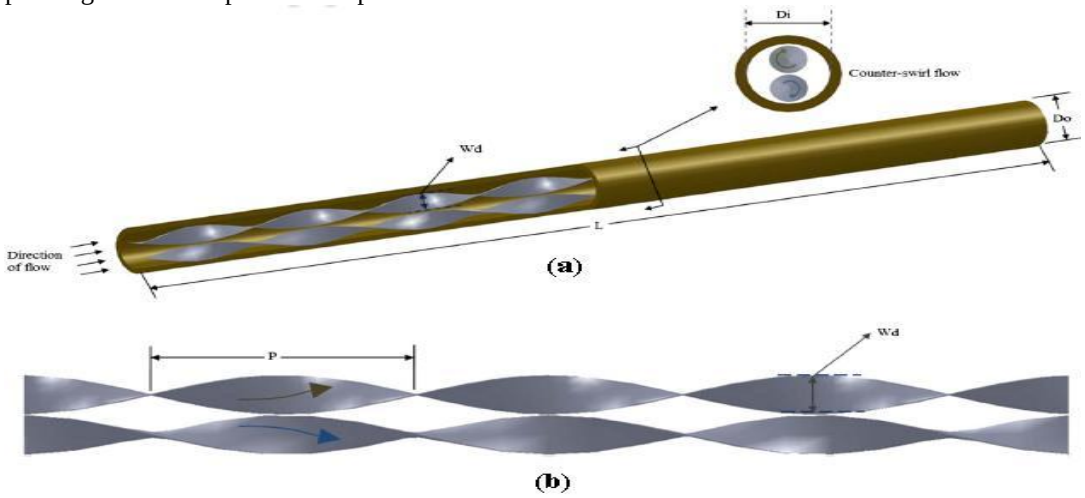

Figure 10. (a) Geometry of test section fitted with double counter twisted tape insert; (b) Geometric parameters of the double counter twisted tape insert. [6]

The double counter twisted tape offered a significant enhancement of heat transfer, friction factor as well as thermal enhancement efficiency compared with the plain tube values as shows in figure 11 and 12. In general observations, it was found that the heat transfer, friction factor and thermal enhancement efficiency increased with decreasing twist ratio. Furthermore, the Nusselt number increased with the increasing Reynolds number while the opposite trends were found for the case of friction factor and thermal enhancement efficiency.

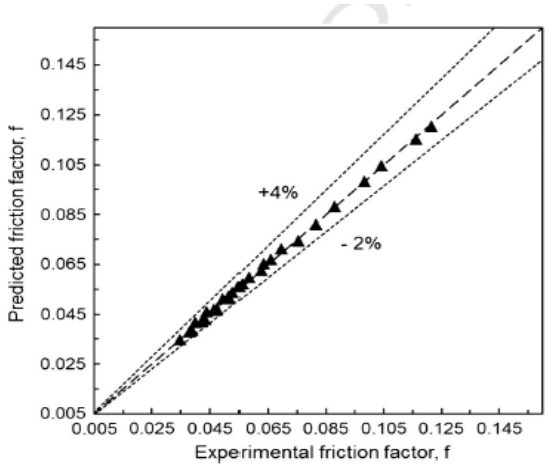

Fig 11 Comparison between the predicted and experimental friction factors

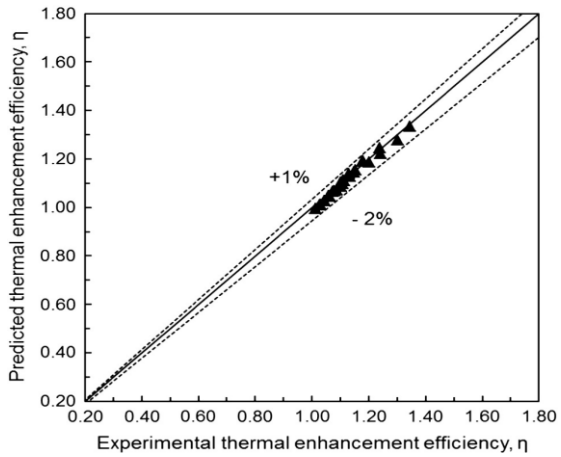

Fig 12 Comparison between the predicted and experimental thermal enhancement Efficiencies.

The thermal enhancement efficiency in the tubes equipped with double counter twisted tapes at constant blower power was achieved to be around 1.01 to 1.34 as shown in figure 12.

VI. PIPE WITH INTERNAL THREADS

To produce the turbulent flow through the pipe for good heat transfer characteristics one of the method used is to use a pipe with internal threads. Shrirao [7] studied heat transfer and friction factor characteristics of horizontal circular pipe using internal threads of pitch 100mm, 120mm and 160mm with air as the working fluid. The transitional flow regime is selected for this study with the Reynolds number range 7,000 to 14,000.

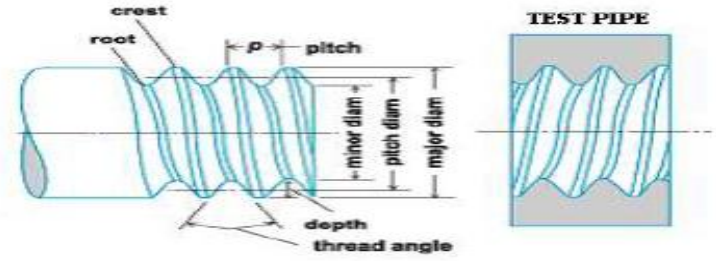

Fig 13 Pipe with internal thread

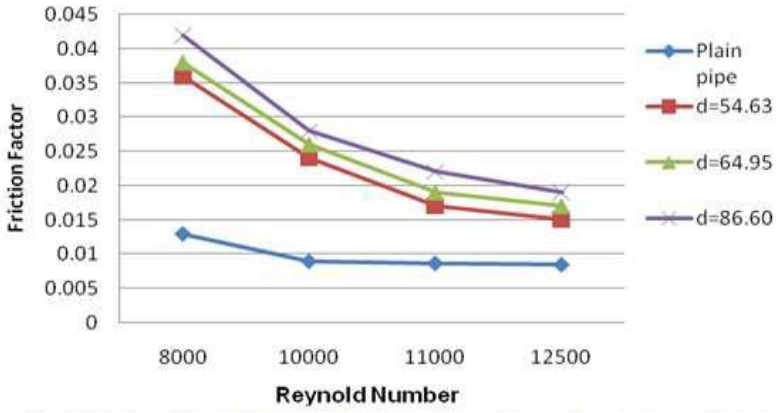

Fig 14 Variation of friction factor vs. Reynolds number for the test pipe using internal threads of varying depth

Figure 14 shows the variation of friction factor Vs Reynolds number for the test pipe using internal threads of varying depth. The friction factor for the test pipe using internal threads of varying depth is more

than that for plain test pipe. Friction factor decreases with increase in Reynolds number for a given depth. This shows that the turbulence formation advanced due to artificial turbulence exerted by internal threads. The friction factor is increases with increasing the depth. This is due to more intense swirl flow in case of more depth.

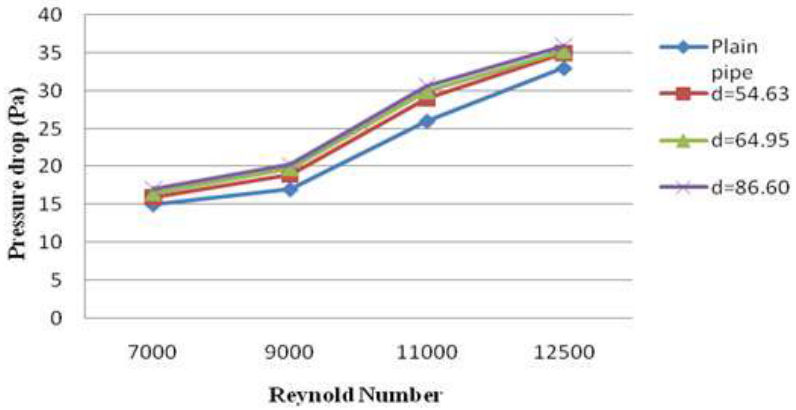

Fig 15 Variation of pressure drop with Reynolds number

Figure 15 shows the variation of pressure drop with Reynolds number. Pressure drop increases with increase in Reynolds number. Maximum pressure drop is observed to be 1.06 times compared to that of plain test pipe for internal thread of depth d = 86.60 mm. The large increase in the pressure drop can be attributed to the plain test pipe for internal thread of depth d = 86.60 mm, and the increased velocity associated more intense swirl flow in case of more depth. The heat transfer enhancement increases with increase in depth of internal threads due to increased turbulence of air. It is due to the swirl flow motion provided by internal threads. The friction factor increases with the increase of depth of internal threads again due to swirl flow exerted by the internal threads.

VII. Conclusion

Laminar flow shows less heat transfer through performance characteristics than that of through turbulent flow. Increase in friction and pressure drop in turbulent flows create dominant effect on heat transfer through the pipe. To produce this turbulent flow various techniques and design strategies are used which are explained in this study. This study shows that turbulent flow increases the Reynolds number. Hence this study helps to design new concept to produce turbulent flow with minimum range of Reynolds number to improve the heat transfer.

REFERENCES

[1] A. Garc, J.P. Solano, P.G. Vicente, A. Viedma, Enhancement of laminar and transitional flowheat transfer in tubes bymeans of wire coil inserts, International Journal ofHeat and Mass Transfer 50 (2007) 3176–3189.

[2] S.S. Hsieh, F.Y. Wu, H.H. Tsai, Turbulent heat transfer and flow characteristics in a horizontal circular tube with strip-type inserts: Part I. Fluidmechanics, International Journal of Heat and Mass Transfer 46 (2003) 823–835.

[3] M.M.K. Bhuiya, M.S.U. Chowdhury , M. Islam , J.U. Ahamed , M.J.H. Khan , M.R.I. Sarker , M. Saha, "Heat transfer performance evaluation for turbulent flow through a tube with twisted wire brush inserts", Elsevier, International Communications in Heat and Mass Transfer 39 (2012) pp- 1505–1512

[4] Halit Bas, Veysel Ozceyhan, "Heat transfer enhancement in a tube with twisted tape inserts placed separately from the tube wall", Elsevier, Experimental Thermal and Fluid Science 41 (2012), pp- 51–58

[5] M.M.K. Bhuiya , M.S.U. Chowdhury, M. Saha, M.T. Islam, "Heat transfer and friction factor characteristics in turbulent flow through a tube fitted with perforated twisted tape inserts", Elsevier, International Communications in Heat and Mass Transfer 46 (2013) 49–57

[6] M.M.K. Bhuiya, A.S.M. Sayem, M. Islamc, M.S.U. Chowdhury, M. Shahabuddin, "Performance assessment in a heat exchanger tube fitted with double counter twisted tape inserts", Elsevier, International Communications in Heat and Mass Transfer (2013) pp-1-9

[7] Pankaj N. Shrirao, Dr. Rajeshkumar U. Sambhe, Pradip R. Bodade, "Experimental Investigation on Turbulent Flow Heat Transfer Enhancement in a Horizontal Circular Pipe using internal threads of varying depth", IOSR Journal of Mechanical and Civil Engineering, Volume 5, Issue 3 (Jan. - Feb. 2013), PP 23-28

[8] Bodius Salam, Sumana Biswas, Shuvra Saha, Muhammad Mostafa K Bhuiya, "Heat transfer enhancement in a tube using rectangular-cut twisted tape insert", Elsevier, 5th BSME International Conference on Thermal Engineering, Procedia Engineering 56 (2013) pp-96 – 103.

OPEN ACCESS

International
Journal
Of Modern Engineering Research (IJMER)

Improvement of Surface Roughness of Nickel Alloy Specimen by Removing Recast Layer In Wire Electric Discharge Machining

Taha Chowdry[1]

[1]*Department of Mechanical Engineering, Islamiah Institute of Technology/ Visvesvaraiah Technological University, India*

Abstract: *In this investigation, experimental work and computational work are combined to obtain improvement in the surface roughness of nickel alloy specimen, the machining is carried out by means of CNC wire electric discharge machining (WEDM). Brass wire is used as the tool electrode and nickel alloy (Inconel600) is used as the work piece material. The machining parameters such as Pulse-On time (T_{on}), Pulse-Off time (T_{off}), Peak Current (I_p), and Bed speed are considered as input parameters for this project. Surface roughness and Recast layer are considered the output parameters. The experiments with the pre-planned set of input parameters are designed based on Taguchi's orthogonal array. The surface roughness is measured using stylus type roughness tester and the thickness of the Recast layer is measured using Scanning Electron Microscope (SEM). The results obtained from the experiments are fed to the Minitab software and optimum input parameters for the desired output parameters are identified. The software uses the concept of analysis of variance (ANOVA) and indicates the nature of effect of input parameters on the output parameters and confirmation is done by validation experiments. Once the recast layer thickness is obtained Chemical Etching and abrasive blasting is performed in order to remove the recast layer and again the surface roughness is measured by using stylus type roughness tester. Finally from the obtained results it was found that there was significant improvement in the Surface roughness of the nickel alloy material. In addition using regression analysis this work is stimulated by computational method and the results are obtained.*

Keywords: *Analysis of variance (ANOVA), Recast layer, Scanning electron microscope (SEM), Surface roughness, Wire electric discharge machining (WEDM)*

I. INTRODUCTION

Industrial technology introduces a variety of superior materials, these materials have better mechanical characteristics such as higher toughness, higher strength, higher hardness etc. Processing these superior materials using traditional machining techniques is difficult. Therefore, nontraditional machining techniques such as wire electrical discharge machining (WEDM) can be applied. This work uses WEDM as the major process of machining materials. The machining technique enables handling these superior materials to fulfill various requirements. No direct contact occurs between electrode and work piece so no stress is created in the processed material. The work piece for processing can consist of any materials as long as the materials have good electrical conductivity. Therefore, WEDM applies widely for processing difficult to machine materials since it performs with superior machining characteristics.

WEDM process is a heat energy process, the processed part surface generates a heat-affected zone (HAZ) of Ni-based super alloy, this zone includes the recast layer structure and surface defects after removal. During the WEDM process, the melting and removal of material progresses between two polarities (electrode and work piece). Some materials experience a resolidification phenomenon. Mixing carbon elements of dielectric fluid, melting electrode, and melting work piece is easy during resolidification, therefore forming the recast structure after the processes. The recast structure has micro-cracks and discharge craters causing bad surface quality that are difficult to remove due to high cohesion and hardness characteristics compared to the base material. The recast structure greatly affects dye fatigue strength and shortens service life. Removing the damaged surface in a post-machining process greatly increases fabricating time and dye cost. Therefore, this study explores chemical etching and abrasive blasting to soften and destroy the recast structure for removing micro-crack and discharge craters. The introduction of the paper should explain the nature of the problem, previous work, purpose, and the contribution of the paper. The contents of each section may be provided to understand easily about the paper.

II. Experimental Methodology

2.1 Taguchi Method

The Robust design method, is pioneered by Dr. Genichi Taguchi, greatly improves engineering productivity. By consciously considering the noise factors (environmental variation during the product usage, manufacturing variation and component deterioration) and the cost of failure in the field, the robust design method helps to ensure customer satisfaction. Robust Design focuses on improving the fundamental function of the product or process. This technique helps to study effect of many factors (variables) on the desired quality characteristic. By studying the effect of individual factors on the result, the best factor combination can be determined. The standardized Taguchi-based experimental design used in this study is an L9 orthogonal array.

2.2 Signal to Noise ratio (S/N ratio)

In the Taguchi method, the term, signal represents the desirable value (mean) for the output characteristic and the term, noise represents the undesirable value (S.D) for the output characteristic. Therefore, the S/N ratio is the ratio of the mean to the S.D. S/N ratio is used to measure the quality characteristic deviating from the desired value. The S/N ratio is defined as smaller the better.

2.3 Chemical Etching

It is the process of using strong acid or mordant to cut into unprotected parts of the metal. In this study the recast layer from the substrate is removed by using an etchant. The etchant consists of sulfuric acid solution that includes nitric acid and sodium chloride. To ensure that all the recast has been removed, the substrate is wiped using a white cloth and if all the recast has been removed the cloth will not change in appearance or color.

2.4 Abrasive Blasting

Abrasive blasting uses a stream of fine grained abrasive mixed with air or some other carrier gas at high pressure. This stream is directed by means of suitably designed nozzle on the work surface to be finished. Metal removal occurs due to erosion caused by the abrasive particles impacting the work surface at high speed.

III. Results And Discussion

The machining experiments have been carried out on FANAUC RC C600 four axis CNC wire EDM, using Brass wire of diameter 0.25mm. Work piece dimensions – 10x10mm, Length 15mm. The experiments have been conducted under flushing dielectric conditions. Deionised water has been used as the dielectric fluid.

Figure 1. Fanauc RC C600 four axis CNC WEDM

In this research work, after conducting the experiments, response values are noted down and analysis is done. Taguchi analysis is conducted to determine the optimal parameters and ANOVA is also performed to estimate magnitude of factors effects on the responses. The response factors or output parameters considered in this project are Surface roughness and Recast layer.

3.1 Machining Data Analysis

The Surface roughness and Recast layer thickness obtained for the corresponding machining experiments are tabulated.Four factors are considered while performing the experiments, they are Pulse-on time, Pulse-off time, Current and Bed speed.

Depending on these factors the surface roughness as well as the recast layer may vary.The data obtained is fed to the Minitab software and the S/N ratio is obtained.Based on the S/N ratio Main effects plots are plotted.From the graphs, the optimum machining parameter values are choosen for conducting the verification experiment.

The response for the verification experiment is expected to be better than the previous designed experiments.Minimum Surface finish and minimum Recast layer thickness is expected from the verification experiment.The obtained result from the verification experiment produces minimum Surface finish and minimum. Recast layer thickness which can be further improved by using different recast layer removal techniques.The different recast layer removal techniques which is used to obtain improved surface finish used are chemical etching and abrasive blasting.

Table 1. Tabulation of surface roughness for different set of input parameters

Exp.no	Pulse on (µs) (A)	Pulse off (µs) (B)	Peak current (amps) (C)	Bed speed (microns/sec) (D)	Response – Ra (µm)	S/N ratio
1	5	20	1	50	1.823	-4.2521
2	5	25	2	75	1.523	-3.1975
3	5	30	3	100	1.928	-5.0021
4	6	20	2	100	1.623	-4.2064
5	6	25	3	50	1.973	-5.9025
6	6	30	1	75	1.541	-3.7561
7	7	20	3	75	1.029	-0.2483
8	7	25	1	100	0.978	0.1932
9	7	30	2	50	2.093	-5.9563

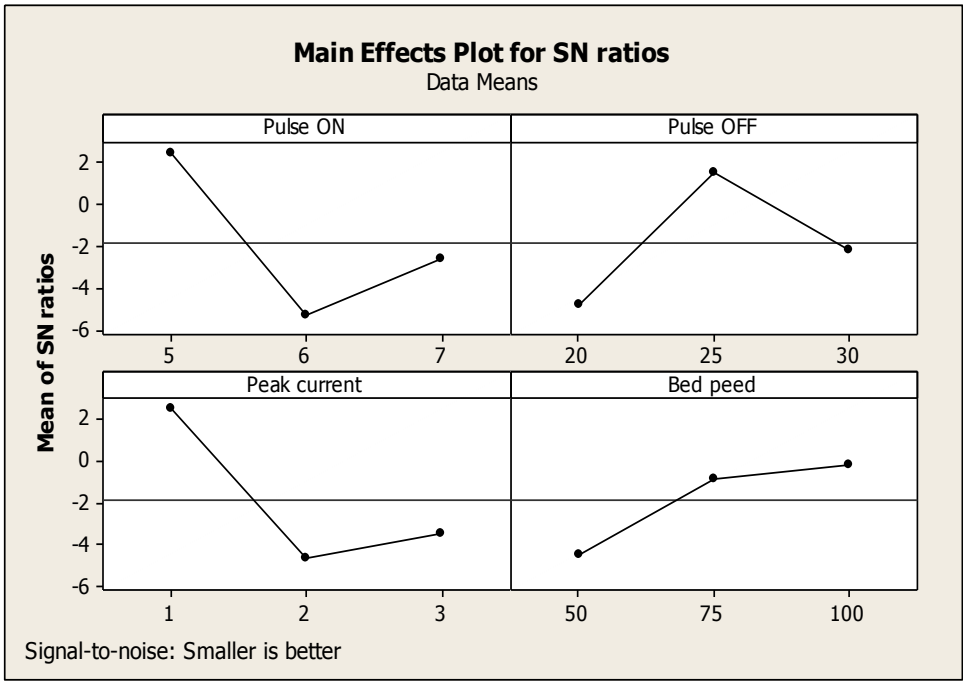

Figure 2.Main effects plot for S/N ratio (Surface Roughness)

Table 2. Response Table for Signal to Noise Ratio of Surface roughness

Level	Pulse ON (µs) (A)	Pulse OFF (µs) (B)	Peak current (amps) (C)	Bed speed (microns/sec) (D)
1	2.408	-4.8532	2.4772	-4.4776
2	-5.5323	-1.5094	-4.6185	-0.9126
3	-2.6697	-2.2413	-3.4435	-0.0194
Delta	7.732	6.3629	7.0957	4.2826
Rank	1	3	2	4

Based on the experiments, the optimum set of parameters is **A2 B1 C2 D1.** Figure 2 shows that Level 2 of A, Level 1 of B, Level 2 of C and Level 1 of D are having the smaller signal to noise ratio. Thus A2 B1 C2 D1 is the best combination i.e. Pulse-ON (6µs), Pulse-OFF (20 µs), Peak current (2 Amps) and Bed speed (50 µ/sec) produce minimum Surface roughness. From the main effects plot and Response table it is considered that the Pulse ON has more effect, Current and Pulse-OFF have lesser effect and Bed speed has least effect on the Surface roughness.

Table 3. Tabulation of Recast Layer for different set of input parameters

Exp.no	Pulse on (µs) (A)	Pulse off (µs) (B)	Peak Current (amps) (C)	Bed speed (microns/sec) (D)	Response– recast layer (µm)	S/N ratio
1	5	20	1	50	2.75	-8.7867
2	5	25	2	75	2.43	-7.7121
3	5	30	3	100	2.896	-9.2360
4	6	20	2	100	4.563	-13.1850
5	6	25	3	50	9.25	-19.3228
6	6	30	1	75	10.53	-20.4486
7	7	20	3	75	12.00	-21.5836
8	7	25	1	100	5.631	-15.0117
9	7	30	2	50	11.5	-21.2140

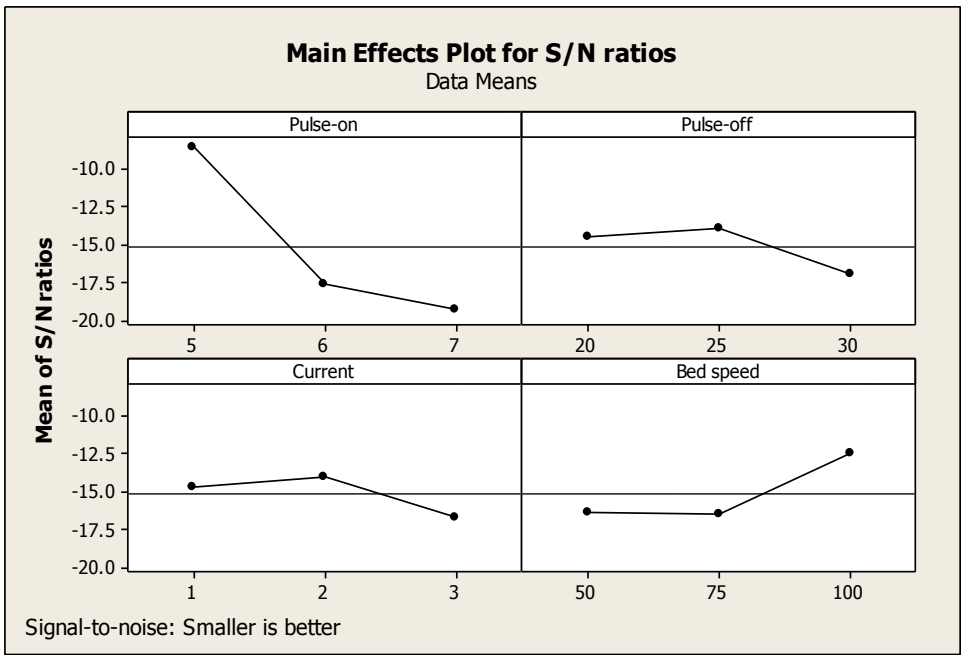

Figure 3. Main effects plot for S/N ratio (Recast Layer)

Table 4. Response Table for Signal to Noise Ratio of Recast Layer

Exp no	Pulse ON (µs) (A)	Pulse OFF (µs) (B)	Current (amps) (C)	Bed speed (microns/sec) (D)
1	-8.578	-14.518	-14.749	-16.441
2	-17.65	-14.016	-14.037	-16.581
3	-19.27	-16.966	-16.714	-12.478
Delta	10.692	2.951	2.677	4.104
Rank	1	3	4	2

Based on the experiments, the optimum set of parameters is **A3 B3 C3 D2.** Figure 3 shows that Level 3 of A, Level 3 of B, Level 3 of C and Level 2 of D are having smaller signal to noise ratio.Thus A3 B3 C3 D2 is the best combination i.e. Pulse-ON (7 µs), Pulse-OFF (30 µs),Current (3 Amps) and bed speed (75 µ/sec) produce the minimum recast layer. From the main effect plot and Response table it is considered that Pulse-ON time has more effect, Pulse-OFF and Bed speed have lesser effect and Current has least effect on the Recast layer.

3.2 Verification Experiment

The purpose of the verification experiment is to validate the conclusions drawn during the analysis phase. The verification experiment is performed by conducting a test with specific combination of parameters and values which are previously evaluated. In thisstudy, after determining the optimum values, a new experiment is designed and executedwith optimum values of the machining parameters. If the observed S/N ratios under theoptimum conditions are close to their respective predictions, then one can conclude thatthe predictive model is a good approximation of the reality.

Table 5. Optimized parameters to obtain minimum Surface roughness

Objective	Pulse ON (µs)	Pulse OFF (µs)	Peak current (amps)	Bed speed (microns/sec)	Obtained Surface roughness (before recast layer removal) (microns)	Obtained Surface roughness (after recast layer removal) (microns)
Minimizing Surface roughness	6	20	2	50	0.81	0.521

Table 6. Optimized parameters to obtain minimum Recast layer thickness

Objective	Pulse ON (µs)	Pulse OFF(µs)	Peak current (amps)	Bed speed (microns/sec)	Recast layer thickness (µm)
Minimizing Recast layer thickness	7	30	3	7	2.45

3.3 Analysis of Chemical Etching

The process of removing a layer of contamination on a metal or plastic surface through chemical erosion is called as chemical etching. Chemical etching of metals, also known as Chemical Milling, Photo-Chemical Machining, has been in existence for quite a long time, first being used for the production of metal 'frames' for holding electronic integrated circuit chips in place and allowing connection to be made to the external pins. Nowadays, it is used to create minute implantable surgical devices, micro machines and, most importantly, railway models.

Chemical milling or industrial etching is a manufacturing process of using baths of temperature-regulated etching chemicals to remove material to create an object with the desired shape. It was developed from armor-decorating and printing etching processes developed during the renaissance as alternatives to engraving on metal. The process essentially involves bathing the cutting areas in a corrosive chemical

known as an etchant, which reacts with the material in the area to be cut and causes the solid material to be dissolved; inert substances known as maskants are used to etch specific areas of the material.

Table 6. Chemical etching performed for various experiments

Exp.no	Recast layer (μm)	Specimen dimension (initial) in mm Before etching	% of Chemical Composition/ 50ml of etchant	Time taken (mins)	Specimen dimension (final) in mm After etching
1	2.75	15.127	25 ml-HNO_3 20ml-H_2SO_4 6gms-NaCl	20	14.352
2	2.43	15.869	20 ml-HNO_3 10ml-H_2SO_4 4gms-NaCl	33	15.569
3	2.859	15.789	15 ml-HNO_3 15ml-H_2SO_4 4gms-NaCl	27	15.049
4	4.563	15.237	20 ml-HNO_3 15ml-H_2SO_4 6gms-NaCl	30	14.972
5	9.25	15.931	15 ml-HNO_3 10 ml-H_2SO_4 2gms-Nacl	45	15.775
6	10.53	15.128	25 ml-HNO_3 10ml-H_2SO_4 4gms-NaCl	30	14.892
7	12.00	15.193	20ml-HNO_3 15ml-H_2SO_4 2gms-NaCl	25	14.861
8	5.631	15.879	15 ml-HNO_3 20ml-H_2SO_4 2gms-NaCl	31	15.456

From table 6 it is found that higher concentration of etchant as in experiment 1 results in lesser time and more material removal rate and lower concentration of etchant as in experiment 5 results in more time and lesser material removal rate.

Table 7. Surface roughness values before and after recast later removal

**Chemical etching*
*** Chemical etching and Abrasive blasting*

Exp.no	Roughness (before recast layer removal) (microns)	Roughness (after recast layer removal by chemical etching) (microns)	Roughness (abrasive blasting performed on etched components) (microns)	Improvement in roughness (microns)
*1	1.823	1.612	-	0.211
**2	1.523	1.445	0.845	0.678
*3	1.928	1.622	-	0.306
**4	1.623	1.572	0.672	0.951
*5	1.973	1.501	-	0.469
**6	1.541	1.406	0.606	0.935
**7	1.029	0.991	0.705	0.324
**8	0.978	0.912	0.684	0.294

From table 7 it can be concluded that the surface roughness of the specimen is considerably improved after the Recast layer has been removed by etching method, further improvement is achived by using abrasive blasting once the recast layer is removed by chemical etching.

3.4 Regression Analysis

Regression analysis is a statistical tool for the investigation of relationships between variables. Usually, the investigator seeks to ascertain the casual effect of one variable upon another, for example the effect of a price increase upon demand, or the effect of changes in the money supply upon the inflation rate. To explore such issues, the investigator assembles data on the underlying variables of interest and employs regression to estimate the quantitative effect of the casual variables upon the variable that they influence.

The investigator also typically assesses the "statistical significance" of the estimated relationships, that is, the degree of confidence that the true relationship is close to the estimated relationship.

In this project, there are four control parameters which are independent variables.They are Pulse ON (Ton), Pulse OFF (Toff), Peak current (Ip) and Bed speed. Each of these factors has relationship with the Surface finish and Recast layer thickness of the work piece.

Table 8 Regression analysis :Experimental and Predicted values of surface roughness

Exp.no	Experimental Values(microns)	Predicted values(microns)	Deviation %
1	1.823	1.621	11.08
2	1.523	1.674	-9.91
3	1.928	1.727	10.42
4	1.623	1.168	28.03
5	1.973	1.858	5.82
6	1.541	1.617	-4.93
7	1.029	1.352	-31.38
8	0.978	1.111	-13.59
9	2.093	1.802	13.9

Exp.no	Experimental values (µm)	Predicted values (µm)	Deviation %
1	2.75	3.29	-19.63
2	2.43	3.36	-38.27
3	2.896	3.43	-18.43
4	4.563	4.2	7.955
5	9.25	9.475	-2.43
6	10.53	6.935	34.14
7	12.00	10.315	14.04
8	5.631	7.775	-38.07
9	11.5	13.05	-13.47

Table 9 Regression analysis : Experimental and Predicted values of Recast layer

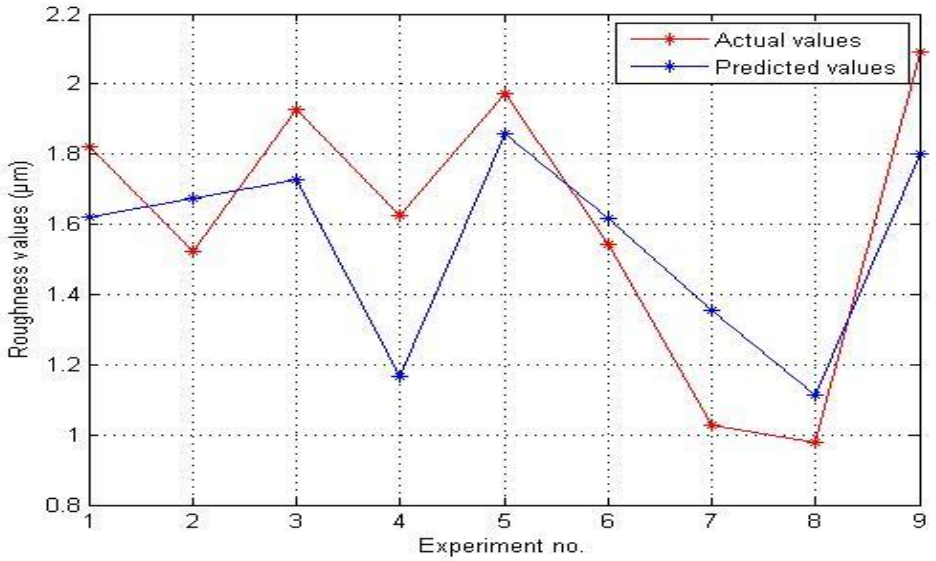

Fig 4.Comparison b/w Experimental and Predicted values of Surface roughness

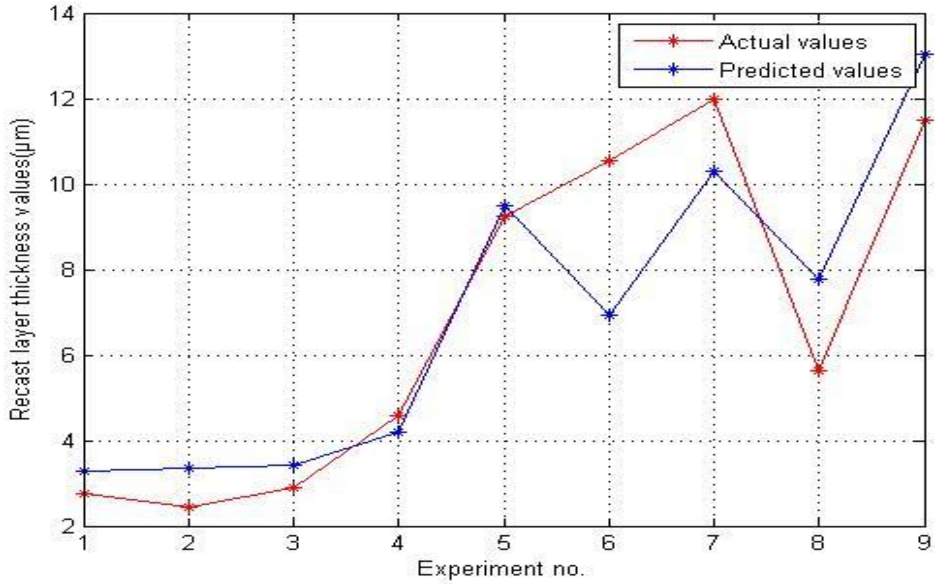

Fig 5.Comparison b/w Experimental and Predicted values of Recast layer

IV. Conclusion

From the results of machining experiments based on L9 orthogonal array and from the results of ANOVA analysis, it can be concluded that while machining the material Inconel-600 with FANUC RB C600 four axis CNC wire cut Electric Discharge Machine, the Pulse ON time has the major effect on Surface roughness and Recast layer thickness. The Pulse OFF time, Peak current and Bed speed have lesser effect on Surface roughness and Recast layer thickness

From the regression analysis results, it can be concluded that the prediction of results or responses with minimum errors are possible using regression analysis with MINITAB and MATLAB software.

REFRENCES

[1] P C Pandey and H S Shan, Modern machining processes, Tata McGraw-Hill Education, 1st edition, New Delhi 1980.

[2] P. K. Mishra, Non conventional machining, Hassan El-Hofy, Narosa Publishing House, New Delhi, 1997.

[3] Yan-Cherng Lin, Optimization of machining parameters in magnetic force assisted EDM based on Taguchi method, Journal of Materials Processing Techonology 2009, pp 3374-3383.

[4] Che-Chung Wang ,Recast layer removal after electric discharge machining via Taguchi analysis, Journal of Materials Processing Technology 2009, pp 4134-4140.
[5] D.K Aspinwall, Workpiece roughness and integrity after WEDM of Ti-6Al-4V and Inconel-718 using minimum damage generator technology, Journal of Material Processing Technology 2008, pp 187-190.
[6] Kung Ling Wu, Study on the characteristics of electric discharge machining using dielectric with surfactant, Journal of Material Processing Technology 2009, pp 3783-3789.
[7] R. Ramakrishnana, L. Karunamoorthy, Modeling and multi-response optimization of Inconel 718 on machining of CNC WEDM process, Journal of Materials Processing Technology, 2008, pp 343–349.
[8] H. Singh, R. Garg, Effects of process parameters on material removal rate in WEDM, Journal of Achievements in Materials and Manufacturing Engineering, Vol-32, Issue-1, 2009, pp 70-74.
[9] Danial Ghodsiyeh, Abolfazl Golshan, Optimizing Finishing process in WED-Machining of Titanium Alloy (Ti6Al4V) by Zinc Coated Brass Wire based on Response Surface Methodology, Indian Journal of Science and Technology, ISSN:0974-6846, Vol.5, Issue.10, 2012, pp 3365-3376.
[10] S. Sarkar, S. Mitra, I.K. Gomes and B. Bhattacharyya, Modeling and Optimization of Wire Electrical Discharge Machining In Single Pass Cutting Operation, Proceedings of the International Conference on Mechanical Engineering, Dhaka, Bangladesh,2005.
[11] S. S. Mahapatra, Amar patnaik, Optimization of Wire Electric Discharge Machining Process Parameters Using Genetic Algorithm, Indian Journal of Engineering and Material Sciences, Vol. 13, 2006, pp 494-502.
[12] A. B. Puri, B. Bhattacharyya, An Analysis and Optimisation of the Geometrical Inaccuracy Due to Wire Lag Phenomenon in WEDM, International Journal of Machine Tools & Manufacture, 2003, Vol. 2, pp 151-159.
[13] Nihat Tosun, The Effects of the Cutting Parameters on Performance of WEDM, KSME International Journal, vol.17, No.6, 2003, pp 816-824.
[14] M.S. Hewidy, T. A. El-Taweel, M. F. El-Safty, Modelling the machining parameters of wire electrical discharge machining of Inconel 601 using RSM, Journal of Materials Processing Technology, 2005, pp 328–336.
[15] S. Sivakiran, C. Bhaskar Reddy, C. Eswara Reddy, Effect Of Process Parameters on MRR in Wire Electrical Discharge Machining of En-31 Steel, International Journal of Engineering Research and Applications, ISSN: 2248-9622, Vol. 2, Issue. 6, 2012, pp 1221-1226.
[16] Atul Kumar, Dr. D. K. Singh, Performance Analysis of Wire Electric Discharge Machining, International Journal of Engineering Research & Technology, Vol. 1, Issue. 4, 2012.
[17] B J Ranganath, Thermal metal cutting process, New Delhi, India, I K International Publishing House Pvt. Ltd, 1st edition, 2008.
[18] Phadke. M. S. Quality Engineering Using Robust Design, Prentice-Hall, EnglewoodCliffs, NJ, 1989.
[19] Taguchi Genichi, Elsayed A Elsayed, Hsiang Thomas Quality Engineering In Production Systems, Mc Graw-Hill Book Company, New York, 1989.
[20] Pujari Srinivasa Rao, Dr. Koona Ramji, Prediction of Material removal rate for Aluminum BIS-24345 Alloy in wire-cut EDM, International Journal of Engineering Science and Technology, Vol. 2, 2010, pp 7729-7739.

OPEN ACCESS

International
Journal
Of Modern Engineering Research (IJMER)

Repairing of Concrete by Using Polymer-Mortar Composites

Yaser M. Abdulateef [1], Besma M. Fahad[2], Khalid M. Eweed[3]

[1]*MSC. Student, Department of Material Engineering, College of Engineering, University of Al-Mustansiriya, Iraq*

[2,3]*Asst. Prof. Department of Material Engineering, College of Engineering, University of Al-Mustansiriya, Iraq*

Abstract: *Replacement of concrete buildings, bridges, roadways and other structures is becoming more and more expensive as costs of materials and labor continue their upward spiral. Polymer-modified or polymer cement mortar (PCM) and concrete (PCC) are a category of concrete-polymer composites which are made from cement mortar or concrete with polymers, The main application of polymer cements is in concrete repair. In this research two sets of mixtures were prepared that consist of mortar and polymer to fabricate the polymer-cement composite. The first set include mortar with ratio (1:1) (cement-sand) without water, while the other set include mortar with ratio (1:2) (cement-sand) without water. The polymer was Quickmast105 epoxy which is added to the mortar after mixing the resin with the hardener in proportion of (1:3). Each set was consist of different percentage of polymer (50:50, 40:60 and 30:70). Tests were conducted, including compression, flexural and bonding strength, were several results obtained including, the highest compressive strength was about 102.889MPa and the highest value of flexural strength was about 57.648MPa for (1:1), the polymer-mortar with 40:60 ratio showed a higher bonding compressive strength. Proportionality between the cement and sand and also between the polymer and mortar plays a major role in adhesion and strength are considered key factors in the bonding and portability to repairs.*

Key Words: *Polymer, mortar, composite, polymer – cement, repairing.*

I. Introduction

Concrete today is an indispensable part of the fabric of modern society, used for everything from mundane road pavements and high rise building structures. Despite its long history of use, our understanding of the material has only really developed in very recent times, particularly with respect to its durability. There was common view that concrete is a durable as well as a maintenance-free constructional material. In recent years this concept has been changed. Many investigations have shown that concrete does not perform as well as it was expected due to the effect of many factors which contribute to or cause the deterioration of concrete structures and that what make it necessary of repairing concrete. [1]

In the last 30 years the construction industry branch having to do with the repair, protection and strengthening of concrete has experienced explosive growth. This has been driven by the need to reverse the deterioration of, damage to, and defects in concrete structures as well as by changes in building use and code requirements. Accordingly, there is great need to improve the materials and techniques used in repair and strengthening.[2] Polymers have been used as additives in cement mortars and concrete since the 1920s. Since then, there has been considerable development of polymer modification for cement and concrete. Commercial products, called cement admixtures, are used in many applications in the construction industry from walls to roads.[3]

Over the past twenty years, many different polymers have been used in a range of applications in the repair and maintenance of buildings and other structures. Without the unique properties of some of the polymer systems, many of the repairs undertaken would, without doubt, have been much more costly and have taken much longer to carry out. The polymers used in concrete repair consist principally of two different types of materials: (Polymers used to modify cementitious systems, and reactive thermosetting resins, mainly epoxy and unsaturated polyester resins).[4] Replacement of concrete buildings, bridges, roadways and other structures is becoming more and more expensive as costs of materials and labor continue their upward spiral. More attention is now being directed to development of materials for repair and restoration of concrete since, when effective, they represent an increasingly economical solution Among the materials being more closely evaluated and more widely accepted are the epoxy resins. Used alone or in combination with other standard construction materials, epoxies have made repairs possible where before only replacement was considered. Although epoxies themselves are somewhat costly, their total cost often becomes minimal when the quality of repair achievable with other materials is considered. It becomes practically insignificant when compared to the cost of new

construction.[5]

Polymer-modified or polymer cement mortar (PCM) and concrete (PCC) are a category of concrete-polymer composites. Polymer modified or polymer cement paste, which is prepared without any aggregate, is sometimes used. Polymer-modified mortar and concrete are prepared by mixing either a polymer or monomer in a dispersed, powdery, or liquid form with fresh cement mortar and concrete mixtures, and subsequently curing. Several types of polymer-modified mortars and concretes, i.e., latex-redispersible polymer powder-, water-soluble polymer-, liquid resin, and monomer-modified mortars and concretes, are produced by using the polymers and monomers.[6] The main application of polymer cements is in concrete repair. The function of the polymer was mainly to reduce concrete permeability and to increase resistance to chloride penetration, toughness and adhesion. .[7]

II. Aims

The aim of this work is to investigate the possibilities of making a new repairing materials by full replacing the water with polymer material and finding out the suitable the suitable percent of mixing and which percent should be avoided to use in bonding the concrete to reduce the cost of concrete repairing.

III. Experimental Procedure

3.1. Materials

3.1.1 Cement:

The cement that used is ordinary Portland cement, commercially known **(TASLUJA)**. It was stored in dry place to minimize the effect of humidity on cement properties and it was tested in (National Center for Laboratories and Construction Research). The chemical and physical properties of cement are given in table (1). It is matched by the Iraqi Reference Guide indicative number (198) and the Ministry of Planning / Central Agency for Standardization and Quality Control Manual 198/1990. [8]

Table (1): Chemical and physical properties of Portland cement.

Chemical composition			Physical composition		
Item	**Content %**	**Spec. Limit**	**Item**	**Test result**	**Spec. Limit**
SiO_2	20.03		Fineness (m^2/kg)	370	230
Al_2O_3	4.35		Autoclave exp.	0.32	0.8%
Fe_2O_3	3.17		Compressive strength (MPa) 3-days age	29.5	15.0
CaO	63.66				
MgO	1.63	5.0 Max	Compressive strength (MPa) 7-days age	35	23.0
SO_3	2.3	2.8 Max			
L.O.I	1.9	4.0 Max	Time of setting Initial (min.)	35	45
I.R.[Insoluble Residue %]	0.99	1.5	Time of setting Final (hour)	5.25	10 Max.

3.1.2 Natural Sand Aggregate

The fine aggregate used in study is according to the Iraqi specification No. 45 of 1984 for Cement. Brought from Ukhaydir area where they were bringing models that are all located within the area of the second gradient specification under Iraqi specification[11] as shown in the table (2)**.**

Table (2): Grading of fine aggregate.

Sieve size (mm)	% Passing by Weight	Specific Limit
4.75	95.3	90-100
2.36	83.7	70-100
1.18	71.9	55-90
0.60	51.8	53-59
0.30	21.2	8-30
0.15	4.7	0-10
Percentage of salts%	0.4	≤0.5

3.1.3 Polymer

The epoxy was resin group type Quickmast 105 (DCP) Company / Jordan. Specific gravity and viscosity of the epoxy resin were 1.04 and 1 poise respectively at 35°C. The ratio between resin and hardener for this epoxy is 3:1 by weight.

IV. Experimental Work

In this work, different mixes of polymer-mortar were prepared to study their mechanical properties of polymer-mortar as a repairing material. Utilization of polymer composite as a repairing material for cracked structural concrete. Experimental work and test procedures are detailed in this work.

Two sets of mixtures were prepared that consist of mortar and polymer to fabricate the polymer-mortar composites. The first set include mortar with ratio (1:1) (cement-sand) without water, while the other set include mortar with ratio (1:2) (cement-sand) without water. Each set was consist of different percentage of polymer (50:50, 40:60 and 30:70). The polymer was epoxy which is added to the mortar after mixing the resin with the hardener in proportion of (3:1). The polymer-mortar mixtures were illustrated in Table (3).

Table 3. Polymer-Mortar Mixtures, [%]

Specimen No.	Mortar %	Epoxy %	Mixture %	Dimensions (mm)	
				Compression	Flexural
1	1:1	1:3	50:50	50x50x50	100x25x25
2	1:1	1:3	40:60	50x50x50	100x25x25
3	1:1	1:3	30:70	50x50x50	100x25x25
4	1:2	1:3	50:50	50x50x50	100x25x25
5	1:2	1:3	40:60	50x50x50	100x25x25
6	1:2	1:3	30:70	50x50x50	100x25x25

The polymer-mortar with different proportions as given in table (3), was prepared by using electrical mixer (Automix, Controls Co. Italy). Firstly the resin mixed with hardener for 2-5 minutes, then cement and sand were separately mixed for 5 minutes. The polymer-mortar mixture were obtained by mixing them for 10 minutes until achieving a homogeneous mix. After complete mixing, the polymer-mortar was poured in molds, the molds were coated with mineral oil to prevent adhesion of polymer-mortar .Polymer-mortar casting was accomplished in three layers. Each layer was compacted by using a vibrating device (Viatest Co. German), for 1-1.5 minutes until no air bubbles emerged to the surface of the casting. The specimens were de-molded after 24±2 hours from casting, and then complete curing at room temperature for seven days to ensure full curing until the time of testing.

V. Tests

Three types of tests for polymer-mortar composites were carried out. The destructive tests consists of compressive strength, flexural strength and bonding compressive strength.

5.1 Destructive Tests

5.1.1 Compressive Strength Test

The compression test was determined according to American Society for Testing and Materials . ASTM C109/C109M-13 (Using 2-in. or [50-mm] cube Specimens).[12] The specimens are loaded uniaxily by the universal compressive machine (Viatest CO. Cyber-Tronic, model DPC 3000. German) of 3000 kN capacity at loading rate of 8.1 KN per second. The test was carried out for all proportions at the same rate of loading.

5.1.2 Flexural Strength Test

This test methods are according to the ASTM D790-02 [13]. A bar of rectangular cross section rests on two supports and is loaded by means of a loading nose midway between the support, using calibrated testing machine (Sercomp, Controls Co. Italy).

5.1.3 Bond Strength test

This test was applied to determine the bond strength of concrete cylinder specimen using polymer-mortar composites as a repairing material under the ASTM C882/C 882M.[14]

The bond strength is determined by using the polymer-mortar to bond two equal sections of a [150 by 75-mm] Portland-cement mortar cylinder, each section of which has a diagonally cast bonding area at a 30° angle from vertical as shown in figure (1).

Fig. 1. Two equal sections of a [150 by 75-mm] Portland-cement mortar cylinder.

Wrap the cylinder parts by using tape and also using plaster to ensure the stability of the parts and also to prevent mixture of polymer-mortar bleeding out from the bonded area. Test procedure starts by mixing the polymer-mortar composite in the proportions as in table (3). A mixing time of 3 minutes should be satisfied. The bond should keep the polymer-mortar mixture injected into a hole, at the bond-line, while keeping the joint horizontal. The assembly should secure with sufficient additional masking tape placed around the wrapped tape and plaster, and making sure that the joint is entirely filled. The bonded cylinder must kept horizontally for 48 hours, then remove all the masking tape. After suitable curing of the bonding agent (for 7 days) , cap the specimens immediately after removal from curing.[15] To ensure that the test cylinder has smooth, parallel, uniform, bearing surfaces that are perpendicular to the applied axial load during compressive strength testing using (Capping).[15] This method is done by remove such coatings or deposits. If necessary, the ends of a specimen may be slightly roughened with a steel file or wire brush to produce proper adhesion of the cap. If desired, capping plates may be coated with a thin layer of mineral oil or grease to prevent the capping material from adhering to the surface of the plate. Prepare sulfur mortar for use by heating to about 130°C. The capping plate or device should be warmed before use to slow the rate of hardening and permit the production of thin caps. Oil the capping plate lightly and stir the molten sulfur mortar immediately prior to pouring each cap. The ends of moist cured specimens shall be dry enough at the time of capping to preclude the formation of steam or foam pockets under or in the cap larger than 6 mm in diameter. This method is shown in figures (2 and 3). To ensure that the cap is bonded to the surface of the specimen, the end of the specimen shall not be oiled prior to the application of the cap.

Fig. 2. Capping plate and device.

Fig. 3. Capping furnace (Controls Co.) Italy.

After the completion of Capping process leave the specimens for a period of 21 days as in figure (4) and then test the specimens in compression accordance with test method.

The area of the elliptical bonding surface of the test cylinders specified in this test method is [9116 mm^2].[14]

After suitable curing of the bonding agent, the test is performed by determining the compressive strength of the bonded cylinder.

Fig. 4. Capped cylinders.

VI. Results And Discussions

6.1 Compressive Strength Test

The compressive strength is considered one of the most important properties of polymer-mortar composites. Generally it is the main characteristic value to assess composite quality in the national and international codes. For this reason, it is if special interest to investigate whether the changes in the mixture composition will affect the early and later compressive strength. The compressive strength results for all proportions are shown in table(4).

Table 4. Results of compressive strength for all proportions.

		Compressive Strength (MPa)	
Polymer Type	**Designation**	**1:1**	**1:2**
Quickmast 105	50:50 at room temperature	87.496	81.464
Quickmast 105	40:60 at room temperature	57.492	70.1996
Quickmast 105	30:70 at room temperature	102.889	101.663

The following observations can be concluded from above results:

- Polymer-mortar composites show an increase in compressive strength, this behavior can be explained due to the presence of polymer in the composite; therefore this property helps to increase the compressive strength.
- Polymer-mortar with low polymer content in the composite having higher compressive strength as in 30:70 proportion, this is due to the good bonding and also good strength.
- The polymer-mortar with 40:60 ratio showed a decrease in compressive strength, this is because of reducing in the adhesion between polymer and mortar particles.
- The percentages with 50:50 gives a moderate values and this behavior this due to the ratio of mortar to the polymer.
-

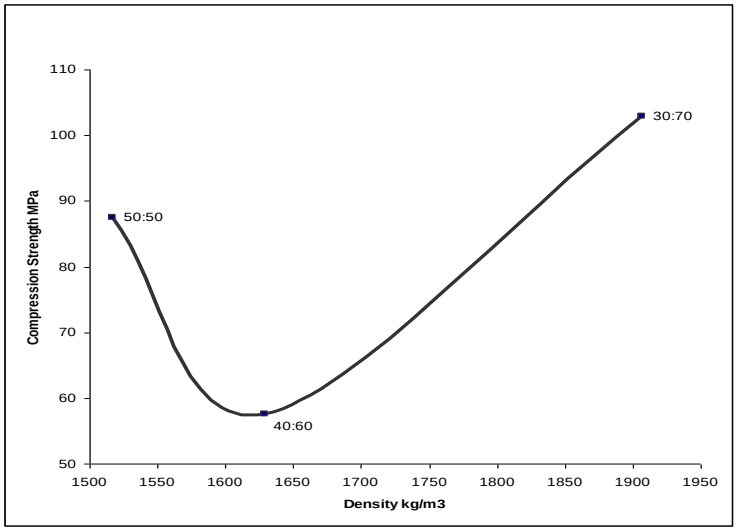

Fig.5. Compressive strength-Density for 1:1 Quickmast 105 at room temperature

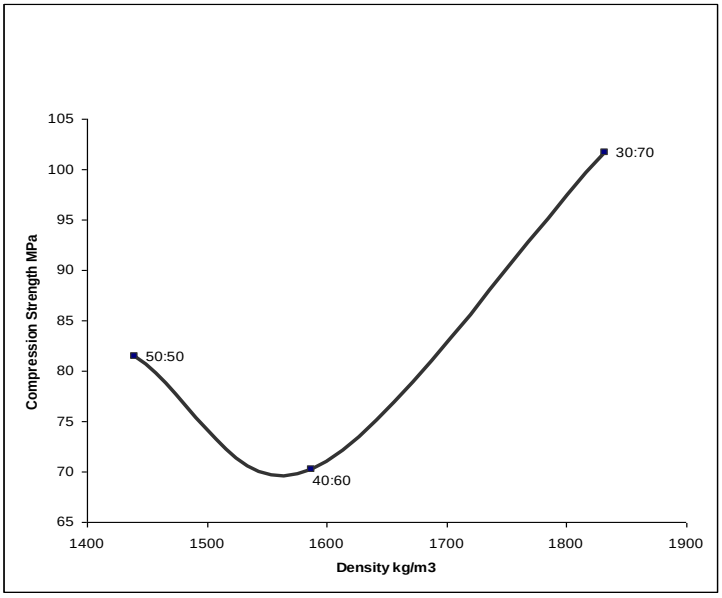

Fig.6. Compressive strength-Density for 1:2 Quickmast 105 at room temperature

- From fig.5. the highest compressive strength at 30:70 polymer-mortar composite (Quickmast 105) is 102.889 MPa for 1:1 at room temperature.
- From fig.6. the highest compressive strength at 30:70 polymer-mortar composite (Quickmast 105) is 101.663 MPa for 1:2 at room temperature.

Figure (7), illustrate the comparison between proportions of polymer-mortar ratios of polymer type Quickmast 105 at room temperature**.**

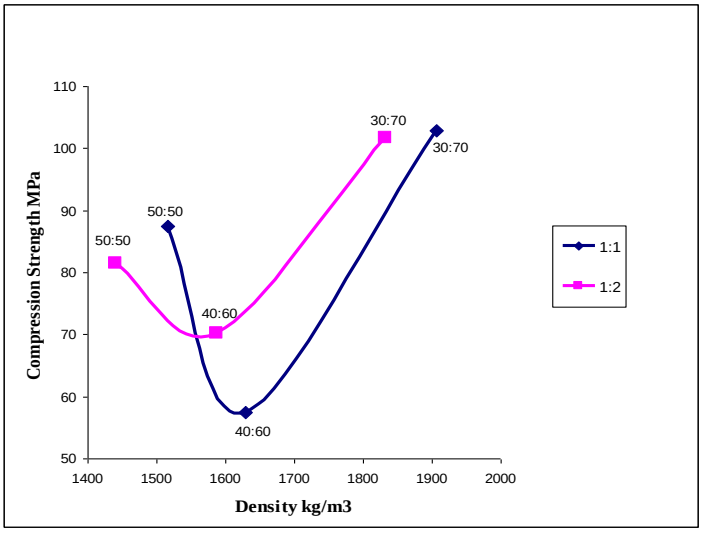

Fig.7. Comparison between the compressive strength of different proportions of polymer-mortar composites at room temperature.

The comparison diagrams showed we can conclude these observations:

- Polymer-mortar with mortar ratio 1:1 is better than that for 1:2 except that for 1:2 of polymer- mortar ratio 30:70 gives higher value.
- For mortar with 1:1 ratio the proportion of 40:60 is the lowest value for two ratios of mortar.

6.2 Flexural Strength Test

The flexural strength represents the highest stress experienced within the material at its moment of rupture. It is measured in terms of stress. A mechanical parameter for brittle material, is defined as a material's ability to resist deformation under load. The transverse bending test is most frequently employed, in which a specimen having a rectangular cross-section is bent until fracture or yielding.

The flexural strength results for all proportions are shown in table (5). Polymer with mortar in different ratios, which are presented in figures (8 and 9).

Table 5.Results of flexural strength for all proportions.

		Flexural Strength (MPa)	
Polymer Type	**Designation**	**1:1**	**1:2**
Quickmast 105	50:50 at room temperature	48.6528	43.1808
Quickmast 105	40:60 at room temperature	48.8064	48.9792
Quickmast 105	30:70 at room temperature	57.648	60.5184

The following observations can be concluded from above results:

- ❖ Polymer- mortar with low polymer content in the composite having higher flexural strength as in 40:60 and 30:70 proportions, this is due to the high ratio of mortar to the polymer this cause a good penetration of polymer to the mortar and this may increase the surface area of the particles and also increase the adhesion strength.
- ❖ The polymer- mortar with 50:50 ratio showed a decrease in flexural strength, this is because of low density and also low compacting between particles.
- ❖ The percentages with 40:60 gives a moderate values and this behavior due to the good bonding and also good strength.

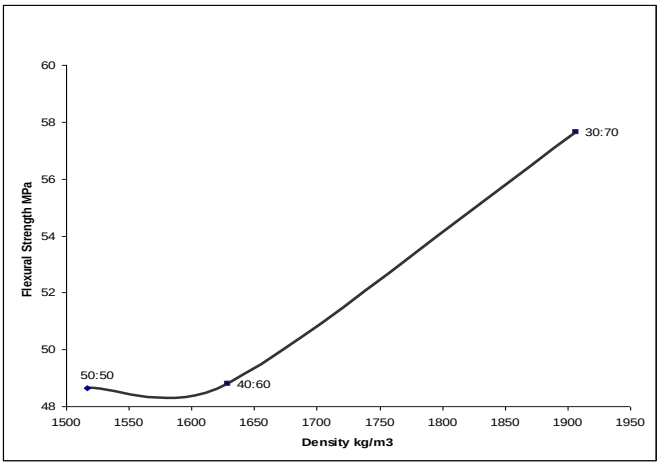

Fig. 8. Flexural strength-Density for 1:1 Quickmast 105 at room temperature

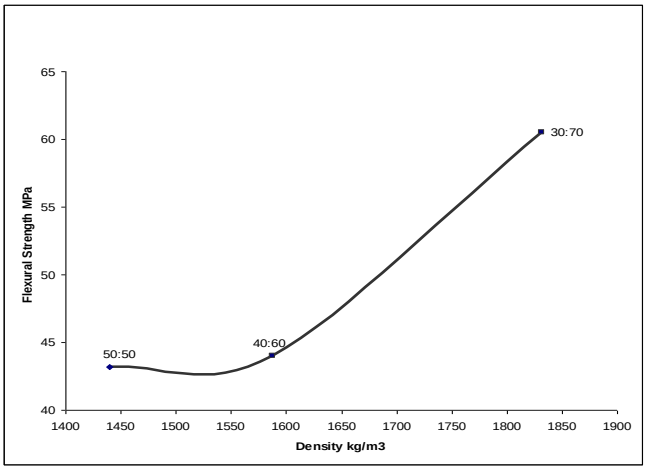

Fig.9. Flexural strength-Density for 1:2 Quickmast 105 at room temperature

- From fig.8. the highest flexural strength at 30:70 polymer- mortar composite (Quickmast 105) is 57.648 MPa for 1:1 at room temperature.
- From fig.9. the highest flexural strength at 30:70 polymer- mortar composite (Quickmast 105) is 60.5184 MPa for 1:2 at room temperature.

Figure (10), illustrate the comparison between proportions of polymer- mortar ratios of polymer type Quickmast 105 at room temperature.

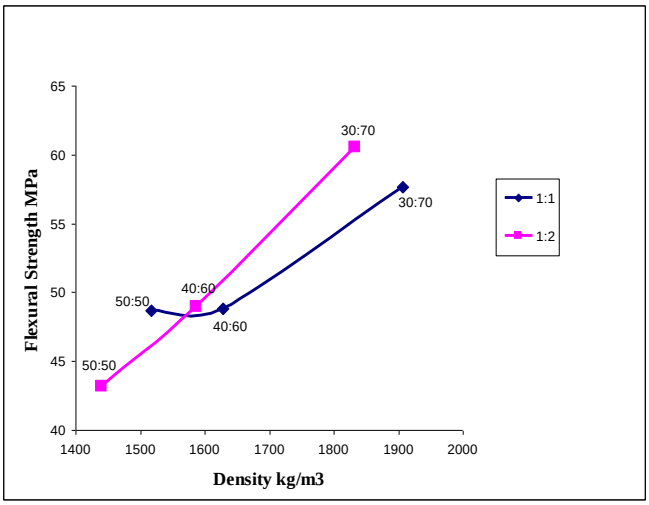

Fig.10. Comparison between the flexural strength of different proportions of polymer-mortar composites at room temperature.

The comparison diagrams showed these observations:

- Polymer-mortar with mortar ratio 1:2 is better than that for 1:1 at room temperature except for 50:50 proportion is lower than that for 1:1.

6.3 Bond Strength of Repaired Concrete Test

Calculate the bond strength of the resin bonding system by dividing the load carried by the specimen at failure by the area of the bonded surface the area of the elliptical bonding surface of the test cylinders specified in this test method is (9116 mm^2). [39] The bond strength after fracture taking place in the main cylinder while the bond region is not affected, this indicate to good bond strength and good repairing material as shown in figure (11), the results are shown in figure (12), and figure (13) for 1:1 and 1:2 respectively.

Fig.11. The bond strength of polymer-mortar.

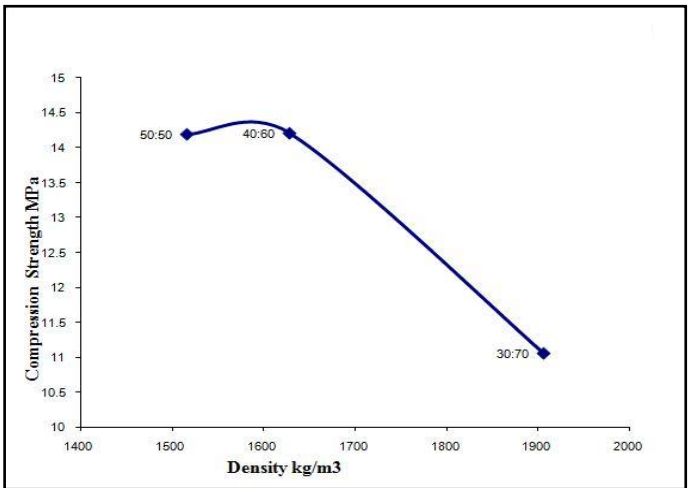

Fig. 12. Bonding Strength – Density diagram for 1:1 Quickmast 105

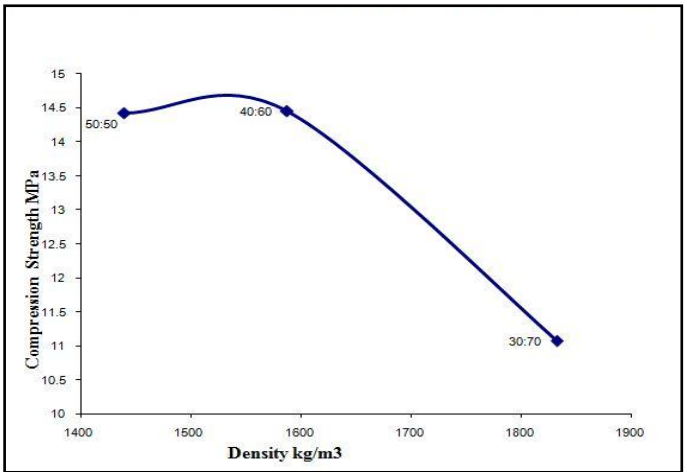

Fig. 13. Bonding Strength – Density diagram for 1:2 Quickmast 105

The following observations can be concluded from above figures:

- Polymer-mortar with low polymer content in the composite having low bonding compressive strength as in 30:70 proportion, this is due to the high ratio of mortar to the polymer this cause a low adhesion and low strength.
- The percentages with 50:50 gives a moderate values and this is because of low density and also low compacting between particles.
- The polymer-mortar with 40:60 ratio showed a higher bonding compressive strength, this is this behavior due to the good bonding and also good strength.
- The bonding strength of 1:2 mortar ratio specimens increased, this is due to good penetration of polymer between sand particle since the sand is added in a high percentages, and so increase the bonding strength between particles.

VII. Conclusion

The following main conclusion were achieved from this study, get a new type of concrete repair materials can be achieved from mixing the polymer with mortar, proportionality between the cement and sand as a mortar and between the polymer and mortar plays a major role in adhesion, the adhesion and strength are considered key factors in the bonding and portability to repairs and also the addition of polymer to mortar increases the compression and flexural strength and reduces their brittle nature.

REFERENCES

[1] Lee Eng Hing, Application of polymer in concrete construction, Faculty of Civil Engineering University Technology Malaysia, November, 2007
[2] Novel cement-based composites for the strengthening and repair of concrete structures Construction and Building Materials, Volume 41, April 2013, Pages 365-373
[3] Edward M Petrie, Polymer modified Portland cement adhesives and grouts, Polymer Modified Cement Special Chem. Sep 17, 2012.
[4] Shaw, J.D.N, Polymers for concrete repair. Civil Engineering, 63–65., 1993.
[5] Epoxies for concrete repair and restoration, By Concrete Construction Staff, The Aberdeen Group, 1979.
[6] Handbook of Polymer-Modified Concrete and Mortars Properties and Process Technology. Yoshihiko Ohama. Copyright. William Andrew Inc. All rights reserved 1995.
[7] Ivan Razl, Flexible Polymer-Cement Based Repair Materials and Their Applications. Concrete Repair Bulletin, 2004.
[8] Iraqi Reference Guide indicative (198) and the Ministry of Planning / Central Agency for Standardization and Quality Control Manual 198/1990.
[9] ASTM C138/C138M Standard Test Method for Density (Unit Weight), Yield, and Air Content (Gravimetric) of Concrete.2010
[10] British standard BS1881 : part 203:1986.2003
[11] ASTM D2240 - 05(2010) Standard Test Method for Rubber Property Durometer Hardness Book of Standards Volume: 09.01
[12] ASTM C 109/C 109M Standard Test Method for Compressive Strength of Hydraulic Cement Mortars (Using 2-in. or [50-mm] Cube Specimens) August 2008.
[13] ASTM D 790 – 02 Standard Test Methods for Flexural Properties of Unreinforced and Reinforced Plastics and Electrical Insulating Materials.2002
[14] ASTM C 882/C 882M Standard Test Method for Bond Strength of Epoxy-Resin Systems Used With Concrete By Slant Shear.2008.
[15] ASTM C 617 – 98 Standard Practice for Capping Cylindrical Concrete Specimens. 2003.

OPEN ACCESS

International
Journal
Of Modern Engineering Research (IJMER)

Enhance the Productivity of the Solar Still by Improving the Operational Parameters

S. Starwin jedidiah[1], I. Daniel Lawrence[2]
[1]*PG Scholar, Dept. of Mechanical Engineering, Anna university regional office Madurai, Tamil Nadu, India*
[2]*Faculty, Dept. of Mechanical Engineering, Anna university regional office Madurai, Tamil Nadu, India*

Abstract: *The productivity of the still is mainly depends upon various operational parameters. In this project a cooling wick is fixed at the top of the glass, and the cooling water is allowed to flow continuously, through the wick, in order to reduce the glass temperature. A mini solar pond and a flat plate collector also integrated with the glass cover cooled solar still in order to increase the inlet water temperature, Here two models were fabricated one is basic model and the another one is still with cooling wick at the top of the glass. Various readings were taken throughout the day and readings were tabulated. The results showing that the glass cooled solar still integrated with flat plate collector gives the higher productivity than the basic solar still. The productivity of the still is improved by 27.32%, the daily water collection of the glass cover cooled solar still integrated with mini solar pond is found that 59.5%.*

Keywords:*solar still,solar pond,flat plate collector,glass cooled solar still.*

I. INTRODUCTION

Solar energy is the best source for the desalination of the saline water. In order to increase the productivity of the solar still so many works are carried out. Sahoo et al [1], suggested that the usage of blackened basin surface and the thermocol insulation at the bottom and the sides of the still can increase the productivity considerably. Bassam et al [2], introduced usage of sponge in solar stills. Solar still with sponge cube gives higher productivity Compared to the basic solar still, (i.e.) 273%. Hiroshi tanaka et al [3], defined that the amount of distillate can be increased 48%, While using internal and external reflectors to the single basin solar still. Palakpatel et al [4] analyzed that the various techniques that can be followed to increase the productivity of the solar still. Mufag Suleiman et al defined that the depth of water has an impact on the productivity of the solar still and also defined that the temperature difference between the glass and the water enhances the water collection. Minasian et al [6] connected a wick type solar still and the hot wastage brine from wick directly fed into basin type solar still, which is giving 85% higher productivity compared to the basin type. Nafey et al [7] have used black rubber and black gravel they have increased the productivity as follows 20%, 19%. Kalidasamurugavel et al [8] also defined that the temperature difference between the glass cover and the basin water temperature increases the condensation rate. Kabeel et al [9] found that the area of evaporation and the glass cover temperature plays an important role on the solar desalination process.

Hintesh et al [10] found that by using a hemispherical shaped solar still his productivity ranges from 1.4 L to 1.6 L. And it is having the productivity of 18 %. So these are the various factors which were having a impact on the field of solar desalination.

II. EXPERIMENTAL SETUP

1. Conventional Solar still

Conventional solar still is the basic form of solar still, which is having single slope and single basin. It is having the basin area of 1m*1m. Basin is made of aluminium sheet of 2mm thickness. The saline water is kept in the storage tank and supplied to the basin via PVC hose. When the evaporation process starts, the water level decreases. In order to maintain the water depth the basin is recharged for every half an hour.

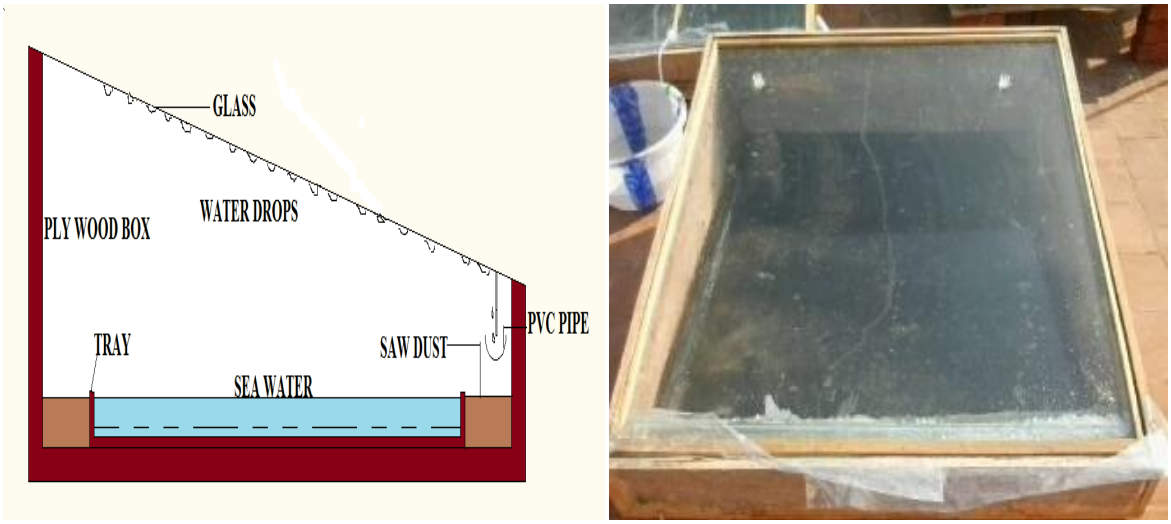

2. Glass cooled Solar still

Single basin solar still is fabricated using the aluminium sheet of 2mm thickness at the dimension of 1m×1m of and height of 50 mm. Since the colour of the aluminium is silvery and here it is painted black for higher heat absorption.

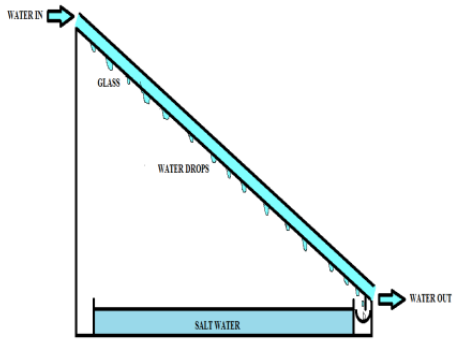

The aluminium basin is painted black in order to increase the absorption of solar radiation. The top of the basin is covered with transparent 5mm window glass inclined to 15% angle with horizontal.

There are certain specifications are needed for the glass to be used in the solar still. They are (a) minimum amount of reflection for solar radiation energy (b) high thermal resistance for heat loss from the basin to the ambient. If the glass to water distances increases, heat loss due to convection become greater which is causing the still efficiency to drop. Here in the glass cooled still one cotton cloth of 2cm wide is fitted on the top of the glass from top to bottom for throughout the length of the glass. And the cover is sealed tightly using silicon sealant to reduce the vapor leakage. A pipe of 10 mm diameter is fitted to the basin for filling saline water. The experiment was carried out by keeping water depth of 1 cm. During the experiment every day the solar radiation, atmospheric temperature and daytime wind speed also measured. The hourly productivity of fresh water output is measured correspondingly, the prevailing conditions are noted down. When the water is maintained at 1 cm of depth, the productivity of fresh water is higher than productivity at 2 cm depth of water.

3. Mini Solar pond

A solar pond is a large area collector of solar energy resembling pond that stores the heat, which is then available to use for practical purposes. Their common features are to store the energy in the incoming solar radiation in the heated depths of the pond, and to suppress the convection currents that would otherwise leads to loss to the surroundings.

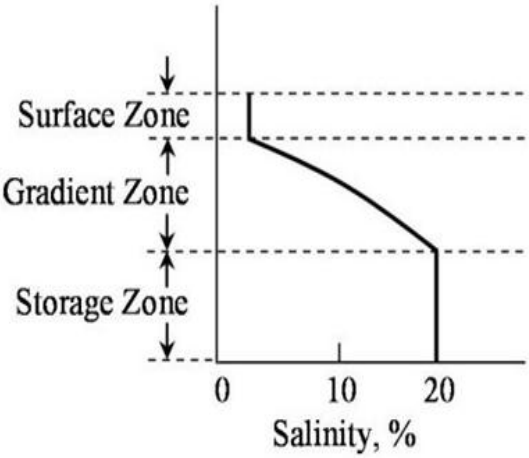

Mainly it consists of three zones they are,

- Relatively fresh water zone.
- Increasing salt.
- Saturated salt water.

The main heat loss from the storage zone has thus been reduced, while there are small heat losses by conduction through bottom and sides of the pond. The storage zone heats up and retains this thermal energy until it is withdrawn for use. Temperatures above 80^0c can be obtained in periods of higher solar radiation.The temperature range at the various zones of the solar pond is given below.

4.Solar Flat plate Collectors

On the many solar collector concepts presently being developed, the relatively simple flat plate solar collector has found the widest application so far. It is the easiest and least expensive to fabricate, install and maintain, moreover it is capable of using both the diffuse and the direct beam solar radiation. Flat plate collectors easily attain temperatures of 40 to 70^0c. Solar collectors transform solar radiation into heat and transfer that heat to medium (water). Then solar heat can be used for heating water.

Flat plate collector consists of an absorber, a transparent cover, a frame, and insulation, transparent cover prevents wind and breezes from carrying the collected heat away. Absorber plates are commonly painted with "selective coatings" because it absorbs and retain heat more than ordinary black paint. Absorber plate is commonly made of aluminium.

III. RESULT AND DISCUSSION

1. Comparison of Basic Solar still and Glass Cooled Solar still

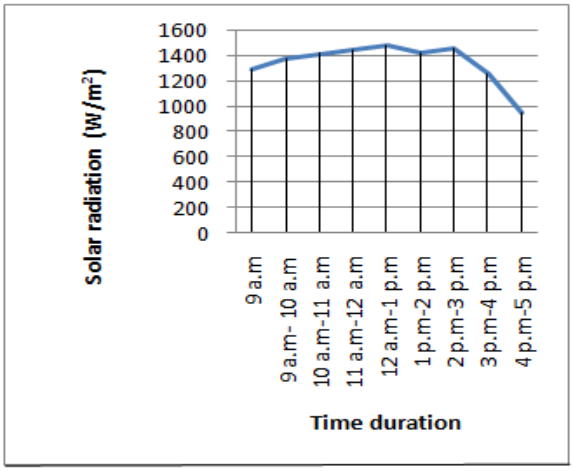

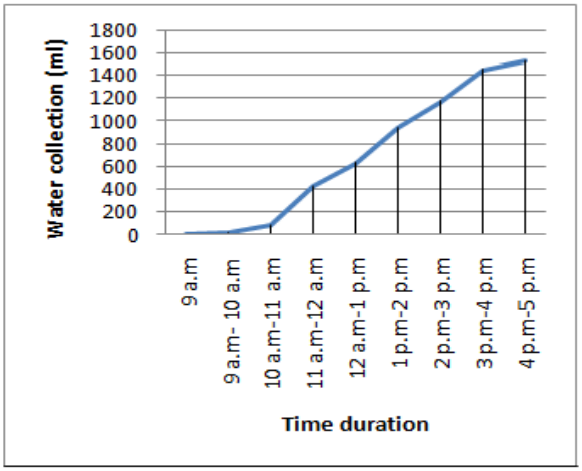

Graph 1. Time Vs Solar radiation**Graph 2.** Time Vs water collection (Basic still)

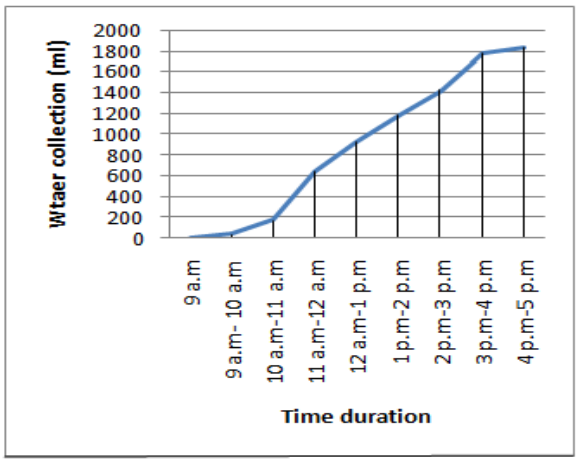

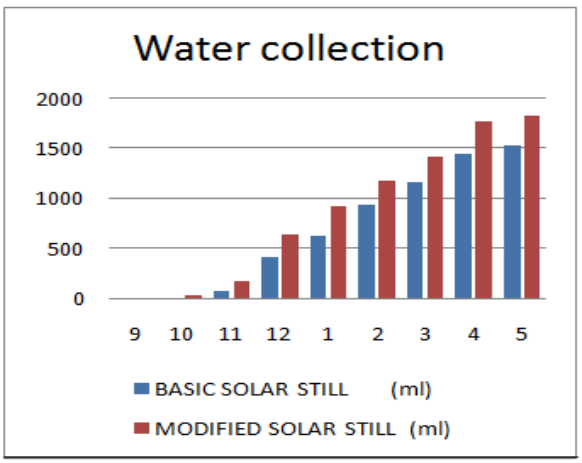

Graph 3 Time Vs Water collection (Modified still) **Graph 4.**Comparison between the Water collection Of Basic Still and Glass cover cooled still

The solar intensity with respect to time is shown in graph 1. The peak solar flux is in 1 pm, in the amount of1490 W/m^2. The cumulative water productivity with respect to time is shown in the graph 2. The daily water productivity of the basic and glass cooled solar still is 1.5liters and 1.7 liters respectively.

2. Comparison of Basic Solar still and Glass cooled Solar still Coupled with Solar pond:

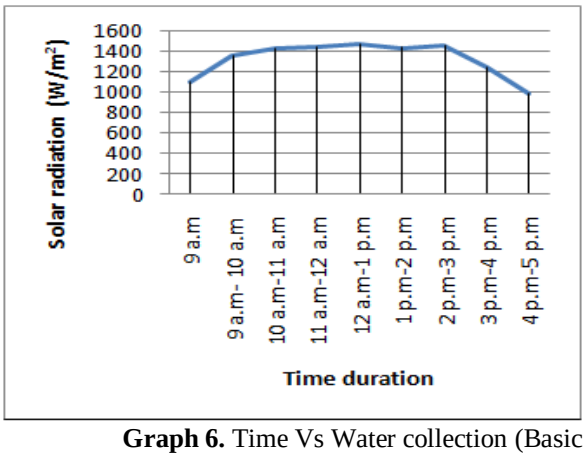

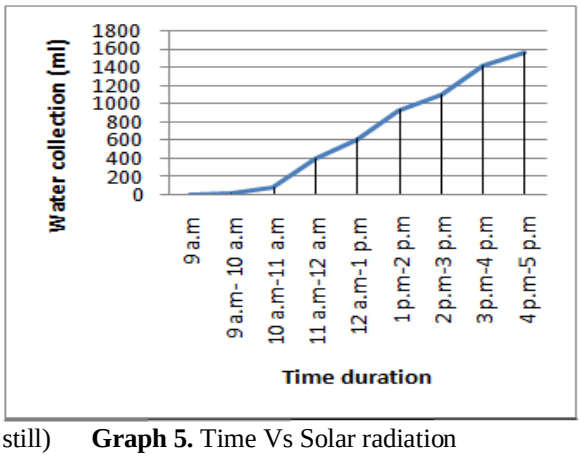

Graph 6. Time Vs Water collection (Basic still) **Graph 5.** Time Vs Solar radiation

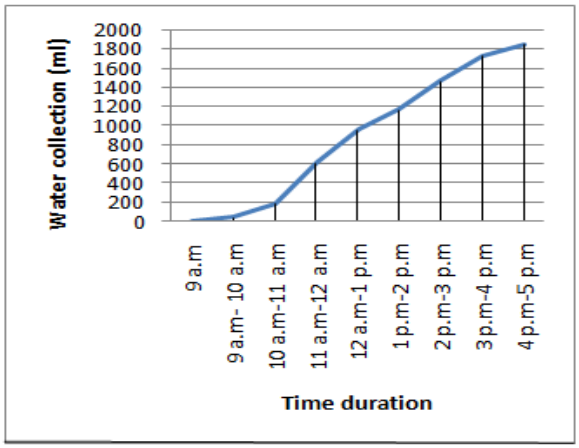

Graph 7. Time Vs Water collection (Glass cover Cooled still with solar pond)

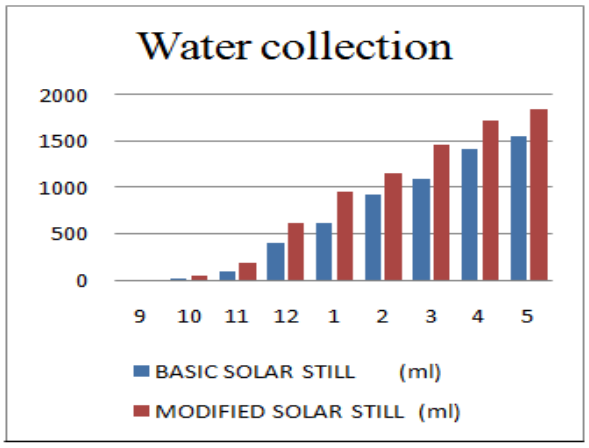

Graph 8. Comparison between water collection of Basic still and Glass cover cooled Solar still with solar pond

Graph 5 shows that the hourly variation of solar radiation with respect to time. The productivity of the basic still and the glass cooled solar still integrated with the solar pond are 1560 ml and 1880 ml respectively. The productivity is improved due to the rise of inlet water temperature.

3. Comparison of Basic Solar still and Glass cooled Solar still Coupled with Flat plate collector

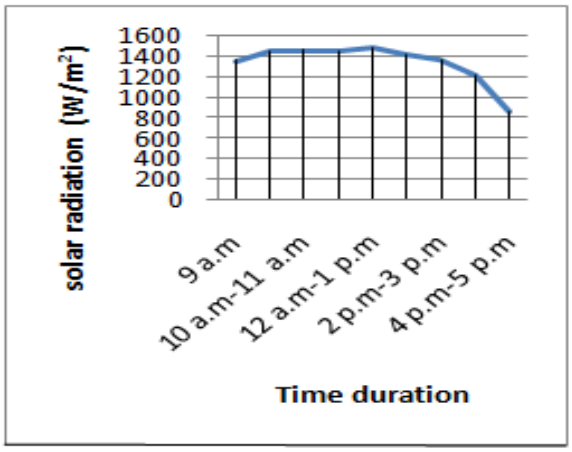

Graph 9.Time Vs Solar radiation

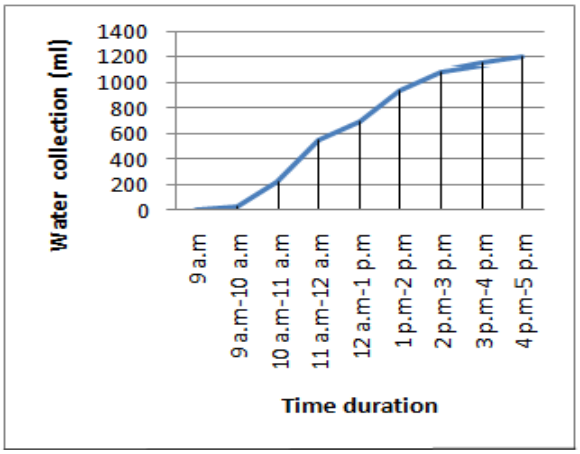

Graph 10. Time Vs Water collection (Basic Still)

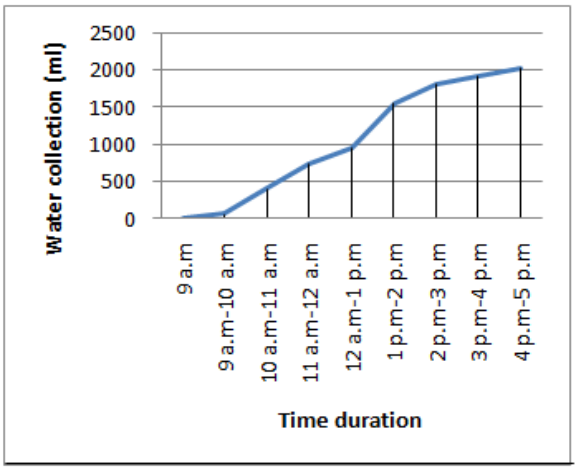

Graph 11. Time Vs Water collection (Glass Cover cooled solar still with flat plate collector)

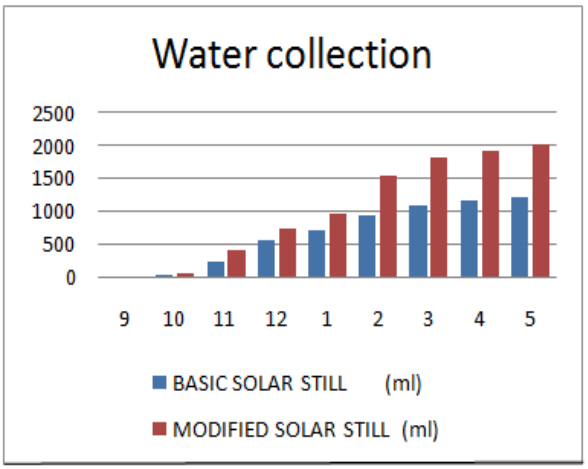

Graph12. Comparison between water collections of Basic still and Glass cover cooled solar still with flat plate collector

Graph 9 indicates the hourly increase and decrease in the solar radiation with respect to time. Condensation rate increases at the evening times due to the temperature difference between the water and the glass temperature. The temperature difference is caused by the reduction of ambient temperature during the evening times. The productivity range in basic and the modified are 1390ml to 2100ml respectively.

IV. CONCLUSION

There are several types of solar stills are available but they are having less productivity. In order to increase the productivity we have designed a new model which is having glass cooled cover. Since here the additional cooling is provided in the glass the productivity of the still is gets increased by 20%, Then the solar still is connected with the solar pond, while the still is connected with the solar pond the productivity is increased by30%, Then the solar still is connected with the solar flat plate collector, Then the productivity of the solar still is increased by 40%. When comparing all the solar stills such as basic solar still, others our modified one gives the higher productivity. Since the combined solar still with the solar pond and the solar flat plate collector gives the higher productivity of 2.1liters per day. Thus our still is having higher productivity than the others.

REFERENCES

[1] Bassam A/K Abu-Hijleh *, Hamzeh M. Rababa_h. Experimental study of a solar still with sponge cubes in basin. Energy Conversion and Management 44 (2003) 1411–1418

[2] Hiroshi Tanaka*, YasuhitoNakatake.Theoretical analysis of a basin type solar still with internal and external reflectors. Desalination 197 (2006) 205-216

[3] Palak $Patel_1$,Ajayaraj s $solanki_2$,Umang R $Soni_3$,Ashish R $Patel_4$, A Review to Increase the Perfomance of Solar Still: Make It Multi Layer Aborber,2 (2014)173-177

[4] A. N. Minasian and a. A. Al-karaghouli. An improved solar still: the wick-basin type.EnergyCoversion Management 36(1995) 213-217

[5] A.S.Nafey[a,*],M.Abdelkader[b] , A.Abdelmotalip[b] ,A.A. Mabrouk[a] ,Solar still Productivity Enhancement. Energy Conversion and Management 42 (2001) 1401-1408

[6] B.B. Sahooa, N. Sahoob, P. Mahantab, L. Borboraa, P. Kalitaa, U.K. Sahab, Performance assessment of a solar still using blackened surface and thermocol insulation, Renewable Energy 33 (2008) 1703–1708

[7] Muafag Suleiman K. Tarawneh *Effect of Water Depth on the Performance Evaluation of Solar Still, 1(2007)*23 – 29*

[8] K. KalidasaMurugavel[a], Kn. K. S. K. Chockalingam[a], K. Srithar[b,*]. Modeling and Verification of Double Slope Single Basin Solar Still Using Laboratory and Actual Solar Conditions,3(2009)228 – 235.

[9] A. E. Kabeel, performance of solar still with a wick, Concave evaporation surface, *Twelfth International Water Technology Conference*, IWTC12 2008, Alexandria, Egypt

[10] 1Hitesh N Panchal, 2Vinod Prajapati, 3RanvirgiriGoswami, 4Nilesh Pancholi,performance analysis of hemispherical solarstill in climate condition of mehsana, gujarat, 1(2012)210-213

International Journal of Modern Engineering Research (IJMER)

Volume : 4 Issue : 11 (Version-3) ISSN : 2249-6645 November- 2014

Contents :

OPEN ACCESS

International
Journal
Of Modern Engineering Research (IJMER)

Effect of Preform Geometry on the Material Behaviour and the Densification Mechanism during Hot Upset Forging of Sintered AISI 9840 P/M Steel Produced Using Elemental Powders

Manoj Kumar[1], Dr. (Mrs.) Shashi Krishna Pandey[2], Dr. (Mrs.) R.Nagalakshmi[3], Dr. K.S. Pandey[4]

[1]*Former, M. Tech. Student, Dept. of MME,National Institute of Technology, Tiruchirappalli-620015,TamilNadu, India,*
[2]*Director, National Institute of Technology, Puducherry, Karaikal 609 605;*
[3]*Manager, Welding Research Institute, Bharat Heavy Electricals Limited, Tiruchirappalli 620014, Tamil Nadu, India,*
[4]*Former Professor, Department of Metallurgical and Materials Engineering, National Institute of technology, Tiruchirappalli-620 015, Tamil Nadu, India.,*

Abstract: *The present investigation pertains to generate experimental data in order to establish the influence of initial preform geometries on the material behaviour and the operative densification mechanism/s during hot upsetforging of sintered AISI 9840 P/M Steel composition prepared from the elemental powders. Powder blend corresponding to AISI 9840= C(0.4%), Mn(0.8%), Si(0.3%), Ni(1.0%),Cr(0.8%), Mo(0.25%) and Fe(96.4%) composition was prepared on a pot mill and the blending was carried out for a period' of 16hrs. while maintaining the powder to ball ratio 1.1: I by weight. Compacts of 27.5mm diameter and 12 - 24mm heights were prepared from the aforesaid blend in the density range of 84±1 percent of theoretical density by applying accurately controlled pressures in the range of 460±10 MPa and by taking pre-weighed powders. Indigenously developed ceramic coating was applied all over the compact surfaces and dried under an ambient conditions for a period of 10- 12 hrs. These ceramic coated compacts were recoated 90° to the previous coating and re- dried under the aforesaid conditions. These ceramic coated preforms were sintered in an electric muffle furnace for a period of 90 minutes at 11500±10°C. Immediately after the completion of the sintering schedule, the preforms corresponding to 0.45, 0.68 and 0.92 initial aspect ratios were axially hot forged to different height strains. Analysis of the experimental data has revealed that the lower aspect ratio preforms densified rapidly compared to higher aspect ratios and the densification curves corresponded to a third order polynomial of the form:*$(\rho f/\rho th) = ao + a_1 \epsilon h + a_2 \epsilon h_2 + a_3 \epsilon h_3$*; where,* $\epsilon h = ln (Ho/H_f)$ *and a0, al, a2 anda3 are empirically determined constants. Further analysis has established that the Poisson's ratio would always remain less than one half and will have the tendency to approach to a limiting value of 0.5 in the near vicinity of the theoretical density. Influence of the preform geometry is established to be quite pronounced and has affected the densification curves and Poisson's ratio with density.*

Key words: *Aspect ratio, ceramic coating, compacts, densification, hot forging.*

I. Introduction

Long before furnaces were developed that could approach the melting points of most of the metals, the, Powder Metallurgy (P/M)principles were invoked to consolidate powders to useful shapes. About 3000 BC, the Egyptians used "sponge iron" for making tools. In this early process, iron oxide was heated in a charcoal and crushed shell fire which was intensified by air blasts from bellows to reduce the oxide to a spongy metallic iron. The resulting hot sponge iron was then hammered to weld the particles together. However. The final shapes were obtained by simple forging procedures described elsewhere [I]. These crude forms of P/Multimately led to the development of one of the commercial methods for producing iron powder. Grinding the sponge iron to fine particles and heating these particles in hydrogen atmosphere removes the oxygen from the oxide and also softens the particles [2].Commercial P/Mnow spans the density spectrum from highly porous metal filters to self-lubricating bearings and P/Mparts with well controlled density to fully dense P/Mwrought metal systems [3]. Manufacturing of precision engineering components from powder metallurgy route has on date become an established mass production technology and the major products of this route include the self-lubricating

bearings, filters, structural andelectrical parts, electrical contacts, cemented carbide, diamond tools and frictional materials. Basically P/M is an art and science of producing fine metal powders and objects finished and semi- finished from individual, mixed or alloyed metal powders with or without the inclusions of non-metallic constituents [4 - 7]. The process has acquired more competitive status in comparison to the other metal forming technologies and powder metallurgy is growing continuously throughout the world. Powder preform forging (PPF) is a process in which sintered or un-sintered metal powders or preforms are hot formed in confined dies. Truly speaking, powder forging is a deformation processing technique aimed at enhancing the density of P/M parts, and, thus, their performance characteristics [4]. A major key factor in successful powder preform forging is the proper preform design. Preform design [8, 9] has a significant effect on metal flow and the distribution of stresses in the deforming preform. These factors, in turn, affect the densification and void fracture of the material. In general, sufficient metal flow must take place to achieve full density and good bonding [10]. However, increasing the amount of metal flow would increase the possibility of fracture. Thus, the preform shape must fall between fracture limits and the threshold for the best properties [11 - 13]. Preform design for each complex part must be taken in account on an individual basis. Nevertheless, some guidelines can always be obtained from the forging of a simple generic shape. An example, reported for flanged hub shape is described elsewhere [12]. Working of a conventional cast or wrought material invariably does not involve any change in the volume of the material. Basically this constancy of volume is one of the most striking factors used in the development of theory of plasticity and the metal working theories. In contrast to the constancy of volume that occurs in working of the conventional material, is the non-constancy of volume or a definite decrease in volume, which occurs in the deformation of P/Mpreforms [9, 14, 15]. The magnitude of the change in volume, i.e., likely to occur in deforming the P/Mpreforms depends upon the preform density and the amount of deformation. Nearly 30 to 40 % of the voids are present in the sintered preforms and, therefore, while deforming them, consideration must be made to the manner in which the voids deform during the compressive mode of loading. Thus, the material and the voids begin to flow under the influence of compressive loading and the deformation of voids continues to increase under the developed shearing stresses, and, also decreases the total volume and the material tends to acquire density close to the theoretical as reported elsewhere [16 - 20]. Densification in P/M preforms during deformation is thus reported to be dependent upon the mode of loading, preform geometry and its initial density, the pore shape, size and its distribution inside the preform [16-24]. However, during hydrostatic deformation, yielding and densification of P/Mpreforms take place as reported elsewhere [16, 17]. The material during upsetting mode laterally expands and when there is a restrain, which can develop hydrostatic pressure as well, and the same would create the feasibility of virtually attaining cent per cent density. The influence of shear mode of deformation has been described by Koerner [25]. The effect of strain induced densification and the stress- induced densification has been shown by Bockstigel and Olsen [18], Kuhn [4] and Fischmeister et.al [19]. However, the amount of flow or strain imparted to a preform is important in achieving high impact strength values [27]. Technical papers dealing on the deformation behaviour of sintered ferrous *P/M* preforms are described elsewhere [28 - 35] and for non-ferrous porous preforms can be referred in the recent literature [13, 36, 37]. The findings of these researchers have shown that the densification is a function of applied stress which induces strains and, therefore, relations have been proposed between the attained density and the true height strains. The present investigation is aimed to establish the feasibility of processing AISI 9840 steel prepared via the *P/M* route by exclusively using the elemental powders. Further, it is to develop the empirical relations for densification during hot forging of sintered *P/M* preforms. Also to study the influence of preform geometry on the densification mechanism. It is also planned to investigate bulging ratio and the densification, Poisson's ratio and densification modes. The AISI 9840 steel composition is Fe - 0.40 % C - 0.80% Mn - 0.30 % is - 0.80 % Cr - 1.0 % Ni - 0.25% Mo. Basically AISI 9840 steels come under the category of triple alloy steels, which include nickel, chromium and molybdenum. These steels exhibit high strength and strength to weight ratio apart from being good corrosion resistant. The presence of various alloying elements and their functions are discussed briefly here in section I.1.

I.1 Functions of Alloying Elements in AISI 9840 Steel

1.1.1 Carbon

Properties of iron-carbon alloys are greatly dependent upon the amount of carbon present in the steel. Once the carbon content is very low in the steel, the steel becomes very soft. However, an increase in the carbon content in the steel enhances its hardness and strength and ultimately the steel becomes very brittle once the carbon content into it exceeds 2.0 per cent. Basically, the carbon content has been taken as the basis for the characterization and classification of the iron-carbon alloys. They have been classified as the irons, steels and the cast irons. Thus, carbon is treated as an essential element in steel. Principally this element is added to increase the solid solution strength and hardness as well as to enhance the hardenability. It also dissolves in iron to form ferrite and austenite. It also combines with iron to form carbide called cementite (Fe_3C) as a component of pearlite.

1.1.2 Nickel

Nickel refines the grain size, improves hardenability and makes austenite to transform sluggishly. It further enhances the strength and toughness of ferrite. Combined with chromium it has a tendency to considerably improve the high temperature resistance to oxidation and corrosion. A nickel addition of 36 % in iron produces an alloy of almost zero expansion. Steels containing nickel in the range of 1.0 to 3.0 % are used for locomotive bodies, boilers, bolts, railway axles and large forgings. Higher amounts of nickel is added to increase the corrosion resistance of high chromium steels. Since it enhances the impact resistance of steel at very low temperatures, and, therefore, the same is extensively used in the manufacture of low temperature steels. Nickel steels were the first alloy steels that were used in large engineering applicationssuch as armor plates, highly stressed bridge members, shafts etc. Further nickel induces improvement in mechanical properties after annealing and normalizing. Therefore, these steels are used for large forgings, castings and structural parts. Nickel is widely used in the production of stainless steels.

1.1.3Manganese

Manganese is present in all grades of steels and is used as a major deoxidizer. Elimination of hot shortness is one among the most important functions of manganese. It strengthens ferrite and is a mild carbide former. It further improves hardenability of steels and also makes austenite sluggish to transform. Apart from these, manganese is one among the least expensive alloying elements and is always present in almost all steels. It is an important alloying element in free cutting steels. This is also found invariably in all structural steels as well. Manganese, basically dissolves in ferrite and, thus, increasing its strength and hardness. Apart from these, it enhances the hardenability to a greater extent. It takes care of the harmful effects of sulphur by forming manganese sulphide. For this purpose the addition of manganese in steels are maintained at least three times that of the sulphur present in the steel.

1.1.4Silicon

Basically silicon dissolves in ferrite increasing its strength and hardness without lowering the ductility. Silicon hardens ferrite and enhances its hardenability moderately. It is a strong deoxidizer for steels and allows the production of sound steel. It is also a very strong graphitizer. Silicon and manganese put together impart high strengths to steels.Silicon-manganese structural and spring steels are the examples. Further, silicon is present in almost all grades of steels. Around 0.3 to 0.5 per cent silicon is added to steel castings in order to enhance their strengths and soundness. However, up to 5 per cent silicon is used in all magnetic steels such as in the steels used for the production of transformers, motors and generators. In these steels, silicon enhances the permeability of the steel and reduces iron losses. Thus, silicon is present in almost all the steels as it is an important alloying element in the steel. Silicon added in the spring steels, chisels and punches in order to enhance their toughness.

1.1.5Chromium

Chromiumis less expensive alloying element in steels than nickel and it is capable of forming simple carbide (Cr) C, (Cr_4C) or complex carbides [(Fe Cr) $_3$c]. These carbides have very high hardness and good wear resistance. Chromium is soluble up to 13% in y - iron and has unlimited solubility in alpha- ferrite. When chromium is present in amounts in excess of 5%, the steel is inherited with the high temperature properties and the. Corrosion resistance improvements. Chromium enhances the hardenability to such an extent that chromium steels arereadily hardened even in very thick sections. Chromium forms carbides which are very hard and wear resistant. Further chromium imparts the steel the desired strength, wear resistance and oxidation resistance at elevated temperatures. Apart from these, chromium is a principal alloying element in all forms of stainless steels.

1.1.6Molybdenum

Molybdenum is relatively expensive alloying element and has limited solubility in Yand alpha-iron and is a strong carbide former. Molybdenum has a strong effect on hardenability and like chromium increases the high temperature hardness and strength of steels. Steels containing molybdenum are less susceptible to temper brittleness compared to other alloy steels. Addition of molybdenum ranging in between 0.15 to 0.30 per cent to steels is done in order to enhance the effects of other alloying elements such as manganese, nickel and chromium. Further this acts as a grain growth inhibitor when the steel is subjected to elevated temperature applications. Molybdenum forms carbides having high red hardness and wear resistance. Further molybdenum resists softening of steel during tempering and heating cycles. Though, molybdenum is a relatively expensive alloying element and are generally found in almost all high strength structural steels. It is an important alloying element in high speed tool steels. Apart from these, molybdenum is commonly added to almost all carburizing steels.

II. Experimental Details

2.1 Materials Required

The materials required to carry out the present investigation were powders of iron, graphite, manganese, silicon, nickel, chromium, and molybdenum respectively. The iron powder was procured from M/**s.**The Sundaram Fasteners Ltd., Hyderabad, Andhra Pradesh, India and the purity of iron powder was found to be 99.6% with 0.4% insoluble impurities. The main alloying powders such as Manganese, silicon, nickel, chromium and molybdenum powders of -37 urn were procured from M/s. The Ghrishma Enterprises, Mumbai, Maharashtra, India. The graphite powder of 2 - 5 µm was supplied by The Asbury Graphite Mills, Inc., and Asbury Warren County, New Jersey, U.S.A., paste of graphite powder in acetone was used during powder compaction. Further, indigenously developed ceramic coating, electrically heated muffle furnace capable of maintaining 1150° ± 10°C temperature, ceramic rectangular boat for charging the indigenously developed ceramic coated preforms inside the furnace and suitable thermocouple for measuring the temperature were required. Apart from these, a hydraulic press of 1.0 MN capacity for powder blend compaction, and a friction screw press of 1.0 MN capacity for carrying out hot upset forgings were required. Suitable die, punch and the bottom insert assembly was required for powder compaction including the flat die set for hot upsetting experiments.

2.2 Powder Characterization

The basic properties such as the flow rates, apparent densities and compressibility tests were carried out for.

Table I. Characteristics of Iron Powder and AISI 9840 steel composition

SI. No.	Property	Iron	AISI 9840 Blend
1.	Flow rate by Hall Flowmeter, Sec/50g	23.80	25.00
2.	Apparent Density, g/cc	3.30	3.35
3.	Compressibility, g/cc at a pressure of 430±10 MPa	6.64 ±0.01	6.65 ± 0.01

Iron powder and the powder blend corresponding to AISI 9840 steel composition and the same are listed in Table I. However, the alloying elemental powders were taken to be of -37µm size, whereas, the sieve size analysis of the iron powder is tabulated in Table II.

Table II. Sieve Size Analysis of Atomized Iron Powder

Sieve Size, µm	-180+ 150	-150+125	-125+106	-106+90	-90+75	-75+63	-63+53	-53+45	-45+37	-37
Wt. % Ret.	3.61	3.62	2.48	0.70	8.33	9.20	16.68	15.83	3.59	35.90
Cum. Wt.%	3.61	7.23	9.71	10.41	18.74	27.94	44.62	60.45	64.04	99.94

2.3 Powder Blend Preparation

Elemental powders of iron, graphite, nickel, silicon, manganese, chromium and molybdenum in the required proportions were pre-weighed and mixed together and kept in a stainless steel pot with porcelain balls of 10mm to 15mm diameter and the pot lid was very securely tightened. The powder to ball ratio was maintained as 1.1: 1 by weight. Now, stainless steel pot was securely placed on the pot mill stand and tightened on it, and the machine was switched on. The blending operation was carried out for a period of thirty hours in order to obtain a homogeneous powder blend Once he uniformity in flow rates and apparent densities were obtained by carrying out an hourly tests on the powder mix,This test was carried out by stopping the pot mill after an interval of 1 hr. and taking out nearly. 100g powder blend for carrying out the flow rate and apparent density tests. Once the tests were completed, the powder blend was returned back to the steel pot. This test was carried out after an interval of every one hour of blending. Once the consistency in readings of flow rates and apparent densities were obtained the blending operation was terminated. Now the powder blend was ready to be used for further processing such as the preparation of the green compacts.

2.4 Compact Preparation

Compacts of 27.5mm diameter and 12 to 24mm heights were prepared from the powder blend of AISI 9840 steel composition in the density range of 84.5 ± 0.5 per cent of theoretical by applying the pressure in the range of 460± 10 MPa and by taking the pre-weighed powder blends. During the compact preparation, the inner die wall, the punch surfaces and the bottom insert surfaces were well lubricated by using graphite paste in acetoneso as to reduce the friction between the die walls and the powder particles and between the die wall and

the moving punch and also to facilitate easy ejection of the compacts at comparatively lower loads without damaging the compact surfaces, and, thus, minimizing the wear and tear of the die and punch surfaces. Compacts of three initial aspect ratios, namely, 0.45, 0.68 and 0.92 respectively were prepared on a 1.0 MN capacity Universal Testing Machine (UTM). Fig.1 shows the schematic diagram of complete powder compaction assembly. The same was used to prepare all the compacts each aspect ratio.

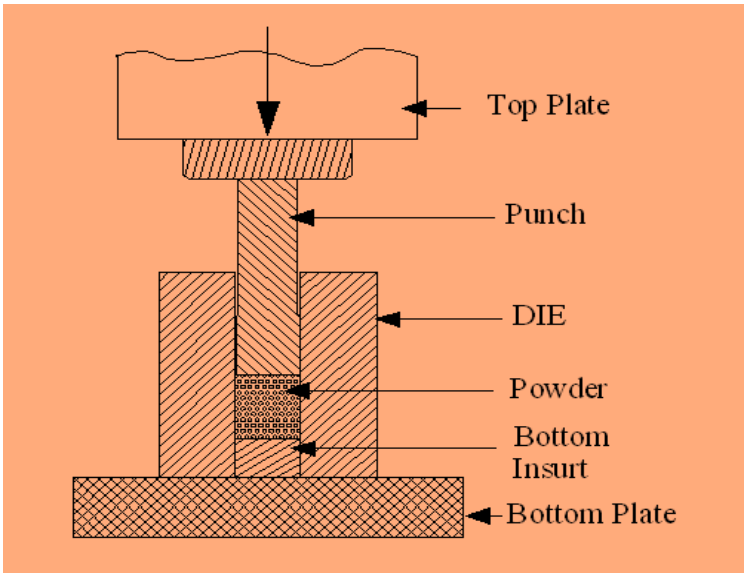

Figure 1 Schematic Diagram of Showing the Complete Powder Compaction Assembly

2.5 Ceramic Coating, Drying, Sintering and Hot Axial Forging

Compacts prepared from AISI 9840 powder blend were coated by indigenously developed ceramic coating [38] and this coating was allowed to dry under an ambient conditions for a period of 10-12 hrs. Immediately after the drying of the ceramic-coated compacts a second coating was applied 90° to the direction of the previous coating and the same was allowed to dry under the aforementioned conditions for a period of 12hrs. Ceramic-coated compacts of AISI 9840 powder blend were kept in a ceramic boat and charged into an electric muffle furnace in the uniform temperature zone for sintering at $1150^0 \pm 10$°C for a period of 90 minutes. Once the ceramic-coated compacts were sintered they were immediately axially hot upset forged to varying strain levels. This exercise was carried out to all preforms of different aspect ratios, namely, 0.45. 0.68 and 0.92 respectively. Immediately after hot upset forging was carried out, the deformed preforms were quenched in oil kept at room temperature. Once the deformed preforms were taken out from the quenchant oil they were thoroughly cleaned. The residual ceramic coating was removed by gentle grinding/machining. The ground and the machined specimens were further smoothened by using emery papers and then they were ready for dimensional measurements and density evaluations. Dimensional measurements such as forged heights (H_f), contact diameters {top (D_t) andbottom (D_{bt})}and bulged diameters (D_b) were made by using digital Vernier calipers. A minimum of three readings were taken and averaged out. Measurements were taken before and after removing the residual ceramic coatings. Virtually no substantial difference in dimensional measurements was found before and after the removal of ceramic coatings. However, the mass in air and water were found out by using single pan electronic balance [39] following the procedure described elsewhere [40].

II. Results and Discussion

3.1 Deformation and Densification

Fig. 2 has been drawn between the fractional theoretical density and the true height strain during the hot upset forming of sintered AISI 9840 P/M steel produced by using elemental powders. These plots also indicate the influence of initial preform aspect ratio, i.e., height to diameter ratio. A general observation of the curves in fig. 2 reveals that the characteristic nature of the curves are quite similar to each other. The preforms of smaller aspect ratio,

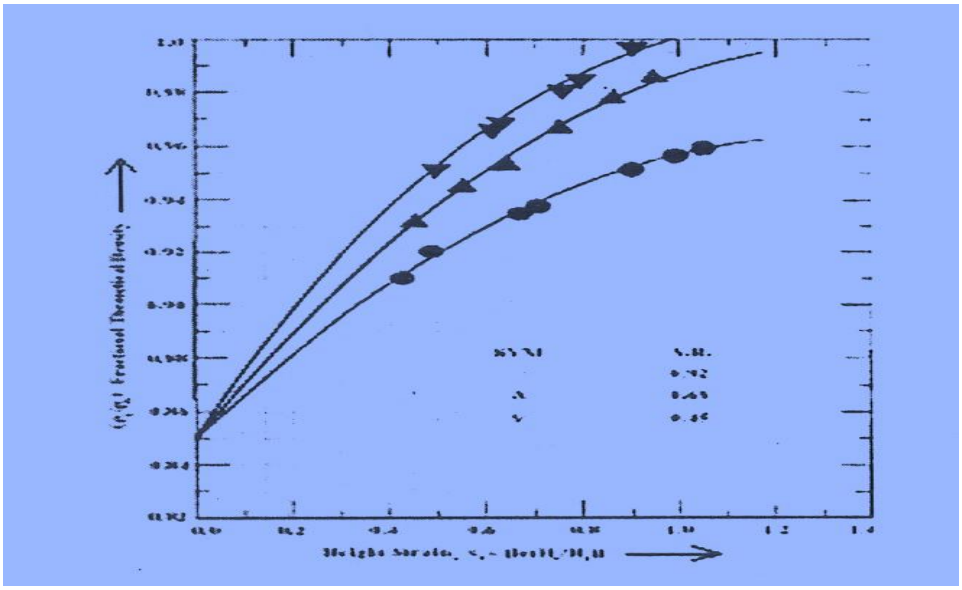

Figure 2 Plots between the Fractional Theoretical Density (ρ_f/ρ_{th}) and the True Height Strain (ϵ_h) During Hot Deformation of Sintered AISI 9840 P/M Steels of Different Initial Aspect Ratios.

i.e., (H_0/D_0) = 0.45 densified much more rapidly compared to the larger aspect ratio preforms, namely, (H_0/D_0) ratios of 0.68 and 0.92 respectively. Further analysis of these curves have revealed that the fractional theoretical density attained followed a third order polynomial with the variable called true height strain, i.e., $\epsilon = \ln (H_0/H_f)$. The equation to which these curves corresponded very closely is mathematically expressed as:

$$(\rho_f/\rho_{th}) = a_o + a_1\epsilon_h + a_2\epsilon_h^2 + a_3\epsilon_h^3 \text{---------- (1)}$$

Where, (ρ_f/ρ_{th}) is the fractional theoretical density and 'a_0', 'a_1', 'a_2' and 'a_3' are found to be empirically determined constants. The values of the constant 'a_0' is found to be in close proximity to the initial preform density for each aspect ratio and, hence, it was concluded that this constant did not participate in the densification mechanism. Densification process in the first phase, is attributed to be linear as the constant 'a_1'is linearly multiplied by the true height strain. Therefore, in the initial stages of the densification, the densification mechanism is absolutely linear However, the value of the constant 'a_2' is always found to be negative, and, therefore, the linearity of densification is disrupted and the curve - flattening step is introduced. Therefore, in the second stage of deformation, the densification starts retarding more and more if the initial aspect ratio has been kept increasing. It is also found that the values of constant 'a_3' are either negative or positive depending upon the preform geometry. When it is found to be positive it has contributed to densification mildly and when the same was found to be negative it has retarded densification further more than what was observed to be only retarding in the second stage of densification. The values of these constants, i.e., 'a_o', 'a_1','a_2'and 'a_3'are listed in Table II along with the values of the regression coefficient R^2.

Table III. Coefficients of the Third order polynomial of the form: $(\rho_f/\rho_{th}) = a_o + a_1\epsilon h + a_2\epsilon h^2 + a_3\epsilon h^3$ for AISI 9840 P/M Steel during Hot Deformation

Aspect Ratio	Constants				Regression Coefficient., R^2
	a_0	a_1	a_2	a_3	
0.45	0.85	0.284	-0.18	0.047	0.9997
0.68	0.85	0.219	-0.09	0.005	0.9999
0.92	0.85	0.164	-0.05	-0.01	0.9999

Table IV provides the level of densities achieved in preforms of three different aspect ratios, namely, 0.45, 0.68 and 0.92 respectively at the prefixed height strains. It is interesting to note that at every prefixed height strain, the densities achieved in lower aspect ratio preforms was higher than the next higher aspect ratio and further higher than the next largest aspect ratio preforms investigated in the present study. This also goes to confirm that the lower aspect ratio preforms densified much more rapidly compared to the larger aspect ratio preforms due to the quick and uniform load

Table IV. Fractional Theoretical Density Levels Achieved at Fixed Height Strains

S1.No.	Fixed Strain	Aspect Ratio		
		0.45	0.68	0.92
1.	0.00	0.85	0.85	0.85
2.	0.10	0.876	0.870	0.865
3.	0.20	0.898	0.889	0.880
4.	0.30	0.919	0.907	0.895
5.	0.40	0.937	0.923	0.908
6.	0.50	0.952	0.938	0.918
7.	0.60	0.966	0.957	0.930
8.	0.70	0.978	0.963	0.937
9.	0.90	0.995	0.980	0.952
10.	1.0	0.999	0.987	0.957

transfer all across the preform thickness. The larger aspect ratio preforms densified poorly compared to the lower aspect ratio preforms due to more dampening behaviour as they contained more number of pores in the thickness direction. These results are in agreements with others [10, 29-34].

3.2 Deformation, Densification, Strains and Concept of Poisson's Ratio

Basically, the Poisson's ratio (Yp) for porous materials under axial compression is defined as the ratio between the diametrical spread out, $€_d = \{\text{In } (D_f/D_o)\}$and the height strain, i.e., $€_h = \{\ln (H_0/H_f)\}$, i.e., $Y_P = €_d/€_h$ which is a very sensitive parameter in metal forming operation when the deforming material is porous. In order to understand its actual significance, a plot between the diameter strain ($€_d$) and the true height strain ($€_h$) has been plotted in fig. 3 for all the

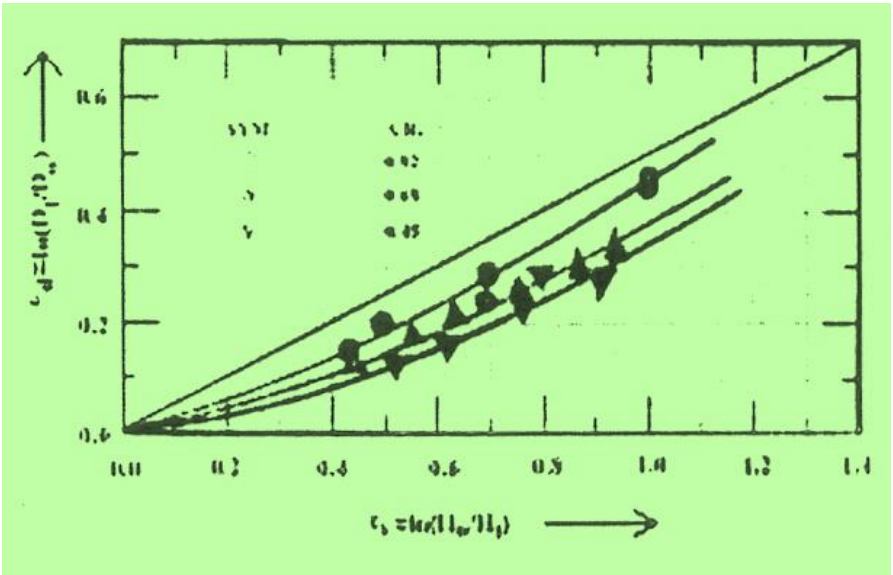

Figure 3 Relationship between True DiameterStrains ($€_d$) and the True Height Strains ($€_h$) during Hot Axial Deformation of AISI 9840 Sintered Powder Preforms

aspect ratios during hot deformation of the sintered AISI 9840 P/M steel, It is observed that al1 the curves exhibit similar characteristic features, but, the curves corresponding to higher aspect ratio preforms are nearer to the theoretical line whereas the lower aspect ratios preform curves is the farthest away from the theoretical line. Interestingly all the data points are below the theoretical line which is the true representation of Poisson's ratio of the. Conventionally dense material under plastic deformation with virtually no friction, thus, yielding a slope of 0.5. Therefore, it can be confidently established that the Poisson's ratio (Yp) for porous materials under plastic deformation can never attain the limiting value of 0.5. Hence, it will always be a quest for the scientist to continue experimenting so as to acquire the value of the Poisson's ratio equal to 0.5 and also to attain the density very much close to one hundred per cent. This limiting value is not attained due to the fact that in the later stages of densification, the flow of pores and materials become simultaneous. This situation generally arises during axial upset forming operation and the same is reported elsewhere [29-37].

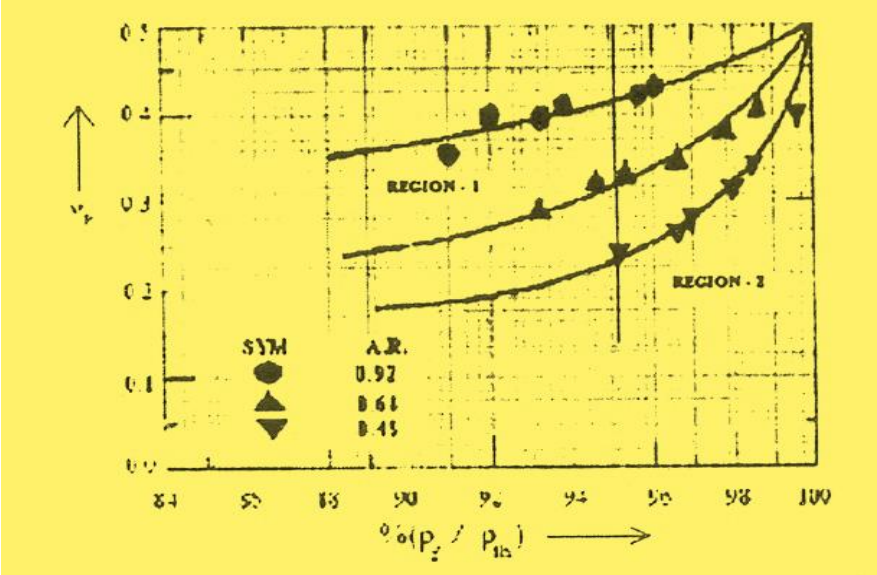

Figure 4 Relationship between Poisson's ratio (Y_p) and percentage theoretical densityattained during hot axial deformation of AISI 9840 powder preforms

In order to establish the true behaviour of Poisson's Ratio with respect to the percentage density achieved, a plot between the Poisson's Ratio and the per cent theoretical density has been drawn and the same is shown in fig. 4. This fig. 4 very clearly shows the influence of initial preform geometries on the actual variation of Poisson's Ratio w.r.t. the attained per cent theoretical density during the hot axial upset forging of sintered AISI 9840 P/M steel preforms. The basic characteristic nature of all these curves are observed to be quite similar to each other, and therefore these curves can be mathematically expressed by a similar expression. A typical curve fitting analysis has revealed that they can be expressed by the following second order polynomial:

$$(p) = b_0 + b_1 (\rho_f/\rho_{th}) + b_2(\rho_f/\rho_{th})^2 \text{---------- (2)}$$

Where, 'b_0', 'b_1' and 'b_2'are empirically determined constants and are found to depend upon the initial preform geometries of the system investigated. All these constants along with the values of the regression coefficients 'R^2'are listed in Table V. Since, the values of the regression coefficient 'R^2' in each case is found to be in extremely close proximity to unity, and, therefore the above empirical relationship arrived at is ably justified. Further, it is observed

Table V Coefficients of the Second order Polynomial of the Form: $(p) = b_0+b_1 (\rho_f/\rho_{th})+b_2(\rho_f/\rho_{th})^2$for AISI 9840 P/M Steel during Hot Deformation

Aspect Ratio	Constants				Regression Coefficient
	b_0	b_1	b_2	b_3	R^2
0.45	0.85	0.284	-0.18	0.047	0.9997
0.68	0.85	0.219	-0.09	0.005	0.9999
0.92	0.85	0.164·	-0.05	-0.01	0.9999

From the above plot that the curves drawn in fig. 4 can be very explicitly sub-divided into two distinct two regions, namely, the Region-1 where densification occurred with a rapid pace,but, with a gradual increase in the values of the Poisson's Ratio and the Region-2 exhibited a rapid rise in the values of the Poisson's Ratio, but, with a minimal increase in attained density. This phenomenon has been true irrespective of the initial preform geometries. Thus, Region-1 is attributed as the region where maximum densification took place. However, Region 2 is described as a region where the pores that are left after the region-1, do not close down and their flow acquires the same status as that of the material flow. In other words, it can be established that the pores have technically stabilized in the structure just like a second phase and thus have become part and parcel of the structure itself. In this region, though the Poisson's ratio tends to approach to a limiting value of 0.5 in the near vicinity of the percentage theoretical density, but, it never attains the limiting value of 0.5. Therefore, it is imperative to conclude that the region 1 is the region of actual densification where the Poisson's ratio could rise steadily and the density enhancement becoming comprehensively rapid, and, hence, it is obvious to predict that in this region the pore closure kinetics is expectedly rapid while there is a gradual change in the geometry of the deforming preform, Now under the aforesaid arguments, it can be categorically stated that the region 2 is a zone

where pore closure kinetics for all practical purposes is a non - operative phenomenon, and, hence, the remaining pores left after region-1 become part and parcel of the structure itself.

3.3 Densification and the Bulging Ratio

In order to establish the relationship between the fractional theoretical density and the bulging ratio, fig.5 has been drawn between the parameters stated above. This figure demonstrates that the characteristic nature of these curves are quite similar to each other, but, the influence of geometry is found to be predominant. The curves of lower aspect ratio preforms are placed higher to the other aspect ratio curves. To further assess the influence of initial aspect ratio on the densification behaviour and bulging ratio, Table VI has been derived from fig. 5. This table shows that as the bulging ratio is kept constant, say for example 1.30, the density attained is 0.978, 0.947, and 0.916 in preforms of initial aspect ratios, i.e., 0.45, 0.68 and 0.92 respectively. This implies that the lower aspect ratio preforms have densified more rapidly compared to higher aspect ratio preforms. Further, as the bulging ratio is enhanced, the density in each aspect ratio has continued to increase. Further analysis of these curves in fig 5 has revealed that they have conformed to a second order polynomial of the form: $(\square_f/\square_{th}) = b_0 + b_1 (D_b/D_0) + b_2 (D_b/D_0)^2$; where, $(\square_f/\square_{th})$ is the fractional theoretical density and 'b_0', 'b_1', and 'b_2' are empirically determined constants and they are found to depend upon the initial preform geometries. Further, the curves start to plateau, i.e., flattening in the final stages of deformation. Yet another mode of analyzing the relationship between the per cent theoretical density attained and the bulging ratio is to plot the curves between Log $\{\%(\rho_f/\rho_{th})\}$ and Log (D_b/D_o). Such plots are shown in fig. 6. The data points on this plot for each aspect ratio exhibit a separate straight line indicating the fact that they actually represent a power law equation of the form: $\%(\square_f/\square_{th}) = A\,(Db/Do)^m$ where 'A' and 'm' are found to be empirically determined.

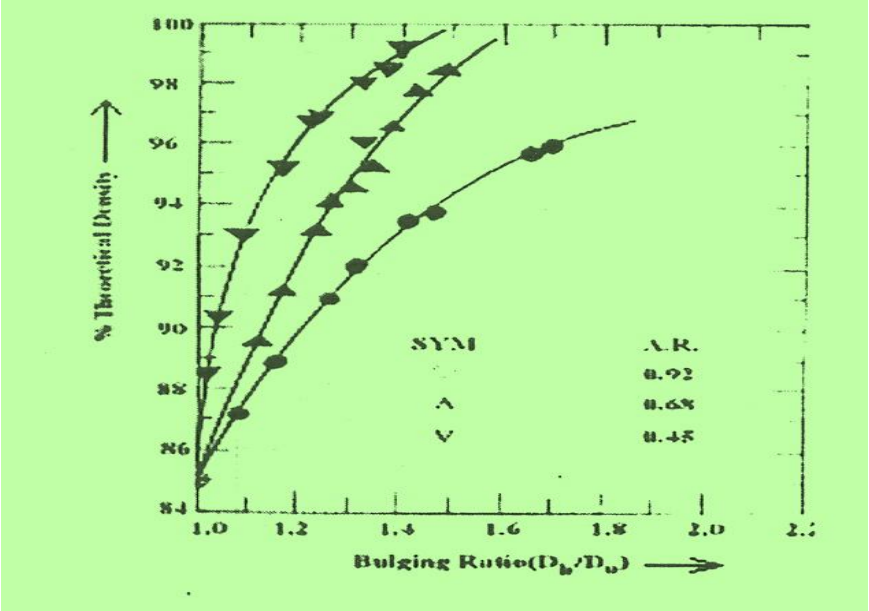

Figure 5 Relationship between Percentage Theoretical Density and Bulging Ratio during Hot Forging of AISI 9840 Powder Preforms.

Table VI. Level of Densification Achieved at Constant Bulging Ratio in the Preforms of Differing Aspect Ratio

S. No.	Bulging Ratio	A.R.=0.45	A.R.= 0.68	A. R.=0.92
1.	1.00	0.850	0.850	0.850
2.	1.05	0.905	0.870	0.863
3.	1.10	0.931	0.888	0.876
4.	1.20	0.961	0.921	0.889
5.	1.30	0.978	0.947	0.916
6.	1.35	0.988	0.960	0.924
7.	1.45	0.995	0.977	0.937
8.	1.50	----	0.984	0.943
9.	1.55	---	0.991	0.948
10.	1.60	---	---	0.953

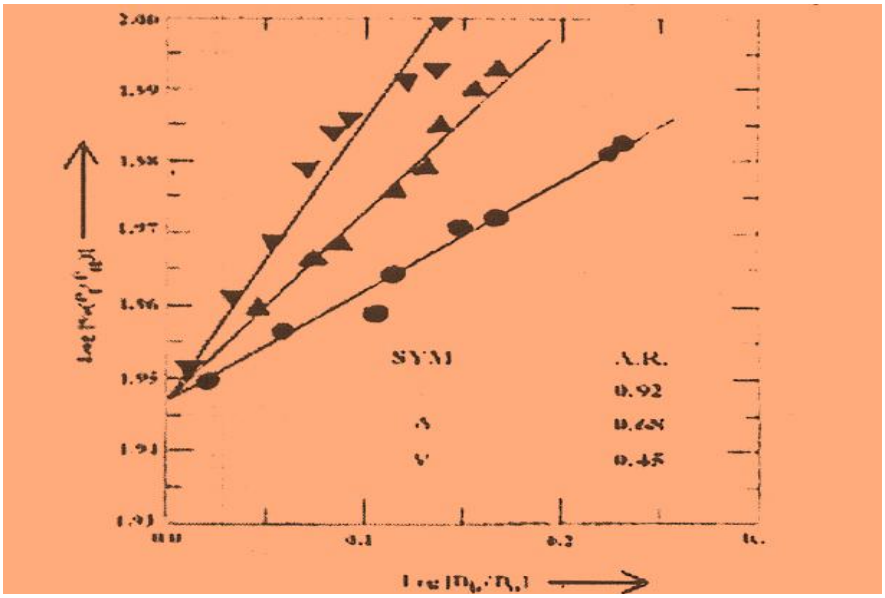

Figure 6: Relationships between Log (Percentage Theoretical Density) and Log (Bulging Ratio) During Hot Forging of AISI 9840 Powder Preforms.

Table VII. Constants of the Power Law Equation of the form: $\%(\rho_f/\rho_{th}) = A\ (Db/Do)^{m}$

Initial Aspect Ratio	Constants	
A. R.	**'A'**	**'m'**
0.45	**88.51**	**0.384**
0.68	**88.51**	**0.256**
0.92	**88.51**	**0.152**

constants and are further found to depend upon the initial aspect ratio of the preforms. The constant 'A' is found to be very close to initial preform density and therefore, is not responsible to contribute to densification whereas the value of 'm' is differing for each aspect ratio and, hence, it is attributed to contribute to densification. All of these constants are tabulated in Table V. Once the constants' A' and 'm' have been determined, the accuracy of the main equation arrived at has been tested. Now for the fixed values of (D_b/D_o), the corresponding values of the percentage theoretical

Table VIII. Measured and Calculated Values of $\%(\rho_f/\rho_{th})$ and also the %age Error Observed

A.R.	(D_b/D_o)	(ρ_f/ρ_{th}) meas.	(ρ_f/ρ_{th}) cal.	%error
0.45	**1.1**	**93.20**	**92.03**	**-1.26**
0.45	**1.2**	**96.05**	**95.15**	**-0.93**
0.45	**1.4**	**99.10**	**100.96**	**+1.88**
0.68	**1.2**	**92.20**	**92.96**	**+0.82**
0.68	**1.4**	**96.90**	**96.70**	**-0.21**
0.68	**1.5**	**98.40**	**98.42**	**+0.02**
0.92	**1.2**	**89.90**	**91.21**	**+1.46**
0.92	**1.5**	**94.30**	**94.36**	**+0.06**
0.92	**1.8**	**96.50**	**97.01**	**+0.53**

density has been taken and also by using the power law equation stated earlier, the corresponding values of the percentage theoretical density have been calculated and the possible error has been assessed. It has been found that the percentage error was confined to the lower values than +1.88 and -1.26. The actual values are shown in Table VIII. In most of the cases the calculated and measured values were in the range of ± 1.5 %. Thus, this demonstrates the accuracy of the above power law equation.

IV. Conclusions

Based on the critical analysis of the experimental and calculated data the following major conclusions can be drawn from the present investigation:

[1]. Densification curves followed a third order polynomial of the form: $(\rho_f/\rho_{th}) = a_o+a_1\epsilon_h+ a_2\epsilon_h^2 +a_3\epsilon_h^3$; where, (ρ_f/ρ_{th}) is the fractional theoretical density obtained at a given true height strain, i.e., $\epsilon_h = \ln (H_0/H_f)$ and 'a_0', a_1, a_2,and 'a_3' are found to be empirically determined constants. The constant 'a_0' was found to be in very much close proximity to the initial preform density, and, therefore, it has not contributed to densification. However, the constant 'a_1' is always positive and has linearly contributed to densification. Its values kept on decreasing as the aspect ratio was enhanced. The always-negative values of 'a_2' have resulted in flattening the curves in the later stages of deformation. 'a_3' is found to increase or decrease the densification rates as its values fluctuated between a very narrow range of negative to positive magnitudes,

[2]. Density levels achieved at any given true height strains were found to be maximum in lower aspect ratio preforms and minimum in the highest aspect ratio preforms. This phenomenon is attributed to the fact that the load transfer across the height direction has been quite uniform and quick in lower height to diameter ratio preforms. Further the poor densification in larger height to diameter ratio preforms is attributed to the cushioning effect of the total porosity content in terms of volume and thus the size effect (preform height) has played the significant role,

[3]. The variation of diameter strain with respect to the height strain has shown that all the data points were below the theoretical line indicating that there is no possibility of Poisson's ratio acquiring a limiting value of 0.5 w0hile deforming porous preforms in the plastic range of deformation. The influence of the preform geometry has played a very distinct role in affecting the positions of the curves,

[4]. The variation of the Poisson's ratio w.r.t. the percentage theoretical density for each aspect ratio is found to be quite similar to each other but the curve corresponding to the larger aspect ratio preform is above all the curves corresponding to lower aspect ratio preforms. Further, the variation of Poisson's ratio is observed to be in such a manner that two clear and distinct regions can be classified. Region 1 is the actual stage of densification where the Poisson's ratio steadily rises and the density enhancement becomes comprehensively rapid and, therefore, it is established that in this region the pore closure kinetics is rapid and effective. However, in Region 2 pore closure kinetics for all practical purposes is non - operative and, therefore, it is established that the flow of material and pores that are left after region I remain in the deforming preforms as part and parcel of the structure itself, and,(Db/D0)

[5]. It has been established that the densification followed a second order polynomial with the bulging ratio (D_b/D_0) of the form: $(\rho_f/\rho_{th}) = b_0 + b_1 (Db/Do) + b_2 (Db/D_0)^2$; where, '$b_0$', '$b_1$' and '$b_2$' are found to be empirically determined constants. Measuring the bulging ratio and knowing the constants 'b_0', 'b_1' and 'b_2' it is possible to predict the densities attained in the preforms without resorting to the tedious mode of measurements. Alternatively, a power law relationship has also been established which can predict the percentage theoretical density in ± 1 per cent range quite accurately. The power law equation is mathematically described as $\% (\square/\square_{th}) = A(Db/Do)^m$ where the symbols have their usual meanings.

REFERENCES

[1]. H. C. P. Carpenter and 1.M.Robertson, "The Metallography of Some Ancient Egyptian Implements", Jl. of Iron and Steel Institute, Vol.121, 1930, pp417 -448.

[2]. P. U1fgummeson, "Modem Atomizing Techniques", Powder Metallurgy, Vol.15, No.29, 1972, pp 67 -94.

[3]. K. S. Pandey, "Powder Preform Forging", Proceedings of the .National Seminar on Advances in Metal Forming, METFORM -2000, MIT Campus, Anna University, March 2000, pp 46-51.

[4]. H. A. Kuhn and C. L. Downey, "How Flow and Fracture Affect Design of Preforms for Powder Forging", Int. JI. Of P/M&Powder/Tech., Vo1.10, 1974, pp 59 -66.

[5]. H. N. Tiwari and R. Saran, "Analysis of Iron Powder Preform Forging", Trans. of PMAI, Vo1.12, 1985, pp 83 -86.

[6]. H. M. Skelly, "Powder Preform Forgings Ma from a Blended Iron Powder", Physical Metallurgy Research Laboratories, Report, MRPIPMPL - 78 -101, 1978, pp 1-15.

[7]. M. l. Koczak and H. Chung, "The Effect of Elemental Alloying and Sintering Temperature on the Cold Forming of Powder Metallurgy Nickel Steels", Powder Metallurgy Int. Yol.7, No.3 1975, pp 71 -74.

[8]. H. A. Kuhn and C. L. Downey, "P/MPreform Design for Hot Forging", Proceedings of APMI - ASM Congress, 1971, pp151 -162.

[9]. H. A. Kuhn, "Deformation Processing of Sintered Powder Materials", Ed. By H. A. Kuhn &A. Lawley, Academic Press, N.Y., 1978, pp 99 - 119.

[10]. K. S. Pandey, "Salient Characteristics of High Temperature Forging of Ferrous Powder Preforms", Key Engineering Materials, Vol.29 -31, Trans. Tech. Publication, 1989, pp, 465 -486.

[11]. P. W. Lee, "Fracture in Cold Forming of Metals - A Criterion &Model", Ph.D. Dissertation, Drexel University, Philadelphia, 1972.

[12]. P. W. Lee and H. A. Kuhn, "Cold Test in Workability", Testing Techniques, G. E. Dieter, Ed. ASM, 1984.

[13]. S. K. Suh and H. A. Kuhn, "Three Fracture Modes and Their Prevention in Forming P/MPreforms", Mod. Dev. In

P/M, Ed. By P. W. Taubenblatand H. H. Hausner, Vo1.9, 1977 MPIF Princeton, NJ, p- 407.
[14]. T. S. Rao and K. S. Pandey, "Development of Theoretical Relations During Deformation of Disc and Ring Shaped Preforms",Trans. of PMAI, Vo1.15, 1988, pp15-22.
[15]. H. A. Kuhn and C. L. Downey, "Deformation Characteristics and Plasticity Theory of Sintered Materials", Int. Journal of P/M, VoJ.7, No.1.1971, pp 15 -26.
[16]. F. Stassi and O. Alia, "Flow and Fracture of Materials according to New Limiting Condition of Yielding", Vol.3, No.11, 1967, pp 28 -37.
[17]. K. J. Kahlow, "Void Behaviour as Influenced by Pressure and Plastic Deformation", Institute of Metal Forming Report, Lehigh University, October 1971.
[18]. S. M. Doraivelu, H. L. Gegel, J. S. Gunasekaran, J. C. Malas and J. T. Morgan, " A New Yield Function for Compressible *PIM* Materials", Int. 11. Of Mech. Sci. Vo1.26, No.9 -12, 1984, pp 527 -535.
[19]. H. F. Fishmeister, B. Aren and K. E. Easterling, "Deformation and Densification of Porous Preforms in Hot Forging", Powder Metallurgy, Vo1.l4, No.27, 1971, pp 144 -163.
[20]. H. W. Ante, "Deformation of Porous Materials", A - Report, Hoeganaes Corporation, Riverton, NJ, 1974, pp 1-
[21]. R. Narayanasamy and K. S. Pandey, "Salient Features in the Cold Upset Forming of Sintered Aluminium - 3.5% Alumina Powder Composite Preforms", Jl. of Mat. Proc. Tech., Vol.72, 1997, pp 201 - 207.
[22]. R. Narayanasamy and K. S. Pandey, "Some Aspects of Work Hardening in Sintered Aluminium and Aluminium-Iron Composite Preforms During Cold Axial Deformation", JI. of Mat. Proc. Tech., Vo1.84, 1998, pp 136 - 142.
[23]. J. R. Inigoraj, R. Narayanasamy and K. S. Pandey, "Strain Hardening Behaviour in Sintered Aluminium - 3.5% Alumina Composite Preforms During Cold Axial Compression with or Without Annealing", JI. of Mal. Proc. Tech., Vol. 84, 1998., pp 143 - 148.
[24]. A J. R Inigoraj, R. Narayanasamy and K. S. Pandey, "Densification in Aluminium and Aluminium-Alumina Sintered Preforms During Cold Deformation", JI. of Metals, Materials and Processing, Vol. 10, 1998, pp.167- 176.
[25]. R. M. Koerner, "Tri-axial Compaction of Metal Powders", Powder Metallurgy International, Vol.3, No.4, 1971, pp.186-188.
[26]. G. Bockstiegel and H. Olsen, "Processing Parameters in the Hot Forming of Powder Preforms", Third European Powder Metallurgy Supplement, Part-I, Powder Metallurgy (U.K.), 1971, pp.127-148.
[27]. K. H. Moyer, "The Effect of Density on the Impact Properties of Iron PIM Forgings", Metals Engineering Quart., August 1972, pp.34-38.
[28]. K. S. Pandey, P. S. Misra and M. L. Mehta, "Effect of Forging Temperature and Carbon Content on the Cracking Behaviour of Iron- Powder Preforms Hot Upset Forged", Trans. of P.M.A.I., VoI.IS, 1988, pp.9-14.
[29]. M. N. Rao and K. S. Pandey, "Working of Porous Solid Cylinders of Eutectoid Composition", 14th National AIMTDR Conference Proc.1990, pp.217-222.
[30]. J. ArivudaiNambi and K. S. Pandey, "Densification Behaviour of Iron and AISI 4340 Powder Preforms During Hot Upsetting", Engineering Today, Vol.1, No.11, Nov.1999, pp.2-4.
[31]. J. ArivudaiNambi and K.S. Pandey, "Assessment of Mechanical Properties of Hot Forged AISI 4340 *PIM* Steel", Engineering Today, Vol., No.12, Dec.1999, pp.19-21.
[32]. S. Senthil Kumar, K. S. Pandey and P. Aravindan, "Densification Mechanism Operative During Hot Forging of Sintered AISI 4140 Steel Composition Using Elemental Powders", National Conference Proceeding on Quality Control in Metallurgical Industries, PSG College of Technology, Coimbatore - 641 004, Conf. Proc. 1999, pp. 76-83.
[33]. N. Ponnusamy, K. S. Pandey and P. Aravindan, "Effect of Manganese Addition in Sintered Fe-1.0%C Hyper Eutectoid Steel During Hot Forging", ibid, pp.496-503.
[34]. K. S. Pandey, "Powder Preform Forging", Proc. of the National Seminar on the Advances in Metal Forming, METFORM - 2000 held at M.LT. Campus, Anna University, March 2000, pp.46-51.
[35]. J. Anusha, J. ArivudaiNambi, K. S. Pandey and P. Aravindan, "Effect of Alteration of Chromium Percentage in AISI 4340 *PIM* Steel and Assessment of Mechanical Properties", ibid, pp.63-68.
[36]. S. Ram Kumar, R. Narayanasamy, K. S. Pandey and K. Mathrubootham, "Effect of Residual Porosity on the Mechanical Properties of Cold Deformed Aluminium and Aluminium - 4% Cu Alloy Powder Preforms", Trans. of P.M.A.I., Vol., 15, 1988,pp.3-8.
[37]. K. S. Pandey, "Some Investigation on the Cold Deformation Behaviour of Sintered AI-4%Cu Alloy Powder Preforms", Quart. Int. JI. of PIM Sci. &Tech., Yoi.2, No.3, 1991, pp.35-42.
[38]. K.S. Pandey, "Special High Temperature Ceramic Coating Indigenously Developed to Protect Preforms Against Oxidation During Sintering", Regional Engineering College, Tiruchirappalli - 620 015, T.N., India, 1986.
[39]. "Instructions Manual for Electronic Balances", Model-180, Adair Dutt& Co (India) Pvt. Limited, Madras.
[40]. Siddhartha Pandey, R. Chandramouli, K. S. Pandey and P. Aravindan, "Densification Behaviour and Properties of Sintered Hot Forged Iron - Carbon - Titanium Carbide particles composites", Proc. Of National Conference on Recent Trends in Manufacturing Technology and Management, Adhiyamaan College of Engineering, Hosur - 635 109, Conf. Proc. 28-29 January 2002, pp.134-141.

OPEN ACCESS

International
Journal
Of Modern Engineering Research (IJMER)

GSM-Microcontroller Based Remote Control of Sprinkler Irrigation

Jagdeep
M.E, I & C, Student , Electrical Engg. Dept., NITTTR, Chandigarh, India
Lecturer, Electrical Engg. Dept., B.K.N Govt. Polytechnic, Narnaul, India

Abstract: *GSM-Microcontroller based Remote Control of Sprinkler Irrigation is a new concept in the field of the irrigation for doing irrigation work remotely without any risk of accident due to electric shock , hard work and working in difficult environment condition. This system discards the conventional methods of irrigation work. In present work the author has designed and developed a automatic sprinkler irrigation system which is controlled and monitored by a microcontroller interfaced with display device , current flow sensor, solenoid valves and GSM modems. Given command to stop , start , interrupt and parameters under monitoring are stored in a memory based upon which microcontroller takes decision to run the system. Provision of protection against dry run and overload of motor coupled with centrifugal pump is also incorporated. Options using selector switches make this system compatible with single phase motor and three phase motor. It obsoletes the mechanical work of farmers by automatically changing over sprinkler water lines in sequence after running for a period of set time decided by farmer and switch off the water pump house motor upon completion of irrigation work using GSM modems interfaced with microcontrollers.*

I. Introduction

1.1 Sprinkler irrigation

This method of irrigation help us to save water and easy to use on uneven land .In sprinkler system , water is piped to one or more central locations in the field and distributed by high-pressure sprinklers using impact mechanism drive of nozzle.

1.2 Need for automation in sprinkler irrigation system

In Conventional farming a crop require irrigation multiple times from cultivation to the harvesting .Irrigation is required by crops in adverse weather conditions. A farmer has to face a lot of unavoidable problems and hardships while doing irrigation work.

1.3 Problems in sprinkler irrigation are

- Water pump houses are generally located far from the fields. To start and stop the motor a farmer have to go to water pump house and he remained to and fro between fields and water pump house for just switching ON/OFF the Motor.
- Sprinkler water pipe lines are required to change over manually after a while to cover all area of crop under irrigation, during this process a farmer is required to take off his clothes to avoid water on clothes & during winter season it is a cumbersome job for a farmer.
- Conventional process causes wastage of time, electrical power & water
- Risk of electric accidents as starter panels are poorly maintained at water pump houses and in most of cases are not earthed properly.
- At night time and in adverse weather conditions a farmer's tendency is to avoid switching off the motor when required causing huge wastage of electric power and precious water.

1.4 Benefits to the farmer using automatic sprinkler irrigation system are

- Saving of time water, Electric power, money& hard labor work.
- No risk of electric accidents , wild animals like snakes etc
- No impact of adverse weather conditions on farmer.

1.5 Selection of GSM technology

GSM (Global System for Mobile Communication) is a public service available at no cost to the user. Nowadays mobile hand set is not new to the farmers. Every where farmers can be seen using mobile phones and they are very much conversant with mobile hand set. There is no extra cost of communication equipments. Using GSM technology, a motor can be controlled and monitored from every corner of the world .It has no bar of distance like Infrared, Bluetooth, Radio waves etc.

II. Basic Design Of The System

The basic design of the GSM based remote control of sprinkler irrigation system is shown in Fig.1.1. The system makes use of a micro-controller that acts as the brain of the entire system. It controls the transmission and receiving of signals commands to the motor, sprinkler system from the mobile device using a GSM modem that allows for the usage of AT commands which can be used to read the messages from the modem. A GSM mobile device is used as first mobile station for transmitting section from which the farmer sends text messages that contain commands and instructions to the second mobile station, which is based on a specific area in the water pump house & agricultural field where the control system is located. The received SMS message is stored in the SIM memory of GSM Modem and is then extracted by the micro-controller and processed accordingly to carry out specific operations. The relay driver (ULN2003) is used to drive the relay circuits which switches the motor connected and solenoid valves in sprinkler water pipe line. The LCD is used to indicate the status of the operation performed by the micro-controller and also its inclusion makes the overall system user-friendly

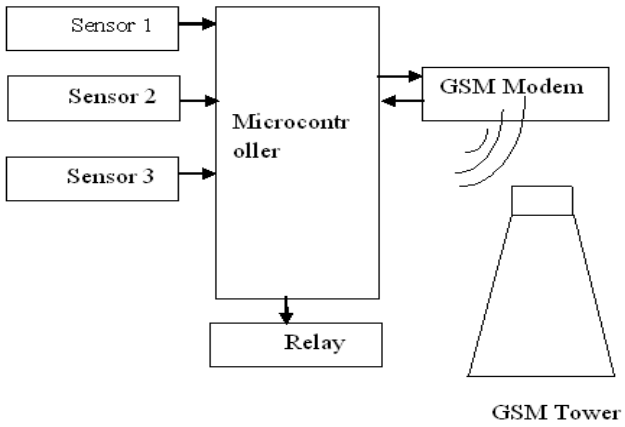

Fig.2.1. GSM based automation.

III. Literature Review

Saito et al. in [1] developed home gateway system for interconnecting home network consisting of IEEE1394 AV network and X10 power line home automation network with Internet. This provided remote access functions from Internet for digital AV appliances like Digital Video Camera, Digital VCR connected to IEEE1394 network and home appliances like TV, desk lamp, electric fan connected to X10 controller

Chen Peijiang et al. in [2] describe a remote monitoring system based on SMS of GSM. The system includes two parts which are the monitoring center and the remote monitoring station. The monitoring center consists of a computer and a TC35 GSM communication module. The computer and TC35 are connected by RS232. The remote monitoring station includes a TC35 GSM communication module, a MSP430F149 MCU, a display unit, various sensors, data gathering and processing unit.

Van Der Werff et al.in [3] proposed a mobile-based home automation system that consists of a mobile phone with Java capabilities, a cellular modem, and a home server. The home appliances are controlled by the home server, which operates according to the user commands received from the mobile phone via the cellular modem. In the proposed system the home server is built upon an SMS/GPRS (Short Message Service/General Packet Radio Service) mobile cell module Sony Ericsson GT48 and a microcontroller Atmel AVR 169, allowing a user to control and monitor any variables related to the home by using any java capable cell phone.

IV. Block Diagram

Approach to achieve objective in this paper is based upon the block diagram in Fig.4.1.Microcontroller receive command from farmer and takes control of electric motor & sprinkler system for irrigation work.

Microcontroller also provides protection to motor in respect of dry run, phase failure and power failure, and underground water pipe line burst due high pressure.

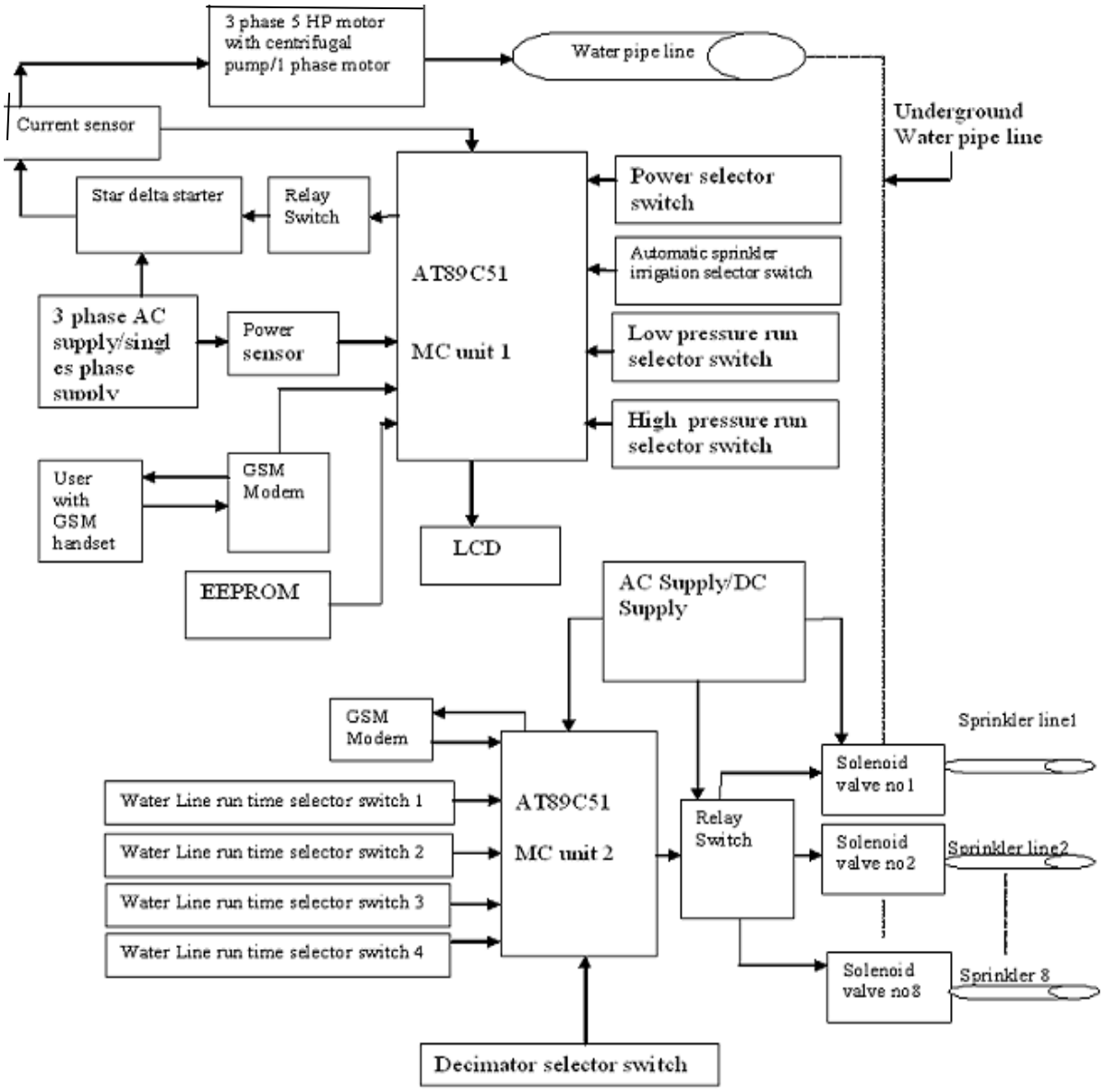

Fig.4.1. Block Diagram of GSM-Microcontroller Based Remote Control of Sprinkler Irrigation.

V. Scope Of The Work

It is evident that lots of problems are faced by the farmers, while doing irrigation works at farms which are generally far away from the house of the farmer. A farmer also has risk of the life due electric shock accident while operating electric motor at his pump house. So it is the need of the hour to design an automatic irrigation system which resolves all the problems faced by a farmer. There are so many wireless technologies available on which purposed work can be carried out, but a farmer in general is not so rich that he can afford a costly technology, so here we need to make use of the devices which are already with the farmers cutting the cost system. GSM technology is preferred over all other wireless communication technologies because every farmer nowadays are using GSM mobile handsets and they are very much conversant in respect of its use.

From the above observations it is evident that various technologies and methodologies have been used in wireless data transmission from one location to another location. It can be observed that GSM based wireless data transmission is very powerful. So GSM-Microcontroller based remote control of sprinkler irrigation system designed is helpful to farmers in controlling irrigation works using a mobile phone.

VI. Methodology

Flow Chart of GSM-Microcontroller Based Remote Control of Sprinkler Irrigation is designed by following the sequential steps mentioned in Fig. 6.1.

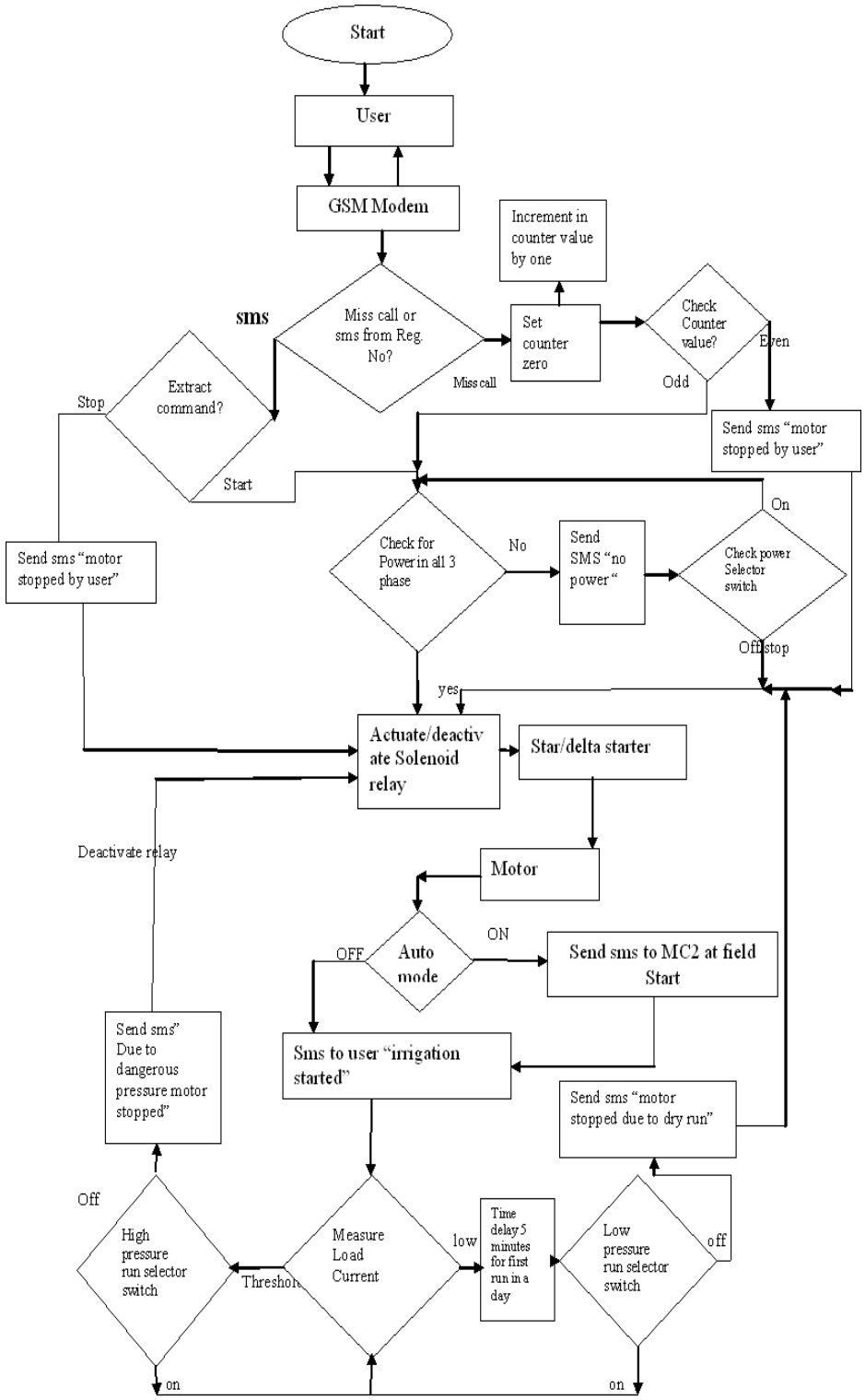

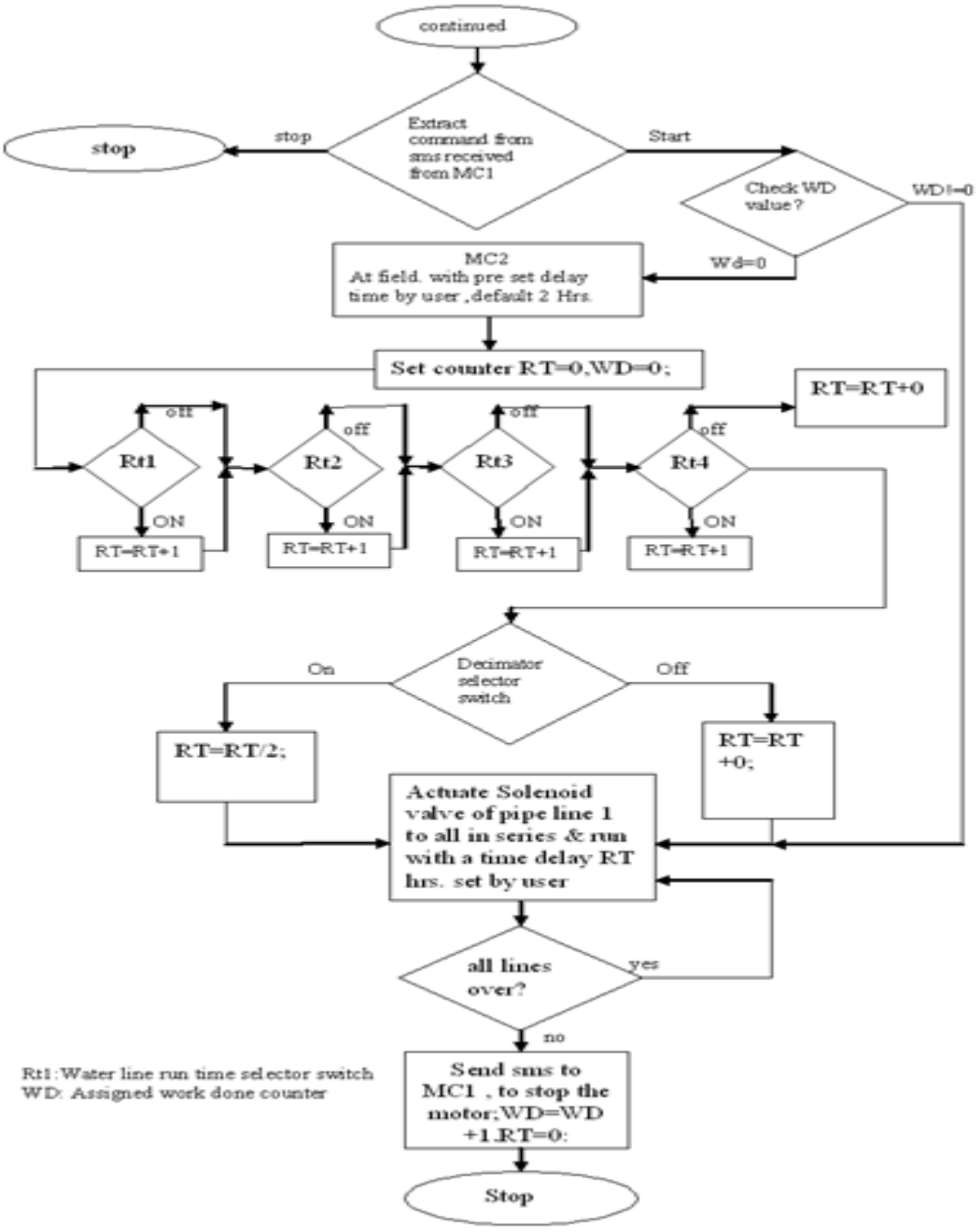

Fig.6.1. Flow Chart Showing Methodology to carry out presented work.

VII. Results

Design & development of GSM Based Remote Control of sprinkler irrigation system has been successfully completed .The output of the implemented system , several testing has been performed to ensure its executed and produce the intended result. The system is designed to receive SMS & miss call from user mobile phone to GSM modem interfaced to the microcontroller circuit. This can be performed by dialing the mobile phone number which has been set in the microcontroller program. The incoming message is deleted by the microcontroller upon completing the requested process, and the message does not longer exist in the connected mobile phone which acts as GSM modem. The system then replies a message to user mobile phone reporting the status of the devices (turned ON or turned OFF). The status message is to remind the user regarding the current state of the irrigation work.

VIII. Discussions

This project work is a small implication of our concept in automation and monitoring a system. The practical applications of this project are immense and can have vast level of implementation. This small concept can be used in fields such as transport, remote sensing, robotics, home automation, and many other related fields where continuous monitoring and regulation is needed. So this is not the end of the project but rather is a step towards exploring other possibilities that it brings with it.

IX. Conclusion

The GSM Based Remote Control of sprinkler irrigation system was successfully developed and met the objectives. The system can automatically switch ON and OFF the motor of the pump house as well sprinkler water line change over process remotely using SMS. The integration of software and hardware has performed a good task in producing the coordination between two units located far away from each other. However, there are several weaknesses had been identified which can be further improved in the future such as the system could provide better performance by intelligently sending notification upon leakage of water in the underground water pipe line, provide a flexible function by supporting both manual and automatic control as well as provide an option for the user to control the appliance through web-based system & system will not work in the absence of cellular service provider signal. In addition, the system is very practical when the pump house location & fields are away from home due to it can control the sprinkler irrigation work remotely as long as the mobile phone gets the signal coverage.

Future Scope

The remote control system run properly and stably and it could implement all the desired and planned functions. This is because the software was designed in a proper way, and the test process run step by step. It is a practically proven application that farmer do not need any other applications to remotely control the irrigation work .With a little change in software & hardware this application can be used in the vehicles for ignition & turning on AC as well as to control the domestic electric appliances remotely users just need to send SMSs with a regular phone.

REFERENCES

[1] Yosuke Tajika, Takeshi Saito, Keiichi Teramoto, Naohisa Oosaka and Masao Isshiki ,"Networked Home Appliance System using Bluetooth Technology Integrating Appliance Control/Monitoring with Internet Service", IEEE Transactions on Consumer Electronics, Vol. 49, No. 4 , pp 1043 – 1048 , 2003.

[2] Chen Peijiang , Jiang Xuehua , "Design and Implementation of Remote Monitoring System Based on GSM" , IEEE Workshop on Computational Intelligence and Industrial Application, 2008 ,Vol. 1 , pp 678 - 681, 2008

[3] Van Der Werff, M. , Gui, X. , Xu, W.L. , "A Mobile-Based Home Automation System" , IEEE conference on Mobile Technology, Applications and Systems , pp 1-5, 2005.

OPEN ACCESS

International
Journal
Of Modern Engineering Research (IJMER)

Interstellar Communication Theories and its Possibilities

Abhinav Sharma[1], B. RanjithReddy[2], A. Ananth Kumar[3]
[1,2,3] *IV B.Tech, Malla Reddy Engineering College, India*

Abstract: *This paper reviews and discusses the research dimensions in four dimensional time travel and time dependencies of future and past on the basis of present. The paper investigates the theories that support time travel in any manner and explore possibilities based on them for interstellar communication.*
Keywords: *cosmological constant, paradox, worm hole, black hole, event horizon, telepathy, parallel universe.*

I. INTRODUCTION

The history of mankind has always seen interest in the measure of time. The biggest factor that made man determine time was the run of nature &his self development .As time passed by he noticed the surroundings around him &he himself metamorphosing into a different self from which he was before one of the important factor that led to the functioning of time was the movement &presence of the sun &the moon .the waxing and waning of the moon & the rising & setting of the sun lead to the invention or so called discovery of the day & night , fortnight &years which then lead to invention of sundials, sand clocks, analog, digital clocks, etc. But as the time passed by man noticed. the days ,the fortnight, the minutes repeated themselves but every time in a different manner, which led to the conclusion that time never repeat itself though time was in perfect cycles. Like the day followed by night &then day followed full moon by half moon &than no moon. it seemed never to be in perfect circles. Even in the nature like the day &night were interfered with solar &lunar eclipses. Similarity if a thing was present in a place for one second, it didn't guarantee zero displacement in the following second. thus time was considered as a phenomenon that never returned in one's life when once passed away , which lead to the human conquest of capturing the past moments and re-living them also to find the mystery of so called unstopping "time".

All the theories that will come across in this thesis directly or indirectly support time travel and explore the possibilities leading to interstellar system and interstellar system travel.

II. FACTORS SUPPORTING TIME TRAVEL

Einstein's theory of relativity &cosmological constant present in Einstein's field equation is the only strong factor that determined scientists around the world a possibility of time travel. the equation appears as such

$$R_{\mu\nu} - \frac{1}{2}R\,g_{\mu\nu} + \Lambda\,g_{\mu\nu} = \frac{8\pi G}{c^4}T_{\mu\nu}$$

Here R and g pertain to the structure of space-time, T pertains to matter and energy (thought of as affecting that structure), and G and c are conversion factors that arise from using traditional units of measurement. When Λ is zero, this reduces to the original field equation of general relativity. When T is zero, the field equation describes empty space (the vacuum).

The solution is lambda known as cosmological constant here ,cosmological constant devices the relation of wormholes& its dimension &also determine the structure of the universe that follows Einstein's theories of special& general relativity, though modern physics tells us that there could be as many as 10 or 11 different dimensions, under normal circumstances humans are able to observe 4dimensions ,we experience 3 dimensions i.e, height, width & depth actively., meaning we can navigate them & one dimension passively, meaning we can detect & observe it, but we can't control how we move through it. the ramification of Albert Einstein's relativity equation are vast, but it ultimately breaks down into this .man& energy are inter changeable & there's only a set amount of matter/energy in the universe .energy only comes into being at the expense of matter &matter only comes into being at expense of energy. These technological advances involve nuclear energy & gives us a framework with which we can understand distant stars. In observing the expansion of the universe, astronomers discovered that it holds a lot more than just the matter & energy we can observe as shown in fig (i) dark energy & dark

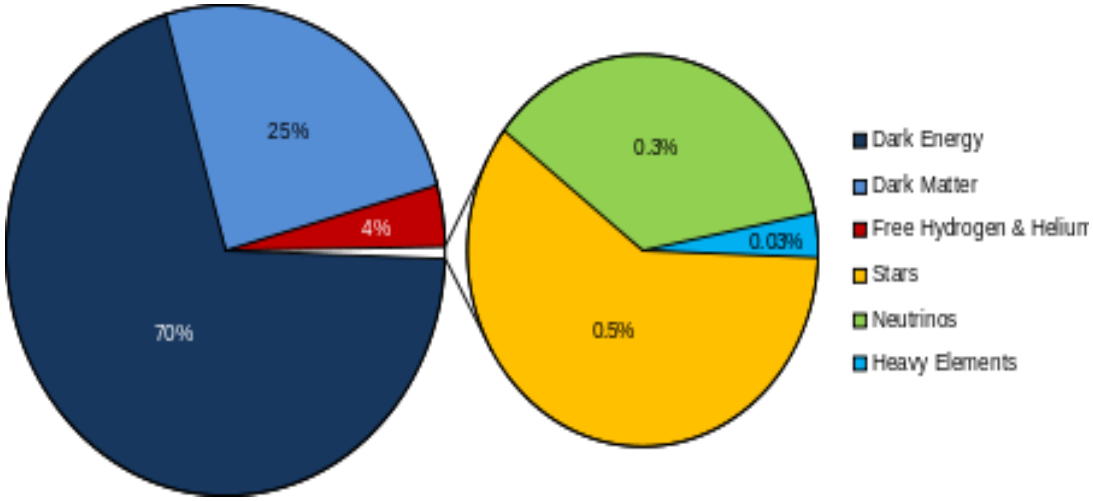

Fig (i)

matter may be impossible to see but have huge consequences on our universe. dark energy, an invisible energy that speeds up expansion, makes up 73% of the universe, dark matter invisible material that may cause the universe to expand on itself makes up 23% of our universe. The remaining 4%is the matter we can see , here dark matter is the matter that neither emits nor scatters light or other electromagnetic radiation , dark energy is a hypothetical form of energy that permeates all of the space & tends to increase the speed of expansion of universe. Einstein's theory of relativity says that time travel is perfectly possible if you're going forward , finding a way to travel backward and breaking of speed of light, which so far seems impossible the factors affecting it shall be discussed later.

The Einstein's theory does not exactly take account of the universe. the universe is in account of Einstein's theory is the persent universe& we know that universe components keep changing whereas the universe remains constant for instance the universe now was not the universe before this second if keeps on changing every second. for clarity we shall see the contradictory pie diagram of the components of universe.

1. When there is tremendous amount of change in 13.7billion years every year there might be small or minute change in the universe which will also affect the (demonstration) of Einstein's equation because the cosmological constant in Einstein's equation depends upon the components of the universe .in common terms cosmological constant is nothing but ratio of dark matter &dark energy which keeps on changing which being the biggest dark drop in the equation.
2. Another backdrop being that Einstein while deriving the equation look the universe as stable which he later quoted as his biggest blunder in his life. & later modified it with some specifications.
3. But for the Einstein's equation to be perfect the universe must rotate around a centralized axis with perfect time period which does not seem to happen as for now. if above stated turns out to be true the cosmological constant will tend to zero. Resulting in a possibility of time travel.

III. Theories Of Time Travelling & Its Defects

1. Wormhole theory (quantum mechanics theory)

A wormhole is any structure connecting two regions or areas otherwise distant or unrelated. That have been by two methods discussed as a possible mode of interstellar travel & even of time travel. Wormhole connect two (otherwise unrelated region to form what is called a multiple connected space).their present paths must be quicker to travel than the paths presented by normal space . For example; the distance from point A to point B can be covered by two methods.

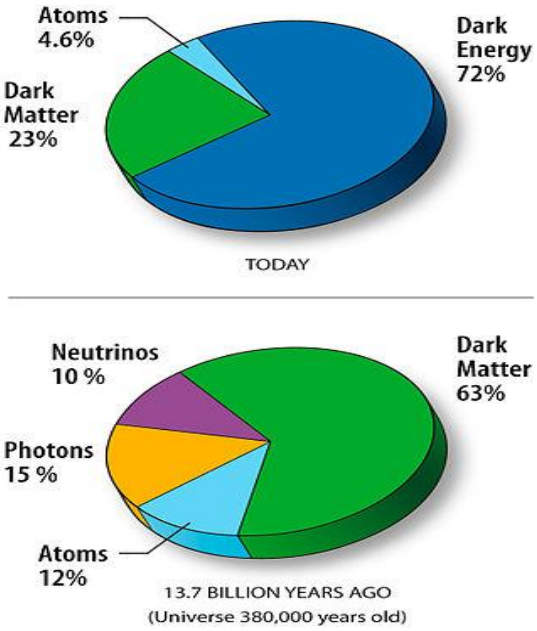

Fig(ii)

Fig (iii)

The blue path is the normal path in which two universes can be a few light years away which is impossible for a man to travel .the zig- zag path as shown in the fig(iii) if human is considered to be a point charge where as the suction path in fig(iv) creates a suction vacuum that pulls the organism in it and makes the person reach the point in fraction of sections instead of light years. the theory of wormhole evolved from the theory of quantum mechanics that a electron travels through an extremely short path under high pressure & settles there instead of travelling the entire distance through the molecules, it acquires the shortest distance possible with about 10^100 times normal energy contributed to the transfer of electron.

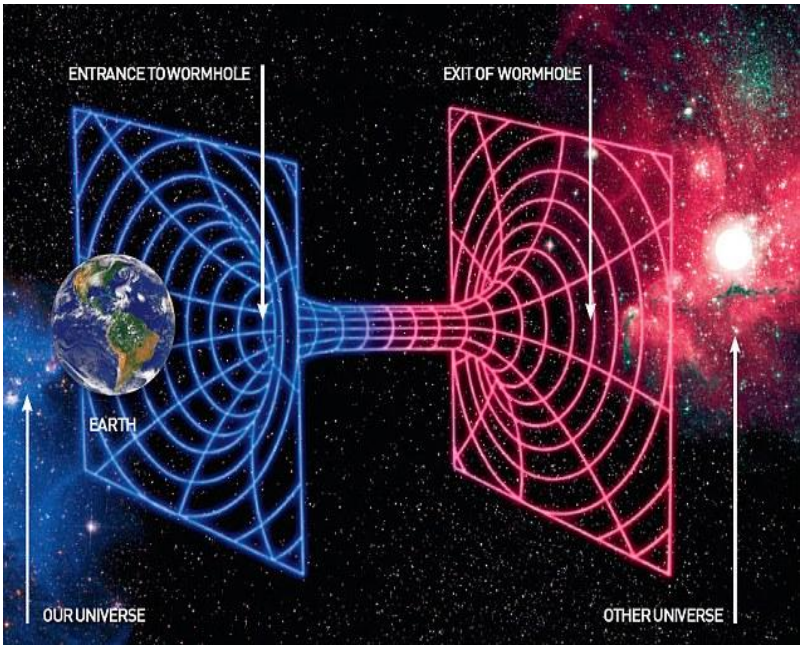

Fig (iv)

Here if the entire galaxy is defined as the space around us & any two definite places in the galaxy are defined as two set of molecules & the organism being man. he can travel through the wormhole & reach the other destination.

After the introduction to wormhole there were 5 types of wormhole introduced
1) Riemann cuts
2) Einstein-Rosen bridge
3) kip throne's wormhole
4) Stephen Hawkins's wormhole
5) Sidney Coleman's wormholes

As we are just talking about the theories we wouldn't like to go in detail to the types wormholes since they are similar types of wormholes with a very little modification in each of them, the Stephen hawking wormhole being the most modified one.

Drawbacks
1. The generation of a human sized wormhole will require energy up to 10^100 times the normal energy required for space travel which is near to impossible for today's man.
2. There are many theories that work on quantum levels but fails when applied to man size bodies.
ex:-Heisenberg's uncertainty principle.
3. The return of man from the destination is in doubt because of two factors.
(a) According to quantum mechanics if an electron alternates a wormhole from one place to other place he may or may not use that wormhole in his return journey to other set of molecules so if at all we introduce a wormhole from earth to some other planet we may need to install another wormhole for our return journey or else we may live there forever.
(b) this wormhole phenomenon also takes account that to return from the destination we would have to generate tremendous amount of energy ie same energy which took for to travel if the place is deficient of energy we would remain in that place &never returning from there.
4. According to Sidney Coleman's wormholes, wormholes are not mathematically predictable. In fact, it would be simple to say that infinite universe connected by infinite wormholes are necessary to keep the cosmological constant (lambda in Einstein field equation) very close to zero. if it was negative, the universe would wrap up into a tiny hypo sphere & if it was positive ,the universe would virtually explode , so the correction imply that only tiny wormholes keep the universe in stable condition which support the 2nd part mentioned above. If at all tiny wormhole are made into existence the tiniest wormhole for a normal human to pass through will require tremendous amount of energy which may not be possibly generated.

2. Einstein's basic equation

Using Einstein basic equation can help astronomers better understand how the universe began –The Big Bang Theory along with events that happen now & might occur in the future. for example, Einstein didn't stop at "E=MC^2" .He expanded the equation to help explain what happens to energy in motion, most of us who study math, science& physics .find it much easier to understand when it is expanded to include 'p' for momentum, however it adds understanding about transfer & transformation of light & energy, in outer space; the energy can be measured as when millions of stars orbit within a black hole. A black hole is a gigantic & mysterious example of how resting mass converts into energy.

A black hole is formed when a large star that has burned up all its fuel collapses upon itself due to the pressure of its own mass , the gravitational field that is formed by the explosion is so strong that it sucks in everything that enters in contact with its "event horizon"(the edge of a black hole from which nothing can get back out),although this kind of black hole crushes any matter that reaches its centre, there are other types of black hole, such as rotating black holes, which astronomers have proposed could serve as perfect for time travel.

Scientists say that "E=MC^2" form the basis of fusion ,which explains not only how energy transfer to light from the sun, but also how nuclear fusion could one day create energy for, nuclear power. and that's just one of many practical & well, universal applications of Einstein's equation because its a mathematical equation that most of us need reminding us from time to time that everything has energy & Einstein's work continues to open doors to exploration of a world here on earth & beyond. Even the radiation pressure that propels spacecraft to study our distant universe is made possibly by Einstein's equation "E=MC^2"
Because atomic nuclei transform mass into energy.

IV. Time Machine Being Developed Now

Messenger telepathy

This kind of machine is being developed at the Princeton University by physicist Dr. Richard Goft. In this experiment he puts two protons such that they are a distance apart, then offer a stimulus to one proton & then the other proton would react to the stimulus before the stimulus receiving proton receives it completely by fraction of nanoseconds. It has not been successful so far but if it succeeds it may lead a different perspective in time-travel as the time signal reaches the proton two will be before the proton one gives a stimulus that results in the travel of proton two into future for further clarity a pictorial representation is given bellow in fig(v).

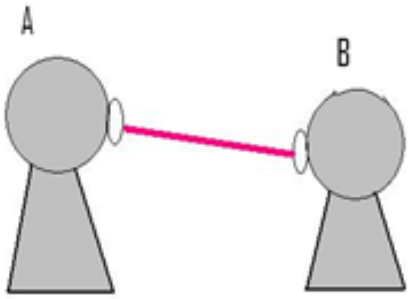

Fig(v)

In the above figure the proton (A) say name it as bob & proton(B) name it as jack when bob gets a stimulus due to the laser which irritates it passes the stimulus to jack .but the proton(B) i.e.; jack receives the stimulus before the stimulus leaves bob. thus jack travel into future, if this phenomenon is made out in macro form it may turn out to be true but it has not been yet proved in micro form.

A similar machine in form of sound signal is being developed in japans .but due to lack of disclosure we can't comment on that.

V. Paradoxes Against And For Time Travel

1. Twin paradox

Paul Langerin, a French physicst devised the twin paradox in 1911 on the basis of Lorentz factor according to this theory ,if one twin lives at the bottom of a mountain &other lives at the top ,the twin who lives at the bottom ,which is nearer to the earth's gravitational pull, will age slowly. The difference, however would be very minimal which result in the twin living above to travel forward in time but that will be less than a nanosecond this theories were proved in an experiment in 1962,when an atomic clock that scientists placed at the bottom of a water tower ,closer to the earth's gravitational pull, ran slower than an atomic clock placed at the top of the water tower .Einstein used the term "time dilation" to describe this phenomenon.

For another example consider a space ship traveling from earth to the nearest star system outside of our solar system: a distance d = 4 light years away, at a speed v = 0.8c (i.e., 80 percent of the speed of light). (to make the numbers easy, the ship is assumed to attain its full speed immediately upon departure—actually it would take close to a year accelerating at 1 g to get up to speed.) The earth-based mission control reasons about the journey this way: the round trip will take $t = 2d/v = 10$ years in earth time (*i.e.* everybody on earth will be 10 years older when the ship returns). the amount of time as measured on the ship's clocks and the aging of the travelers during their trip will be reduced by the factor $\epsilon=\sqrt{1-v^2/c^2}$, the reciprocal of the lorentz factor. in this case $\varepsilon = 0.6$ and the travelers will have aged only $0.6 \times 10 = 6$ years when they return.

The ship's crew members also calculate the particulars of their trip from their perspective. they know that the distant star system and the earth are moving relative to the ship at speed v during the trip. in their rest frame the distance between the earth and the star system is $\varepsilon d = 0.6d = 2.4$ light years (length contraction), for both the outward and return journeys. each half of the journey takes $2.4/v = 3$ years, and the round trip takes $2 \times 3 = 6$ years. their calculations show that they will arrive home having aged 6 years. the travelers' final calculation is in complete agreement with the calculations of those on earth, though they experience the trip quite differently from those who stay at home.

If twins are born on the day the ship leaves, and one goes on the journey while the other stays on earth, they will meet again when the traveler is 6 years old and the stay-at-home twin is 10 years old. the calculation illustrates the usage of the phenomenon of length contraction and the experimentally

verified phenomenon of time dilation to describe and calculate consequences and predictions of Einstein's special theory of relativity.

As we all know that atomic clock is the most accurate clock in the world it ticks 9billion times per second i,e $1/10^{(4)}$ billionth of a nano second which are only 6 in the world. it requires large amount of cesium to make it & if misses a beat, its something to worry about

Now, if both twins send a video feed of themselves to each other, what do they see in their screens? Or, if each twin always carried a clock indicating his age, what time would each see in the image of their distant twin and his clock?

Shortly after departure, the traveling twin sees the stay-at-home twin with no time delay. At arrival, the image in the ship screen shows the staying twin as he was 1 year after launch, because radio emitted from Earth 1 year after launch gets to the other star 4 years afterwards and meets the ship there. During this leg of the trip, the traveling twin sees his own clock advance 3 years and the clock in the screen advance 1 year, so it seems to advance at $\frac{1}{3}$ the normal rate, just 20 image seconds per ship minute. This combines the effects of time dilation due to motion (by factor ε=0.6, five years on earth are 3 years on ship) and the effect of increasing light-time-delay (which grows from 0 to 4 years).

Of course, the observed frequency of the transmission is also $\frac{1}{3}$ the frequency of the transmitter (a reduction in frequency; "red-shifted"). This is called the realistic dopler effect. The frequency of clock-ticks (or of wave fronts) which one sees from a source with rest frequency f_{rest} is

$$f_{\text{obs}} = f_{\text{rest}}\sqrt{(1 - v/c) \,/\, (1 + v/c)}$$

As for the screen on Earth, it shows that trip back beginning 9 years after launch, and the traveling clock in the screen shows that 3 years have passed on the ship. One year later, the ship is back home and the clock shows 6 years. So, during the trip back, *both* twins see their sibling's clock going 3 times faster than their own. Factoring out the fact that the light-time-delay is decreasing by 0.8 seconds every second, each twin calculates that the other twin is

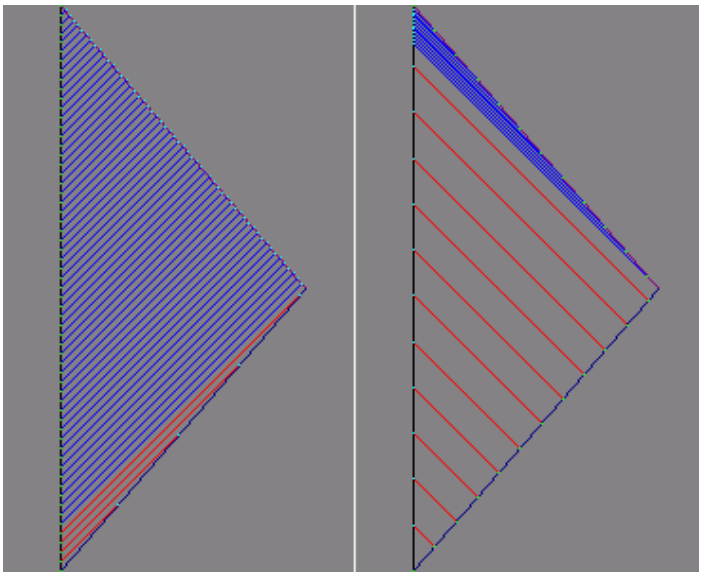

Fig (vi)

aging at 60% his own aging speed The *x*–*t* (space–time) diagrams at left show the paths of light signals traveling between Earth and ship (1st diagram) and between ship and Earth (2nd diagram). These signals carry the images of each twin and his age-clock to the other twin. The vertical black line is the Earth's path through spacetime and the other two sides of the triangle show the ship's path through spacetime (as in the Minkowski diagram above). As far as the sender is concerned, he transmits these at equal intervals (say, once an hour) according to his own clock; but according to the clock of the twin receiving these signals, they are not being received at equal intervals.

After the ship has reached its cruising speed of 0.8*c*, each twin would see 1 second pass in the received image of the other twin for every 3 seconds of his own time. That is, each would see the image of the other's clock going slow, not just slow by the ε factor 0.6, but even slower because light-time-delay is

increasing 0.8 seconds per second. This is shown in the figures by red light paths. At some point, the images received by each twin change so that each would see 3 seconds pass in the image for every second of his own time. That is, the received signal has been increased in frequency by the Doppler shift. These high frequency images are shown in the figures by blue light paths.

Drawbacks

1) The change cannot be shown significantly even in the atomic clock.
2) It may not be possible to construct such huge building just for the sake of time travel
3) The time travel is less than a nano second which does not hold good for micro objects too.

2. Grandfather paradox

This was great counter to all those minds which though they could construct a time machine it was stated by one of the greatest mind Stephen Hawkins ,it states that if you travel into time & go back to your home & kill a person who happens to be your grandfather before your father has been (conceived) then how do you seem to exist .it killing yourself by means of yourself.

How does nature counter that if all we travel into time is the question & may be nature has no alternate to so it does not allow time travel but hawking countered his own statement by introducing the theory of presence of multiple universe according to this statement he says that the universe we live in is one period of time somewhere there exists another universe which runs before our time & yet another universe which runs after our time .he proposed the presence of multiple universes as such where each universe was in a particular period of time .here the 'grandfather paradox' do exist because when you will travel in time you will be actually traveling to a different universe there if you kill your grandfather you will only cease to exist in that particular universe that you belong so but this theory seems to be highly impossible because of at parallel universe exists it may require light years together to go through them

VI. CONCLUSION

Presently the science and technology of space travel and time travel seems to be a very rigid and unappending but seemingly possesses a wide application in future technology and if developed seemingly faster than now can be advanced to analyze the future happenings and the untold mysteries of the past which always seem to fascinate human beings in some or the other way.

Acknowledgements

1. C. Silpa, assistant professor, malla reddy engineering college
2. A. Indra Kumar, assistant professor, malla reddy engineering college

REFERENCES

[1]. concepts of physics , h.c verma
[2]. "universe". Encyclopedia Britannica. "the whole cosmic system of matter and energy of which earth, and therefore the human race, is a part"
[3]. "space and time warps". hawking.org.uk.
[4]. concepts of simultaneity: from antiquity to einstein and beyond. the johns hopkins university
[5]. www.discoveryscience.com

OPEN ACCESS

International
Journal
Of Modern Engineering Research (IJMER)

A Technical Review of Biodiesel Fuel Emissions and Performance on Industrial and Automobiles Application

S. K. Sharma[1], Ankur Dixit[2], Priyanka Goyal[3], S. Maheshwari[4],

[1,2,4] *Department of Mechanical & Automation Engineering, Amity School of Engineering & Technology, Amity University Noida Uttar Pradesh, India*

[3]*Amity Institute of Aerospace Engineering, Amity University Noida, Uttar Pradesh, India*

Abstract: *Biofuels play an important role in many developing countries as a clean liquid fuel which helps to address the energy, costs and global warming as compared to petroleum fuels. Biodiesel can be blended to any level to any petroleum diesel to create a biodiesel blend. Blending of biodiesel with small amount of petroleum product gives control to air pollution. Additives plays and important role in minimizing the NOx Emission which result in sigh of relief who are opting biodiesel as an alternative fuel. In the future the biodiesel play an important role in reduce the greenhouse gases In this review article the reports on regulated and non-regulated emission, durability, economy and performance on biodiesel by various researchers have seen cited since 2000.*

Keywords: *Biodiesel, Emissions, Performance Parameter*

I. Introduction

Due to increase in pollution and increase in price of petroleum products together with environment concerns caused by the combustion of fossils fuels, the research on alternative fuels plays an important role**. [7-9]**.Biodiesel is considered as the prime alternative for diesel fuel. It can be described as fatty acid, alkyl esters (methyl or ethyl) from the oils of vegetables andfats from animals. It is from sustained renewable sources, can be decomposed (biodegradable) and with more oxygen content. Most of the researchers have foreseen that there can be reduction in emissions of greenhouse gases with the usage of this fuel topromote environment safety and improve the economic distribution. Although there is an increasednumber of literatures related with engine researchon performance and emissions after using biodiesel as fuel, but few of them only have analysed**. [11, 12, 15].**

Biodiesel is a fuel replacement for diesel, it is generally manufactured from oils like cooking oil, soybean oil and animals fats. **[6,7**] It is not possible to use vegetable oil or animal fat directly as a fuel which is even not compatible as they can cause various number of engine problems such as incomplete combustion, poor atomization of fuel, lubrication contamination etc., that is due to high viscous property of these oils. Therefore, many methods are used by which the viscosity of these oils is reduced, such as micro emulsification, oil blending, transesterification etc. **[10-12].** Among all these mentioned processes the transesterification process is most preferred for industrial production of biodiesel. Biodiesel is also obtained from alcohols other than oil of vegetables and fats from animal, which is used in compression ignition engines or blended with diesel oil. The ASTM International defines this fuel as a combination of long chain monoalkylic esters from fatty acids obtained from the renewable resources to be used in compression ignition engines**. [1-4]**

Biofuels offers an attractive alternative to fossil fuels, but a consistent scientific framework is needed to ensure policies that maximize the positive and minimize the negative aspects of biofuels. Many countries are moving towards the partial and gradual replacement of fossil fuels with biofuels, majorly ethanol for petroleum replacement replacements. And biodiesel for diesel the increased move towards biofuels is spurred by global, political, economic and environmental events, especially due to rising rate of crude oil prices. **[2, 4, 5].**

Table: 1 Biodiesel Production in Different Countries **[45]**

Country	**Source of Biodiesel**
USA	Soyabean
Europe	Rapeseed oil (>80%) and sunflower oil
Spain	Linseed and olive oil
Brazil	Soyabean
Canada	Vegetable oil/Animal fat
Germany	Rapeseed oil
China	Guang pi

Australia	Animal fat, beef tallow and rapeseed oil
Malaysia	Palm oil
Ireland	Animal fat and beef tallow
Italy	Sunflower oil
France	Sunflower oil

Table: 2 Classification of Biodiesel **[5]**

First Generation Biofuels (From Grains Seeds or sugars)	**Second Generation Biofuels** (Extracted from residues of crops, woody crops or energy grasses, and lignocelluloses biomass)
Petroleum-gasoline substitutes: Ethanol or butanol by fermentation of starches (wheat, corn or potato) or sugars (Sugar beets, sugar cane).	Biochemically produces petroleum-gasoline substitutes: Ethanol or butanol by enzymatic hydrolysis
Petroleum diesel substitutes: Biodiesel by transesterification of plant oils, also called fatty acid methyl ester (FAME) and fatty acid ethyl ester (FAEE)	Thermo chemically produced petroleum gasoline substitutes: Methanol, Mixed Alcohols, Ficher-Tropsch gasoline
Pure plant oils (straight vegetable oil)	Thermo chemically produced petroleum-diesel substitutes – Fischer-Tropsch diesel – Dimethyl ether (also a propane substitute) – Green diesel

Table: 3 Demand of petrol and diesel and biofuels requirements **(Source: Planning commission Govt. of India, 2003)**

Year	**Petrol Demand**	**Ethanal blending Requirement (in metric ton)**			**Diesel demand**	**Biodiesel blending Requirement (in metric ton)**		
		5%	**10%**	**20%**		**5%**	**10%**	**20%**
2006-07	10.07	0.50	1.01	2.01	52.32	2.62	5.23	10.46
2011-12	12.85	0.64	1.29	2.57	66.91	3.35	6.69	13.38
2016-17	16.40	0.82	1.64	3.28	83.58	4.18	4.18	16.72

II. Blending Methods

There are numerous ways by which blending of biodiesel can be accomplished with diesel fuel through mixing fuels in tanks at manufacturing point till delivery to tanker trucks. **[13].**

Mixing by splash [14]

The most common method of blending biodiesel with the different diesel products is mixing through Splash, but this method does not have much accuracy. It is done in a way that biodiesel is mixed in a truck containing diesel fuel with a pressurized pumped due to which splashing of two liquids takes place. The temperature range of biodiesel is approximately 18-20 degree Celsius whereas diesel is colder i.e. less than 8 degree Celsius. **[13].**

Mixing through Injection [13]

In this method, the biodiesel in blended with diesel fuel in the containers at a manufacturing point prior to delivery to the tanker truck. It is done by the valve mechanism which is used to ensure that the particular quantity of biodiesel component is injected along with the diesel fuel.

In-line Mixing Method [13]

In-line mixing process involves the two storage tanks, one containing the biodiesel and other containing refinery produced diesel fuel, which together is passed through the hose or silicon made pipe and collect in a third final product tank. So both the fuels get mixed within the silicon pipe in-line. This type of blending is used where large amount of biodiesel has to be blended. To avoid the risk of shock crystallization, it is better to keep the temperature of biodiesel less than 6 degree Celsius.

Blends of Biodiesel

The blends of biodiesel and conventional petroleum based diesel are produced by mixing these fuels in suitable and appropriate proportions. "B" system is used all over the world which represents the amount of biodiesel in any fuel mixtures, like 100% of biodiesel is referred to as B100, B20 signifies that 20% of biodiesel

is blended with 80% of petroleum diesel, similarly B5 represents that blended fuel contains 5% biodiesel and 95% Diesel. The most common blending of biodiesel is B2 in which 2% of biodiesel is blended with 98% of petroleum diesel. B2 is generally used in tractors, off-road heavy equipment's vehicles, on road light duty fleets tech vehicles.

III. Impact Of Biodiesel On Engine Performance

Effect of biodiesel on engine power

A survey is done to study the biodiesel fuel effects on power and torque from engine, It is shown that there are more than 25 literatures which gives the effects of pure biodiesel fuel on power from engine and around 70 percent of those literatures agreed to the point that power delivered by engine is reduced due to lose in heating value of the biodiesel. Some of the researcher has also found it lower than expected. (I.e. the loss in heating value of the biodiesel when compared with diesel**). [18-36].** Ultu et al. **[22]** found that the decrease in power and torque values of engine by using oil waste after frying and alkyl ester was around 4.3 percent in power and 4.5 percent in torque because of their higher viscosity and higher density. The same range between power loss and the decreasing heating value was reported in **[36].** Hansen et.al **[25]**had observed that there was loss in the brake torque of 9.1 percent for pure biodiesel when compared with diesel fuel (D2) at engine speed of 1900 rpm due to the heating value variation of about 13.3 percent, and also variations in density value and viscosity of the fuel.

It is seen that there is no significant difference between the power output of pure biodiesel and diesel**. [37-42**]Lin et al. **[37]** observed the maximum and minimum differences between the power and torque at full load between petroleum fuel and four kinds of vegetable oil methyl ester fuels, that were only 1.49% and -0.64%, 1.39% and -1.25%, which is due to high break specific consumption of fuel, high viscosity, high rate of combustion for biodiesel and higher oxygen content. Some of the researchers have seen that there is increase in either power or torque value of engine for 100 percent biodiesel fuel. It has been observed that brake power of engine and torque is increased with increase in biodiesel fuel percent in blends**. [43-44]**.

Effect of Properties of biodiesel on engine power

The biodiesel fuel properties i.e. heat value, lubricity and also viscous property has a major effect on power from engine. The heat value is one of the major parameter which is used for measuring energy inwork production. Lower the heat value of the fuel, lesser will be the engine power. Most of the researcher has found that power of engine is reduced with the use of biodiesel. The high viscous property of biodiesel fuel improves its spray penetrating capacity and thereby enhances the mixing of A/F. However few researchers have found that increased viscosity results loss in power, because more viscosity reduces the efficiency of combustion, due to poor injection of fuel and its atomization in chamber **.**High lubricate property of biodiesel fuel results in decreasedloss in friction and enhances the effective braking power**. [46-47].**

IV. Emissions From Biodiesel

Particulate matter of biodiesel

It is overwhelming argument that usage of alternative fuel (biodiesel) in place of diesel fuel causes the reduction in the particulate emissions from engine. **[18, 19, 20, 21-27, 48-75].** Wu et al. founded that the emissions performance for five pure samples of biodiesel on Cummins engine (ISBe6 direct ignition) with intercooler and turbocharger reduces the emissions by 53 percent to 69 percent when comparing with petroleum diesel fuel. Lin et al. [37] pointed that there has been decrease in smoke emissions ranging from 50% to 72.73. % for eight types of VOME fuels comparing with the Pd. A few researchers have observed that not much difference was there in emissions of particulate matter for biodiesel in relative with diesel fuel. And also even there might be little bit of difference. **[76].** Most of the researchers contributed that high viscous property of biodiesel which causepoor atomization of fuel and deterioration in quality of combustion. **[18, 77-78]**

Table: 4 Overview on durability of biodiesel and its blends **[61-75]**

Content and Feedstock	Ref. diesel	Engine Tested	Operation Conditions	Durations	Test Results
20% Rice bran oil	Conventions	4-cylinder, NA, WC, DI	Ten nonstop running cycles	100hr	CD: Significantly lower; Wear Lower
20% Linseed oil	Agricultural	1-cylinder, WC, portable	1500 rpm	512hr	IJ:no coking, no filter plugging; Wear: lower
20% Linseed oil	Agricultural	1-Cylinder, WC,	1500 rpm	512hr	Wear :lower

100%, 15%,7.5%, palm oil		Portable 4-cylinder, NA, WC, IDI, 1.8L	2000 rpm	100hr	The reduction of wear with the increased content of biodiesel
100%, 50% soybean oil	No.2 (EN 590)	TC, DI, 1.9L	NEDC driving cycle	1250 km, 750km	Wear: higher except Piston
100% Waste olive oil	No.2 (EN-590)	3-cylinder,WC,DI, 2.5L	8-15 kw and 1800-2100 rpm	50hr	CD: no visual difference; wear; no visual difference
100% rapeseed oil	No.2 (EN 590)	6-Cylinder WC, DI, 11L		110hr	CD: similar; IJ: Cleaner than that of D2
100% Mahua, karanja oil	High Speed Diesel		Static immersion test at ambient temperature	300D	No Corrosion on piston metal and piston liner

NOx Emission of Biodiesel

Many researchers have founded that withthe use of only biodiesel in engines as fuel causes the more Nox emissions **[18, 19, 20, 21, 59-64,].** For an example, maximum 15% increased NOx emissions for 100% pure biodiesel was observed at high load condition which results in 12% oxygen content of the B100 and high temperature in combustion chamber. **[69].** in many literatures it was found that the diesel and biodiesel was similar in Nox Emissions. The 29% of literature pointed that Nox emissions reduces when using biodiesel. Dorado et al**, [79]** found that Nox emissions decrease by 20% for biodiesel from waste olive oil with an 8 mode test cycles. NOx exhaust emissions from biodiesel B-20 are comparable if not lower than engine out Emissions from an engine fueled with regular diesel fuel this has been attributed to the lower volatility of B-20 compared to regular diesel**. [14-17]**

CO Emission of Biodiesel

Most of the researchers have recommended that the CO emissions are reduced when diesel is replaced by pure biodiesel. **[18-22,24,28-32,59-71].** One of the researcher Krahl et al**. [80]** founded that 50% of reduction in carbon monoxide emissions for biodiesel from rapeseed oil compared to low and ultra-low Sulphur diesel. Rehman et al. [29] have seen that reduction range for carbon monoxide gas was around 73 to 94 percent for the methyl ester of karanja (B100 pure biodiesel and other blends with20%, 40%, 60%, and 80% of biodiesel content) in comparison with diesel. It was surprising that some authors found that CO emission is significantly increased. The primary reasons given by them are that high viscousproperty and bad spray quality for biodiesel fuel, which can lead to bad atomization of fuel and worse combustion**. [54].**

Hydrocarbon Emissions of Biodiesel

It has been observed that emissions of hydrocarbonhave reduced byusing pure biodiesel in place of diesel fuel**. [20, 23, 28, 32, 55, 57, 59, 60, 65-71]**. Wu et al. reported that 5 different biodiesels reduces HC Emissions by 45-67% on an average compared to Biodiesel. Some other authors also reported considerable decrease similarly. One of the researchers has reported that HC emissions are reduced by 60% by using biodiesel incompared with diesel fuel. Lin et al has found that the emissions of THC were reduced within range of around 22.47 percent to 33.15 percent for the eight types of VOME. It had been observed that fuel from polanga, from karanja and Jatropha and also their blends in comparing with the diesel fuel in an engine of three cylinders during biodiesel reduction by 20.73%, 20.64% and 6.75%. **[27, 59, 37].** Many of the researchers believe that the HC emissions decrease with increase in biodiesel percentage in the blend. Several researcher shows that nothing much significant difference are observed between the biodiesel and the diesel fuel. The emissions of THC for biodiesel was found increased in many literatures. The 10 percent increase in hydrocarbon emission is obtained for alkyl ester of methane of Jatropha oil in comparison with the diesel fuel**. [51, 36, 71]**

V. Conclusion And Further Research

Biodiesel produced from renewable sources. It is represent from more sustainable energy and plays a significant role in provide an energy requirement in transportations, industrial applications. Therefore most of the work has been done on its emission and performance from past 12 years. Therefore it can be use with diesel engines without major alterations to engine. It is also biodegradable and free from sulphur and aromatics, it is safer to handle and transportation. Biodiesel run in any unmodified diesel engine, addition of 2% biodiesel helps in improvement of lubricity of biodiesel. The following conclusions could be drawn in this literature work:

1. It is seen that the emissions of Carbon monoxide reduces with the usage of biodiesel because of the high contentof oxygen. Also it lowers the hydrocarbons as compared to the petroleum diesel fuel.
2. Many researchers have shown those emissions of aromatic and also some polyaromatic compound for biodiesel reduces as compared to the petroleum diesel fuel.
3. The majority of the literatures agreed that particulate matter emission for biodiesel have been reducing as compared to the petroleum products.
4. Most of the studies suggest that Nox emissions are increase when using biodiesel. This is due to because biodiesel contain high oxygen content, more ever different properties like Cetane number, injection characteristics have impact on biodiesel.
5. It is also seen that usage of biodiesel fuel will give reduction in the carbon deposit to the parts of engine as compared with petroleum diesel fuel.
6. Few researchers concluded the CO2 emissions reduce a biodiesel fuel because of low ratio of carbon to HC. But some of them found that CO2 emissions increase because of combustion went effectively. But within the case of biodiesel CO2 emission reduce effectively from the life cycle circulation of CO2.

Overall when biodiesel blend with small portion with the diesel give best result in comparing the emission and life of the engine and is technically feasible as an alternative fuel for compression ignition engine without any minor or major modification. Most of the developers found that for pure biodiesel the engine should be redesigned. The further improvement in the biodiesel should be change it property and quality also the additives especially for NOx emissions. The further research should be done on low temperature performance of biodiesel because presently biodiesel have high viscous property than the diesel fuel which effects the emissions because of different sizes in the drops of fuel. The Study on emissions of non-regulated should be carried out especially for carbonyl compound emissions.

REFERENCES

[1] Knothe G, Dunn RO, Bagby MO (1997) "Biodiesel: the use of vegetable oils and their derivatives as alternative diesel fuels: In Fuels and Chemicals from Biomass, 1st edn. American Chemical Society, New York

[2] Van Gerpen J, Shanks B, Pruszko R, Clements D, Knothe G (2004) Biodiesel production technology. National Renewable Energy Laboratory, NRRL/SR-510-36244

[3] Introduction to Biodiesel Production3. Van Gerpen J, Shanks B, Pruszko R, Clements D, Knothe G (2004) Biodiesel analytical methods. National Renewable Energy Laboratory, NRRL/SR-510-36240

[4] Romano SD, González Suárez E, Laborde MA (2006) Biodiesel. In: Combustibles Alternatives, 2nd edn. Editions Cooperatives, Buenos Aires.

[5] Biodiesel Production Technologies: status, Prospects and implications for trade and development (2008), United Nation Conference on Trade and Development, New York and Geneva.

[6] Clean cities, a review, U.S. Department of Energy, Energy Efficiency and Renewable Energy, Fact sheet, April 2008.

[7] F. Ma, M.A, Hanna, "Biodiesel production: a review", Bio resource. Techno. 70 (1999) 1-15

[8] S. Angina, P. Ram, "Triglycerides-based diesel fuels", Renewable and Sustainable Energy Rev. 4 (2000) 111-133.

[9] V.A.N. Gerpen, "Biodiesel processing and production, Fuel Process". Techno.86 (2005) 1097-1107.

[10] S. Naga Sarada, M. Shailaja, A.V. Sita Rama Raju, "Optimization of injection pressure for a compression ignition engine with cotton seed oil as an alternate fuel", International journal of Engineering Science and Technology Vol. 2, No.6, 2010, pp. 124-149.

[11] Graboski M.S, McCormick R.L, "Combustion of fat and vegetable oil derived fuels in diesel engines", PRog Energy Combust 1998; 24:125-64.

[12] http://www.accenture.com/SiteCollectionDocuments/PDF/Accenture_Energy_APAS_Core_Blending_Biofuels.pdf Blending biofuels in the European Union review by Accenture.

[13] Sandra Rintoul, "Technical article on The Ideal Measurement Solution for Biofuels Blend Quality and Wastewater testing", American Laboratory, On-Line Edition, April 2009.

[14] C.D. Rakopoulos, K.A. Antonopoulos, D.C. Rakopoulos, D.T. Hountalas, E.G. Giakoumis, "Comparative performance and emissions study of a direct injection Diesel engine using blends of Diesel fuel with vegetable oils or bio-diesels of various origins", Renew Energy 0196-8904, 2006 Elsevier Ltd.

[15] M. Senthil Kumar, A. Ramesh, B. Nagalingam, "An experimental comparison of methods to use methanol and Jatropha oil in a compression ignition engine", Biomass and Bioenergy 25 (2003) 309 – 318 2003 Elsevier Ltd.

[16] McCormick, A. Williams, J. Ireland, Brimhall, and R.R. Hayes, "Effects of Biodiesel Blends on Vehicle Emissions" October 2006 Fiscal Year 2006 Annual Operating Plan Milestone 10.4" NREL/MP-540-40554.

[17] R.L. McCormick, J.R. Alvarez, and M.S. Graboski "NOX Solutions for Biodiesel" Final Report 6 in a series of 6, NREL/SR-510-.31465.

[18] Aydin H, Bayindir H. "Performance and emission analysis of cottonseed oil methyl ester in a diesel engine". Renewable Energy 2010; 35:588–92.

[19] Hazar H. "Effects of biodiesel on a low heat loss diesel engine". Renewable Energy 2009; 34:1533–7.

[20] Ozsezen AN, Canakci M, Turkcan A, Sayin C. "Performance and combustion characteristics of a DI diesel engine fueled with waste palm oil and canola oil methyl esters". Fuel 2009; 88:629–36.

[21] Karabektas M. "The effects of turbocharger on the performance and exhaust emissions of a diesel engine fuelled with biodiesel". Renewable Energy 2009; 34:989–93.
[22] Utlu Z, Koc¸ AK MS. "The effect of biodiesel fuel obtained from waste frying oil on direct injection diesel engine performance and exhaust emissions". Renewable Energy 2008; 33:1936–41.
[23] Ozgunay H, C¸ olak S, Zengin G, Sari O, Sarikahya H, Yuceer L. "Performance and emission study of biodiesel from leather industry pre-fleshings". Waste Manage 2007; 27:1897–901.
[24] Murillo S, Mıguez JL, Porteiro J, Granada E, Moran JC. "Performance and exhaust emissions in the use of biodiesel in outboard diesel engines". Fuel 2007; 86:1765–71.
[25] Hansen AC, Gratton MR, Yuan W. "Diesel engine performance and NOx emissions from oxygenated biofuels and blends with diesel fuel". Trans ASABE 2006; 49:589–95.
[26] Kaplan C, Arslan R, Surmen A. "Performance characteristics of sunflower methyl esters as biodiesel". Energ Source Part a 2006; 28:751–5.
[27] Reyes JF, Sepulveda MA. PM-10 emissions and power of a diesel engine fueled with crude and refined biodiesel from salmon oil. Fuel 2006; 85:1714–9.
[28] Carraretto C, Macor A, "Mirandola A, Stoppato A, Tonon S. Biodiesel as alternative fuel": experimental analysis and energetic evaluations. Energy 2004; 29:2195–211.
[29] Raheman H, Phadatare AG. "Diesel engine emissions and performance from blends of karanja methyl ester and diesel". Biomass Bioenerg 2004; 27:393–7.
[30] Ulusoy Y, Tekin Y, C¸ etinkaya M, Kapaosmano˘glu F. "The engine tests of biodiesel from used frying oil". Energ Source Part a 2004; 26:927–32.
[31] C¸ etinkaya M, Ulusoy Y, Tekin Y, Kapaosmano˘glu F. "Engine and winter road test performances of used cooking oil originated biodiesel". Energ Convers Manage 2005; 46:1279–91.
[32] Lin Y-C, Lee W-J, WuT-S, WangC-T. "Comparison ofPAHand regulated harmful matter emissions from biodiesel blends and paraffinic fuel blends on engine accumulated mileage test". Fuel 2006; 85:2516–23.
[33] Buyukkaya E. "Effects of biodiesel on a DI diesel engine performance, emission and combustion characteristics". Fuel 2010; 89:3099–105.
[34] Choi S-H, Oh Y. "The emission effects by the use of biodiesel fuel. International Journal of Modern Physics" B 2006; 20:4481–6.
[35] Da Silva Fernando N, Antonio SP, Jorge RT. "Technical feasibility assessment of oleic sunflower methyl ester utilization in diesel bus engines". Energy Convers Manage 2003; 44:2857–78.
[36] Yucesu HS, Cumali I˙. "Effect of cotton seed oil methyl ester on the performance and exhaust emission of a diesel engine". Energy Source Part a 2006; 28:389–98.
[37] Lin B-F, Huang J-H, Huang D-Y. "Experimental study of the effects of vegetable oil methyl ester on DI diesel engine performance characteristics and pollutant emissions". Fuel 2009; 88:1779–85.
[38] Ghobadian B, Rahimi H, Nikbakht AM, Najafi G, Yusaf TF. "Diesel engine performance and exhaust emission analysis using waste cooking biodiesel fuel with an artificial neural network". Renewable Energies 2009; 34:976–82.
[39] Qi DH, Geng LM, Chen H, Bian YZH, Liu J, Ren XCH. "Combustion and performance evaluation of a diesel engine fueled with biodiesel produced from soybean crude oil". Renewable Energies 2009; 34:2706–13.
[40] Lapuerta M, Herreros JM, Lyons LL, Garcia-Contreras R, Brice Y. "Effect of the alcohol type used in the production of waste cooking oil biodiesel on diesel performance and emissions. "Fuel 2008; 87:3161–9.
[41] Keskin A, Guru M, Altıparmak D. "Influence of tall oil biodiesel withMgandMo based fuel additives on diesel engine performance and emission". Bio resource Technol 2008; 99:6434–8.
[42] O˘guz H, O˘gut H, Eryilmaz T. "Investigation of biodiesel production, quality and performance in Turkey". Energ Source Part A 2007; 29:1529–35.
[43] Song J-T, Zhang C-H. "An experimental study on the performance and exhaust emissions of a diesel engine fuelled with soybean oil methyl ester". P I Mech Eng D-J Aut 2008; 222:2487–96.
[44] Al-Widyan MI, Tashtoush G, Abu-Qudais M. "Utilization of ethyl ester of waste vegetable oils as fuel in diesel engines". Fuel Process Technol 2002; 76:91–103.
[45] Divya Bajpai., V.K. Tyagi, "Biodiesel: Source, Production, Composition, Properties and its Benefits". Journal of Oleo Science, Vol. 55, No. 10, pp487-502, 2006.
[46] Oner C, Altun S, "Biodiesel production from inedible animal tallow and an experimental investigation of its use as alternative fuel in a direct injection diesel engine". Appl Energ 2009; 86:2114–20.
[47] Monyem A, Van Gerpen JH, Canakci M. "The effect of timing and oxidation on emissions from biodiesel-fueled engines". Transactions ASAE 2001; 44:35–42.
[48] Senatore A, Cardone M, Rocco V, Prati MV. "A comparative analysis of combustion process in DI diesel engine fueled with biodiesel and diesel fuel". SAE Paper 2000, 2000-01-0691.
[49] Hass MJ, Scott KM, Alleman TL, McCormick RL. "Engine performance of biodiesel fuel prepared from soybean soapstock: a high quality renewable fuel produced from a waste feedstock". Energy Fuel 2001; 15:1207–12.
[50] Sahoo PK, Das LM, Babu MKG, Naik SN. "Biodiesel development from high acid value polanga seed oil and performance evaluation in a CI engine". Fuel 2007; 86:448–54.
[51] Baiju B, Naik MK, Das LM. "A comparative evaluation of compression ignition engine characteristics using methyl and ethyl esters of Karanja oil. Renewable Energy" 2009; 34:1616–21.
[52] Puhan S, Vedaraman N, Sankaranarayanan G, Bharat Ram BV. "Performance and emission study of Mahua oil (Madhuca indica oil) ethyl ester in a4-stroke natural aspirated direct injection diesel engine". Renewable Energy 2005; 30:1269–78.

[53] Wu F, Wang J, Chen W, and Shuai S. "A study on emission performance of a diesel engine fueled with five typical methyl ester biodiesels". Atmospheric Environment 2009; 43:1481–5.
[54] Ulusoy Y, Arslan R, Kaplan C." Emission characteristics of sunflower oil methyl ester: Energy Source Part a 2009; 31:906–10.
[55] Lin C-Y, Li R-J. "Engine performance and emission characteristics of marine fish-oil biodiesel produced from the discarded parts of marine fish". Fuel Process Technology 2009; 90:883–8.
[56] Tziourtzioumis D, Demetriades L, Zogou O, Stamatelos AM. "Experimental investigation of the effect of a B70 biodiesel blends on a common-rail passenger car diesel engine". P I Mech Eng D-J Aut 2009; 223:671–85.
[57] Nabi MN, Najmul Hoque SM, Akhter MS. Karanja (Pongamia Pinnata), "biodiesel production in Bangladesh, characterization of karanja biodiesel and its effect on diesel emissions." Fuel Process Technology 2009; 90:1080–6.
[58] Zheng M, Mulenga MC, Reader GT, Wang M, Ting DS-K, Tjong J. "Biodiesel engine performance and emissions in low temperature combustion". Fuel2008; 87:714–22.
[59] Tat ME, Van Gerpen JH, Wang PS. "Fuel property effects on injection timing, ignition timing, and oxides of nitrogen emissions from biodiesel-fueledengines". Transaction ASABE 2007; 50:1123–8.
[60] Chung A, Lall AA, and Paulson SE. "Particulate emissions by a small non-road diesel engine: Biodiesel and diesel characterization and mass measurements using the extended idealized aggregated theory". Atmospheric Environment 2008; 42:2129–40.
[61] Kalligeros S, Zannikos F, Stournas S, Lois E, Anastopoulos G, Teas Ch., and et al. "An Investigation of using biodiesel/marine diesel blends on the performance ofa stationary diesel engine". Biomass Bioenerg 2003; 24:141–9.
[62] Lapuerta M, Armas O, Ballesteros R. "Diesel particulate emissions from biofuels derived from Spanish vegetable oils". SAE Paper 2002, 2002-01-1657.
[63] Jung H, Kittelson DB, Zachariah MR. "Characteristics of SME biodiesel-fueleddiesel particle emissions and the kinetics of oxidation". Environment Science Technology 2006; 40:4949–55.
[64] Assessment and Standards Division (Office of Transportation and Air Quality of the US Environmental Protection Agency), "A comprehensive analysis of Biodiesel impacts on exhaust emissions", United States Environmental Protection Agency, 2002, EPA 420-P-02-001.
[65] Monyem A, Van Gerpen JH. "The effect of biodiesel oxidation on engine performance and emissions". Biomass Bioenerg 2001; 20:317–25.
[66] Graboski MS, McCormick RL, Alleman TL, Herring AM. "The effect of biodiesel composition on engine emissions from a DDC series 60 diesel engine". Natl Renewable Energy Lab 2003. NREL/SR-510-31461.
[67] Wang WG, Lyons DW, Clark NN, Gautam M, Norton PM. "Emissions from nine heavy trucks fuelled by diesel and biodiesel blend without engine modification". Environment Science Technology 2000; 34:933–9.
[68] Cardone M, Prati MV, Rocco V, Seggiani M, Senatore A, Vitolo S. "Brassica Carinata As an alternative oil crop for the production of biodiesel in Italy": engine performance and regulated and unregulated exhaust emissions. Environment Science Technology 2002; 36:4656–62.
[69] Kado NY, Kuzmicky PA. "Bioassay analyses of particulate matter from a diesel Bus engine using various biodiesel feedstock fuels. Natl Renewable Energy Lab2003. NREL/SR-510-31463.
[70] Lapuerta M, Armas O, Ballesteros R, Carmona M. "Fuel formulation effects on Passenger car diesel engine particulate emissions and composition". SAE paper2000, 2000-01-1850.
[71] Armas O, Hernandez JJ, Cardenas MD. "Reduction of diesel smoke opacity from vegetable oil methyl esters during transient operation". Fuel2006; 85:2427–38.
[72] Yamane K, Ueta A, Shimamoto Y. "Influence of physical and chemical properties of biodiesel fuels on injection, combustion and exhaust emission characteristics in a direct injection compression ignition engine". International Journal of Engine Research 2001; 2:249–61.
[73] Lapuerta M, Armas O, Herreros JM. "Emissions from a diesel-biodiesel blending an automotive diesel engine". Fuel 2008; 1:25–31.
[74] Lapuerta M, Armas O, Ballesteros R, Fernandez J. "Diesel emissions from biofuels derived from Spanish potential vegetable oils". Fuel 2005; 84:773–80.
[75] Dincer K. "Lower emission from biodiesel combustion". Energ Source Part a2008; 30:963–8.
[76] Qi DH, Chen H, Geng LM, Bian YZH. "Experimental studies on the combustion characteristics and performance of a direct injection engine fueled with biodiesel/diesel blends". Energy Conversation Manage 2010; 51:2985–92.
[77] Senthil Kumar M, Ramesh A, Nagalingam B. "A comparison of the different methods of using Jatropha oil as fuel in a compression ignition engine". J Eng Gas Turb Power 2010; 132:032801–32811.
[78] Banapurmatha NR, Tewaria PG, "Hosmath RS. Performance and emission characteristics of a DI compression ignition engine operated on Honge, Jatropha and sesame oil methyl esters". Renewable Energy 2008; 33:1982–8.
[79] Dorado MP, Ballesteros E, Arnal JM, Gomez J, Lopez FJ. "Exhaust emissions form diesel engine fueled with Trans esterified waste olive oil". Fuel 2003; 82:1311–5.
[80] Krahl J, Munack A, Schroder O, Stein H, Bunger J. Influence of biodiesel and different designed diesel fuels on the exhaust gas emissions and health effects. SAE paper 2003, 2003-01-3199.

OPEN ACCESS

International
Journal
Of Modern Engineering Research (IJMER)

The Bloch Space of Analytic functions

S. Nagendra[1], Prof. E. Keshava Reddy[2]
[1]*Department of Mathematics, Government Degree College, Porumamilla*
[2]*Department of Mathematics, JNTUA*

Abstract: *We shall state and prove a characterization for the Bloch space and obtain analogous characterization for the little Bloch space of analytic functions on the unit disk in the complex plane. We shall also state and prove three containment results related to Bloch space and Little Bloch space.*
Keywords: *Bloch Space, Analytic Functions, Mobius Transformation*

I. INTRODUCTION

We let $= \{ z \in C / |z| < 1 \}$ D

For w∈D, the Mobius transformation ϕ_w is defined by

$$\phi_w(z) = \frac{w - z}{1 - \overline{w}z} \quad for \quad z \in D$$

Then

$$1 - |\phi_w(z)|^2 = 1 - \phi_w(z).\overline{\phi_w(z)}$$

$$= 1 - \left(\frac{w - z}{1 - \overline{\omega} z} \right) \left(\frac{\overline{w} - \overline{z}}{1 - w\overline{z}} \right)$$

$$1 - |\phi_w(z)|^2 = \frac{\left(1 - |w|^2\right)\left(1 - |z|^2\right)}{\left|1 - \overline{w}z\right|^2} \qquad - (1)$$

So, the function ϕ_w maps D on to itself and ∂D on to itself. It is easy to verify that ϕ_w is its own inverse. Noting that $\phi_w^1(z) = \frac{\left(|w|^2 - 1\right)}{\left(\left|1 - \overline{w}z\right|\right)^2}$, the above identity states:

$$\left(1 - |z|^2\right)\left|\phi_w^1(z)\right| = 1 - |\phi_w(z)|^2 \qquad - (2)$$

Bloch space B is the space of all analytic functions f on D for which

$$\sup_{z \in D} \left(1 - |z|^2\right) \left| f^1(z) \right| < \infty$$

and B becomes a Banach space with respect to the semi norm

$$\| f \|_B = \sup_{z \in D} \left(1 - |z|^2\right) \left| f^1(z) \right|$$

Using (2), we have

$$\begin{aligned}\|fo\phi_w\|_B &= \underset{z\in D}{Sup}\left(1-|z|^2\right)\left|\left(fo\phi_w\right)^1(z)\right| \\ &= \underset{z\in D}{Sup}\left(1-|z|^2\right)\left|f^1(\phi_w(z))\right|\left|\phi_w^1(z)\right| \\ &= \underset{\phi_w(z)\in D}{Sup}\left(1-|\phi_w(z)|^2\right)\left|f^1(\phi_w(z))\right| \\ &= \|f\|_B \\ \therefore \|fo\phi_w\|_B &= \|f\|_B \qquad - \ (3)\end{aligned}$$

Thus Bloch space is a Mobius invariant space.

In the next section, we shall state and prove a criterion for containment in the Bloch space and little Bloch space.

II. CHARACTERIZATION FOR BLOCH AND LITTLE BLOCH SPACE

A. THEOREM 1

For an analytic function f on D

$$f \in B \Leftrightarrow Sup\left\{\frac{\left(1-|z|^2\right)\left(1-|w|^2\right)}{\left|1-\overline{w}z\right|}\left|\frac{f(z)-f(w)}{z-w}\right| : z,w\in D,\ z\neq w\right\}<\infty$$

Proof : Suppose for an analytic function f on D

$$Sup\left\{\frac{\left(1-|z|^2\right)\left(1-|w|^2\right)}{\left|1-\overline{w}z\right|}\left|\frac{f(z)-f(w)}{z-w}\right| : z,w\in D,\ z\neq w\right\}<\infty$$

$$\Rightarrow \quad \frac{\left(1-|z|^2\right)\left(1-|w|^2\right)}{\left|1-\overline{w}z\right|}\left|\frac{f(z)-f(w)}{z-w}\right|<\infty,\ \ \forall\, z,w\in D, z\neq w$$

Taking limit as w→z, we get

$$\begin{aligned}&Sup\left(\frac{\left(1-|z|^2\right)^2\left|f^1(z)\right|}{\left(1-|z|^2\right)}\right)<\infty \\ &\Rightarrow \underset{z\in D}{Sup}\left(1-|z|^2\right)\left|f^1(z)\right|<\infty \\ &\Rightarrow f\in B\end{aligned}$$

For the next part, suppose $f \in B$

$$\begin{aligned}&\Rightarrow \underset{z\in D}{Sup}\left(1-|z|^2\right)\left|f^1(z)\right|<\infty \\ &\Rightarrow \left(1-|z|^2\right)\left|f^1(z)\right|\le \|f\|_B,\ \forall\, z\in D \qquad - \ (4)\end{aligned}$$

Then for each $u \in D$, we have

$$f(u) - f(0) = \int_0^1 f^1(tu)\,u\,dt$$

$$\Rightarrow \quad |f(u) - f(0)| = \left| \int_0^1 f^1(tu)\,u\,dt \right|$$

$$\leq \int_0^1 \left| f^1(tu) \right| |u|\,dt$$

$$\leq \int_0^1 \frac{\|f\|_B}{1 - t^2|u|^2} |u|\,dt \qquad (\because (4))$$

$$\leq \int_0^1 \frac{\|f\|_B |u|}{1 - t|u|}\,dt$$

$$\therefore \ |f(u) - f(0)| < \|f\|_B \int_0^1 \frac{|u|}{1 - t|u|}\,dt = \|f\|_B |u| \frac{\left(\log(1 - t|u|)\right)_0^1}{-|u|}$$

$$= \|f\|_B \log\left(1 - |u|\right)^{-1} = \|f\|_B \log\left|\frac{1}{1 - |u|}\right|$$

$$< \|f\|_B \log\left|\frac{1 + |u|}{1 - |u|^2}\right|$$

$$\leq \|f\|_B \left(\frac{1 + |u|}{1 - |u|^2} - 1 \right) \qquad (\therefore \log x \leq x - 1,\ x > 0)$$

$$\leq \|f\|_B \left(\frac{1 + |u| - 1 + |u|^2}{1 - |u|^2} \right)$$

$$\leq \|f\|_B \left(\frac{1 + |u| - 1 + |u|}{1 - |u|^2} \right)$$

$$\therefore \ |f(u) - f(0)| \leq \|f\|_B \frac{2|u|}{1 - |u|^2}, \quad \forall\ u \in D$$

Now for z, $w \in D$ replace f in the above inequality by $f o \phi_w$ and let u = ϕ_w(z). Using

$\phi_w(\phi_w(z)) = z$ and identities (1) and (3) we have

$$\left| (f o \phi_w)(u) - (f o \phi_w)(0) \right| \leq \|f o \phi_w\|_B \cdot \frac{2|\phi_w(z)|}{1 - |\phi_w(z)|^2}$$

$$\Rightarrow \left|f(z)-f(w)\right| \le \frac{\|f\|_B \dfrac{2|w-z|}{|1-\bar{w}z|}}{\dfrac{\left(1-|w|^2\right)\left(1-|z|^2\right)}{|1-\bar{w}z|^2}}$$

We briefly discuss the little Bloch space B0. The set of all analytic functions f on D for which

$$\lim_{|z|\to\bar{1}} \left(1-|z|^2\right)\left|f^1(z)\right|=0$$

For an analytic function f on D and 0 < t < 1 the dilate ft is the function defined by $f_t(z) = f(tz)$. It is known that for an analytic function f on D:

$$f \in B_0 \quad iff \quad \|f-f_t\|_B \to 0 \quad as\ t \to \bar{1}$$

$$\therefore \frac{\left(1-|z|^2\right)\left(1-|w|^2\right)}{|1-\bar{w}z|}\left|\frac{f(z)-f(w)}{z-w}\right| \le 2\|f\|_B \qquad -\ (5)$$

$$\therefore Sup\left\{\frac{\left(1-|z|^2\right)\left(1-|w|^2\right)}{|1-\bar{w}z|}\left|\frac{f(z)-f(w)}{z-w}\right| : z, \atop w\in D,\ z\neq w\right\} \le 2\|f\|_B < \infty$$

In analogy to theorem (1), we have the following result.

B. THEOREM 2

For an analytic function f on D

$$\lim_{|z|\to\bar{1}} Sup\left\{\frac{\left(1-|z|^2\right)\left(1-|w|^2\right)}{|1-\bar{w}z|}\left|\frac{f(z)-f(w)}{z-w}\right| : z, w\in D,\ z\neq w\right\}=0$$

Proof:

Taking limit as $w\to z$ in the condition of the statement, we get

$$\lim_{|z|\to\bar{1}} Sup\left\{\frac{\left(1-|z|^2\right)^2}{|1-|z|^2|}\left|f^1(z)\right|\right\} = 0$$

$$\therefore \lim_{|z|\to\bar{1}} \left(1-|z|^2\right)\left|f^1(z)\right| = 0$$

$$\Rightarrow f \in B_0$$

Suppose $f \in B_0$, then $f - f_t \in B$

Applying inequality (5) for $f_t \in B$, we have

$$\frac{\left(1-|z|^2\right)\left(1-|w|^2\right)}{|1-\bar{w}z|}\left|\frac{f_t(z)-f_t(w)}{z-w}\right| \le \frac{\left(1-|z|^2\right)\left(1-|w|^2\right)}{|z-w||1-\bar{w}z|}\cdot\frac{2\|f_t\|_B\, t|z-w||1-t^2\bar{w}z|}{\left(1-t^2|z|^2\right)\left(1-t^2|w|^2\right)}$$

$$= \frac{2t}{\left(1-t^2\right)^2}\|f\|_B\left(1-|z|^2\right) \quad - \quad (6)$$

Applying inequality (5) for $f - f_t \in B$, we have

$$\frac{\left(1-|z|^2\right)\left(1-|w|^2\right)}{|1-\bar{w}z|}\left|\frac{(f-f_t)(z)-(f-f_t)(w)}{z-w}\right| \le 2\|f-f_t\|_B \quad - (7)$$

Inequality (6), (7) and triangle inequality imply that

$$\frac{\left(1-|z|^2\right)\left(1-|w|^2\right)}{|1-\bar{w}z|}\left|\frac{f(z)-f(w)}{z-w}\right|$$

$$= \frac{\left(1-|z|^2\right)\left(1-|w|^2\right)}{|1-\bar{w}z||z-w|}\left|(f-f_t)(z)-(f-f_t)(w)+f_t(z)-f_t(w)\right|$$

$$\le \frac{\left(1-|z|^2\right)\left(1-|w|^2\right)}{|1-\bar{w}z||z-w|}\left|(f-f_t)(z)-(f-f_t)(w)\right|$$

$$+ \frac{\left(1-|z|^2\right)\left(1-|w|^2\right)}{|1-\bar{w}z||z-w|}\left|f_t(z)-f_t(w)\right|$$

$$\le 2\|f-f_t\|_B + \frac{2t}{\left(1-t^2\right)^2}\|f\|_B\left(1-|z|^2\right)$$

Now first letting $|z| \to \bar{1}$ and then $t \to \bar{1}$, we get

$$\lim_{|z|\to 1^-} Sup\left\{\frac{\left(1-|z|^2\right)\left(1-|w|^2\right)}{|1-\bar{w}z|}\left|\frac{f(z)-f(w)}{z-w}\right| : z, w \in D,\ z \neq w\right\} = 0$$

In the next section, we shall prove three results related to containment of Bloch and Little Bloch space

III. CONTAINMENT RESULTS OF BLOCH AND LITTLE BLOCH SPACE

Let ϕ be a bounded analytic function on D, then there exists a constant

$$M > 0 such that |\phi(z)| \le M, \forall z \in D$$

From Cauchy's integral formula, we have

$$\phi'(z) = \frac{1}{2\pi i}\int_C \frac{\phi(w)\,dw}{(w-z)^2}$$

where C is any closed disc of radius r in neighbourhood of 1 and containing z, then $\left|\phi'(z)\right| \le \frac{4M}{r}$ in the concentric disc of radius $\frac{r}{2}$. This implies that $\phi'(z)$ is bounded in any neighbourhood of 1 contained in D whenever so is $\phi(z)$.

A. THEOREM 3

If $f \in B$ then $f + k \in B$ where $k \in C$ is a constant

Proof: It is very easy to see that

$$f'(z) = (f+k)'(z)$$

Therefore $\sup_{z\in D}\left(1-|z|^2\right)\left|f'(z)\right| = \sup_{z\in D}\left(1-|z|^2\right)\left|(f+k)'(z)\right|$

Hence $f + k \in B$ whenever $f \in B$

B. THEOREM 4

If $f \in B_0$ is bounded and ϕ is any bounded and analytic function on D then $\phi f \in B_0$.

Proof: $f \in B_0 \Rightarrow \lim_{|z|\to 1^-}\left(1-|z|^2\right)\left|f'(z)\right| = 0$

$$(\phi f)'(z) = \phi(z) f'(z) + f(z)\phi'(z)$$

Note that $\Rightarrow \left|(\phi f)'(z)\right| \le \left|\phi(z)\right|\left|f'(z)\right| + \left|f(z)\right|\left|\phi'(z)\right|$

$$\Rightarrow \left(1-|z|^2\right)\left|(\phi f)'(z)\right| \le \left(1-|z|^2\right)\left|\phi(z)\right|\left|f'(z)\right| + \left(1-|z|^2\right)\left|f(z)\right|\left|\phi'(z)\right|$$

Taking limit as $|z| \to 1^-$, the first term on RHS tends to 0 because of the hypothesis and ϕ is bounded and the second term since f and ϕ' bounded in the neighbourhood of 1 as ϕ is bounded on D tends to 0.

Hence $\lim_{|z|\to 1^-}\left(1-|z|^2\right)\left|(\phi f)'(z)\right| = 0$

Therefore $\phi f \in B_0$.

C. THEOREM 5

If f, g are bounded functions of B_0, then $fg \in B_0$.

Proof: From the definition of B_0,

$$\lim_{|z|\to 1^-}\left(1-|z|^2\right)\left|f'(z)\right| = 0$$

$$\lim_{|z|\to 1^-}\left(1-|z|^2\right)\left|g'(z)\right| = 0$$

Note that $0 < \left(1-|z|^2\right)\left|(fg)'(z)\right| \le \left(1-|z|^2\right)\left|g'(z)\right|\left|f(z)\right| + \left(1-|z|^2\right)\left|f'(z)\right|\left|g(z)\right|$

Taking limit as $|z| \to 1^-$, we get

$$\lim_{|z|\to 1^-}\left(1-|z|^2\right)\left|(fg)'(z)\right| = 0$$

$$\therefore fg \in B_0.$$

IV. CONCLUSION

I invite interested readers to pursue geometric interpretation of characterization theorems that we proved in this paper and also similar containment results related to the Bloch space.

REFERENCES

[1] J.M. Anderson, J. Clunie and Ch. Pommerenke, On Bloch functions and normal functions, Proc. of the American Mathematical Society 85,1974, 12-37.
[2] Jose. L. Fernandez, J, On coeffients of Bloch functions, London math. Soc. (2). 29 (1984), 94-102.
[3] R. Aulaskari, N. Danikas, and R. Zhao, The Algebra Property of The Integrals of Some Banach spaces of Analytic functions by N. Danikar, Aristotle univ. of Thessaloniki.
[4] Theory of function spaces by Kehe Jhu.
[5] Bloch functions : The Basic theory by J.M.Anderson edited by S.C. Power, series C: Mathematical and Physical Sciences Vol. 153.
[6] Multipliers of Bloch functions by Jonathan Arazy, Report 54, 1982.
[7] The Bloch space and Besov spaces of Analytic functions by Karel Stroethoff, Bull. Austral. Math. Soc. Vol. 54, 1996, 211-219.

OPEN ACCESS

International
Journal
Of Modern Engineering Research (IJMER)

ANN Based Prediction Model as a Condition Monitoring Tool for Machine Tools

Lokesha[1], P B Nagaraj[2], Pushpalatha M N[3], P Dinesh[4]
[1,2,4] *Department of Mechanical Engineering, M S Ramaiah Institute of Technology, Bangalore*
[3] *Department of Information Science, M S Ramaiah Institute of Technology, Bangalore*

Abstract: *In today's world of manufacturing, a machine tool has an important role to produce best quality and quantity in phase with the demand. Machine tool in good working condition enhances the productivity and provides an opportunity for the overall development of the industry. Several parameters such as vibration of a machine tool structure, temperature at cutting zones, machined surface roughness, noise levels in the moving parts etc. provide the information of its working condition which is related to its productivity. Surface roughness of the machined part is one of the parameters to indicate machine tool condition. In the recent trends, soft computing tools have emerged as an aid for the condition monitoring of machine tools. In the present work, experiments have been conducted based on Taguchi technique for turning operation with different process input parameters using carbide cutting tool insert and the surface roughness of the turned parts were measured as output characteristic. Relation between input and output was established and a prediction model for surface roughness was built by using artificial neural network (ANN) backpropagation learning algorithm. The predicted values of surface roughness from the prediction model in comparison with the experimental values are found to be in close agreement. This establishes the use of ANN in developing prediction models for better monitoring of the condition of a machine tool for enhancing the productivity.*

Keywords: *Artificial neural network , Condition monitoring, Productivity.*

I. Introduction

Various soft computing techniques are being used in the study of condition monitoring for prediction of health of a machine tool. Surface roughness is one of the parameters that can be used to indicate the condition of a machine tool which also depends on process parameters such as cutting speed, depth of cut, feed rate and tool overhang .The combination of these process parameters result in an optimized machine tool condition for an enhanced productivity and quality of product and also indicating its condition.

Several experimental studies have been conducted to analyze the surface finish under different cutting conditions. A study on EN8 material during face turning operation with a coated ceramic cutting tool under the influence of process parameters such as depth of cut, feed rate and cutting speed revealed that the effect of increase of feed rate is more on the surface roughness than the cutting speed [1]. Further, an experimental study was carried out on AISI 1045 steel material to investigate the effect of cutting speed, depth of cut, feed rate and tool geometry on surface roughness in a turning operation and predict the optimal process parameters. Number of trials were decided based on the Taguchi orthogonal array L25 and the optimal input parameters were investigated with the help of ANOVA technique with 95% confidence level. The study revealed the effect of each of the optimal parameters on surface roughness [2].An experimental work carried out to analyze the surface finish and temperature variation in the cutting tool for a turning operation revealed the quality of surface finish of the work piece with different machining condition [3]. Similarly, an experimental study conducted to analyze the influence of variation of cutting speed, depth of cut, feed rate and cutting tool overhang on surface roughness revealed that the better surface finish is achieved with less feed rate and smaller tool overhang [4]. Focusing the effect of other parameters which affect the machining condition such as vibration, an experiment was carried out to investigate the influence of machine tool vibration on surface roughness with input variables as constant cutting speed and depth cut, along with variable feed rate and cutting tool insert nose radius and the study revealed that the larger insert nose radius with lower feed rate produces better surface finish [5].

II. Ann Based Prediction Model

The focus of present study was to develop an ANN based prediction model which establishes a relationship between input and output parameters. The prediction model was developed by using

backpropagation ANN training algorithm. The backpropagation algorithm is generally referred as feed forward, multilayered network with number of hidden layers.

The multilayer feed forward networks consists of a set of sensory units or source nodes that constitute the input layer, one or more hidden layers of computation nodes, and an output layer of computation nodes. The input signal propagates through the network in a forward direction, layer-by-layer basis and these neural networks are commonly referred to as multilayer perception (MLPs). Multilayer perceptron utilizes the backpropagation algorithm for training the network [6].

The error back-propagation learning consists of two passes, a forward pass and a backward pass. In the forward pass an activity pattern is applied to the sensory nodes of the network, and its effect propagates through the network, layer by layer. Finally a set of outputs is produced as the actual response of the network. During the forward pass the synaptic weights of the network are all fixed. During the backward pass, on the other hand, the synaptic weights are all adjusted in accordance with an error-correction rule. Specifically, the actual response of the network is subtracted from a target response to produce an error-signal. This error signal is then propagated backward through the network, against the direction of synaptic connections. The synaptic weights are adjusted to make the actual response of the network move closer to the desired response in a statistical sense.

Following are the steps of the backpropagation algorithm [7]

Step1 – Initialize the weights.
Initializes the weights and bias to small random numbers, like -1.0 to +1.0 or -0.5 to +0.5

Step2 – Propagate the inputs forward.
Input is fed to the input layers of the network. The input will remain small in the input layers, i.e., for an input unit k, its output O_k is equal to its input value I_k. The net input to a unit in the hidden or output layers is computed as a linear combination of its inputs. Given a unit k in a hidden or output layer, the net input I_k, to unit k is

$$I_k = \sum_i w_{ik} O_i + \theta_k$$

Where w_{ik} is the weight of the connection from unit i in the previous layers to unit k, Oi is the output of unit i from the previous layer and θ_k is the bias of the unit. The bias acts as a threshold in that it serves to vary the activity of the unit.
Given the net input I_k to unit k, then O_k, the output of the unit k, is computed as

$$O_k = \frac{1}{1 + e^{-I_k}}$$

The above function is also called as a squashing function because it maps a large input domain into smaller range of 0 to 1.

Step3 – Back propagate the error.
For a unit k in the output layer, the error Err_k is computed by

$$Err_k = O_k(1 - O_k)(T_k - O_k)$$

Where, O_k is the actual output of unit k and T_k is the known target value of the given input.
Error of a hidden layer unit k is

$$Err_k = O_k(1 - O_k) \sum_j Err_j w_{kj}$$

Where, w_{kj} is the weight of the connection from unit k to a unit j in the next higher layer and Err_j is the error of unit j.
The weights and bias are updated to reflect the propagated errors.
Weights are updated by the following equation, where Δw_{ik} is the change in weight w_{ik}.

$$\Delta w_{ik} = (l) Err_k O_i$$
$$w_{ik} = w_{ik} + \Delta w_{ik}$$

l is the learning rate, a constant having a value between 0.0 to 1.0.
Biases are updated by the following equation, where $\Delta\theta_j$ is the change in bias θ_j.

$$\Delta\theta_j = (l) Err_j$$
$$\theta_j = \theta_j + \Delta\theta_j$$

Here the weights of biases are updated after the presentation of each input which is known as case updating. Alternatively the weights and bias increments could be accumulated in variables, so that the weights and biases are updated after all of the training inputs have been presented. This strategy is called epoch updating, where one iteration through the training set is an epoch.
Step4 – Termination conditions.

The training terminates, when:

- All the Δw_{ij} in the previous epoch were so small so as to be below some specified threshold
- The percentage of tuples misclassified in the previous epoch is below some threshold
- A pre-specified number of epochs have expired.

Machine tool condition monitoring has been also carried out with several soft skill techniques. ANN has emerged a popular tool as it can relate several input parameters with an output without much mathematical complexities. ANN is a computational model used to predict a function that depends on large number of unknown inputs. It is a system of interconnected neurons which computes and predicts the values from inputs and has the capability of machining learning and pattern recognition. This tool is generally used to solve the wide variety of problems which are difficult to solve with the help of ordinary rule based programming.

There are number of ANN applications in condition monitoring. A study conducted and discussed the maintenance and system health management with the use of methods and techniques from the field of Artificial Intelligence (AI), particularly experience-based diagnosis and condition-based maintenance and the study revealed that the development of CBM systems is directed towards the ability to diagnose any abnormalities and to calculate the remaining useful life (RUL) using Artificial Intelligence (AI) techniques. AI encompasses the application of Neural Networks (NN), Case Based Reasoning (CBR), and Fuzzy Logic tools and techniques which are ideally suited to efficiently handle the large amounts of data generated through the processes [8]. An experimental study conducted by considering cutting speed, depth of cut and feed rate as process variables, with and without the application of damping material between the cutting tool and tool holder. A 3k factorial design is used to select the machining parameters and ANOVA to analyze the effect of parameters on performance. Regression equations and a multi layer artificial neural network (ANN) are developed for tangential and axial vibration levels and compared with the experimental findings, which are found to be satisfactory and to be used as alternate technique to predict the vibration level [9]. Considering the development of computer applications in the field of condition monitoring, an experimental investigation has been carried out to develop software allowing the cutting conditions optimization and the process monitoring to prevent any trouble during machining operations. The micro movement of the tool is measured using eddy current sensor during the machining operation with different process parameters and the stability of the tests was confirmed against the surface finish. Determination of stable and unstable condition of the process due to vibration generated in the space region for different width of cut and cutting speed is carried out by using fuzzy classification method based on fuzzy rules [10].

III. Experimental Setup

The experimental study has been carried out on the prediction of surface roughness under various conditions of machining parameters such as cutting speed, depth of cut and feed rate for a plane dry turning operation on lathe. Machining of mild steel specimens under different machining conditions was carried out and the surface roughness was measured. Using this data an ANN model was obtained for predicting the surface roughness for several other machining conditions and experimental values were compared with ANN predicted values which were found to be in good agreement.

Number of trials with selected process parameters of cutting speed (A), feed rate (B) and depth of cut (C) were designed by using L9 Taguchi orthogonal array. Taguchi orthogonal array is an effective technique which has the capability of checking the interaction among the selected parameters. The design of experimental work for the present study resulted in nine trials. Tables 1 and 2 provide the selected parameters and parameters set for each trial respectively.

Table 1 Process parameters for experiments

Range	Cutting speed (A)	Feed rate (B)	depth of cut (C)
	m/min	mm/rev	mm
1	250	0.05	0.50
2	420	0.11	0.75
3	710	0.22	1.00

Table 2: Number of trials for the experimental work as per Taguchi L9 orthogonal array

Trial No.	A	B	C
1	250	0.05	0.50
2	250	0.11	0.75
3	250	0.22	1.00
4	420	0.05	0.75
5	420	0.11	1.00
6	420	0.22	0.50
7	710	0.05	1.00
8	710	0.11	0.50
9	710	0.22	0.75

The experimental work was carried on HMTLT-20 engine lathe with dry run condition using a carbide cutting tool insert for mild steel material. Figure 1 shows the experimental setup.

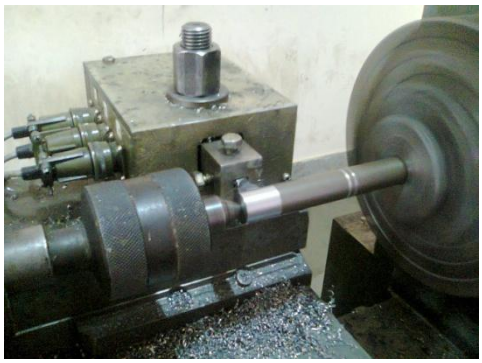

Fig 1: Details of experimental setup

A 20mm diameter mild steel specimen was turned for a length of 40mm in each trial. Surface roughness of turned portion of the work piece was measured using SURFCOM 130A instrument. Table 3gives the measured surface roughness value for each trial.

Table 3: Surface roughness determined experimentally

Trial No.	Surface roughness Microns
1	2.06
2	4.03
3	6.44
4	3.66
5	6.78
6	4.63
7	5.14
8	3.05
9	4.95

IV. Training And Testing Of Ann Model

The experiments were carried out as discussed in the previous section. The set of data from the Tables 2 and 3 were used to train the ANN network. Further, using the same experimental setup, three more trials were conducted for the conditions as in Table 4 for obtaining data to be compared with ANN based prediction of surface roughness

Table 4: Input process parameters for testing trials

Test trial No.	Cutting speed m/min	Feed rate mm/rev	depth of cut mm
1	250	0.22	0.50
2	420	0.11	0.75
3	710	0.11	1.00

The neural network used for obtaining the prediction model consists of three layers, namely input layer, hidden layer and output layer. The number of neurons in the input layer has been set to three depending on number of input process parameters, cutting speed, feed rate and depth of cut. Two neurons were used in the hidden layer by considering the minimum error in the prediction and one neuron was used in the output layer as there is only one output parameter, surface roughness.

V. Results And Discussion

The ANN model network for the present work has been developed with the help of ANN based WEKA machine learning tool. The architecture of the network is as shown in the figure 2. It consists of three inputs, cutting speed, feed rate and depth of cut and one output, surface roughness.

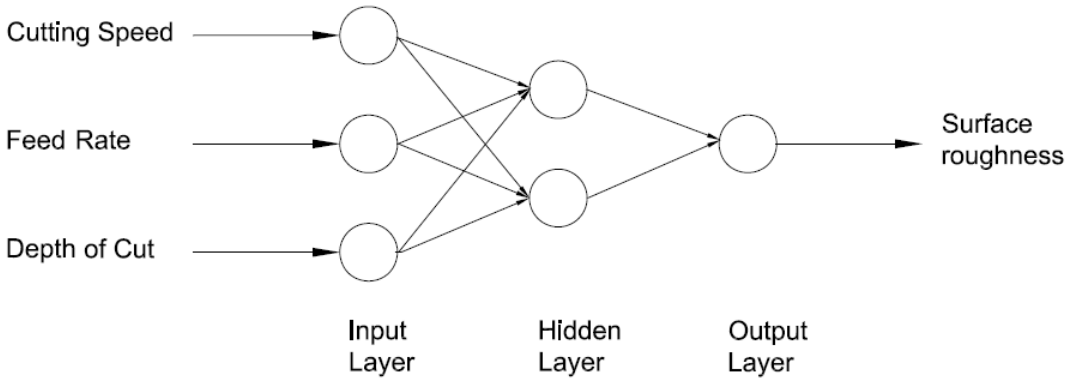

Figure 2: ANN prediction model for surface roughness

The developed ANN prediction model was successfully used to predict the surface roughness for the trials as per Table 4.The surface roughness for the test trials were also measured physically with the help of SURFCOM 130A instrument. Table 5 gives the results in terms of predicted value, measured value and percentage of error for the surface roughness of the specimens.

Table 5: Comparison of measured value and predicted value

Test trial No.	Measured Surface Roughness Microns	Predicted Surface Roughness Microns	Absolute Prediction error(APE)	Accuracy in %	Percentage of Error
1	3.86	3.65	5.44	94.55	5
2	4.5	4.82	7.11	92.88	-7
3	4.93	5.62	13.99	86	-14

The Absolute Prediction Error is calculated used the below equation,

$$\text{Absolute Prediction Error (APF)} = \frac{\text{Measured Value} - \text{ANN predicted value}}{\text{Measured value}} \text{X100}$$

Accuracy is used to check the closeness of the predicted and measured value. The accuracy is calculated using below equation.

Accuracy = (1-APE) X 100

VI. Conclusions

The present study of predicting surface roughness using ANN establishes the use of ANN as prediction tool in condition monitoring process as surface roughness is a good indicator of machine health. The development of ANN based prediction models are sure to help industries in establishing a better and efficient method of condition monitoring of machine tools leading to enhancement of its productivity. The present work can extended to include more number of process parameters covering a wider range of machining conditions.

References

Journal Papers:

[1] K. Adarsh Kumar, Ch.Ratnam, BSN Murthy, B.Satish Ben, K. Raghu Ram Mohan Reddy, Optimization of surface roughness in face turning operation in machining of EN8, International Journal of Engineering Science & Advanced Technology" , Volume2, Issue4,807 – 812, 2012

[2] FarhadKolahan, Mohsen Manoochehri and Abbas Hosseini, Simultaneous optimization of machining parameters and tool geometry specifications in turning operation of AISI 1045 steel, World Academy of Science, Engineering and Technology, 2011

[3] M. Davami and M. Zadshakoyan, Investigation of Tool Temperature and Surface Quality in Hot Machining of Hard-to-Cut Materials, World Academy of Science, Engineering and Technology 22 2008

[4] Safeen Y. Kassab&Younis K. Khoshnaw, The Effect of Cutting Tool Vibration on Surface Roughness of Workpiece in Dry Turning Operation, Eng. & Technology, Vol.25, No.7, 2007.

[5] Muhammad Munawar, Nadeem A, Mufti, and Hassan Iqbal, Optimization of Surface Finish in Turning Operation by Considering the Machine Tool Vibration using Taguchi Method, Mehran University Research Journal of Engineering & Technology, Volume 31, No. 1, January, 2012.

[8] Peter Funk and Mats Jackson; Experience Based Diagnostics and Condition Based Maintenance Within Production Systems. In COMADEM 2005, The 18th International Congress and Exhibition on Condition Monitoring and Diagnostic Engineering Management, editor: David Mba, pages 7, United Kingdom, August 2005.

[9] S SAbuthakeer , P V Mohanram& G Mohan Kumar, Prediction and Control of Cutting Tool Vibration in CNC Lathe with ANOVA and ANN, International Journal of Lean Thinking, Volume 2, Issue 1, June 2011.

[10] Arnaud Devilliez& Daniel Dudzinski, Tool vibration detection with eddy current sensors in machining process and computation of stability lobes using fuzzy classifiers, Mechanical Systems & Signal Processing, Volume 21, Issue 1, Pages 441-456, January 2007.

Books:

[6] Simon Haykin., 2001, Neural Networks- A comprehensive Foundation, Second Edition.

[10] Jiawei Han and Micheline Kambar, Data mining Concepts and Techniques, Second Edition.

OPEN ACCESS

International
Journal
Of Modern Engineering Research (IJMER)

MCDM Techniques for the Selection of Material Handling Equipment in the Automobile Industry

Kavishwar Roy Gaurh[1], Imtiyaz Khan[2], M. K. Ghosh[3]
[1]*M.Tech Scholar, Industrial Engineering & Management,*
[2]*Senior Lecturer, Department of Mechanical Engineering*
[3]*Professor, Department of Mechanical Engineering MIT Mandsaur, 458001*

Abstract: *Material Handling Equipments are utilized in different shops of an automobile industry. For culling congruous Material Handling Equipment, it is felt that some Multi Criteria Decision Making Methods must be used due to their ability of converting an intricate quandary to a paired comparison. These methods are predicated on some relative Criteria and Sub-criteria. Certain methods such as; Analytic Hierarchy Process (AHP), Fuzzy Analytic Hierarchy Process (FAHP), and Technique for Order Preference by Similarity to Ideal Solution (TOPSIS) Method have to be utilized for solving the quandary of Material Handling Equipment cull in different shops of automobile industry. For solving these quandaries, some criteria (Material, Move, and Method) are culled.*
The main conclusions drawn from this study are that, Method criteria is more consequential for culling Material Handling Equipment, and Conveyor System is more efficient and precise Equipment for Handling the Material in shop floor of any automobile industry. The focus of this research is in the area of Cull of Material Handling Equipment in automobile industry. Cull of congruous Material Handling Equipment is very paramount for reducing manufacturing cycle time, and cost of manufacturing.

Key Words: *Material Handling, Analytic Hierarchy Process , Fuzzy Analytic Hierarchy Process and Techniaue for Order Preference bv Similaritv to Ideal Solution.*

I. Introduction

Material Handling is the field concerned with solving the pragmatic problems involving the movement, storage in a manufacturing plant or warehouse, control and protection of materials, goods and products throughout the processes of cleaning, preparation, manufacturing, distribution, consumption and disposal of all related materials, goods and their packaging. The focus of studies of Material Handling course work is on the methods, mechanical equipment, systems and related controls used to achieve these functions. The material handling industry manufactures and distributes the equipment and services required to implement material handling systems, from obtaining, locally processing and shipping raw materials to utilization of industrial feed stocks in industrial manufacturing processes. Material handling systems range from simple pallet rack and shelving projects, to complex conveyor belt and Automated Storage and Retrieval Systems (AS/RS); from mining and drilling equipment to custom built barley malt drying rooms in breweries. Material handling can also consist of sorting and picking, as well as automatic guided vehicles.

The automotive industry is involved in the design, development, manufacturing, marketing and sale of motor vehicles. The automobile industry plays an important role in overall business cycle developments. The automobile industry is having a strong multiplier effect on the growth of a country. It plays a major role in developing transport sector in one hand and help industrial sector on the other to grow faster and thereby generate a significant employment opportunities.

II. Literature Review

There are some Criteria and Sub-criteria that can be used for solving the problem of Material Handling Equipment Selection in Automobile Industry.:-

1. Material: - This is most important criteria for material handling equipment selection. One should know about what type of material is required for handling.
2. Move: - It is necessary to know about when and where the material is to be moved.
3. Method: - it is also important to select the most appropriate and efficient method for handling the material. Selection of effective method minimizes the cost of production and consume less time.

The material handling principles provide fundamentals of material handling practices.
Planning principle
Standardization principle
Work principle
Ergonomic principle
Unit load principle:-
Space utilization principle
System principle
Automation principle
Environment principle
Life cycle cost principle

III. The Analytic Hierarchy Process

The AHP was developed in the 1980s by Saaty. It is a systematic decision making method which includes both qualitative and quantitative techniques.
The application of the AHP to the complex problem usually involves four major steps :-

1. Break down the complex problem into a number of small constituent elements and then structure the elements in a hierarchical form.
2. Make a series of pair wise comparisons among the elements according to a ratio scale.
3. Use the eigenvalue method to estimate the relative weights of the elements.
4. Aggregate these relative weights and synthesize them for the final measurement of given decision alternatives.

Various steps of Analytic Hierarchy Process are as follows:-
Assessment of a_{ij} values

Value of a_{ij}	Interpretation
1	Equal importance of i and j
2	Between equal and weak importance of i over j
3	Weak importance of i over j
4	Between weak and strong importance of i over j
5	Strong importance of i over j
6	Between strong and demonstrated importance of i over j
7	Demonstrated importance of i over j
8	Between demonstrated and absolute importance of i over j
9	Absolute importance of i over j

1. State the problem and define the objective.
2. Develop the hierarchy from the top through the intermediate levels to the lowest level of the hierarchy.
3. Construct a pair-wise comparison matrix using a scale of relative importance. Determine the maximum Eigen value λ_{max} that is the average of matrix.
4. Calculate the consistency index CI = $(\lambda_{max} - n) / (n - 1)$. The smaller the value of CI, the smaller is the deviation from the consistency.
5. Calculate the consistency ratio CR = CI/RI. Usually, a CR of 0.1 or less is considered as acceptable.
6. Compare the pair-wise alternatives with respect to how much better they are in satisfying each of the attributes.
7.

IV. The Fuzzy AHP Method

The fuzzy AHP technique can be viewed as an advanced analytical method developed from the traditional AHP. Despite the convenience of AHP in handling both quantitative and qualitative criteria of multi-criteria decision making problems based on decision maker's judgments, fuzziness and vagueness existing in many decision-making problems may contribute to the imprecise judgments of decision makers in conventional AHP approaches. So, many researchers who have studied the fuzzy AHP which is the extension of Saaty's theory, have provided evidence that fuzzy AHP shows relatively more sufficient description of these kind of decision making processes compared to the traditional AHP methods.

In complex systems, the experiences and judgments of humans are represented by linguistic and vague patterns. Therefore, a much better representation of this linguistics can be developed as quantitative data; this type of data set is then refined by the evaluation methods of fuzzy set theory. On the other hand, the AHP

method is mainly used in nearly crisp (non-fuzzy) decision applications and creates and deals with a very unbalanced scale of judgment. Therefore, the AHP method does not take into account the uncertainty associated with the mapping. The AHP's subjective judgment, selection and preference of decision-makers have great influence on the success of the method. The conventional AHP still cannot reflect the human thinking style. Avoiding these risks on performance, the fuzzy AHP, a fuzzy extension of AHP, was developed to solve the hierarchical fuzzy problems.

Various steps used in fuzzy AHP are as follows:-

1. Determine objective and choosing alternatives.
2. Determines criteria to be used in the ranking process.
3. Structuring decision hierarchy.
4. Approved decision hierarchy.
5. Assigning weights to criteria and alternatives via FAHP.
6. Approving weights used.
7. Ranking the alternatives.
8. Choosing the highest ranking from the set of alternatives.

Table 1 Proposed TFN and linguistic variables (Supiah et al., 2005)

Saaty's scale of relative importance	Definition	Triangular Fuzzy Number (TFN)	Linguistic variables
1	Equal importance	(1,1,1)	Least importance
3	Moderate importance of one over another	(2,3,4)	Moderate importance
5	Essential or strong importance	(4,5,6)	Essential importance
7	Demonstrated importance	(6,7,8)	Demonstrated importance
9	Extreme importance	(9,9,9)	Extreme importance
2,4,6,8	Intermediate values between two adjacent judgements	(1,2,3), (3,4,5), (5,6,7) and (7,8,9)	Intermediate values between two adjacent judgements

V. Technique for Order Preference by Similarity to Ideal Solution (TOPSIS) Method

TOPSIS (Technique for Order Preference by Similarity to Ideal Solution) was developed by Hwang and Yoon.

This method considers three types of attributes or criteria:-

- Qualitative benefit attributes/criteria.
- Quantitative benefit attributes.
- Cost attributes or criteria.

TOPSIS assumes that we have m alternatives (options) and n attributes/criteria and we have the score of each option with respect to each criterion.

The basic concept of this method is that the selected best alternative should have the shortest distance from the ideal solution and the farthest distance from the negative-ideal solution in a geometrical sense. TOPSIS assumes that each attribute has a tendency toward monotonically increasing or decreasing utility. Therefore, it is easy to locate the ideal and negative-ideal solutions.

Various steps used in TOPSIS method are as follows:

1. Construct normalized decision matrix. This step transforms various attribute dimensions into non-dimensional attributes, which allows comparisons across criteria. Normalize scores or data as follows:

$r_{ij} = x_{ij} / (\Sigma x^2_{ij})^{1/2}$ for i = 1, …, m; j = 1, …, n.

2. Construct the weighted normalized decision matrix. Assume we have a set of weights for each criteria w_j for j = 1,…n. Multiply each column of the normalized decision matrix by its associated weight. An element of the new matrix is:

$v_{ij} = w_j \times r_{ij.}$

3. Determine the ideal and negative ideal solutions.

Ideal solution-

$A^* = \{ v_1^*, \ldots, v_n^* \}$, where

$v_j^* = \{ \max (v_{ij}) \text{ if } j \in J ; \min (v_{ij}) \text{ if } j \in J' \}$

Negative ideal solution-

$A' = \{ v_1', \ldots, v_n' \}$, where
$v' = \{ \min (v_{ij}) \text{ if } j \in J ; \max (v_{ij}) \text{ if } j \in J' \}$
4. Calculate the separation measures for each alternative.
The separation from the ideal alternative is:
$S_i^* = [\Sigma (v_j^* - v_{ij})^2]^{½}$ $i = 1, \ldots, m.$
Similarly, the separation from the negative ideal alternative is:
$S'_i = [\Sigma (v_j' - v_{ij})^2]^{½}$ $i = 1, \ldots, m.$
5. Calculate the relative closeness to the ideal solution C_i^*
$C_i^* = S'_i / (S_i^* + S'_i)$, $0 < C_i^* < 1$
Select the option with C_i^* closest to 1.

VI. Numerical analysis

6.1 Body Shop

a) Analytic Hierarchy Process

Table 6.1 **Comparison matrix for Criteria-**

	Material	Move	Method	Priority Weights
Material	1	1/5	1/6	0.081
Move	5	1	1/2	0.342
Method	6	2	1	0.577

b) Fuzzy Analytic Hierarchy Process

Table 6.2 **Comparison matrix for Criteria-**

	Material	Move	Method
Material	(1,1,1)	(1/4,1/5,1/6)	(1/5,1/6,1/7)
Move	(4,5,6)	(1,1,1)	(1,1/2,1/3)
Method	(5,6,7)	(1,2,3)	(1,1,1)

c) Technique for Order Preference by Similarity to Ideal Solution (TOPSIS) Method:-

The calculation of TOPSIS method is as follows:-

Table 6.3 **Decision matrix for Alternatives-**

Alternative/Criteria	Material (0.081)	Move (0.342)	Method (0.577)
Conveyor	7	4	9
Industrial Truck	6	8	5
Hoist	5	6	7

6.2 Paint Shop

a) Analytic Hierarchy Process:-

The calculation of AHP method is as follows:-

Table 6.4 **Comparison matrix for Criteria-**

	Material	Move	Method	Priority Weights
Material	1	1/5	1/6	0.078
Move	5	1	1/3	0.287
Method	6	3	1	0.635

b) Fuzzy Analytic Hierarchy Process:-

Table 6.5 **Comparison matrix for Criteria-**

	Material	Move	Method
Material	(1,1,1)	(1/4,1/5,1/6)	(1/5,1/6,1/7)
Move	(4,5,6)	(1,1,1)	(1/2,1/3,1/4)
Method	(5,6,7)	(2,3,4)	(1,1,1)

c) Technique for Order Preference by Similarity to Ideal Solution (TOPSIS) Method:-

Table 6.6 **Decision matrix for Alternatives-**

Alternative/Criteria	Material (0.078)	Move (0.287)	Method (0.635)
Conveyor	8	3	9
Industrial Truck	4	7	6
Cranes & Hoist	6	5	4

6.3 Trim Shop

a) Analytic Hierarchy Process:-

The calculation of AHP method is as follows:-

Table 6.7 **Comparison matrix for Criteria-**

	Material	Move	Method	Priority Weights
Material	1	1/5	1/6	0.078
Move	5	1	1/3	0.287
Method	6	3	1	0.635

b) Fuzzy Analytic Hierarchy Process:-

Table 6.8 **Comparison matrix for Criteria-**

	Material	Move	Method
Material	(1,1,1)	(1/4,1/5,1/6)	(1/5,1/6,1/7)
Move	(4,5,6)	(1,1,1)	(1/2,1/3,1/4)
Method	(5,6,7)	(2,3,4)	(1,1,1)

c) Technique for Order Preference by Similarity to Ideal Solution (TOPSIS) Method:-

Table 6.9 **Decision matrix for Alternatives-**

Alternative/Criteria	Material (0.078)	Move (0.287)	Method (0.635)
Conveyor	5	6	8
Forklift	9	7	4
Hoist	7	5	6

6.4 Final Assembly Shop

a) Analytic Hierarchy Process:-

Table 6.10 **Comparison matrix for Criteria-**

	Material	Move	Method	Priority Weights
Material	1	1/5	1/6	0.078
Move	5	1	1/3	0.287
Method	6	3	1	0.635

b) Fuzzy Analytic Hierarchy Process:-

Table 6.11 **Comparison matrix for Criteria-**

	Material	Move	Method
Material	(1,1,1)	(1/4,1/5,1/6)	(1/5,1/6,1/7)
Move	(4,5,6)	(1,1,1)	(1/2,1/3,1/4)
Method	(5,6,7)	(2,3,4)	(1,1,1)

c) Technique for Order Preference by Similarity to Ideal Solution (TOPSIS) Method:-

Table 6.12 **Decision matrix for Alternatives-**

Alternative/Criteria	Material (0.078)	Move (0.287)	Method (0.635)
Conveyor	3	6	9
Industrial Truck	7	8	4
Cranes & Hoist	5	4	6

VII. Computational Result

For Body Shop:-

Table 1 Preference Ratio and Ranking of Alternatives in Body Shop-

	AHP Method		Fuzzy AHP Method		TOPSIS Method	
Alternatives	Preference Ratio	Ranking	Preference Ratio	Ranking	Preference Ratio	Ranking
Conveyor	0.664	1	0.662	1	0.613	1
Industrial Truck	0.244	2	0.245	2	0.387	3
Hoist	0.092	3	0.093	3	0.48	2

For Paint Shop:-

Table 2 Preference Ratio and Ranking of Alternatives in Paint Shop-

	AHP Method		Fuzzy AHP Method		TOPSIS Method	
Alternatives	Preference Ratio	Ranking	Preference Ratio	Ranking	Preference Ratio	Ranking
Conveyor	0.709	1	0.71	1	0.675	1
Industrial Truck	0.09	3	0.092	3	0.515	2
Hoist	0.197	2	0.198	2	0.2	3

For Trim Shop:-

Table 3 Preference Ratio and Ranking of Alternatives in Trim Shop-

	AHP Method		Fuzzy AHP Method		TOPSIS Method	
Alternatives	Preference Ratio	Ranking	Preference Ratio	Ranking	Preference Ratio	Ranking
Conveyor	0.698	1	0.697	1	0.852	1
Industrial Truck	0.095	3	0.096	3	0.201	3
Hoist	0.206	2	0.207	2	0.458	2

For Final Assembly Shop:-

Table 4 Preference Ratio and Ranking of Alternatives in Final Assembly Shop-

	AHP Method		Fuzzy AHP Method		TOPSIS Method	
Alternatives	Preference Ratio	Ranking	Preference Ratio	Ranking	Preference Ratio	Ranking
Conveyor	0.709	1	0.71	1	0.823	1
Industrial Truck	0.09	3	0.092	3	0.278	3
Hoist	0.197	2	0.198	2	0.367	2

Thus, it is clear that the Conveyor System is more important Material Handling Equipment in the shop floor of an automobile industry.

VIII. Conclusion

Various Material Handling Equipments such as: Conveyors, Industrial Trucks, Cranes and Hoists are used in Automobile Industries. For selecting the best equipment, certain Multi Criteria Decision Making Methods (based on different criteria and sub-criteria) are employed. These methods based on pair wise comparison matrices and after calculating the weights of all selected alternatives, it can be concluded that, the Method criteria is more important for selecting Material Handling Equipment, and Conveyor System is more efficient and accurate Material Handling Equipment for any Automobile Industry.

Today various Automobile Industries are present in India for manufacturing variety of vehicles. In Automobile Industry proper and accurate handling of material is very necessary for reducing cost of manufacturing, and manufacturing cycle time. It is also important for increasing the capacity of production, and for improving the working conditions.

REFERENCES

[1] Allegri, T. H., (1981), ‘‘Materials Handling: Principles and Practice’’, CBS Publishers & Distributors, New Delhi
[2] Graehl, D., (1992), Insights into carrier control: “A Simulation of a Power and Free
[3] Hwang, C. L., and Yoon, K., (1981) “Multiple Attribute Decision Making: Methods and Applications”, Springer-Verlag, New York
[4] Momani, Amer M., and Ahmed, Abdulaziz A., (2011), “Material Handling Equipment Selection using Hybrid Monte Carlo Simulation and Analytic Hierarchy Process”, World Academy of Science, Engineering and Technology, 59
[5] Ramanathan, R., (2001), “A note on the use of the Analytic Hierarchy Process for Environmental Impact Assessment”, Journal of Environmental Management, 63, pp. 27−35
[6] Saaty, T. L., (1980), “The Analytic Hierarchy Process”, McGraw-Hill, New York
[7] Saaty, T. L., and Alexander, J., (1989), Conflict Resolution: “The Analytic Hierarchy Process”, New York: Praeger
[8] Solutions for the Automotive Industry (SAI), available at

http://www.belden.com/marketsolutions/Industrial/upload/Automotive-brochure-Hirschmann.pdf, accessed on 20th April, 2012

[9] Supiah, S., NorBaharim, H., Azmi, A. R., and Gesiri, G., (2005), "Southern Johor River Ranking Using HIPRE 3", *Proceedings of the International Conference on Reservoir Operation and River Management*, Guangzhou & Three Gorges, China

[10] Tompkins, J. A., White, Y. A., Bozer, E. H., and Frazelle, J. M., (2003), "*Facilities Planning*", New York: Wiley, pp. 137-287

[11] Zahir, S., (1999), "Clusters in group: Decision Making in the Vector Space Formulation of the Analytic Hierarchy Process", European Journal of Operational Research, 112, pp. 620−634

[12] Zeleny, M., (1982), "*Multiple Criteria Decision Making*", McGraw Hill, New York

[13] Zhu, K. J., Jing, Y., and Chang, D. Y., (1999), "A Discussion on Extent Analysis Method and Applications of Fuzzy-AHP", European Journal of Operational Research, 116, pp. 450-456

OPEN ACCESS

International
Journal
Of Modern Engineering Research (IJMER)

Buckling Analysis of Cold Formed Steel Compression Members at Elevated Temperatures

A.A.Patil[1], J.G. Solanki[2]

[1]*M.tech Student, Structural Engineering Department, Veermata Jijabai Technological Institute, India*
[2]*Asst. Professor, Structural Engineering Department, Veermata Jijabai Technological Institute, India*

Abstract: *Cold-formed steel members have been widely used in residential, industrial and commercial buildings as primary load bearing structural elements due to their advantages such as higher strength to weight ratio over the other structural materials such as hot-rolled steel, timber and concrete. However, they are susceptible to various buckling modes including local and distortional buckling. Fire safety design of building structures has received greater attention in recent times as fire events can cause loss of property and lives. Therefore it is essential to understand the fire performance of light gauge cold-formed steel structures under fire conditions. The buckling behavior of cold-formed steel compression members under fire conditions is not well investigated yet and hence there is a lack of knowledge on the fire performance of cold-formed steel compression members. Therefore, this paper deals with behavior of cold formed steel compression member under fire and to analyze the effect of fire on critical buckling load of compression member. Eigen value analysis for Lipped channel sections made of various thicknesses and both low and high strength steels was carried out through finite element method. The ultimate load carrying capacity results from experimental investigation and finite element analyses were then compared.*

Keywords: *Light gauge cold-formed steel, elevated temperatures, critical buckling load, reduced mechanical properties, finite element analysis.*

I. INTRODUCTION

In recent times light gauge cold-formed steel construction has replaced the conventional hot-rolled steel construction in many cases due to its many advantages. However, cold-formed steel structures are subjected to a more complex behavior than traditional hot-rolled steel structures. They are subjected to various buckling modes including local, distortional, and global and their interactions. Previous research was mostly concerned about local and global buckling modes and there is a wealth of knowledge on these modes at ambient temperature. [1]–[7].On the other hand, some research was mostly concerned about reduced mechanical properties of cold formed steel compression members at elevated temperatures [8],[9]. Structures can accidentally catch fire or are deliberately set on fire which can cause loss of life and property, not only because of fire but also due to the structural failure. Therefore, it is necessary to fully understand the structural behavior of light gauge cold-formed steel structures at elevated temperatures. Current knowledge on the structural behavior of light gauge cold-formed steel members under fire conditions is limited. The effects of fire conditions on the buckling behavior of light gauge cold-formed steel compression members are not known. Therefore, this research was conducted to investigate the buckling behavior of light gauge cold-formed steel compression members at ambient and elevated temperatures. This paper presents the details of an analytical study of light gauge cold-formed steel lipped channel compression members at ambient and elevated temperatures for low and high strength steels. The experiments were undertaken at varying temperatures up to 800°C by Thanuja Ranawaka [10]. The paper also describes a finite element model developed using ABAQUS for a range of lipped channel sections with various thicknesses. Finally the ultimate load carrying capacity results from experimental investigation and finite element analyses were then compared.

II. Experimental Investigation

Experimental investigations were carried out by Thanuja Ranawaka [10] for lipped channel sections made of low (G250 with the nominal yield strength of 250 MPa) and high (G550 with the nominal yield strength of 550 MPa) strength steels. The sections were designed to fail by pure distortional buckling at ambient and elevated temperatures.

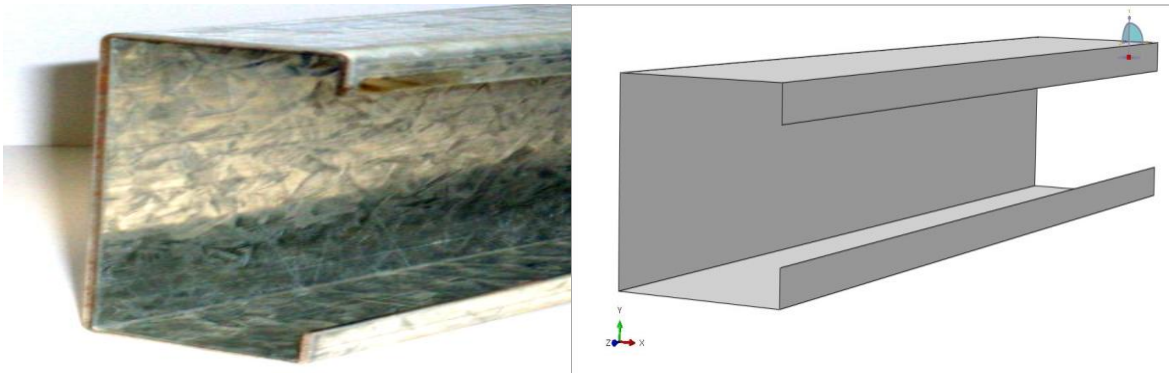

Fig. 1 Cross-section of a Lipped Channel Section

Table 1 Measured specimen dimensions

Steel grade (MPa)	Temperature °C	Web(mm) b	Flange(mm) f	Lip(mm) l	Thickness (mm)	Length (mm)
G250	20	30.84	31.6	5.7	0.79	190
	200	30.96	31.4	5.5	0.8	190.2
	350	30.92	31.4	5.45	0.79	190.1
	500	30.84	31.1	5.53	0.79	190
	650	30.82	31.1	5.41	0.79	190
	800	30.91	31.6	5.47	0.79	190.1
G550	20	31.07	31.5	5.47	0.8	190.2
	200	30.86	31.1	5.46	0.81	190
	350	30.92	30.95	5.53	0.8	189.9
	500	30.86	31.7	5.7	0.8	190.1
	650	30.8	31.7	5.48	0.8	190.2
	800	30.87	31.4	5.43	0.81	190.1

Where, b - web width, f - flange width, I-lip width

2.1 Mechanical properties

The mechanical properties have a significant effect on the behavior of light gauge cold-formed steel compression members. The mechanical properties are also essential for finite element and finite strip analyses under various temperatures. Therefore tensile coupon tests were carried out by Thanuja Ranawaka to determine the mechanical properties of light gauge cold-formed steels at ambient temperature (20°C), and obtained results are given in Table 2. The mean value of the measured Young's modulus was about 200,000 MPa for both steel grades. Table 2 values were then used in the finite element analysis.

Table 2 Mechanical properties at various temperatures

Temperature(°C)	Modulus Of Elasticity (ET)(MPa)	Yield Strength (fyT) (MPa)
20	200000	300
200	172000	283
350	130000	246
500	88000	179
650	43267	96.5
800	11647	30

Where, ET - Young's modulus at specified temperature
fyT - Yield strength at specified temperature

2.2 Finite Element Analysis

ABAQUS was used as finite element analysis tools to investigate the behavior of cold-formed steel compression members at ambient and elevated temperatures. S4R element type was selected to adequately simulate the buckling deformation and yielding of light gauge cold-formed steel compression members. A

uniformly distributed compression load i.e. Shell edge load was applied to the upper and lower nodes of the member.

A 2 mm X 2 mm mesh was selected for all the sections (see Figure 1). The column is restrained in x and y direction at both ends (u=0, v=0) and at middle only z direction is restrained (w=0).Compressive load of magnitude 1000 KN is applied at both ends as shown in (see figure 2).

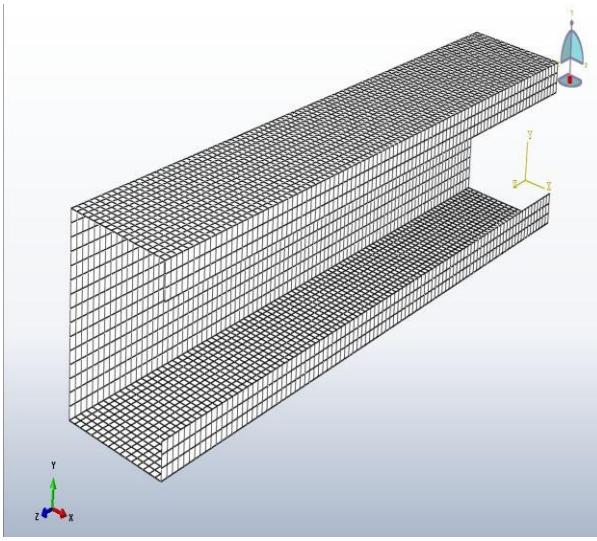

Fig.1 Finite element meshing using S4 Element

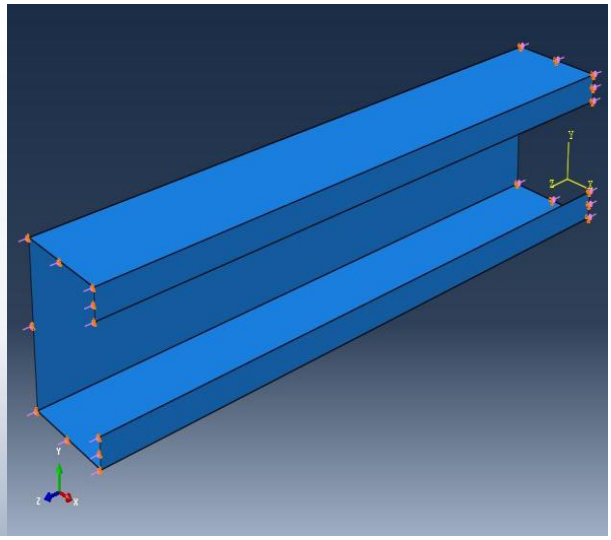

Fig.2 Loading and boundary condition

2.3 Linear Eigen Value Buckling Analysis

Buckling is that mode of failure when the structure experiences sudden failure when subjected to compressive stress. When a slender structure is loaded in compression, for small loads it deforms with hardly any noticeable change in the geometry and load carrying capacity. At the point of critical load value, the structure suddenly experiences a large deformation and may lose its ability to carry load. This stage is the buckling stage. In Abaqus, Linear Eigen Value Buckle step is used to calculate critical buckling load which is nothing but ultimate load. Two types of analysis were employed by using the developed finite element model: elastic buckling and nonlinear static analyses. Elastic buckling analysis gives the elastic buckling loads and corresponding buckling modes. The lowest Eigen vector obtained from elastic buckling analysis was used to calculate the critical buckling load.

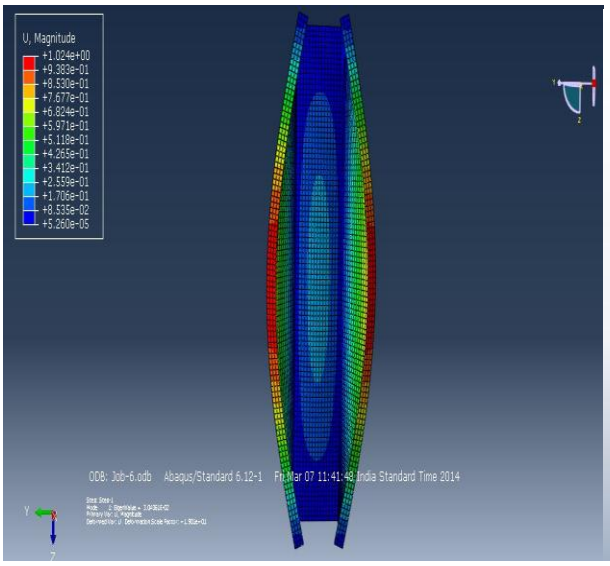

Fig.3a) First Buckling mode of column section in Abaqus at ambient temperature

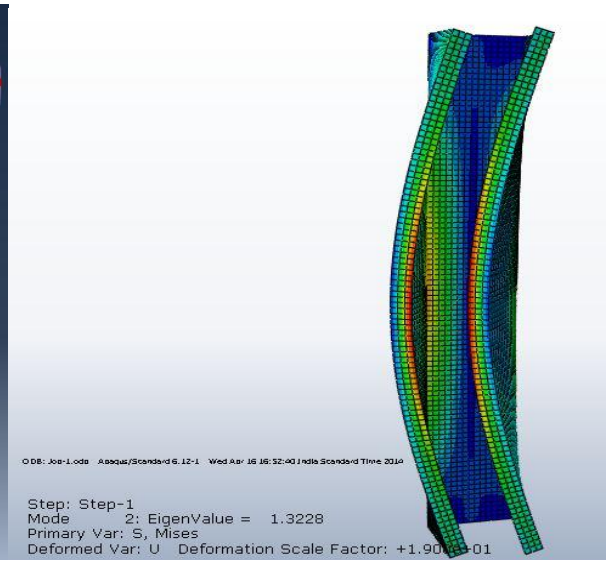

Fig.3b) First Buckling mode of column section in Abaqus at elevated temperature

III. Results And Discussion

Table 1 Ultimate loads of 0.6 mm G250 steel columns

Temp. (°C)	Experimental Ultimate Load (KN)	FEA Ultimate Load (KN)
20	14.2	14.53
200	12.5	11.95
350	9.8	8.92
500	6.75	6.19
650	3.38	2.96
800	0.93	0.8

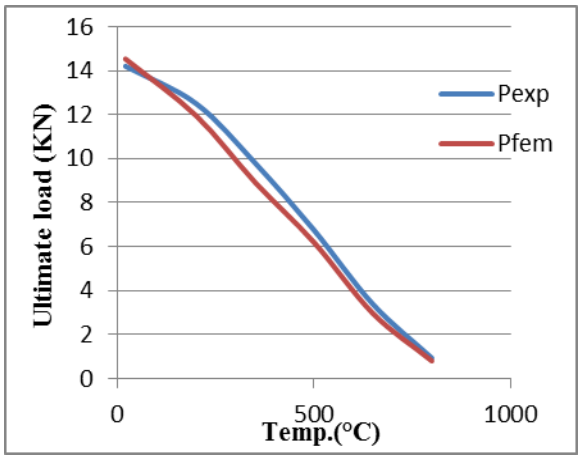

Fig.4 Ultimate load vs. temperature for 0.6 mm G250 steel column

Table 2 Ultimate loads of 0.6 mm G550 steel columns

Temp. (°C)	Experimental Ultimate Load (KN)	FEA Ultimate Load (KN)
20	16.55	15.32
200	14.6	13.20
350	11.65	10.76
500	8.35	7.38
650	4.35	4.01
800	1.14	1

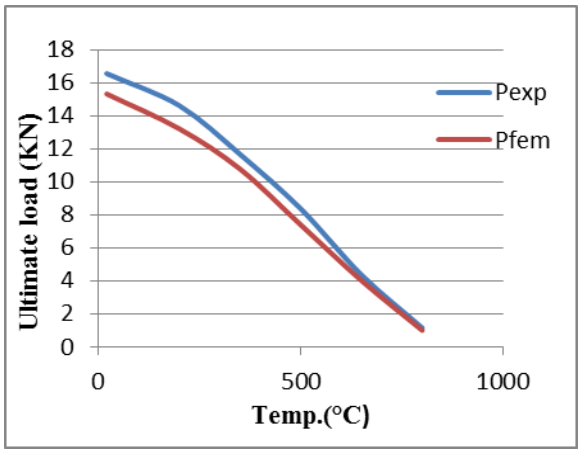

Fig.5 Ultimate load vs. temperature for 0.6 mm G550 steel column

Table 3 Ultimate loads of 0.8 mm G250 steel columns

Temp. (°C)	Experimental Ultimate Load (KN)	FEA Ultimate Load (KN)
20	20.8	20
200	17.7	17
350	15.6	13
500	11.46	9.5
650	4.1	3.7
800	1.4	1.3

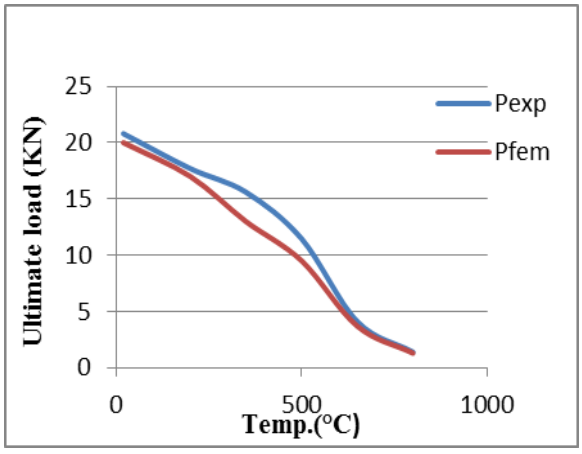

Fig.6 Ultimate load vs. temperature for 0.8 mm G250steel column

Table 4 Ultimate loads of 0.8 mm G550 steel columns

Temp. (°C)	Experimental Ultimate Load (KN)	FEA Ultimate Load (KN)
20	27.43	25.43
200	26.5	24.67
350	23.1	21.2
500	13.2	11
650	4.25	5
800	1.74	1.39

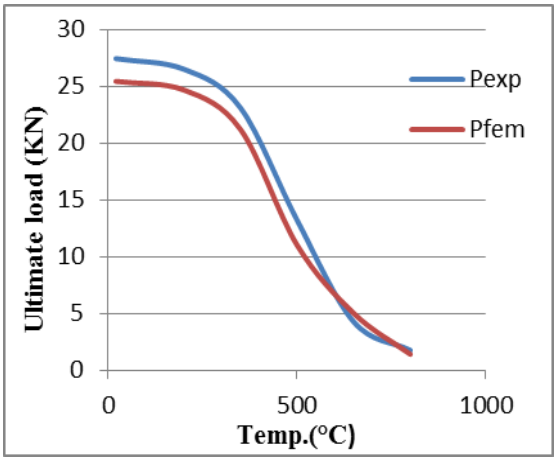

Fig.7 Ultimate load vs. temperature for 0.8 mm G550 steel column

Table 5 Ultimate loads of 0.95 mm G250 steel columns

Temp. (°C)	Experimental Ultimate Load (KN)	FEA Ultimate Load (KN)
20	26.89	25.67
200	24.64	23.89
350	20.29	19.34
500	14.24	13.47
650	7.26	7.08
800	2.02	2

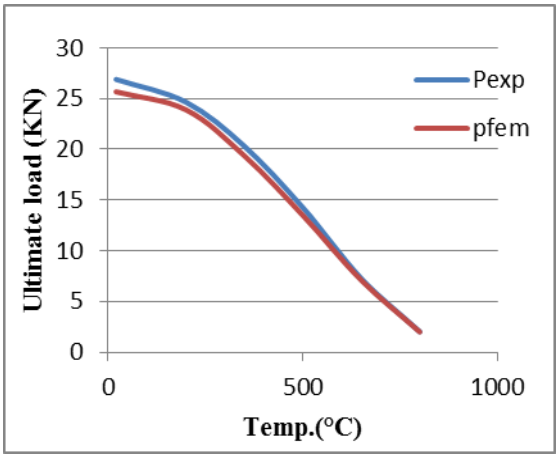

Fig.8 Ultimate load vs. temperature for 0.95 mm G250 steel column

Table 6 Ultimate loads of 0.95 mm G550 steel columns

Temp. (°C)	Experimental Ultimate Load (KN)	FEA Ultimate Load (KN)
20	36.35	34.97
200	31.79	30.23
350	24.8	22.56
500	17.16	15.33
650	9.07	8.87
800	2.4	1.87

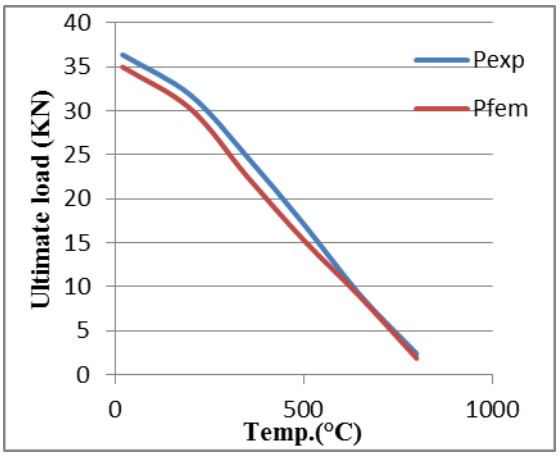

Fig.9 Ultimate load vs. temperature for 0.95 mm G550 steel column

IV. CONCLUSIONS

The most valuable outcomes obtained from this research are as follows:

1) Mechanical properties deteriorate at different rates at elevated temperatures and it appears that (ET/fyT) ratio has an effect on the buckling capacity.
2) Ductility of cold-formed steels was noted to increase with increasing temperature with significant increases beyond 500°C. However, the lowest ductility was observed at 200°C. A significant increase in the ductility was seen for the temperatures beyond 500°C.
3) The ultimate loads of the low and high strength steel specimens at varying temperatures are compared and it can be seen that the strength reduction with increasing temperature was not uniform. The compression strength reduced at a lower rate at low temperatures (up to 350°C), but reduced at a higher rate at high temperatures (350°C to 650°C).
4) It was found that ambient temperature results showed that columns failed by both flanges moving inwards or outwards (see figure 3a) while many columns failed due to one flange moving outward while the other flange moving inward at elevated temperatures (see figure 3b).

REFERENCES

[1] Chen, J. and Young, B. (2006a), "Design Cold-formed Steel Lipped Channel Columns at Elevated Temperatures", Engineering Structures, Vol. 29. pp 2445-2456.
[2] Chen, J. and Young, B. (2006b), "Corner Properties of Cold-Formed Steel Sections at Elevated Temperatures", Thin-Walled Structures, Vol. 44, Issue 2, pp 216-223.
[3] Chen, J. and Young, B. (2007a), "Experimental investigation of cold-formed steel material at elevated temperatures", Thin-Walled Structures, Volume 45, Issue 1, pp 96-110.
[4] Chen, J. and Young, B. (2007b), "Cold-formed steel lipped channel columns at elevated temperatures", Engineering Structures, Volume 29, Issue 10, pp 2445-2456.
[5] Dolamune Kankanamge (2009), "Flexural Behaviour of Cold-formed Steel Beams at Elevated Temperatures", PhD thesis, Queensland University of technology, Brisbane, Australia.
[6] Lee, J. (2004), "Local Buckling Behaviour and Design of Cold-Formed Steel Compression Members at Elevated Temperatures", PhD thesis, Queensland University of Technology, Brisbane, Australia.
[7] Liu, Y. and young, B. (2003), "Buckling of Stainless Steel Square Hollow Section Compression Members", Journal of Construction Steel Research, Vol. 59, Issue 2, pp165-177.
[8] Makelainen, P. and Miller, K. (1983), "Mechanical Properties of Cold-formed Galvanized Steel Z32 at Elevated temperatures", Helsinki University of technology, Finland.
[9] Ranawaka, T. and Mahendran, M. (2009), "Experimental study of the mechanical properties of light gauge cold-formed steels at elevated temperatures", Fire Safety Journal, Volume 44, Issue 2, pp, Pages 219-229
[10] Thanuja Ranawaka and Mahen Mahendran (2004), "Design of Cold-Formed Steel Compression Members Subject to Distortional Buckling at Elevated Temperatures", Seventeenth International Specialty Conference on Cold-Formed Steel Structures Orlando, Florida, Vol. 59, pp. 1517-1532.

OPEN ACCESS

International
Journal
Of Modern Engineering Research (IJMER)

A Review of FDM Based Parts to Act as Rapid Tooling

Imtiyaz Khan[1], Dr. A. A. Shaikh[2]

[1]*Senior Lecturer, Mechanical Engineering Department, MIT Mandsaur, M.P, India*
[2]*Professor, Mechanical Engineering Department, Sardar Vallabhbhai National Institute of Technology, Surat, Gujarat, India*

Abstract: *Fused Deposition Modeling (FDM) is one from basic Rapid Prototyping (RP) technologies used in technical practice. In this contribution are presented basic information about parameters such as layer thickness, part build orientation, raster angle, raster width and air gap. This study provides insight into complex dependency of strength on process parameters. In this paper microphotographs are used to show the mechanism of failure. The major reason for weak strength is attributed to distortion within or between the layers.Developing a curved layer deposition methodology can improve part quality by reduced lamination, reduction in the staircase effect which leads to improved dimensional accuracy of the part. Less effort has been made to increase the range of FDM materials to include metals or metal based composites with the help of metal based composite direct rapid tooling will allow fabrication of injection moulding dies and inserts with desired thermal and mechanical properties suitable for using directly in injection moulding machines for short term or long term production runs.*

Keywords: *Rapid Prototyping; Fused Deposition Modeling; Rapid Tooling; Staircase Effect.*

I. Introduction

As a matter of fact the new market realistic require faster product development and reduced time to meet market demand (like: high quality, greater efficiency, cost reduction and a ability to meet environmental and recycling objectives) to reduce the product development time and cost of manufacturing, new technology of Rapid Prototyping (RP) has been developed. Rapid Prototyping Manufacturing (RPM) has been widely used in the modern industry, but it is difficult to achieve higher precision parts in FDM currently. Therefore, how to improve part quality can be said as hotspot in industrial applications of RPM, especially when rapid prototyping parts will be used as die, injection molding and EDM electrode, etc., the quality of which plays decisive role to that of final product in mass production. Stereo lithography (SL), selective laser sintering (SLS), fused deposition modeling (FDM) and laminated object manufacturing (LOM) is four relatively matured RPM processes that dominate the current commercial market [1-3], among which FDM, arepresentative rapid prototyping technology (RPT) with no use of toxic materials, has been increasingly widely used in offices. But now the FDM systems currently only fabricate parts in elastomers, ABS and investment casting wax using the layer by layer deposition of extruded materials through a nozzle using feedstock filaments from a spool [4]. Most of the parts fabricated in these materials can only be used for design verification, form and fit checking and patterns for casting processes and medical applications[5]. For FDM, the two concerns are how to develop new metal materials that can directly manufacture metal parts used in tooling, etc., and how to improve dimension accuracy. As to developing new metal materials, literature [6] presented the detailed formulation and characterization of the tensile properties of the various combinations of the nylon type matrix consisting of iron particles, and the feedstock filaments of this composite have been produced and used successfully in the unmodified FDM system for direct rapid tooling of injection moulding inserts, while literature [7] presented an investigation on thermal and mechanical properties of new metal-particle filled ABS (acrylonitrile-butadine-styrene) composites for applications in FDM rapid prototyping process. As to improving dimensional accuracy, literature [8] presented experimental investigations on influence of important process parameters viz. layer thickness, part orientation, raster angle, air gap, and raster width along with their interactions on dimensional accuracy of FDM processed ABS400 part, and it is observed that shrinkage is dominant along length and width direction of built part, while literature [9] presented a powerful tool, the Taguchi method, to design optimization for quality. In this study, not only can the optimal process parameters for FDM process be obtained, but also the main process parameters that affect the performance of the prototype can be found. Although great progress has been made in this field, most of the literatures focus only on improving dimensional accuracy. In fact, the part errors in FDM are classified into dimension error, shaped error and surface roughness. This paper, taking FDM

for example, aims to analyze the reasons which lead to errors and propose corresponding measures to improve part accuracy.

II. Previous Work Done

2.1. FDM Machine Structure

FDM mainly involves a feeder role or coil which is perpetually fed into an extrusion head or nozzle. Before the material reaches the nozzle, it is heated to soften the material to a molten state when it can be deposited onto the platform [10]. This is done with the avail of heating elements in nozzle which melts the material. This nozzle is controlled by a computer availed manufacturing package which can be habituated to move the nozzle in horizontal, vertical directions. As the molten material ejects out of the nozzle, it is then spread onto the platform in the desired shape as a layer. The deposition platform is then lowered to a height equipollent to one layer height of the component and the deposition process is reiterated over the anteriorly deposited layer [11]. This process is reiterated layer by layer starting from the base and worked its way to the top to consummate the whole model

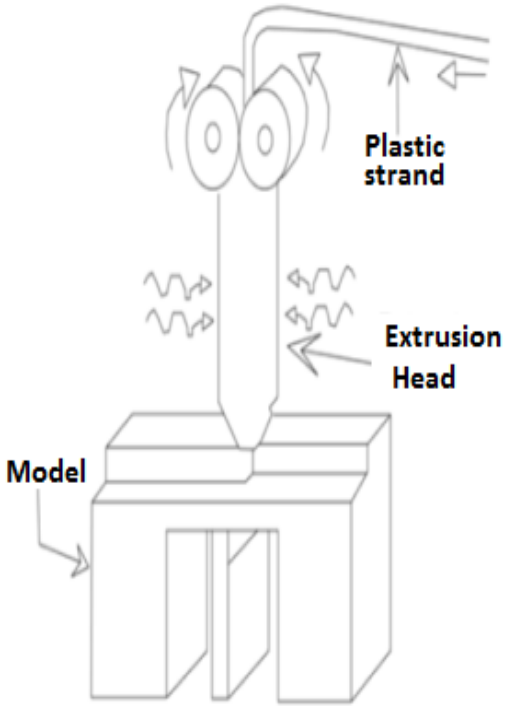

Fig. 2.1.1 FDM Schematic [12]

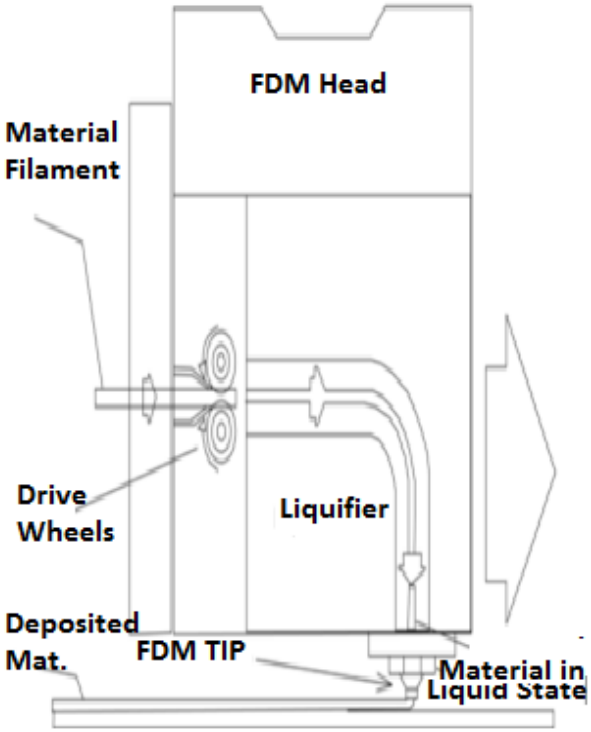

Fig. 2.1.2 Deposition Head [12]

The deposition head of the machine mainly consists of the drive block, the tip and the heating compartment. The raw material is fed into the machine with the avail of the drive blocks which contain wheels mounted on back of head [13]. These drive blocks are responsible for loading and unloading of the raw materials from the rolls and can be computer controlled for precision. A heating element is utilized as bubbles wrap for the heating compartment and withal blends in an L shape angle. This is done to divert the horizontal flow of the filament to a vertical direction which can be then utilized as an area to melt the material. External threading is done on the tips so that they can be screwed in with the internal screws on the heating compartment [14].

2.2. Process parameters

When preparing to build FDM parts many fabrication parameters are needed. To achieve optimum quality, parameters are set differently according to requirements of applications. Some parameters are -

a. Orientation: Part builds orientation or orientation referrers to the inclination of part in a build platform with respect to X, Y, Z axis. Where X and Y-axis are considered parallel to build platform and Z-axis is along the direction of part build.

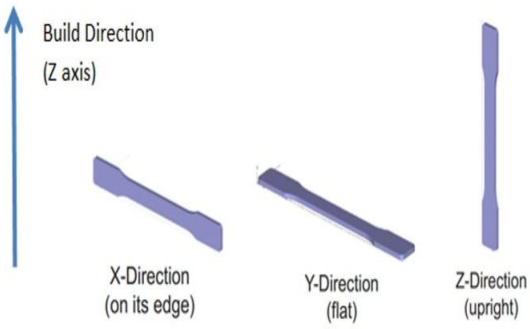

Fig. 2.2.1 Orientation [15]

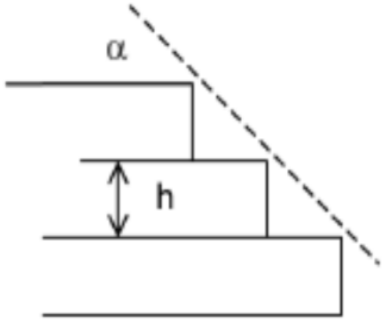

Fig. 2.2.2 Layer Thickness [16]

b. **Layer Thickness:** Slice height is the thickness of each layer measured in the vertical or Z direction as shown in fig. Varying the slice height would most likely have the same effect as varying the bead width of ABS plastic.

c. **Raster Angle:** Denotes the raster orientation which is measured from the X-axis on the bottom part layer as shown in figure 3.7. Also it refers to the direction of the beads of material (roads) relative to the loading of the part. The deposited roads can be built at different angles to fill the interior part. The effect of this filling according to the raster angle applied was also investigated, where using loose angles at (45o/90o) and tighter angles at (45o/-45o) of deposited roads.

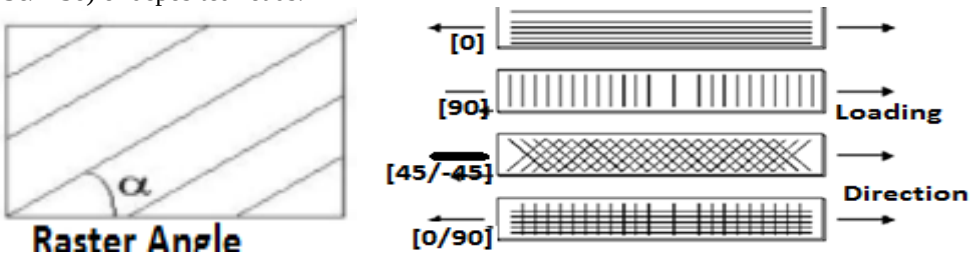

(a) (b)

Fig. 2.2.3 (a) & (b) Raster Angle [17-18]

d. Part Raster Width (raster width): Denotes the raster width or road width which refers to the width of the deposition path related to tip size. Also refers to the tool path width of the raster pattern used to fill interior regions of the part curves as shown in figure 3.5. Narrow and wide filling pattern (roads) were considered to be examined [18].

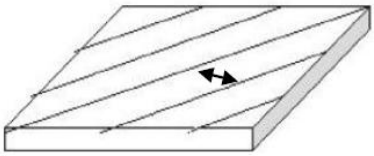

Fig. 2.2.4 Raster Width [17]

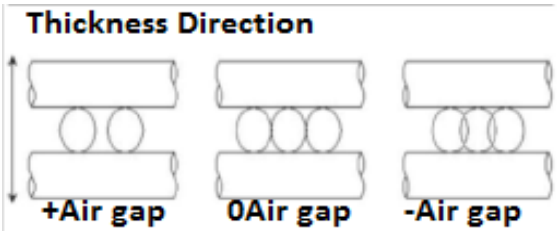

Fig. 2.2.5 Air gap [17]

e. Raster to Raster gap (air gap): Air gap is the space between the beads of FDM material as shown in Fig.2.2.5. The default is zero, meaning that the bead just touches. It can be modified to leave a positive gap, which means that the beads of material do not touch. The positive gap results in a loosely packed structure that builds rapidly. The air gap value can also be modified to leave a negative gap, meaning that two beads partially occupy the same space. This results in a dense structure, which requires a longer build time.

From the published literature on FDM it appears that the [19] heat is dissipated by conduction and coerced convection and the reduction in temperature caused by these processes forces the material to expeditiously solidify onto the circumventing filaments. Bonding between the filaments is caused by local remelting of anteriorly solidified material and diffusion. This results in uneven heating and cooling of material and develops non-uniform temperature gradients. As a result, uniform stress will not be developed in the deposited material and it may not regain its pristine dimension thoroughly. Speed at which nozzle is depositing the material may alter the heating and cooling cycle and results in different degree of thermal gradient and thus withal affects the component precision [20]. At lower slice thickness, nozzle deposition speed is more gradual as

compared to higher slice thickness. Withal during deposition, nozzle ceases depositing material in arbitrary manner (in between depositing a layer and after consummately depositing a layer) and return to accommodation location for tip cleaning. While depositing the material at the turns near the boundary of part, nozzle speed has to be decremented and then increase to uniform speed [21]. If deposition path length is minuscule, this will result in non-uniform stress to build up especially near the component boundary. The pattern used to deposit a material in a layer has a consequential effect on the resulting stresses and deformation. Higher stresses will be found along the long axis of deposition line. Therefore, short raster length is preferred along the long axis of part to reduce the stresses [22]. Stress accumulation additionally increase with layer thickness and road width [23]. But the thick layer additionally designates fewer layers, which may reduce the number of heating and cooling cycles. Withal, a more minuscule road width will input less heat into the system within the designated period of time but requires more loops to fill a certain area. More loops betokens more time required for deposition of single layer and more non uniform nozzle speed. This will keep the deposited material above its desired temperature for regaining its pristine shape and in the mean time incipient material will be deposited and contraction of antecedently deposited material will be constrained. The gap between two rasters in a single layer and voids between rasters (Fig. 2.2.7) of two adjacent layers withal effect the heat dissipation and thus may decrease the residual stress. For the case of thickness, it seems that increase is mainly caused due to obviation of shape error and positive slicing method [24,25]. Consider (Fig.2.2.8) which shows that height of part (H) is function of its inclination (h) with reverence to base (build platform), length (L) and thickness (T). Diffusion of material between neighbouring rasters additionally engenders the bump (Fig. 2.2.9) because of overfilling at contact area which results in uneven layer.

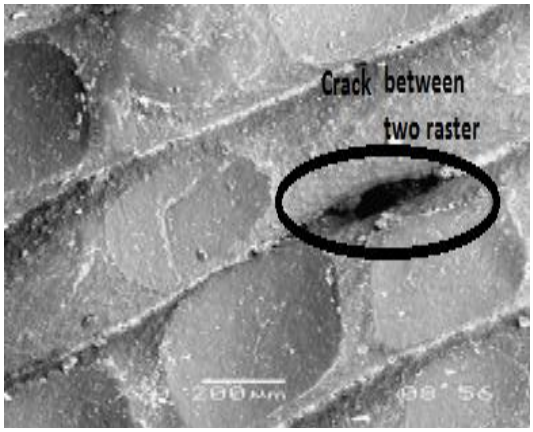

Fig.2.2.6. Crack between two rasters [9]

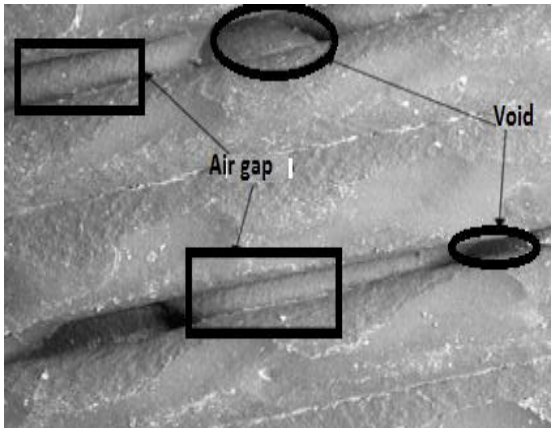

Fig.2.2.7. Air gap [9]

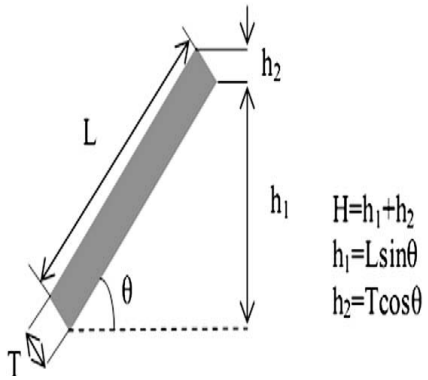

Fig. 2.2.8. Orientation of part with respect to the base (H is height of part) [9]

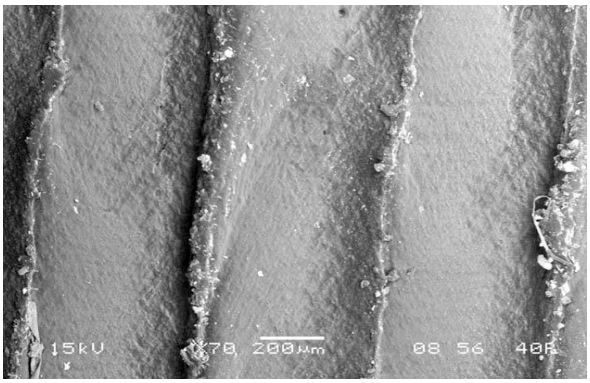

Fig.2.2.9. Overfilling at the contact of two raster [9]

2.3. Stair Case Effect

In FDM printing of components by stacking layer one on top of other. In this method rate of product development expeditious but bring some shortfalls additionally. One of the main areas of inhibition which particularly subsist in FDM is the "stair case effect". This is mainly due to the deposition method of the process, printing of horizontal layers one on top of the other. The CAD model is first converted into the STL format which is then sliced in flat horizontal layers with each layer having its own shape. The STL file is fundamentally is one which consists of all the points which make up the shapes in each layer and all layers when put together stacks up as a model. The extrusion head, which is responsible for depositing the material on the surface layer

by layer, follows the path information stored in the STL file and builds the whole part with an effect in which curved surfaces appear to be a little short or over shoot the genuine dimension of the component. "Stair case" effect, shown in the fig. 2.3.1

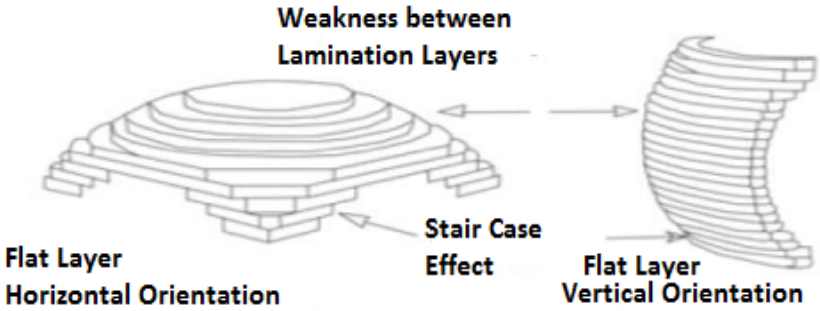

Fig.2.3.1 Stair case effect [12]

Stair case effect is more prominent when a more sizably voluminous diameter nozzle is utilized for material deposition. The straightforward solution to this situation would be to utilize low diameter nozzle which will print thin layers. In order to achieve more preponderant finish and reduced stair case effect, it would take more number of layers to print the same part which results in time consumption. To achieve high precision & surface finish prefer reduced layer thickness, as shown in the fig. 2.3.2 [12].

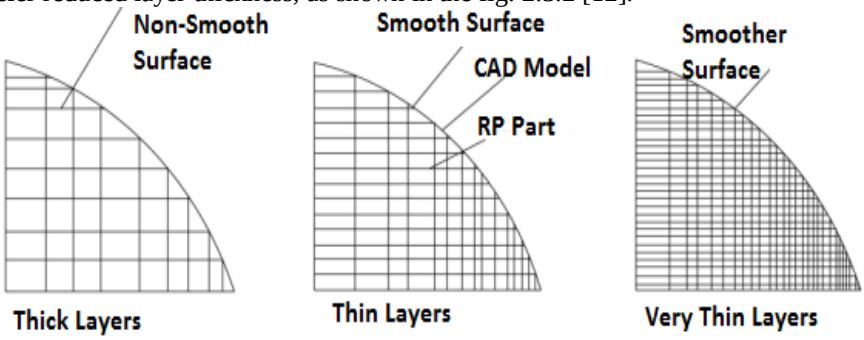

Fig. 2.3.2 Layers and finish quality [12]

2.4. Application of RP for Tooling

Today a great demand subsists on RPT-technologies to fortify product development by tooling or tooling inserts that sanction the engenderment of more astronomically immense series and at the same time enables the engenderment of those components in materials and with technologies akin to the ones used later for series engenderment runs. The most eminent advantage is the integration of engenderment orchestrating and testing within the product development period [26]. These processes can be relegated into two categories of Direct Rapid Tooling and Indirect Rapid Tooling, Fig.2.4.2 predicated on the number of intermediate steps taken along with the mundane RP operations to build the final implement. Direct Rapid Tooling involves fabrication of rapid tooling inserts directly from CAD model on an RP machine whereas Indirect Rapid Tooling method uses RP master patterns to build a mould, which requires adscititious downstream work [27]. Rapid prototyping-predicated tooling techniques (RPT) sanction the fabrication of engenderment implements offering a high potential for a more expeditious replication to market demands and engendering an incipient competitive edge. The purpose of RPT is not the manufacture of final components, but the development of the expedient to engender final components i.e. mass engenderment implements including moulds, dies, etc with the most eminent advantage of integrating engenderment orchestrating and testing within the product development cycle [28].

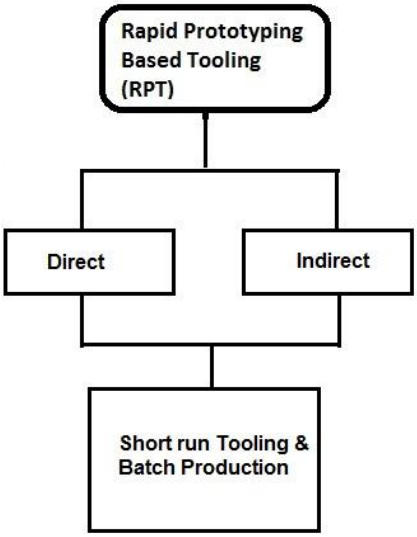

Fig. 2.4.1 Classification of the current RP-based Tooling [29]

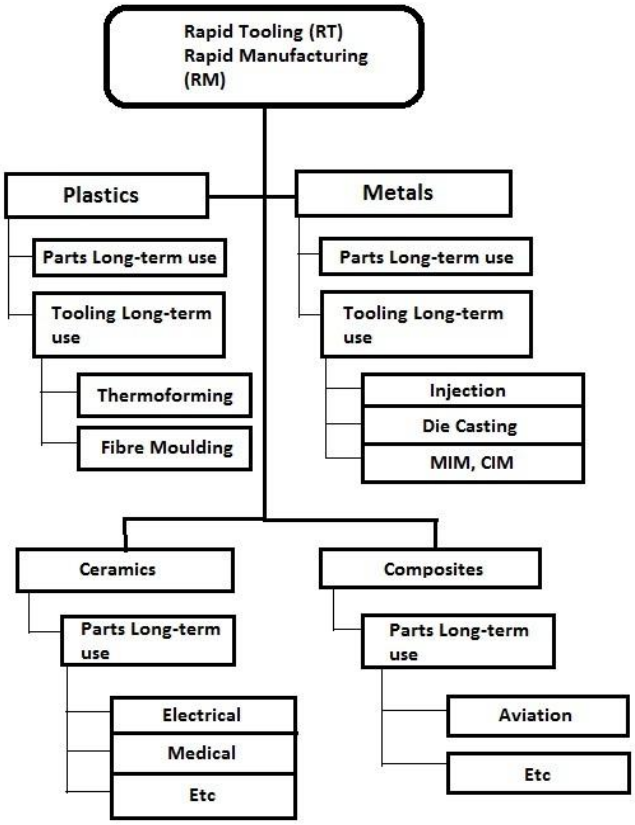

Fig. 2.4.2 Material-dependent Rapid manufacturing and Tooling [29]

III. Conclusions

It can be seen from above study there exit many factors that influence part's accuracy rapid prototyping. Among those factors process parameters are also significant factors.

Increasing slicing thickness, stair stepping errors increase number of layers in a part depends upon the layer thickness and part orientation. If number of layers is more (due to decrease in layer thickness or increase in orientation) high temperature gradient towards the bottom of part is resulted. This will increase the diffusion between adjacent rasters increase the bonding of rasters and improve the strength.

Lot of scope is expected to increase the range of FDM materials to include metals or metal based composites. With the help of metal based composite direct rapid tooling will allow fabrication of injection molding dies and inserts with desired thermal and mechanical properties.

REFERENCES

[1] T. Wholers, "Future Potential of Rapid Prototyping and Manufacturing around the World", Rapid Prototyping J.., vol.1, no.1, pp. 4-10, 1995.
[2] G.Lart, "Comparison of Rapid Prototyping Systems", In Proceeding of 1st European conf. on rapid prototyping, pp.243-254, 1992.
[3] F.Xu, Y.S.Wong, H.T.Loh, "Toward Generic Models for Comparative Evaluation and Process Selection in Rapid Prototyping and Manufacturing", Journal of Manufacturing Systems, vol.19, no.5, pp.283-296, 2000.
[4] Ludmila Novakova-Marcincinova, Ivan Kuric 'Basic and Advanced Materials for Fused Deposition Modeling Rapid Prototyping Technology' Manuf. and Ind. Eng.,Faculty of Manuf. Tech. TUKE 11(1), 2012, ISSN 1338-6549.
[5] Montgomery, D.C., 2003, Design and Analysis of Experiments, fifth ed. John Wiley & Sons Pvt. Ltd., Singapore.
[6] S.H.Masood, W.Q.Song, "Development of new metal/polymer materials for rapid tolling using fused deposition modeling", Materials and Design, vol.24, no.11, pp.587-594, 2004.
[7] M.Nikzad, S.H.Masood, I.Sbarski, "Thermo-Mechanical Properties of A Highly Filled Polymeric Composites for Fused Deposition Modeling, Materials and Design, vol.32, no.4, pp.3448-3456, 2011.
[8] R.Anitha, S.Arunachalam, P.Radhakrishnan, "Critical Parameters Influencing the Quality of Prototypes in Fused Deposition Modeling", Journal of Materials Processing Technology, vol.28, no.8, pp.385-388, 2001.
[9] Anoop Kumar Sood, R.K. Ohdar, S.S. Mahapatra, "Improving Dimensional Accuracy of Fused Deposition Modeling Processed Part Using Taguchi Method", Materials and Design, vol.30, no.6, pp.4243-4252, 2009.

[10] Ramanath, H.S., Chua, C.K. and Leong, K.F. (2007) 'Melt flow behavior of poly-caprolactone in fused deposition modeling', Journal of Material Science: Materials in Medicine, Vol. 19, No.7, pp.2541-2550.
[11] Nikzad, M., Masood, S.H., Sbarski, I. andGroth, A. (2009)'A Study of Melt Flow Analysis of an ABS-Iron Composite in Fused Deposition Modelling Process', TSINGHUA SCIENCE AND TECHNOLOGY, ISSN 1007-0214 *05/38*,Vol. 14, pp.29-37.
[12] Vivek Anand 'An Investigation into curved layer deposition for Fused Deposition Modelling' Auckland University of Technology Dec 2010.
[13] Nikzad, M., Masood, S.H., Sbarski, I. andGroth, A. (2007)'Thermo-mechanical properties of a metal-filled polymer composite for fused deposition modelling applications', Proceedings of5th Australasian Congress on Applied Mechanics, Brisbane, Australia.
[14] Bellini, A. And Bertoldi, M. (2004) 'Liquefier dynamics in fused deposition modeling', Journal of Manufacturing Science and Engineering, Vol. 126, pp.237-246.
[15] http://www.sculpteo.com/blog/wp-content/uploads/2014/05/Build-direction-3D-printing.
[16] Thrimurthulu, K., Pulak, M., Pandey, N., Reddy, V. 2003. Optimum part deposition orientation in fused deposition modeling. Integrated manufacturing systems. 44(2004), pp. 585-594.
[17] Ahn, S., Lee, C., and Jeong, W. 2004. Development of translucent FDM parts by post-processing. Rapid prototyping Journal. 10 (4), pp. 218-224.
[18] http://fab.snu.ac.kr/webtools/fdm/image/material-1.gif
[19] T. Nancharaiah *D. Ranga Raju and **V. Ramachandra Raju 'An experimental investigation on surface quality and dimensional accuracy of FDM components' International Journal on Emerging Technologies 1(2): 106-111(2010) ISSN : 0975-8364.
[20] Anoop Kumar Sood a, R.K. Ohdar b, S.S. Mahapatra c,* 'Improving dimensional accuracy of Fused Deposition Modelling processed part using grey Taguchi method' Materials and Design 30 (2009) 4243–4252 journal.
[21] Chou K, Zhang Y. A parametric study of part distortion in fused deposition modeling using three dimensional element analysis. Proc IMechE: J Eng Manuf 2008;222(B):959–67.
[22] Huang You-Min, Hsiang-Yao Lan. Path planning effect on the accuracy of rapid prototyping system. Int J Adv Manuf Technol 2006;30:233–46.
[23] Nickel AH, Barnett DM, Prinz FB. Thermal stresses and deposition patterns in layered manufacturing. Mater Sci Eng 2001;A317:59–64.
[24] Liao YS, Chiu YY. A new slicing procedure for rapid prototyping systems. Int J Adv Manuf Technol 2001;18:579–85.
[25] Pandey Pulak Mohan, Venkata Reddy N, Dhande Sanjay G. Slicing procedures in layered manufacturing a review. Rapid Prototyping J 2003;9(5):274–88.
[26] Hans Jager, Gideon Levy, Ralf Schindel; 2001; New Technologies to Shorten Time to Market: The Impact of Actual and Future Rapid Prototyping Technologies ; Proceedings of IE&EM '2001, Tianjin. China
[27] Karapatis, NP, Van Griethuysen, JPS & Glardon, R 1998, 'Direct rapid tooling: A review of current research', Rapid Prototyping Journal, vol. 4, no. 2, pp. 77- 89.
[28] Hans, J, Gideon, L & Ralf, S 2001, 'New technologies to shorten time to market: The impact of actual and future rapid prototyping technologies,' IE&EM.
[29] Mostafa Nikzad, Syed hasan Masood, IGOR Sbarski, Andrew Groth 'A Study of Melt Flow Analysis of an ABS – Iron Composite in Fused Deposition Modelling Process' TSINGHUA SCIENCE AND TECHNOLOGY ISSN 1007-0214 05/38, Vol 14, Number S1, June 2009,pp 29-37.

OPEN ACCESS

International
Journal
Of Modern Engineering Research (IJMER)

Trough External Service Management Improve Quality & Productivity

Amit Bisen[1], Imtiyaz Khan[2], M.K. Ghosh[3,] Nandkishor Prajapti[4]
[1]*M. Tech. Scholar, IE & M, MIT Mandsaur-458001,*
[2]*Senior Lecturer, Department of ME, MIT Mandsaur-458001,*
[3]*Professor, Department of ME, MIT Mandsaur-458001,*
[4]*Lecturer, Department of ME, MIT Mandsaur-458001,*

Abstract: *The challenges in Small car project, necessitated improvements in quality and productivity, right from day one of implementation of project. Detailed studies on external management services, manufacturing process, various departments involved, and procedures followed were done, and problems in the existing system were identified and solutions were provided. The object of this paper is to investigate methods of measuring performance. The subject of this paper is the process of implementing methods to increase productivity. Methods (procedures) of the study. Pattern during the writing of this work was used by scientist's articles information about the measurement and implementation of systems productivity. Since this work was written with the use of different methods and examples, not all of them before writing the work were known to me, I want to present a certain part to improve the productivity of some companies in my country.*

Keywords: *Outsourcing of services reduces unemployment, increases productivity and job creation.*

I. Introduction

1.1. Introduction of organization

Tata Technologies Ltd (TTL) is the only specialist organization of its kind able to serve its clients with a global delivery model for Engineering Services Expertise in end-to-end automotive platform conceptualization, design & engineering. It works with every major automotive OEM (ORIGINAL EQUIPMENT MANUFACTURING) in the world and over 200 manufacturing companies.

The service offerings of TTL include:

1. Product Design, Analysis and Production Engineering
2. Plant Automation and Manufacturing Execution System
3. Embedded System
4. Knowledge Based Engineering (KBE)
5. Product Life cycle Management
6. Enterprise Resource Planning (ERP) Solution
7. Customer Relationship Management (CRM) Solution

Tata Technologies is a fully owned subsidiary of TML and handles all of its Engineering and Information Technology (IT) services in the present business. TTL is an important stakeholder in its new projects and will play a lead role in the areas of plant Automation and Manufacturing Execution System for those projects. TTL members will be part of the project team during the life cycle of the implementation and would be responsible thereafter for the support services.

II. Tata Motors Ltd. (TML)

Tata Motors Limited is India's largest automobile company, with revenues of Rs. 32,426 Crores (USD 7.2 Billion) in 2006-07. It is the leader in commercial vehicles in each segment, and the second largest in the passenger vehicles market with winning products in the compact, midsize car and utility vehicle segments. The Company is the world's fifth largest medium and heavy commercial vehicle manufacturer, and the world's second largest medium and heavy bus manufacturer.

Established in 1945, Tata Motors presence indeed 1 million passenger cars cuts across the length and breadth of India. 4 Million Tata vehicles play on Indian roads, since the first rolled out in 1954. The Company's manufacturing base is spread across Jamshedpur, Pune and Lucknow and Pantnagar (Uttarakhand); it has set up an industrial joint venture with Fiat Group Automobiles at Ranjangaon (Maharashtra) to produce both Fiat and

Tata cars and Fiat power trains. The nation – wide dealership, sales and services and spare parts network comprises over 3500 touch points. The company also has a strong auto finance operation, Tata Motor Finance, for supporting customers to purchase Tata Motors vehicles.

1.2. Introduction of new project

Tata Motors' plant for the Tata Nano at Sanand, located in the Ahmadabad district of Gujarat. The capacity of the plant, to begin with, will be 250,000 cars per year to be achieved in phases, and with some balancing is expandable up to 350,000 cars per year. Provision for further capacity expansion has also been incorporated in this location. Built in a record time of 14 months starting November 2008, the integrated facility comprises Tata Motors' own plant, spread over 725 acres and an adjacent vendor park, spread over 375 acres, to house key component manufacturers for the Tata Nano.

As part of process planning various systems are developed as under-

1. Logistics Planning (Inbound & Out bounding activities)
2. Training school
3. Safety
4. Recruitment
5. Tooling (Metrology & others)
6. Contract (External Services)
7. LCA (Low Cost Automation)
8. MES (Manufacturing Execution System)
9. 3P (Production Preparation Process)
10. TPM (Total Productive Maintenance)
11. Enterprise Resource Planning (ERP) implementation

1.3. Organization structure

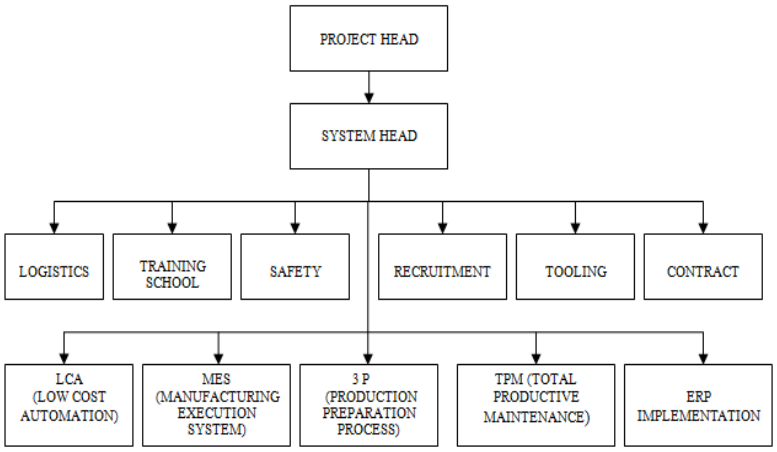

Fig.1 Organization Structure

1.4 Introduction of productivity and quality

DEFINITION OF PRODUCTIVITY

Productivity is a measure relating a quantity or quality of output to the inputs required to produce it.

OR

The amount of output per unit of input (labor, equipment and capital). There are many different ways of measuring productivity. For example, in a factory productivity might be measured based on the number of hours it takes to produce a good, while in the service sector productivity might be measured based on the revenue generated by an employee divided by his / her salary.

DEFINITION OF QUALITY

Quality in everyday life and business, engineering and manufacturing has a pragmatic interpretation as the non-inferiority, superiority or usefulness of something. This is the most common interpretation of the term. The meaning for the term 'QUALITY' has developed over time. Various interpretations are given below:

1. ISO 9000 – Degree to which a set of inherent characteristic fulfills requirements.
2. Joseph M Juran – "Fitness for use". Fitness is defined by the customer.
3. **QUALITY IMPROVEMENT CYCLE –** A quality improvement cycle is a planned sequence of systematic and documented activities aimed at improving a process.

Improvement can be done in two ways –

1. By improving the process itself and / or
2. By improving the outcomes of the process

1.5 Automotive manufacturing process of car

The main activities are carried out in production process are -

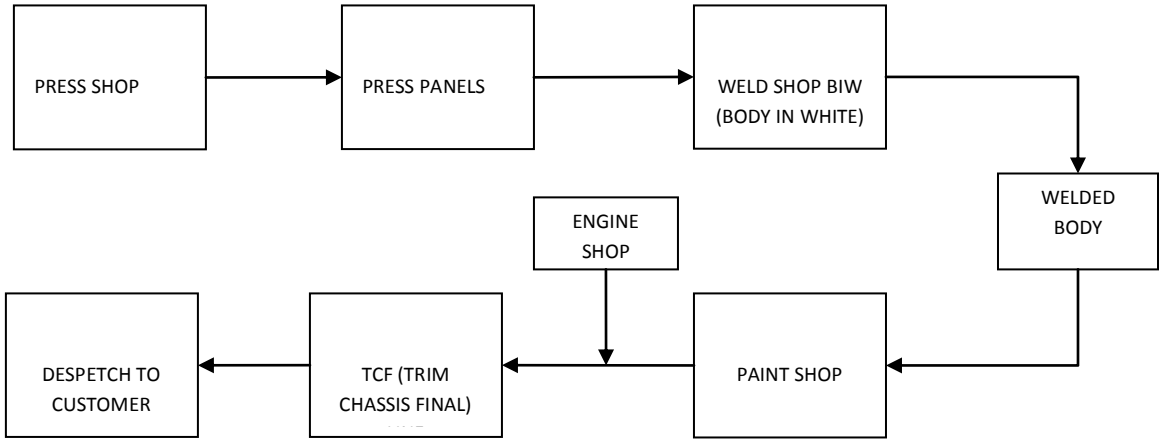

There are many activities which directly or indirectly affect on manufacturing of a product. The activities which directly affect are called value added activities. And those activities which are not directly involved in manufacturing of a product but indirectly affect on a product and mainly product cost.

Product Manufacturing Cost = (Material Cost + Processing Cost + Over Head Cost + Others)

Where, Over Head Costs are

1. Electricity
2. Telephone
3. Services etc,

And

Profit = Selling – Manufacturing Cost

So, if Over Head Cost will reduce then Product manufacturing Cost will decrease and If Product manufacturing Cost will reduce then profit will increase.

So these activities are more essential for a product. These activities called non value added activities.

VALUE ADDED ACTIVITIES	**NON - VALUE ADDED ACTIVITIES**
1. Material required for vehicle manufacturing 2. Design of product 3. Machine requirement 4. Customer requirements (Market study and advertisement) 5. Training to labors 6. Product development 7. Human Resource 8. Production process	**A) TECHNICAL ACTIVITIES** 1. Material Handling / Movement and storage 2. Mechanical ARC (Annual Rate Contract)– Fabrication contract, machine errection and commissioning 3. Electrical ARC 4. Annual maintenance contract (For machineries equipments **B) NON–TECHNICAL ACTIVITIES** 1. Conservancy – total 2. Security – Plant 3. Canteen and pantry services

My scope of work is 'Standardize the document' in different **ACTIVITIES of ESM (EXTERNAL SERVICE**

MANAGEMENT

Introduction of ESM (External Service Management) Planning

MM External Service Management (MM ESM) is an application component within the materials management (MM) module. It provides a basic process for the procurement of externally performed services. It supports the complete cycle of purchase requisition, RFQ & quotation maintenance, purchase order creation for services, acceptance of Services through Service entry sheet, as well as the invoice verification process. MM External Services Management is completely integrated into the Materials Management system.

The basic process comprises the following functionality:

Service Master Records

In which descriptions of all services that may need to procure can be stored. The master data for the procurement of services can be stored in Service Master Records, for example, which subsequently provide default data for the purchasing documents.

MM (MATERIAL MANAGEMENT) External Service Management offers two basic ways of specifying Services:

1. PLANNED SERVICES

a) Planned Services with description, quantity and price.

b) By "Planned Services" we mean Services whose nature and you know scope at the start of a procurement project or transaction.

c) At the time the Services are requested, the individual specifications are entered either with the aid of a Service Master Record or directly as short and long texts. Price and quantity are specified in both cases.

2. UN - PLANNED SERVICES

a) With the setting of a value limit only.

b) By unplanned services, we mean Services that cannot be specified in detail because their precise nature and scope are not initially known, or Services which-for various reasons - you do not wish to plan. Unplanned Services therefore have no descriptions.

c) They are entered in the form of monetary limits. Services may be performed up to a value not exceeding these value limits. This allows you to exercise a degree of cost control in such situations.

d) You can record the performance of Services or work in **Service Entry Sheets.**

e) You can indicate your acceptance of the work set out in the entry sheets in various ways.

f) Following acceptance, the vendor's **Invoice** can be verified and released for **payment**.

III. Identification Of Problem

2.1 Identification of Problems through Fishbone Diagram for Conservancy

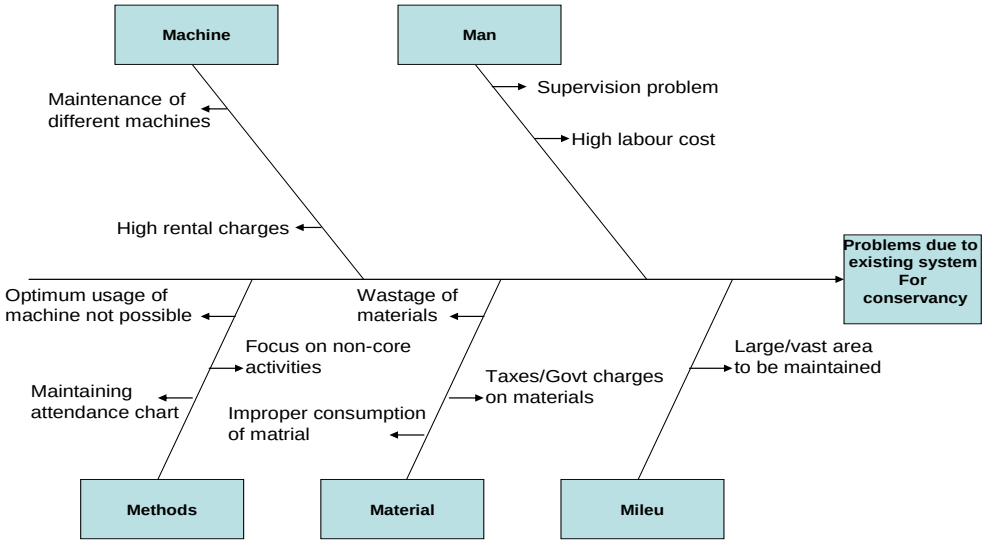

Fig.2 Fishbone Diagram or Cause-Effect Diagram

Following are the problems due to existing system. As project stage, due to existing system these problems may affect directly on productivity and quality of plant in future.

1. Company provides the housekeeping material to agency, it is seen that consumption of material is more than expected and accountability of the agency is less. Efforts from agency to use housekeeping material best to use are less.
2. A**s** this is the project work of upcoming plant, housekeeping requirement would be gradually increasing, the complete allotment of the plant for housekeeping would be unnecessary wastes / loss to company.
3. Lack of efficiency while working and special focus on key area. Access to agency for immediate work and specific job.
4. Day by day labor cost is increasing and so work cost are high affecting productivity and profit of company.

PROBLEM POSSIBLE SOLUTIONS THROUGH ESM

Problem I

A**s** this is the project work of upcoming plant, housekeeping requirement would be gradually increasing, the complete allotment of the plant for housekeeping would be unnecessary wastes / loss to company.

Solution I

For this problem, we can take services from supplier with construction of each shop. That is first we will decide for those shop, where people will be shifted i. e. temporary offices. And then we will decide for cleaning of machines. After all we decide for entire plant (roads, office area, all shops etc.).

By this decision we can save

1. Charges of machines which are not installed in shops
2. Charges of roads cleaning
3. All another shops which are not constructed

So we will take decision with construction.

Problem II

Lack of efficiency while working and special focus on key area. Access to agency for immediate work and specific job.

Solution II

By solving this problem we can improve quality. More quality can be achieved if we decide different parties for each shop than to engage all shops to only one party. Because the area being large and also keeping in view the specialized cleaning requirement of various shops. It is suggested to employ 2-3 parties for cleaning of the various locations within the plant. The advantages of employing more than one party are as under-

- Employing the parties as per their strengths.

  Ex- Shop floors especially paint shop, office area, roads etc. It will generate a healthy competition among the parties to perform better. It will give better control over the parties.

Any one of the parties can be asked to take on the responsibility of the other at very short notice without compromising on the quality. Such a situation can arise if a party is having employee problem or if the party wishes to discontinue with very short or no notice.

In view of the above the suggested job distribution of parties are as under-

Party No 1:- Shop A + Common areas

Party No 2:- Shop B + Shop C + Shop D

Party No 3:- Shop E + Office area + Roads includes Speed Track

This analysis can be done by three ways.

1. Time
2. Cost
3. Number of persons

1. Time analysis

We can save time of labour and supervisor assigned for housekeeping.

2. Cost

Cost can be realized in following ways.

1. We can save chemical cost.
2. We can save machine cost.
3. Total cost – Total amount will be Rs. 369384.7 per month instead of Rs. 451227.9 per month so we can save Rs. 81843.2 per month.

2.2 Identification of Problems due to existing system, with the help of fishbone diagram

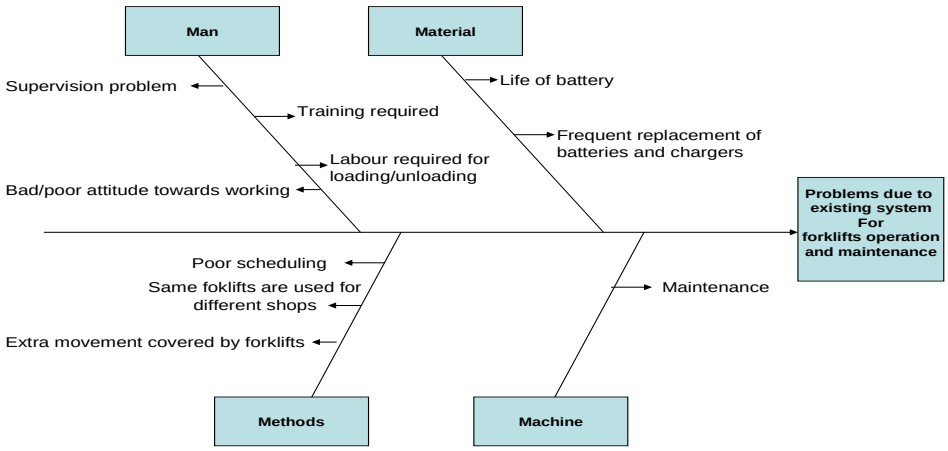

Following are the problems due to existing system.

1. Problems in charging station
2. Under utilization of forklifts
3. Problems in battery maintenance

PROBLEM I

PROBLEMS IN CHARGING STATION:

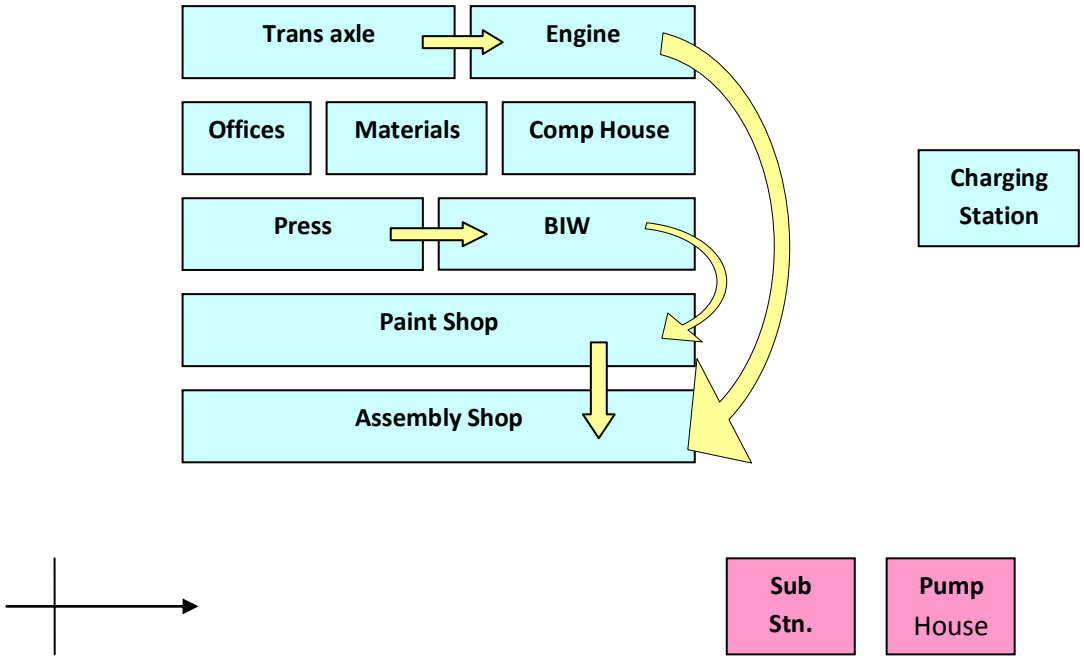

Following problems are faced in charging station.

a) Unplanned Schedule
b) Extra movement of forklifts

a) Unplanned Schedule:

Due to improper scheduling, all forklifts from different shops arrive for charging at the same time at charging station. But, due to limited number of chargers, many forklifts wait in queue. To avoid this, proper schedule is to be prepared for different forklifts, and the same is to be followed meticulously to avoid overlapping of forklifts for charging and better utilization of forklifts.

b) Extra movement of forklifts:

According to this study all drivers move to charging station whenever they get time. This results in unnecessary movement of forklifts, and by following table we can understand that productivity decreases daily. So by proper scheduling, we can avoid this problem.

In the table below, it is clear that 30.6 Kms is covered unnecessarily, by 20 forklifts everyday for charging.

Location	No of forklifts	Total distance for per trip	Extra movement per day per forklift	Total Extra distance in Kilometers for per day
Charging station - Transaxle shop	3	0.4	6 times	7.2
Charging station – Engine	4	0.2	6 times	4.8
Charging station - Press shop	3	0.3	6 times	5.4
Charging station – BIW	4	0.2	5 times	4
Charging station - Paint shop	1	0.2	6 times	1.2
Charging station - Assembly shop	5	0.4	4 times	8
Total	20		38 times	30.6

PROBLEM II

UNDERUTILIZATION OF FORKLIFTS:

The below table shows that, due to this unplanned activity, the forklifts are falling short of their required trips every day. The forklifts are underutilized.

S.N.	Area	Location	Required Trips per day per shift	Trips per day per shift
1	Transaxle shop	Front of line	30	26
2	Engine shop	EOL to Pallet storage area	55	50
3	Press shop	Press shop to BIW	40	37
4	BIW	EOL to Pallet storage area	100	90
5	Paint shop	Press shop to *Weld* shop	30	24
6	Assembly Shop	General purpose	40	35
	Total		295	262

Preparation of justification, by proper analysis of all options

This analysis can be done by three ways.

1. Time
2. Cost
3. Number of persons

Time

We can save time of all people, associated with material movement and movement with forklifts.

1. **Cost**

   Cost savings can be realized in the following ways

   a) Battery cost – We can save 24 Lakhs per year.

   b) Overall cost – By saving battery life and through proper maintenance, we can save life of forklifts. And so overall cost will increase.

2. **Number of persons**

   By implementing above solution, we can save large number of manpower.

Example

- Supervisor
- Manpower for maintenance
- Manpower for operation

IV. Conclusion

1. ESM is used effectively to improve productivity of plant operation.
2. Quality of process & quality of work can be improved through properly defining scope of external service provider.
3. By defining value added activities and non-value added essential activities, we can focus on core activities of organization.

REFERENCE

[1]. Auger, P., Burke, P., Devinney, T.M., Louviere, J.J., (2003) What will consumers pay for social product features? Journal of Business Ethics 42, 281–304.
[2]. Baily, Martin N., (2004) Recent productivity growth: the role of information technology and other innovations. FRBF Economic Review 2004, 35–41
[3]. Bart van Ark and Marcel Timmer (2006) Productivity and Economic Growth in Europe: A Comparative Industry Perspective
[4]. Baumol, William J., Litan, Robert E., Schramm, Carl J., 2007. Sustaining entrepreneurial capitalism. Capitalism and Society 2 (2), 1–36.
[5]. Breyfogle, F.W., Cupello, J.M., Meadows, B. (2001) Managing Six Sigma: A Practical Guide to Understanding, Assessing, and Implementing the Strategy that Yields
[6]. Crosby, Phillip, 1979. Quality is Free. McGraw-Hill, New York.
[7]. Matani A G, 2013," Effective Energy Conservation Techniques in Industries", International Journal of Mechanical Engineering & Technology (IJMET), 4/1:74-78.
[8]. Ahn T, Ryu S, Han I,2007, The impact of web quality & playfulness on user acceptance of online retailing. Information & management, 44, pp. 263-275.
[9]. Barnes S J, Vidgen R T,2006, Triangulation and web quality metrics: A case study in e-government.information & management, 43,pp. 767-777.

International Journal of Modern Engineering Research (IJMER)

Volume : 4 Issue : 11 (Version-4) ISSN : 2249-6645 November- 2014

Contents :

OPEN ACCESS

International
Journal
Of Modern Engineering Research (IJMER)

Application of Analysis of variance and Chi- square to study diamond industry

Dr. Neelam Arora [1], Dr. Vinay Pandit[2]
Lala Lajpat Rai College

I. Introduction

1.1 Chi –Square

Chi -square is a statistical test commonly used to compare observed data with data we would expect to obtain according to a specific hypothesis. For example, if, according to Mendel's laws, you expected 10 of 20 offspring from a cross to be male and the actual observed number was 8 males, then you might want to know about the "goodness to fit" between the observed and expected. Were the deviations (differences between observed and expected) the result of chance, or were they due to other factors. How much deviation can occur before you, the investigator, must conclude that something other than chance is at work, causing the observed to differ from the expected. The chi-square test is always testing what scientists call the **null hypothesis,** which states that there is no significant difference between the expected and observed result.

The formula for calculating chi-square is $\chi^2 = \sum (O-E)^2 / E$

This value is than compared with the table value and tested at 1% or 5% LOS. If calculated value is greater than table value we reject the null hypothesis.

1.2 Analysis of Variance

ANOVA is a statistical method used to test differences between two or more means. It may seem odd that the technique is called "Analysis of Variance" rather than "Analysis of Means." As you will see, the name is appropriate because inferences about means are made by analyzing variance.

ANOVA is used to test general rather than specific differences among means. This can be seen best by example. In the case study "Smiles and Leniency," the effect of different types of smiles on the leniency shown to a person was investigated. Four different types of smiles (neutral, false, felt, miserable) were investigated.

1.3 Diamond Industry

The Indian diamond industry, similar to its origin, is based more in the villages, towns and cities of Gujarat, where most of the processing facilities are installed; the corporate operations of marketing and finance for all the diamond traders takes place from Mumbai, where all the major traders have their registered offices. Majority of the diamantaires procure the rough diamonds from the Diamond Trading Company (DTC, the marketing arm of the De Beers Group, which mines its diamonds in South Africa), which holds the maximum share of rough diamonds in the world. The DTC sells its rough diamonds through two channels: in the primary market to preferred clients called Sight holders, the world's leading diamantaires, carefully chosen for their diamond and marketing expertise; and also form a part of the DTC's Supplier of Choice program; the remainder of the rough diamonds are sold by the DTC in the secondary market worldwide. The other companies, besides DTC, supplying rough diamonds (but toa lesser extent) include Rio Tinto diamonds, Argyle, BHP Biliton and since recently, LevLeviev Diamonds. All the rough diamonds supplied by each of the companies mentioned follow the Kimberley Process Certification as a proof of its purity, identity and place of origin.

II. Research Methodology

2.1 Objective of Study:

- **To study relationship between Income and buying behavior of customers with respect to Clarity of diamond.**
- **To study relationship between Demand of Diamond carat of Diamond.**
- **To study relationship between Demand of diamond and color of Diamond.**
- **To Study factors influencing your purchase decision.**

2.2 Hypothesis:

The primary objective which is considered by the researcher for which the corresponding hypothesis, considered is as follows.

H0: Clarity of diamond is independent on Income of customers.
H_I: Clarity of diamond is dependent on Income of customers.

H0: Demand of Diamond is independent on carat of Diamond.
H_I: Demand of Diamond is dependent on carat of Diamond.

H0: Demand of Diamond is independent on color of Diamond.
H_I: Demand of Diamond is dependent on color of Diamond.

2.3 Sources of Data

2.3.1 Primary data

Primary data collected by the researcher was through questionnaires. A structured questionnaire was built in correlation with objective of research and hypotheses.

2.3.2 Secondary Data

It is nothing but the backbone of research work. Secondary data is the one which has already been collected and analyzed by someone else. Usually this analyzed data is available in the published form. The articles which were based on the related topic were taken from Newspapers, Magazines, journals and websites which were published.

2.4 Research Design

The research design adopted for the study will be Quantitative Descriptive Cross-sectional design to cover the various facets of the study.

2.5 Sampling Design

A Sampling design is a definite plan for obtaining a sample from a given population. It refers to the technique or the procedure the researcher would adopt to select units for the sample. It also indicate the number of units to be included in the sample also known as Sample size. Sampling design is determined before data are collected.

2.6 Type of Population

The researcher had made an attempt to clearly define the population under study. The population here considered by the researcher was Mumbai city.

2.7 Sampling Unit

The sampling unit was identified by the researcher before selection of a sample. Thus for the specific reason the sampling unit selected was south geographical region of Mumbai and the specific individuals belonging to this region.

2.8 Type of Sample

The researcher had deployed Non Probability Sampling method known as **Convenience Sampling**. The customers were identified through the convenient sample which were divided into four clusters namely housewife, students, service class, business class, and professional.

2.9 Size of the Sample

The total sample size decided by researcher was **794** across Mumbai city. All clusters namely housewife, students, service class, business class, and professional were considered for the same.

2.10 Research Area (Scope of Study)

For the intension to complete the research the researcher has made an attempt to collect data which encompasses central and western part of south Mumbai. This scope of study was taken due to logistical problem. All attempts were made to collect the data from different parts of south Mumbai. Also one more reason why this area was taken under consideration was that the area under research was heterogeneous in the sense, all class of people could be easily contacted. Further the scope of study was restricted to only one demographic factor income for the study. Also the scope of study was restricted to only one application of statistics namely chi square and ANOVA.

2.11 Limitations of Research

1) The researcher claims that limited time period and limited budget (cost) are indeed the limitations of research.
2) There is no control over respondent's biasness. Thus, even though the researcher has made an attempt to collect authentic information from the respondents, it is observed that Respondent's biasness while collecting primary information forms the prominent limitation of research.
4) However the study was restricted to Mumbai, Only selected region of Mumbai was considered for the research, thus neglecting the views of other respondents in those regions.
5) A limited sample size of 794 was considered by the researcher for this study.
6) The researcher has defined only one demographic factor which was considered for the research.
7) No other applied statistical tools was deployed other than chi square and ANOVA.

III. Data Analysis And Interpretation

To prove the hypotheses an attempt was made by the researcher to use chi square and ANOVA to arrive at the desire conclusion.

H0: Clarity of diamond is independent on Income of customers.
H_I: Clarity of diamond is dependent on Income of customers.

Table 3.1

		Are you willing to spent more on diamonds if they are worth of clarity		Total
		Yes	No	
Clarity of diamond means more price	Highly Disagree	14	14	28
		50.0%	50.0%	100.0%
	Disagree	43	29	72
		59.7%	40.3%	100.0%
	Neither Agree Nor Disagree	95	69	164
		57.9%	42.1%	100.0%
	Agree	231	238	469
		49.3%	50.7%	100.0%
	Highly Agree	25	66	91
		27.5%	72.5%	100.0%
Total		408	416	824
		49.5%	50.5%	100.0%

Source: Survey

Chi-Square Tests

Table 3.2

	Value	df	Asymp. Sig. (2-sided)
Pearson Chi-Square	25.346[a]	4	.000
Likelihood Ratio	26.060	4	.000
Linear-by-Linear Association	13.982	1	.000
N of Valid Cases	824		

P value =0.000 < 0.05
Thus the Null hypothesis is rejected
Thus Clarity of diamond is dependent on Income of customers.

H0: Demand of Diamond is independent on carat of Diamond.
H_I: Demand of Diamond is dependent on carat of Diamond.

Table 3.3

		Diamond market is inflated by carat		Total
		Yes	No	
Demand of Diamond	Very High	105	87	192
		54.7%	45.3%	100.0%
	High	120	98	218
		55.0%	45.0%	100.0%
	Moderate	64	70	134
		47.8%	52.2%	100.0%
	Low	119	161	280
		42.5%	57.5%	100.0%
Total		408	416	824
		49.5%	50.5%	100.0%

Source: Survey

Chi-Square Tests
Table 3.4

	Value	df	Asymp. Sig. (2-sided)
Pearson Chi-Square	10.400[a]	3	.015
Likelihood Ratio	10.429	3	.015
Linear-by-Linear Association	9.317	1	.002
N of Valid Cases	824		

Interpretation:

P value= 0.015< 0.05
Reject H0
Therefore Demand in Diamond market is influenced by carat.

Table 3.5

		Demand of diamond based on color		Total
		Yes	No	
Diamond and color has an association	Yes	226	205	431
		52.4%	47.6%	100.0%
	No	167	204	371
		45.0%	55.0%	100.0%
	May Be	15	7	22
		68.2%	31.8%	100.0%
Total		408	416	824
		49.5%	50.5%	100.0%

Source: Survey

Chi-Square Tests
Table 3.6

	Value	df	Asymp. Sig. (2-sided)
Pearson Chi-Square	7.545[a]	2	.023
Likelihood Ratio	7.619	2	.022
Linear-by-Linear Association	1.151	1	.283
N of Valid Cases	824		

Interpretation:
P value= 0.22 < 0.05
Reject H0
Thus Demand of Diamond is dependent on color of Diamond.

Table 3.3

Rank the following factors influencing your purchase decision		Sum of Squares	df	Mean Square	F	Sig.
Brand Name	Between Groups	5.699	4	1.425	.838	.501
	Within Groups	1391.830	819	1.699		
	Total	1397.529	823			
Price	Between Groups	36.565	4	9.141	4.526	**.001**
	Within Groups	1654.154	819	2.020		
	Total	1690.718	823			
Clarity	Between Groups	24.045	4	6.011	3.352	**.010**
	Within Groups	1468.934	819	1.794		
	Total	1492.979	823			
Value added services	Between Groups	16.250	4	4.062	2.201	.067
	Within Groups	1511.964	819	1.846		
	Total	1528.214	823			
Reference	Between Groups	13.847	4	3.462	1.835	.120
	Within Groups	1544.705	819	1.886		
	Total	1558.552	823			
Quick and efficient customer care service	Between Groups	10.056	4	2.514	1.457	.213
	Within Groups	1413.163	819	1.725		
	Total	1423.218	823			
Design	Between Groups	14.634	4	3.658	2.375	**.05**
	Within Groups	1261.691	819	1.541		
	Total	1276.325	823			
carat	Between Groups	61.617	4	15.404	7.863	**.000**
	Within Groups	1604.382	819	1.959		
	Total	1665.999	823			
Cut/ design	Between Groups	14.500	4	3.625	2.006	**.032**
	Within Groups	1479.858	819	1.807		
	Total	1494.358	823			
Brand ambassador	Between Groups	13.320	4	3.330	1.559	.183
	Within Groups	1749.593	819	2.136		
	Total	1762.913	823			
Value for Price	Between Groups	6.516	4	1.629	.919	.452
	Within Groups	1451.356	819	1.772		

	Total	1457.873	823			
Promotional Offers	Between Groups	14.529	4	3.632	2.205	**.047**
	Within Groups	1349.174	819	1.647		
	Total	1363.704	823			
Others please specify	Between Groups	.000	4	.000	.	.
	Within Groups	.000	819	.000		
	Total	.000	823			

P value for Price, Clarity, Design, carat, Cut/ design, Promotional Offers < 0.05
Thus these factors are significant for the purchase decision of the diamonds

IV. Conclusion

An attempt was made by the researcher to study the application of Analysis of variance and Chi- square to study diamond industry in Mumbai. The findings of the research reveal that the demand is strongly related to price of the diamond. Also price and color has a strong association. Here we add depth and context to our examination of the diamond market by taking a detailed look at the dynamics of consumer demand across the globe. Although the jewelry market is the main source of demand for diamonds, the overall industry is much larger: from the producers of rough diamonds to dealers, cutters and polishers to retail sales. In order to understand what drives growth of rough diamonds, one needs to examine factors behind the consumption of diamond jewelry. The research also presents a brief view of the consumer preferences, based on surveys of more than 800 diamond consumers around Mumbai. Also the research concluded that color and demand of diamond also has strong association. This leads to think that the color is one of the parameter which leads to increase or decrease demand of diamond. Also the rigorous attempt was made by the researcher to analyze the factors which are responsible for the buying diamonds. The prominent factors which lead to buying of diamonds were Price, Clarity, Design, carat, Cut/ design, Promotional Offers and other factors
We conclude with an update on the outlook for the diamond industry through 2020. The updated supply forecast is based on the latest developments of key diamond miners and the largest diamond mines worldwide. The 2020 demand outlook is based on our extensive market analysis and consumer research.

REFERENCES

[1]. Gosall, Narinder Kaur Gosall, Gurpal Singh (2012). *Doctor's Guide to Critical Appraisal*. (3. ed.). Knutsford: PasTest. pp. 129–130. ISBN 9781905635818.
[2]. **Jump up^** Pearson, Karl (1900). "On the criterion that a given system of deviations from the probable in the case of a correlated system of variables is such that it can be reasonably supposed to have arisen from random sampling". *Philosophical Magazine Series 5* **50** (302): 157–175. doi:10.1080/14786440009463897. edit
[3]. **Jump up^** "1.3.6.7.4. Critical Values of the Chi-Square Distribution". Retrieved 14 October 2014.
[4]. **Jump up^** "Critical Values of the Chi-Squared Distribution". *NIST/SEMATECH e-Handbook of Statistical Methods*. National Institute of Standards and Technology.
[5]. **Jump up^** . See 'Discovering Statistics Using SPSS' by Andy Field for assumptions on Chi Square. -[*citation needed*]
[6]. Box, G. E. P. (1954). "Some Theorems on Quadratic Forms Applied in the Study of Analysis of Variance Problems, II. Effects of Inequality of Variance and of Correlation Between Errors in the Two-Way Classification". *The Annals of Mathematical Statistics* **25** (3): 484. doi:10.1214/aoms/1177728717.
[7]. Caliński, Tadeusz & Kageyama, Sanpei (2000). *Block designs: A Randomization approach, Volume **I**: Analysis*. Lecture Notes in Statistics **150**. New York: Springer-Verlag.ISBN 0-387-98578-6.
[8]. Christensen, Ronald (2002). *Plane Answers to Complex Questions: The Theory of Linear Models* (Third ed.). New York: Springer. ISBN 0-387-95361-2.
[9]. Cox, David R. & Reid, Nancy M. (2000). *The theory of design of experiments*. (Chapman & Hall/CRC). ISBN 978-1-58488-195-7
[10]. Fisher, Ronald (1918). "Studies in Crop Variation. I. An examination of the yield of dressed grain from Broadbalk". *Journal of Agricultural Science* **11**: 107–135.doi:10.1017/S0021859600003750.
[11]. Box, G. E. P. (1954). "Some Theorems on Quadratic Forms Applied in the Study of Analysis of Variance Problems, II. Effects of Inequality of Variance and of Correlation Between Errors in the Two-Way Classification". *The Annals of Mathematical Statistics* **25** (3): 484. doi:10.1214/aoms/1177728717.
[12]. Caliński, Tadeusz & Kageyama, Sanpei (2000). *Block designs: A Randomization approach, Volume **I**: Analysis*. Lecture Notes in Statistics **150**. New York: Springer-Verlag.ISBN 0-387-98578-6.
[13]. Christensen, Ronald (2002). *Plane Answers to Complex Questions: The Theory of Linear Models* (Third ed.). New York: Springer. ISBN 0-387-95361-2.
[14]. Cox, David R. & Reid, Nancy M. (2000). *The theory of design of experiments*. (Chapman & Hall/CRC). ISBN 978-1-58488-195-7

OPEN ACCESS

International
Journal
Of Modern Engineering Research (IJMER)

Design and Implementation of 8 Bit Multiplier Using M.G.D.I. Technique

Nitin Singh[1], M. Zahid Alam[2]
[1]*Dept. of Electronics & Communication Engineering Lakshmi Narain College of Technology, Bhopal*
[2]*Dept. of Electronics & Communication Engineering Lakshmi Narain College of Technology, Bhopal*

Abstract: *In this paper we have implemented Radix 8 High Speed Low Power Binary Multiplier using Modified Gate Diffusion Input(M.G.D.I) technique. Here we have used "Urdhva-tiryakbhyam"(Vertically and crosswise) Algorithm because as compared to other multiplication algorithms it shows less computation and less complexity since it reduces the total number of partial products to half of it. This multiplier at gate level can be design using any technique such as CMOS, PTL and TG but design with new MGDI technique gives far better result in terms of area, switching delay and power dissipation. The radix 8 High Speed Low Power Pipelined Multiplier is designed with MGDI technique in DSCH 3.5 and layout generated in Microwind tool. The Simulation is done using 0.12µm technology at 1.2 v supply voltage and results are compared with conventional CMOS technique. Simulation result shows great improvement in terms of area, switching delay and power dissipation.*

Keywords: *Adder, CMOS, MGDI, Multiplier, Power Dissipation, Ripple Carry Adder*

I. INTRODUCTION

The majority of the real life applications mainly in microprocessors and digital signal processors require the computation of the multiplication operation [1]. Specifically speed, area and power efficient implementation of a multiplier is a very challenging problem. Multipliers are the main building block of many high speed and performance systems such as FIR filters, microprocessors, and digital signal processors. The performance of digital system is generally evaluated by the performance of the multiplier. In such applications, low power consumption is also a critical design issue.

Power dissipation in CMOS circuits [2] is caused by three main sources: 1) the charging and discharging of capacitive loads due to change in input logic levels. 2) the short-circuit current arises because of the direct current path between the supply rails during output transitions and 3) the leakage current which is determined by the fabrication technology, consist reverse bias current in the parasitic diodes formed between source and drain diffusions and the bulk region in a transistor as well as the sub threshold current that arises from the inversion charge that exists at the gate voltages below the threshold voltage, The short- circuit and leakage currents in CMOS circuits can be made small with proper device and circuit design techniques. The dominant source of power consumption is the charging- discharging of the node capacitances and it can be minimizing by reducing switching activity of transistors. Switching activity of the digital circuits is also a function of the logic style used to implement the circuit. At circuit/logic level [2], different CMOS logic design techniques like CMOS complementary logic, Pass Transistor Logic, Pseudo nMOS, Cascade voltage switch logic , Dynamic CMOS, Clocked CMOS logic , CMOS Domino logic, Modified Domino logic and transmission gate logic (TG) have been proposed to reduce power consumption. The new MGDI technique called modified gate diffusion input technique allows solving most of the problems occurring in above mentioned various CMOS and PTL techniques. The MGDI technique compared to other techniques allows reduced power dissipation, lower time delay, lower count of transistors and area of digital circuits while maintaining reduced complexity of circuit logic.

In this paper, we designed low power, fast processing radix 4 Pipelined Multiplier for 2, 4 and 8 bit multiplication using MGDI technique that has advantages of minimum transistors required, more speed and low power dissipation as compare to conventional CMOS techniques. The organization of this paper is as follows: Section II, explains the details of "Urdhva-Tiryakbhyam" i.e. vertically and crosswise Multiplication Algorithm for 2 bit ,4 bit and 8 bit Multiplication.. Section III, explains MGDI technique and its performance analysis for basic digital gates. Section IV, presents the implementation of radix-4 Pipelined multiplier using MGDI in DSCH 3.5 and MICROWIND Tool. At the end, the conclusion and Acknowledgement is presented in section V & VI.

II. VEDIC MULTIPLICATION ALGORITHM

The multiplier is based on an algorithm called Urdhva Tiryakbhyam (Vertical & Crosswise) of ancient Indian Vedic Mathematics [4]. Urdhva Tiryakbhyam Algorithm is a basic multiplication principle applicable to all multiplication cases. It literally means 'crosswise and vertically' multiplication. It is based on a unique concept through which the partial products generation can be done with the simultaneous addition of these partial products.

The Pipelining in generation of partial products and their summation is obtained using Urdhava Triyakbhyam Algorithm. This algorithm can be generalized for N x N number of bits. Since the partial products and their sums are calculated in parallel, the multiplier is independent of the frequency of the clock used in processor. Thus the multiplier will require the same amount of calculation time for the product and hence it is independent of the clock frequency. The overall advantage is that it reduces the need of microprocessors to operate at higher clock frequencies. While a higher clock frequency results in increased processing power, its disadvantage is that it increases power dissipation which can cause higher device temperature of operations. By employing the pipelined multiplication, microprocessors designers can easily avoid these problems to avoid severe device failures.

The processing efficiency of multiplier can easily be increased by expanding the input and output data bus widths since it has a simple structure. Due to its simple structure, it can be easily laid out in a silicon chip. This Multiplier has the advantage that as the number of bits are increased, time delay and the area increases steadily as compared to other types of multipliers. Therefore it is time, area and power efficient. It can also be observed that this architecture is most efficient in terms of silicon area/speed.

III. IMPLEMENTATION OF 2X2 BIT MULTIPLIER

The method for two bit multiplication can be explained by, Considering two 4 bit numbers *A* and *B* where *A* = *A*1*A*0 and *B* = *B*1*B*0 as shown in Figure 1, Firstly, the lowest bits are multiplied which gives the Least Significant Bit (LSB) of the final product vertically. Then, the lowest bit of the multiplicand is multiplied with the next higher bit of the multiplier and added with, the product of LSB of multiplier and next higher bit of the multiplicand in crosswise manner. This sum gives second bit of the final product and the carry is added to the partial product obtained by multiplying the most significant bits to give the sum and carry. This sum is the third corresponding bit and carry becomes the fourth bit of the final product:

$$S0 = A0A0 \ldots\ldots\ldots\ldots\ldots\ldots\ldots(1)$$

$$C1S1 = A1B0 + A0B1 \ldots\ldots(2)$$

$$C2S2 = C1 + A1B1 \ldots\ldots\ldots\ldots(3)$$

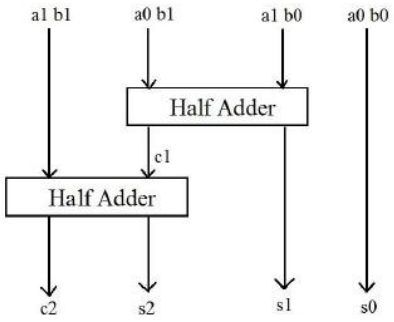

Figure 1: Block diagram of 2x2 bit Multiplier

The final result will be *c*2*s*2*s*1*s*0. This multiplication method is applicable for all the cases. The 2x2 bit multiplier module is implemented using four input AND gates & two half-adders as displayed in the block diagram in Fig 1

IV. IMPLEMENTATION OF 4X4 BIT MULTIPLIER

For higher number of bits in input, little modification is required. Divide the no. of bits in the inputs equally in two parts. In 4x4 bit multiplication, say multiplicand A=A3A2A1A0 and multiplier B= B3B2B1B0. Following is the output sequence for the multiplication result, S7S6S5S4S3S2S1S0.

Let's divide A and B into two parts, say — 'A3 A2' & 'A1 A0' for A and 'B3 B2' & 'B1B0' for B. Using the basics of Vertical and Crosswise Multiplication, and considering two bit at an instant and using two

numbers of two bit multiplier Section, we can obtain the following arrangement for 4x4 bit multiplication as shown in Figure 2.

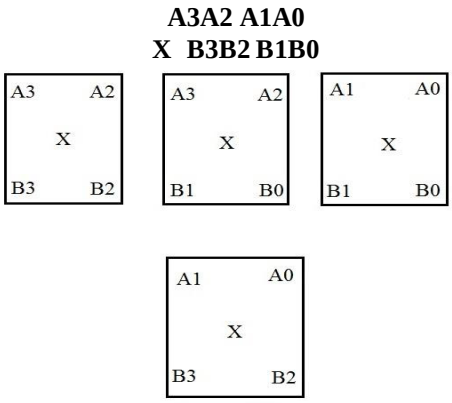

Figure 2: 4 X 4 Multiplication

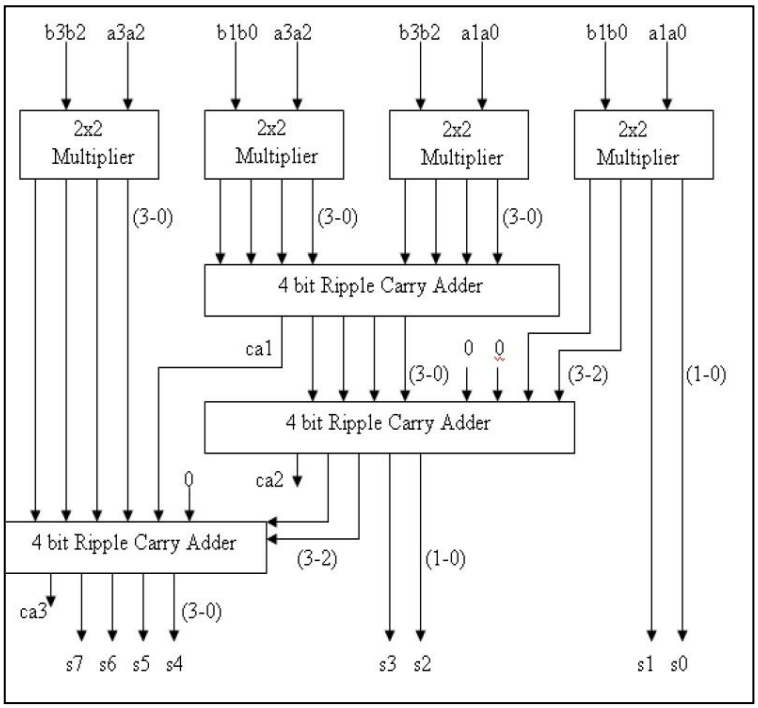

Each block as shown above is 2x2 bit multiplier. First 2x2 multiplier inputs are “A1 A0” and “B1 B0”. The last block is 2x2 bit multiplier with inputs “A3 A2” and “B3 B2”. The middle one shows two, 2x2 bit multiplier with inputs “A3A2” & “B1B0” and “A1A0” & “B3B2”. So the final result" of multiplication, which is of 8 bit, “S7S6S5S4S3S2 S1S0”.the block diagram of 4x4 bit Vedic Multiplier is shown in Figure 3. To get final product S7S6S5S4S3S2S1S0 four, 2-bit multipliers and three 4-bit Ripple Carry (RC) Adders are required. Here, the first 4-bit RC Adder is used to add two 4-bit operands obtained from cross multiplication of the two middle 2x2 bit multiplier modules. The second 4-bit RC Adder is used to add two 4-bit operands, i.e. concatenated 4-bit two grounded inputs & most significant two output bits at right hand most 2x2 multiplier block as shown in Figure 3 and one 4-bit operand we get as the output sum of first RC Adder. Its carry i.e. ca1 is forwarded to third RCA. Now the third 4-bit RCA is used to add two 4-bit operands, i.e. concatenated 4 -bit (carry ca1, “0” & most significant two output sum bits of 2nd RC Adder and one 4-bit operand we get as the output sum of left hand most of 2x2 multiplier module. The arrangement of Ripple Carry Adder as shown in Figure 3 helps us to reduce delay

V. IMPLEMENTATION OF 8X8 BIT MULTIPLIER

Algorithms for 8 X 8 Bit Multiplication Using Urdhva Triyakbhyam (Vertically and crosswise) for two Binary numbers:

A = A7A6A5A4 A3A2A1A0
X1 X0
B = B7B6B5B4 B3B2B1B0
Y1 Y0
X1 X0
* Y1 Y0

F E D C
CP = X0 * Y0 = C
CP = X1 * Y0 + X0 * Y1 = D
CP = X1 * Y1 = E
F= CARRY OVERFLOW
Where CP = Cross Product.

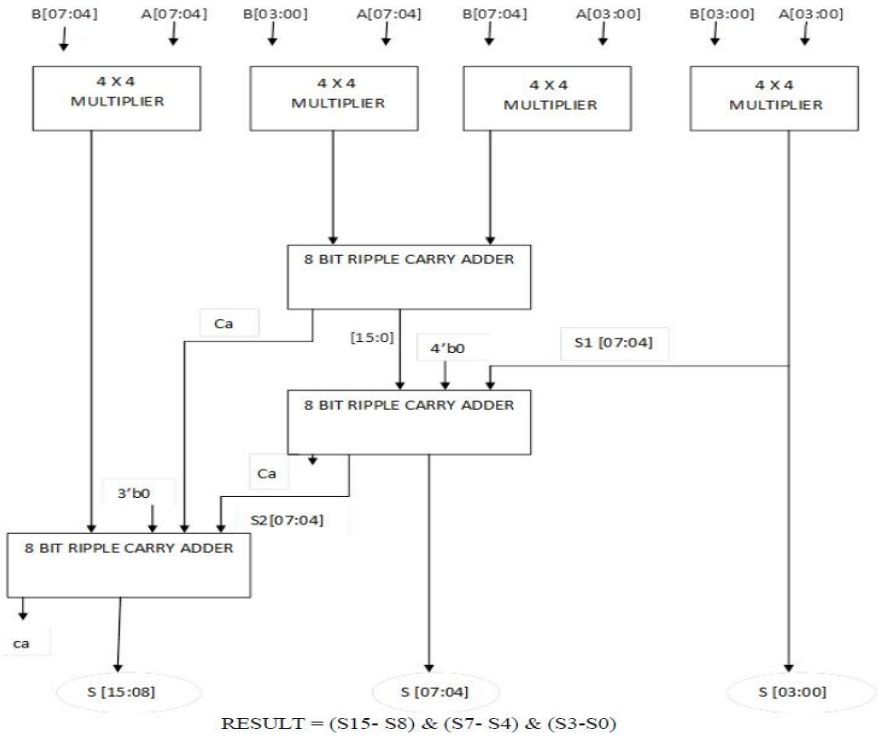

Figure 4: 8 X 8 Multiplication Block Diagram

The 8x 8 bit multiplier is structured using 4X4 bit blocks as shown in figure 4.7. In this figure the 8 bit multiplicand A can be decomposed into pair of 4 bits AH-AL. Similarly multiplicand B can be decomposed into BH-BL. The 16 bit product can be written as:

P = A x B= (AH-AL) x (BH-BL)
= AH x BH+AH x BL + AL x BH+ AL x BL

The outputs of 4X4 bit multipliers are added accordingly to obtain the final product with the help of three ripple carry adders. Now the basic building block of 8x8 bits Vedic multiplier is 4x4 bits multiplier which implemented in its structural model. For bigger multiplier implementation like 8x8 bits multiplier the 4x4 bits multiplier units has been used as components which are implemented in DSCH3.5 and MICROWIND 3.1 and the structural modelling of above design shows fastest design

VI. MGDI LOGIC DESIGN TECHNIQUE

First the GDI basic cell was introduced by Arkadiy Morgenshtein in 2002 [5]. The basic GDI cell (figure 2) contains one nMOS and one pMOS transistors with four terminals: G, P, N and D. Input G is the common gate input of nMOS and pMOS transistors, input P is the outer diffusion node of pMOS transistor, input N is the outer diffusion node of MOS transistor, and output D is the common output diffusion node of both transistors. The GDI primitive cells are designed in twin-well CMOS or silicon on insulator (SOI) technologies.

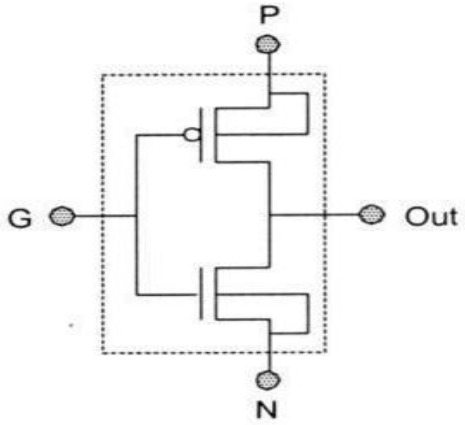

Figure.5. Basic GDI cell

With few improvements in GDI technique, paper [8] presented MGDI cell for all basic gates with minimum power dissipation. Figure 3 shows the design of MGDI basic gates for inverter, 2 input AND, OR, NAND, NOR, and 3 transistor XOR gates. The operation of OR gate is described here. For OR gate, the source of pMOS is connected with input "B" and the source of nMOS is connected with input "A". The gate terminal G is connected with "A". When both the inputs are at low level then pMOS will operates in linear whereas nMOS is cut-off. When A is at high and B is at low level then pMOS is in linear region and nMOS is in linear region thereby producing the output as 1. Similarly for A at low level and B is at high level then pMOS is in linear and nMOS is also in linear region again producing the output as 1 Similarly when A and B both are at high level , then pMOS and nMOS are again in linear region thereby producing the output as 1.

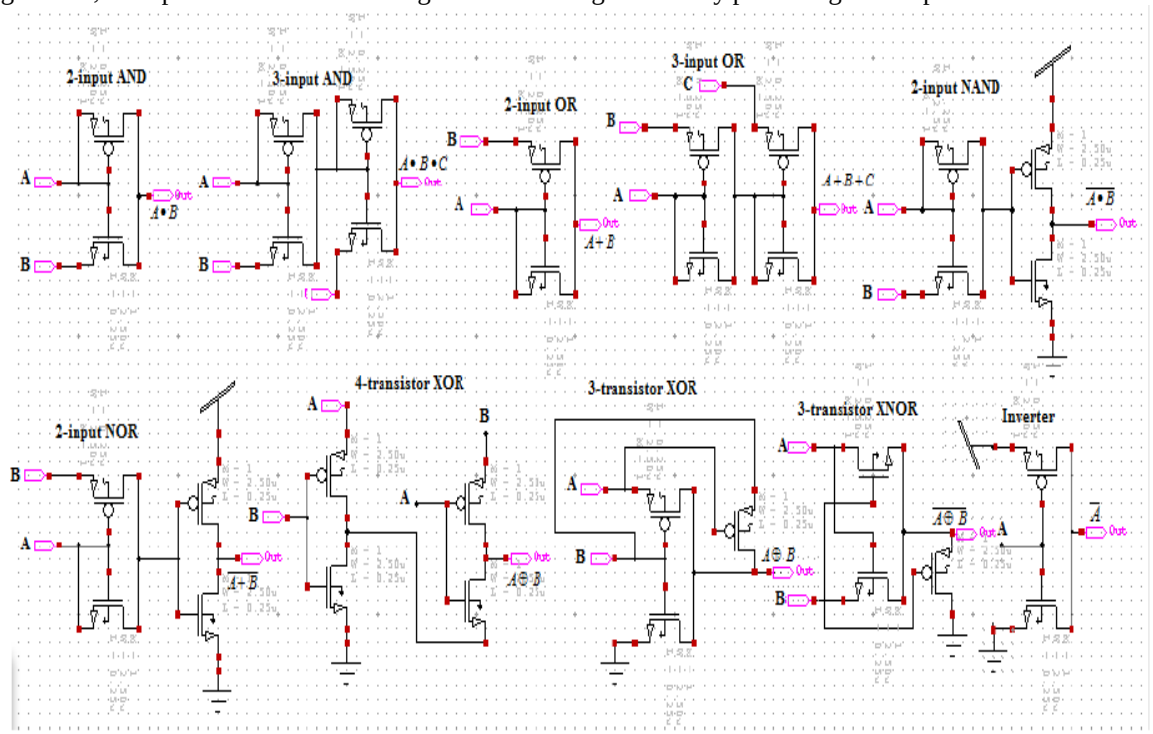

Figure.6 Basic Digital Gates using MGDI technique

The comparative performance analysis [8] of MGDI, and CMOS logic is presented in Table 1. The comparative performance is done with respect to switching delay, transistor count and average power consumed by MGDI, and CMOS logic. The Comparative Table No.1 shows that the MGDI performance is better when compared to CMOS logic. CMOS technique uses double number of transistor compare to MGDI to realize any digital gates. The transistors used to design XOR and XNOR has only three transistors in MGDI whereas CMOS logic uses eight transistors.

VII. Implementation Of Pipelined Multiplier Using MGDI Cell

Binary Pipelined Multiplier for 2x2 bit 4x4 and 8x8 bit multiplication is designed using MGDI cell. First Basic gates, Half Adder, Full Adder and Ripple Carry Adder are designed using MGDI cell in MICROWIND & DSCH tools with 0.12µm technology with 1.2v supply voltage. The W/L ratio of both nMOS and pMOS transistors are taken as 1.0/0.12µm. To establish an unbiased testing environment, the simulation of multiplier designs have been carried out using comprehensive input bits, which covers every possible transition for multiplier and multiplicand bits. The cell delay are been measured from the instant inputs reach 50% of the voltage supply level to the instant the latest of the output signals reach the same voltage level. All the transitions from an input bit combination to another have been tested and the delay at each transition has been measured. The average has been considered as the cell delay. The power dissipation of multiplier is also measured for these input patterns and its average power has been reported.

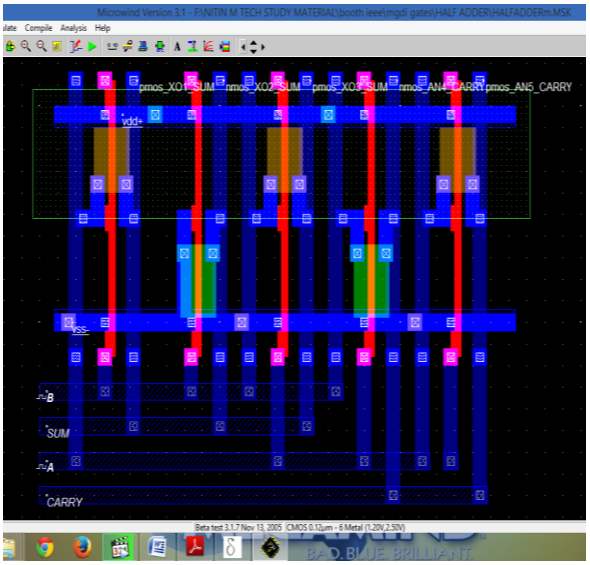

Figure 7 Layout of MGDI Half Adder

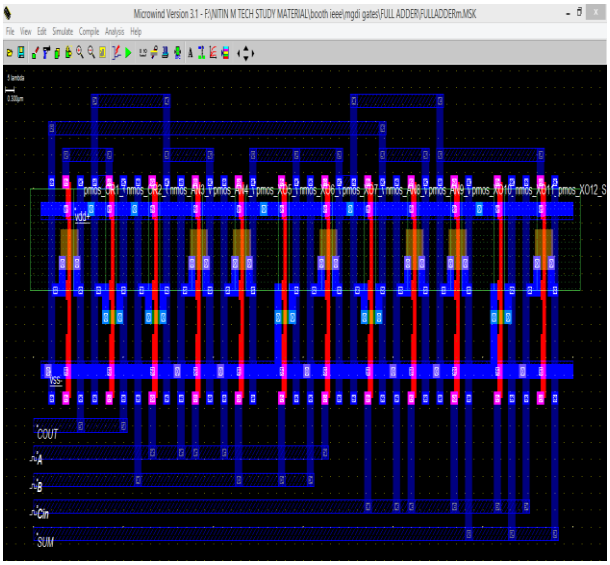

Figure 8 Layout of MGDI Full Adder

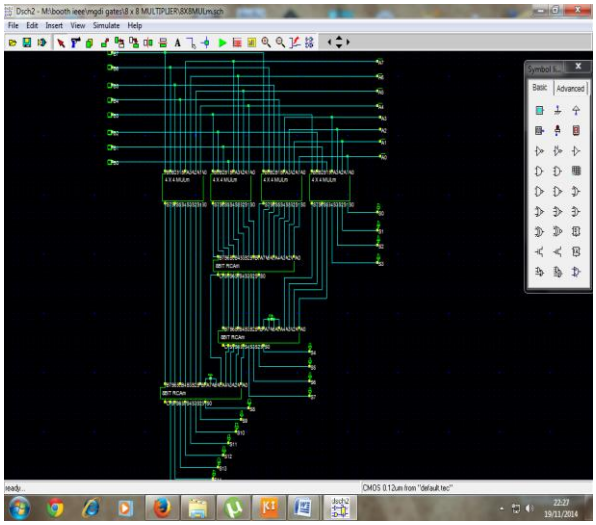

Figure 9 Layout of MGDI 4 X 4 Multiplier

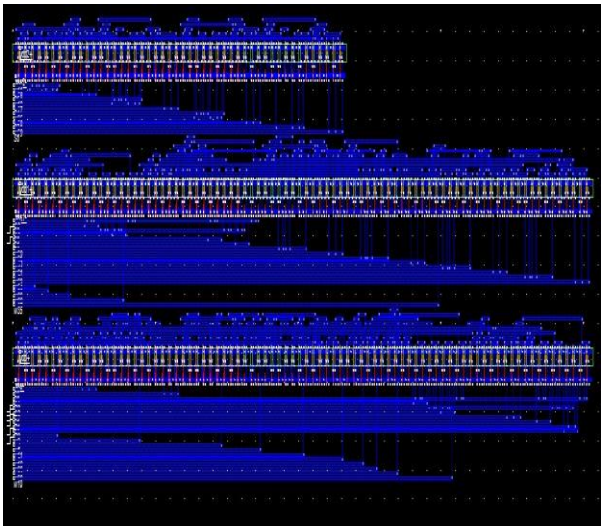

Figure 10 Layout of MGDI 8 X 8 Multiplier

VIII. Simulation Results

Schematic of Multipliers are designed using DSCH 3.5 VLSI CAD tool and simulation is done while the Layout is generated using MICROWIND 3.1. For 8-bit multiplication, figure 9 shows simulation result for input multiplicand bit $(19)_{10}$ = $(00001011)_2$ and multiplier bit $(11)_{10}$ = $(00010011)_2$ and its output is $(209)_{10}$ = $(0000000011010001)_2$

TABLE NO.1

S.No.	Primitive Cell	Switching Delay (ns)		Power Dissipation		Area (um)		Transistors Used	
		CMOS	MGDI	CMOS	MGDI	CMOS	MGDI	CMOS	MGDI
1	2-INPUT AND GATE	0.51	0.2	0.528	0.379	67.23	29.7	6	2
2	2-INPUT OR GATE	0.59	0.23	0.977	0.098	97.7	29.8	6	2
3	INVERTER	0.2	0.2	0.867	0.923	27.2	27.2	2	2
4	2-INPUT NAND GATE	0.35	0.41	1.615	0.779	107.7	65.03	4	4
5	2-INPUT NOR GATE	0.35	0.42	0.887	0.608	58.3	63.02	4	4
6	2-INPUT XOR GATE	0.61	0.27	0.0978	0.589	91	45.7	6	3
7	2-INPUT XNOR GATE	0.35	0.25	0.833	0.531	58.3	41	4	3
8	2:1 MULTIPLEXER	0.34	0.2	0.94	0.517	97.7	32.4	6	2

Table 2
ANALYSIS OF 4X 4 MULTIPLIER

S.NO.	PARAMETERS	CMOS TECH.	MGDI TECH.
1	SWITCHING DELAY (Min. , Max)	0.79,15.29 ns	0.29,8.91 ns
2	VERILOG FILE SIZE (Lines)	970	257
3	NO. OF SYMBOLS USED	913	241
4	COMPILED CELLS	429	216
5	ROUTED WIRES	88	109
6	NO. OF NMOS TRANS. USED	399	92
7	NO. OF PMOS TRANS. USED	399	124
8	ELECTRICAL NODES COMPILED	542	130
9	AREA (μm^2)	20649.2	5770.1
10	TRANSISTORS USED	798	218

Table 3
ANALYSIS OF 8 X 8 MULTIPLIER

S.NO.	PARAMETERS	CMOS TECH.	MGDI TECH.
1	SWITCHING DELAY (Min., Max)	0.79,40.5 ns	0.3,20.5 ns
2	VERILOG FILE SIZE (Lines)	3880	1261
3	NO. OF SYMBOLS USED	3652	1193
4	COMPILED CELLS	1716	1152
5	ROUTED WIRES	352	136
6	NO. OF NMOS TRANS. USED	1596	488
7	NO. OF PMOS TRANS. USED	1596	664
8	ELECTRICAL NODES COMPILED	2168	714
9	AREA (μm^2)	82596	31779.2
10	TRANSISTORS USED	3192	1152

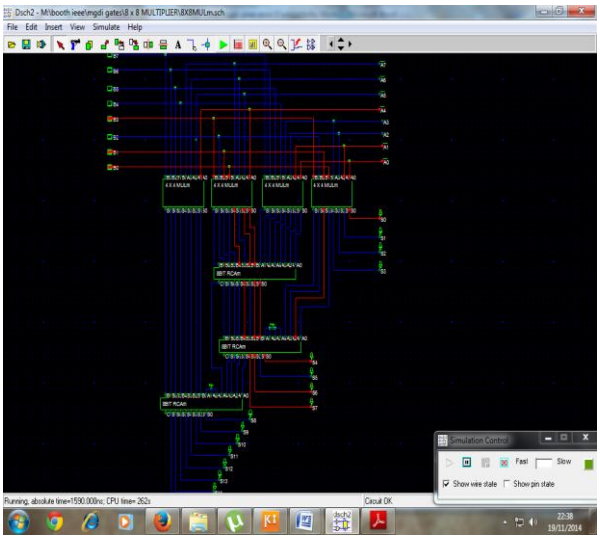

Figure 11 Simulation result $(19)_{10}$ x $(11)_{10}$

IX. Conclusion

This paper has presented the architecture design, logic design and circuit implementation of 8 Bit Pipelined Multiplier. The objective for Area, delay and power in Multipliers was carried out for bit multiplication using CMOS and MGDI techniques and Comparison with CMOS Technique are shown in Table1, Table 2 and Table 3.The Pipelined Multiplier with MGDI technique gives less delay and less power dissipation with higher-speed of operation as compared to CMOS Technique.

Acknowledgment

I would like to say thanks to my guide Associate Professor. Mr. M.Zahid Alam who gave their knowledge and time in order to complete this paper. This paper will never complete without the support faculty member of ECE department of L.N.C.T College, Bhopal.

REFERENCES

[1] Massoud Pedram, "*Design Technologies for Low Power VLSI*", to spear in Encyclopedia of Computer Science and Technology, 1995.

[2] Anantha P Chadrakasan and Robert W Brodersen, "*Minimizing Power Consumption in CMOS Circuits*", Proceedings of IEEE, Vol.83, No.4,April 1995.

[3] Book by Dimitris Soudris, Christian Piguet and Costas Goutis,"*Designing CMOS circuits for Low Power*", May 2002

[4] Pushpalata Verma (June 2012), "Design of 4x4 bit Vedic Multiplier using EDA Tool "International Journal of Computer Applications (0975 – 888) Volume 48– No.20, 32.

[5] Arkadiy Morgenshtein, Alexander Fish, and Israel A. Wagner, "*Gate Diffusion Input (GDI)-A Power-Efficient method for digital combinatorial circuits"* IEEE Transactions on VLSI systems, vol.. 10,No. 5, October 2002

[6] PhD Thesis by Gary W. Bewick, "*Fast Multiplication: Algorithms and Implementation*", Feb 1994

[7] R.Uma and P. Dhavachelvan, "*Modified Gate Diffusion Input Technique: A New Technique for Enhancing Performance in Full Adder Circuits*", 2nd International

[8] I.S. Abu I.S.Abu-Khater, A. Bellaouar, and M. I. Elmastry, "Circuit techniques for CMOS low-power high-performance multipliers," IEEE J. Solid-State Circuits, vol. 31, pp. 1535–1546, Oct. 1996.

[9] Chidgupkar, P. D. and Karad, M.T., "*The Implementation of Vedic Algorithms in Digital Signal Processing*", Global Congress on Engineering Education, Vol. 8, No.2, 2004.

[10] Himanshu Thapliyal and Vishal Verma ,"*High Speed Efficient Signed/Unsigned N X N Bit Multiplier Based On Ancient Indian Vedic Mathematics*"proceedings of the 7th IEEE VLSI Design & Test Workshop, Bangalore, August 2003.

OPEN ACCESS

International
Journal
Of Modern Engineering Research (IJMER)

A Study on Mathematical Statistics to Evaluate Relationship between Attributes

Dr. Vinay Pandit
Lala Lajpat Rai College

I. Introduction

The **goodness of fit** of a statistical model describes how well it fits a set of observations. Measures of goodness of fit typically summarize the discrepancy between observed values and the values expected under the model in question. Such measures can be used in statistical hypothesis testing, e.g. to test for normality of residuals, to test whether two samples are drawn from identical distributions (see Kolmogorov–Smirnov test), or whether outcome frequencies follow a specified distribution (see Pearson's chi-squared test).

When an analyst attempts to fit a statistical model to observed data, he or she may wonder how well the model actually reflects the data. How "close" are the observed values to those which would be expected under the fitted model? One statistical test that addresses this issue is the chi-square goodness of fit test. This test is commonly used to test association of variables in two-way tables (see "Two-Way Tables and the Chi-Square Test"), where the assumed model of independence is evaluated against the observed data. In general, the ***chi-square test statistic*** is of the form.

$$X^2 = \sum \frac{(\text{observed} - \text{expected})^2}{\text{expected}}$$

II. Objective Of Research

1. To study the test of goodness of fit to find relation between location and frequency of visit.
2. To study the test of goodness of fit to find relation between location and customer service provided by Future group.
3. To study the test of goodness of fit to find relation between frequency of visit and customer service provided by Future group.

III. Scope

1) The researcher has made an attempt to collect data which is representative of central and western part of South Mumbai. This scope of study was taken due to logistical problem and also Mumbai is and miniature of Maharashtra.
2) Here after, the researcher will include whether study is restricted to one brand, one company, specific age group etc.
3) The scope of this research is to identify the buying behaviour of customers of Central. This research is based on primary data and secondary data. This study only focuses on urban buying behaviour of customers.
4) The study does not say anything about rural buying behaviour of customer because rural norms/status/attitude & acceptance of the rural customers differs with urban customers.
5) The scope of study was only restricted to only chi square test of goodness of fit.

IV. Hypothesis

Hypothesis 1

H_0-There is no relationship between location & frequency of visit.
H_1-There is a relationship between location & frequency of visit.

Hypothesis 2

H_0 - There is no relationship between location and customer service provided by Central.
H_1 – There is a relationship between location and customer service provided by Central.

Hypothesis 3

H_0 - There is no relationship between frequency of visit and customer service provided by Central.
H_1 – There is a relationship between frequency of visit and customer service provided by Central.

V. Data Collection

Primary Source:

The primary data was collected by means of a survey. Questionnaires were prepared and customers of the Central at two branches were approached to fill up the questionnaires. The questionnaire contains 20 questions which reflect on the type and quality of services provided by the Central to the customers. The response of the customer is recorded on a grade scale of strongly disagree, disagree, uncertain, agree and strongly agree for each question. The filled up information was later analysed to obtain the required interpretation and the findings.

Secondary Source:

In order to have a proper understanding of the customer service of Central a depth study was done from the various sources such as books, magazines; a lot of data is also collected from the official websites of the Central and the articles from various search engines like Google, yahoo search and answers.com. the concept of test of goodness of fit was also referred from reference books.

VI. Research Instrument

To collect the appropriate data the researcher has used the questionnaire as the research instrument. The questionnaire so formed includes both open ended and close ended questions.Close ended questions were used so that appropriate statistics could be calculated.Open ended questions were used to find out the reviews of the respondents so that a proper recommendation could be made by the researcher.

VII. Research Design

The research design is exploratory as well as descriptive when it comes to evaluating customer perception of customer service of the Central. Descriptive research answers the questions who, what, where, when and how.

VIII. Sampling Plan / Sampling Technique

8.1 Sampling Plan

Since it is not possible to study whole universe, it becomes necessary to take sample from the universe to know about its characteristics.

Contact Method: Personal Interview.

8.2 Sample Size

The survey was conducted in the city of Mumbai with two branches of Central, with 100 customers as respondent.

IX. Testing Of Hypothesis

The researcher has made an attempt to test the hypothesis using chi square test.

X. Research Limitations

- The study was restricted to test of goodness of fit only for chi- square test of independence
- The study is only for the Central confined to a particular location and a very small sample of respondents. Hence the findings cannot be treated as representative of the entire retail industry.
- Respondents may give biased answers for the required data. Some of the respondents did not like to respond.
- Respondents tried to escape some statements by simply answering “neither agree nor disagree” to most of the statements. This was one of the most important limitations faced, as it was difficult to analyse and come at a right conclusion.
- In our study we have included 100 customers because of time limit.

XI. Data Analysis

Hypothesis 1:

H_0-There is no relationship between location & frequency of visit.

H_1-There is a relationship between location & frequency of visit.

Table 1: observed values

Frequency of visit	Location		
	Yes	No	Total
Twice a week	6	5	11
During special offers	12	13	25
Once a week	7	2	9
Whenever need arises	41	14	55
Total	66	34	100

Source: Survey

Table 2: Expected values:

Frequency of visit	Location	
	Yes	No
Twice a week	11/100x66=7.26	11/100x34=3.74
During special offers	25/100x66=16.5	25/100x34=8.5
Once a week	9/100x66=5.94	9/100x34=3.06
Whenever need arises	55/100x66=36.3	55/100x34=18.7

$\chi^2=\sum \frac{(\text{Observed-Expected})^2}{\text{Expected}}$

$=\{[6-7.26]^2/7.26\}+\{[5-3.74]^2/3.74\}+\{[12-16.5]^2/16.5\}+\{[13-8.5]^2/8.5\}+\{[7-5.94]^2/5.94\}+\{[2-3.06]^2/3.06\}+\{[41-36.3]^2/36.3\}+\{[14-18.7]^2/18.7\}$

$=0.22+0.42+1.23+3.56+1.46+0.37+0.61+1.18$

$\chi_{cal}=9.05$

D.F. = (rows–1) (columns–1)

= 3 x 1

= 3

$\chi^2_{critical}$ at 5% level of significance and 3 degree of freedom= 7.816

$\chi^2_{cal}>\chi^2_{critical}$

Therefore reject H_0.

Therefore, there is a relationship between location and frequency of visit.

Hypothesis 2:

H_0 - There is no relationship between location and customer service provided by Central.

H_1 – There is a relationship between location and customer service provided by Central.

Table 3 Observed values:

Customer service provided	Location		
	Yes	No	Total
Strongly disagree	5	3	8
Disagree	11	5	16
Neither disagreeNor agree	25	15	40
Agree	21	9	30
Strongly Agree	4	2	6
Total	66	34	100

Source: Survey

Table 4: Expected values

Customer service provided	Location	
	Yes	No
Strongly disagree	8/100x66=5.28	8/100x34=2.72
Disagree	16/100x66=10.56	16/100x34=5.44
Neither disagreeNor agree	40/100x66=26.4	40/100x34=13.6
Agree	30/100x66=19.8	30/100x34=10.2
Strongly Agree	6/100x66=3.96	6/100x34=2.04

$\chi^2 = \sum \frac{(\text{Observed-Expected})^2}{\text{Expected}}$

$=\{[5-5.28]^2/5.28\}+\{[11-10.56]^2/10.56\}+\{[25-26.4]^2/26.4\}+\{[21-19.8]^2/19.8\}+\{[4-3.96]^2/3.96\}+\{[3-2.72]^2/2.72\}+\{[5-5.44]^2/5.44\}+\{[15-13.6]^2/13.6\}+\{[9-10.2]^2/10.2\}+\{[2-2.04]^2/2.04\}$

$\square^2_{cal}$ **=0.72**

D.F. = (rows–1) (columns–1)

= 4 x 1

= 4

$\chi^2_{critical}$ at 5% level of significance and 3 degree of freedom= 9.49

$\chi^2_{cal} < \chi^2_{critical}$

Therefore reject H_1.

Therefore, there is no relationship between location and customer service provided by Central.

Hypothesis 3:

H_0 - There is no relationship between frequency of visit and customer service provided by Central.

H_1 – There is a relationship between frequency of visit and customer service provided by Central.

Table 5: Observed values

Customer service provided	Frequency of visit				
	Excellent	Good	Average	Fair	Total
Twice a week	3	2	3	2	12
During special offers	3	12	7	2	24
Once a week	1	2	6	0	9
Whenever the need arises	4	26	19	6	55
Total	11	44	35	10	100

Source: Survey

Table 6: Expected values

Customer service provided	Frequency of visit			
	Excellent	Good	Average	Fair
Twice a week	12/100x11= 1.32	12/100x44= 5.28	12/100x35= 4.2	12/100x10= 1.2
During special offers	24/100x11=2.64	24/100x44= 10.56	24/100x35= 8.4	24/100x10= 2.4
Once a week	9/100x11= 0.99	9/100x44= 3.96	9/100x35= 3.15	9/100x10= 0.9
Whenever the need arises	55/100x11= 6.05	55/100x44= 24.2	55/100x35= 19.25	55/100x10= 5.5

$\chi^2 = \sum \frac{(\text{Observed-Expected})^2}{\text{Expected}}$

$=\{[3-1.32]^2/1.32\}+\{[3-2.64]^2/2.64\}+\{[1-0.99]^2/0.99\}+\{[4-6.05]^2/6.05\}+[\{2-5.28]^2/5.28\}+\{[12-10.56]^2/10.56\}+\{[2-3.96]^2/3.96\}+\{[26-24.2]^2/24.2\}+\{[3-4.2]^2/4.2\}+\{[7-8.4]^2/8.4\}+\{[6-3.15]^2/3.15\}+\{[35-19.25]^2/19.25\}+\{[2-1.2]^2/1.2\}+\{[2-2.4]^2/2.4\}+\{[0-0.9]^2/0.9\}+\{[6-5.5]^2/5.5\}$

χ^2_{cal} **=22.98**

D.F. = (rows–1) (columns–1)

= 3 x 3

= 9

$\chi^2_{critical}$ at 5% level of significance and 9 degree of freedom= 16.92

$\chi^2_{cal} > \chi^2_{critical}$

Therefore reject H_0.

Therefore, there is a relationship between frequency of visit and customer service provided by Central.

XII. Findings Of The Report

- Central is undoubtedly number one retailer in India. It has built very emotional & cordial relationship with its customers.
- They are also intending to build long term relationship with all its stakeholders which are very essential for successful business venture.
- In order to attract customer they should provide good parking facility

- Cleanliness and hygienic environment is also the major concern for Central. Management needs to be focus on it.
- Store layout should also be developed in an efficient manner so that customer can get things easily.
- According to research I found that most of the people were affected & attracted with offers and schemes. So, Central should employ those people who are well trained to provide information to customer regarding new things to enhance its customer services.
- Consumer chooses malls to shop because they all want variety and brands. According to customers it is economical as compared to other places.
- We can also say that location, variety conveniences and economical products are not the only thing which attracts the customer but good customer service is one of the crucial factors that attract customers.

XIII. Conclusion

- As most of the retail industries did market research before entering into market. Same thing was done by Central. Location, market, consumer perception analysis was done by Central.
- In one year, much more diversification was done in it. And to retain customers they use many loyalty programs & IT techniques.
- Central, a part of future group is a hypermarket offering a huge array of goods of good quality for all at affordable prices. Central with over 214 outlets in different part of India is present in both the metro cities as well as in small towns.
- Central can attract more customers by different variety and assortments.
- They can improve customer satisfaction by providing home delivery services.
- We can conclude that Central has one of the major retail industries in India.
- Working environment is good and also the various facilities are provided to increase the customer services.
- There exist a healthy & strong relationship between employees and managers.
- The employees accept their responsibility wholeheartedly and perform the services in well manner that satisfied the customers.

XIV. Recommendations

- Advertising is the basic and most prominent tool to increase the awareness of product. So, Central should use this tool to increase their share in the market.
- Retail business is successful only when they have a good customer services. Customer loyalty can only be gain by providing good or satisfied services to the customers.
- Most respondents take on the spot decision of buying different products because of the various attractive products displays. So pretty combination with good services should be done to retain customers.
- Quality plays a major role because most respondent said that they want a quality product and that's also the one of the reason for most of the respondents sticking to particular brand.
- Customers are very price conscious they are having many options in the market. The following steps should opt :-
- Should follow more of high low pricing rather than everyday low pricing
- Should go for a weekly coupon system as it holds more of the loyal customers.
- Should provide good customer services so that customer likes to visit again.
- There should be a proper assortment of various product categories.
- Proper training should be provided to the customer so that they can deal with customer efficiently
- Various offers can be provided to them to attract new customers.
- Quality in product should be reached up to mark.

REFERENCES

[1]. Anderson, G. (1994). "Simple tests of distributional form", Journal of Econometrics, 62, 265-276.
[2]. Mann, H. B. and Wald, A. (1942). "On the choice of the number of class intervals in the application of the chi-square test". Annals of Mathematical Statistics , 13, 306-317. 21
[3]. McCulloch, J. H. (1994). Financial applications of stable distributions. In Statistical methods in finance (Maddala, G.S., and Rao, C.R., Eds.) Elsevier, pp.393-425.
[4]. Noceti, P, Smith, J. and Hodges, S. (2003). "An evaluation of tests of distributional forecasts", Journal of Forecasting , 22, 447-455.
[5]. Rachev, Svetlozar T. and Mittnik, S. (2000). Stable Paretian models in finance . Wiley.
[6]. Ramberg, J.S., Dudewicz, E.J., Tadikamalla, P.R. and Mykytka, E. (1979). "A probability distribution and its uses in fitting data". Technometrics , 21, 201-214.

OPEN ACCESS

International
Journal
Of Modern Engineering Research (IJMER)

Improving the Stability of Cascaded DC Power Supply System by Adaptive Active Capacitor Converter

B. Prudvi Kumar Reddy[1], B. Amruth Kumar Reddy[2]
[1]M.Tech Student, Dr.K.V.S.R College of Technology, Kurnool, Andhra Pradesh
[2] EEE Department, .K.V.S.R College of Technology, Kurnool,, Andhra Pradesh

Abstract: *When all links are changes in the cascade is the corner of the shape in the dc division energy orbit (DEO). When resistances are intermission betwixt one by one stylish changes in that would possibly end up so the cascaded orbits are unsteady. They are antecedent we can place in a nearer to the useful in the cascaded orbit can be got in compelled to vary the supply they have load changes in the internal structure of the same regions in the electrical device they can be opposed in a quality of the characteristic of dc DEO. Throughout the Associate in nursing adaptation active device in the (AACC) we can know another determined in the cascaded orbit. Therefore the AACC was connected by side by side in the cascaded orbit's they can mediate in between the carries and completely a requirement of a notice then they carries the voltage with none modification in this subsystems. Then it will have a stylish to the customary have basic units to measuring in the dc DEO. When the AACC is additionally a similar bus device to cut back the output resistance of the supply device, therefore averting in a interiority have their load changes in the input resistance, of the cascaded orbit have their solutions then they becomes constant. We have important carrier device it will computing in the AACC adaptation in line with they have output energy to the cascaded orbit, they have energy vesting in the AACC that's way they will reduced and therefore they have a lot of energy in a reacting to the orbit so it is a best in the orbit of a submissive device. What\'s many, since no capacitance have a requirement among an AACC, when the cascaded orbits have their quantity of it slowly it will extend in time. They have activity fundamental truth to stop their magnificence thought in the AACC are mentioned throughout of this project, it can have four thousand eight hundred and zero watts cascaded orbit was contain a strive of process to move in a full-bridge changes they can be styli shed and evaluated. So when the simulation solutions have to clear the performance of the arrangement of AACC.*

Index Terms: *Active capacitor converter, adaptive control, cascaded System, modularization, stability.*

I. INTRODUCTION

The dc division energy orbit (DEO) has been used widely in such applications as space stations, aircraft, communication systems, industrial autonomous production lines and defense electronic power systems for the last 20 years [1]–[5], due to its flexile system configuration, high-efficiency energy conversion, and high-density power delivery capability .One of the dc DEO'S attractive characteristics is modularity design[6], in which each Subsystem is first designed individually as a module, and then all subsystems are integrated to form a dc DEO. The modularization characteristic of dc DEO cuts down the system's development cycles and costs effectively. In a dc DPS, there are various ways to connect the subsystems, among which, a typical connection style is cascaded Converters.

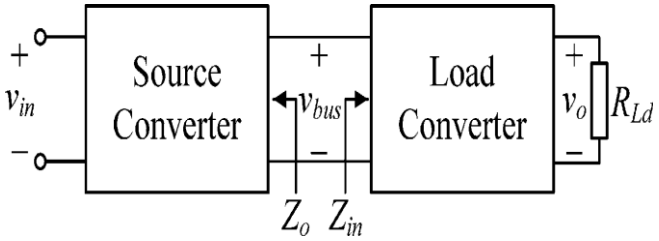

Fig. 1. Cascaded power supply system.

The cascaded system may have stability problem due to the interaction between the subsystems, even though each subsystem is individually well designed to be stable on its own [7]–[12].This problem was first analyzed by idle brook [13]. It was shown that for the typical cascaded system shown in Fig. 1, the ratio of the source converter's output impedance *Zo* and the load converter's input impedance *Z*in, *Zo* /*Z*in , can be equivalently represented as the loop gain of the cascaded system. It was also pointed out that if both the ource converter and the load converter are stable individually, and *Zo* is less than *Z*in in the entire frequency ranges, the stability of the cascaded system will be guaranteed. This is the so-called Middle brook criterion. Subsequently, various impedance criteria aiming at a more accurate and practical prediction of the subsystem interaction had been developed in the last two decades [14]–[19].Solutions for solving the instability problem have been proposed and can be broadly classified into two types: passive [20]–[22] and active [23]–[29] methods. Passive methods employ passive components, such as resistors, capacitors, and inductors, to improve system stability. A resistive load was added to modify load dynamic characteristics in [20], thereby improving system stability. Both *RC* and *RL* dampers were introduced to minimize the output impedance peak of the source converter in [21] and [22], thus ensuring *Zo* be less than *Z*in in the entire frequency ranges. The passive methods incur significant power dissipation. Active methods for stabilizing the system are based on modifying the control of the source converter [23]–[26]and/or load converter [27], or adding a power buffer between the source and load subsystems [28], [29]. The former approach, however, is usually complex in implementation and sometimes proposed conflicting with other control objectives. For the latter approach, the power buffer is connected in series in-between the subsystems, and would affect the impedance interaction during the transient that may not be acceptable in some applications. All the aforementioned solutions need to change the internal structure, including the main circuit and/or control circuit, of the dc DEO's subsystems, leading to redesign of the subsystems that have already been modularly designed. This contradicts with the objective of the modularity design of dc DPS and increases the system's development cycles. This paper introduces an adaptive active capacitor converter (AACC) connected in parallel with the remediate bus of the cascaded system. The AACC is equivalent to an adaptive bus capacitor varied with the cascaded system's output power; which reduces the output impedance of the source converter to avoid interacting with load converter's input impedance. As a result, the cascaded system becomes stable. The AACC only needs to detect the intermediate bus voltage without changing anything of the existing subsystems; hence, it serves as a standard stabilizer for dc DEO. Meanwhile, the equivalent capacitor of the AACC is adaptive, ensuring a minimal additional power loss and a better dynamic response of the system than that using a passive capacitor. Furthermore, as no electrolytic capacitor is required in the AACC, the lifetime of the cascaded system is prolonged. This paper first analyzes the impedance characteristics and instability problem of the cascaded system in Section II, and presents the concept, operating principle, ad control strategy of AACC in Section III. The design procedure and a design ample of AACC are given in Section IV. Section V shows he experimental results that verify the effectiveness of the proposed method. Finally, Section VI concludes this paper

II. Impedance Characteristics And Instability Problem Of Cascaded System

A. Review of Subsystem's Impedance Characteristics and Cause of Instability

For cascaded systems, the impedance characteristics of subsystems and the cause of instability have been studied extensively during the last two decades [30]–[35]. Some general conclusions are summarized as follows:

1) Impedance characteristic of *Zo* : *Zo* is the source converter's output impedance independent of its load resistor. As shown in the dotted line of Fig. 2, *Zo* is similar to the output impedance of an *LC* filter. If*f* < *fc S*, *Zo* presents

the characteristic of an inductor; and if *f* > *fc S*, *Zo* presents the characteristic of source converter's output filter capacitor. Here, *fc S* is the cutoff frequency of the source converter's voltage loop. Note that *Zo* 's peak value ,*Zo* peak, appears at *fc S* and is inversely proportional to source converter's output filter capacitor [30].

2) Impedance characteristic of *Z*in : In Fig. 2, the solid line

Represents *Z*in that is the input impedance of load converter

Operating in continuous current mode (CCM). If*f* < *fc L*, *Z*in behaves as a negative resistor, whose value equals to $-V2$

bus/*Po* [31], where *V*bus is the intermediate bus voltage and *Po* is the load converter's output power

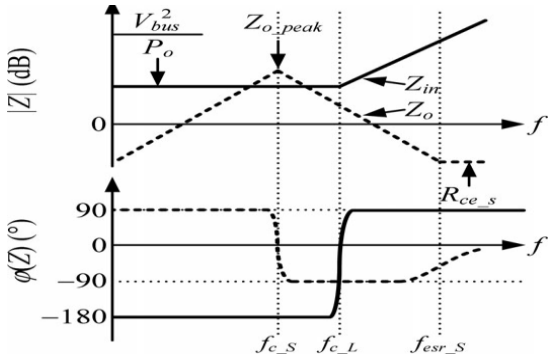

Fig. 2. Impedance interaction of the cascaded system.

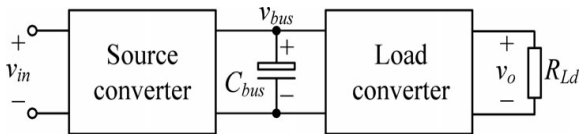

Fig. 3. Cascaded system with additional intermediate bus capacitor

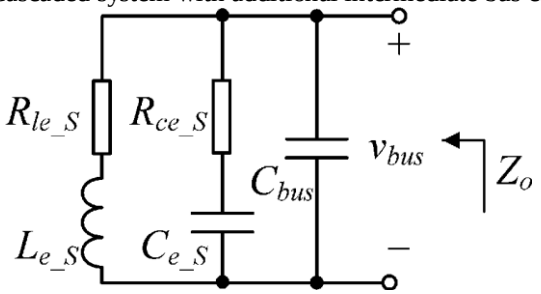

Fig. 4. Equivalent model of *Zo* with additional intermediate bus capacitor

and if *f* > *fc L*, *Z*in behaves as an inductor. Here, *fc L*is the cutoff frequency of the load converter's voltage loop. Note that when *f* < *fc L* , the magnitude of *Z*in is inversely proportional to *Po* [32].

3) Cause of instability: In a cascaded system, as shown in

Figs. 1 and 2, if *Zo* is intersected with *Z*in and *fc S* is less than *fc L* , the cascaded system will be unstable [33].In this case, the oscillation frequency is *fc S* that is unaffected by system's power [34].

The above analysis indicates that *Zo* is not affected by *Po* , and when *f* < *fc L* , the magnitude of *Z*in is inversely proportional to *Po* . Thus, the cascaded system is most likely to be unstable at full load because *Z*in is minimal and easily intersected with *Zo*at this condition. Note that the above conclusions are general and applicable to all dc–dc converters.

B. Solving the Instability Problem by Adding Intermediate Bus Capacitor

There is nothing more desirable than a total separation between *Zo* and *Z*in to ensure that the cascaded system is stable. Since |*Zo* peak| is inversely proportional to source converter's output filter capacitor [30], one intuitive way is to reduce the source converter' output impedance by adding an intermediate bus capacitor *C*bus to the cascaded system, as shown in Fig. 3.Here, *C*bus can be treated as an additional output filter capacitor of the source converter, and the equivalent *LC* output impedance model of source converter with *C*bus is given in Fig. 4. In Fig. 4, *Le S* is the equivalent filter's inductor, *Ce S* is the equivalent filter's capacitor, *Rle S* is the parasitic resistor of

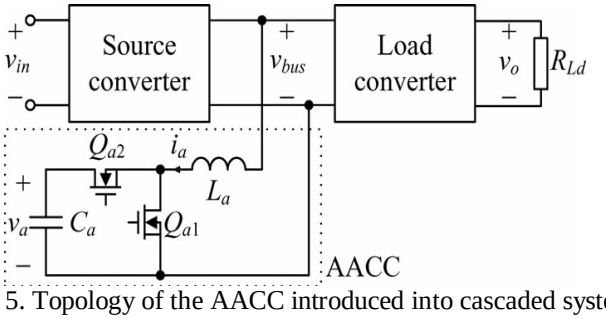

Fig. 5. Topology of the AACC introduced into cascaded system

Le S , and *Rce S* is the equivalent series resistor (ESR) of *Ce S* that can be measured from Fig. 2. Also, *Ce S*, *Le S* , and *Rle S* are expressed in (1)–(3), respectively

$$Ce\ S = 1/2\pi Rce\ S\ fesr\ S \quad (1)$$

$$Le\ S = 1/(2\pi fc\ S)2\ Ce\ S \quad (2)$$

$$Rle\ S = Le\ S/Ce\ S \cdot |Zo\ \text{peak}| - Rce\ S \quad (3)$$

where *f*esr *S* is the zero caused by the ESR of *Ce S* .

According to (1)–(3), the peak value of *Zo* in Fig. 4 is derived as

$$|Zo\ \text{peak}| = Le\ S/(Ce\ S + C\text{bus})\ (Rle\ S + Rce\ S)\ . \quad (4)$$

Thus, in order to ensure that *Zo* < *Z*in in the entire frequency ranges, |*Zo* peak| must satisfy

$$|Zo\ \text{peak}| \leq V\ 2\text{bus}/Po \quad . (5)$$

From (4) and (5), the required value of *C*bus can be obtained as

$$C\text{bus} \geq Le\ SPo/V\ 2\text{bus}\ (Rle\ S + Rce\ S) - Ce\ S. \quad (6)$$

According to (6), the required *C*bus increases with the increase of *Po* , so, if a capacitor is employed, its value must be selected by (6) at full load. However, a larger *C*bus results in a smaller bandwidth of the source converter that is already modularly designed, leading to a poor dynamic performance [35].Since the required *C*bus is relatively large, it inevitably adopts electrolytic capacitor, indicating a significant reduction of the lifetime [36].

In fact, the value of *C*bus could be selected adaptively according to *Po* , as shown in (6), which keeps *C*bus at its minimal required value for different loads. In this way, the cascaded system does not only ensure stable, but also achieves a better dynamic response.

III. Topology And Control Of The Proposed AACC

A. Topology of AACC

The adaptively varying *C*bus mentioned in Section II can be

Emulated by a converter, as shown in the dashed block in Fig. 5.The converter is referred to as AACC. The AACC is composed of switches *Qa*1 and *Qa*2 , inductor *La* , and capacitor *Ca*. It is connected to the intermediate bus of the cascaded system. By controlling *La* 's current appropriately, the terminal characteristic at the bus side of AACC will present an adaptively varying *C*bus that ensures the stability of the cascaded system and improves the dynamic response.

The AACC is also suitable for the cascaded system with multiple load converters. In this case, the AACC has the same operation principle with the system of Fig. 5, which just makes the source converter's output impedance lower than the total input impedance of the multiple load converters [17].

This paper analyzes the case shown in Fig. 5, but the conclusion applies to the system with multiple load converters.

B. Control of AACC

Since the function of AACC is to emulate the adaptive *C*bus, the current of *La, ia* , should be controlled as

$$ia\ (t) = C\text{bus}(dv\text{bus}/dt) \quad . (7)$$

According to (6) and (7), it can be known that *ia* varies with *Po* . Considering *Po* can be reflected by the oscillation rippleof *v*bus, Δ*v*bus [37], *ia* could be controlled by Δ*v*bus, whose control cicuit is realized by a simple analog circuit, as shown inFig. 6. The control circuit for *ia* would only need to detect *v*bus without changing any part of the existing subsystems. Thus, the AACC can be designed as a standard module for dc DPS.As shown in Fig. 6, *v*bus first goes through a differential circuit (sub circuit A) to get the form of *ia* ref (*dv*bus/*dt*), defined as *v*1 . Meanwhile, Δ*v*bus is extracted from *v*bus by the filter comprising *C*2 and *R*5 , and then it is sent to the rectifier circuit and a peak value detection circuit, producing Δ*v*bus's magnitude*v*2 . Then, *v*2 is compared with the preset allowable voltage ripple Δ*V*bus allow, and the error is amplified by amplifier A4. The output of A4, *v*3 , is the magnitude of *ia* ref . Therefore, *ia* refis adaptively varied by *Po*: a large *Po* brings a larger Δ*v*bus, leading to a larger *ia* ref , which means a larger equivalent *C*bus of AACC; and on the contrary, a smaller *Po* gives a smaller equivalent *C*bus of AACC. Effectively, if *Po* is small enough, Δ*v*bus will be less than Δ*V*bus allow and *ia* ref will be zero, which means that *C*bus is no longer required at this time. Multiplying *v*1 with *v*3 by the multiplier, and the output,

ia ref *s* , is the required current, as seen in (7). In sub circuit C, *ia* ref *s* is filtered by *R*13 and *C*5 to produce *ia* ref , and only the Oscillation frequency component of *ia* ref *s* is retained. For proper operation of the AACC, *va* must be regulated at a value higher than *v*bus. A voltage closed loop must be included in the controller to enforce this (sub circuit D). Specifically, *va* is sensed and compared with the voltage reference *Va* ref , and the amplified error signal *v*4 is obtained. The sum of *ia* ref and *v*4with the weighted resistors *R*17 and *R*18, respectively, is used as the current reference of *ia* . The UC3525 controller is employed as the current regulator of *ia* and drive circuit of AACC. Also,*Qa*1 and *Qa*2 are switched in a complementary manner. The shutdown signal of UC3525 is generated by sub circuit F that determines the working mode of AACC automatically. If the

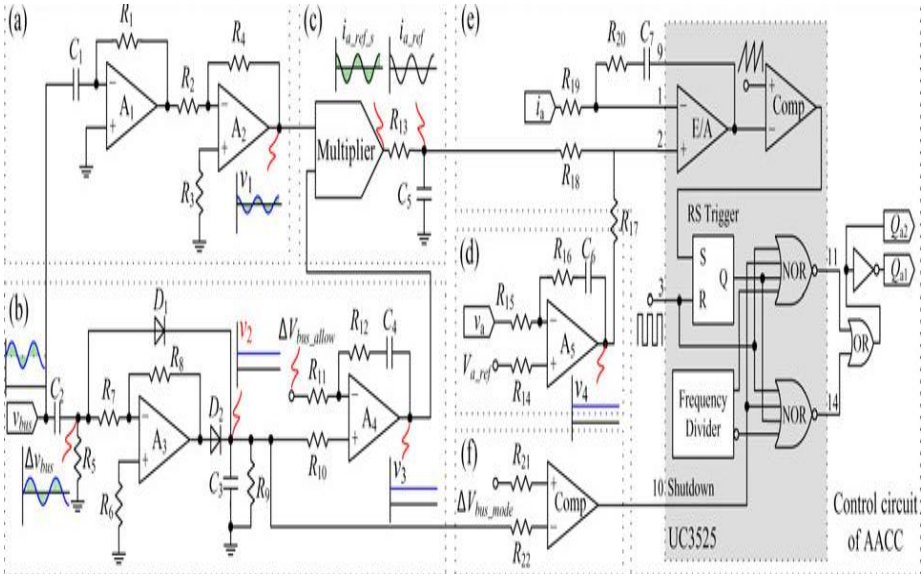

Fig. 6. Control circuit of the AACC

Cascaded system is unstable, the magnitude of Δ*v*bus, *v*2 , will be larger than the permitted value, denoted as Δ*V*bus mode, and the shutdown signal of UC3525 will become low. In this case, the AACC works normally. Otherwise, the shutdowns signal will go high, shutting down the AACC. Here, Δ*V*bus mode is set at a value below Δ*V*bus allow to ensure that AACC works well.

IV. Design Of AACC

A. Output Filter Capacitor Ca

With AACC, ignoring the switching harmonics of the cascaded system's intermediate bus voltage, *v*bus can be expressed as

$$v\text{bus} = V\text{bus} + \Delta V\text{bus allow} \sin \omega t. \quad (8)$$

where *V*bus is the average value of *v*bus, and ω is the angular frequency of the ripple in *v*bus, i.e., $\omega = 2\pi fc\ S$.
The instantaneous input power of AACC can be obtained by (7) and (8), i.e.,

$$pa\ (t) = v\text{bus}ia$$

$$= (V\text{bus} + \Delta V\text{bus allow} \sin \omega t)C\text{bus}\Delta V\text{bus allow}\omega \cos \omega t. \quad (9)$$

Generally, Δ*V*bus allow _ *V*bus; thus, (9) can be simplified as

$$pa\ (t) = V\text{bus}C\text{bus}\Delta V\text{bus allow}\omega \cos \omega t. \quad (10)$$

According to (7) and (10), the waveforms of the instantaneous input power *Pa* ,inductor current *ia* , and output filter capacitor voltage *va* of AACC are depicted in Fig. 7. It can be seen that *Ca* is discharged from *Tos* /4 to 3*Tos* /4, and *va* decreases; and *Ca* is charged from 3*Tos* /4 to 5*Tos* /4, and *va* increases. Consequently, the maximum and minimum values of *va* occur, respectively, at*Tos* /4 and 3 *Tos* /4.
The energy charging *Ca* from 3*Tos* /4 to 5*Tos* /4

$$\Delta E_a(t) = \int_{\frac{3Tos}{1}}^{t} P_a\ (t)dt$$

$$= \int_{3Tos/1}^{t} V_{bus}\, C_{bus} \Delta V_{bus\_allow}\, \omega \cos \omega t \, dt$$

$$= 2V_{bus} C_{bus} \Delta V_{bus\_allow} \sin^2 \left(\frac{\omega}{2t} + \pi/4\right) \quad (11)$$

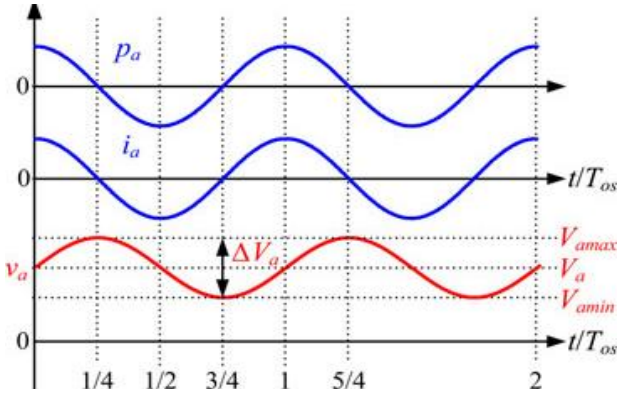

Fig. 7. Waveforms of instantaneous input power, inductor current, and output filter capacitor voltage of the AACC.

Here, Δ*Ea* (*t*) can also be expressed as

[ΔEa (t)=1/2CaV]_a^2(t) -1/2CaV]_(a min) ^2

where *Va* min is the minimum voltage of the capacitor *Ca* .

Putting (12) in (11) gives

[1/2Ca [V〗 _a^2(t) - V_ (a min) ^2] =2 VbusCbus ΔVbus_allow Sin2 (ω⁄2t +π⁄4)

(13)

From (13), we have

$$V_a(t) = \sqrt{\frac{4VbusCbus\Delta Vbus_{allow} Sin2\left(\frac{\omega}{2t}+\frac{\pi}{4}\right)}{Ca} + V_{a\,min}^2} \quad (14)$$

Substitution of *t* = 5*Tos* /4 into (14), the maximum voltage of the capacitor *Ca* can be derived as

$$V_{a\,max} = \sqrt{\frac{4V_{bus}C_{bus}\Delta V_{bus\_allow}}{C_a} + V_{a\,min}^2} \quad (15)$$

The average voltage of *Ca* can be approximated as

Vabc = (Va min + Va max)/2

$$= V_{a\,min} + \frac{\sqrt{4\,V_{bus}\,C_{bus}\Delta V_{bus_{allow}}\frac{}{C_a} + V_{amin}^2}}{2} \quad (16)$$

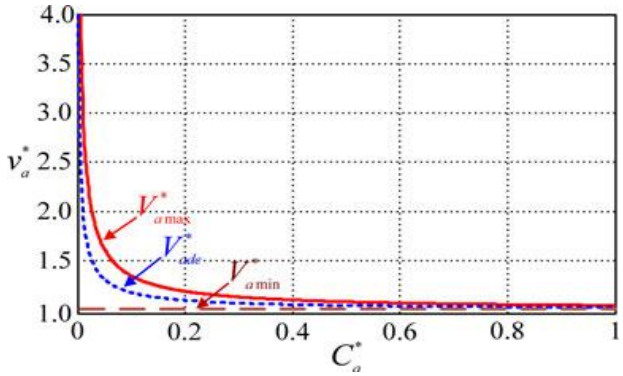

Fig. 8. Plots of *V a* max, *V a* min, and *V a*dc as functions of *C a* .

To ensure the proper operation of AACC, the instantaneous Voltage of *Ca* must always be higher than the input voltage of AACC, i.e.,

$$va\ (t) \geq V\text{bus}. \qquad (17)$$

We set *Va* min at *V*bus and Δ*v*bus allow at 1% × *V*bus, and the Normalized *Va* max and *Va* dc with base of *V*bus are

$$V\_(a\ max)\text{^}*=V\_(a\ max)/V\_bus=\sqrt{(4\%/C\_a\text{^}*)}+1 \qquad (18)$$

$$V\_abc\text{^}*=V\_abc/V\_bus\ =1/2+\sqrt{(4\%/C\_a\text{^}*\ )}+1/4 \qquad (19)$$

Where *C a* is the normalized *Ca* with base of *C*bus. According to (18) and (19), $V * a$ max and $V * a$dc as functions of $C * a$ are plotted in Fig. 8. Here, *Va* max increases as *Ca* reduces. In order to adopt film capacitors or ceramic capacitors instead of electrolytic capacitors, the value of *Ca* should be small enough However, this will result in high *Va* max. A high *Va* max induces high voltage stress on *Qa*1 and *Qa*2 . Thus, *Ca* needs to be selected eclectically. Note that *Ca* must be selected at full load because it is the worst case for the cascaded system and the required *Ca* has the maximum value.

*B. Selection of Qa*1 *and Qa*2

According to Fig. 5, the voltage stress of *Qa*1 and *Qa*2 is the Maximum voltage of *va* , i.e.,

$$VQa\ 1 = VQa\ 2 = Va\ \text{max}. \qquad (20)$$

The current stress of *Qa*1 and *Qa*2 is the maximum current of *La* , and can be derived from (7) and (8), i.e.,

$$IQa\ 1 = IQa\ 2 = \omega C\text{bus max}\Delta V\text{bus allow} \qquad (21)$$

Where *C*bus max is the required value of *C*bus at full load.

The power devices for *Qa*1 and *Qa*2 could be chosen according to (20) and (21).

C. Inductor of AACC

Two factors must be taken into consideration when choosing the value of *La* . One is to ensure that the inductor current is

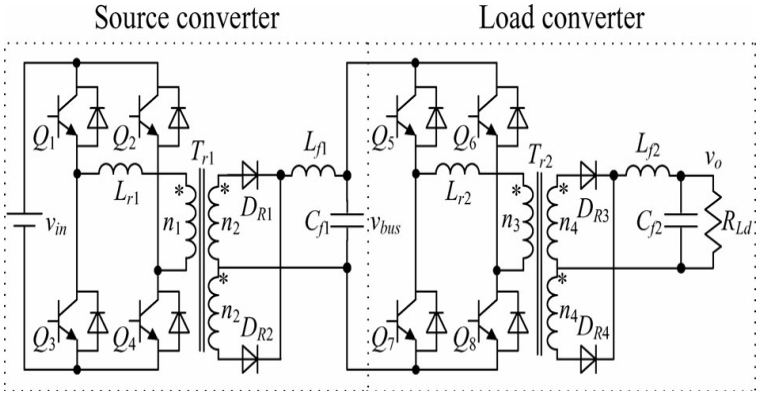

Fig. 9. Cascaded system consisting of two phase-shifted full-bridge converters.

Capable of tracking the current reference and the other is that the inductor current ripple should be kept small.

Here, the AACC's inductor current, *ia* , needs to track the Oscillation ripple, whose oscillation frequency is the cutoff frequency of the source converter's voltage loop gain. Hence, the switching frequency of AACC, *fsa* , should be chosen much higher than the oscillation frequency *fc S* . In this case, the tracking speed of *ia* is ensured and it would be sufficient to choose the value of *La* with sole consideration given to the inductor current ripple.

As the two power switches of AACC operate in a complementary manner, the AACC is operating in continuous current conduction mode. Thus, the duty cycle of *Qa*1 is

$$dQa\ 1\ (t) = 1 - V\text{bus}\ va\ (t)\ . \qquad (22)$$

When *Qa*1 is turned ON and *Qa*2 is turned OFF, the voltage across *La* is *V*bus. This voltage causes *ia* to increase. The rippleof *ia* can be expressed as

$$\Delta iLa = V\text{bus}/La \cdot dQa\ 1\ (t) \cdot 1/fsa \qquad (23)$$

Substitution of (22) into (23) gives

$$La = (va\ (t) - V\text{bus})\ V\text{bus}/va\ (t)\Delta iLa\ fsa \qquad . (24)$$

It can be seen from (24) that *La* varies with *va* (*t*) in a oscillation period.

D. Design Example

In this part, an AACC is designed for a cascaded system, as seen in Fig. 9, the system is composed by two phase-shifted full-bridge converters. Table I gives its parameters. In Fig. 9, both the source converter and load converter's voltage regulator are employing a PI controller. In this paper, *fc S*and phase margin of source converter are set at 550 Hz and 45◦, respectively, and *fc L* and phase margin of load converter are set at 5 kHz and 45◦, respectively. According to the circuit and control parameters of the cascaded system, the Bode plots of the source converter's output impedance *Zo* and the load converter's input impedance *Z*in at different loads are plotted in Fig. 10. It can be seen that when the load is lower than 35% full load, *Zo* peak is less than *Z*in , and the cascaded system is stable. Otherwise, there is interaction between *Zo* and *Z*in , the system

TABLE I. Circuit Parameters of Source Converter and Load Converter

Source converter (360 V – 48 V 480 W 100 kHz)			
Parameter	value	Parameter	value
Q_1~ Q_4	IRF840	L_{f1}	150 μH
D_{R1}~ D_{R2}	DSEP15-06	C_{f1}	680 μF
Winding Turns Ratio of T_{r1}	5 : 1	L_{r1}	2 μH
K_p	3	K_i	1000
Load converter (48 V – 12 V 480W 100 kHz)			
Parameter	value	Parameter	value
Q_5~ Q_8	IXTP44N10T	L_{f2}	2.2 μH
D_{R3}~ D_{R4}	DSA60C100PB	C_{f2}	4700 μF
Winding Turns Ratio of T_{r2}	3 : 1	L_{r2}	1 μH
K_p	8	K_i	1500

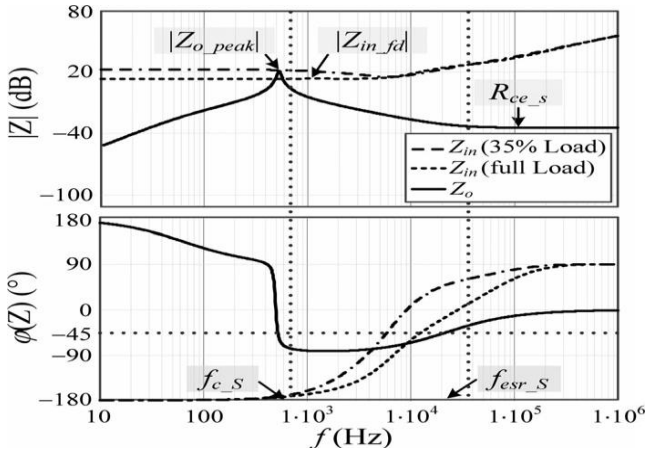

Fig. 10. Impedances of the source and load converters at different loads

Will become unstable, and the AACC is needed. In practice, the impedance characteristics of *Zo* and *Z*in can be measured by a network analyzer without knowing the intrinsic parameters of the subsystems. From Fig. 10, it can be seen that, *Zo* peak = 13.5 Ω, the input impedance of load converter at full load *Z*in *f d* is equal to4.8 Ω, *Rce S* = 0.017 Ω, *fc S* = 550 Hz, and *f*esr *S* = 22.5 kHz. Using (1)–(3) and (7), we can calculate the oscillation angular frequency and *C*bus max, i.e., $\omega = 2\pi f c\ S$ = 3455 rad/s and *C*bus max = 1950 μF.
Setting Δ*v*bus allow at 1%*V*bus, the main circuit parameters of AACC can be designed as follows:

1) We choose *Ca* = 20 μF (film capacitors, EACO-STH 200 V/20 μF), then $C * a$ = 20 μF/1950 μF = 0.01.
2) Considering *V*bus = 48 V and (18), *VQa*1 = *VQa*2 =*Va* max 110 V. By (21), *IQa*1 = *IQa*2 = 3 A. Here,FDMS2572 (4.5 A/150 V) with *Rds*(ON) of 0.09 Ω isadopted.
3) Considering *fc S* = 550 Hz, *fsa* is chosen as 100 kHz that is much higher than 550 Hz.
4) Setting Δ*iL* max = 20%*IQa*1 = 0.6 A and from (14) and (24), the curve of minimum value of *La*, *La* min, in an oscillation period can be plotted in Fig. 11, where the

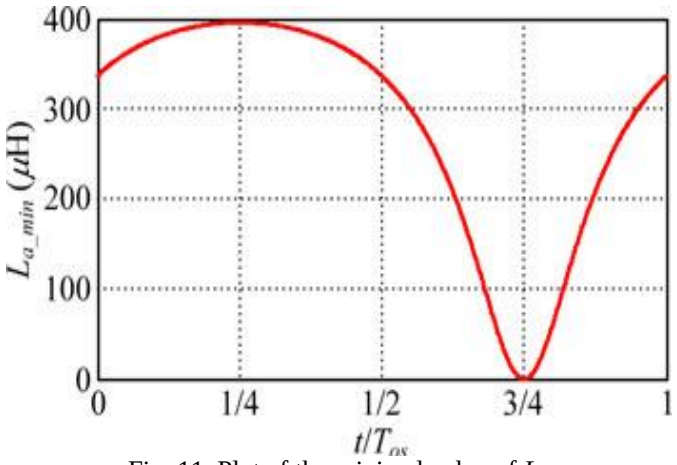

Fig. 11. Plot of the minimal value of *La*

TABLE II. Components of Aacc, Passive Capacitor Solution, and The Original cascaded System

Components of AACC			
Main circuit		Control circuit	
Component	Part number	IC	Quantity
Q_{a1}	FDMS2572 (4.5A/150V)	TL074	2
Q_{a2}	FDMS2572 (4.5A/150V)	TL072	1
L_a	NCD EE33/14/13	LM393	1
C_a	EACO-STH 200 V/20 μF	SG3525	1
Components of passive capacitor solution			
Component	Part number		Quantity
C_{bus} (1950 μF)	*Jianghai* CD29S PJ 100 V/390 μF		5
Components of original cascaded system			
Source converter			
Main circuit		Control circuit	
Component	Part number	IC	Quantity
Q_1~ Q_4	IRF840 (8A/500V)	TL074	1
D_{R1}~ D_{R2}	DSEP15-06A (15A/600V)	TL072	1
T_{r1}	NCD EE42/21/20	LM393	3
L_{r1}	NCD EE25/10/7	TLP521-1	1
L_{f1}	NCD EE55/28/25	HCPL3120	4
C_{f1}	*Jianghai* CD294 100 V/680 μF	UCC3895	1
Load converter			
Main circuit		Control circuit	
Component	Part number	IC	Quantity
Q_5~ Q_8	IXTP44N10T (44A/100V)	TL074	1
D_{R3}~ D_{R4}	DSA60C100PB (60A/100V)	TL072	1
T_{r2}	NCD EE42/21/20	LM393	3
L_{r2}	NCD EE25/10/7	TLP521-1	1
L_{f2}	NCD EE42/21/20	HCPL3120	4
C_{f2}	*Jianghai* CD294 50 V/4700 μF	UCC3895	1

Maximum value of *La* min is 395 μH. Here, we choose
La = 395 μH.

Considering the cost is a matter of concern in practical, Table II lists the selected components of AACC, passive capacitor solution, and the original cascaded system. Currently, the cost of AACC is slight higher than the passive capacitor solution, and accounts for about 9% of the original cascaded system.

V. Experimental Verification

In order to verify the validity of the proposed AACC, a prototype has been built and tested. The parameters of the prototype have been given in Section IV-D. Fig. 12 shows the steady-state experimental waveforms of the source converter and load converter operating individually. Fig. 13(a) and (b) shows the individual dynamic waveforms of the source and load converters when their load steps between full load and 10% full load, respectively. As seen from the figures, both source and load converters are stable and working well.

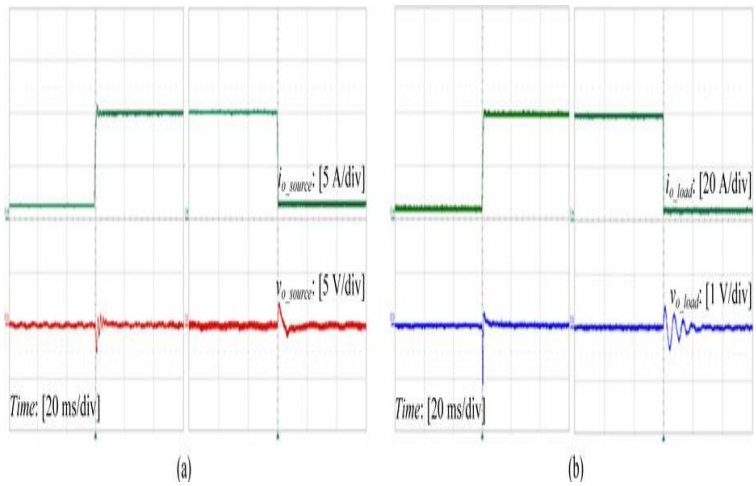

Fig. 13. Individual dynamic waveforms of the source and load converters when their load steps between full load and 10% full load: (a) source converter and (b) load converter

Considering that the cascaded system can be stable with a 1950 μF passive capacitor (Cbus max) or AACC in the full load range. Fig. 18 compares their dynamic performance when the load steps between full load and 10% full load. It shows that the system with AACC has a faster dynamic response than that of the system using the passive capacitor solution. According to the reason can be explained as follows. The equivalent capacitor of AACC is adaptively varied by the load. Its value is always smaller than 1950 μF and approaches zero when the system is stable. And a smaller Cbus, of course, means a faster dynamic performance for the cascaded system. In addition, compared with Figs. 13 and 18(b), it seems that the cascaded system with AACC has a similar dynamic performance with its individual subsystems.

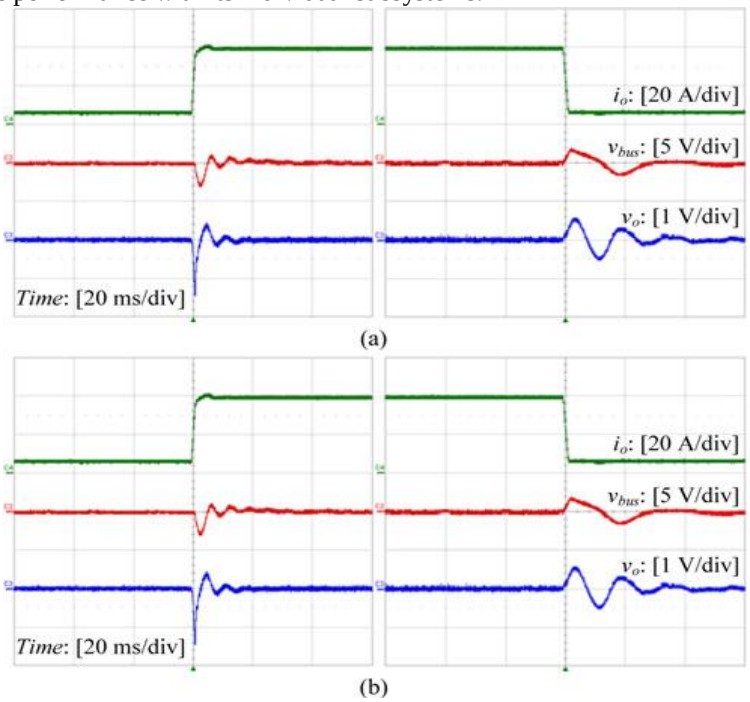

Fig. 14. Waveforms of cascaded system when the load steps between full load and 10% full load: (a) with the AACC (b) without the AACC

VI. Conclusion

When the AACC is a good suggests that to resolve the instability downside of the dc distributed power supply. In the presents days they will offers the AACC as identical adjective bus capacitance will be changeable per then the cascaded system have their output power, so we can avert the electrical resistance can communicate to the cascaded system with the quantity of the output electrical resistance in the supply convertor. Betting in the edge of the undisturbed conditions in the cascaded system, therefore the AACC is adjectively functionaries. Once the move in the cascaded system was broad in the AACC supply to the additional power of the produce to

the bigger importance capacitance. Once they can moves in the cascaded system have a very small value, when the AACC can supply less power in the produce have smaller importance capacitance. Once there is no moves in a cascaded system they have a periodic voltage among in a permutable to the opportunity, of the AACC are going to be stop working. They can have employment in the AACC doesn't solely make sure the undisturbed conditions in a cascaded system, however additionally unpleasant situation in the important loss. When the energy has a lot of reactions in the cascaded system have additionally then see a better change in the employment of a yielding capacitance. Moreover, there is an electrolytic employed during AACC of the incorporates a hopeful effect in a organized period.

They will tally in the present technique, the projected convertor solely has they discover the cascaded system to the bus voltage while not dynamic something in the present subsystems, thus they will be a stylish to the customary can be measuring in the dc DPS. Then AACC will been ascertain carefully see the power values that is four thousand eight hundred zero watts and we can see different voltage ratings in the cascaded system. After we can see the exacta output results of the experimental in the validity of the analysis.

REFERENCES

[1] F. Blaabjerg, A. Consoli, J. A. Ferreira, and J. D. van Wyk, "The future of electronic power processing and conversion," *IEEE Trans. Power Electron.*, vol. 20, no. 3, pp. 715–720, May 2005.

[2] J. D. van Wyk and F. C. Lee, "Power electronics technology—Status and future," in *Proc. CPES*, 1999, pp. 61–70.

[3] K. T. Kornegay, "Design issues in power electronic building block (PEBB) system integration," in *Proc. IEEE VLSI*, Apr. 1998, pp. 48–52.

[4] T. Ericsen, "Power electronic building blocks—A systematic approach to power electronics," in *Proc. IEEE Power Eng. Soc. Summer Meeting*, 2000, pp. 1216–1218.

[5] D. Boroyevich, I. Cvetkovi c, D. Dong, R. Burgos, F. Wang, and F. C. Lee, "Future electronic power distribution systems—A contemplative view," in *Proc. IEEE OPTIM*, May 2010, pp. 1369–1380.

[6] S. Luo, "A review of distributed power systems part I: DC distributed power system," *IEEE Aerosp. Electron. Syst. Mag.*, vol. 20, no. 8, pp. 5–16, Aug. 2005.

[7] L. R. Lewis, B. H. Cho, F. C. Lee, and B. A. Carpenter, "Modeling, Analysis and design of distributed power systems," in *Proc. IEEE PESC*, Jun. 1989, pp. 152–159.

[8] G. A. Franz, G. W. Ludwig, and R. L. Steigerwald, "Modeling and simulation of distributed power systems," in *Proc. IEEE PESC*, 1990, pp. 606–610.

[9] S. Schulz, B. H. Cho, and F. C. Lee, "Design considerations for a distributed power system," in *Proc. IEEE PESC*, 1990, pp. 611–617.

[10] B. H. Cho and B. Choi, "Analysis and design of multi-stage distributed power systems," in *Proc. Int. Telecomm. Energy Conf.*, Kyoto, Japan, Nov. 1991, pp. 220–226.

[11] A. Emadi, "Modeling of power electronic loads in ac distribution systems using the generalized state-space averaging method," *IEEE Trans. Ind. Electron.*, vol. 51, no. 5, pp. 995–1000, Oct. 2004.

[12] A. Khaligh, "Realization of parasitics in stability of dc–dc converters loaded by constant power loads in advanced multiconverter automotive systems," *IEEE Trans. Ind. Electron.*, vol. 55, no. 6, pp. 2295–2305, Jun. 2008.

[13] R. D. Middlebrook, "Input filter considerations in design and application of switching regulators," in *Proc. IEEE IAS*, 1979, pp. 366–382.

[14] C. M. Wildrick, F. C. Lee, B. H. Cho, and B. Choi, "A method of defining the load impedance specification for a stable distributed power system," *IEEE Trans. Power Electron.*, vol. 10, no. 3, pp. 280–285, May 1995.

[15] P. Huynh and B. H. Cho, "A new methodology for the stability analysis of large-scale power electronics systems," *IEEE Trans. Circuits Syst. I,Fundam. Theory Appl.*, vol. 45, no. 4, pp. 377–385, Apr. 1998.

[16] S. D. Sudhoff, S. F. Glover, P. T. Lamm, D. H. Schmucker, and D. E. Delisle, "Admittance space stability analysis of power electronic systems," *IEEE Trans. Aerosp. Electron. Syst.*, vol. 36, no. 3, pp. 965–973, Jul. 2000.

[17] X. Feng, J. Liu, and F. C. Lee, "Impedance specifications for stable DC distributed power systems," *IEEE Trans. Power Electron.*, vol. 17, no. 2, pp. 157–162, Mar. 2002.

[18] X. Wang, R. Yao, and F. Rao, "Three-step impedance criterion for small signal stability in two-stage dc distributed power systems," *IEEE Trans. Power Electron. Lett.*, vol. 1, no. 3, pp. 83–87, Sep. 2003.

[19] T. Suntio, I. Gadoura, and K. Zenger, "Input filter interactions in peakcurrent-mode-controlled buck converter operating in CICM," *IEEE Trans. Ind. Electron.*, vol. 49, no. 1, pp. 76–86, Feb. 2002.

[20] X. Wang, D. Vilathgamuwa, and S. Choi, "Decoupling load and power system dynamics to improve system stability," in *Proc. IEEE PEDS*, 2005, pp. 268–273.

BIOGRAPHIES

B. Prudvikumarreddy is born in 1990 in India. He is graduated from JNTUA University in 2012. Presently he is doing Post graduation in Power Electronics and Electrical Drives Specialization at J.N.T.U.A, Anantapur His main areas of interest include Induction motor drives, Electrical machines, Power Electronics, & power systems.

B. AmruthKumarreddy is born in 1987 in India. He is graduated from JNTUH University in 2008 and pursued Post graduation from the JNTUA University. He is currently working as a Assistant professor in the department of electrical and electronics engineering Dr. K.V.S.R institute of technology, kurnool, Andhra Pradesh, India. He has 5 years of teaching experience. He has attended several National workshops. His main areas of research include Induction motor drives, Electrical machines, FACTS and power convertors.

OPEN ACCESS

International
Journal
Of Modern Engineering Research (IJMER)

Dynamic Traffic Management Services to Provide High Performance in IntelRate Controller Using Fuzzy Logic

M.Vasuki[1], N.Balkis[2], V. Jayalakshmi[3]

[1,] *Associate Professor, Department of MCA, Sri Manakula Vinayagar Engineering College. Puducherry, India*
[2,3]*Department of MCA, Sri Manakula Vinayagar Engineering College. Puducherry, India*

Abstract: *Traffic is the chief puzzle problem in which every country faces to elaborate sending a number of packets throughout the world. This paper proposes a new speculation for distributed traffic management by availing the presumption of fuzzy logic. The routers are established by using an IntelRate Controllers to manage the traffic congestion in the networks dynamically. Fuzzy logic is used to previse the maximum allowable sending rate by observing the queue size of router. The network traffic control protocol is unique to estimate the network parameter which involves link latency, bottleneck bandwidth or packet loss rate in order to compute the allowed source sending rate. The fuzzy logic based controller can measure queue size directly, it neglects various potential performance issues arising due to parameter estimation as reduce consumption of computation and memory resource in router. A network parameter, the queue size can be viewed accurately and if action should be taken to regulate the source sending rate and it increases the resilience of the network to traffic congestion. Using the fuzzy logic technique, QoS (Quality of Service) can achieve better performance than the existing protocol that depends on the estimation of network parameter, to make the network more adaptive for current traffic conditions.*

Keywords: *congestion control, fuzzy logic control, QoS (Quality of Service), max-min fairness, robustness, traffic management.*

I. INTRODUCTION

Traffic congestion control is one of the effective approaches to manage the network traffic [1], [2]. Network traffic management can be used to prevent and control a network traffic from congestion and degradation in throughput delay performance. An explicit congestion controller depend on estimation of network parameters (such as link latency, bottleneck bandwidth, packet loss, or the number of flows) which is used to compute the allowed source sending rate and it will measured accurately. The Intel Rate controller can be used to avoid the good stability and robustness in the network traffic. the Intel Rate controller can be approximated by a PI (Proportional-Integral) controller but with time-varying gains, which allows the controller to outperform its counterparts and finally by comparing with API-RCP (Adaptive PI Rate Control Protocol) by using OPNET simulation[3].

The back-pressure algorithm is a well known throughput-optimal algorithm and its delay performance may be quite poor. when the traffic load is not close to network capacity with the following two reasons. First, each node has been maintained as a separate queue in the network, and only one queue is distributed at a time. Second, the back-pressure routing algorithm may send some packets along very long routes. The user introduce some solving solutions to address both the above issues, and hence, make better improvement in the delay performance of the back-pressure algorithm. One of the recommended solutions also reduce the complexity of the queuing data structures to be maintained at each node [4]. Recently, explicit Control Protocol (XCP), Rate Control Protocol (RCP), and Adaptive Proportional- Integral Rate Control Protocol (API-RCP) have been proposed for congestion control, with the main target to achieving the fair and maximum bandwidth utilization. However, it shows both RCP and XCP may suffer continuous oscillations due to misestimating the bottleneck link capacity, and API-RCP may experience oscillations because of its PI adaptively scheme which involves switching nonlinearity. To avoid these problems, one way of designing the congestion control based on the IQSize (Instantaneous Queue Sizes) in the routers. The new scheme achieves high link utilization and smooth dynamics by fixing the bottleneck queue at a desired size. It maintains good fairness by allocating the bottleneck bandwidth equally to the competing flows. these are all performed to verify the effectiveness of the theoretical design of the network traffic [5].Next generation IP-based networks will has guaranteed of quality

of service (QoS) by deploying technologies such as differentiated services (DiffServ) and multi-protocol label switching (MPLS) for traffic engineering and network-wide resource management.

A number of issues still exist regarding edge-to-edge intra-domain and inter-domain QoS provisioning and management for the subscription to QoS-based services. It will then move to examine the architectures and the frameworks for the management and control of QoS-enabled networks, including the following aspects: approaches and algorithms for off-line traffic engineering and provisioning through explicit MPLS paths or through hop-by-hop IP routing; approaches for dynamic resource management to big deal with traffic fluctuations outside an envelope; a service management framework supporting a "resource provisioning cycle"; the derivation of expected traffic request from subscribed SLSs and approaches for SLS invocation admission control; observing architecture for scalable information collection supporting traffic engineering and service management; and realization issues given the current state-of-the-art of management protocols and monitoring support. [6].

A new active queue management scheme, fuzzy explicit marking (FEM), implemented within the differentiated services (Diffserv) framework to provide the congestion control using a fuzzy logic control approach. Network congestion control remains a critical and high priority issue. RED (random early detection) and its variants are one of these alternatives to provide QoS in TCP/IP Diffserv networks. The proposed fuzzy logic approach for congestion control allows the use of linguistic knowledge to capture the dynamics of nonlinear probability marking functions and it also gives the effective implementation. By using the multiple inputs to capture the network traffic more accurately, by enabling the elegant tuning for packet marking manners for aggravated flows, and thus provide better QoS to different types of data streams, such as TCP/FTP traffic, it maintains high utilization [7].These has been widely examined with various proposed solutions such as AQM(Active Queue Management) schemes [8]-[10] whose control protocols are also implicit in nature.

A class of explicit congestion protocols has been proposed to signal network traffic level by using the multiple bits. Examples are the XCP [6], RCP [11], JetMax [12], MaxNet [13].The explicit protocol is used to compute the sending rates based on the queue size, to estimate the number of active flows in a router and consumes memory resources and others. for examples are the rate-based controllers [14]-[16] for packet switching networks and also ER (Explicit Rate) allocation algorithm [17] for ATM (Asynchronous Transfer Mode) networks. The API-RCP controller [15], both the original and the improved method [18] faces some memory problem when dealing with many flows arriving to a router each and every hour [19]. In some other controllers (eg., [17]), the TBO (Target Buffer Occupancy) is designed as high as 3 times of the BDP, which can cause a large queuing delay and degrading network performance, and it becomes even in the high-speed networks.

The ER allocation algorithms in ATM networks will also shares the same problems (e.g., [17], [20]) because they just need to compute the link bandwidth and the numbers of active VCs (Virtual Circuits). Some others (e.g., [21]) adjust the source sending rates in binary-feedback switches according to a queue thresholds, which may cause un fairness as well as high cell loss rate [2], [22].

A. Existing system

In existing adjust the source sending rates in binary-feedback switches or explicit feedback switches according to a few queue thresholds, which may cause unfairness as well as high cell loss rate. From the perspective of network and service management, the mentioned congestion control approaches have QoS (Quality of Service) problems in that they cannot guarantee a certain level of performance under some situations due to design drawbacks. There are many different approaches to improve QoS. For example, admission control, as a network traffic management approach, can guarantee QoS by checking the availability of network bandwidth before establishing a connection, e.g., [23]- [25] Service priority as another approach can be used to improve QoS by providing different service priorities to different users. This paper focuses on congestion control as an approach to address the QoS (Quality of Service) problems in that they cannot guarantee a certain level of performance under some situations due to design drawbacks large queuing delay and thus degrading network performance.

B. Proposed system

FLC (Fuzzy Logic Control) [26] has been considered for IC (Intelligence Control). It is a methodology used to design robust systems that can contend with the common adverse synthesizing factors such as system nonlinearity, parameter uncertainty, measurement and modeling imprecision [27]. In addition, fuzzy logic theory provides a convenient controller design approach based on expert knowledge which is close to human decision making, and readily helps engineers to model a complicated non-linear system.

In fact, fuzzy logic control has been widely applied in industrial process control and showed extraordinary and mature control performance in accuracy, transient response, robustness and stability [28], [29] .Fuzzy Smoother mechanism that can generate relatively smooth flow throughput. Finally, we will employ OPNET modeler to verify the effectiveness and superiority of our scheme. FLC has found its applications to network congestion control since 1990. In early stage, it was used to do rate control in ATM network, e.g., [30], [31], to guarantee the QoS. The rest of the paper is organized as follows. After a description of network model and assumptions in Section II, Section III introduces the design rationale and the controller implementation procedure. Section IV and Section V illustrate the simulation performance of the IntelRate controller. Finally, we conclude this paper with Section VI. For the remainder of the paper, the following notations and symbols pertain.

A	Edge value of MFs (Membership Functions) of e (t) , beyond which the MFs of e (t) saturate
B	Buffer capacity
c (t)	Service rate (output link capacity) of a router
C	Edge value of MFs of $g(e(t))$, beyond which the MFs of $g(e(t))$ saturate
D	Outermost edge value of MFs of u (t)
$e(t)$	Queue error which is one input of the IntelRate controller
$g(e(t))$	Integration of e (t) which is the other input of the IntelRate controller
m	Multiple of TBO to design the width limit for the MFs of input $e(t)$ and $g(e(t))$
N	Number of LVs (Linguistic Values)
q_0	TBO of a router
$q(t)$	IQSize (Instantaneous Queue Size) of a router
$u(t)$	The controller crisp output for each flow
$u'(t)$	Current source sending rate
$v(t)$	Aggregate uncontrolled incoming traffic rate to a router
$y(t)$	Aggregate controlled incoming traffic rate to a router (also aggregate controller output)
μ_{Pi}^{j}	Input fuzzy set of the IntelRate controller
μ_{U}^{j}	Output fuzzy set of the IntelRate controller
T_{fi1}	Time delay of a packet from source I to a router
T_{fi2}	Time delay of a packet from a router to its destination i
T_{bi}	Feedback delay of a packet from destination I back to source i
T_{pi}	RTPD (Round Trip Propagation Delay)
T_i	RTT (Round Trip Time)

II. LITERATURE SURVEY

Literature survey is the documentation of a comprehensive review of the published and unpublished work from secondary sources data in the areas of specific interest to the researcher. The library is a rich storage base for secondary data and researchers used to spend several weeks and sometimes months going through books, journals, newspapers, magazines, conference proceedings, doctoral dissertations, master's theses, government publications and financial reports to find information on their research topic. With computerized databases now readily available and accessible the literature search is much speedier and easier and can be done without entering the portals of a library building.

The researcher could start the literature survey even as the information from the unstructured and structured interviews is being gathered. Reviewing the literature on the topic area at this time helps the researcher to focus further interviews more meaningfully on certain aspects found to be important is the published studies even if these had not surfaced during the earlier questioning.

So the literature survey is important for gathering the secondary data for the research which might be proved very helpful in the research. The literature survey can be conducted for several reasons. The literature review can be in any area of the business.

In this paper, we referred the "Congestion avoidance and control" was developed in the year 1988 by the author V. Jacobson to avoid the congestion in the network and followed by "Modified TCP congestion avoidance algorithm" was developed in the year 1990 by the author V. Jacobson."Feedback control of congestion in packet switching networks: the case of a single congested node" was developed in the year 1993 by the author L. Benmohamed and S. M. Meerkov." Enhanced PRCA (proportional rate control algorithm)"

was developed in the year 1994 by the author L. Roberts.The fuzzy logic traffic controller is proposed to perform traffic and functions by using, "Design of fuzzy traffic controller for ATM Networks" was developed in the year 1996 by the author R. Chang and C. Cheng."Self-similarity in world wide web traffic: evidence and possible causes" was developed in the year 1997 by the author M. E. Crovella and A. Bestavros, this will shows evidence that WWW traffic exhibits is consistent with self-similar traffic model. "Fuzzy Control" was developed in the year 1998 by the author K. M. Passino and S. Yurkovich."Proposals to add explicit congestion notification (ECN) to IP" was developed in the year 1999 by the author K. K. Ramakrishnan and S. Floyd."A neural-fuzzy system for congestion control in ATM networks", was developed in the year 2000 by the author S. J. Lee and C. L. Hou, the neural-fuzzy scheme for rate-based feedback congestion control in ATM."Providing appropriate exercise levels for the elderly" was developed in the year 2001 by the author T. Kiryu, I. Sasaki, K. Shibai, et al."Passive estimation of round-trip times" was developed in the year 2002 by the author H. Jiang and C. Dovrolis."Dynamics of TCP/AQM and a scalable control" was developed in the year 2003 by the author S. H. Low, F. Paganini, J.Wang,et al."Network Congestion Control: Managing Internet Traffic" was developed in the year 2004 by the author M. Welzl."Design of adaptive PI rate controller for best effort traffic in the Internet based on phase margin" was developed in the year 2007 by the author Y. Hong and O. Yang."A game-theoretic model for capacity-constrained fair bandwidth allocation" was developed in the year 2008 by the author Y. Yan, A. El-Atawy, and E. Al-Shaer.

The policy management will provides the ability to (re-)configure the differentiated services networks so that will desired QoS goals can be achieved with the help of "Policy conflict analysis for diffuser quality of service management" was developed in the year 2009 by the author M. Charalambides, P. Flegkas."Explicit congestion control (XCC) algorithms for time varying capacity media" was developed in the year 2011 by the author F. Abrantes, J. Araujo, and M. Ricardo.

III. Background Details

A. Traffic management principles and modelling

Consider a backbone network interconnected by a number of geographically distributed routers; the hosts are attached to the access routers which cooperate with the core routers to enable end-to-end communications. Congestion control protocol occurs when many flows traverse a router and because it's IQSize (Instantaneous Queue Size) to exceed the buffer capacity and make a bottleneck in the Internet. Any router may become bottleneck along an end-to-end data path. Each router can be able to manage its traffic. Below is the general operation principle of our new traffic control algorithm. Inside each router, our distributed traffic controller acts as a data rate regulator by measuring and monitoring the IQSize. As per its application, every host requests a sending rate it desires by depositing a value into a dedicated field Req_rate inside the packet header. This field can be updated by any router en-route. Each router has the data path and it allows you to compute the source transmission rate according to the IQSize and then compare it with the rate already recorded in Req_rate field. After the packet arrives at the destination, the value of the Req_rate field reflects the allowed data rate from the most congested router along the path if the value is not more than the desired rate of the source. The receiver then sends this value back to the source via an ACK (ACKnowledgment) packet, and the source would update its current sending rate accordingly. If no router modifies Req_rate field, it means that all routers en route allow the source to send its data with the requested desired rate.

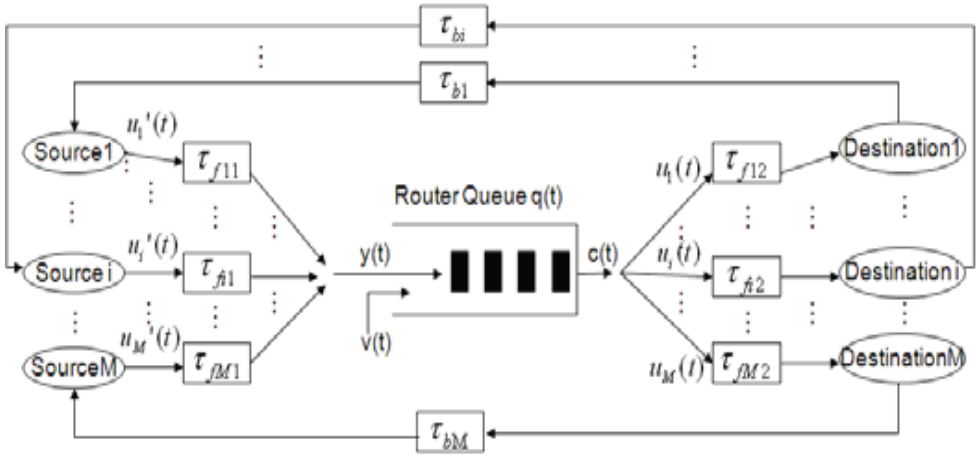

Fig. 1. System model of an AQM router

Some of the assumptions are used in this paper to pertain:

- *Every source requests a desired sending rate from the network according to its application.*
- *A destination always has enough buffer space to receive data from its source. This is because we do not want the destination to impose any constraint on the source sending rate when we verify the effect of our new control scheme in a bottlenecked router.*
- *The propagation delay and the queuing delay along the data path are the two dominant components of the RTT while other components like processing delay of a packet in routers or hosts are negligible in comparison.*
- *The queuing discipline of routers is FIFO (First-In-First-Out).*
- *Long-lived flows with infinitely long files are used to approximate the greedy behavior of a source when active. This would generate the severest traffic in order for us to verify the robustness of the new scheme.*

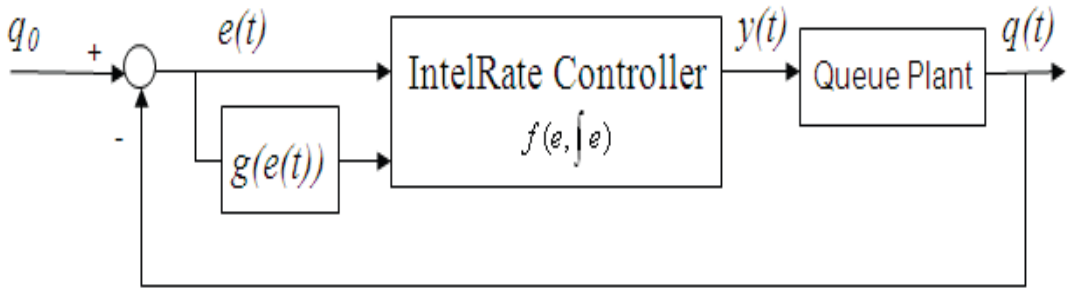

Fig. 2. The IntelRate closed-loop control system.

B. Traffic attributes

To set a connection on ATM network, user can specify the following parameters. It relates the input traffic characteristics and desired Quality of Service.

Peak Cell Rate (PCR): It can be used to find the maximum instantaneous rate at which the user will transmit.

Sustain Cell Rate (SCR): The average rate can be measured over a long interval.

Cell Loss Ratio (CLR): The percentages of cells are lost in the network due the error and congestion. So it cannot be delivered to the destination.

$$\text{Cell Loss Ratio} = \frac{\text{Lost Cells}}{\text{Transmitted Cells}}$$

Each ATM cells has a "Cell Loss Priority (CLP)" bit in the header. During congestion, first drop the network cells that have CLP bit set. Since the loss of CLP=0 cell is more harmful to the operation of the application. CLR can be specified separately for cells with CLP=1 and for those with CLP=0.

Cell Transfer Delay (CTD): the experienced delay cells are used between the network entry and exit points is called cell transfer delay. It includes queuing delay propagation delay in various intermediate switches; queuing points are used at service time.

Cell Delay Variation (CDV): It can be used to measure the variance of CTD. High variation implies lager buffering for delay sensitive traffic such voice and video. Multiple ways can be used to measure CDV. "peak-to-peak" are used, in this CDV consist of computing the difference between the (1-α)-percentile and the minimum of the cell transfer delay for some small value of α.

Cell Delay Variation Tolerance (CDVT) and Burst Tolerance (BT): source transmitting the Intel cell time.

Maximum Burst Size (MBS): Maximum number of back- to- back cell are used to send at the peak cell rate without violating the sustained cell rate. It related to the PCR, SCR and BT as follows:

$$\text{Burst Tolerance} = (\text{MBS-1})\left(\frac{1}{\text{SCR}} - \frac{1}{\text{PCR}}\right)$$

MBS is more intuitive than BT, MBS used signaling messages. BT can be easily calculated from MBR, SCR, and PCR.

Minimum Cell Rate (MCR): The minimum rate desired by a user.

The first six of the above network parameters were specified in UNI version3.0. MCR are recently added and it will appear in the next version of the traffic management document.

C. Service categories

There are five categories of services. The QoS parameters for these categories are summarized in Table 1 and are explained below:

Constant Bit Rate (CBR): It can be used for emulating circuit switching. The cell rate is constant. Cell loss ratio is specified for CLP=0 cells and may or may not be specified for CLP=1 cells. Examples: CBR are telephone, video conferencing, and television applications are used.

Variable Bit Rate (VBR): It allows users to send the variable rate. Statistical multiplexing may be used as small nonzero random loss. Depending upon whether or not the application is sensitive to cell delay variation and it can be subdivided into two categories: Real time VBR and Non-real time VBR. In non-real time VBR, only mean delay is specified. In real time VBR, maximum delay and peak-to-peak CDV are specified; an example of real time VBR is interactive compressed video while that of non-real time VBR is multimedia email.

Available Bit Rate (ABR): It can be used design the normal data traffic such as file transfer and email. It does not require the standard cell transfer delay and cell loss ratio to be minimized; it's desirable for switches to minimize the delay and loss as much as possible. It depend upon the congestion state of the network, the source is required to control its rate. The users are allowed to declare a minimum cell rate, which is guaranteed to the VC by the network. Most VCs will ask for an MCR of zero with higher MCR may be denied connection if sufficient bandwidth is not available.

Unspecified Bit Rate (UBR): It can be used to design the data applications. We can use any left-over capacity and it should not be sensitive to cell loss or delay. Connections are not rejected on the basis of bandwidth shortage and not policed for their usage behavior. During congestion, the cells are lost but the sources are not expected to reduce their cell rate.

D. Fuzzy logic

It's a form of multi-valued logic; it deals with reasoning that is approximate rather than fixed and exact. Compared to traditional binary sets (where variables may take on true), fuzzy logic variables may have a truth value that ranges in degree between 0 and 1.Fuzzy logic has been extended to handle the concept of partial truth, where the truth value may range between completely true and completely false. When linguistic variables are used, these degrees may be managed by specific functions. Irrationality can be described in terms of what is known as the fuzzy objective. The term "fuzzy Logic" was introduced with the 1965 proposal of fuzzy set theory by Lotfi A. Zadeh. Fuzzy logic has been applied to many fields, from control theory to artificial intelligence. Fuzzy logic had, however, been studied since the 1920s, as infinite-valued logic - notably by Łukasiewicz and Tarski.

Some of the rules are applied on fuzzy input sets:

A	If e(t) is 'VS' OR p(t) is 'LL', then r(t) is MI
B	If e(t) is 'VS' AND p(t) is 'AA', then r(t) is MI
C	If e(t) is 'VS' AND p(t) is 'LL', then r(t) is MI
D	If e(t) is 'SS' AND p(t) is 'HH', then r(t) is MI
E	If e(t) is 'SS' AND p(t) is 'AA', then r(t) is OO
F	If e(t) is 'SS' AND p(t) is 'LL', then r(t) is OO
G	If e(t) is 'MM' AND p(t) is 'HH', then r(t) is OO
H	If e(t) is 'MM' AND p(t) is 'AA', then r(t) is OO
I	If e(t) is 'MM' AND p(t) is 'LL', then r(t) is OO
J	If e(t) is 'LL' AND p(t) is 'HH', then r(t) is OO
K	If e(t) is 'LL' AND p(t) is 'AA', then r(t) is OO
L	If e(t) is 'LL' AND p(t) is 'LL', then r(t) is MX
M	If e(t) is 'VL' AND p(t) is 'HH', then r(t) is MX
N	If e(t) is 'VL' AND p(t) is 'AA', then r(t) is MX
O	If e(t) is 'VL' AND p(t) is 'LL', then r(t) is OO
P	If e(t) is 'VL' OR p(t) is 'HH', then r(t) is MX

IV. THE INTELRATE CONTROLLER DESIGN

Figure 2 contains the components of our fuzzy logic traffic controller for controlling traffic in the network system defined in Fig. 1. Called the Intel Rate, it is a TISO (Two-Input Single-Output) controller. The TBO (Target Buffer Occupancy) q0. 0 is the queue size level and it can be used to achieve the congestion control protocol. The queue deviation e (t) = q0 −q(t) is one of the two inputs of the controller. To remove the steady state error, we can choose the integration of e(t) as the other input of the controller, i.e. g (e (t)) =_ e (t) dt. The aggregate output is y (t) =ui (t − τi). In heavy traffic situations, the IntelRate controller would compute

the sending rate ui(t) for flow i according to the current IQSize. q(t) can be stabilized around q0. IQSize q(t) is the only parameter that can be used in the each router.

It measures the order to complete the closed –loop control.FLC is a non-linear mapping of inputs into outputs, which consists of four steps, i.e., rule base building, fuzzification, inference and defuzzification. The concepts of fuzzy set and logic of FLC were introduced in 1965 by Zadeh, and it was basically extended from two-valued logic to the continuous interval by adding the intermediate values between absolute TRUE and FALSE. In the sequel, we formulate our new controller by following those four steps along with designing the fuzzy linguistic descriptions and the membership functions. The parameter design issues and the traffic control procedure are also discussed at the end of the section.

A. linguistic description and rule based

We define the crisp inputs e(t), g(e(t)) and output u(t) with the linguistic variables é (t), ǵ (e (t)) and ú (t), respectively. There aren N (N = 1, 2, 3, . . .) LVs (Linguistic Values) assigned to each of these linguistic variables. Specifically, we let Pi ={ pi j : j= 1, 2,…,N} be the input LVs with i = 1 for é (t) and i = 2 for ǵ (e (t)), and let U ={U j: j = 1, 2, … ,N} for ú (t). For example, when N = 9, we can assign the following values for both the inputs e (t) and g(e(t)). P i1 ="Negative Very Large (NV)," P i2i ="Negative Large (NL)," P 3i ="Negative Medium (NM)," P 4ii ="Negative Small (NS)," P 5i ="Zero (ZR)," P 6i ="Positive Small (PS)," P 7i ="Positive Medium (PM)," P 8i ="Positive Large (PL),"and P 9i ="Positive Very Large (PV)," i = 1, 2. Similarly, we can designate the output when N = 9 with the following linguistic values. U1="Zero (ZR)," U2="Extremely Small (ES)," U3="Very Small (VS)," U4="Small (SM),"U5="Medium (MD)," U6="Big (BG)," U7="Very Big (VB)," U8="Extremely Big (EB)," and U9="Maximum (MX)."

Table I illustrates the controller rule base using N = 9. The rule base is the set of linguistic rules used to map the inputs to the output using the "If. . . Then. . . " format, e.g. "If e(t) is ZR (Zero) and g(e(t)) is PS (Positive Small), Then u(t) is BG (Big)." In the following sections, we refer to a rule in this table by the notation (P $^{j}_{1}$, P $^{k}_{2,}$ U ^{l}), where j, k, l = 1, 2. . . N, e.g. (P $^{5}_{1}$, P $^{2}_{2,}$ U ^{2}) = (ZR, NL, ES).

TABLE I. RULE TABLE FOR INTELRATE CONTROLLER (9 LVS)

Allowed Throughput *u(t)*		*e(t)*								
		NV	NL	NM	NS	ZR	PS	PM	PL	PV
g(e(t))	NV	ZR	ZR	ZR	ZR	ZR	ES	VS	SM	MD
	NL	ZR	ZR	ZR	ZR	ES	VS	SM	MD	BG
	NM	ZR	ZR	ZR	ES	VS	SM	MD	BG	VB
	NS	ZR	ZR	ES	VS	SM	MD	BG	VB	EB
	ZR	ZR	ES	VS	SM	MD	BG	VB	EB	MX
	PS	ES	VS	SM	MD	BG	VB	EB	MX	MX
	PM	VS	SM	MD	BG	VB	EB	MX	MX	MX
	PL	SM	MD	BG	VB	EB	MX	MX	MX	MX
	PV	MD	BG	VB	EB	MX	MX	MX	MX	MX

B. Membership function, Fuzzification and reference

Intel Rate controller employs the isosceles triangular and trapezoid-like functions as its MFs (Membership Functions).Figure 3 describes the MFs used to determine the certainty of a crisp input or output.

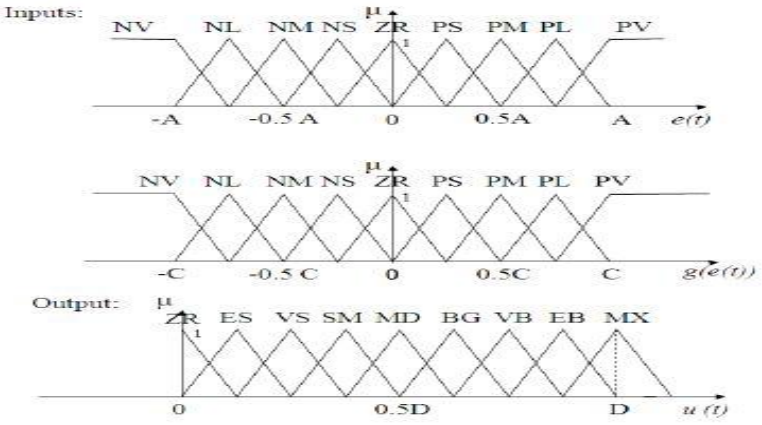

Fig.3 Membership functions without FS.

The above figure describes the usual way of designing MFs with FLC to determine the certainty of a crisp input or output, where e(t) and g(e(t)) have the same number of MFs and there is no boundaries for the input g(e(t)). While Fig. 4 is used to illustrate the design of a general FS, the designated values are actually come from an example of N = 9 LVs with the absolute values of both the upper and lower limits of g(e(t)) set to mq0.

In this e(t) is bounded by the physical size of a queue, we have the boundaries according to the limits $q0-B \leq e(t) \leq q0$. The vertical dashed lines in Fig. 4 denote those boundaries of inputs or output.

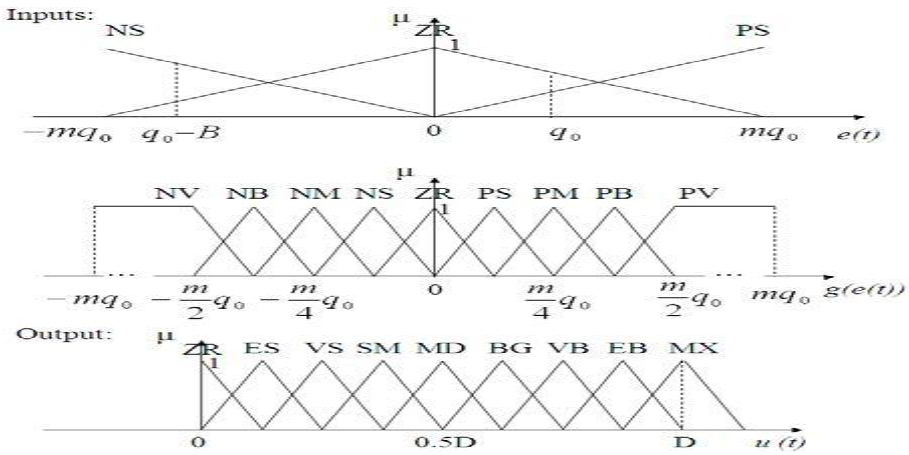

Fig.4 Membership functions with FS.

C. Defuzzification

Using the defuzzification algorithm, the IntelRate controller applies the COG (Center of Gravity) method to obtain the crisp output with the equation [26].

D. Design parameters

From our design above, one can see there are different parameters which ultimately will affect the performance of our traffic controller.

E. The control procedure

The traffic-handling procedure of the IntelRate controller in a router is,

- The router extracts Req_rate from the congestion header of the packet.
- Sample IQSize q(t) and update e(t) and g(e(t)).
- Compute the output u(t) and compare it with Req_rate.
- If an operation cycle d is over, update the crisp output u(t) and the output edge value of D.

This procedure allows the router to perform the max-min fairness in that the greedy flows are always restricted to u(t) by a router under heavy traffic conditions while those small flows is used.

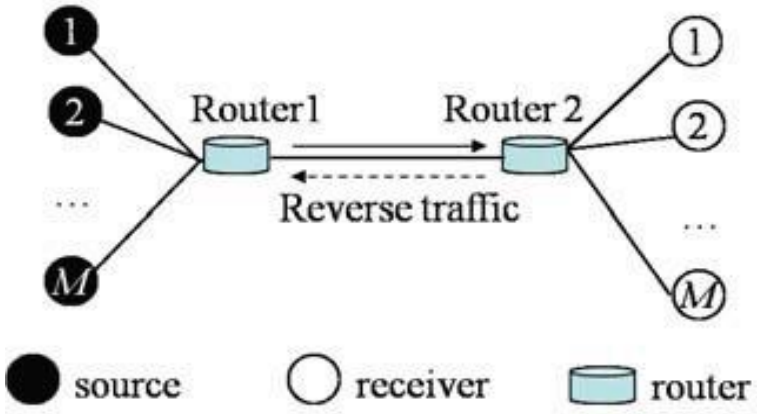

Fig. 5. Simulation network.

The desired sending rate is smaller than u(t) along their data path have no such a restriction. When the packet arrives at the destination, the receiver extracts Req_rate from the header and records it into the ACK packet before sending it back to the source.

V. An Algorithm Implementation Of Allocation And Reduce Packet Loss Rate and Utilization

ER Allocation Algorithm(Explicit-Rate)

In an explicit rate (ER) allocation algorithm for the MAX-MIN flow control of elastic traffic services with minimum rate guarantee in the setting of the ATM ABR (Available Bit Rate) service. The proposed ER algorithm is simple in that the number of operations required to compute it at a switch is minimized, scalable in that per-VC (virtual circuit) operations including per-VC queuing, per-VC accounting and per-VC state management are virtually removed, and stable in that by employing it the user transmission rates and the network queues are asymptotically stabilized at a unique equilibrium point at which MAX-MIN fairness with minimum rate guarantee and target queue lengths are achieved respectively. To improve the speed of convergence we normalize the controller gains of the algorithm by the estimate of the number of locally-bottlenecked VCs. The estimation scheme is also computationally simple and scalable since it does not require per-VC accounting either. We analyze the theoretical performance of the proposed algorithm and verify its agreement with the practical performance through simulations in the case of multiple bottleneck nodes. We believe that the proposed algorithm will serve as an encouraging solution to the MAX-MIN flow control of elastic traffic services, the deployment of which has been debated long due to their lack of theoretical foundation and implementation complexity.

ER allocation algorithm is as follows.

$$r[k + 1] = r[k] - \sum_{i=0} \alpha_i (q[k - i] - q_T) - \sum_{j=0} \beta_j r[k - j]$$

Fig. 7. ER Allocation Algorithm.

VI. Performance Evaluation

In this Intel Rate controller capacity demonstrate the performance evaluations through a series of experiments.

A. Simulated Network

Each and every controller is evaluated by the following performance measures.

- Source throughput is defined the average number of bits successfully sent out by a source per second, i.e. bits/second. Consider the bit is successfully sent out if it is part of a packet that has been successfully sent.
- IQ Size is the length of the bottleneck buffer queue seen by a departing packet.
- Queuing delay is the waiting time of a packet in the router queue before its service.
- Queuing jitter is the variation of queuing delay due to the queue length dynamics, and it can be defined as the variance of the queuing delay.
- Link utilization is the ratio between the current actual throughput in the bottleneck and the maximum data rate of the bottleneck. It is expressed as a fraction less than one or as a percentage.
- Packet loss rate is the ratio between the number of packet dropped and the number of total packets received per second by the bottleneck.

- A feasible allocation of rates is 'max-min fair' if and only if an increase of any rate within the domain of feasible allocations must be at the cost of a decrease of some already smaller or equal rates.

B. Robustness to Large Network Charges

In the real world Internet traffic is always dynamic. The performance of the controllers is faced with drastic network changes as in Fig.5 the variations of the number of flows or the available bandwidth is been investigated.

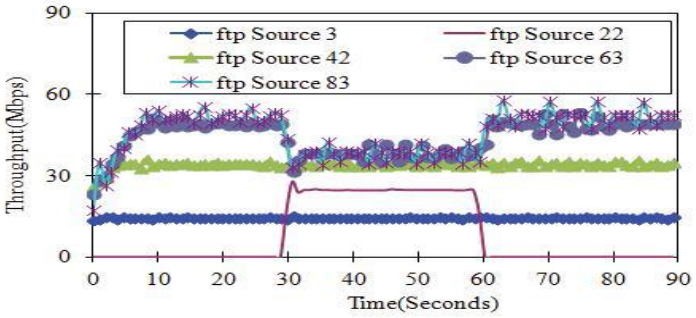

Fig. 8 Source and IQ Size dynamics under traffic change.

C. Queuing Jitter Control

One main source of the network latency oscillations comes from the dynamics of queuing delay in the routers. In Fig.8, we want to check under heavy traffic condition show the queuing delay fluctuates under the different TBO sin the Intel Rate controller, and how big the queuing jitters can be used.

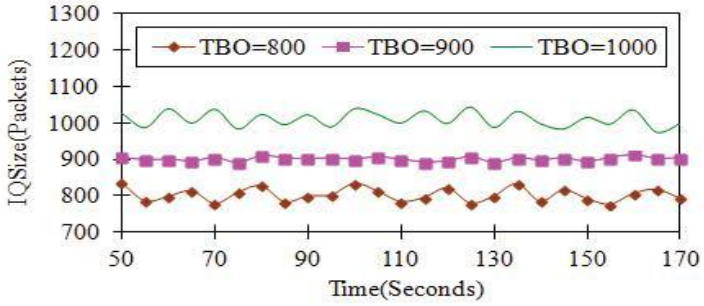

Fig.9 IQSize and queuing delay under different TBOs.

E. Effect of Short-Lived Traffic

The experiment shows that the long-lived flow scans accommodate the large short-lived http flows upon their arrivals. They simply regard the http flows as the long-lived ftp flows.

F. Utilization and Packet Loss Rate

The utilization and packet loss rate performance of the Intel Rate controller with respect to bottleneck bandwidth or the different settings of TBOs. First we check the system utilization and packet loss rate under the different bottleneck bandwidth from 45Mbpsto 10Gbps. The simulation results show that the Intel Rate controller is able to maintain the ideal zero packet loss rate with 100% link utilization despite the different bottleneck. In this buffer never overflows and packets are never lost upon heavy traffic. In the meanwhile, the stable feature in IQ Size and throughput guarantees the full bandwidth utilization.

VII. Conclusion

The IntelRate Controller has managed the internet traffic in order to reduce the QoS for different application. The IQSize has used for effective buffer capacity and max-min fairness is used to monitor the url to avoid the congestion with high performance speed dynamically. The IntelRate controller can overcome some fundamental deficiency such as potential performance problem or high router resource consumption and memory resource in router. The intelligent Fuzzy Logic Control (FLC) will tackle the non-linearity of the traffic control system.

REFERENCES

[1] M. Welzl, *Network Congestion Control: Managing Internet Traffic*. JohnWiley & Sons Ltd., 2005.

[2] R. Jain, "Congestion control and traffic management in ATM networks: recent advances and a survey," *Computer Networks ISDN Syst.*, vol. 28, no. 13, pp. 1723–1738, Oct. 1996.

[3] J. Liu and O. Yang, "Characterization of the IntelRate controller for high-speed networks," in *Proc. 2011 Commun. Netw. Services Research Conf.*, pp. 63–68.

[4] Bui, L. ; Srikant, R. ; Stolyar, A.," Novel Architectures and Algorithms for Delay Reduction in Back-Pressure Scheduling and Routing ," INFOCOM 2009 *Commun. Netw. Services Research Conf.*, pp. 33

[5] W. Hu and G. Xiao, "Design of congestion control based on instantaneous queue size in the routers," in *Proc. 2009 IEEE GLOBECOM*, pp. 1–6.

[6] G. Pavlou, "Traffic engineering and quality of service management for IP-based NGNs," in *Proc. 2006 IEEE/IFIP Netw. Operations Manage. Symp.*, p. 589..

[7] C. Chrysostomou, A. Pitsillides, G. Hadjipollas, *et al.*, "Fuzzy explicit marking for congestion control in differentiated services networks," in *Proc. 2003 IEEE Int. Symp. Computers Commun.*, vol. 1, pp. 312–319.

[8] S. Floyd, "High-speed TCP for large congestion windows," RFC 3649, Dec. 2003.

[9] W. Feng and S. Vanichpun, "Enabling compatibility between TCP Reno and TCP Vegas," in *Proc. 2003 Symp. Applications Internet*, pp. 301– 308.

[10] M. M. Hassani and R. Berangi, "An analytical model for evaluating utilization of TCP Reno," in *Proc. 2007 Int. Conf. Computer Syst. Technologies*, p. 14-1-7.

[11] N. Dukkipati, N. McKeown, and A. G. Fraser, "RCP-AC congestion control to make flows complete quickly in any environment," in *Proc. 2006 IEEE INFOCOM*, pp. 1–5.

[12] Y. Zhang, D. Leonard, and D. Loguinov, "JetMax: scalable max-min congestion control for high-speed heterogeneous networks," in *Proc. 2006 IEEE INFOCOM*, pp. 1–13.

[13] B. Wydrowski, L. Andrew, and M. Zukerman, "MaxNet: a congestion control architecture for scalable networks," *IEEE Commun. Lett.*, vol. 7, no. 10, pp. 511–513, Oct. 2003.

[14] L. Benmohamed and S. M. Meerkov, "Feedback control of congestion in packet switching networks: the case of a single congested node," *IEEE/ACM Trans. Netw.*, vol. 1, no. 6, pp. 693–708, Dec. 1993.

[15] Y. Hong and O. Yang, "Design of adaptive PI rate controller for besteffort traffic in the Internet based on phase margin," *IEEE Trans. Parallel Distrib. Syst.*, vol. 18, no. 4, pp. 550–561, 2007.

[16] W. Hu and G. Xiao, "Design of congestion control based on instantaneous queue size in the routers," in *Proc. 2009 IEEE GLOBECOM*, pp. 1–6.

[17] S. Chong, S. Lee, and S. Kang, "A simple, scalable, and stable explicit rate allocation algorithm for max-min flow control with minimum rate guarantee," *IEEE/ACM Trans. Netw.*, vol. 9, no. 3, pp. 322–335, June 2001.

[18] Y. Hong and O. Yang, "An API-RCP design using pole placement technique," in *Proc. 2011 IEEE ICC*, pp. 1–5.

[19] B. Ribeiro, T. Ye, and D. Towsley, "Resource-minimalist flow size histogram estimator," in *Proc. 2008 ACM SIGCOMM Conf. Internet Measurement*, pp. 285–290.

[20] Y. H. Long, T. K. Ho, and A. B. Rad, "An enhanced explicit rate algorithm for ABR traffic control in ATM networks," *Int. J. Commun. Syst*, vol. 14, pp. 909–923, 2011.

[21] L. Roberts, "Enhanced PRCA proportional rate control algorithm," AFTM- R, Aug. 1994.

[22] S. J. Lee and C. L. Hou, "A neural-fuzzy system for congestion control in ATM networks," *IEEE Trans. Syst. Man Cybern. B., Cybern.*, vol. 30, no. 1, pp. 2–9, 2000.

[23] A. Vashist, M. Siun-Chuon, A. Poylisher, *et al.*, "Leveraging social network for predicting demand and estimating available resources for communication network management," in *Proc. 2011 IEEE/IFIP Int. Symp. Integrated Netw. Manage.*, pp. 547–554.

[24] D. Toelle and R. Knorr, "Congestion control for carrier ethernet using network potential," *Proc. 2006 IEEE/IFIP Netw. Operations Manage. Symp.*, pp.1–4.

[25] Y. Yan, A. El-Atawy, and E. Al-Shaer, "A game-theoretic model for capacity-constrained fair bandwidth allocation," *Int. J. Netw. Manage.*, vol. 18, no. 6, pp. 485–504, Nov. 2008.

[26] K. M. Passino and S. Yurkovich, *Fuzzy Control*. Addison Wesley Longman Inc., 1998.

[27] E. Jammeh, M. Fleury, C. Wagner, *et al.*, "Interval type-2 fuzzy logic congestion control for video streaming across IP networks," *IEEE Trans. Fuzzy Syst.*, vol. 17, no. 5, pp. 1123–1142, 2009.

[28] T. W. Vaneck, "Fuzzy guidance controller for an autonomous boat," *IEEE Control Syst. Mag.*, vol. 17, no. 2, pp. 43–51, Apr. 1997.

[29] T. Kiryu, I. Sasaki, K. Shibai, *et al.*, "Providing appropriate exercise levels for the elderly," *IEEE Eng. Med. Biol. Mag.*, vol. 20, no. 6, pp. 116–124, 2001.

[30] C. Chang and R. Cheng, "Traffic control in an ATM network using fuzzy set theory," in *Proc. 1994 IEEE INFOCOM*, vol. 3. pp. 1200–1207.

[31] J. Harju and K. Pulakka, "Optimization of the performance of a ratebased congestion control system by using fuzzy controllers," in *Proc. 1999 IEEE IPCCC*, pp. 192–198.

OPEN ACCESS

International
Journal
Of Modern Engineering Research (IJMER)

A CPW-Fed Wideband And Multiband Rectangular Microstrip Patch Antenna For Wireless Applications

D. Ujwala[1], A. Gnandeep Reddy[2], K. Gopivasanth Kumar[3], K. Harika[4], N.Jaswanth[5], G. Gopinath Chowdary[6]

[1]*Assistant Professor,Department of ECE,K L University,A.P.,India*
[2,3,4,5,6] *Students,B.Tech,Department of ECE,K L University,A.P.,India*

Abstract: *In this paper a rectangular patch antenna is proposed for both the multiband and wide band operations with a coplanar waveguide (CPW) feeding. The proposed antenna has a size of 30x40x1.57mm^3 including the ground plane and it is designed on FR4 substrate with a dielectric constant of 4.4. The proposed antenna resonates at four distinct frequency bands, centered at 3.03, 4.84, 7.94 and 8.85 GHz. The return loss for the above mentioned frequency bands can be controlled and can be adjusted with parametric analysis of E-slot. The various terms and parameters associated with the antenna like return loss, radiation patterns, VSWR, current distributions and gain are analyzed and are optimized by the simulations carried out using finite element method based Ansoft High Frequency Structural Simulator(HFSS).*

Keywords: *Coplanar waveguide feed line, E-slot antenna, Antenna Performance characteristics.*

I. INTRODUCTION

The aim of this paper is to design an antenna with a low profile and high gain which can be in turn used for wireless applications. In order to achieve these attractive features such as low profile and high gain we prefer the micro strip path antennas which are most suited for millimeter wave frequency band applications and widely used for mobile communications, wireless communications and aerospace applications [1]. This Microstrip patch antennas are very simple in their construction using the conventional microstrip fabrication technique. The antennas in future must not only have multiband operation, should also possess wider bandwidths, simple structures and should have the ability to integrate with the RF circuits [2]. The Phenomenon of frequency agility, broad bandwidth, feed line flexibility and beam scanning can be easily obtained from these antennas [3]. Generally, the dimensions of microstrip patch antennas are around a half waveguide wavelength[4] and there are many miniaturization techniques that can be adopted in reducing such dimensions, they are classified as 1) Using high permittivity substrates 2) Increasing electrical length 3)Short circuits 3) Superstrates 4) Using magnetic substrates[5].

In the proposed antenna design a coplanar waveguide transmission line is employed, which enables us to design a wide range of characteristic impedances and the CPW structures usually provide wider bandwidths [6] and have many attractive features including low radiation losses, less dispersion and easy integration.

In this paper, an E- shaped slot is cut on the ground plane for multi and wide band operations; this E-shaped slot on ground plane also creates a longer current path. There are varieties of configurations that can be realized for generating multi wide operations in a single antenna are already proposed. e.g., using coupled V-slot [7], double L- slit[8] ,U- slot antenna[9] inverted- L monopole antenna [10] etc. Most of these antennas could not cover low frequency applications but can be used for multi wide band operations.

Antenna Geometry

The Antenna Structure shown in the Figure 1 represents the antenna Configuration and figures 1(a) ,1(b) represents ground Plane (Bottom view) and patch(Top view) respectively. An E-Shaped slot is cut on the ground plane to create a longer current path and at the same time to achieve both wideband and multiband operations. The proposed antenna is designed on a FR4 Substrate with an overall area of 30x40mm^2 and thickness of 1.57mm.The whole system is fed by coplanar waveguide feeding and the design of antenna is optimized using the Ansoft High Frequency Structural Simulator with the main dimensions shown in the figures 1(a) and 1(b).

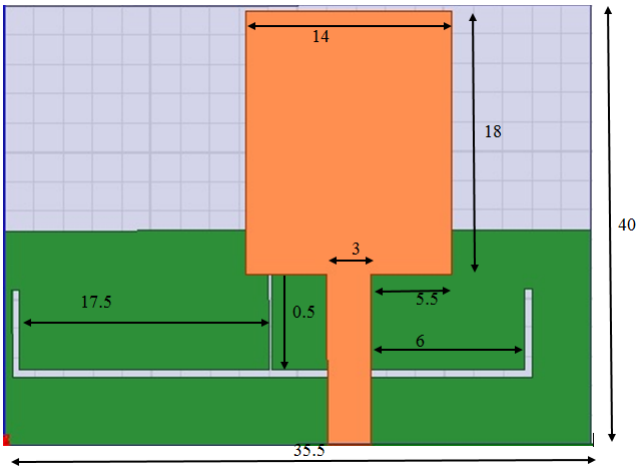

Figure1: Proposed Antenna Geometry

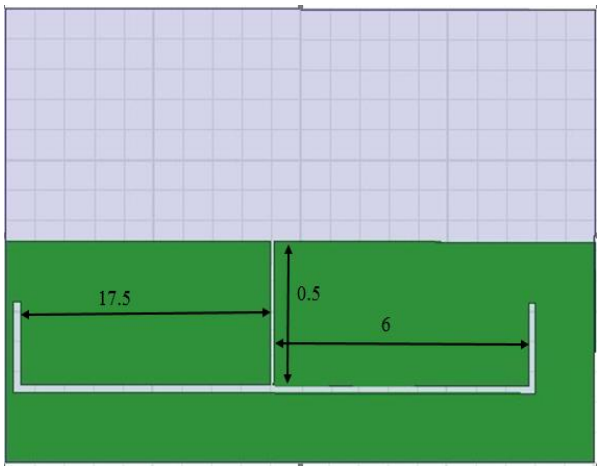

Figure 1(a): E-Slotted Ground

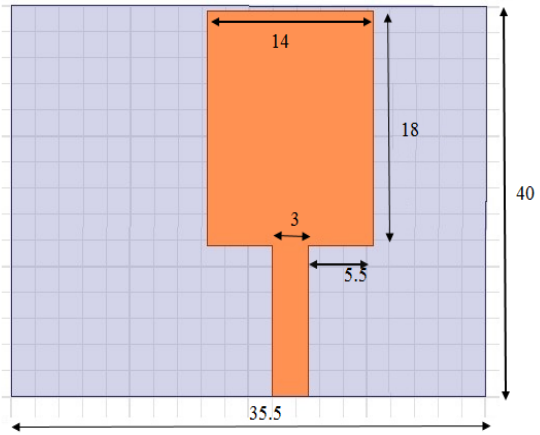

Figure 1(b): Top View Plane

II. Results And Discussions

The Proposed antenna is resonated at four different frequencies 3.03GHz, 4.84GHz, 7.94GHz and 8.85GHz and the corresponding return loss at these four frequencies are -12.94dB at 3.03GHz, -21.39 dB at 4.84GHz ,-20.25 dB at 7.94GHz and -14.93 dB at 8.85GHz. As shown in the figure 2.

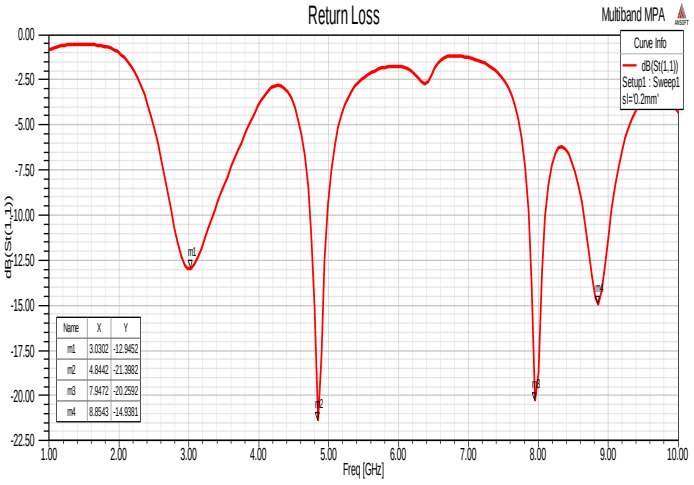

FIGURE 2: RETURN LOSS (DB) VERSUS FREQUENCY (GHZ)

The voltage Standing wave Ratio,a function of reflection coefficient which represents the power power reflected from the antenna. The Impedance matching will be perfect when the value of VSWR lies between 1 and 2. Figure 3 represents the VSWR plot. The values of VSWR at four resonant frequencies are 1.58,1.18,1.21 and 1.43 respectively.

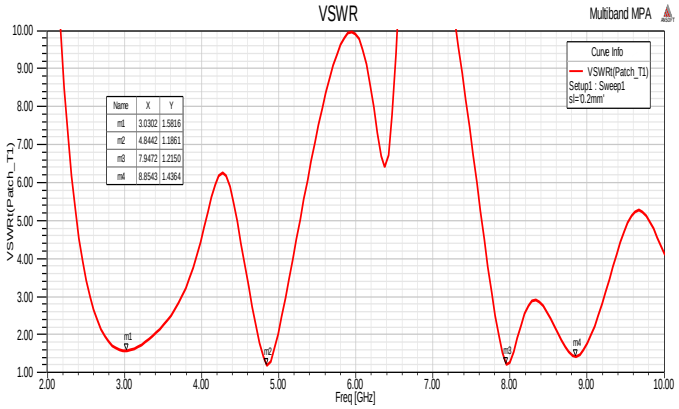

Figure 3: VSWR versus Frequency(GHz)

The E-plane Radiation patterns at 4.8Ghz and 7.94Ghz for phi=0 degrees and phi=90 degrees are shown in figure 4.

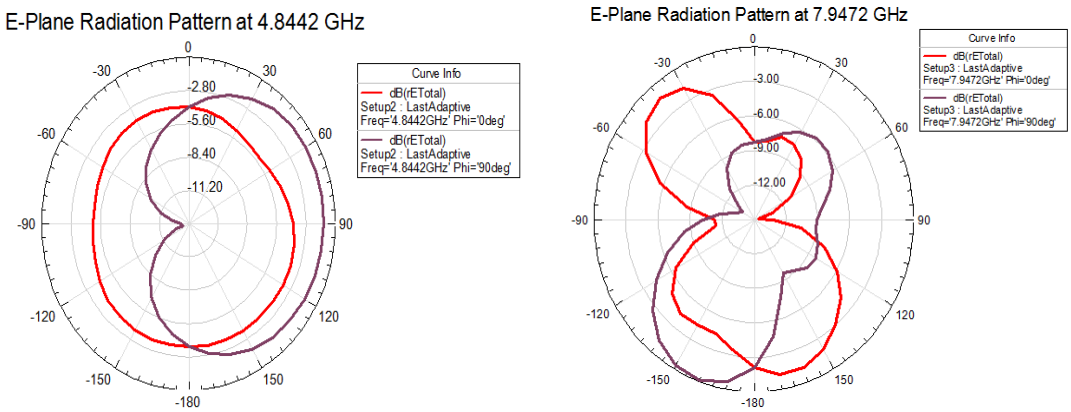

Figure 4: E-plane Radiation patterns at 4.84GHz and 7.94 GHz

The H-plane radiation patterns at 4.8 Ghz and 7.94 Ghz for Theta=0 degrees and Theta=90 degrees are shown in figure 5.

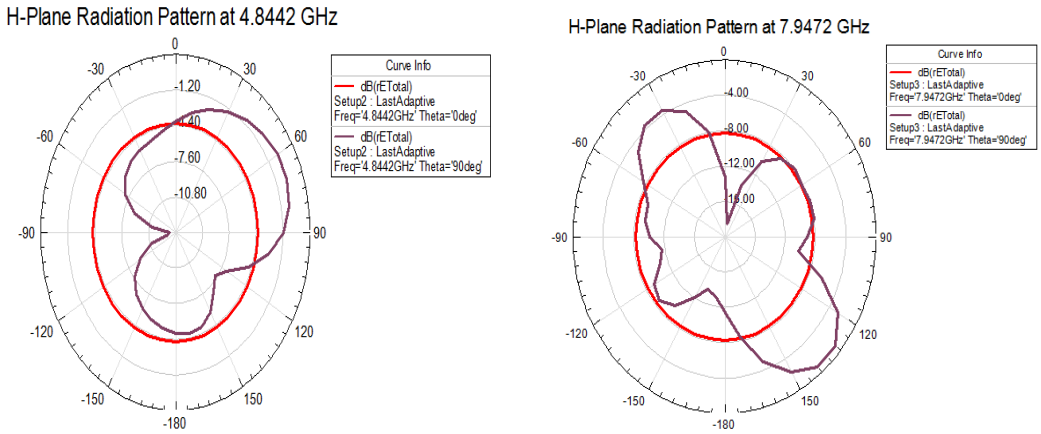

Figure 5: H-plane Radiation patterns at 4.84GHz and 7.94 GHz

The behaviour of antenna can be further studied using current distribution. The current distribution on the circuit can be measured directly by using a magnetic probe composed of an antenna in the vicinity of the circuit. However, the direct estimation of the current distribution is difficult for the case of the multilayer circuit. Here we used single patch element on the substrate, so the electric current can be estimated easily at resonant frequencies. The resonant frequencies 3.03,4.84,7.94,8.85GHz are been used for current distribution studies. The surface current distributions at 4.84 and 7.94GHz resonant frequencies is shown in the figure 6(a) and 6(b).

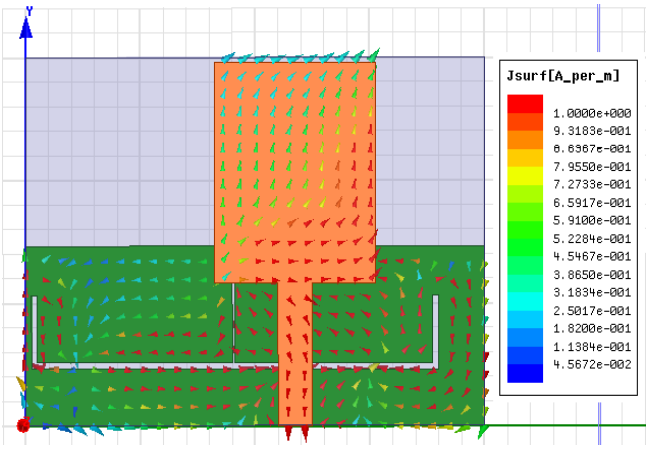

Figure 6(a): Surface Current distribution at 4.84GHz Frequency

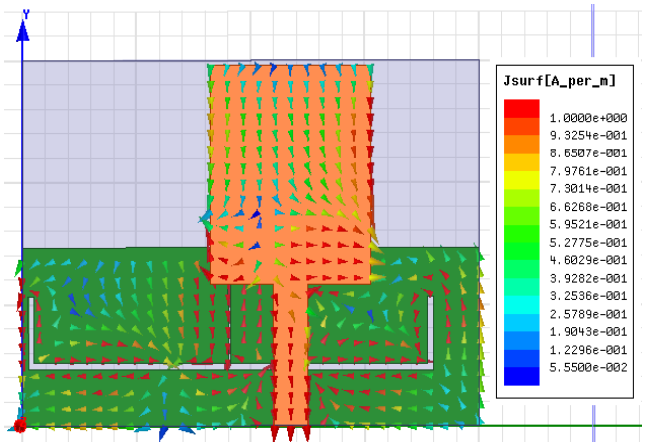

Figure 6(b): Surface Current distribution at 7.94GHz frequency

The simulated peak gain of the proposed Antenna is observed and displayed as shown in the figure 7 for both 4.84 and 7.94GHz resonant frequencies as 2.4 and 3.6 dBi respectively.

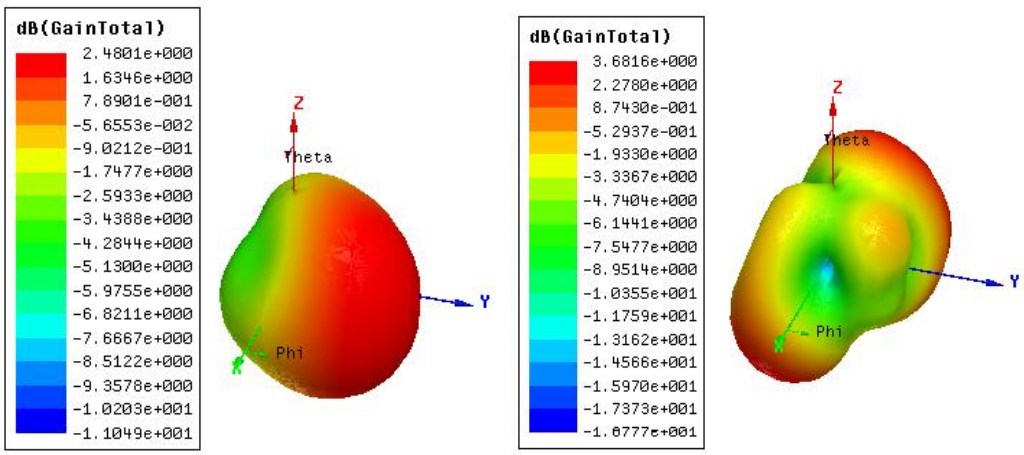

Figure7: Antenna Gain at 4.84 and 7.94GHz Frequencies

III. Conclusion

The Technique of using an E-shaped slot in the ground plane for a rectangular microstrip patch antenna with CPW feeding is to obtain both multiband and wideband characteristics in a single antenna is examined. Investigation on antenna shows that wide impedance bandwidths are achievable by varying size and shape of the ground plane. Along with the conventional parametric studies the current distribution analysis is also done in order to further realize the antenna performance. The Simulation results show that the proposed antenna presented in this paper has a high gain, high efficiency and stable radiation pattern at all the four resonant frequencies.

Acknowledgement

The Authors would like to acknowledge their gratitude towards the management and Department of ECE, K L University for their support during the work.

REFERENCES

[1]. D.Ujwala,B.Jyothi, B.T.P.Madhav, "Design and Analysis of Compact CPW-Fed UWB Antenna for Wireless Communication Applications", International Journal of Current Research and Review ,Volume no:4,Issue:7,April 2012.

[2]. Hattan F. Abutarboush, Member, IEEE, H. Nasif, R. Nilavalan, Senior Member, IEEE, and S. W. Cheung, Senior Member, IEEE "Multiband and Wideband Monopole Antenna for GSM900 and Other Wireless Applications" IEEE Antennas and Wireless propagation letters, vol. 11, 2012 pp.539-542.

[3]. B.T.P.Madhav, D.Ujwala, Habibullah Khan,Atluri Lakshmi Tejaswani, Sriram Guntupalli and Atluri Bala-Substrate permittivity effects on the performance of Slotted Aperture Stacked Patch Antenna, International Journal of Applied EngineeringResearch,Vol:8,No:8,August-13,PP:909-916.

[4]. D.Ujwala, A.Gnandeep Reddy, K.Gopivasanth Kumar,J.Kowsik, K.Sai Chandra-"Wideband Coaxial Fed Rotated Stacked Patch Antenna for Wireless Applications"International Journal of Engineering Research and Applications,Vol.4,Issue 3,March 2014 pp:102-105.

[5]. M.C.Pang and K.L.Wong-"Broadband Circularly polarized microstrip antenna with a Dual perpendicular feed" Microwave Optical Technology Letters,Vol.24,No.6,March 2000,pp:420-422.

[6]. Jyh-Ying Chiou, Jia-Yi Sze, and Kin-LuWong, "A broad-band CPW fed strip-loaded square slot antenna," IEEE Trans. Antennas Propagation., vo1.51, pp. 719-721,2003.

[7]. S.-W. Qu and Q. Xue, "A Y-shaped stub proximity coupled V-slot microstrip patch antenna," IEEE Antennas Wireless Propag. Lett., vol. 6, pp. 40–42, 2007.

[8]. T.-H. Kim and D.-C. Park, "Compact dual-band antenna with doubleL-slits for WLAN operations," IEEE Antennas Wireless Propag. Lett.,vol. 4, pp. 249–252, 2005.

[9]. H. F. Abutarboush, R. Nilavalan, D. Budimir, and H. Al-Raweshidy,"Double U-slots patch antenna for tri-band wireless systems," Int. J.RF Microw. Comput.-Aided Eng., vol. 20, no. 3, pp. 279–285, May 2010.

[10]. W. Ni and N. Nakajima, "Small printed inverted-L monopole antennafor worldwide interoperability for microwave access wideband operation,"Microw., Antennas Propag., vol. 4, no. 11, pp. 1714–1719, Nov.2010.

D. Ujwala born in A.P, India in 1987. Completed B.Tech in 2008 from Koneru Lakshmaiah College of Engineering affiliated to Acharya Nagarjuna University. Worked as Associate Software Engineer for K L University from 2009-2010. Completed her M.Tech, Communication and Radar Systems from K L University in 2012. Currently working as Assistant Professor in K L University.

A. Gnandeep Reddy was born in A.P.,India in 1994.He is pursuing his B.Tech in Electronics and Communication Engineering from School of Electrical Sciences,K L University.with the Specialization in Communication Systems. He is a member of IETE.Till date,He has published 2 papers in International Journals and Presented Technical Papers in National Level Technical Symposiums of reputed institutions like NIT,Warangal.Vignan University,Guntur.His Research interests include Antennas, RF System Design, Transmission Line modeling and Satellite Communications.

K. Gopivasanth Kumar was born in A.P.,India in 1994.He is pursuing his B.Tech in Electronics and Communication Engineering from K L University with the specialization in Communication Systems.He has published 2 papers in International Journals and presented papers in National Level Technical Symposiums of reputed institutions like IIIT,Hyderabad and NIT,Warangal.His research interests include RF and Microwave Engineering,Antennas and VLSI Design.

K. Harika was born in A.P., India. pursuing her B.Tech in Electronics and Communication Engineering from School of Electrical Sciences, K L University. She is a member of IETE. She has presented various Technical papers in National Level Technical Symposiums. Her research interests include Wireless Communications and Antenna Design.

N. Jaswanth was born in A.P, India. He is pursuing his B.Tech in Electronics and Communication Engineering from School of Electrical Sciences, K L University with the specialization in Signal Processing. He is a member of IETE. His research interests include Image Processing, Digital Signal Processing and Antennas.

G. Gopinadh Chowdary was born in A.P., India in 1994.He is pursuing his B.Tech in Electronics and Communication Engineering from K L University with the specialization in Networking. He is a member of IETE. His research interests include Medical Image Processing, Satellite Communications and Digital Electronics.

OPEN ACCESS

International
Journal
Of Modern Engineering Research (IJMER)

Optimization of Turning Parameters Using Taguchi Method

Sharda R. Nayse[1], M. G. Rathi[2]

[1]*Student, Department of Mechanical Engineering, Government Engineering College Aurangabad, (MS), India.*
[2]*Associate professor, Department of Mechanical Engineering, Government Engineering College Aurangabad, (MS), India.*

Abstract: *Today in manufacturing and metal industries customer satisfaction is very important to make own place in competitive market and also to make mirror image with faith in the heart of customer, because customer gives preference to buy good quality product. In the metal and manufacturing industries for the product low surface roughness is very important. Lowest surface roughness assures not only good quality but also reduces manufacturing cost. In this paper the main objective is to study effect of cutting speed, feed rate and depth of cut on surface roughness of mild steel in turning operation and as a result of that the combination of optimum level of factors was obtained to get lowest surface roughness. Experiments have been conducted using Taguchi's experimental design technique. An orthogonal array, signal to noise ratio, and analysis of variance are employed to investigate cutting characteristics of mild steel using high speed steel. Experimental results show that among the cutting parameter cutting speed is the most significant machining parameter for surface roughness followed by feed rate and depth of cut.*

Keywords: *Surface roughness, Turning operation, S/N Ratio.*

I. Introduction

The machining processes generate a wide variety of surface textures. Surface texture consists of the repetitive and random deviations from the ideal smooth surface. These deviations are

- Roughness: small, finely spaced surface irregularities (micro irregularities)
- Waviness: surface irregularities of greater spacing (macro irregularities)
- Lay: predominant direction of surface texture

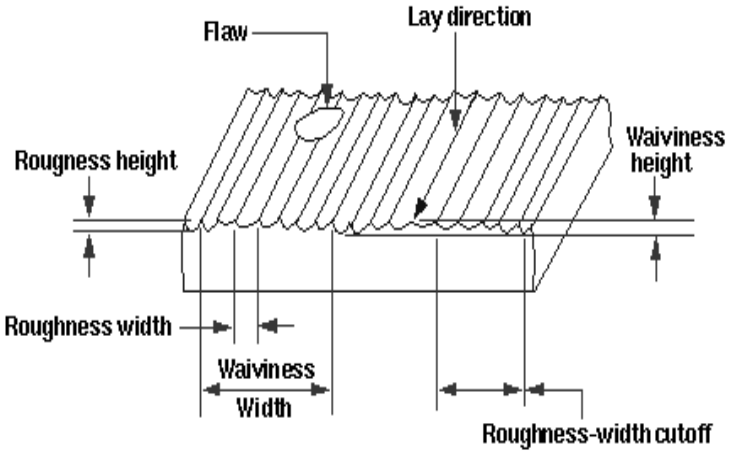

Fig 1: Surface characteristics

Three main factors make the surface roughness the most important of these parameters:

- Fatigue life: The service life of a component under cyclic stress (fatigue life) is much shorter if the surface is high.
- Bearing properties: A perfectly smooth surface is not a good because it cannot maintain a lubricating film.
- Wear: High surface roughness will result in more intensive surface wear in friction.

Factors Affecting Quality of Turning Process:

The three key mechanical inputs in metal removal operations are speed, feed and depth of cut. Manipulating the speed, feed and depth of cut can maximize the benefits of a particular cutting fluid and can increase productivity. However, like most decisions, the choice of feed, speed and depth of cut must be based on the customer's objectives. What is their goal in this application? Do they want to manufacture parts faster or maximize tool life? How important is the surface finish and dimensional accuracy of the part? Answers to these questions will drive their decisions on feed, speed and depth of cut.

Definitions:

- Speed: speed is the rate of rotation of the spindle where the tool is held. It is measured in revolutions per minute (RPMs).
- Feed: feed is the rate at which the tool is moved into the part or part into the tool. Feed is measured in feet, inches or millimeters per time period.
- Depth of Cut (DOC): the measurement (normally in inches or millimeters) of how wide and deep the tool cuts into the work piece.

II. Taguchi Method

Taguchi methods are statistical methods developed by Genichi Taguchi to improve the quality of manufactured goods, and more recently also applied to engineering, biotechnology, marketing and advertising. Professional statisticians have welcomed the goals and improvements brought about by Taguchi methods, particularly by Taguchi's development of designs for studying variation, but have criticized the inefficiency of some of Taguchi's proposals. The performance measure, signal to noise ratio (S/N) proposed by Taguchi is used to obtain the optimum parameter combinations. The larger S/N means the relation to the quality will become better.

In Taguchi method desirable performance is classified in three categories such as the smaller-the-better quality, the larger-the-better-quality, and the nominal-the-best. Signal to noise analysis is designed to measure quality characteristic. It is given by

$$S/N = -10\log_{10}(MSD)$$

Where MSD= Mean Square Deviation

For the smaller the better characteristic,

$$MSD = (Y_1^2 + Y_2^2 + Y_3^2 + \cdots\cdots\cdots\cdots)/n$$

Larger the better characteristic,

$$MSD = (1/Y_1^2 + 1/Y_2^2 + 1/Y_3^2 + \cdots\cdots\cdots\cdots)/n$$

Nominal the best characteristic,

$$MSD = [(Y_1 - m)^2 + (Y_2 - m)^2 + (Y_3 - m)^2 + \cdots\cdots\cdots\cdots)]/n$$

Where Y_1, Y2, Y3 are the responses and n is the number of tests in a trial and m is the target value of the result. Smaller surface roughness values represent better or improved surface quality of the product. Therefore, a smaller-the-better quality characteristic was implemented and introduced in this study.

Quality implies delivering products and services that meet customer's standards and fulfill their needs and expressions. Quality has been traditionally assured by Statistical Process Control a collection of powerful statistical methods facilitating the production of quality goods by intelligently controlling the factors that affect a manufacturing process.

Experiments are carried out by researchers or engineers in all fields of study to compare the effects of several conditions or to discover something new. If an experiment is to be performed most efficiently, then a scientific approach to planning it must be considered. The statistical design of experiments is the process planning experiments so that appropriate data will be conducted, the minimum number of experiments will be performed to acquire the necessary technical information, and suitable statistical methods will be used to analyze the collected data.

The statistical approach to experimental design is necessary if we wish to draw meaningful conclusions from the data. Thus, there are two aspects to any experimental design: the design of the experiment and the statistical analysis of the collected data. They are closely related, since the method of statistical analysis depends on the design employed.

An outline for an experimental design is shown in figure 2:

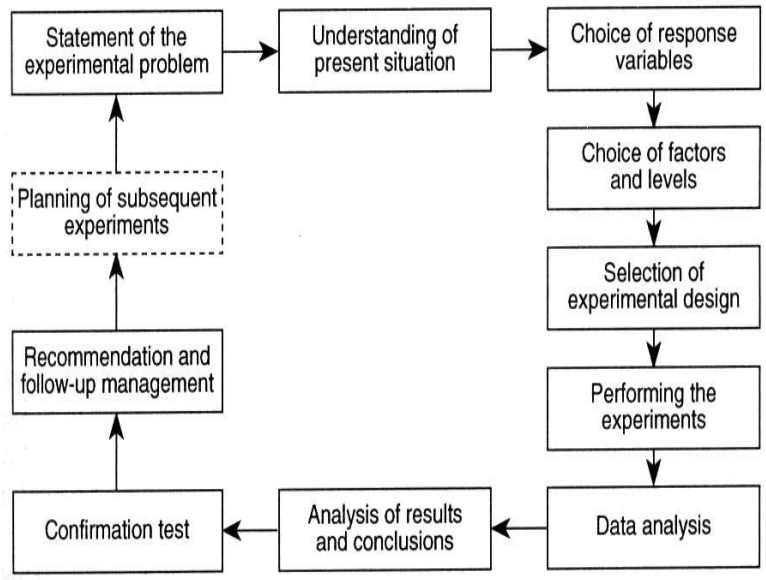

Fig 2: Outline of experimental design procedure

III. Experimental Design

In this study, the main objective is to study the effect of cutting speed, feed rate and depth of cut on the surface roughness of turned specimen of mild steel using Taguchi's L_9 orthogonal array design. The values of the input process parameters for the turning operation are as under:

Table I: Input Parameters

Notations	Factors	Level 1	Level 2	Level 3
A	Cutting Speed (rpm)	190	300	500
B	Feed (mm/rev)	0.044	0.088	0.132
C	Depth of Cut (mm)	0.2	0.4	0.6

Table Ii: Layout of L_9 Orthogonal Array

Trial	Cutting Speed (rpm) (A)	Feed (mm/rev) (B)	Depth of Cut (mm) (C)
1	Level 1	Level 1	Level 1
2	Level 1	Level 2	Level 2
3	Level 1	Level 3	Level 3
4	Level 2	Level 1	Level 2
5	Level 2	Level 2	Level 3
6	Level 2	Level 3	Level 1
7	Level 3	Level 1	Level 3
8	Level 3	Level 2	Level 1
9	Level 3	Level 3	Level 2

TABLE III: LAYOUT OF EXPERIMENTAL DESIGN ACCORDING TO L_9 ARRAY

Trial No.	A Cutting Speed (rpm)	B Feed (mm/rev)	C Depth of Cut (mm)	Surface Roughness (microns)	S/N Ratio
1	190	0.044	0.2	1.63	-4.26
2	190	0.088	0.4	2.16	-6.70
3	190	0.132	0.6	2.83	-9.04
4	300	0.044	0.4	2.09	-6.40
5	300	0.088	0.6	2.69	-8.61
6	300	0.132	0.2	2.11	-6.50
7	500	0.044	0.6	2.91	-9.28
8	500	0.088	0.2	1.90	-5.58
9	500	0.132	0.4	2.40	-7.60

IV. Analysis Of Variance

Analysis of variance is standard is a standard technical technique to interpret experimental results. It is extensively used to detect differences in average performance of groups of items under investigation. It breaks down the variation in the experimental result into accountable sources and thus finds the parameters whose contribution to total variation is significant. Thus analysis of variance is to study the relative influences of multiple variables, and their significance. The importance of ANOVA is to determine two estimates of population variance viz., one based on between samples variance and the other based on within sample variance. Then said to estimates of population variance are compared with F-test. At pre-determined level of significance, the null hypothesis is rejected, otherwise accepted.

For this ANOVA table is prepared. In this ANOVA table, the sum of squares (SS) due to independent variable and the sum of squares due to error is separately given. Degree of freedom (DOF) is the number of way one can select the components for a set up under restriction. In the case of analysis, there is loss of one degree in sum of squares due to regression. Mean sum of squares (MSS) are obtained by dividing SS by the DOF, each for regression and error. The MSS related to error is called as variance.

TABLE IV: RESULTS OF ANOVA

Factors	Degree of Freedom	Sum of Squares	Mean Square	% Contribution	F-Ratio
Cutting Speed (rpm)	2	1.17	0.59	3.225	0.0834
Feed (mm/rev)	2	1.94	0.97	5.348	0.13720
Depth of Cut (mm)	2	19.028	9.514	52.451	1.34569
Error	2	14.14	7.07	38.977	
Total	8	36.278	4.535		

V. Conclusions

In this study, the Taguchi method is used to study the effect of parameters like cutting speed, feed and depth of cut on the surface roughness of mild steel in turning and to find out optimum combination parameters at which lower surface roughness value is obtained. In this study, at cutting speed (190 rpm), feed (0.044mm/rev) and depth of cut (0.2 mm) the lower value of surface roughness is obtained. Hence in this study, $A_1B_1C_1$ is the best combination.

REFERENCES

[1] http://www.quakerchem.com

[2] Raghuwanshi B. S, A course in Workshop Technology Vol. II (Machine Tools), Dhanpat Rai & Company Pvt. Ltd, 2009.

[3] C. Vidal, C Infante, P. Pecas, P. Vilaca, "Application of Taguchi Method in the optimization of an aeronautic aluminum alloy," Departmento de agenharia Mecanica, Instituto Superior Tecnico, Av. Rovisco Pais, 1096-001 Lisboa, Portugal.

[4] Mahapatra S. S, Parametric Analysis and Optimization of Cutting parameters for Turning Operations based on Taguchi Method, Proceedings of the International conference on Global manufacturing and Innovation, pp. 27-29, July 2006.

[5] Wang, W. H., and Tarng, Y. S., 1998, "Design Optimization of Cutting Parameters for turning operations based on the Taguchi method". *Journal of Materials Processing Technology, pp. 84, pp. 122-129.*

[6] Taguchi G. Introduction to quality engineering. New York: Mc Graw Hill; 1990.